Fibroblast Spheroids:

A Useful Assay for Drug Screening in Idiopathic Pulmonary Fibrosis?

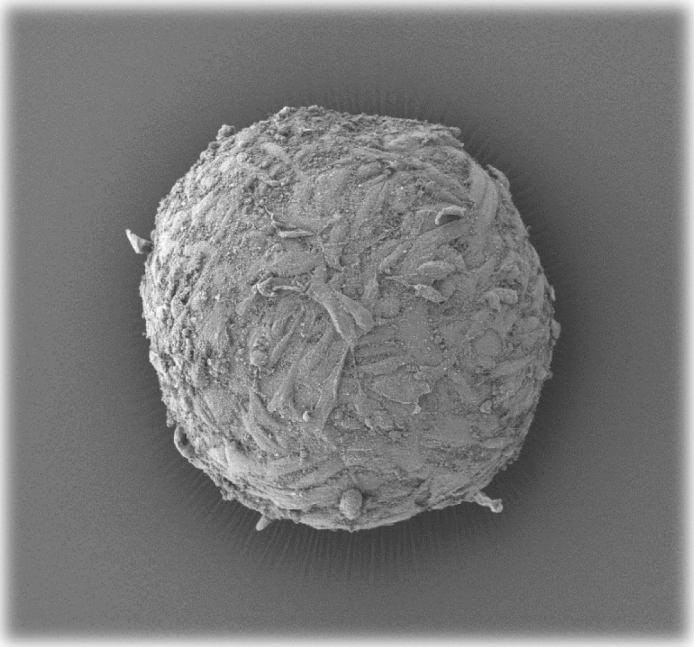

By Nisha Kanda

A thesis submitted to University College London, for the degree of Doctor of Philosophy

Centre for Inflammation and Tissue Repair (CITR),
Rayne Institute, University College London,
5 University Street, London, WC1E 6JF

DECLARATION

I, Nisha Kanda, confirm that the work presented in this thesis is entirely my own. Where information has been derived from other sources, I confirm that this has been indicated in this thesis.

ACKNOWLEDGEMENTS

I would like to take this opportunity to thank a number of people within the Centre for Inflammation and Tissue Repair (CITR) at University College London (UCL, UK) and Fibrosis Discovery Performance Unit (DPU) at GlaxoSmithKline (GSK, Stevenage, UK) for giving invaluable support throughout the course.

Firstly, I would like to express my sincere gratitude to Dr. Chris J. Scotton (my primary supervisor) for his motivation, enthusiasm, patience, immense knowledge, and his wonderful guidance throughout the four years. Despite his absence from UCL in my final year, he was always able to provide support in every possible way and for that reason I am extremely grateful to him and could not have imagined a better mentor for my PhD. I would also like to thank Chris for his critical appraisal of this thesis.

Prof. Rachel Chambers (my secondary supervisor) for her scientific insight and for her humble support in the absence of Chris during my MPhil/PhD upgrade and in my final year; Dr. Andy Blanchard (my industrial supervisor) and Dr. Carmel Nanthakumar for their guidance and support in several aspects of my project and for their immense help during my work at GSK.

Dr. Paul Mercer (UCL) and Dr. Robin McAnulty (UCL) for their support and guidance in several scientific aspects; Dr. Richard Hatley (GSK, Stevenage) for providing the compounds; Dr. Elaine Gower, Dr. Susan Boyce, and Mr Prabin Rai (GSK, Stevenage) for their humble support in the lab at GSK; Mark Turmaine (UCL) for training me on electron microscopy and for processing the samples; Mr Elliott Harrison and Dr. Gino Miele (Epistem, UK) for performing the microarrays.

My colleagues at UCL (including the ones who have left our group) for all their support, assistance, advice, and for becoming great friends. These include (in no particular order): Robert Alexander, Natalia Smoktunowicz, Manuela Platè, Linda Franklin, Sharada Karanam, Ellen Forty, Ricardo Jose, David Pearce, Jessica Eley, Lizzy Peix, Jo Barnes, Hannah Woodcock, Iona Evans, Noura Al-Juffali, Katrina McNulty, Katerina Jenkins, Steve Bottoms, and Michal Sulikowski.

BBSRC and GSK for their funding.

Finally, I would like to take this opportunity to thank God and the most important people in my life, my family, because without them this achievement would have simply been impossible. There are no words to explain how grateful I am to them and how much I love and appreciate them all for being a huge part of my life.

I would like to thank my parents for giving me the strength, motivation, encouragement, and guidance throughout life. I would also like to thank them, as well as my siblings (Mohit, Chanda, Reinu, and Vanita) for their unconditional love and support, for always having faith in me, for always motivating me, for tolerating all of my stressful outbursts, and for always being there through the most challenging years of my life.

Last but definitely not the least I would like to thank Snaha Patel for her friendship, immense support, and motivation during my BSc degree, MSc degree, and during the first three years of my PhD which is one of the many reasons why throughout life I will always remain grateful to her and I will always consider her as a member of my family.

This thesis is dedicated to…

My Family & Chris

…because without them this achievement

would have been impossible.

TABLE OF CONTENTS

LIST OF FIGURES

LIST OF TABLES

ABSTRACT

Introduction: Idiopathic pulmonary fibrosis (IPF) is characterised by excessive deposition of extracellular matrix proteins and destruction of the lung architecture. The aetiology of this disorder is unknown and few effective therapies are available. Several models have been established to identify key pathological cells and mediators that may be important in IPF, however these models lack the classical histopathological features seen in IPF, such as fibrotic foci. The aim of this project was to develop a novel 3-D *in vitro* assay system which more closely mimics a fibrotic focus, for pre-clinical drug evaluation.

Methods: Primary human lung fibroblasts were isolated as outgrowths from small (<1 mm^3) lung explants (non-IPF and IPF patients). Non-IPF (n = 10) and IPF (n = 10) fibroblasts were cultured in non-adherent 96-well plates to generate fibroblastic spheroids. Spheroid formation and phenotypic features were characterised using time-lapse videomicroscopy, histological analysis, (including TUNEL assay) and, electron microscopy. RNA was extracted from the spheroids and microarray analysis and qRT-PCR were used to analyse mRNA levels. Total collagen was measured using HPLC analysis of hydroxyproline levels while active TGFβ within the spheroid homogenates and supernatants were measured using the transformed mink lung epithelial cell bioassay. A medium-throughput screen of potential anti-fibrotic compounds (using a focused GSK compound library known as the fibrosis toolbox) was also performed, using hydroxyproline levels as the endpoint measure.

Results: Non-IPF and IPF fibroblasts were able to form non-proliferating spheroids within 24 hours of incubation, with clear organisation and orientation of cells within the spheroid. IPF spheroids had a myofibroblastic phenotype with increase expression of αSMA. TUNEL assay identified increased numbers of apoptotic cells in non-IPF spheroids in comparison to IPF spheroids, which may be due, in part, to autocrine/paracrine COX1-mediated PGE_2 generation. The mink lung cell assay demonstrated that non-IPF and IPF spheroids spontaneously produced high levels of active TGFβ, which was partially dependent on β3 and β8 integrins. Antagonising TGFβ signalling did not however affect spheroid collagen production. Microarray data analysis illustrated a limited number of differentially expressed genes, with the majority involved in encoding proteins that play a key role in metabolic pathways. The fibrosis toolbox identified potential target molecules that impact on collagen biosynthesis including EP2/4 compounds, an integrin αv inhibitor, Smo antagonists, MCP-1 inhibitor, and mTORC 1/2 inhibitors.

Conclusions: Fibrotic fibroblast spheroids mimic some of the key characteristics of fibroblasts in fibrotic foci of IPF lungs (i.e. increased collagen production, elevated levels of active TGFβ and resistance to apoptosis). In addition, microarray and medium-throughput screening identified several potential targets. Therefore, fibrotic fibroblast spheroids may represent a novel assay system for pre-clinical drug evaluation, and warrant further investigation.

ABBREVIATIONS

3-Hyp	3(S)-hydroxy-L-proline
4-Hyp	4(R)-hydroxy-L-proline
5-LOX	5-lipoxygenase
6MWT	6 minute walk test
AA	Arachidonic acid
ACE	Angiotensin converting enzyme
AEC	Alveolar epithelial cells
ALK	Activin-like kinase
ANG	Angiotensin
ATI	Alveolar epithelial cells type I
ATII	Alveolar epithelial cells type II
ATP	Adenosine triphosphate
ATS	American Thoracic Society
αSMA	Alpha smooth muscle actin
BALF	Bronchoalveolar lavage fluid
BCA	Bicinchoninic acid
BM	Basement membrane
BMP	Bone morphogenetic protein
BSA	Bovine serum albumin
CAD	Caspase-activate DNase
cAMP	Cyclic adenosine monophosphate
CASP1	Caspase 1
CCL	Chemokine (C-C motif) ligand
CCR	Chemokine (C-C motif) ligand receptor

COMP	Collagen and cartilage oligomeric matrix protein
COX	Cyclooxygenase
CS	Citrate synthase
Ct	Threshold cycle
CTGF	Connective tissue growth factor
DAB	3,3'-diaminobenzdine
DAPI	4',6-diamidino-2-phenylindole
DDR	Discoidin domain receptor
DLCO	Diffusing capacity of the lung for carbon monoxide
DMEM	Dulbecco's modified eagle's medium
DMSO	Dimtheyl sulfoxide
DNA	Deoxyribonucleic acid
DNMT	DNA methyltransferase
DPBS	Dulbecco's phosphate-buffered saline
DTT	Dithiothreitol
ECL	Enhanced chemiluminescence
ECM	Extracellular matrix
EDTA	Ethylenediaminetetracetic acid
EIF4A2	Eukaryotic translation initiation factor 4A2
ELISA	Enzyme-linked immunoassay
EM	Electron microscopy
EMT	Epithelial-mesenchymal transition
EP	Prostaglandin E receptor
ER	Endoplasmic reticulum
ERK	Extracellular signal-regulated kinase

ERS	European Respiratory Society
ET	Endothelin
FACIT	Fibril-associated collagens with interrupted triple helices
FasL	Fas ligand
FBS	Foetal bovine serum
FC	Fold change
FDR	False discovery rate
FGF	Fibroblast growth factor
FP	Prostaglandin F receptor
FVC	Forced vital capacity
GAG	Glycosaminoglycan
GDF	Growth and differentiation factors
GLI	Glioma-associated oncogene homolog
GPCR	G-protein coupled receptor
HAT	Histone acetyletransferase
HBEC	Human bronchial epithelial cells
HDAC	Histone deacetylase
HLF	Human lung fibroblast
HPLC	High pressure liquid chromatography
HRCT	High resolution computed tomography
HSP47	Heat shock protein 47
IFN	Interferon
IIP	Idiopathic interstitial pneumonia
IL	Interleukin
ILD	Interstitial ling disease
IMPDH2	Inosine-5’-monophosphate 2

IPF	Idiopathic pulmonary fibrosis
JAK	Janus kinase
JNK	c-Jun amino-terminal kinase
kDa	Kilodalton
LAP	Latency-associated peptide
LLC	Large latency complex
LOX	Lysyl oxidase
LOXL	Lysy oxidase like protein
LTGF	Latent TGFβ binding protein
MACIT	Membrane-associated collagens with interrupted triple helices
MAPK	Mitogen activated protein kinase
MCP1	Monocyte chemotactic protein 1
MEK	Mitogen activated protein kinase kinase
MHC	Major histocompatibility complex
MIF	Macrophage migration inhibitory factor
MM	Mismatch probe
MMP	Matrix metalloproteinases
MSB	Martius scarlet blue
MTHFR	Methylenetetrahydrofolate reductase
MT-MMP	Membrane-type metalloproteinases
mTOR	Mammalian target of rapamycin
mTORC	Mammalian target of rapamycin complex
NAC	N-acetylcysteine
NBD-Cl	4-Chloro-7-nitrobenzofurazan
NCS	Neonatal calf serum
NSB	Non-specific binding

NSIP	Non-specific interstitial pneumonia
OD	Optical density
P3H	Prolyl 3-hydroxylase
P4H	Prolyl 4-hydroxylase
P4HA1	Prolyl 4-hydroxylase subunit alpha 1
PAI	Plasminogen activator inhibitor
PAR	Proteinase activated receptor
PBS	Phosphate buffered saline
PCA	Principle component analysis
PCP	Procollagen carboxy terminal proteinase
PDE	Phosphodiesterase
PDGF	Platelet derived growth factor
PDI	Protein disulphide isomerase
PDK1	Phosphoinositide dependent protein kinase 1
PF	Pulmonary fibrosis
PFA	Paraformaldehyde
PG	Prostaglandin
PGE_2	Prostaglandin E2
PGES	Prostglandin E2 synthase
pHLF-Di	Primary human lung fibroblasts isolated from digested lungs
pHLF-Ex	Primary human lung fibroblasts isolated from lung explants
PI3K	Phosphatidylinositol-3 kinase
PICP	Procollagen type I carboxy-terminal pro-peptide
PIIICP	Procollagen type III carboxy-terminal pro-peptide

PIP2	Phosphatidylinositol 4,5-bisphosphate
PIP3	Phosphatidylinositol 3,4,5-trisphosphate
PKB	Protein kinase B
PLA_2	Prospholipase A2
PM	Perfect match probe
PTEN	Phosphatase and tensin homolog
QC	Quality control
qRT-PCR	Real time quantitative reverse transcription polymerase chain reaction
RAPTOR	Regulatory-associated protein of mTOR
RAS	Renin-angiotensin system
RGD	Arg-Gly-Asp sequence
RICTOR	Rapamycin-insensitive companion of mTOR
RIN	RNA integrity number
RMA	Robust multi-array average
RNA	Ribonucleic acid
RTK	Receptor tyrosine kinase
RT-PCR	Reverse transcription polymerase chain reaction
ROS	Reactive oxygen species
SDS-PAGE	Sodium dodecyl sulphate polyacrylamide gel electrophoresis
SEM	Scanning electron microscopy
SFTA2	Surfactant protein A2
Shh	Sonic hedgehog
SLC	Small latency complex
Smo	Smoothelin
SPTLC2	Serine palmitoyltransferase

SYNJ2	Synaptojanin 2
TβR	TGF-beta receptor
TBS	Tris-buffered saline
TBST	Tris-buffered saline tween
TdT	Terminal deoxynucleotidyl transferase
TEM	Transmission electron microscopy
TGFβ	Transforming growth factor beta
TIMP	Tissue inhibitors of metalloproteinase
TLC	Total lung capacity
TMLEC	Transformed mink lung epithelial cell
TNF-α	Tumour necrosis factor alpha
TOP1	Topoisomerase 1
tPA	Tissue plasminogen activator
TSP-1	Thrombospondin-1
TUNEL	Terminal deoxynucleotidyl transferase dUTP nick ended labelling
UIP	Usual interstitial pneumonia
uPA	Urokinase plasminogen activator
UPR	Unfolded protein response
UBC	Ubiquitin C
VEGF	Vascular endothelial growth factor
XDH	Xanthine dehydrogenase
ZO-1	Zonula occludens -1

CHAPTER 1: INTRODUCTION

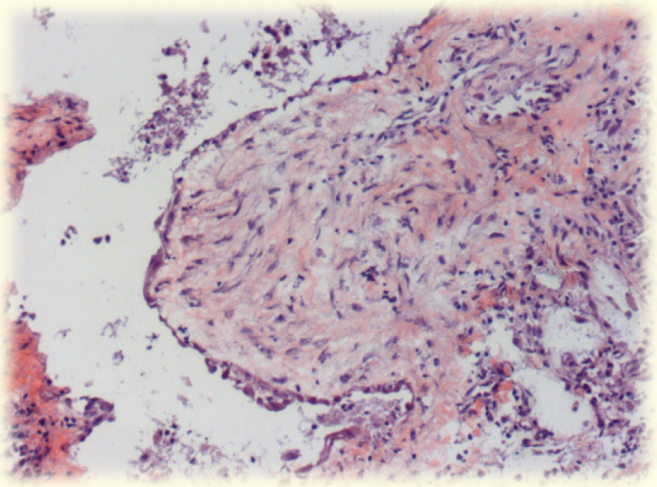

1.1. Anatomy and Physiology of Normal Lungs

1.1.1. Lung structure and function

Lungs are the sole respiratory organs found in mammals and their principal function involves the transport of atmospheric oxygen into the bloodstream and removal of carbon dioxide via diffusion. The basic structure of the lung is shown in **Figure 1.1**, illustrating a branching system composed of the trachea, bronchi, bronchioles, and alveoli. However, several cells play critical roles in maintaining its structure and function including epithelial cells, endothelial cells, smooth muscle cells, stem and progenitor cells, macrophages, and fibroblasts. Thus lungs are highly complex organs, not least from a cellular perspective.

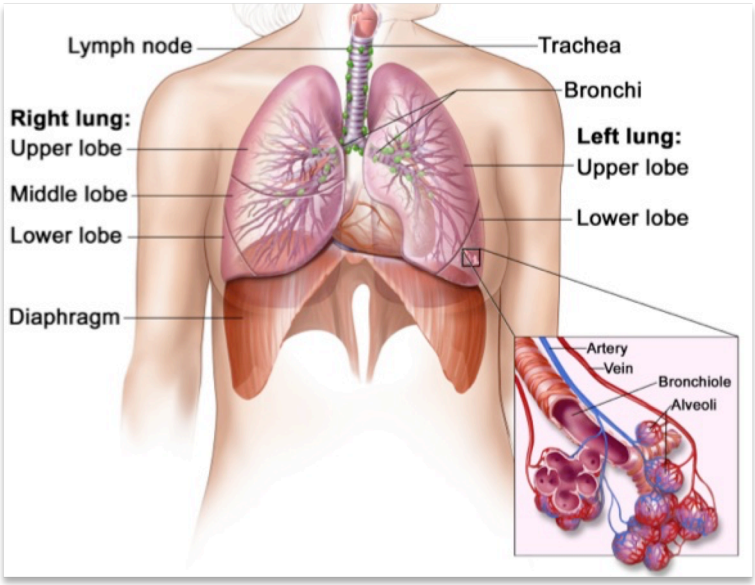

Figure 1. 1: Basic schematic of human lung structure.

Reproduced from (Winslow, 2006) with the permission of Terese Winslow, the National Cancer Institute © 2006.

Gas exchange takes place at the alveoli. Each alveolus is approximately 200μm in diameter, composed of a simple epithelium which is surrounded by a network of capillaries. To appreciate the efficiency of the gas exchange it is important to note that respiratory gases need to pass through the microvascular endothelium (0.04-0.2μm), interstitial space (0.02-0.2

μm), alveolar epithelium (0.05-0.3 μm), and the surface lining of surfactant (0.01 μm). Thus, the total distance between the airspace and the microvasculature is approximately between 0.2 and 0.6 μm (Adds et al., 2001). Epithelial and endothelial cells share the same basement membrane and together they form a total gas exchange surface of ~70 m^2 (Selman and Pardo, 2006).

Since there is a direct contact between the lungs and the external environment, the lungs are constantly exposed to several noxious substances such as pollutants, microorganisms, cigarette smoke, and dust. Thus, it is vital that the structure and defence mechanism of the lungs remain robust enough to withstand the effects of such contaminants in order to maintain its respiratory function. Any alterations in the lung architecture, such as excessive deposition of extracellular matrix (ECM) in the pulmonary interstitium, can reduce the efficacy of gas exchange (Laurent and Shapiro, 2006) leading to severe pathological conditions such as pulmonary fibrosis (PF; discussed in detail in **Section 1.2**).

1.1.2. Normal pulmonary extracellular matrix

ECM encompasses components of the interstitial connective tissue and the basement membrane (Dunsmore and Rannels, 1996) which play a key role in the physical and mechanical properties of all organs including the lungs. The tensile strength in the large airways and the trachea is achieved by the cartilage which is composed of collagen and cartilage oligomeric matrix protein (COMP) (Vuga et al., 2013). Furthermore, the basement membrane in the airways (located beneath the alveolar epithelial layer) consists of several ECM proteins including collagen type IV, laminin, fibronectin, and entactin all of which are involved in regulating the diffusion of gases across the epithelial layer. Moreover, ECM in the pulmonary interstitium (predominately composed of fibrillar collagens, elastic fibres, and proteoglycans) acts as a spatiotemporal natural scaffold which is able to modulate several cellular functions including cell migration, proliferation, and differentiation (Dunsmore and Rannels, 1996; Mammoto et al., 2013). Thus, ECM proteins play essential roles in normal lung structure and function. Although there are several ECM components in the lung this thesis will mainly focus on the most abundant ECM constituent, collagen, and its effects on pathological conditions (i.e. idiopathic pulmonary fibrosis, IPF, discussed in detail in **Section 1.2.1**).

1.1.3. Collagens, the most abundant ECM proteins

Structure and collagen types

Collagens are characterised by a unique triple helical structure composed of three alpha chains each containing domains with repeats of an amino acid sequence, Gly-X-Y, where positions X and Y are usually composed of lysine and L-proline residues of which some are hydroxylated during posttranslational processes (Schegg et al., 2009). Maintenance of this triple helical structure is vital for several biological functions including adhesion, collagen-mediated cellular and/or enzymatic function, and ECM assembly (Travis et al., 2013). Currently 28 types of collagens have been identified (**Table 1.1**) which are encoded by at least 44 different genes (Schegg et al., 2009), giving each type a distinctive amino acid sequence and molecular structure. Collagen types can be categorised into two groups based on their biochemical properties: neutral-salt soluble collagen (composed of immature precursor with very few crosslinks) and acid–soluble collagen (composed of mature fibres with several intra-molecular crosslinks). Approximately, 1-5 % of adult lung collagen is considered to be neutral salt collagen (Last and Reiser, 1984; Kliment et al., 2011). Thus, in order to determine the majority of collagen content in the lung a harsh technique (e.g. acid hydrolysis) is required. In our lab, this is done by incubating tissues/cells at 110 ^{o}C overnight in 6 M hydrochloric acid (HCl; details of this method are described later in **Section 2.12**).

Nevertheless, collagens may also be categorised into seven groups based on their domain structure: fibrillar collagen (main structural components of connective tissues), FACITs (fibril-associated collagens with interrupted triple helices), network-forming collagens, transmembrane collagens also known as MACITs (membrane-associated collagens with interrupted triple helices), MULTIPLEXINs (multiple triple-helix domains and interruptions), anchoring fibrils, and beaded-filament forming collagens (**Figure 1.2; Table 1.1**). Approximately 90 % of the collagens in the human body are fibrillar collagen types I, II, and III (Lodish et al., 2000), and more than 95 % of the total lung parenchymal collagen is type I and III with a ratio of 2:1 (Last and Reiser, 1984). These are synthesised by fibroblasts and distributed in blood vessels, the tracheobronchial tree, and alveolar interstitium. The amount of collagen deposited by fibroblasts in the lung is regulated by a carefully controlled process which affects the balance between collagen synthesis and degradation. During a pathological maturation and remodelling phase the process of collagen synthesised is greater in comparison to its degradation causing an elevation in the net collagen level.

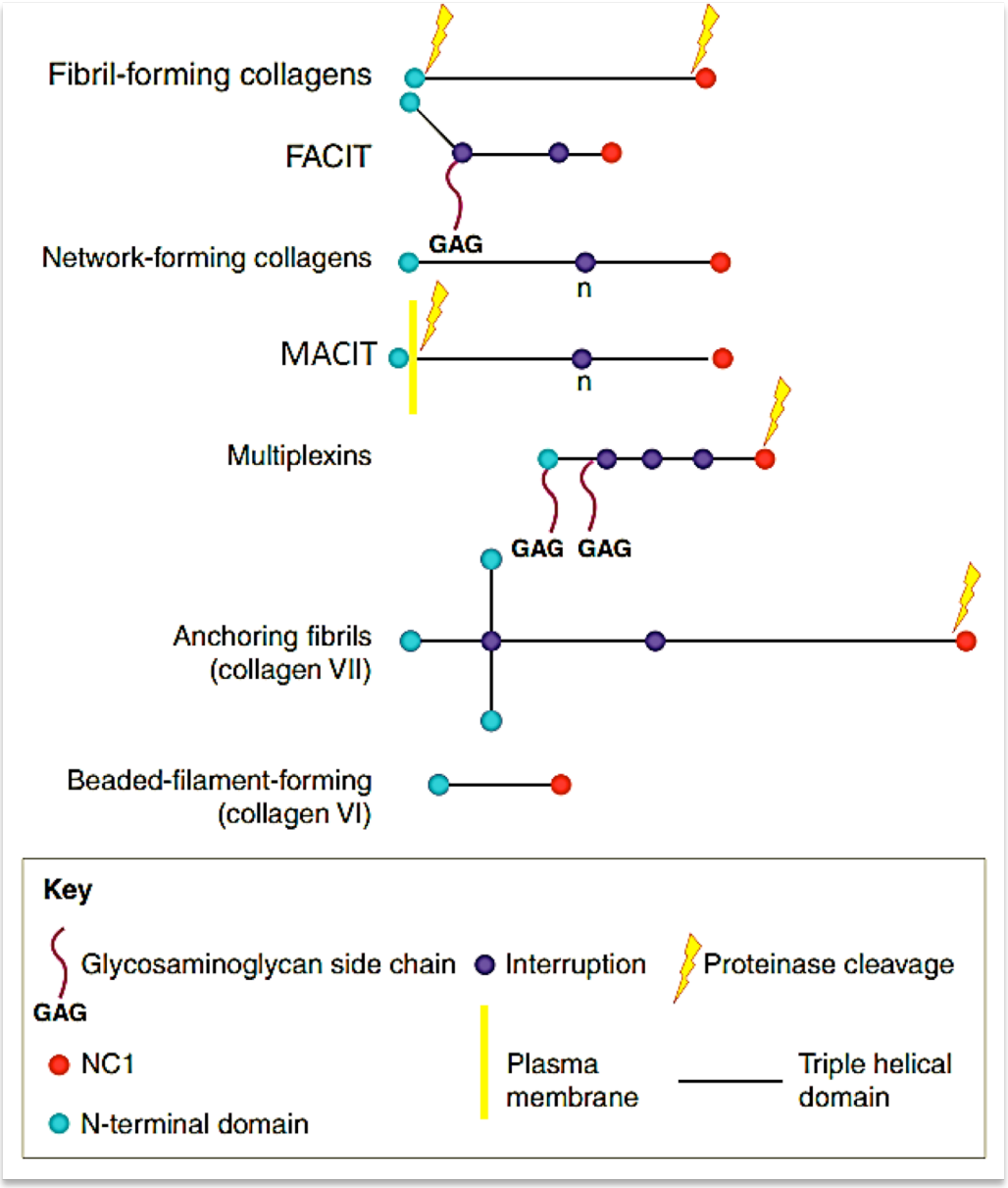

Figure 1. 2: Collagen types based on domain structure.

Collagens are categorised into seven groups based on their domain structures. 1) Fibril-forming collagens are initially synthesised as procollagens which contain C- and N-terminal propeptides which are eventually cleaved off; 2) FACIT (fibril-associated collagens with interrupted triple); 3) Network-forming collagens which form an interlaced network in the basement membrane; 4) MACIT (transmembrane-associated collagens with interrupted triple helices) which are also referred to as transmembrane collagens composed of long interrupted triple helical extracellular domains and a short cytosolic N-terminal domain; 5) Multiplexins, also known as endostatin producing collagens; 6) Anchoring fibrils, which contain collagen VII as a major component; 7) Beaded-filament-forming collagens. NC1 refers to a non-collagenous domain 1 which does not contain the original triple helical structure.

Adapted from: (Kadler et al., 2007)

Table 1. 1: Collagen types and distributions

	Class	Molecular Composition	Distribution
I	Fibrillar	$[\alpha1(I)]_2$, $[\alpha2(I)]$	Abundant; widespread in connective tissues
II	Fibrillar	$[\alpha1(II)]_3$	Cartilage, vitreous humor
III	Fibrillar	$[\alpha1(III)]_3$	Skin, muscle, blood vessels
IV	Network	$[\alpha1(IV)]_2$, $[\alpha2(IV)]$	Basement membrane
V	Fibrillar	$[\alpha1(V)]_3$	Co-distributes with type I especially embryonic tissues
VI	Beaded-filament	$[\alpha1(VI)]$, $[\alpha2(VI)]$, $[\alpha3(VI)]$	Widespread, especially muscles
VII	Anchoring fibrils	$[\alpha1(VII)]_2$, $[\alpha2(VII)]$	Basement membrane
VIII	Network	$[\alpha1(VIII)]_3$	Descement's membrane
IX	FACIT	$[\alpha1(IX)]$, $[\alpha2(IX)]$, $[\alpha3(IX)]$	Co-distributes with collagen II
X	Network	$[\alpha1(X)]_3$	Hypertrophic cartilage
XI	Fibrillar	$[\alpha1(XI)]$, $[\alpha2(XI)]$, $[\alpha3(XI)]$	Co-distributes with collagen II
XII	FACIT	$[\alpha1(XII)]_3$	Found with collagen I
XIII	MACIT	-	Neuromuscular junctions, skin
XIV	FACIT	$[\alpha1\{XIV)]_3$	Found with collagen I
XV	MULTIPLEXIN	-	Located between collagen fibrils close to the basement membrane; eyes, muscles.
XVI	FACIT	-	Integrated into collagen fibrils
XVII	MACIT	$[\alpha1(XVII)]_3$	Localised to epithelia
XVIII	MULTIPLEXIN	-	Associated with basement membranes
XIX	FACIT	-	Rare; localised to basement membrane zones;
XX	FACIT	-	Widespread distribution
XXI	FACIT	-	Widespread distribution
XXII	FACIT	-	Localised at tissue junctions
XXIII	MACIT	-	Limited tissue distribution; exists as a transmembrane and shed form
XXIV	Fibrillar	-	Selective expression in developing cornea and bones
XXV	MACIT	-	Precursor protein for CLAC
XXVI	FACIT	-	-
XXVII	Fibrillar	-	Embryonic cartilage, developing dermis, cornea, retina, arteries; restricted to cartilage found in adults
XXVIII	-	-	Basement membrane around Schwann cells

Reproduced and adapted from (Lodish et al., 2000)

Collagen biosynthesis

The biosynthetic pathway for collagen type I has been most intensively studied. **Figure 1.3** illustrates a simplified schematic for collagen synthesis. Following transcription and translation, precursor collagen chains known as nascent procollagens are synthesised in the endoplasmic reticulum (ER). These chains then undergo several posttranslational modifications including hydroxylation of L-proline (Mizuno et al., 2003) and lysine residues (Risteli et al., 2004). Two enzymes play a vital role in this process. These are prolyl 4-hydroxylase (P4H) (Kukkola et al., 2003) and prolyl 3-hydroxylase (P3H) (Vranka et al., 2004) which require an essential co-factor (ascorbic acid, vitamin C) to result in the formation of 4(R)-hydroxy-L-proline (4-Hyp) and 3(S)-hydroxy-L-proline (3-Hyp), respectively. 4-Hyp is the main component of all collagen types, comprising around 13.5 % of its amino acid composition; thus the amount of 4-Hyp is used as a measure of total collagen content in tissue samples (Kliment et al., 2011). Hydroxylation of lysine residues occurs via the activity of lysyl hydroxylases. Both hydroxyproline and hydroxylysine contribute to the stability of the triple helix structure where hydroxylysine is vital for cross-linking of collagen molecules (Reiser et al., 1992).

Further modifications to the procollagen chains include glycosylation of hydroxylysine residues which involves the addition of the monosaccharide Gal(β1-*O*) or the disaccharide Glc(α1-2)Gal(β1-*O*) via the activity of galactosyltransferase and glucosyltransferase (Spiro, 1969). Some studies have demonstrated that lysyl hydroxylase 3 may also catalyse a modest glucosyl and galactosyltransferase activity, supporting that this enzyme is multifunctional (Heikkinen et al., 2000). In addition, oligosaccharide chains are added to certain asparagine residues in the C-terminal propeptide (segment located at the C-terminus of the procollagen).

Several folding proteins and/or chaperones in the ER also play a role in collagen synthesis. For example, protein disulphide isomerase (PDI) associates with the C-propeptides on procollagen and catalyses the formation of disulphide bonds which proceed towards the N-terminus and facilitates trimer formation (Wilson et al., 1998). PDI is considered as a multifactorial protein as it not only catalyses the formation of disulphide bonds but also acts as a subunit for P4H during proline hydroxylation, and behaves as a molecular chaperone during procollagen chain assembly (Wilson et al., 1998). Another protein chaperone essential for correct folding of the triple helix is heat shock protein (HSP)-47 (Nagata, 1996; Lamande and Bateman, 1999; Sauk et al., 2005; Taguchi and Razzaque, 2007).

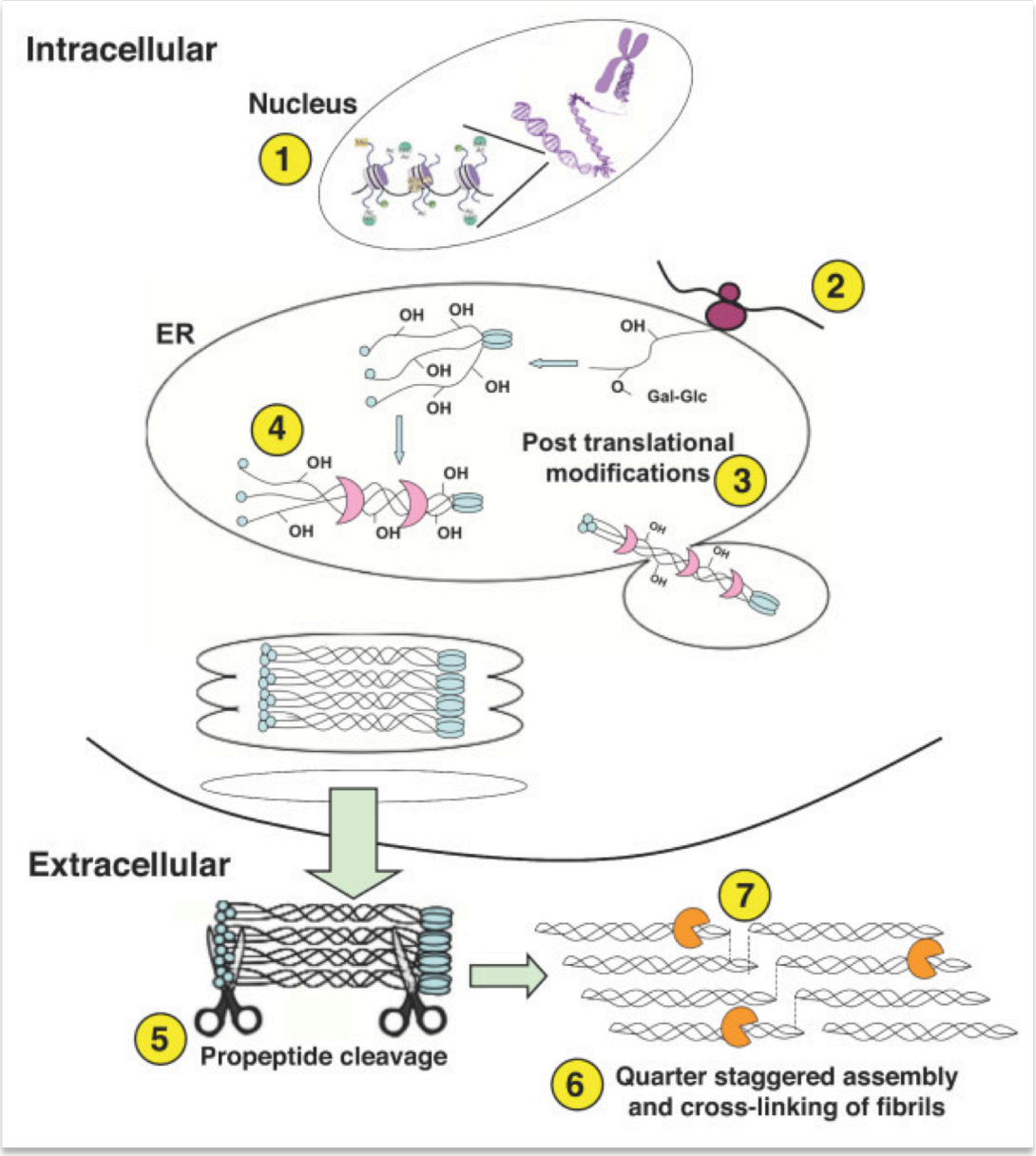

Figure 1. 3: Collagen synthesis.

Collagen genes are transcribed and mRNA is transported from the nucleus to the ribosomes of the rough endoplasmic reticulum. 2) Procollagen chains are synthesised. 3) Procollagen chains undergo posttranslational modifications including hydroxylation, glycosylation, and disulphide bond formation. 4) Heat shock protein 47 (HSP47) chaperone associates with the chains to *allow* correct folding of the triple helix (pink crescent symbol). 5) Procollagen secreted into the extracellular matix (ECM). C- and N-propeptidases cleave the C- and N-terminals of the procollagen chains. 6) Lysyl oxidases (LOX) catalyse the formation of crosslinks between collagen molecules. 7) Matrix metalloproteinases (MMPs) promote the degradation of collagen (orange Pacman symbol).

Following posttranslational modifications in the ER and Golgi apparatus, the triple helix procollagen is secreted into the extracellular space, whereby proteolytic enzymes cleave the C- and N-terminal propeptides resulting in the formation of collagen (also referred to as tropocollagen). This cleavage allows the collagen molecules to polymerise into fibrils in the ECM. Furthermore, lysyl oxidases (LOX; copper dependent enzyme) in the ECM catalyse the formation of reactive aldehydes, spontaneously forming crosslinks between the triple-helical collagen molecules and stabilises the collagen fibrils (Lodish et al., 2000; Maki et al., 2005). Currently, five LOX enzymes have been identified of which LOXL2 has shown to be associated with lung fibrosis (Barry-Hamilton et al., 2010).

Signal transduction processes in the pulmonary ECM

The pulmonary ECM is able to interact dynamically with its surrounding cells, activating a variety of signalling pathways which influence cell morphology and behaviour (e.g. proliferation, migration, differentiation, and adhesion). In addition, the intracellular cytoskeleton may exert forces which affect the orientation of matrix macromolecules. Thus, the communication between cells and ECM is bi-directional which is essential for several biological processes, epitomised by efficient gaseous exchange. This bi-directional signalling is regulated via the activation of transmembrane linker cell surface receptors known as integrins. These are able to associate with most ECM proteins as well as mediate cell-to-cell interaction. Structurally, integrins are composed of noncovalently-associated alpha and beta subunits. The molecular interactions between integrin receptors and their respective ligands involves the recognition of the Arg-Gly-Asp (RGD) sequence, which is known to be present in several ECM components including collagen, fibronectin, fibrinogen, and vitronectin. Integrins $\alpha v\beta 3$ and $\alpha v\beta 5$ are receptors for vitronectin (Horton, 1997), thrombin, fibronectin, thrombospondin, and fibrinogen. Furthermore, within the integrin family four collagen receptors have been identified of which $\alpha 1\beta 1$ and $\alpha 2\beta 1$ integrins have been most intensively studied. These integrins are expressed on cardiac, dermal, and lung fibroblasts (Gullberg et al., 1992; Caniggia et al., 1995; Eckes et al., 2006; McCall-Culbreath and Zutter, 2008). Furthermore studies have shown that during collagen matrix contraction, $\beta 1$ integrins mediate lung fibroblast cell survival via the phosphatidylinositol-3-Kinase/Akt/protein kinase B (PI3K/Akt/PKB) signalling pathway (Tian et al., 2002). As well as direct interaction with ECM protein, integrins also interact with profibrotic cytokines (i.e. transforming growth factor beta, TGFβ) resulting in the activation of downstream signalling pathways which in turn lead to further production of ECM proteins and ECM remodelling. The importance of abnormal integrin signalling and elevated

TGFβ levels has been implicated in several pathological conditions including fibrosis, which will be discussed in greater detail in later sections.

As well as integrins, studies have demonstrated three other receptors which directly associate with collagen molecules. These are discoidin domain receptors (DDRs), glycoprotein VI (GPVI; an activating receptor on platelets), and leukocyte-associated immunoglobulin-like receptor I (LAIR-1; an inhibitory receptor located on immune cells). DDRs are a unique subfamily of receptor tyrosine kinases (RTKs). Unlike most RTKs, DDRs are activated by mature collagen containing a specific DDR binding site (GVMGFO motif) (Carafoli and Hohenester, 2013). Extracellular domains of DDRs mediate binding of this receptor to the GVMGFO motif. These domains include an N-terminal discoidin (DS) domain, a DS-like domain and a short juxtamembrane (JM) region (Leitinger, 2003; Ichikawa et al., 2007; Carafoli et al., 2009). Two DDRs have been identified: DDR1 and DDR2. DDR1 is primarily located on epithelial cells of most tissues (including lungs, kidneys, gastrointestinal tract, and mammary glands) and activated by collagen types I, VI, and VIII. On the other hand DDR2 is expressed in mesenchymal cells (such as smooth muscle cells and fibroblasts) and activated by collagen types I and III (Shrivastava et al., 1997; Vogel et al., 1997; Ruiz and Jarai, 2011). Nevertheless, recent studies have demonstrated that the expression of DDR1 increases on the surface of human lung fibroblasts following collagen I-induced DDR2 activation via a JAK/ERK1/2-mediated mechanism As well as increasing receptor expression, DDRs are able to activate several downstream signalling molecules including Shp-2, Src, MAPK, and NF-kB pathways (Leitinger, 2011; Ruiz and Jarai, 2011) in order to regulate matrix remodelling (via matrix metalloproteinases; MMPs), cell adhesion, migration, and proliferation (Vogel et al., 1997).

ECM degradation – role of matrix metalloproteinases

Degradation of pulmonary ECM proteins is primarily mediated by matrix metalloproteinases (MMPs) with some contributions from serine proteinases including tissue plasminogen activator (tPA), urokinase plasminogen activator (uPA), and plasmin (Mutsaers et al., 1997). MMPs are a family of 24 secreted and membrane-bound proteinases in humans which are synthesised by several cells in the lungs including fibroblasts, myofibroblasts, epithelial cells, and macrophages. They are zinc-dependent endopeptidases which are secreted as zymogens (inactive enzyme precursors) and require cleavage in order to become activated (Greenlee et al., 2007). The activity of these degrading proteins is dependent on numerous mediators including cytokines, proteases, growth factors, mechanical forces, and lipid mediators.

Furthermore, MMP activity is also regulated by tissue inhibitors of metalloproteinases (TIMPs). Thus, the balance between MMPs and TIMPs play a critical role in ECM remodelling. As well as degrading ECM components, MMPs have also been recognised to alter cell-cell and cell-matrix interactions ultimately making cell receptors available to growth factors bound to ECM (e.g. TGFβ). The balance between collagen production and degradation in pathological conditions (i.e. idiopathic pulmonary fibrosis) will be discussed below.

1.2. Pulmonary Fibrosis

Wound healing is an absolutely critical biological process involved in direct replacement of damaged or dead cells with connective tissue, following injury. The end result of this process involves the formation of a scar. Scars have many useful purposes including the reinforcement of the initial clot formation to prevent blood loss at the site of injury, creating a barrier to prevent pathogen invasion, and providing a provisional matrix for subsequent reepithelialisation (Hecker and Thannickal, 2011). However, abnormalities in the wound healing process can lead to fibrosis affecting the overall function of the organ. Fibrosis typically results from conditions persisting for several weeks, months, or years in which tissue destruction and repair occur simultaneously leading to excessive connective tissue deposits. Fibrosis can occur in virtually any tissue or organ in the body including lungs, liver, kidney, and skin.

Pulmonary fibrosis (PF) is the end stage of a heterogeneous group of lung disorders, known as interstitial lung diseases (ILDs) which are characterised by fibroblast proliferation and excessive deposition of extracellular matrix (ECM) proteins within the pulmonary interstitium. There are around 200 lung diseases within this group, all of which share features of clinical presentation, however the pathological features and aetiology of each disease are different making them independent from one another (Sureshbabu et al., 2011).

Several ILDs have causes which have been well characterised, including environmental exposures (e.g. asbestosis), drug toxicity, radiation, and systemic fibrotic conditions (e.g. systemic sclerosis, rheumatoid arthritis, and collagen vascular disease). Despite this, the aetiology of the most common form of ILDs, known as idiopathic interstitial pneumonias (IIPs) are still unknown. Many IIPs exhibit similar clinical, pathological, and radiological features. This

makes diagnosis, prognosis, and treatment of IIPs extremely challenging. However, in 2002 the American Thoracic Society (ATS) and European Respiratory Society (ERS), which has recently been updated in 2013 and is illustrated in Table 1.2, introduced a criterion for the characterisation and diagnosis of major IIPs.

Table 1.2: Categorisation of major idiopathic interstitial pneumonias

	Clinical-Radiological-Pathological Diagnoses	Associated Radiologic and/or Pathologic-Morphologic Patterns
Chronic fibrosing IP	Idiopathic pulmonary fibrosis	Usual interstitial pneumonia
	Idiopathic nonspecific interstitial pneumonias	Non-specific interstitial pneumonia
Smoking-related IP*	Respiratory bronchiolitis-interstitial lung disease	Respiratory bronchiolitis
	Desquamative interstitial pneumonia	Desquamative interstitial pneumonia
Acute/subacute IP	Cryptogenic organising pneumonia	Organising pneumonia
	Acute interstitial pneumonia	Diffuse alveolar damage

* Desquamative interstitial pneumonia can occasionally occur in non-smokers.

Reproduced and adapted from (Travis et al., 2013) with permission of the American Thoracic Society (ATS).

1.2.1. Idiopathic Pulmonary Fibrosis

Idiopathic pulmonary fibrosis (IPF) is the most common and lethal form of IIP affecting approximately 5 million people worldwide (Meltzer and Noble, 2008). It is an irreversible, chronic, and progressive parenchymal lung disorder which leads to respiratory failure due to destruction of functional alveolar units (**Figure 1.4**) (Selman et al., 2011).

Statistics show that the survival rate of patients diagnosed with IPF is much worse in comparison to several cancers (**Figure 1.5**) with over 5000 deaths recorded each year within the UK (Hodgson et al., 2002; Gribbin et al., 2006; Raghu et al., 2006, 2011). The prevalence of

IPF is rising and currently it is estimated to be 7.4 per 100,000 people/year in the UK, 6.8-16.3 per 100,000 people/year in the US, and 11.5 per 100,000 people/year in the European Union (EU; **Table 1.3**) (Rafii et al., 2013). Furthermore, no distinct pattern of social, geographical, or racial distribution occurs.

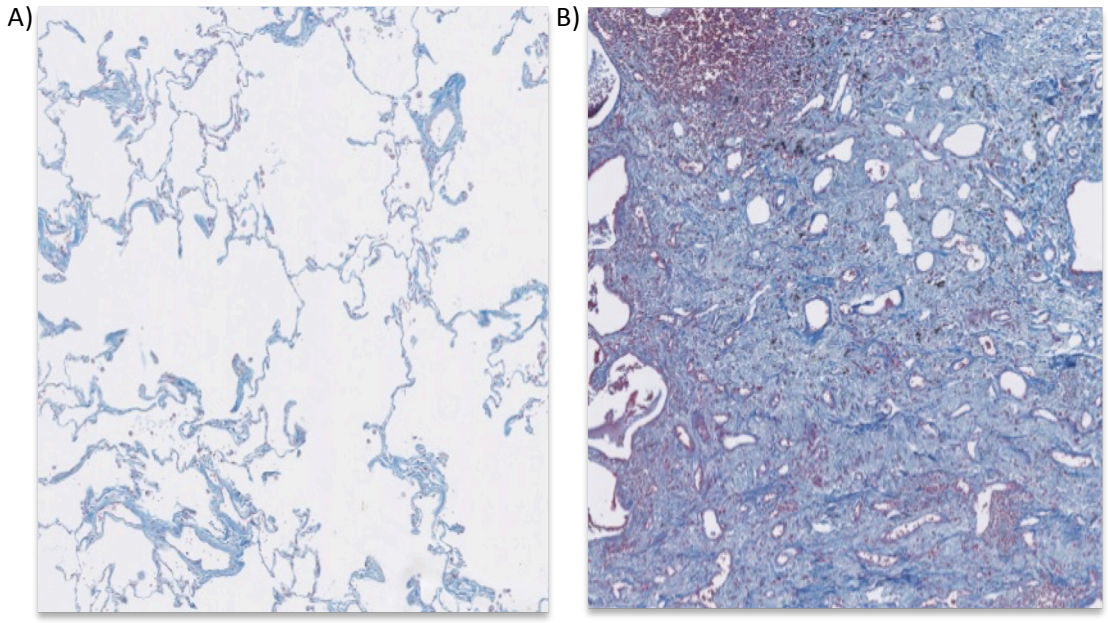

Figure 1. 4: Alveolar architecture of control (or non-IPF) and IPF lung.

Martius Scarlet Blue (MSB) staining illustrating collagen deposition in lung sections from A) non-IPF patient and B) IPF patient. Original magnification, 5x

IPF is commonly diagnosed in patients aged between 40 to 70 years, with prevalence higher in men in comparison to women (ratio of approximately 1.7:1) (Raghu et al., 2006; Han et al., 2008). The incidence rises with age and approximately two-thirds of IPF patients are older than 60, giving a mean diagnosis age of 66 years (Navaratnam et al., 2011). Additionally, the risk of mortality as a result of IPF also rises with age (Erbes et al., 1997) suggesting that age-related changes affecting normal cellular activity are most likely to be important in the development of IPF (Collard, 2010).

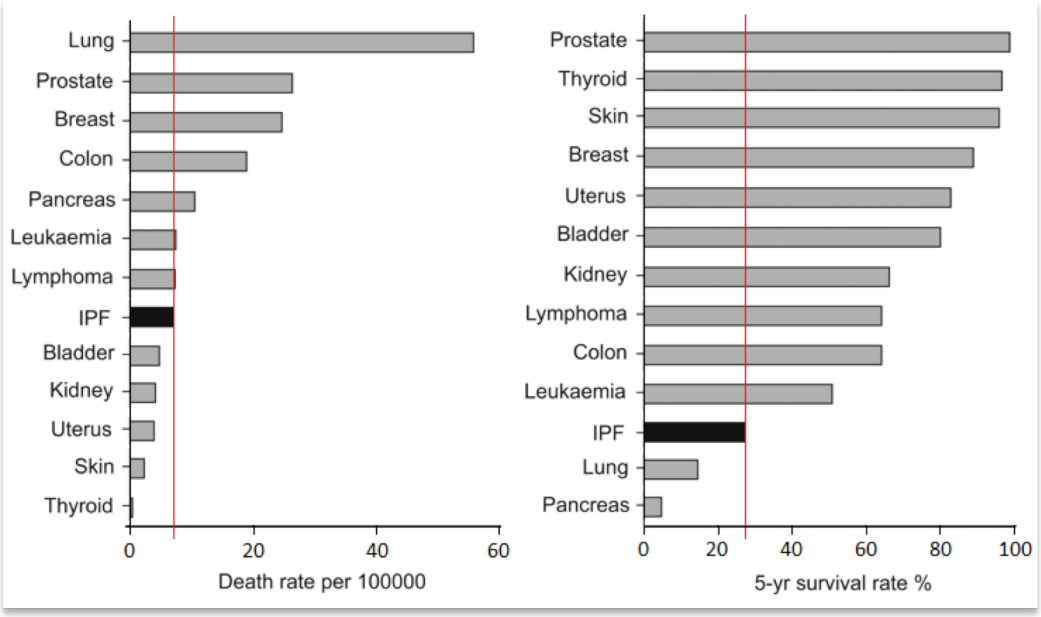

Figure 1. 5: Comparison of death rate and five year survival rate for idiopathic pulmonary fibrosis (IPF) and different forms of cancer.

Statistics are from the US National Cancer Institute.

Reproduced and adapted from (Vancheri et al., 2010) with permission of the European Respiratory Society (ERS)

Table 1.3: Incidence of idiopathic pulmonary fibrosis

Country or region of study (data source)	Incidence per 100,000	Authors
US (healthcare claims database)	6.8-16.3	(Raghu et al., 2006)
UK (primary care database including diagnostics and prescribing data)	7.44	(Navaratnam et al., 2011)
Greece (survey of pneumonology departments)	3.38	(Kadler et al., 2007)
Finland (hospital diagnostic coding databases)	16-18	(Hodgson et al., 2002)
EU (review of medical literature)	11.5	(Orphanet Report Series, 2013)

Reproduced and adapted from (Rafii et al., 2013)

Once diagnosed, the progression of the disorder is variable and unpredictable from patient to patient. Some remain asymptomatic for 2-3 years, whilst in others the disease is short lived with rapid deterioration (accelerated form) (Selman et al., 2007). However, the majority of IPF patients experience a slow progression with clinical and functional deterioration which ultimately leads to chronic respiratory failure. Nevertheless, a subpopulation of IPF patients may experience a steady progression with episodes of rapid deterioration, known as acute exacerbations leading to an increase in morbidity as well as mortality (**Figure 1.6**) (Raghu et al., 2011). Such patients develop severe dyspnoea resulting in hypoxia within 30 days and require hospitalisation for mechanical ventilation. Acute exacerbations may result from known factors such as heart failure, infection, or pulmonary embolism, however in some cases the cause is unknown. In general, the median survival is 2-3 years following diagnosis (the worst prognosis of all IIPs).

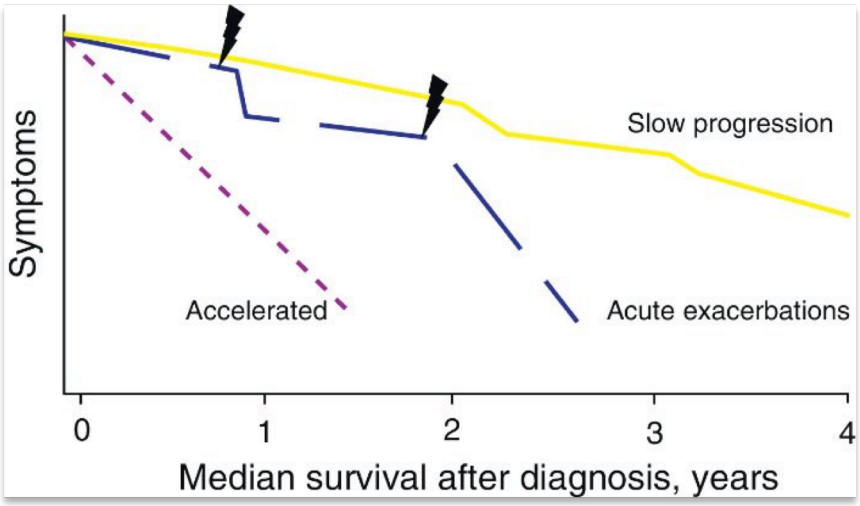

Figure 1. 6: Progression of idiopathic pulmonary fibrosis

Majority of patients experience a slow progression of the disease (yellow) whilst a minority of patients have a rapid progression (dotted purple line) following diagnosis. A subpopulation of patients experience a slow progression with episodes of rapid deterioration, known as acute exacerbations (dotted blue line).

Reproduced from (Xaubet et al., 2013) with permission of Elsevier.

1.2.2. Diagnosis of IPF

Patients are diagnosed with this disorder based on the clinical, histopathological and radiographical evaluations. Clinical presentations include chronic and progressive dyspnoea (shortness of breath) induced by 6-minute-walk (6mw) test, dry cough, impaired gas exchange

(measured by diffusing capacity of the lung for carbon monoxide, $_{DL}$CO), and reduced lung volume (i.e. forced vital capacity, FVC; and total lung capacity, TLC). Furthermore, fever, weight loss, finger clubbing, fatigue, and malaise have also been reported (ATS and ERS, 2002).

Lung biopsies from IPF patients show the histological appearance of usual interstitial pneumonia (UIP). These are heterogeneous appearances of fibrosis and honeycombing (bronchial epithelium lining fibrotic airspaces, which are often filled by numerous inflammatory cells as well as mucin), alternating with areas of less affected or unaffected lung parenchyma. The areas which are more severely affected are the subpleural and paraseptal parenchyma. In addition, high-resolution computerised tomography (HRCT) scans also show the presence of UIP which are characterised by reticular opacities (**Figure 1.7**). This is often associated with abnormal airway dilation (traction bronchiectasis). In addition, the lungs of some patients also show mild inflammation consisting of patchy lymphoplasmacytic interstitial infiltrate. The analysis of these features is necessary to make a definite diagnosis (ATS and ERS, 2002; Sureshbabu et al., 2011).

Figure 1. 7: High resolution CT scan illustrating usual interstitial pneumonia

Subpleural reticular opacities and areas of honeycombing.

Reproduced from (Cottin et al., 2014) with permission of the European Respiratory Society (ERS).

Furthermore, small regions of active fibrosis (fibrotic foci) are present in the lungs of IPF patients. These are clusters of activated myofibroblasts that underlie hyperplastic alveolar epithelial cells (**Figure 1.8**), located in areas with collagen deposition. These histological hallmarks were considered to be discrete sites of lung injury. However, Cool et al. (2006) demonstrated that these are in fact an extremely complex and interconnected, non-malignant continuous reticulum, which extend from the pleura into the lung parenchyma (Cool et al., 2006).

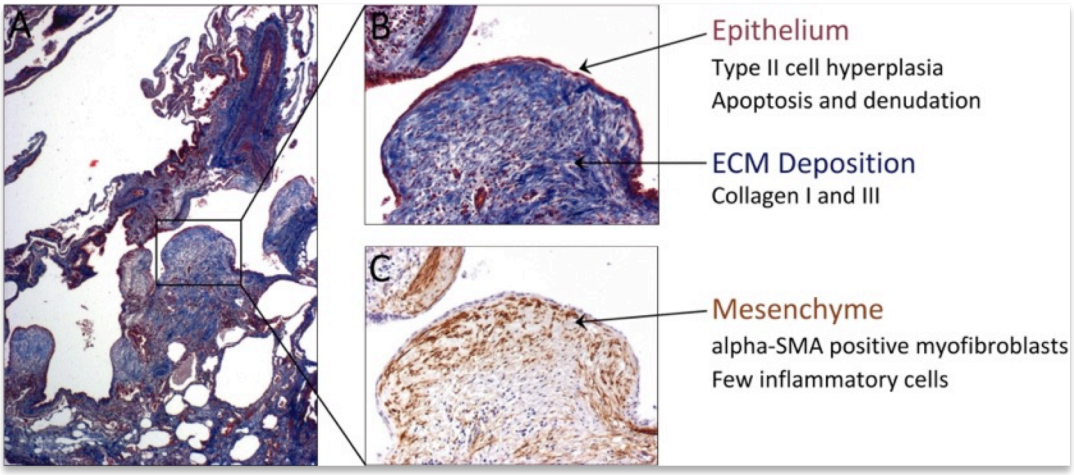

Figure 1. 8: Fibrotic focus – a histological hallmark of idiopathic pulmonary fibrosis

A) Histological analysis (Martius Scarlet Blue staining) of a human IPF lung tissue illustrating dense collagen deposition (blue) within the pulmonary interstitium (original magnification x10). B) Fibrotic focus, highly synthetic for collagen. C) These are clusters of myofibroblasts (positive for αSMA, immunohistochemistry) underlying hyperplastic epithelial cells (original magnification x20).

Reproduced from (Datta et al., 2011) with permissions of John Wiley and Sons.

A few studies have explored the relationship between the number of fibrotic foci and the severity of the disorder. For instance, King et al. (2001) used surgical biopsy specimens from 87 patients with UIP to investigate which histopathological feature of UIP affects survival. The results demonstrated that patients with more fibrotic foci had a poorer outcome (King Jr. et al., 2001). In addition Nicholson et al. (2002) also confirmed the prognostic significance of fibrotic foci by retrospective analysis of 53 patients with UIP (Nicholson et al., 2002). Furthermore, in 2003 Flaherty et al. (2006) discovered that patients with collagen vascular disease have fewer fibrotic foci in comparison to IPF patients, with better survival of the former (Flaherty et al., 2003). This was also demonstrated by Enomoto et al. (2006). Thus, the

number of fibrotic foci present within the lungs of the patients correlates with the progression of the disorder (Enomoto et al., 2006). As the disease progresses, there is a loss of lung elasticity and alveolar surface area, which results in the impairment of gas exchange and pulmonary function, leading to respiratory failure (ATS and ERS, 2002; Chambers, 2008).

1.2.3. Pathogenesis of IPF

Despite having an unknown aetiology, a number of risk factors have been implicated in IPF development. These include cigarette smoking (Baumgartner et al., 1997), viral infections (Tang et al., 2003), drug toxicity, and prolonged environmental exposure (e.g. wood or metal dust; (Raghu et al., 2011). Furthermore, genetic predispositions to PF have also been proposed based on several studies of PF patients with the familial form. Such include mutations in genes encoding surfactant protein A2 (*SFTA2)* (Thomas et al., 2002), mucin 5B (*MUC5B)* (Seibold et al., 2011), and telomerase (*TERT* and *TERC*) (Armanios et al., 2007; Tsakiri et al., 2007). Moreover polymorphisms in tumour necrosis factor (TNF)-α and TGFβ1 have also been identified (Whyte et al., 2000; Xaubet et al., 2003). However, the precise genetic factor(s) that determine the clinical manifestations as well as the phenotypic expression of sporadic IPF remain unknown and are also extremely challenging to determine due to the late onset of the disease presentation. Nevertheless, genetic predisposition appears to be responsible for ~5 % of IPF cases suggesting the aetiology of IPF is likely to be multifactorial (Noble et al., 2012).

Additionally, several other hypotheses have been postulated to explain the possible pathogenesis of this fatal disease. Originally it was thought that IPF is a chronic inflammatory disease initiated following alveolar injury (alveolitis) resulting in the recruitment of inflammatory cells and the release of inflammatory and profibrotic mediators leading to fibrogenesis. However, lack of clinical benefit in response to anti-inflammatory drugs and immunosuppressive reagents suggests that the progression of IPF is not dependent on typical inflammation (Gross and Hunninghake, 2001; Thannickal et al., 2004).

Many studies now focus on a more recent concept suggesting that IPF is an 'epithelial-fibroblastic disorder' whereby continuous micro-repetitive injury to the epithelial cells within the lung causes abnormal wound healing responses including aberrant proliferation and differentiation of fibroblasts, formation of fibrotic foci, and excessive deposition of ECM components. Furthermore, in this hypothesis, inflammation is considered to be a secondary event (Chakraborty et al., 2014). Several *in vitro* and *in vivo* studies of PF support this

hypothesis, with the most common *in vivo* model involving the administration of bleomycin (discussed in detail in **Section 1.3**) (Gross and Hunninghake, 2001; Selman and Pardo, 2002; Selman et al., 2011). However, the underlying mechanisms involved in the development of fibrotic foci are still unclear.

1.2.4. Alveolar epithelial cells

In normal lungs, over 90% of the alveolar surface consists of alveolar epithelial cells (AEC) type I (AT1) which interface with the pulmonary capillaries resulting in an intact thin surface readily permeable to gases. On the other hand, approximately 5% of the alveolar surface is composed of AEC type II (AT2). Morphologically these cells appear as large rounded cells which are in close proximity to mesenchymal cells, and play a vital role in synthesising surfactant (Sirianni et al., 2003; Selman and Pardo, 2006). In addition, ATII cells also act as limited progenitor cells which are able to regenerate AT1 during injury, and synthesise some of the vital components of the basement membrane (including collagen IV, fibronectin, and laminin) in order to maintain the integrity of the alveolar epithelium (Chakraborty et al., 2014). Furthermore, ATII cells minimise alveolar fluid by aiding the transport of sodium from apical to basolateral cell surfaces (Shannon and Hyatt, 2004; Selman and Pardo, 2006).

Under normal wound healing conditions, fibroblasts (discussed in more detail in **Section 1.2.5**) are activated to myofibroblasts, recruited to the injury site, and initiate the formation of a provisional matrix (which acts as a scaffold for normal tissue repair), and contract to promote wound closure. Following this, the cells undergo apoptosis and are cleared from the wound area. Subsequently, ATII cells proliferate and differentiate for the regeneration of the denuded epithelium. Thus, under normal conditions, epithelial cells and fibroblasts maintain the lung homeostasis and initiate repair mechanisms in response to injury without affecting its structure and function. However, as mentioned above, in IPF patients AECs undergo phenotypic changes as a result of repetitive injury to the epithelial layer (Kasper and Haroske, 1996; Chilosi et al., 2002). Abnormalities in AECs have been illustrated in lung biopsies from IPF patients (Uhal et al., 1998; Barbas-Filho et al., 2001; Maeyama et al., 2001; Plataki et al., 2005) including the presence of hyperplastic AT2 (Corrin et al., 1985), bronchiolar-like epithelial cells (bronchiolarisation) AECs (Kawanami et al., 1982; Sutinen et al., 1980) (Sutinen et al., 1980; Kawanami et al., 1982), and squamous metaplasia lining regions of honeycomb fibrosis. Furthermore, several studies have demonstrated that AECs are not only more susceptible to apoptosis (Kasper and Haroske, 1996) but also continue to undergo cell death in the absence

of the initial injury stimulus (King Jr. et al., 2011). The key question here is does AEC damage occur at the early stage of the disease (the triggering event) or as part of the evolution of IPF (a secondary process). It has been hypothesised that AEC cell death is involved in the initial event in the pathogenesis of IPF as studies have demonstrated AEC death in normal areas of the lung parenchyma. Furthermore, *in vivo* models of fibrosis have illustrated that mice are protected from bleomycin-induced fibrosis when epithelial cell apoptosis is inhibited (Kuwano et al., 1999a), suggesting a possible therapeutic target for IPF patients.

Several mediators also play a key role in AEC apoptosis including TGFβ (Lee et al., 2004), Fas ligand (FasL) (Maeyama et al., 2001), reactive oxygen species (ROS) (Waghray et al., 2005), and angiotensin II (ANGII). More recently, studies have illustrated that IPF AECs express markers of ER stress and the unfolded protein response (UPR) which may result in altered processing of surfactant protein (Korfei et al., 2008; Lawson et al., 2008). Moreover, defects in the regulation of developmental/embryological pathways may explain the irregular behaviour of AECs (Konigshoff and Eickelberg, 2010). For instance, several studies have shown that epithelial cells from IPF patients overexpress β-catenin suggesting that the Wnt pathway is switched on within these cells (Konigshoff et al., 2008). Despite the progression in the number of *in vitro* and *in vivo* studies performed to understand the cause of AEC death, currently the precise cellular mediators that culminate in the initial AEC dysfunction and death remain completely unknown and require intense investigation.

1.2.5. Fibroblasts and Myofibroblasts: matrix producing cells

As already mentioned, mesenchymal cells (i.e. fibroblasts and myofibroblasts) have a fundamental role in the pathogenesis of IPF and over the past 30 years it has been generally accepted that these cells play an essential role in the establishment of tension during wound healing and pathological conditions (Hinz, 2007; Hinz et al., 2007). In normal lung tissue, fibroblasts are predominately located in the parenchymal interstitium (accounting for 30-50% of total interstitial cells) and in the subepithelial layer of the conducting airways, which places them in a prime location to interact with endothelial and epithelial cells (Tomasek et al., 2002). However, in IPF lungs the fibroblast cell number is far greater (Jordana et al., 1994), localised to sites of active fibrosis as well as fibrotic foci. In addition, during a wound healing process or a pathological environment these cells are known to differentiate into a more contractile phenotype (myofibroblasts) which are considered as the principal effector cells responsible for the deposition of ECM proteins (including collagen). Myofibroblasts are elongated spindle-like

shaped contractile cells which share features of both fibroblasts and smooth muscle cells, and are characterised by the presence of stress fibres and the expression of alpha-smooth muscle actin (αSMA) as well as several other markers (**Figure 1.10**).

Fibroblasts express several receptors for major profibrotic mediators including platelet derived growth factor (PDGF), connective tissue growth factor (CTGF), TGFβ (Farkas et al., 2010), and protease activated receptor (PAR)1 (Scotton and Chambers, 2007; Chakraborty et al., 2014). In addition, these cells also express receptors for proinflammatory/antifibrotic mediators, including tumour necrosis factor (TNF)-*α*. It is believed that AEC injury results in the release of profibrotic mediators, which promote the migration, proliferation, and activation of fibroblasts to myofibroblasts. Furthermore, matrix metalloproteinases (MMPs), such as MMP2, MMP3, and MMP9, are also released by both epithelial cells and fibroblasts, which affect ECM remodelling and disrupt the basement membrane in lungs of IPF patients (discussed later) (Lovgren et al., 2011).

Origin of myofibroblasts

Three possible origins for myofibroblasts have been proposed (**Figure 1.9**). Initially it was thought that myofibroblasts originate from resident fibroblasts which are able to differentiate in the presence of profibrotic mediators (as mentioned above). However, prior to the formation of myofibroblasts, it has been proposed that resident fibroblasts differentiate into proto-myofibroblasts. These are cells which, unlike myofibroblasts, contain stress fibres that do not express αSMA (**Table 1.4**). Several *in vivo* studies support the existence of proto-myofibroblasts – for example, these cells have been detected in lung alveolar septa (Kapanci et al., 1992) as well as the early phases of granulation-tissue formation (Hinz et al., 2001b). The distinction between fibroblasts and proto-myofibroblasts is clearly visible *in vivo* and it has been proposed that these cells may function as an independent cell type (Tomasek et al., 2002). This proposal is based on the fact that proto-myofibroblasts (in normal tissues) are always present in areas where there is a need to create mechanical tension (Serini and Gabbiani, 1999). However, nearly all fibroblasts acquire proto-myofibroblastic features once the cells are grown in culture (in the presence of foetal bovine serum, FBS) on plastic (Hinz, 2006). Thus, as well as cell signalling molecules and cytokine (e.g. PDGF), mechanical tension may also promote the formation of proto-myofibroblasts (Hinz et al., 2004; Desmouliere et al., 2005).

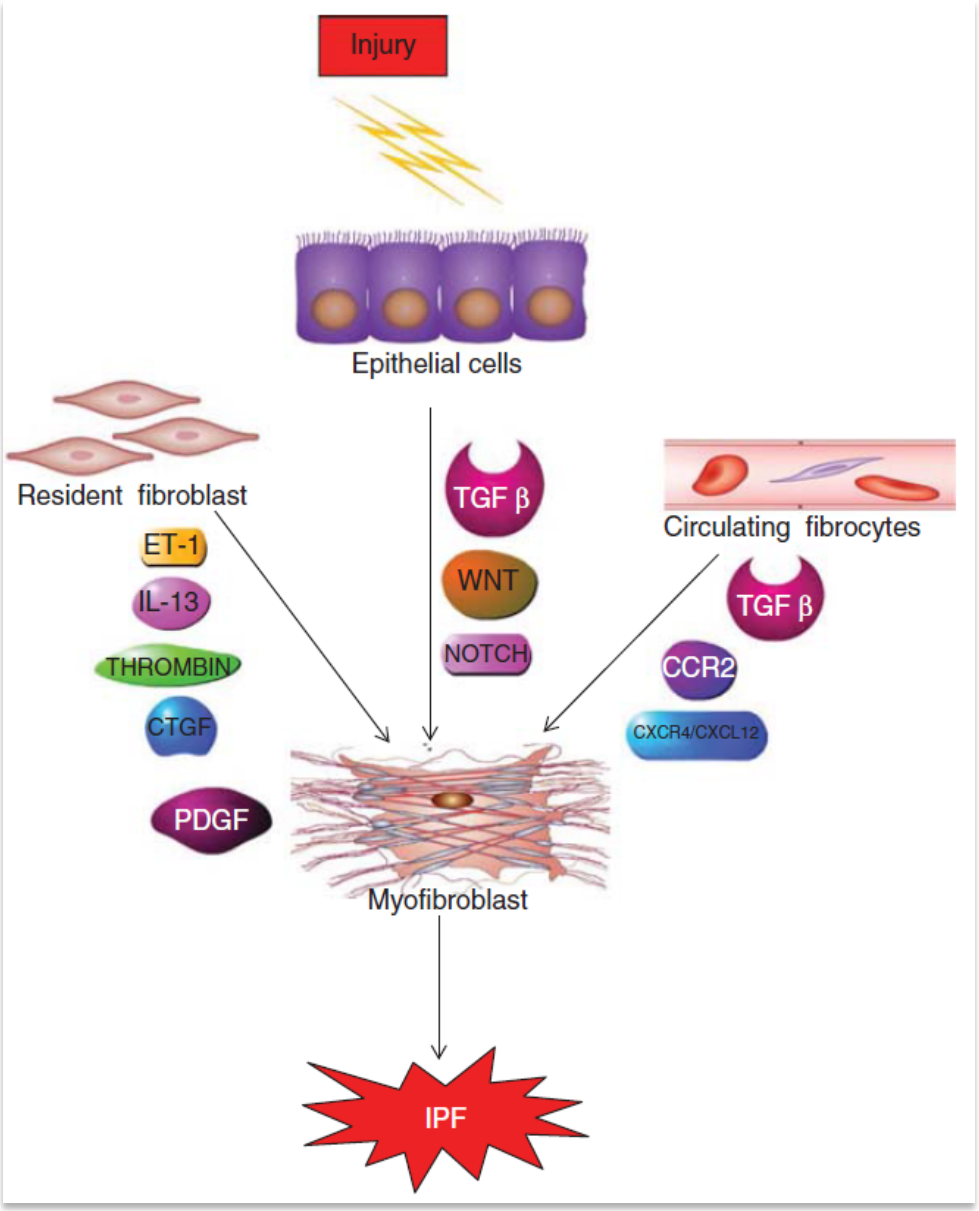

Figure 1. 9: Proposed origin of myofibroblasts in the pathogenesis of IPF

Myofibroblasts may originate from three proposed sources: resident lung fibroblasts which differentiate under the influence of pro-fibrotic mediators; epithelial cells in response to injury via epithelial-mesenchymal transition; mesenchymal cells derived from circulating fibrocytes or from bone-marrow-derived progenitor cells which differentiate in the presence of pro-fibrotic mediators. During normal tissue repair, myofibroblasts undergo apoptosis, however in IPF patients, myofibroblasts proliferate excessively with excess ECM deposition leading to remodelling of the lung architecture.

Reproduced and adapted from (Chakraborty et al., 2014) with permissions of Informa Ltd.

Table 1.4: Fibroblast-myofibroblast features in different situations

	In vivo	Closest *In vitro* model
Fibroblast	Normal connective tissue	Low stiffness substrates ± TGFβ Free-floating collagen gels ±TGF-β
Proto-myofibroblast (stress fibres that express cytoplasmic actins)	Specialised normal connective tissue (e.g. alveolar septum), early granulation tissue (e.g. open wound)	Medium stiffness substrates
Differentiated myofibroblast (stress fibres that express α-SMA)	Specialised normal connective tissue (e.g. bone marrow stroma, liver capsule); Late contracting granulation tissue (e.g. open wound); Fibrocontractive diseases	Medium stiffness substrates ±TGFβ High stiffness substrates ± TGFβ Attached collagen gels ± TGFβ

Reproduced and adapted from (Tomasek et al., 2002) with permission of Nature Publishing Group.

In vivo, proto-myofibroblasts proceed to differentiate into myofibroblasts which are characterised by *de novo* expression of αSMA. Under the influence of high tension, αSMA is recruited to the stress fibres (Goffin et al., 2006). Studies have illustrated that the level of αSMA expressed in myofibroblasts correlates with the contractility of the cell (Zhang et al., 1996; Hinz et al., 2001a), however the precise mechanism involved in this correlation is currently unknown.

As well as resident fibroblasts, myofibroblasts have also been suggested to originate from AECs. It has been proposed that in response to injury AECs are able to transdifferentiate into mesenchymal cells (Kim et al., 2006), a process known as epithelial-mesenchymal transition (EMT; **Figure 1.10**). This cell plasticity has been observed in distinct cellular processes including embryonic development and metastasis. Furthermore, EMT has also been described to occur in *in vivo* and *in vitro* models of fibrosis, whereby in the presence of TGFβ epithelial cells acquire migratory capacity and invasive properties (Kasai et al., 2005; Wu et al., 2007).

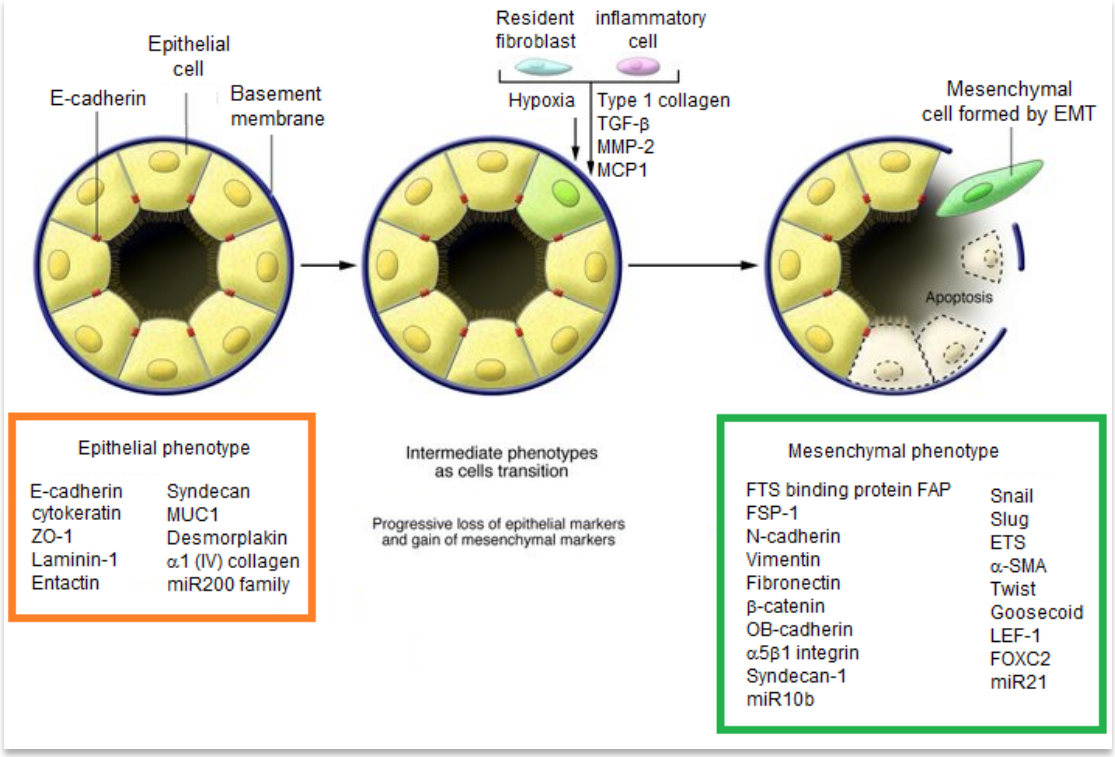

Figure 1. 10: Epithelial-mesenchymal transition.

Markers used by researchers to determine cell phenotype are listed. In the presence of resident fibroblasts or inflammatory cells a number of mediators are released (e.g. TGFβ, Type 1 collagen, MMP2, or MCP1), which results in the loss of epithelial cell markers and gain of mesenchymal markers (e.g. αSMA), process known as EMT. Epithelial cells are more susceptible to apoptosis in comparison to mesenchymal cells.

Reproduced from (Kalluri and Weinberg, 2009) with permission of American society for clinical investigations.

Moreover, decrease in expression of epithelial cell markers has also been described. Such markers include junction associated proteins (such as E-cadherin, zonula occludens [ZO]-1), and cytokeratins). In addition, increase in expression of mesenchymal markers (including αSMA, MMP2 and MMP9), and excess collagen production have also been illustrated (Gharaee-Kermani et al., 2009), which occurs via a Smad3-dependent mechanism (Hu et al., 2003). More importantly, approximately 80 % of the hyperplastic epithelial cells overlying fibrotic foci co-express epithelial and mesenchymal markers in IPF lung biopsies which provides strong evidence of EMT during the development of lung fibrosis (Willis and Borok, 2007), and it has been proposed that following injury EMT may result as an attempt to escape epithelial cell apoptosis (Vega et al., 2004). If this proposal is correct then EMT may be considered as an epithelial cell injury marker and inhibition of EMT may in fact result in

adverse effects in IPF (Kage and Borok, 2012). However, further studies are necessary before making any firm conclusions.

Recent research has demonstrated that TGFβ-induced EMT may be reversed in the presence of fibroblast growth factor (FGF)-1 which promotes ERK phosphorylation and Smad2 dephosphorylation (Ramos and Becerril, 2010). This implies that inhibiting global TGFβ activity may affect the tissue homeostasis and suggests that FGF-1 may have a therapeutic role in the treatment of PF. The regulation of TGFβ will be discussed in detail in the next section. Other signalling pathways which also promote EMT are Wnt and Notch signalling.

Despite having numerous data supporting EMT, some studies have shown contradictory results. For instance, Rock *et al.* (2011) illustrated that ATII cells (expressing surfactant protein C) did not transdifferentiate into myofibroblasts following bleomycin administration as there was no change in expression for αSMA or vimentin. In addition, cells expressing Scgb1a1 (a marker for bronchiolar clara cells and possibly alveolar progenitor cells) also showed negative results with regards to EMT (Rock et al., 2011). However, since this was demonstrated only in the bleomycin model of fibrosis (which is the most accepted model of PF), it has been suggested that other fibrogenic models may show different results (Degryse et al., 2010; Kage and Borok, 2012), therefore further investigations are required.

Circulating fibrocytes also show evidence for being the source for myofibroblasts in IPF patients. These are bone marrow-derived progenitor cells characterised by the expression of mesenchymal markers (i.e. type I collagen, and fibronectin) and haemopoietic cell markers (i.e. CD34 and CD45) (Strieter et al., 2009). In response to injury, fibrocytes are thought to migrate to affected areas within the lung and differentiate into myofibroblasts. Chemokine receptors (i.e. CXCR4) are expressed by human fibrocytes which have affinity for the chemokine CXCL12, suggesting a crucial role of CXCR4-CXCL12 axis in the trafficking of the cells into the lungs of IPF patients. In addition, AECs express CXCL12 which may therefore be involved in forming the chemotactic gradient required for the $CXCR4^{+}$ fibrocyte trafficking (Andersson-Sjoland et al., 2008; King Jr. et al., 2011).

More recent studies have suggested that myofibroblasts may also originate from pericytes (Hung et al., 2013a). These are specialised mesenchymal cells that share a basement membrane alongside endothelial cells and commonly express several markers including αSMA, PDGFRβ, GFAP, CD146, P75 NGFR, and angiopoietin 1.

Myofibroblasts in IPF

As stated above, myofibroblasts are the principal cells for collagen production. The first study to show direct evidence for this in fibrotic lung was conducted by Zhang *et al* (1994) which involved *in situ* hybridisation on bleomycin-induced lung tissue sections illustrating colocalisation of *ACTA2* and *COL1A1* mRNA (Zhang et al., 1994). This has also been confirmed in our lab with colocalisation of αSMA and collagen-I and collagen-III in IPF lung tissue serial sections (see **Section 3.2**). However, the precise mechanisms which lead to elevated ECM synthesis by myofibroblasts are not completely understood. One hypothesis suggests that myofibroblasts undergo phenotypic changes which result in permanent 'reprograming' of the cells, promoting fibrogenesis. This theory is supported by studies on fibroblasts/myofibroblasts isolated from IPF lung tissues illustrating highly synthetic capacity for collagen and other ECM proteins, as well as greater contractility of collagen matrices (Miki et al., 2000) in the presence of pro-fibrotic mediators, compared to cells isolated from control lungs (Hetzel et al., 2005).

In addition, over expression of molecules involved in developmental pathways is evident in IPF fibroblasts (similar to AECs, mentioned above). Such include β-catenin in the Wnt signalling pathway (Coward et al., 2010) and components of the Sonic hedgehog signalling pathway (i.e. Sonic hedgehog, SHH; glioma-associated oncogene homolog, GLI-1 and GLI-2; Smoothened, Smo; and Patched-1) (Bolanos et al., 2012). Furthermore, IPF cells also produce low levels of anti-fibrotic mediators such as prostaglandin (discussed further in **Section 1.2.7**) (Keerthisingam et al., 2001; Kohyama et al., 2001; Lama et al., 2002; Kolodsick et al., 2003; Moore et al., 2003) and unlike AEC, myofibroblasts are more resistant to apoptosis (Xu et al., 2003; Ramos and Becerril, 2010). In fact, myofibroblasts provoke AEC apoptosis, obstruct epithelial cell regeneration, and denude the basement membrane. This provides evidence of epithelial-mesenchymal crosstalk. Several mediators have been suggested to modulate this imbalance in apoptosis of epithelial cells and fibroblasts, some of which have already been discussed above including TGFβ (Zhang and Phan, 1999; Hagimoto et al., 2002), FIZZ1 (Chung et al., 2007), IL-1β (Zhang et al., 1997), IL-6 (Moodley et al., 2003), and TNF-α (Piguet et al., 1993; Frankel et al., 2006). However the precise molecular pathway(s) involved in this aberrant epithelial-mesenchymal crosstalk is currently an area of intense investigation.

IPF fibroblasts also have enhanced an migratory and proliferative phenotype in comparison to control cells (Suganuma et al., 1995; Ramos et al., 2001). However, some studies have illustrated that IPF fibroblasts proliferate at a lower rate when the disease is at a more

advanced stage (Raghu et al., 1988; Hetzel et al., 2005). To some extent this has also been assessed in our lab, which also supports a slower proliferation rate of IPF fibroblasts in comparison to controls (unpublished data) *in vitro*. These contradictory data suggest that *in vitro* cell isolates grown on tissue culture treated plastic may not provide a true representation of the disease pathology as seen *in vivo* as the cells may undergo phenotypic modulation due to the change in microenvironment.

Collagen turnover in IPF

Collagen in normal lungs exists in a dynamic equilibrium where synthesis and degradation are regulated by carefully controlled processes involving the activity of several enzymes as well as growth factors, cytokines, proteases, lipid mediators, and mechanical forces (see **Section 1.1.3**). Early studies in our lab have illustrated that collagen synthesis and degradation occurs rapidly in normal adult rat tissues (McAnulty and Laurent, 1987). However, in fibrotic lung this balance is disrupted with excessive collagen deposits resulting in gross thickening of the alveolar interstitium leading to the remodelling, destruction of the lung architecture, and progressive loss of alveolar function. Several studies (including past and current research in our lab) have illustrated this in both *in vitro* and *in vivo* models of PF by measuring pro-collagen synthesis, which reflects total collagen content (see **Section 1.1.3**).

An imbalance in the ratio of collagen type I and III has been reportedly observed in lung biopsies of patients with IPF, whereby collagen type III elevates excessively in early fibrosis (Kirk et al., 1984). However, once fibrosis has been established the collagen I to collagen III ratio alternates with higher levels of collagen I observed. Since collagen I and III are insoluble proteins and cannot be measured directly from the patient without invasive biopsy, studies analyse their production by determining the levels of procollagen carboxy-terminal pro-peptides (PICP and PIIICP, respectively) which are considered as surrogate markers for collagen synthesis (reviewed in (Dancer et al., 2011)). Both PICP and PIIICP are elevated in BALF of IPF patients. In addition, PICP levels in the epithelial lining fluid as well as BALF had a significant negative correlation with $_{DL}$CO (Lammi et al., 1999). Collagen III is predominantly located in the thickened alveolar septa and interstitium, although collagen type I appears to be the major collagen at later stages in the disease course. This has been demonstrated both immunohistochemically and by *in situ* mRNA studies on lung tissue (Raghu et al., 1985). Increased levels of other ECM constituents, including collagen types V, VI, and VII, fibronectin, elastin, and proteoglycans are also present at high levels in IPF (Pardo et al., 2008).

As well as synthesising collagen and other ECM proteins, fibroblasts host the synthesis of matrix degrading proteins, such as MMPs in order to control tissue architecture and matrix turnover during the initiation and resolution phases following injury. MMP levels in IPF lungs are elevated in comparison to control lungs. Since MMPs degrade collagen, increased levels of MMPs would suggest greater degradation of ECM protein. However this does not seem to occur in fibrotic lungs as the concentration of TIMPs (endogenous MMP inhibitors) is also high (Selman, 2000). This has been demonstrated by many studies including one by Montano *et al.* (1989) illustrating high collagenase inhibitory activity in biopsies from IPF patients in comparison to control subjects (Montaño et al., 1989). Additionally, Fukuda *et al.* (1998) showed co-localisation of MMP1, MMP2, and MMP9 with TIMP-2 at the epithelium surrounding the fibrotic lesions in IPF lungs. High levels of TIMP-2 suggest that the activity of MMP-1, -2, and -9 are inhibited, thus the matrix is not degraded (Fukuda et al., 1998). Furthermore, immunohistochemical analysis of IPF tissue has demonstrated high expression levels of TIMP-1, TIMP-3, and TIMP-4 in interstitial macrophages, vessels, and epithelial cells, respectively (Selman, 2000).

Therefore, the dysregulated balance between MMPs and TIMPs are considered to aid persistent matrix deposition in IPF lungs. Later studies have also reported a role of MMP3 in fibrotic diseases. Overexpression of MMP3 has been detected in IPF BALF (Richter et al., 2009) as well as the lungs of *in vivo* model of PF whereby mice lacking MMP3 were protected from PF in comparison to wild type (Yamashita et al., 2011). Other MMPs shown to be elevated in BALF of IPF patients include MMP7 (Fujishima et al., 2010), MMP8 (Henry et al., 2002), and MMP12 (Lanone et al., 2002) (**Table 1.5**). In addition, membrane-type MMPs (MT-MMPs) are also elevated in IPF patients. MT-MMPs participate in the activation of pro-MMP2 to form MMP2. MT1-MMP and MT2-MMP are expressed in AECs, MT3-MMP in fibroblasts from fibroblastic foci and AECs, and MT5-MMP is expressed in basal bronchiolar epithelial cells. Furthermore, TGFβ1 upregulates MT3-MMP levels (both mRNA and protein) in lung fibroblasts (García-Alvarez et al., 2006).

Table 1. 5: Elevated MMPs shown in IPF patients

	Substrate	Studied in IPF patients	Cellular source	References
MMP1	Collagen I and III; pro-TNFα	Lung tissue mRNA and protein; BALF; plasma	Fibroblasts, epithelial cells, endothelial cells, macrophages	(Nkyimbeng et al., 2013)
MMP2	Collagen IV	Lung tissue protein	Fibroblasts, fibrocytes, hyperplastic epithelial cells	(Nkyimbeng et al., 2013)
MMP3	Collagen II, IV, IX, fibronectin, proteoglycan, laminin, elastin, gelatins, MMP1, MMP7, MMP9	BALF	Epithelial cells	(Matrisian, 1990; Murphy et al., 1992; Richter et al., 2009)
MMP7	Collagen IV, laminin, fibronectin, gelatine, elastin, osteopontin, FasL, integrin β4,E-caderin, pro-HB EGF, plasminogen, pro-TNFα, syndecan, IGFBP3, pro-MMP1, pro-MMP2, pro-MMP9	Lung tissue mRNA and protein; BALF; plasma	Epithelial cells, fibrocytes	(Rosas et al., 2008; McKeown et al., 2009; Nkyimbeng et al., 2013)
MMP8	Collagen I	BALF	Neutrophils and to less extent fibrocytes, fibroblasts, endothelial, epithelial, and plasma cells	(Henry et al., 2002; McKeown et al., 2009)
MMP9	TGFβ	Lung tissue protein	Macrophages, neutrophils, endothelial cells, fibroblasts, fibrocytes, alveolar epithelial cells, Clara cells, smooth muscle cells	(McKeown et al., 2009; Nkyimbeng et al., 2013)
MMP12	FasL	Lung tissue mRNA and protein		(Nkyimbeng et al., 2013)
MMP13	Collagen I, II and III	Lung tissue mRNA and protein; BALF	Macrophages, T-lymphocytes, plasma cells	(Henry et al., 2002; Nkyimbeng et al., 2013)

Despite several studies focusing on the roles of MMPs in IPF, there are several potentially important MMPs which currently remain poorly studied. For instance, microarray studies on IPF tissue have shown upregulated MMP-10 and MMP-28 expression however their cellular sources, substrates and function are unknown. MMP-28 may potentially be of interest as studies have proposed that this may play a role in EMT and proteolytic cleavage of TGFβ (Illman et al., 2006). Further work to elucidate the significance of these novel MMPs is currently ongoing.

1.2.6. Transforming growth factor-beta (TGFβ)

TGFβ is a multifactorial protein belonging to a wider TGFβ superfamily composed of several other factors including bone morphogenetic proteins (BMPs), growth and differentiation factors (GDFs), activins, inhibins, and nodal. TGFβ is considered to be a potent cytokine which exerts several cellular effects including differentiation and proliferation during development, immune responses, wound healing, and tumour-cell growth/inhibition. The importance of this cytokine in normal embryonic, foetal, and adult organ development has been well described. In particular, the role of TGFβ in the production, organisation, and degradation of connective tissue for organ homeostasis has been widely appreciated.

TGFβ exists in three isoforms within the human body: TGFβ1, -2, and -3, each having distinct non-overlapping roles *in vivo* (Shi and Massague, 2003). Many different cell types express all three isoforms and during normal lung development the expression levels of all three types are elevated (Bartram and Speer, 2004). However, TGFβ1 is known to be the most abundant and best characterised. From this point forward TGFβ1 will be abbreviated as just TGFβ, unless otherwise stated. Most cells express TGFβ receptor (TβR)-I and TβR-II (Shi et al., 2011). Despite having a widespread expression, activation of the receptors is localised within regions where latent TGFβ is converted to active TGFβ (described in detail later).

Role of TGFβ in normal and fibrotic lungs

In the lung, cellular sources of TGFβ include fibroblasts, myofibroblasts (Kelley et al., 1991), type II AECs (Xu et al., 2003), endothelial cells (Grotendorst et al., 1989b), monocytes, neutrophils, and macrophages (Grotendorst et al., 1989a). Once synthesised and activated, TGFβ can regulate several effects some of which have already been described above. Moreover, TGFβ is a potent chemoattractant and mitogen for fibroblasts and myofibroblasts

(Postlethwaite et al., 1987) stimulating a fibroproliferative response. Furthermore, TGFβ also elicits several negative growth responses in epithelial and endothelial cells. For instance, *in vitro* TGFβ prevents the formation of active cyclin E/CDK2 complex in mink lung epithelial cells, which in turn results in the induction of G1 cell cycle arrest and inhibits mink lung cell proliferation (Koff et al., 1993). And as stated before, TGFβ has also promotes EMT. Since TGFβ is multifactorial and often elevated during abnormalities in tissue growth, it is considered as one of the most important molecular regulators of tissue homeostasis.

There is a great deal of evidence showing the profibrogenic effects of this cytokine in *in vitro* models, *in vivo* models, and in IPF patients. For instance, TGFβ stimulates the production of various collagen types as well as other ECM proteins (such as elastin, tenascin, vitronectin, fibronectin, and proteoglycans) by mesenchymal cells (Saharinen et al., 1999). Furthermore, TGFβ is also able to attenuate MMP production, stimulate the synthesis of TIMPs (Edwards et al., 1987), increases the expression of HSP47 to enhance the efficacy of procollagen processing, and sensitise fibroblasts to its own effects and maintain them in an activated state by an autocrine mechanism which results in further production of TGF-β (Van Obberghen-Schilling et al., 1988; Pannu et al., 2007). This therefore suggests that excess activation of TGFβ contributes to the formation of a pro-fibrotic environment.

TGFβ synthesis and activation

TGFB1 not only encodes the 12.5 kDa C-terminal TGFβ moiety, but also an N-terminal prodomain called latency-associated peptide (LAP; 25kDa) which plays a key role in facilitating the release of the entire TGFβ-LAP molecule from the cell into the ECM (**Figure 1.11**). The TGFβ monomers dimerise by a single disulphide bond while two disulphide bonds form between the larger LAP monomers (Gentry et al., 1988). Once the homodimeric LAP-TGFβ pro-peptide complex enters the Golgi apparatus, furin-type endopeptidases cleave the pro-peptide causing LAP to surround TGFβ and remain non-covalently associated. This LAP-TGFβ complex (also known as the small latency complex, SLC) is released into the ECM. However most cells secrete latent TGFβ as a large-latency complex (LLC) which is comprised of the LAP-TGFβ dimer covalently associated to a 120-240kDa glycoprotein known as latent TGFβ binding protein (LTBP) (Gleizes et al., 1997; Worthington et al., 2011). Studies have shown that abnormalities in LTBP lead to misfolding of the SLC within the Golgi apparatus. Thus, LTBP is necessary for direct processing and secretion of TGFβ from most cells (Miyazono and Heldin, 1991; Miyazono et al., 1991). Once the LLC is secreted from the cell, the LTBP plays a crucial role in

targeting the latent-TGFβ complex to the ECM (Taipale et al., 1994; Koli et al., 2001). The amino terminus of LTBP is covalently cross-linked to components of the ECM via tissue transglutaminase (Nunes et al., 1997). In the LLC, TGFβ is in its inactive state and is unable to associate with its receptor.

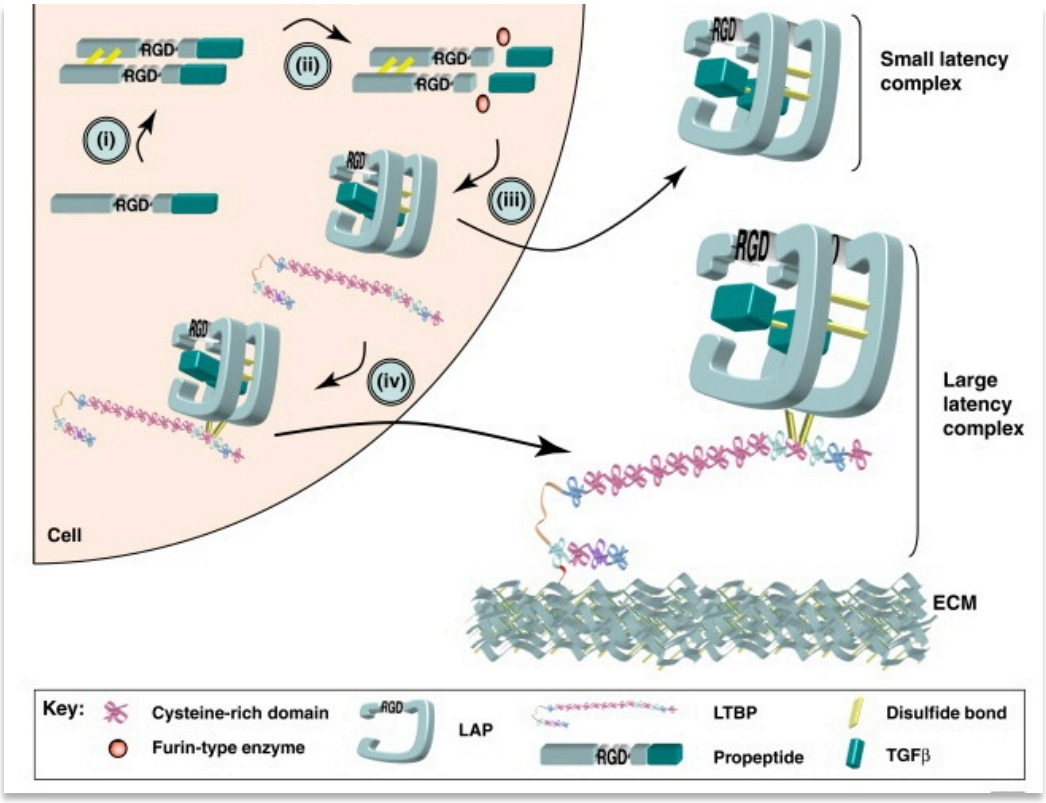

Figure 1. 11: TGF-beta synthesis

TGFβ is transcribed as a propeptide consisting of a C-terminal TGFβ moiety and an N-terminal RGD sequence containing latency associated peptide (LAP). This RGD sequence is only present in TGFβ1 and TGFβ3 isoforms (not TGFβ2). (i) The propeptide forms a homodimer. (ii) In the Golgi, furin enzyme cleaves the propeptide. (iii) TGFβ and LAP remain non-covalently associated with each other and form a small-latency complex (SLC). (iv) SLC associates with latent TGFβ binding protein (LTBP) via a disulphide bridge and forms a large latency complex.

Reproduced from (Worthington et al., 2011) with permissions of Elsevier Ltd.

The majority of cultured cells are unable to secrete significant levels of latent TGFβ or activate TGFβ in the absence of an exogenous stimulus. Nevertheless, numerous physiological conditions are able to promote TGFβ activation *in vitro*. Such conditions include heat, pH, radiation, enzymatic processing, detergents, urea, and shear stress (Brown et al., 1990).

Furthermore, several exogenous stimuli also promote TGFβ activation. These include reactive oxygen species (ROS), MMPs, thrombospondin-1 (TSP-1), and integrins. TSP-1 and integrin mediated TGFβ activation will be discussed in a little more detail in this section.

TSP-1 is a large, disulphide-linked homotrimeric protein which is elevated during development and in response to injury. It is considered to be a major activator for both small and large forms of latent TGFβ (Raugi et al., 1987; O'Shea et al., 1990; Reed et al., 1995; Yehualaeshet et al., 1999) in many fibrotic diseases including systemic sclerosis (SSc), kidney fibrosis, liver fibrosis, and lung fibrosis (reviewed in (Nakerakanti, 2012)). Binding of TSP-1 to LAP-TGFβ latent complex is mediated by two sequences: WxxW which directly associates to the active TGFβ dimer, and KRFK motif which binds to the LSKL sequence located on the amino terminal of LAP. Studies have suggested that the association of TSP-1 KRFK motif with the LSKL sequence of LAP results in a conformation change in the TGFβ latency complex leading to the release of active TGFβ dimer. However, a mimetic LSKL peptide is able to inhibit TSP-1 mediated TGFβ activation *in vitro* by competitively associating to the KRFK sequence of TSP-1, preventing it from associating to the LAP LSKL motif (Xie et al., 2010).

Over the past decade integrin-mediated TGFβ activation has been studied by many research groups. Integrins are heterodimeric type-1 transmembrane cell adhesion receptors composed of non-covalently associated α and β subunits. They have a key role in mediating interactions between the ECM and the cytoskeleton. 24 integrins have been identified in mammals, and *in vitro* studies have illustrated that 6 integrins (αvβ1, αvβ3, αvβ5, αvβ6, αvβ8 and α8β1) are able to recognise and interact with a tri-peptide RGD motif located in LAP (only on the latent form of TGFβ1 and TGFβ3, not TGFβ2). However, the activation of TGFβ has only been demonstrated *in vivo* by integrins αvβ3, αvβ5, αvβ6, and αvβ8. The physiological relevance of the latent TGFβ interaction with integrins αvβ1 and α8β1 is not known (Jenkins et al., 2006).

Integrins αvβ3 and αvβ5 are expressed in many cells including fibroblasts. Both integrins are able to activate TGFβ, and it is believed that αvβ5 causes the transformation of fibroblasts to myofibroblasts via TGFβ activation (Zhou et al., 2010). In addition, immunohistochemistry on IPF tissue has demonstrated that αvβ5 localises with αSMA within the fibrotic foci suggesting that αvβ5 may have an important role in the development of IPF possibly by activating TGFβ within the fibrotic foci (Scotton et al., 2009). However, recent studies involving the bleomycin model have demonstrated that mice lacking both αvβ3 and αvβ5 are not protected from bleomycin-induced PF (Atabai et al., 2009; Worthington et al., 2011). Nevertheless, it is

important to note that in the bleomycin model of PF, mice do not develop fibrotic foci. Therefore, more studies are required to investigate the precise role of these integrins in fibrosis. Unlike αvβ3 and αvβ5, the expression of αvβ6 is limited to epithelial cells. Studies have shown that upon tissue injury, the expression of this integrin is upregulated. In addition, Itgb6$^{-/-}$ mice have reduced activation of TGFβ and are protected from bleomycin-induced PF (Munger et al., 1999). Integrin αvβ6 may also have a vital role in the development and progression of PF.

It had been assumed that the mechanism by which integrins activate TGFβ involves cleavage of TGFβ. However, cell culture models have demonstrated that in the presence of protease inhibitors, αvβ5 and αvβ6-mediated latent TGFβ activation is not inhibited, suggesting that the activation is independent of cleavage. It is now presumed that binding of integrins to the RGD motif induces a conformational change to the latent TGFβ structure, allowing the active TGFβ to interact with its receptor on neighbouring cells (Munger et al., 1999; Wipff et al., 2007; Hinz and Gabbiani, 2010).

Cell contraction plays a vital role in αvβ5- and αvβ6-mediated TGFβ activation. *In vitro* work has demonstrated that TGFβ activation is dependent on an intact actin cytoskeleton. Treating cells with an actin polymerisation inhibitor (i.e. cytochalasin D) causes a decrease in integrin-mediated TGFβ activation. Furthermore, treatment of myofibroblasts with inhibitors of cell contraction (i.e. blebbistatin) also reduces TGFβ activation via αvβ5. Moreover, treating myofibroblasts with agents that promote cell contraction enhances αvβ5-mediated TGFβ activation. Such agents include endothelin-1, thrombin, and angiotensin-II. In addition, seeding myofibroblasts on to substrates that facilitate cell contraction (i.e. stiff silicone substrates) promotes the activation of TGFβ in the presence of αvβ5 in comparison to myofibroblasts seeded on to more flexible substrates (that do not support contraction of the cells). All these *in vitro* studies support that cell contraction is important in TGFβ activation (Wipff et al., 2007; Worthington et al., 2011). In addition, over the past few years the role of proteinase-activated receptor (PAR)-1 in promoting integrin-mediated activation has also been studied whereby αvβ6 and αvβ5 are activated downstream of PAR1 signalling (**Figure 1.12**) (Chambers et al., 2000; Jenkins et al., 2006; Scotton et al., 2009).

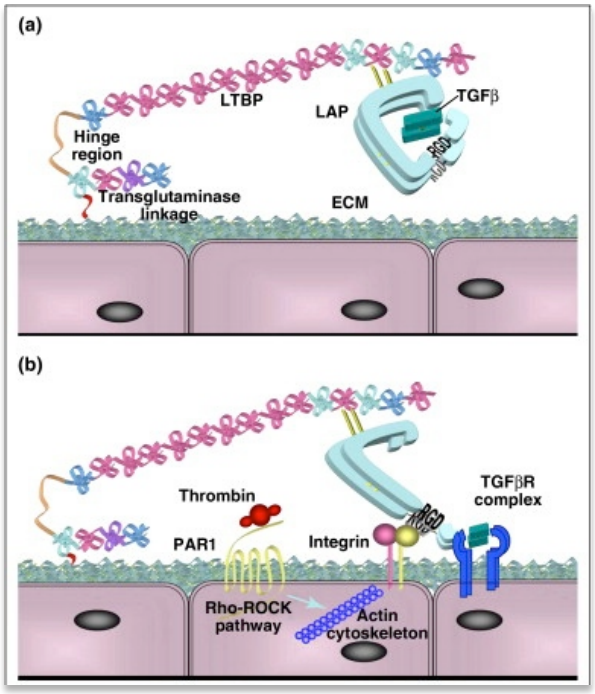

Figure 1. 12: Integrin-mediated TGF-beta activation via proteinase activated receptor (PAR)-1.

(A) Structure of the latent TGFβ complex (B) Thrombin mediated PAR1 activation triggers the Rho-ROCK pathway, which in turn activates myofibroblast-expressed integrin αvβ3 or αvβ5, or epithelial-expressed avβ6. These integrins recognise the RGD sequence on the latency associated peptide (LAP), resulting in a conformational change to the latent complex, releasing the active TGFβ. Active TGFβ bind to its receptor on neighbouring cells, triggering Smad-dependent and Smad-independent intracellular pathways.

Reproduced from (Worthington et al., 2011), with permission of Elsevier Ltd.

TGFβ signalling pathways

Following TGFβ activation, various proteoglycans enhance the delivery of active TGFβ to its receptor. The best characterised are glypcians. These are small proteoglycans composed of heparin sulphate glycosaminoglycan (GAG) side chains associated to the extracytoplasmic surface of the cell membrane by glycosylphosphatidyl intositol anchors (Cheifetz et al., 1988; Kayed et al., 2006). Glypcians behaves as a co-receptor for not only active TGFβ, but also several other growth factors including PDGF (Higashiyama et al., 1993), VEGF (Dougher et al., 1997), BMPs (Paine-Saunders et al., 2000), activins (Nakamura et al., 1991), and Wnt family of secreted glycoproteins (Reichsman et al., 1996; Kayed et al., 2006).

Once TGFβ associates with its receptor, several intracellular signalling processes are initiated including the canonical pathway which involves the activation of Smad protein. In brief, active TGFβ associates with the homodimeric serine threonine transmembrane kinase receptor (i.e. Tβ-RII). This promotes the recruitment of homodimer Tβ-RI (activin-like kinase-5, ALK-5) which interacts with the Tβ-RII dimer resulting in the formation of a tetrameric cell surface complex. This promotes the Tβ-RII kinase to phosphorylate the serine and threonine residues in the short juxtamembrane glycine/serine rich (GS) domains of the Tβ-RI (Souchelnytskyi et al.,

1996). This results in a conformational change in Tβ-RI (Huse et al., 2001) causing the activation of its kinase activity. Activation of ALK-5 kinase activity results in the recruitment and phosphorylation of R-Smad (Smad 2/3) which occurs with the help of SARA (Smad anchor for receptor activation). Phosphorylated Smad 2/3 then form a heteromeric complex with co-Smad (Smad 4) in the cell cytoplasm. This Smad complex then translocates into the nucleus and binds to specific DNA-binding sites on the promoter regions of target genes with the help of intranuclear transcriptional partners. Such genes including those encoding CTGF, collagen type I, and integrin β6. Thus, activation of TGFβ via αvβ6 creates a positive feedback loop (Margadant and Sonnenberg, 2010). This creates a profibrotic environment, which exists in IPF patients and it has been suggested that this may be involved in driving the progression of the disease.

In addition, the Smad-dependent TGFβ signalling pathway may also promote the synthesis of plasminogen activator inhibitor 1 (PAI-1). This protein is the principle inhibitor for serine proteinases tissue- and urokinase-plasminogen activator (tPA and uPA). Both tPA and uPA are involved in the conversion of plasminogen to plasmin which promotes fibrin degradation. In addition, studies have demonstrated that plasmin also plays a key role in MMP activation (including MMP2, MMP3, MMP9, MMP12, and MMP13 (reviewed in (Liu, 2008)). Thus, inhibition of tPA and uPA activity via PAI-1 not only inhibits fibrinolysis, but also reduces collagen degradation. In BALF of IPF patients, PAI-1 expression is elevated. This has also been demonstrated in murine models of PF.

Activation of ALK-1 also contributes to the fibrotic response by promoting the expression of target genes. This occurs as a result of phosphorylation and activation of the non-receptor tyrosine kinase, c-Abl (cellular Abelson non-receptor kinase) (Wilkes and Leof, 2006; Rahimi and Leof, 2007), which activates several downstream molecules including protein kinase C-δ (PKC-δ), and EGR transcription leading to Smad2/3-independent collagen synthesis (Bhattacharyya et al., 2009). In addition, TGFβ also modulates the activity of several other non-canonical (or Smad-independent) pathways including phosphatidylinositol-3-kinase(PI3K)/AKT pathway, Rho-like GTPase signalling pathway, and mitogen activated protein kinase (MAPK) pathway (Moustakas and Heldin, 2005; Zhang, 2009; Mu et al., 2012).

As well as promoting gene transcription, studies have shown that activated TGFβ receptor complexes may be internalised via lipid rafts and caveolin-1 where they are poly-ubiquitinated by E3 ubiquitin ligase (recruited by Smad 7 and Smurf 2) and destined for degradation (Di

Guglielmo et al., 2003; Razani et al., 2001). Thus, TGFβ activation and degradation is a carefully controlled process and alterations in these mechanisms play a role in the pathogenesis of IPF (Kardassis et al., 2009; Heldin and Moustakas, 2012; Choi et al., 2014).

Inhibiting the activity of active TGFβ signalling has been studied in various diseases, which have mainly focused on developing TGFβ receptor inhibitors, such as SB-525334A (GlaxoSmithKline, UK) and SD-208 (Scios Inc., USA). Such inhibitors attenuate bleomycin-induced PF (Higashiyama et al., 2007). In addition, studies also aim to develop agents that may target the activation of TGFβ, such as αvβ5 and αvβ6 inhibitors which could possibly reduce fibrotic responses.

1.2.7. Prostanoids

Alterations in the levels of antifibrotic mediators within the lung may result in PF, and studies have investigated the potential role of prostanoids in the pathogenesis of IPF. Prostanoids are a subclass of eicosanoids composed of prostaglandins (PG) and thromboxanes which are synthesised via the metabolism of arachidonic acid (AA). The major prostanoid within the lung is prostaglandin E2 (PGE_2) which is produced by several cells including epithelial cells, fibroblasts, and alveolar macrophages (Churchill et al., 1989; Hempel et al., 1994a, 1994b; Jordana et al., 1994; Kolodsick et al., 2003). This section summarizes our current understanding regarding the role of PGE_2 in modulating lung fibrosis. In addition, other prostanoids such as PGI_2 and $PGF_{2\alpha}$ will also be briefly discussed.

PGE_2 biosynthesis, regulation and receptor signalling

Figure 1.13 summarises the prostanoid synthesis pathway. AA is a polyunsaturated fatty acid located in phospholipids of cell membranes. Free AA is liberated from the membrane via the activity of phospholipase A2 (PLA_2) in response to various pathological and physiological stimuli. Following this, the free AA is metabolised via the 5-lipoxygenase (5-LOX) pathway or the cyclooxygenase (COX) pathway. The former pathway occurs primarily in leukocytes and macrophages, giving rise to leukotrienes (Ford-Hutchinson et al., 1994). However, it has been shown that AECs may also produce cycterinyl leukotrienes at low concentrations (Vannella et al., 2010). On the other, the COX pathway yields prostanoid products. The initial step of this pathway involves the *bis*-dioxygenation and subsequent reduction of AA via the activity of COX

enzymes (the rate-limiting enzymes), resulting in the production of PGH_2. Currently two COX enzymes have been studied extensively, COX1 and COX2.

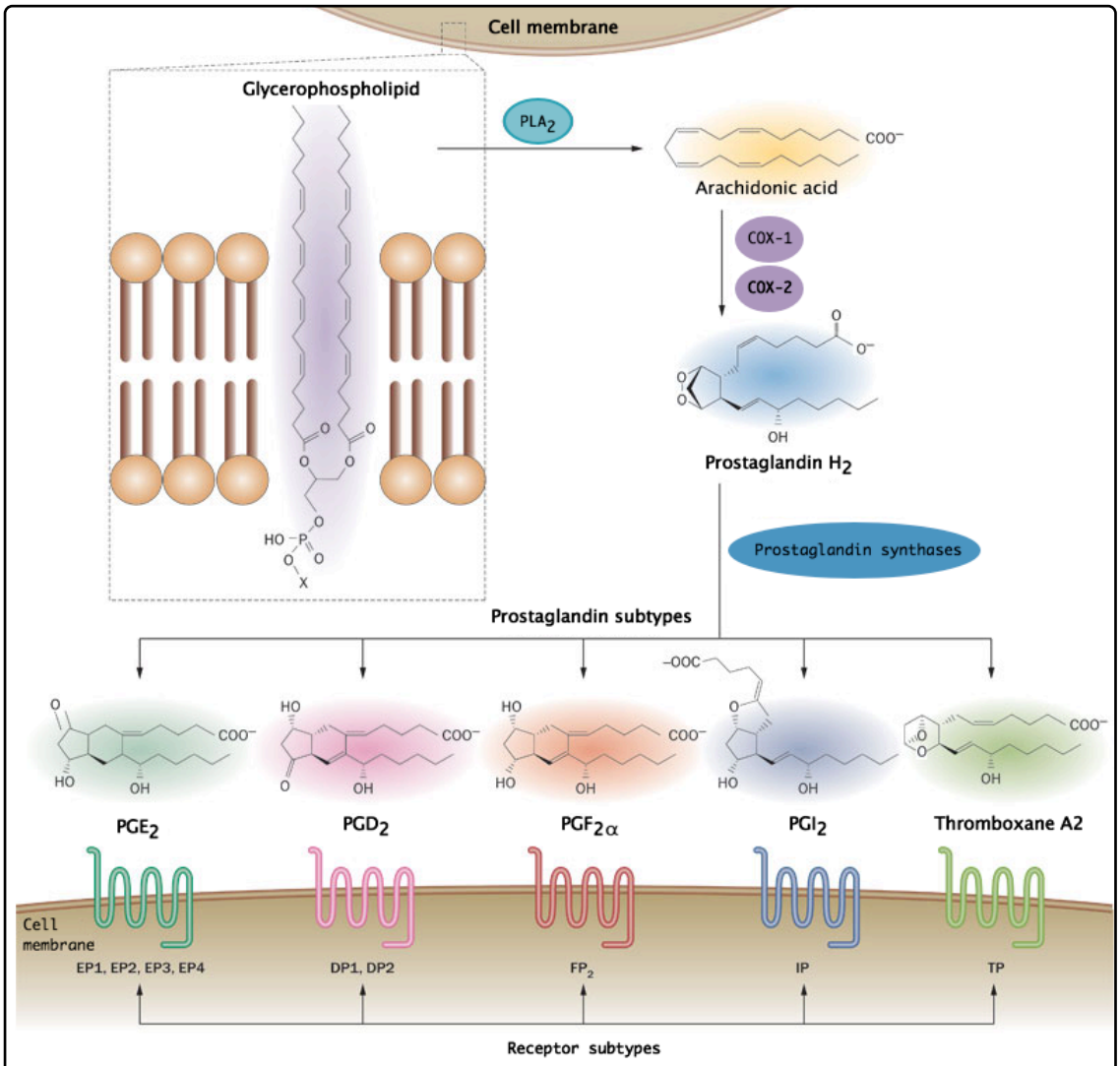

Figure 1. 13: Prostaglandin biosynthetic pathway.

Arachidonic acid is released from cell membranes via the activity of phospholipase A_2 (PLA_2). Cyclooxygenase (COX)-1 and COX-2 catalyse the production of prostaglandin H_2 from the arachidonic acid. Specific prostaglandin synthases then promote the formation of PGE_2, PGD_2, $PGF_{2\alpha}$, PGI_2, or thromboxane A2. Each of these prostanoids have specific G-protein coupled receptors to which they associate to and activate downstream signalling pathways.

Reproduced from (Rahnama'i et al., 2012) with permission of Nature publishing group.

COX1 is expressed constitutively whereas COX2 expression is transient and induced via several inflammatory mediators in the majority of cell types (excluding AECs and bronchial epithelial

cells which express COX2 constitutively) (Walenga et al., 1996; Ermert et al., 1998; Simon, 1999). Stimuli include TGFβ, IL-1β, hepatocyte growth factor (HGF), lipopolysaccharide, and plasmin (Brock et al., 2003; Coward et al., 2010). These mediators not only promote the binding of transcription factors to the COX2 promoter regions (i.e. NFkB, AP-1, and cAMP response elements or CREs) (Appleby et al., 1994), but also regulate histone acetylation and chromosome accessibility (Coward et al., 2009). In contrast, transcriptional silencing of the COX-2 gene can result from epigenetic changes including hypermethylation of the CpG islands in the 5'UTR (Song et al., 2001). Other regulatory mechanisms affecting COX-2 expression include proteosomal protein degradation pathways, miRNA inhibition of translation, differential utilization of polyadenylation sites, and suicide inactivation of COX catalytic activity (Harper and Tyson-Capper, 2008; Mbonye and Song, 2009).

Following PGH_2 production, specific prostanoid end-products are synthesised via the activity of cell-specific distal prostaglandin synthase enzymes (Hara et al., 2010), and are then able to associate to their receptors to promote the activation of several signalling pathways. Three isoforms of PGE_2 synthase (PGES) have been identified in murine and mammalian tissues: microsomal PGES (mPGES)-1, mPGES-2, and cytosolic PGES (cPGES). As stated in the names, mPGES-1 and mPGES-2 are located in the microsomes whereas cPGES is situated in the cytosol. In general, cPGES and mPGES-2 are constitutively expressed whereas mPGES-1 expression is induced. Studies have illustrated cPGES is capable of catalysing the conversion of COX1-derived PGH2 to PGE_2. However, cPGES is unable to convert PGH_2 derived from COX2 activity. On the other hand, mPGES-1 converts COX2-derived PGH_2 (not COX1). Interestingly, mPGES-2 may couple with either COX1- or COX2-derived PGH2, although it is slightly more partial towards COX1 (Samuelsson et al., 2007; Hara et al., 2010).

Knockout mice for the genes encoding all three isotypes have been developed. mPGES-2 deficient mice showed no effect on physiological and pathophysiological conditions; mPGES-1-deficient mice showed reduced response to inflammatory stimuli, suggesting that mPGES-1 regulate inflammation-induced PGE_2 synthesis; and cPGES deficiency is perinatally lethal with the mice displaying poor lung development, retarded growth, and delayed skin maturation (Nakatani et al., 2007). Similarly to the COX enzymes, it is generally accepted that mPGES-2 catalyses the production PGE_2 for housekeeping functions, while mPGES-1 forms PGE_2 in response to stimuli (Samuelsson et al., 2007).

Four receptors for PGE_2 have been identified: EP1, EP2, EP3, and EP4, all of which are G-protein coupled receptors composed of 7-transmembrane-spanning domains (Narumiya et al., 1999). The intracellular signalling pathways activated in response to the EP receptors dictate their cellular functions. For instance, EP2 and EP4 receptors stimulate the activity of adenylate cyclase which in turn increases intracellular concentrations of the second messenger cyclic adenosine monophosphate (cAMP), triggering the relaxation of smooth muscle cells. Although EP2 and EP4 receptors activate the same downstream signalling pathway, structurally these receptors are different. Of the six loops between the transmembrane domains only the second cytoplasmic loop appears to be the same in both receptors which suggests that this part of the receptor is crucial for the common intracellular signalling (Brock, 2014). On the other hand, activation of EP1 and EP3 receptors causes an increase in intracellular Ca^{2+} concentration and decreases cAMP levels, respectively, thus promoting smooth muscle cell contraction (reviewed in (Bozyk and Moore, 2011)).

The role of prostanoids in normal lung homeostasis

In a healthy lung microenvironment, homeostasis is considered to be dependent on epithelial-mesenchymal crosstalk (Selman et al., 2001; Selman and Pardo, 2002). The homeostatic signalling of PGE_2 in AECs and fibroblasts is illustrated in **Figure 1.14**. Several pieces of evidence support this concept including *in vitro* studies whereby AECs from control animals were able to inhibit fibroblast proliferation. In addition, AECs extend through the basement membrane making contact with fibroblasts in normal lung sections. Inhibition of fibroblast proliferation by AECs is dependent on the ability of the AECs to synthesise PGE_2 (Lama et al., 2002; Moore et al., 2005a; Huang et al., 2007, 2008a) and studies have demonstrated that in the presence of PGE_2 Epac-1 (exchange protein activated by cAMP-1) is activated downstream of EP2 receptor signalling which exclusively inhibits fibroblast proliferation (Huang et al., 2008a). As well as the inhibition of fibroblast proliferation, PGE_2 plays an essential role in regulating apoptosis. In normal human lung fibroblasts, PGE_2 potentiates FasL induced apoptosis via EP2/EP4 receptor signalling with reduced activity of the prosurvival molecule protein kinase B (Akt) (Huang et al., 2009).

Activation of EP2 receptor signalling via PGE_2 also inhibits TGFβ-induced fibroblast differentiation as well as attenuating collagen synthesis (Kolodsick et al., 2003) which occurs independently of Smad-signalling. Instead, PGE_2 is able to alter the architecture of the cytoskeleton leading to the disruption of focal adhesion formation. These cytoskeletal changes

were detected by analysing the expression of adhesion dependent signalling molecules (i.e. FAK, paxillin, STAT-3, and Akt) (Thomas et al., 2007). In addition, EP2 receptor signalling activates PTEN, and as a result fibroblast proliferation is inhibited (White et al., 2005, 2006). Therefore, PTEN activation via PGE_2 is another mechanism by which prostanoids inhibit myofibroblast differentiation. Furthermore, amplification of cAMP generated by PGE_2 reduces collagen synthesis (Huang et al., 2007, 2008a), promotes collagen degradation (Baum et al., 1980), inhibits fibroblast chemotaxis, and reduces the expression of growth factor receptors (Boyle et al., 1999). This can be achieved by using phosphodiesterase 4 (PDE4) inhibitors which inhibit cAMP breakdown (Kohyama et al., 2002b; Dunkern et al., 2007; Togo et al., 2009).

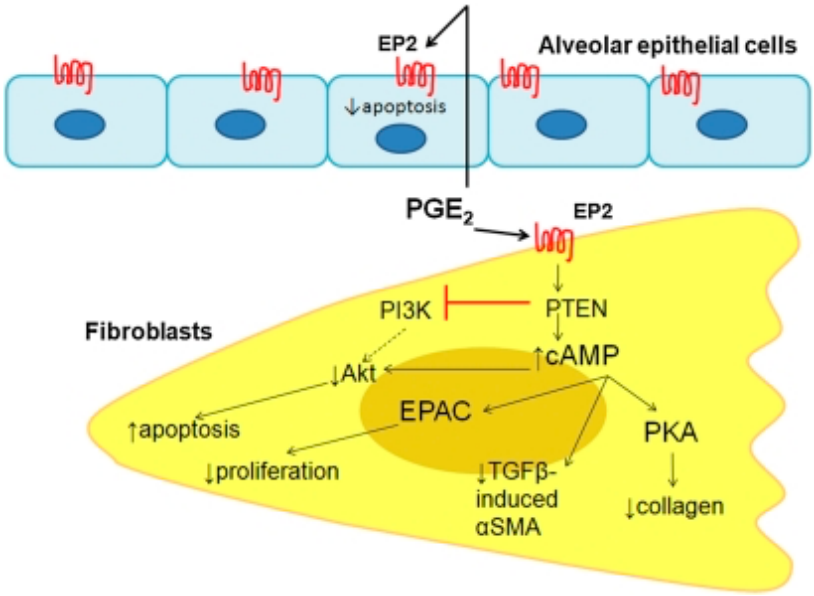

Figure 1. 14: PGE_2 signalling in AECs and fibroblasts in monolayer cultures.

Studies hypothesise that in monolayer cultures, PGE_2 protects AECs from apoptosis and limits fibroblast proliferation, collagen production, and differentiation via EP2 receptor signaling.

Reproduced from (Bozyk and Moore, 2011) with permission of American Thoracic Society

PGE_2 levels in IPF

Imbalance of eicosanoid synthesis has been shown in human and animal lung fibrosis studies, whereby reduced PGE_2 levels and increased leukotriene levels in BALF and lung homogenates of IPF patients have been detected in comparison to healthy controls (Wardlaw et al., 1989; Peters-Golden et al., 2002). Reduced PGE_2 levels are consistent with finding of decreased COX-

1 and COX-2 expression in IPF patients (Petkova et al., 2003; Coward et al., 2009; Maher et al., 2010). In addition, studies have illustrated that IPF fibroblasts are unable to upregulate the expression of COX-2 in response to an exogenous stimulus. The reduced COX-2 expression correlates with increased fibroblast proliferation and promotes collagen production following TGFβ stimulation (Wilborn et al., 1995; Keerthisingam et al., 2001; Maher et al., 2010). In addition, COX-2 deficiency promotes bleomycin-induced PF in mice (Keerthisingam et al., 2001; Hodges et al., 2004). A more recent study has illustrated that the role of mPGES-1 in PF whereby mPGES-1 knockout mice exhibited more severe fibrotic lesions, reduced PGE_2 concentrations, and decreased expression levels for EP2 and EP4 receptors following the administration of bleomycin, in comparison to wild type mice (Wei et al., 2014). In addition, diminished PGE_2 contributes to the apoptosis paradox seen in IPF patients (i.e. increased AEC apoptosis and diminished apoptosis in fibroblasts). However, fibrotic fibroblasts are resistant to the pro-apoptotic effects of PGE_2. Reduced COX-2 expression in IPF fibroblasts is one factor which is considered to promote fibroblast survival (Maher et al., 2010).

Recent studies on animal models as well as human tissues have increased our understanding of the role and regulation of PGs in fibrotic lung diseases including the identification of many soluble mediators and epigenetic changes which may possibly explain the decline in PG synthesis (Coward et al., 2009; Huang et al., 2010). For instance, AEC injury results in the release of chemokines such as CCL2 (Moore et al., 2001) and studies have illustrated that in the presence of CCL2, PGE_2 production via AECs is diminished and fibroproliferation is elevated (Moore et al., 2003). This is one mechanism which explains the reason why CCR2 (CCL2 receptor) knockout mice are protected from fibrotic injury (Moore et al., 2001; Gharaee-Kermani et al., 2003).

Fibrotic lung injury also promotes plasma leakage and activation of the coagulation cascade. However, the extravascular fibrin is not effectively cleared in fibrotic lungs due to the increase in expression of PAI-1 (Chapman et al., 1986; Idell et al., 1989; Bertozzi et al., 1990). As already mentioned before, PAI-1 prevents plasmin production by inhibiting the activity of uPA and tPA and thus inhibits fibrinolysis. Studies have shown that under normal wound healing responses plasmin is able to upregulate COX2 expression and stimulate PGE_2 synthesis in AECs, fibroblasts, and fibrocytes (in mice and human lungs) via hepatocyte growth factor (HGF; plays a key role in mediating lung epithelial cell growth) (Hojo et al., 1997). This supports the notion that increased levels of PAI-1 diminish PGE_2 synthesis. In addition, studies have also illustrated that PGE_2 is able to mediate HGF activation in a positive antifibrotic feedback loop in normal

lung. Thus, it's likely that this feedback loop is missing in lungs of IPF patients (Marchand-Adam et al., 2003).

More recently, studies have been focusing on possible epigenetic changes which may contribute to diminished COX2 expression. For instance, Coward et al. (2009) illustrated reduced COX2 mRNA levels in fibrotic fibroblasts however the mRNA degradation rates were the same in comparison to control fibroblasts, which suggested that reduced COX2 expression may be a result of defects during transcription. To further investigate this the same study. showed that despite having appropriate levels of transcription factors involved in driving COX2 expression (i.e. CREB1, CEBPb, NFκB, and p65), these factors were unable to associate with their binding sites on the COX2 promoter. This correlated with reduced levels of histone acetyltransferase (HAT) and increased recruitment of histone deacetylase (HDAC) leading to a decrease in levels of H3 and H4 acetylation (both of which are required for normal COX2 transcription process). However, when the IPF fibroblasts were treated with HATs along with HDAC inhibitors, the level of histone H3 and H4 acetylation increased and cytokine-induced COX2 expression was restored. These results support the concept that diminished COX2 expression is IPF is due to epigenetic abnormalities in the form of histone hypoacetylation (Coward et al., 2009).

Furthermore, epigenetic changes in EP receptors (in particular EP2) leading to decreased receptor expression have been described in fibrotic fibroblasts (Moore et al., 2005a; Huang et al., 2008b; Sagana et al., 2009). Such changes include DNA hypermethylation at CpG islands in the promoter region of prostaglandin EP2 receptor gene (*PTGER2*). This hypermethylation is greater in comparison to control fibroblasts and results from increased Akt signaling and decreased PTEN activity. However, treating IPF fibroblasts with a DNA methylation inhibitor (i.e. 5-aza-2'-deoxycytidine) reduces *PTGER2* methylation, elevates *PTGER2* mRNA levels as well as EP2 protein expression, and restores PGE_2 response in the fibrotic fibroblasts (i.e. reduces fibroblast proliferation and collagen synthesis). DNA methyltransferase (DNMT)-specific siRNA also has similar results (Huang et al., 2010). These results suggest that the expression of EP2 receptors is tightly controlled. Taken together, these epigenetic changes demonstrated in IPF fibroblasts prevent COX-2 gene transcription in IPF and contribute to diminished production of PGE_2. Thus, these could be potential therapeutic target for the treatment of IPF.

Other prostanoids in IPF

As well as PGE_2 other prostanoids have also been reported to play a role in PF, and have recently become of great interest. These are PGI_2 (prostacyclin) and $PGF_{2\alpha}$. Similar to PGE_2, PGI_2 also mediates antifibrotic effects (i.e. inhibit fibroblast proliferation, migration, and collagen synthesis) by increasing intracellular cAMP levels via the activation of its G-protein coupled receptor (IP) (Stratton et al., 2001; Kohyama et al., 2002a; Soberman Peter, 2006). PGI_2 levels in IPF fibroblasts are low in comparison to control cells *in vitro*. In addition, IP knockout mice are more susceptible to developing severe PF in response to bleomycin in comparison to the wild type (Lovgren et al., 2006). Furthermore, a synthetic prostacyclin agonist (iloprost) attenuates bleomycin-induced lung fibrosis in mice (Murakami et al., 2006). Such results support that as well as PGE_2, PGI_2 may also potentially be a therapeutic target of interest for the treatment of IPF.

Unlike PGE_2 and PGI_2, $PGF_{2\alpha}$ is a profibrotic mediator, as in the bleomycin induced PF model $PGF_{2\alpha}$ facilitates PF via PGF receptors (FP). In addition, the levels of $PGF_{2\alpha}$ are elevated in BALF of IPF patients and studies have illustrated that $PGF_{2\alpha}$ is able to stimulate collagen production by lung fibroblasts. Such results support that this prostaglandin may contribute to disease progression (Aihara et al., 2013).

1.2.8. Therapeutic interventions of IPF

As already mentioned, in spite of extensive studies into understanding the pathogenesis of IPF, the mechanism is still not completely understood. Nevertheless, several studies have helped enhance our understanding in the complexity of this deadly disorder which has led to the identification of putative targets for the treatment of IPF. Over the past ten years the number of high-quality clinical trials has slowly increased. However, none of the trials have shown worthwhile treatment effects on patients with the severe form of IPF which emphasises the desperate need in determining the precise mechanism involved in the progression of this fatal disease. Compounds which have failed clinical trials include corticosteroid monotherapy (i.e. prednisone), anticoagulant therapy (i.e. warfarin), Azathioprine (immunosuppressant), cyclophosphamide (chemotherapeutic agent), Everolimus (rapamycin derivative with immunosuppressive and anti-fibroproliferative properties), Bosentan (endothelin receptor antagonist), sildenafil (PDE5 inhibitor), interferon gamma (IFNγ), Etanercept (TNFα antagonist),

and Imatinib (an anti-proliferation protein tyrosine kinase inhibitor of PDGFR) (reviewed in (Ahluwalia et al., 2014)) .

Furthermore, a three-drug regimen involving an immunosuppressive drug, a glucocorticoid, and an antioxidant (i.e. azathioprine; prednisone; and N-acetylcysteine, NAC) was tested in the PANTHER clinical trial which was randomised, double-blinded, and with placebo controls. Unfortunately however, due to increased mortality and hospitalisation with the three-drug regimen, the trial was stopped at interim analysis. Nevertheless, the NAC only part of this study continued. Previous studies have demonstrated that oxidative stress may contribute to the aberrant AEC injury seen in IPF. Since the lungs of IPF patients exhibit an elevated oxidant burden (with increased reactive oxygen species, ROS, and reduced levels of the antioxidant glutathione) it was hypothesised that treating IPF patients with the anti-oxidant NAC would reduce this oxidant burden. However the results from the trial published earlier this year illustrated that NAC alone also had no significant benefit with respect to the preservation of FVC in IPF patients (with mild-to-moderate impairment in lung function) (The Idiopathic Pulmonary Fibrosis Clinical Research Network, 2014).

Despite several failed trials, recently a few compounds have shown some positive results in clinical trials. For example Pirfenidone (5-methyl-1-phenyl-2-[1H]-pyridone), which is the only drug which has been approved for IPF patients with mild-to-moderate form of the disease in Europe, Canada, India, Japan., and USA. This compound has shown anti-fibrotic, anti-oxidant, and anti-inflammatory actions *in vitro* and in several animal models of fibrosis in lungs, liver, and kidney (Gurujeyalakshmi et al., 1999; Iyer et al., 1999; García et al., 2002; Oku et al., 2002; Cho et al., 2007). For instance, in retinal pigment epithelial cells Pirfenidone is able to block nuclear translocation of Smad proteins (Choi et al., 2012) and inhibit TGFβ induced HSP47 and collagen I over expression in A549 cells (Hisatomi et al., 2012) as well as human lung fibroblasts *in vitro* (Nakayama et al., 2008). Thus, Pirfenidone is able to inhibit TGFβ-induced fibrogenesis. In addition, using the bleomycin hamster model of lung fibrosis Pirfenidone attenuates pro-collagen I and III mRNA accumulation, hydroxyproline content, prolyl hydroxylase activity, lipid peroxidation (a marker for inflammation index), and TGFβ mRNA and protein levels (Iyer et al., 1999). Moreover, Pirfenidone inhibits the synthesis of PDGF in lung macrophages (Gurujeyalakshmi et al., 1999); reduces the influx of macrophages, neutrophils, and lymphocytes in BALF at early time points (Corbel et al., 2001); reduces hydroxyproline content, inflammatory edema, interleukin (IL)-1β, IL-6, IL-12, and interferon (IFN)-γ (Oku et al.,

2008); and attenuates the elevation of lung FGF, lung stromal cell derived factor-1α, and IL-18 (Iyer et al., 1999; Oku et al., 2008).

The effect of Pirfenidone on IPF patients has been evaluated in three phase 3 clinical trials, one of which was performed in Japan with 275 participants and the other two trials (known as CAPACITY studies 004 and 006) were conducted in the North America, Europe, and Australia involving a total of 435 and 344 patients, respectively. The CAPACITY 004 trial involved assigning patients into three groups: placebo, high dose Pirfenidone (2403 mg/day), and low dose Pirfenidone (1197 mg/day) which were administered orally. CAPACITY 006 trial only involved two groups: placebo and high dose Pirfenidone (Noble et al., 2011). Both the Japanese trial and CAPACITY 004 showed positive results with reduced decline in forced vital capacity (FVC) at 52 and 72 weeks in patients treated with Pirfenidone, respectively. However, no such results were shown in CAPACITY 006, encouraging US regulations to generate an additional trial with more patients recruited in order to support the approval of Pirfenidone. This trial was known as the ASCEND (a randomised, double blinded, placebo control trial), which not only looked at the FVC but also investigated the effects of the drug (high dose; 2403 mg/day) on mortality rate at 52 weeks, 6MW distance, dyspnoea, and progression-free survival. In addition, this trial differed from the CAPACITY trials as it modified the selected eligibility criteria in order to only enrol patients that are at a higher risk of disease progression. The results from this trial illustrated that Pirfenidone was able to reduce disease progression (reflected by exercise tolerance, lung function, and progression-free survival) and cause fewer deaths in patients with IPF in comparison to placebo controls (King et al., 2014). These trials support that Pirfenidone may be a useful means of therapy for the treatment of IPF. However, one of the limitations of these studies is that in all four trials the patients showed no sign of improvement in respiratory symptoms and/or quality of life (Poletti et al., 2014). In addition, the recruited patients in all trials had mild-to-moderate forms of the disease. Thus, the effect of this drug on patients with the severe form is currently unknown and needs investigation.

Another compound that has shown clinical benefits is Nintedanib (also known as BIBF 1120). This compound is an inhibitor of tyrosine kinase receptors including PDGFR and FGFR, and VEGFR (Hilberg et al., 2008; Wollin et al., 2014), all of which have been implicated in the pathogenesis of IPF (Kaner et al., 2000; Allen JT, 2002). Two multinational replicated Phase III studies of Nintedanib (INPULSIS-1 and -2), which involved the administration of this drug at a concentration of 150mg twice daily, have recently been completed (Richeldi et al., 2014). The dose of the compound was used based on a previous phase II trial (TOMORROW; random,

double-blinded, placebo controlled trial) illustrating that at 150mg Nintedanib reduced the FVC decline and reduced the frequency of acute exacerbations (Richeldi et al., 2011). However since the TOMORROW trial consisted of a small number of patients, the study was repeated in two trials with a larger group of patients at 205 different sites in 24 different countries to evaluate the efficacy and safety of the compound. The primary end point was the annual rate of decline in FVC. Both trials illustrated positive results with a significantly reduced rate of decline in FVC, thus Nintedanib may also be used to reduce the progression of IPF. However, the rate of acute exacerbations in patients treated with this compound was inconsistent. This was partly due to the fact that exacerbations are particularly rare in IPF patients recruited in clinical trials, thus this area is difficult to assess and characterise (Richeldi et al., 2014). Furthermore, patients in these trials did experience some adverse side effects including diaorrhea and myocardial infarction.

Many other clinical trials are currently still running which involve compounds targeting various pathways that have been implicated in fibrosis. One example is STX-100, currently running in Phase II trials; this is a monoclonal antibody against $\alpha v\beta 6$. As already stated $\alpha v\beta 6$ is able to activate latent TGFβ which is a potent pro-fibrotic cytokine. Since TGFβ is also an important mediator for homeostatic functions including the regulation of inflammation and the suppression of tumourigenesis, global inhibition of TGFβ may lead to adverse effects. Thus, studies have generated a monoclonal antibody for one of the mediators involved in the activation of TGFβ (i.e. $\alpha v\beta 6$) which is specifically upregulated at sites of injury and has low expression in lungs of normal donors. Thus it is suggested that targeting avb6 will block TGFβ activation specifically in the lungs of IPF patients and not affect the activity of global TGFβ. Other compounds currently being evaluated in Phase II trials include FG-3019 (CTGF-neutralising antibody), BMS-986020 (LPA1 receptor antagonist), and simtuzumab (monoclonal antibody directed against LOXL2.

Despite having a slight increase in the number of high quality clinical trials over the past decade only a few have reached Phase II/III with a few positive effects shown only in mild-to-moderate forms of IPF. The failures in the majority of clinical trials suggest that *in vivo* and *in vitro* models of PF only partially recapitulate the complex pathogenesis of IPF; hence these models may be imperfect for determining potential therapies (Moore et al., 2013; Spagnolo et al., 2014). The current types of *in vivo* and *in vitro* models of fibrosis will be discussed in the next two sections.

1.3. Current models of PF

1.3.1. *In vivo* models of fibrosis

Several animal models are used in research to understand fibrotic responses and to study pulmonary fibrosis in greater detail. This has allowed researchers to identify key cells that may be involved in the disease (described above). However there are a number of disadvantages of using such models, which are summarised in **Table 1.6**. The most common *in vivo* model for fibrosis involves the use of bleomycin. This is an antibiotic, which was originally isolated from *Streptomyces verticillatus* in 1966. It works by binding to guanosine-cytosine-rich areas within the DNA strands and inducing DNA strand breaks. The DNA cleavage is dependent on metal ions (primarily iron) and oxygen. It has been suggested that bleomycin is able to chelate iron resulting in the production of a pseudoenzyme which is then able to react with oxygen. This reaction leads to the production of superoxide and hydroxide free radicals, which in turn result in DNA single-strand breaks at 3'-4' bonds in deoxyribose (Dorr, 1992; Hecht, 2000).

Bleomycin is a useful anti-neoplastic agent and it was initially discovered to work against skin tumours and squamous cell carcinomas. However, increasing the dose of this drug results in pulmonary toxicity, which in turn can lead to fibrosis (Moore and Hogaboam, 2008). Several experimental animals develop fibrosis when treated with this drug including mice, hamsters, rats, guinea pigs, rabbits, dogs, and primates. When this drug is administered via intravenous (i.v.), intraperitoneal (i.p.), or subcutaneous delivery it is assumed that initial lesions to the pulmonary endothelium allows the compound to enter the lung interstitium resulting in subsequent type I epithelial cell damage. However, intranasal (i.n.) and intratracheal (i.t.) administration results in direct epithelial cell damage. In addition, metaplasia in type II epithelial cells is also induced and some inflammatory cells (neutrophils and macrophages) infiltrate into the affected area. Another route of administration of bleomycin is via oropharyngeal instillation. This is currently used in our laboratory as it is considered to be a more representative model of human disease since it causes more homogenous injury in mice with presence of peripheral and subpleural fibrosis (Egger et al., 2013; Scotton et al., 2013). Fibrotic lesions develop within two weeks following administration of bleomycin (Scotton et al., 2009). In addition, histological analyses show damaged basement membrane, clusters of mesenchymal cells, intra-alveolar buds, collagen deposition, and obliteration of the alveolar space all of which are also present within the lungs of IPF patients (Moeller et al., 2008;

Mouratis and Aidinis, 2011). These observations illustrate that bleomycin is able to reproduce many typical features of the human disease (Moeller et al., 2008). Furthermore, the use of this model has contributed tremendously to elucidate the roles of several cytokines, growth factors, as well as some signalling pathways that may be involved in PF.

Despite this there are many disadvantages, one of which includes the lack of some of the pathological features (e.g. fibrotic foci, and the progressive and irreversible nature of the fibrotic condition) shown in lungs of IPF patients. Furthermore, studies suggest that most of the inflammatory responses shown upon the administration of bleomycin are similar to that of acute lung injury (a condition characterised by damage to the alveolar epithelial cells, infiltration of inflammatory cells, oedema, and formation of hyaline membranes) in comparison to fibrosis. This limitation makes it problematic to use this model for drug development, as it would be difficult to interpret the drug benefits against the normal lung repair mechanism. Another weakness of this model is that it is limited to specific mice strains. This is due to the fact that the lungs of other mice strains are able to produce bleomycin hydroxylase which inactivates bleomycin (Moeller et al., 2008). Despite these disadvantages, the bleomycin model (intratracheal administration) remains a vital tool for future use, as it has shown some critical aspects of PF and may be used to assess the efficacy of the compounds (with a potential to be used clinically) in general as proof of principle (Degryse and Lawson, 2011). However, new models should be developed that not only show the pathological features seen in IPF patients, but also be a useful tool to analyse new therapeutic compounds.

Table 1. 6: Summary of common murine models of pulmonary fibrosis

	Advantages	Disadvantages
Single dose intratracheal bleomycin	- Clinic ally relevant - Ease of delivery - Low cost - Quick development of fibrosis - Widely used and accepted in literature	- Lack of some UIP features - Mouse strain dependent
Silica	- Persistent fibrosis - Clinically relevant as a model for the human disease silicosis	- Lack of some UIP features - Prolonged time to develop fibrosis - Expensive - Requires specialised equipment - Mouse strain dependent
Fluorescenin isothiocyanate (FITC)	- Immunofluorescence allows for identification of deposition - Quick development of fibrosis - Persistent fibrosis - Not mouse strain development	- Lack of some UIP features - Reports of variability in FITC response
Radiation	- Clinically relevant as a model for radiation pneumonitis and fibrosis	- Prolonged time to develop fibrosis - Mouse strain dependent
Viral vector delivery of transgenes	- Allows targeted study of specific fibrosis-related genes	- Mouse immune system identifies viral vectors rendering subsequent exposures less potent - Transgenes are typically expressed at greater than physiological level
Transgenic models	- Allows targets study of specific fibrosis-related genes	- Costly and difficult to engineer mouse - Transgenes are typically expressed at greater than physiological levels

Reproduced and adapted from (Degryse and Lawson, 2011; Henry et al., 2002) with permissions of Wolters Kluwer Health.

1.3.2. *In vitro* models of fibrosis

Using animal models and humans in research for drug screening is often restricted by feasibility of testing procedures, availability of test subjects, and ethical concerns. Many studies also use cadaveric tissues, however the disadvantages of using tissues to understand disease pathology are the limited availability of donors and the complications that may arise whilst maintaining the viability of the tissue. In addition, other factors of the donor (such as genetic variations) may go undetected which could affect the experimental result. These limitations have encouraged many researchers to develop *in vitro* models in order to study mechanisms of diseases and hopefully become a useful tool for drug screening. Such *in vitro* models have many advantages including repetitive and quantitative investigations on cell physiology in drug discovery. In addition, *in vitro* models are less expensive in comparison to *in vivo* models. The different types of *in vitro* models used to study PF will be discussed below.

2D monolayer cultures

Two-dimensional (2D) *in vitro* models of mammalian cells have been used extensively in research. This involves seeding cells suspended in media (composed of growth factors) onto a tissue culture treated plastic or glass substrate to determine cellular characteristics (e.g. proliferation, apoptosis, mRNA and protein expression of a target molecule of interest, etc.). The simplicity of a 2D culture has aided in understanding individual cellular phenomena and has led to the identification of several fibrotic mediators some of which have already been described. However, there are many disadvantages of using monolayer cultures. For example, in a normal physiological environment cells are surrounded by a complex and 'crowded' environment composed of various cell secreted factors and a mixed population of cells which interact heterotypically, influencing their respective function. However, in a 2D monolayer culture this does not occur (Baker and Chen, 2012) and the cells are unable to recapitulate some of the characteristic features seen in lung of patients diagnosed with IPF (i.e. fibrotic foci, a key histological feature which correlate with the progression of IPF).

Another disadvantage of 2D *in vitro* systems is that fibroblasts are unable to lay down significant amounts of collagen, even in the presence of ascorbic acid (co-enzyme essential for rendering collagen triple helix) (Murad et al., 1983; Chen and Raghunath, 2009). The reason for this lies in the delayed procollagen C-proteinase (PCP) activity under the aqueous culture conditions which leads to the accumulation of unprocessed procollagen in the cell culture

medium and following every media change this unprocessed pro-collagen is discarded (Lareu et al., 2007a, 2007b). To address this issue, a hyperconfluent cell culture fibroplasia model (involving exogenous treatment with TGFβ) has been developed which stimulates proliferation and collagen synthesis (Clark et al., 1997). However, collagen cross-linking is still difficult to detect in this model.

Another disadvantage of 2D *in vitro* system is the use of a stiff substrate. It is becoming increasingly accepted that as well as chemical compositions, mechanical cues inherent to stiff substrates are just as essential in affecting cellular behaviour (such as growth, differentiation, protein and DNA synthesis, and apoptosis) (Hinz et al., 2001b; Tomasek et al., 2002; Hinz and Gabbiani, 2003a, 2003b; Georges and Janmey, 2005; Engler et al., 2006; Janmey et al., 2009; John et al., 2010). Studies have shown that in most normal tissues the elastic modulus ranges from 0.5-15 kPa whereas in a fibrotic tissue the stiffness can be 10-100 times greater (Discher et al., 2005; Georges and Janmey, 2005; Wells, 2008; Janmey et al., 2009; Hinz, 2010; Balestrini et al., 2012). However, the elasticity for a stiff surface such as polystyrene plastic is ~10^6 kPa which is 100,000 times stiffer than a fibrotic tissue (Gilbert et al., 2010). Therefore, growing cells on a stiff surface (i.e. tissue culture treated plastic or glass) has been described as highly nonphysiological. Several studies on fibroblasts isolated from various tissues across many species support that fibroblasts show distinct functional behaviours which are dependant on substrate stiffness. For instance, Jesudason et al. (2010) illustrated that mechanical forces regulate elastase (protein involved in the degradation elastin) activity within mouse lung parenchyma (Jesudason et al., 2010). In addition, Goffin et al. (2006) identified αSMA as a mechanicosensitive protein which is recruited to stress fibres under significant mechanical load (Goffin et al., 2006; Hinz, 2006). Decreasing the stiffness of the substrate and by inhibiting myosin contraction diminishes stress fibre tension and results in the removal of αSMA from the stress fibres (Goffin et al., 2006). Similar results have also been demonstrated by Balestrini et al whereby explanting fibroblast outgrowth on tissue culture plastic or stiff collagen-coated silicone substrate (i.e. 100 kPA) resulted in increased expression of αSMA and increases cell proliferation in comparison to the soft substrate (i.e. 5 kPa) (Balestrini et al., 2012). One interesting finding from this study was that lung fibroblasts grown on stiff matrix for three weeks sustained their myofibroblastic phenotype even after the cells were returned to a healthy soft substrate for two weeks. In addition, culturing lung fibroblasts for three weeks on soft substrates partially protected the cells from myofibroblast activation after shifting the cells to stiff substrates. Thus, culturing cells on to a stiff substrate may have a permanent

impact on cell behaviour which does not resemble normal cellular behaviour evident in control tissues *in vivo*. Nevertheless, despite having many disadvantages 2D monolayer cultures are still used in labs to determine behaviour of normal and pathological cells.

Scar-in-a-jar (SIAJ) assay

The SIAJ *in vitro* assay has become increasingly popular in many labs in particular at GSK (Stevenage, UK) for screening compounds. This assay is similar to a 2D culture as it involves seeding a monolayer of fibroblasts into a tissue culture treated plastic substrate. However, the uniqueness of this model is that it involves the addition of Ficoll which is a non-interacting, neutral hydrophilic polysaccharide capable of causing macromolecular crowding (a feature absent in the classical 2D monolayer culture) promoting collagen synthesis at a faster rate, thus reducing incubation time. Therefore, this assay allows *in situ* assessment of the area of collagen type I deposited per cell and it is also possible to detect collagen cross-linking. Furthermore, this assay is considered to be high-throughput for compound screening as the effect of compounds on TGFβ-induced collagen synthesis, αSMA expression, proliferation, and cell toxicity can be measured simultaneously within a single well (Chen and Raghunath, 2009). Although this model produces high collagen levels at a fast rate and is considered a far better system to identify therapeutic targets compared to the standard 2D monolayer *in vitro* culture, the SIAJ model also has several disadvantages some of which have already been described (i.e. the assay only involves one cell type, cells are grown on a stiff substrate/plastic, the cells require exogenous TGFβ to promote collagen synthesis, and the model is unable to recapitulate fibrotic foci).

Precision cut lung slices

Over the past few year, the development of more complex three dimensional (3D) *in vitro* models that mimic microenvironments observed in normal tissues have now become of great interest (Elliott and Yuan, 2011). One such model developed is known as the precision cut lung slice. This model involves embedding donor lungs into low melting point agarose (inserted through the trachea) to preserve the opened alveoli and provide better tissue compliance, prior to slicing. The lung slices are then cultured at air-liquid interface and treated with compounds to investigate their effects. TGFβ1-induced fibrosis has been studied on precision lung slices for up to 7 days of culture whereby increased thickness of alveolar septa was evident, and concentration dependent (Lin et al. 1998). Furthermore, elevated collagen VI and αSMA expression has also been reported (Kasper et al. 2004). This model offers a large range

of applications for biomechanical, physiological, toxicological, and pharmacological studies. Furthermore, the greatest advantages of this model are the preservation of the differentiation state of quiescent tissue and the possibility to analyse multiple cell type interactions, similar to *in vivo* lungs. In addition, studies have illustrated that the precision cut lungs slices behave in a similar way to that seen *in vivo*. However, one of the major disadvantages of this model is the lack of tissue availability due to limited number of donors. Therefore, a more robust 3D system is necessary which not only mimics some of the key features seen in IPF lungs, but is also reproducible and easily used for high-throughput screening of potential compounds for the treatment of IPF.

1.4. Spheroids and Microfluidic devices

1.4.1. Spheroids

Spheroids are defined as spherical aggregates of cells in culture which are able to retain a 3D architecture (Takezawa et al., 1993). The aggregates are organised in a complex network involving cell-to-cell and cell-to-matrix interactions (Berahim et al., 2011). It is believed that cells within the spheroids are able to form gap and tight junctions, which contribute to the formation of the spheroid (Takezawa et al., 1993). Since the early 1970s, spheroids have been utilised in research areas of tissue engineering, as they seem to mimic morphological and physiological characteristics of cells in living tissues/organs thus aid in understanding the pathology of various diseases (Corbeil et al., 1977; Culo et al., 1980; Kunz-Schughart et al., 1998). One of the major benefits of establishing spheroids is that certain cellular mechanisms (i.e. cell growth, proliferation, and differentiation) can be studied in a reproducible format (Kunz-Schughart et al., 1998).

Spheroid forming techniques

There are several fabrication methods which have been developed to form spheroids some of which are illustrated in **Figure 1.15**. The most classical method used to produce spheroids involves culturing cells in a round-bottom 96 well plate with a non-adherent surface. Pre-coating the tissue culture treated plate with agarose can generate this non-adherent surface (Takezawa et al., 1993). This approach is simple to carry out and forms reproducible spheroids

of the same size. The static liquid overlay method is similar to this method as it also involves culturing cells on non-adherent substrates. However, in this method the cells are cultured on a larger surface which eventually results in the mass production of spheroids. However unlike the previous approach described, this technique does not allow precise control for the size of the spheroids.

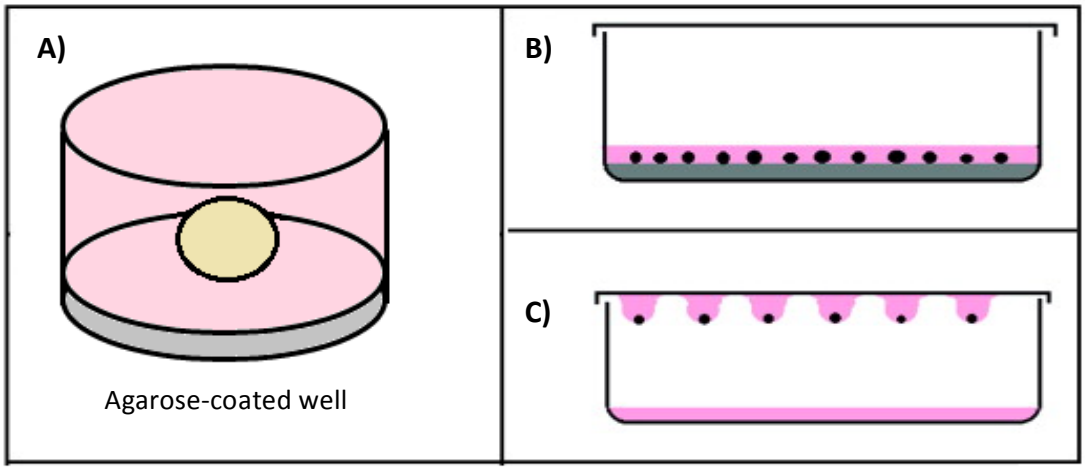

Figure 1. 15: Spheroid formation methods

(A) Non-adherent surface technique (in this case agarose coated wells); (B) Liquid overlay technique; (C) Hanging drop technique. B and C are reproduced from (Fennema et al., 2013) with permission of Elsevier Ltd.

Another common method used is the 'hanging drop' approach. This involves placing a drop of cell suspension on to an inverted dish which is then placed above a reservoir to prevent evaporation. This would allow the cells in the drop to adhere to one another forming a spheroid. Unlike the previous methods described, this approach is slightly more tedious (in particular when collecting the spheroid for analysis) and less high-throughput. To address these issues, manufacturers have recently developed commercially-available 96- and 384-microwell plate formats which provide more control with regards to the size of the spheroid and are theoretically less labour intensive (Tung et al., 2011; Hsiao et al., 2012).

Current literature on cells cultured as spheroids

Spheroid culture is a versatile and powerful biomimicry tool used in many areas of basic science and regenerative medicine. Cancer cells, embryonic cells, and dermal fibroblasts have been studied extensively as spheroids (Culo et al., 1980; Takezawa et al., 1993; Matsuo et al.,

1997). For instance, Culo et al. (1980) used four mouse tumours to form multicellular tumour spheroids in order to investigate tumour growth in normal and immunised mice. In addition, Kaufman et al. (1981) analysed the physiology of multicellular spheroids from hamster lung fibroblast cells, where they demonstrated that in the presence of non-toxic indirect radiosensitiser agents; the radioresistance of these cells was significantly modified. Furthermore, studies on periodontal fibroblasts have demonstrated the growth of spheroids on collagen-based and synthetic membranes. In addition, spheroids formed from mesenchymal stem cells (MSCs) derived from human umbilical cord blood appear to exhibit increased therapeutic potential for myocardial infarction (Lee et al., 2012) supporting the idea that spheroid systems may provide a great promise for drug screening (Bichay et al., 1990).

Spheroid cultures have also been pivotal in the analysis of a new immune-activation phenomenon, known as nemosis. This process is described as programmed cell death of activated cancer-associated fibroblast spheroids in the absence of apoptotic markers. This cell death results from the production of COX2, MMP1, MMP10, MT-MMP1, proinflammatory cytokines (e.g. IL-1, IL-6, IL-8) and chemokines (such as RANTES) (Vaheri et al., 2009). Furthermore, studies have illustrated that integrin-fibronectin association plays a key role in fibrocyte spheroid formation as fibronectin knockout cells or antibodies against integrins $\alpha 5$ and $\beta 1$ impair spheroid formation and promote nemosis (Salmenperä et al., 2008; Vaheri et al., 2009).

Over the past decade, studies have also demonstrated the feasibility of co-culturing fibroblast spheroids with other cell types, including human bladder cancer cells (Schuster et al., 1994), hepatocytes (Takezawa et al., 1992), cholangiocarcinoma cell line (Kubota et al., 1992), esophageal squamous carcinoma cells (Shima et al., 1995), human keratinocytes (Butt et al., 1996), breast tumour cells (Kunz-Schughart et al., 2001; Kaur et al., 2011; Li and Lu, 2011). More recently, Saleh et al. (2011), analysed the effects of co-culturing human bone-marrow MSC spheroids with human umbilical vein endothelial cells (HUVECs), and demonstrated an increase in proliferation and differentiation of MSC, as well as enhanced Wnt/BMP signalling (Saleh et al., 2011). However, human lung fibroblasts (and IPF fibroblasts in particular) have never been reported in spheroid studies.

1.4.2. Microfluidics

Many researchers are also greatly interested in cell-based microfluidic technologies in order to develop culture conditions and methodologies in various scientific areas ranging from fundamental biological studies to drug discovery (Whitesides, 2006; Kang et al., 2008; Satoh et al., 2009). There are many advantages of using microfluidic systems, one of which involves precise control of fluidic elements. For instance, in order to understand the effect of soluble factors on cell behaviour (such as proliferation, differentiation, and migration), gradient and focusing flow generators have been used, which control spatial distribution of the soluble factors (Jeon et al., 2000). In addition, these systems may be customised easily and be attractive for studies that require analysis of several drugs. Furthermore, due to the fact that the microfluidic experiments run on micro-scale, the amount of reagent required is very small; thus the use of these systems may be more economical (Elliott and Yuan, 2011). Single cell lines have been studied by many researchers using microfluidic systems. However, researchers now focus on developing systems that culture more than one cell type on a range of different matrices (natural or artificial) (Scotton, 2011) . For instance, Hermanns et al. (2004) demonstrated the feasibility of culturing two cell types (i.e. human lung epithelial cells with pulmonary microvascular endothelial cells) on opposite sides of a polycarbonate membrane filter, which not only formed a functional barrier between the cells, but also tight junctions (Hermanns et al., 2004).

In addition, recently Huh et al. (2010) created an *in vitro* biomimetic microsystem (lung-on-a-chip) which reconstituted the functional alveolar-capillary interface of the human lung (**Figure 1.16**). This microdevice comprised three polydimethylsiloxane (PDMS) layers. PDMS is a silicone-based polymer which is the most commonly used material in microfluidic systems, as it is biocompatible, optically transparent for microscopy studies, and permeable to oxygen (Elliott and Yuan, 2011). The three layers were sandwiched together to form parallel microchannels, separated by a 10 μm thick porous PDMS membrane, pre-coated with ECM. Endothelial (HUVEC) and immortalised epithelial cells (A549) were then cultured on opposite sides of membrane (lower and upper surfaces, respectively), and once the cells were confluent, the medium from the upper chamber was removed to establish a more physiological system, air liquid interface. Moreover, in order to mimic physiological breathing movements, computer-controlled vacuum was applied to side chambers which allowed cyclic-stretching of the membrane (Huh et al., 2010).

This lung-on-a-chip model not only mimicked certain physiological features, but also provided some promising results which suggest that biomimetic microsystems may be the way forward to understand diseases and for high-throughput drug screening. However, further refinement to this system is required to establish this (such as using primary human epithelial cells in place of immortalized cell lines) (Scotton, 2011).

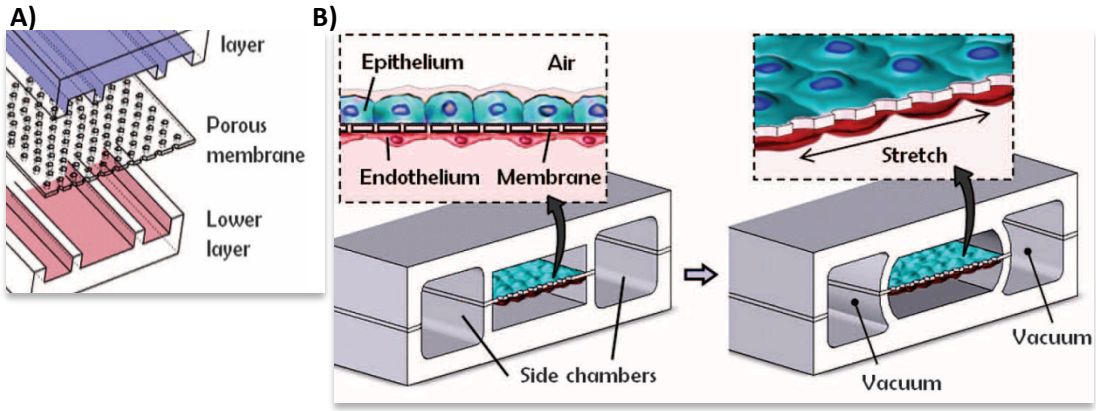

Figure 1. 16: Human breathing lung-on-a-chip micro device.

(A) The device is composed of 3 PDMS layers, with the centre layer being a porous 10 mm thick membrane coated with ECM. (B) Structure of the chambers illustrating the epithelial and endothelial cells cultured of opposite sides of the membrane. Applying vacuum to the side chambers allows the membrane to stretch, which mimics the physiological system.

Reproduced from (Huh et al., 2010) with permission of The American Association for the Advancement of Science (AAAS).

As well as developing microfluidic systems, which involve co-culturing one or two different cell types as monolayers, some studies have also developed devices that involve culturing spheroids. For instance, Hsiao et al. (2009) developed a microfluidic device which was able to culture 3D multi-cell type spheroids composed of prostate cancer cells, endothelial cells, and osteoblasts. The device consisted of two PDMS layered microchannels separated by a semi-permeable polycarbonate membrane (10 μm thickness with 5 μm pore). The upper microchannel composed of 28 dead-end side-chambers, which were 200 x 200 x 200 μm (l x w x d). The lower channel was used for perfusion of media. The membrane and the 28-side channels were first coated with a low-cellular attachment, followed by seeding cells into the device, which resulted in the formation of equally sized spheroids within 24 hours (**Figure 1.17**).

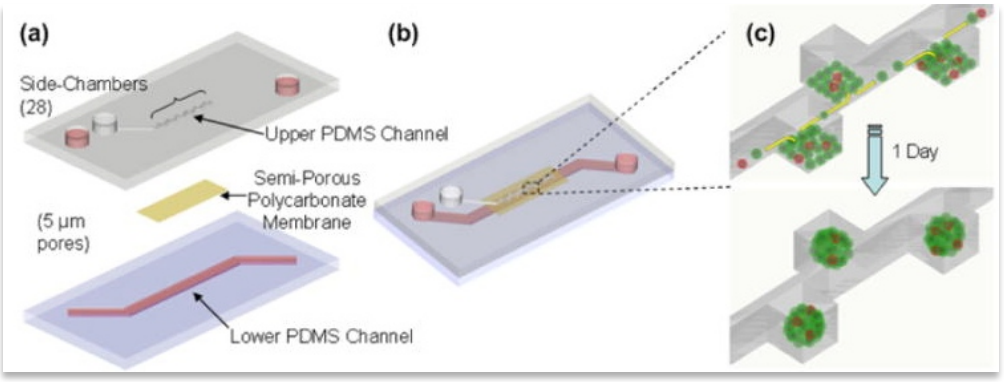

Figure 1. 17: Spheroid formation using microfluidic device.

(A) & (B) The device consists of 2 PDMS layers. Upper layer consisted of 28 dead-end side chambers and the lower layer was used for media perfusion. Both layers were separated by a semi-porous polycarbonate membrane. The channels and membrane were coated with a low-cellular attachment surface. (C) Cells were then cultured into the device, and equally sized spheroids formed in each chamber within 24 hours.

Reproduced from (Hsiao et al., 2009) with permission of Biological Engineering Society.

Despite great success in co-culturing two cell lines in microfluidic devices and forming spheroids of different cell types, to date there is no evidence of whether it is feasible to form spheroids from lung fibroblasts and co-culture them with lung epithelial cell. Forming such a model could answer many unanswered questions regarding crosstalk between epithelial and mesenchymal cells in particular during fibrosis and could potentially lead to the development of new therapeutic targets.

1.5. Summary, hypothesis, and aims for this thesis

IPF is a fatal interstitial lung disease, with an unknown aetiology. The incidence of IPF in the UK is increasing rapidly in patients aged between 55-75 years and unfortunately there is no truly effective treatment available to halt disease progression. A number of animal models have been developed to understand the pathology of the disease, which has suggested that this disorder results due to the dysregulation of epithelial-mesenchymal crosstalk following repetitive injury to the AECs. However, the lack of key histopathological features in these murine models is a great limitation for developing effective therapies.

Based on our current understanding about the disease and possible cells and mediators involved, this project focused on the development of organotypic cell culture approaches in order to understand the disease progression in greater detail, which could hopefully provide a useful tool for drug screening. Hence, the aim of this project was to develop a novel *in vitro* 3D model which mimics a particular characteristic feature seen in IPF patients - the fibrotic focus.

This thesis therefore addressed the following hypothesis:

'3D spheroid cultures of fibroblasts will provide a more representative *in vitro* model system for drug screening in IPF'

The following aims were examined:

1. Investigate the morphological characteristics of non-IPF primary human fibroblasts derived from lung explants (pHLF-Ex) and digested lungs (pHLF-Di) and explore the spheroid-forming capacity of non-IPF and IPF fibroblasts.

2. Determine some of the key fibroblast characteristics in spheroids (e.g. apoptosis, proliferation, collagen synthesis, TGF-beta production).

3. Investigate transcriptional differences between non-IPF and IPF spheroids by performing microarray data analysis on samples from multiple donors.

4. Investigate the feasibility of identifying specific targets by screening known compounds using a GSK compound library

CHAPTER 2: MATERIALS AND METHODS

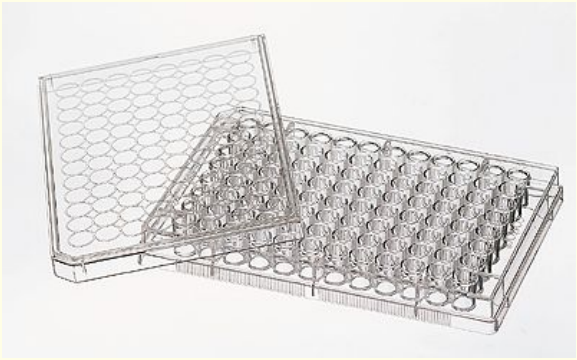

2.1. General plastic ware, chemicals, and cell culture reagents

Sterile tissue culture plates and flasks were all purchased from Nunc (Roskilde, Denmark). Sterile polypropylene centrifuge tubes and pipettes were purchased from Falcon (New Jersey, USA). Whatman cyclopore 0.2 µm polyester syringe filters were from Whatman (UK). Collagen-coated transwells (12 mm polystyrene inserts with 0.4µm pore PTFE membrane, collagen coated, sterile) were purchased from VWR International Ltd (UK). Other disposable plasticware was purchased from Sterilin (Ashford, UK). Deionised water was prepared using a Millipore Water Purification System (Millipore R010 followed by Milli-Q Plus; Millipore Ltd, UK) for the preparation of dilutions and buffers.

Sterile Dulbecco's Modified Eagle Medium (DMEM; high glucose, sodium pyruvate, no L-glutamine), F12K culture media, Dulbecco's Phosphate Buffered Saline (DPBS), Hank's Balanced Saline Solution (HBSS), Trypsin Neutralising Solution (TNS), penicillin-streptomycin, L-glutamine, 0.25% trypsin-EDTA, amphotericin B, Foetal Bovine Serum (FBS), Neonatal Calf Serum (NCS), and geneticin (G418) were purchased from Gibco Life technologies (UK). DCCM-1 culture media was obtained from Biological Industries Ltd. (Glasgow, UK). Bronchial epithelial cell growth medium (BEGM), Bulletkit growth factors, and HEPES buffer were purchased from Lonza (UK). Pronase was purchased from Roche (UK). DMSO and L-Ascorbic acid 2-phosphate sesquimagnesium salt hydrate were purchased from Sigma Aldrich (UK).

2.2. Cell lines and primary cells

The A549 cell line was obtained from the American Type Culture Collection (ATCC) via LGC Promochem (Middlesex, UK). Human transformed mink lung epithelial cells (TMLC) were a kind gift from Dr D. Rifkin (New York University, New York, USA). Human bronchial epithelial cells (HBECs) were isolated and cultured in our laboratory with the help of Dr Manuela Platè (UCL, UK). Primary human lung fibroblasts (pHLFs) from six donors were a kind gift from GSK (Stevenage, UK); 10 donors were a kind gift from Dr Robin McAnulty (UCL, CITR, UK); and five further donors were isolated during this project. The method used to isolate the fibroblasts from the lungs was the same for each donor and is described in **Section 2.3**. Lung samples

were obtained from 11 patients with IPF (6 male, 5 female; mean age, 65 yrs) following diagnostic surgical lung biopsy or lung transplant. All fibrotic samples used in this study were classified using the diagnostic criteria of the American Thoracic Society/European Respiratory Society (ATS/ERS) consensus criteria: namely, a pattern of usual interstitial pneumonia (UIP) (Raghu et al., 2011). Control lung samples were obtained from lungs of 10 patients (8 male, 2 female; mean age, 36 yrs) following cancer resection surgery (uninvolved tissue) or from patients who died as a result of an accident or suicide with no signs of lung disease. Three control samples were obtained from National Disease Research Interchange (NDRI). Approval for the use of all material was obtained from the Royal Brompton & Harefield NHLI and the ethics committee of University College London and University College London Hospital. Informed consent was received from each subject.

2.3. Isolation of primary cells

2.3.1. Primary human lung fibroblasts from explants (pHLF-Ex)

Under sterile conditions, peripheral lung tissue was cut into small explants (less than $1mm^3$) and placed into petri dishes with 2 ml of 20 % FBS in DMEM (containing 400 U/ml penicillin streptomycin, 4 mM L-glutamine and 0.1 % amphotericin B). The petri dishes were incubated at 37 ^oC with 10 % CO_2 for 24 hours before the addition of further 8 mL of media. Every 2-3 days the petri dishes were topped up with 200 μL of amphotericin B and 400 U/mL penicillin streptomycin (1:1 ratio). Upon reaching 80-90 % confluence (after 2-4 weeks) the medium was removed and washed with trypsin-EDTA once, followed by an additional treatment with fresh trypsin-EDTA at 37 ^oC. The cells were inspected after approximately three minutes, using an Olympus TCK-2 inverted phase contrast light microscope (Olympus Optical Ltd, UK) for shape change (rounding up) and detachment from the plastic. Trypsin was subsequently neutralised with DMEM/10 % FBS. The cells were then centrifuged at 300 *g* for 5 minutes. Supernatant was discarded and the pellet was re-suspended in DMEM/10 % FBS. The cells were counted on a Glasstic® microscope slide (Hycor Biomed, USA) or using a Handheld Automated Cell Counter (Sceptor, Millipore, UK) and seeded at appropriate densities. Non-IPF pHLF-Ex were used between passages 3-6 and IPF pHLF-Ex were used between passages 4-12.

2.3.2. Primary human lung fibroblasts from digested lung (pHLF-Di)

Peripheral lung tissue was first washed with either sterile saline (Baxter, Austria) or HBSS to remove erythrocytes. This involved injection through the large airways in order to achieve better distribution of the saline and prevent any tissue damage. This was done until the cell count was $<1x10^4$ cells/mL (excluding erythrocytes). The tissue was then injected with 0.25 % trypsin (from bovine pancreas, Sigma, UK) in HBSS through the large airways and parenchyma and incubated at 37 °C with 5 % CO_2 for 45 minutes. The activity of trypsin was then neutralised using NCS containing 250 µg/mL DNase1. The tissue was minced into small pieces, and agitated for 5 minutes. Following this, the tissue suspension was filtered through 400 µm and 40 µm filters (BD) to remove any large multicellular pieces of tissue and then centrifuged at 400 *g*, 12 °C, for 10 minutes. The supernatant was discarded and the cell pellet was re-suspended in DCCM-1 medium, supplemented with 50 µg/mL DNase1. The cell suspension was then seeded into tissue culture treated flasks, followed by incubation at 37 °C with 5 % CO_2 for two-three hours to allow adherent cells (i.e. fibroblasts and macrophages) to adhere to the flask, incubated at 37 ^oC with 10 % CO_2. Confluence of the fibroblasts (80-90 %) was achieved within 1 week, and the cells were then trypsinised (as mentioned in **Section 2.3.1**). pHLF-Di were used between passages 2-6.

Both pHLF-Ex and pHLF-Di were morphologically characterised by immunocytochemical staining (**Section 2.4**) for a selection of smooth muscle cell (i.e. smoothelin), endothelial and fibroblast markers such as a-smooth muscle actin (αSMA).

2.3.3. Primary human bronchial or bronchiolar epithelial cells (HBECs)

Under sterile conditions, bronchi/bronchioles were removed from the lung and cut into small pieces (1 mm^3). These were then placed into a 50 mL falcon tube with 0.15 % pronase in DMEM (containing 200 U/mL penicillin-streptomycin, 4 mM L-glutamine, and 0.1 % amphotericin B) and incubated overnight at 4 ^oC on a rotary mixer. Following 16-18 hours of incubation, the tissue was agitated to dislodge the bronchiolar epithelial cells from the basement membrane and any remaining pieces of solid tissue were removed and discarded. 10 % FBS was added to the medium to inactivate the proteolytic activity of the pronase and the mixture was centrifuged for 5 minutes at 150 *g*. The supernatant was discarded from the cell pellet followed by resuspension in pre-warmed (37 ^oC) BEGM (BEBM + Bulletkit growth factors). The cells were then seeded into sterile flasks at $1x10^6$ cells per 25 cm^2. The medium

was replaced the following day to remove non-adherent and dead cells. Cells were then grown to 80 % confluence, with the medium being changed every 2-3 days. Purity of the cell population was examined using both positive and negative immuno-based staining.

Flasks were passaged as follows: The medium was removed from flasks and the monolayers were washed briefly with HEPES buffer. Trypsin was then added and the cells incubated for five minutes at 37 °C with 5 % CO_2. After incubation, the cells were examined using an Olympus TCK-2 inverted phase contrast light microscope (Olympus optical Ltd, UK) to verify cellular detachment. Trypsin was then inactivated by the addition of an equal volume of TNS. The suspension was then centrifuged at 150 *g* for 5 minutes. The supernatant was discarded and the cell pellet was resuspended with fresh media. Cells were passaged 1:5 and used up to passage 4. For experiments, trypsinised HBECs were resuspended into DMEM and 10 % FBS and seeded at a density of $1x10^4$ cells per spheroid (see **Section 2.5** for spheroid formation). The cells were incubated for 24 hours to allow adherence at 37 ^oC with 10 % CO_2 before analysis.

2.4. Immunocytochemistry

Immunocytochemistry was performed to characterise the phenotype of the cell isolates, using antibodies detailed in **Table 2.1**. Cells were seeded into a 96 well plate (density 10,000 cells per well) or a glass chamber slide (50,000 cells per well) for 24 hours. Cells were then serum starved for 24 hours followed by TGFβ (1 ng/mL) activation for a further 24 hours. Cell were then washed with DPBS and fixed with methanol for two minutes. These were then blocked with 5 % serum (from same species as secondary antibody) and 3 % BSA in DPBS for 30 minutes, followed by incubation with primary antibody diluted in DPBS with 3 % BSA, overnight at 4 ^oC (**Table 2.1**).

The cells were then washed three times with DPBS, followed by incubation with fluorescently labeled secondary antibody for 1 hour at room temperature. Note, for cell in the 96-well plate DAPI was added at the same time as the secondary antibody at a dilution of 1:10,000. However, for chamber slides Prolong-gold anti-fade with DAPI was used to mount the slides after incubating the cells in the secondary antibody. A Zeiss Axioskop 2 microscope and Qicam 12-bit color fast camera was used to visualize and capture images of cell in the chamber slides.

ImageXpress Micro XL was used to visualize and capture images of the cells seeded in the 96 well plates. Quantification analysis was performed using MetaXpress version 5.3.0.1.

Table 2. 1: List of primary antibodies used for immunostaining

	Recognises	Raised in	Supplier	Dilution used	Secondary species
cytokeratin	Human	Mouse	Dako, UK	1:200	Goat
α-smooth muscle actin (αSMA)	Human	Mouse, monoclonal	Sigma Aldrich, UK	1:200	Goat
Smoothelin	Human	Mouse, monoclonal	Abcam, UK	1:40	Goat
Ki-67	Human	Rabbit, monoclonal	Abcam, UK	1:100	Goat
Collagen I	Human	Rabbit, polyclonal	Abcam, UK	1:200	Goat
Collagen III	Human	Rabbit, polyclonal	Abcam, UK	1:2000	Goat

2.5. 3D culture

2.5.1. Spheroid formation

4 % agarose (Sigma Aldrich, UK) was prepared in Milli-Q water. This was then diluted to 2 % agarose using DMEM (1:1 ratio). Using an Eppendorf Multipette, 50 μL of this mix was placed into each well of a flat-bottom 96 well plate to form a thin film of agarose as a non-adhesive surface. The plates were left at room temperature for approximately 15 minutes to allow the agarose to set. Following trypsinisation pHLF (non-IPF and IPF) were re-suspended in DMEM (containing 50 U/mL penicillin streptomycin, 2 mM L-glutamine) and 0.4 % FBS, supplemented with 100 μM L-Ascorbic acid 2-phosphate sesquimagnesium salt hydrate. The cells were counted using a Handheld Automated Cell Counter (Sceptor) to get a cell count of $1x10^5$ cell/mL. 100 μL of the cell suspension were seeded into the agarose coated at a density of $1x10^4$ cells per well. The plates were then incubated at 37 ^oC with 10 % CO_2 to allow the cells to aggregate and form spheroids. Samples were collected for analysis following 24 to 96 hours of incubation.

2.5.2. Compound treatment

Indomethacin was purchased from Sigma (UK). SC-560, CAY10404, LSKL (thrombospondin-1 inhibitor) and SLLK (control peptide for thrombospondin-1 inhibitor) were purchased from Cambridge Bioscience (UK). NS398 was obtained from VWR (UK). All other compounds were a kind gift from GSK (Stevenage, UK). All compounds were serially diluted by a factor of 3 in DMSO 10 times from a starting concentration of 0.01 M. The compounds were then further diluted 1:100 in media (DMEM supplemented with 2 mM L-glutamine, 50 U/mL penicillin, 50 μg/mL streptomycin and 0.4 % FBS). The diluted compounds were then added into each well before spheroid formation (prophylactic treatment, time zero) or 24 hours after spheroid formation (therapeutic treatment) to give a final concentration range of 300 pM to 10 μM. Each spheroid was treated with the compounds for 24 hours before analysis.

2.5.3. IncuCyte Zoom

To monitor spheroid formation and the effect of compounds, the plates were cultured in the IncuCyte Zoom (Essen bioscience, UK), composed of a microscope gantry that resides in the cell incubator capable of taking live content phase contrast imaging of the cell aggregation/spheroid formation over time. Magnification of the IncuCyte Zoom was set to x4. Phase object area is defined as the total area of a well containing cells. A reduction in phase contrast object area represented the aggregation of the cells into a more compact form (i.e. spheroids). Each treatment had eight replicates for statistical analysis.

2.6. Histological evaluations of spheroids

2.6.1. Spheroid fixation and paraffin embedding

Spheroids were collected and washed with DPBS followed by fixation with 4 % PFA (diluted in PBS; Sigma Aldrich, UK) for 20 minutes. They were then dehydrated with 70 % ethanol for 5 minutes before the addition of ultra-low melting point agarose in order to form small agarose plugs. These plugs were then left to cool at room temperature and then placed in processing cassettes (Histosette II®; Simport, Quebec, Canada) and dehydrated using a Leica TP1050 tissue processor (Leica Microsystems, Buckinghamshire, UK). This involved dehydrating the

spheroids by incubating them in increasing concentrations of IMS (70 %, 2hrs; 80 %, 1 hr 30 min; 90 % 1 hr 30 min; and 100 %, 1 hr 15 min 4 times). Following this the spheroids were incubated in xylene (3X 1 hr) and then paraffin wax (3X 1 hr). Subsequent the spheroids were embedded into paraffin wax. The paraffin wax blocks were cooled to 4 ^{o}C and 2 μm sections were cut using Shandon A5235 Retraction microtome (Thermo Shandon, Cheshire, UK) and Tissue-Tek® AccuEdge® blades (VWR, UK) and placed on poly-lysine coated microscope slides (VWR, UK).

2.6.2. H&E and MSB staining

The architecture of the spheroids was analysed using two staining techniques: haemotoxylin and eosin (H&E, **Table 2.2**) staining and a modified trichrome stain (martius scarlet blue, MSB staining, **Table 2.3**). H&E was used to visualise the cellular structure of the tissue and spheroids. Gill II haematoxylin (Bios. Laboratories, USA) stains the nucleus of the cells blue whereas eosin Y (1% aqueous; Bios. Laboratories, USA) stains the cytoplasm of cells pink.

MSB was used to visualise the architecture of connective tissue. Nuclei stain brown/red, muscles stain red, fibrin stains light pink, and collagen stains blue. For the demonstration of collagen the pivotal stage is the Chicargo sky blue 6GX dye. This is the largest dye molecule used in the technique and the stain product is dependent upon the permeability of collagen. Automated staining of sections was performed using a Sakura Tissue-Tek DRS 2000 Diversified Stainer (Miles Diagnostics/Bayer, UK). All chemicals used to prepare the solutions for MSB were purchased from Sigma Aldrich (UK).

Table 2. 2: Solutions and incubation times for H&E staining

Step No.	Solution	Time
1	Xylene	3 min
2	Xylene	3 min
3	100% IMS	2 min
4	90% IMS	2 min
5	70% IMS	2 min
6	50% IMS	2 min
7	dH2O	1 min
8	Haematoxylin	5 min
9	Wash in H_2O	10 sec
10	Wash in H_2O	10 sec
11	Acid alcohol 1% HCl in 70% alcohol)	8 sec
12	Wash in H_2O	30 sec
13	Wash in H_2O	2 min
14	Eosin	6 min
15	Wash in H_2O	15 sec
16	50% IMS	30 sec
17	70% IMS	45 sec
18	90% IMS	1 min
19	100% IMS	1 min
20	100% IMS	2 min
21	Xylene	1 min
22	Xylene	2 min
23	Xylene	2 min

Table 2. 3: Staining sequence for Martius Scarlet Blue

Step No.	Solution	Time
1	Xylene	3 min
2	Xylene	3 min
3	100% Industrial Methylated Spirit (IMS)	2 min
4	90% IMS	2 min
5	70% IMS	2 min
6	Lugol's Iodine	5 min
7	3% Sodium thiosulphate	3 min
8	Wash in H_2O	2 min
9	Celestine blue	5 min
10	Wash in H_2O	1 min
11	Rinse in distilled H_2O	30 sec
12	Haemotoxylin	5 min
13	Wash in H_2O	30 sec
14	Acid alcohol (1% HCl in 70% alcohol)	3 sec
15	Wash in H_2O	8 min
17	90% IMS	30 sec
18	0.2% Orange G in picric alcohol	8 min
19	Distilled H_2O	5 sec
20	Red mixture (0.5% ponceaux de xylidine; 0.5% acid fushsin in 1% glacia; acetic acid)	7 min
21	Distilled H_2O	5 sec
22	1% Phosphotungstic acid	30 sec
22	Distilled H_2O	20 sec
22	0.5% Chicago Sky Blue 6BX (Direct Blue) in 1% glacial acetic acid	80 sec
22	1% Acetic acid	20 sec
22	70% IMS	20 sec
22	90% IMS	20 sec
22	100% IMS	1 min
22	Xylene	2 min
22	Xylene	2 min
23	Xylene	2 min

2.6.3. Immunohistochemistry

Paraffin embedded spheroid sections on poly-lysine coated slides (**Section 2.6.1**) were first de-waxed using a Sakura Tissue-Tek DRS 2000 Diversified Stainer. This involved incubation of the slides for 3 minutes in xylene (twice), followed by rehydration by incubating the sections in decreasing concentrations of IMS (100 %, 90 %, 70 %, 50 % in distilled water). Each rehydrating step involved 2 minute incubation. The slides were then placed into distilled water for one minute prior to immunostaining.

The sections were then washed in 1x Tris buffered saline (TBS; 1:20 dilution using 20x TBS containing 0.05 % Tris-base and 16 % NaCl in deionised water at pH 7.6) for five minutes. An Immedge pen (Vector Laboratories, USA) was used to draw around each section on the slide in order to make a hydrophobic boundary. The sections were then incubated in 0.05% saponin (Sigma Aldrich, UK) for 30 minutes at room temperature for antigen retrieval followed by washing in TBS twice for five minutes. Following antigen retrieval, the sections were immunostained using either the avidin-biotinylated enzyme complex kit (Vector Laboratories, USA) or ImmPress reagent kit (Vector Laboratories, USA).

Avidin-biotinated enzyme complex kit

During the early stage of this project the avidin biotinated enzyme complex kit was used which involved firstly incubating the sections in 3 % hydrogen peroxide (H_2O_2) for 30 minutes to neutralise endogenous peroxidase followed by five minute washes in TBS, twice. Following this, the sections were incubated with ~16 % serum of the secondary species (as displayed in **Table 2.1**) and avidin block (4 drops/mL, as stated in manufacturer's instructions) diluted in TBS, for 20 minutes at room temperature. The sections were then drained and incubated in either polyclonal non-immune control IgG (used as an isotype specific negative control) or primary antibody (**Table 2.4**) diluted in 1 % BSA, 1 % serum of secondary species, and biotin block (4 drops/mL, as stated in manufacturer's instructions) in TBS, overnight at 4 ^{o}C. After the overnight incubation, the slides were washed twice in TBS for five minutes followed by incubation in secondary antibody (either goat anti-rabbit IgG conjugated to biotin or goat anti-mouse IgG conjugated to biotin (1 µg/mL; Dako, Denmark) in 1 % BSA diluted in TBS, for two hours at room temperature. The sections were then washed twice in TBS for five minutes and then incubated with 0.5 % streptavidin/HRP (Dako) diluted in TBS containing 1 % BSA for 30 minutes at room temperature. The sections were washed again three times in TBS for five

minutes followed by 10 minutes incubation in 3,3'-diaminobenzdine (DAB) solution (DAB substrate kit; Vector Laboratories, USA) as instructed by the manufacturer's protocol. The sections were then submerged in tap water prior to counterstaining with haemotoxylin (using Sakura Tissue-Tek DRS 2000 Diversified Stainer). The slides were the coverslipped using an automatic coverslip machine, Sakura Coveraid SCA5600 (Bayer Diagnostics, UK) and HiQA coverslip tape (CellPath, Powys, UK).

ImmPress reagent kit

During half way through my project we decided to use the ImmPress reagent kit. This staining system involves novel conjugation and micropolymer chemistries to create a ready-to-use, one-step, biotin-free detection system which is highly sensitive. The unique micropolymer is attached to the affinity purified secondary antibodies (provided with the kit), which results in low background in comparison to the previous kit.

Following antigen retrieval, the sections were incubated in 3 % H_2O_2 for 30 min (same as before) followed by five minute washes in TBS. The sections were then blocked with 2.5 % normal horse serum block from 30 min (provided by the ImmPress reagent kit), followed by incubation in primary antibody (diluted in 1 % BSA in TBS) overnight at 4^{o}C. The slides were then washed in TBS twice for five minutes and subsequently treated with the secondary antibody (provided by the kit) for 30 min at room temperature. The sections were then washed again for five minutes in TBS followed by treatment with ImmPact NovaRed Peroxidase Substrate (Vector laboratories, USA) for 2 min. The sections were then submerged in tap water prior to counterstaining (as stated above).

2.7. Electron microscopy (EM)

Cells were seeded for spheroid formation as stated in **Section 2.5.1**. Following 24 hours of incubation, the spheroids were washed twice in PBS followed by 24 hour fixation at 4 ^{o}C with 2 % paraformaldehyde (PFA) and 1.5 % glutaraldehyde diluted in 0.1M sodium cacodylate buffer, pH 7.3. Samples were then processed for EM which was kindly performed by Dr. Mark

Turmaine (Department of Anatomy and Developmental Biology, UCL). This initial step involved washing the spheroids in 0.1 M sodium cacodylate buffer (pH 7.4) twice for 30 minutes.

For scanning electron microscopy (SEM), the spheroids were then post-fixed in 1 % osmium tetraoxide (OsO_4) and 1.5 % potassium ferrocyanine in 0.1m cacodylate buffer at 3 ^{o}C for 1 ½ hours followed by washing in 0.1 M sodium cacodylate buffer and rinse in ddH_2O. The spheroids were then dehydrated through a graded ethanol-water series to 100 % ethanol. The spheroids were critical point-dried using CO_2 and mounted on aluminium stubs using sticky carbon taps. The mounted samples where then coated with a thin layer of gold/palladium (Au/Pd; approximately 2nm thick) using a Gatan ion beam coater. Imaging was performed using Jeol 7401 FEGSEM (Jeol, UK).

For transmission electron microscopy (TEM), the spheroids were post-fixed in 1 % OsO4 and 0.1 M sodium cacodylate (pH 7.3) at 3oC for 1 ½ hours followed by washing in 0.1 M sodium cacodylate (pH 7.4). The samples were then Enbloc stained with 0.5 % uranyl acetate dH20 at 3^{o}C for30min. After rinsing with dH2O, the spheroids were dehydrated in a graded ethanol-water series and infiltrated with Agar 100 resin to hardened. A representative area was selected and ultra thin sections were cut at 70-80 nm using a diamond knive on a Reichert ultracut S microtome. Sections were collected on 200 mesh copper and stained with lead citrate. The sections were then viewed with a Joel 1010 transition electron microscope and the images recorded using a Gatan Orius CCD camera (Gatan, UK).

2.8. TUNEL assay

2.8.1. Principle of technique

TUNEL (Terminal deoxynucleotidyl transferase dUTP nick ended labelling) assay is a common assay used to assess cell death by detecting fragmented DNA. This assay is dependent on the activity of terminal deoxynucleotidyl transferase (TdT) which is able to catalyse the addition of dUTP molecules (conjugated to a fluorescent marker) to the fragmented DNA which can be analysed using a fluorescence microscope.

2.8.2. Reagents

Proteinase K (26 μg/mL in 10 mM TRIS 5 mM EDTA, pH7.4); TUNEL labelling mix and TUNEL enzyme (Roche, UK); DNase I recombinant, grade I (3000 U/mL– 3 U/ mL in 50 mM Tris-HCl, pH 7.5, 1 mg/mL BSA); Prolong anti-fade gold (with DAPI; Invitrogen, UK).

2.8.3. Procedure

The procedure was followed as stated in the manufacturer's instruction leaflet. Briefly, this involved de-waxing paraffin embedded spheroids sections and incubating with proteinase K for 15 minutes. For the positive control, the slides were incubated with DNase I recombinant for 10 min at 15-25 °C to induce DNA strand breaks, prior to the labelling procedure. The labelling procedure involved incubating all sections with the TUNEL reaction mixture (5 μL TUNEL enzyme and 45 μL TUNEL label solution per section) for 1 hour at 37 ^{o}C in a humidified atmosphere in the dark. For the negative control, the sections were incubated with the TUNEL label solution only. Each section was then mounted under coverslip using Prolong anti-fade gold (with DAPI). Sections were analysed under the microscope with an excitation wavelength in the range of 450–500 nm and detection in the range of 515–565 nm (green). The percentage of TUNEL positive cells was counted using the publically available NIH Image J software.

2.9. Western blotting

2.9.1. Reagents, buffers, and equipment

Reagents: Bicinchoninic acid (BCA) protein assay (Pierce, USA); phosphosafe extraction buffer (Merck, Germany); Complete Mini Protease Inhibitor Cocktail (Roche, UK) dissolved in 500μL deionized water; Bovine serum albumin (BSA; Millipore, UK); PageRuler Plus Prestained Protein Ladder, 250 kDa to 10 kDa (Fermentas, UK); 1 % Ponceau S solution (Sigma Aldrich, UK); ECL (Amersham, USA).

Gels and membranes: Pre-cast 8-16 % Tris-HEPES polyacrylamide gradient gels (Nucep, USA); Hybond-ECL, GE Healthcare Amersham^{TM} 0.45 μm nitrocellulose membrane (VWR, UK); filter paper (Whatman, USA); Hyperfilm ECL (Amersham, USA).

Buffers: 5X Laemmli buffer: 100 mM dithiothreitol (DTT), 1 M Tris pH 6.8, 10 % w/v sodium dodecyl sulphate (SDS), 20 % w/v glycerol and, bromphenol blue to color; Running buffer: 0.1 M Tris, 0.1 M HEPES, 0.1 % w/v SDS; TBS-Tween (TBST): 10 nM Tris pH 8, 150 nM NaCl, 0.1 % v/v Tween-20; Transfer buffer: 25 mM Tris, 0.2 M glycine, 1 % w/v SDS, 20 % v/v methanol; Blocking buffer: 5 % w/v non-fat milk powder in TBS-Tween. All buffers were made using deionised water.

Equipment: Novex semi-dry blotter (Invitrogen, UK); Titertek Multiscan MCC/340 plate reader (Labsystems, Finland); automated film developer (Kodak, UK)

2.9.2. Sample preparation

Spheroids were washed with cold PBS and lysed in ice cold phosphosafe extraction buffer with protease inhibitors (1:20 dilution from stock). Spheroids were homogenized with a hand held pestle (Eppendorf, UK) to ensure complete lysis and lysates were transferred to microcentrifuge tubes. All samples were stored at -20 °C before use.

BCA protein assay was used to determine protein concentration in each spheroid lysate sample. The assay works on the basis of biuret reaction whereby proteins are able to reduce Cu^{2+} (copper ion) to Cu^{+} (cuprous ion) in alkaline conditions. Two bicinchoninic acid molecules are able to chelate with Cu^{+} resulting in the formation of an intense purple colour and its absorbance can me read be at 562 nm. The amount of BCA-Cu^{+} complex formed within each sample is directly proportional to protein concentration. This assay was performed as instructed by the manufacturer. Briefly, bovine serum albumin (BSA) was used to generate standard protein controls with concentration ranging from 2 mg/mL to 0.0039 mg/mL. In a 96 well plate, 10 μL of the standard control or sample were placed into each well in duplicates. Each well was then treated with 200 μL of freshly prepared BCA working reagent (combination of reagent A and reagent B, at a 50:1 ratio). The components were then gently mixed and incubated for 30 minutes at 37 ^{o}C. The absorbance was then read using a plate reader. A standard curve was generated by plotting the BSA standard concentration against absorbance values which was used to determine the protein concentration of each samples based on its absorbance value. Each sample was then diluted as appropriate with deionised water to get a final protein concentration of 7 μg. This was then mixed with 5x Laemmli buffer, followed by incubation at 100 ^{o}C for five minutes in order to reduce any disulphide bonds. The samples

were then loaded onto a pre-cast 8-16 % Tris-HEPES polyacrylamide gradient gel, alongside with a protein ladder. Electrophoresis was performed at 120 V for 45 minutes.

2.9.3. Protein transfer

A horizontal semi-dry transfer method was used to transfer the electrophoresed protein form the gel onto a 0.45 μm nitrocellulose membrane. Prior to transfer, the gel was equilibrated in transfer buffer for 20 minutes and the nitrocellulose membrane was also soaked in transfer buffer. Transfer sandwiches were then made in the following order (from bottom to top): electrode, filter paper, nitrocellulose membrane, gel, filter paper, electrode. The proteins were transferred at a constant voltage of 20 V for one hour. Following this the quality of the transfer was assessed by using a rapid stain in 1 % Ponceau S solution which stains proteins without having any effect on the downstream immunoblot. The membrane was then destained by rinsing in water.

2.9.4. Chemiluminescence

Following protein transfer, the membrane was incubated in blocking buffer for 1 hour at room temperature with gentle motion to block against non-specific antibody binding. The membrane was then incubated overnight at 4 °C with primary antibodies against proteins of interest diluted in blocking buffer. After the overnight incubation, the membrane was washed three times for five minutes in TBST and then incubated with a species specific horseradish peroxidase (HRP)-linked secondary antibody (diluted in blocking buffer). The membrane was then washed three times for five minutes in TBST and positive bands were developed by enhanced chemiluminescence (ECL) as per manufacturer's instructions. Immunoreactive bands were visualized by exposing Hyperfilm ECL to the membrane and developing the film on an automated film developer. Exposure time was adjusted according to the strength of the signal.

2.9.5. Densitometric analysis

Semi-quantitative analysis of Western blots was performed using densitometry. A flatbed scanner (Epson, UK) was used to scan the blots. NIH Image J was used to calculate the optical density of each band, according to a calibration curve of different densities (Kodak photographic step tablet, Kodak, UK). The optical density of each band was normalized to its loading control (extracellular regulated kinase-2, ERK2).

2.10. qRT-PCR

2.10.1. Reagents and primers

RNaseZap (Sigma Aldrich, UK) was used to thoroughly clean all equipment and filtered nuclease free pipette tips (Continental Lab Products, UK) were used to minimise RNA degradation. Trizol (Sigma Aldrich, UK); molecular biology grade chloroform and 2-propanol, (Sigma Aldrich, UK); Nuclease free water (Ambien UK); 0.1 % diethyl pyrocarbonate (DEPC; Sigma, UK) water (prepared in deionised water, left overnight at room temperature, and subsequently autoclaved to deactivate DEPC); Glycoblue coprecipitant (15 mg/mL; Ambion, Life technologies, UK); DNase free kit (Primer design, UK); qScript cDNA SuperMix ® kit (Quanta Biosciences, UK); MESA FAST qPCR MasterMix plus for SYBR green assay no ROX w/o UNG (Eurogentec, UK). GeNorm kit (composed of 12 housekeeping genes to select the best reference primers for normalisation of mRNA levels) was from Primer design.

All other primers used in real-time (RT)-PCR studies were designed by myself or Dr. Chris Scotton using an internet based software. Accession numbers were located from www.ncbi.nlm.gov/gene. This number was then entered into primer BLAST (www.ncbi.nlm.gov/tools/primer-blast). The parameters were set at: product size 80-130 bp; primer size 18-22 nucleotides long; primer melting temperature 58 °C to 62 °C with an optimum of 60 °C and a maximum temperature difference of 0.5 °C; primer GC % was 40 % to 60 % with an optimum of 50 %; maximum self-complimentary was set at 6.0 and maximum 3' self-complementarity of 2.0 and finally, the maximum poly-X was set at 3 to avoid runs of nucleotides. A BLAST search was also performed to check that the forward and reverse primers were specific for the intended sequence. The primers were manufactured by Invitrogen, UK. Primer sequences are listed in **Table 2.4**.

Table 2. 4: Sequences for primers used

Primer	Forward sequence	Reverse sequence
ACTA2	5'ATCCTGACTGAGCGTGGCTATT 3'	5'GGCCATCTCATTTTCAAAGTCC 3'
COL1A1	ATGTAGGCCACGCTGTTCTT	GAGAGCATGACCGATGGATT
COL3A1	CCAGGAGCTAACGGTCTCAG	CAGGGTTTCCATCTCTTCCA
ITGAV	TCTGTGCCGCGCCTTCAACC	AACATCCGGGAAGACGCGCTG
ITGB5	AACCGCCAAGGACTGCGTCATG	TTTCCACACTCTGGCTCCCTGAGG
ITGB3	TGCGAGTGTGACGACTTCTC	GTCCAGTCGGAGTCACACAG
ITGB8	GGTCCAGAATGTGGATGGTGT	TCAACTGAGCAGCCTTTGCT
PTGS1	TCAGGGAGTCTCGGGAGATG	ATTCCTCCAACTCTGCTGCC
PTGS2	ACGCTTTATGCTGAAGCCCT	CCACAGCATCGATGTCACCA
PTGER1	TGCCCATCTTCTCCATGACG	CCACGAACAGCAGGAAGGT
PTGER2	CAGTCTCCCTGCTCTTCTGC	GCACCGAGACAATGAGAAGC
PTGER3	CAGTGTTCCTCAACCTTGATGTG	CACAATGTGCAGTTGCCCTC
PTGER4	TGCTCTTCTTCAGCCTGTCC	AGACTGCAAAGAGCGTGAGG
LOXL2	CCAGTGTGGTCTGCAGAGAG	CCTGTGCACTGGATCTCGTT
MMP1	GGACCAACAATTTCAGAGAGTACAA	CCACTGAAGGTGTAGCTAGGG
MMP2	AGTTGGCAGTGCAATACCTGA	GGCAGTCCAAAGAACTTCTGC
MMP7	TGCCAACAGTTTAGAAGCCAA	TTCTGCAACATCTGGCACTC

2.10.2. RNA isolation, purification and quantification

Spheroids were made as previously described. The spheroids were transferred into Eppendorf tubes (10 spheroids per tube). The medium was removed and 0.5mL of TRIzol was added. TRIzol is a solution of phenol and guanidine isothiocyanate which disrupts cell membrane and dissolves cell components leaving RNA integrity intact. The spheroids were homogenised using handheld homogeniser in TRIzol. To isolate RNA from TRIzol the samples were left for five minutes at room temperature and then 200 μL of chloroform was added. The mixture was mixed vigorously and left for 10 minutes at room temperature to allow separation of upper aqueous and a lower organic layer. The samples were then centrifuged for 15 minutes at 12,000 *g* at 4°C and the aqueous phase containing RNA was transferred to a new Eppendorf tube containing 200 μL isopropanol and 1.5 μL Glycoblue. Glycoblue is composed of glycogen

which is covalently linked to a blue dye which is able to facilitate nucleic acid precipitation allowing the pellet to become easily visible.

The RNA was allowed to precipitate for 10 minutes at room temperature and was then centrifuged at 12,000 g for 15 minutes at 4°C. The supernatants were discarded and the RNA pellet was re-suspended in 80 % ethanol in DEPC-treated deionised water (BDH VWR International, UK). Following further 15 minutes centrifugation at 12,000 *g* at 4 °C, the supernatants were discarded, the pellets air dried and then re-suspended in 12.5 μL of nuclease free water. Contaminating genomic DNA was removed using DNAfree kit as stated in manufacturer's instructions.

Although RNA is thermodynamically stable, it can be rapidly degraded into shorter RNA fragments in the presence of ubiquitous RNase which can potentially lead to misleading results. Therefore for microarray analysis in particular, it was vital to measure the degree of RNA degradation. A Bioanalyzer (Agilent, UK) was used to determine the RNA integrity. This device involves a combination of microfluidic chips, gel filled channels for voltage-induced size separation of RNA fragments, RNA stained with an intercalating dye, and laser-induced fluorescence (LIF) detection. The amount of fluorescence detected correlated with the amount of RNA of a given size which was demonstrated on an electropherogram (**Figure 2.1**) (Schroeder et al., 2006) and gel-like images. This was used to generate an algorithm to calculate the RNA integrity number (RIN) which was independent of RNA concentration. A RIN value of between 7 and 10 indicated good RNA quality.

The concentration and purity of the RNA was further quantified using a Nanodrop 8000 spectrophotometer. The ratio of the A_{260}/A_{280} was used as a measure of protein contamination of the sample. A ratio of 2 was considered ideal with a range from 1.7 to 2 considered acceptable.

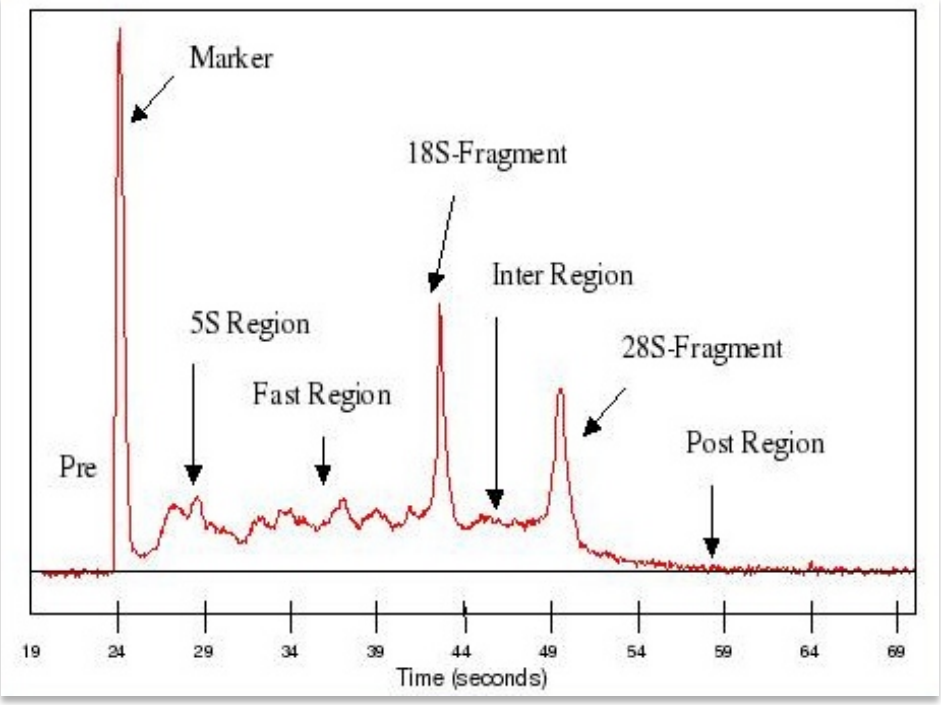

Figure 2. 1: Example of an electropherogram trace.

The 5S region covers the 5S and 5.8S rRNA fragments. The 18S and 28S peaks illustrate the level of 18S rRNA and 28S rRNA, respectively. 5S, 5.8S, and 28S rRNA are located in large ribosomal subunit, whereas 18S rRNA is found in the small ribosomal subunit. Peaks in the fast- and inter-regions indicate amount of degraded RNA (Schroeder et al., 2006).

2.10.3. cDNA synthesis

cDNA was prepared by reverse-transcription (RT) using qScript cDNA SuperMix kit. Following the manufacturer's instructions up to 1µg of RNA sample was made up to volume of 16 µL with nuclease-free water. 4 µL of qScript cDNA SuperMix (5x reaction buffer containing optimized concentrations of $MgCl_2$, dNTPs (dATP, dCTP, dGTP, dTTP), recombinant RNase inhibitor protein, qScript reverse transcriptase and random primers, was then added to each sample, to achieve a final volume of 20µL. Samples were then incubated for five minutes at 25 °C, 30 minutes at 42 °C and five minutes at 85 °C.

2.10.4. Real time qRT-PCR

Real time qRT-PCR was performed with 0.4 ng of cDNA using SYBR green I and primers (forward and reverse each at a final concentration of 800 nM; 10 μL reaction) on a Mastercycler EP Realplex (Eppendorf, Germany). Cycling conditions were as follows: activation of SYBR Green 95 °C for 10 minutes; cDNA amplification 95 °C for 10 seconds, 62 °C for 45 seconds for 40 cycles followed by melting curve analysis. The efficiency of each primer pair was assessed by determining the relationship of primer threshold cycle (Ct) values with cDNA concentration using a series of half-log dilutions of template cDNA. Ct values were defined as the earliest point of the linear region of the logarithmic amplification plot reaching a threshold level of detection. The log of cDNA concentrations was plotted against Ct values, and the slope of the plot was used to ascertain primer efficiency. Primer efficiency was given by the equation: Efficiency= $10^{(-1/slope)}$ and were only used if the value was close to two indicating PCR efficiency of ~100 %. To examine the quantitative differences in target mRNA expression in each sample, Ct values were determined from the linear region of the logarithmic amplification plot. Each sample was also tested for the expression of the housekeeping genes which were selected based on GeNorm analysis. The Ct values of the housekeeping genes were used to normalise between samples. Statistical analysis was performed using the ΔCt values. The melting curve of the product obtained from the PCR was analysed to confirm its specificity. This curve was generated based on the temperature required to denature half of the dsDNA sequence of the PCR product (melting temperature; Tm) which was measured as a decrease in fluorescence. The value was dependent on the nucleotide sequence and a single melting curve represented a single PCR product.

2.10.5. GeNorm

This kit is composed of 12 housekeeping genes (*18S, ACTB, ATP5B, B2M, CYC1, EIF4A2, GAPDH, RPL13A, SDHA, TOP1, UBC*, and *YWHAZ*). RT-qPCR was performed on cDNA samples from both non-IPF (n=3) and IPF (n=4) spheroids to measure mRNA levels of each reference gene. The software qBASE+ (Primer design, UK) was used to analyse the Ct values and determine the average expression stability of all reference targets across all samples. GeNorm M value of <0.5 was considered as a stable housekeeping gene. Based on the analysis three housekeeping genes were selected for normalisation of RT-qPCR data set (*EIF4A2, TOP1,* and *UBC*; **Figure 2.2**).

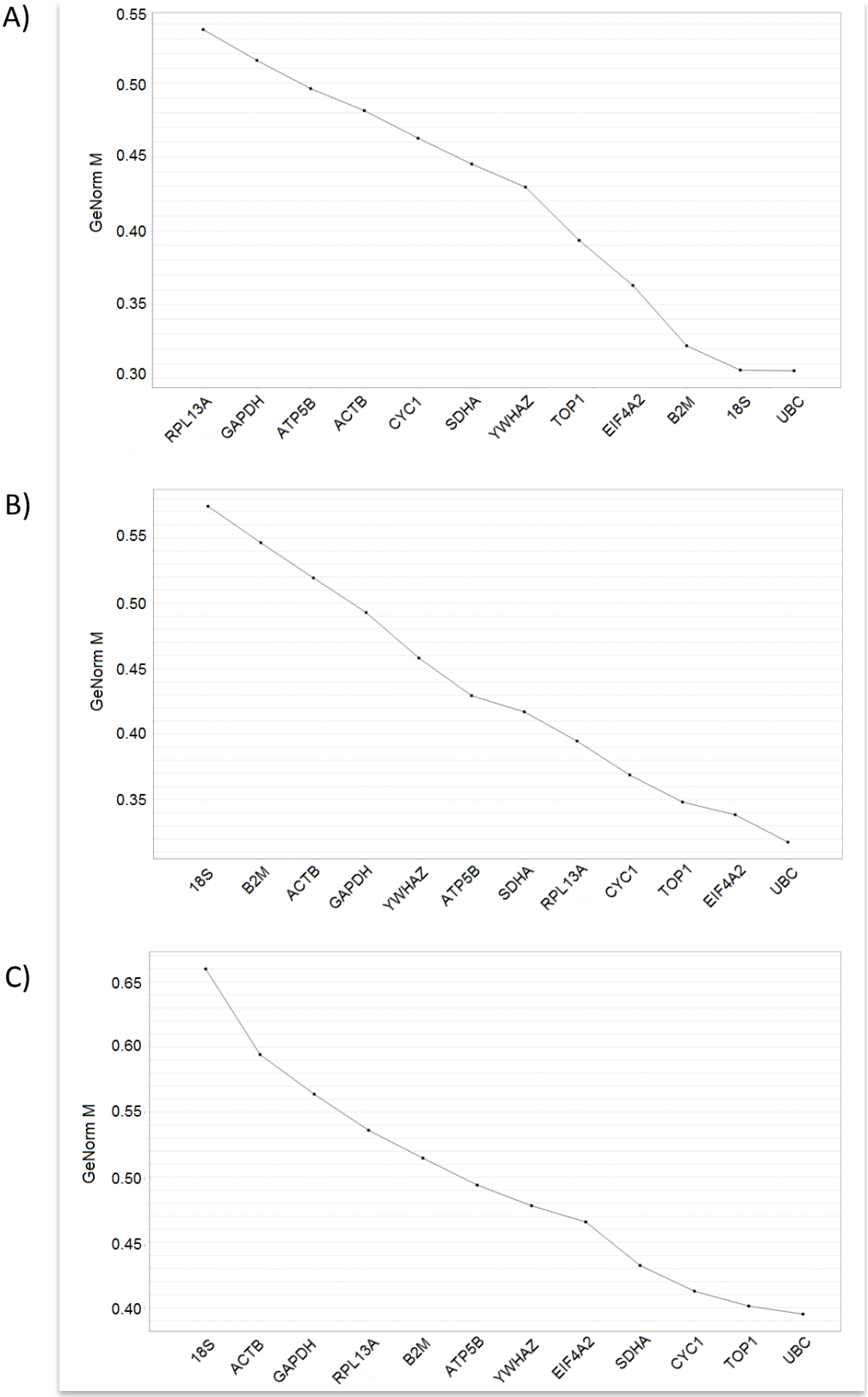

Figure 2. 2. Average expression stability of reference genes using GeNorm and qBase+.

GeNorm M <0.5 indicates the gene expression is stable under the specific experimental conditions. A) Non-IPF spheroid (n=3); B) IPF spheroids (n=4); C) non-IPF and IPF spheroids.

2.11. Measurement of TGFβ activity with TMLEC bioassay

2.11.1. Principle of technique

To determine the levels of active TGFβ in cell culture supernatants or spheroid homogenate, transformed mink lung epithelial cell (TMLEC) bioassay was performed. This assay was originally set up by Abe *et al.* (1994) and utilises the ability of TGFβ to specifically induce PAI-1 expression. TMLECs are stably transfected with an expression construct containing a truncated PAI-1 promoter which is fused to the firefly luciferase reporter gene. Exposure of these cells to TGFβ increases the activity of luciferase in a dose-dependent manner. Luciferase is a monomeric 61 kDa protein which is able to catalyse the oxidation of luciferin to oxyluciferin (by using ATP•Mg2+ as a cosubstrate) resulting in the emission of light which can be read using a luminometer. Importantly, other known PAI-1 expression inducers (such as PDGF-BB, EGF, bFGF and rIL-1β) have shown minimal effect on this promoter fragment. Thus, this assay is highly specific for TGFβ activity (Abe et al., 1994).

2.11.2. Preparation of samples

Following spheroid formation, the supernatant was removed, diluted 1:4 with DMEM (supplemented with 2 mM L-glutamine, 50 U/mL penicillin, 50 μg/mL streptomycin), and stored at -20 ^{o}C until needed. On the other hand, the spheroids were washed twice with DMEM and then homogenised in 200 μL fresh media (without FBS). The homogenates were also stored at -20 ^{o}C until needed.

2.11.3. Culturing TMLEC and measuring luciferase activity

TMLECs were seeded into a tissue culture flask in the same media as fibroblasts (DMEM with 2 mM L-glutamine, 50 U/mL penicillin, 50 μg/mL streptomycin, and 10 % FBS) with the addition of 250 μg/mL Geneticin (G418; Life technologies, UK), incubated at 37 ^{o}C with 10 % CO_2 atmosphere. Once confluent, the cells were trypsinised with Trypsin-EDTA and centrifuged (5 min at 300g) and the pellet was re-suspended in fresh media. The cells were then seeded into a flat bottom 96 well plate at a density of $1.6x10^4$ cells/mL. The cells were then incubated at 37^{o}C with 10 % CO_2 atmosphere for three hours or overnight to allow adherence. Once adhered, the media was aspirated and the cells were washed using serum-free media. 100 μL

recombinant porcine TGFβ1 standards (0.1-1 ng/mL in the same culture medium as the samples) or samples were added in duplicate to the plated TMLECs. The cells were then incubated for 14 hours at 37 ^{o}C with 10 % CO_2. Following incubation, media were aspirated and cells were washed in twice PBS. Subsequently 100 μL of luciferase reporter gene assay lysis buffer (Roche, UK) was added to each well. The plate was then placed into -80 ^{o}C freezer for a minimum of 30 minutes. The lysates were then thawed and agitated for 25 minutes to allow complete lysis of the cells. 20 μL of each lysate was then transferred into the corresponding well of a 96-well opaque white optiplate (Nunc, UK). The luciferase substrate (Promega, UK) was automatically added and a luminescence reading was obtained using the Tropix TR717 Microplate Luminometer (Applied Biosystems, UK).

2.12. Measurement of procollagen accumulation

2.12.1. Principle of technique

Hydroxyproline accumulation in spheroids was used as a measure of pro-collagen production. Hydroxyproline represents approximately 13.5 % of the primary sequence of procollagen and is essential for the formation of the collagen triple helix. Hydroxproline is not present in significant levels in any other proteins. Levels of hydroxyproline in cell culture hydrolysates were quantified by reverse-phase high performance liquid chromatography (HPLC) following derivitisation with 7-chloro-4-nitrobenzo-oxa-1,3-diazole (NBD-Cl) (Sigma; #17239-0050) to generate a chromophore detectable at 495 nm wavelength. The specificity of the reaction is further ensured by keeping the derivation time to 20 minutes at 37 ^{o}C, a time-point that has been confirmed experimentally to be maximal for hydroxyproline derivatisation with NBD-Cl for up to 20 nmol hydroxyproline.

2.12.2. Sample preparation

Cultured non-IPF and IPF spheroids (as described in **Section 2.5**) were used to study procollagen accumulation. Following treatment of the compound for 24 hours, the media was removed from each well and the spheroids were washed in PBS and placed into sterile 2 mL polypropylene microcentrifuge tubes (Fisher; UK). Each tube contained two spheroids and 200 μL of 6 M HCl. These were then hydrolysed at 110 ^{o}C for 16 hr. 100 μL of the hydrolysate were

transferred to 1.5 mL centrifuge tubes and evaporated to dryness using speedvac concentrator (Savant SPD 131DDA, Thermo Electron Corporation, Cambridge, UK). Milli-Q water (100 μL) was added to the dried aliquot of hydrolysate and left to rehydrate at 4 °C overnight or 30 minutes at room temperature.

Standard sample preparation: 250 μM of Trans-4-hydroxy-L-proline (PHPRO; Sigma Aldrich, UK) was diluted 1:100 using Milli-Q water (Milli-Q Plus; Millipore Ltd., UK). The final amount of Hydroxyproline (Hyp) standard loaded onto the column was 50 pmol.

2.12.3. Derivitising samples

100 μL of each sample and standard were buffered with 0.4 M potassium tetraborate (adjusted to pH9.5 with HCl) and then reacted with 100 μL NBD-Cl (36 mM in methanol) to a final concentration of 12 mM NBD-Cl. These were Vortex mixed thoroughly and incubated at 37 ^{o}C (in the dark) for 20 minutes. The reaction was stopped by adding 50 μL 1.5 M HCl. Following this, 150 μL of a concentrated solution (3.33X) of HPLC running Buffer A (5.68 *g* sodium acetate dissolved in 150 mL Milli-Q water and 65 mL acetonitrile, corrected to pH6.4 with orthophosphoric acid and made up to 250 mL) was added and mixed thoroughly. The samples were then filtered through a HPLC low dead volume filter (pore size 0.22 μm, type GV; Millipore Ltd, UK) into a polypropylene insert. The insert was placed into a brown glass Amber Snap Seal vial (Laboratory Sales Ltd., Rochdale, UK). These vials were then placed in the automatic sampler in the HPLC apparatus and the samples were sequentially injected onto the HPLC column and eluted with an acetonitrile gradient as described below.

2.12.4. Chromatography conditions

The HPLC apparatus used for measurements was Agilent series 1100 (Agilen Technologies, USA) with a reverse-phase cartridge column (LiCrospher 100 Rp-18 (10 μm), LiChroCART 250 mm length x 4 mm diameter, 5 μm particle size; Merck, UK). The column was continuously maintained at 40 ^{o}C in a heated column oven. At the beginning of each batch of samples, the HPLC system was equilibrated in running buffer A for minimum of 40 minutes. NBD-Cl derivatives of standards and samples were individually injected onto the column and eluted with an acetonitrile gradient, which was achieved by changing the relative proportions of running buffers A and B over time. Chromatographic conditions and buffers used in this process are summarised in **Table 2.5**.

Table 2. 5: Conditions and buffers for the separation of hydroxyproline by reverse-phase HPLC

Column	LiChrospher, 100 RP-18, 250 x 4 mm, 5 μm		
Mobile phase	*Buffer A* - aqueous acetonitrile (8 % v/v) 50mM sodium acetate, pH 6.4 *Buffer B* - aqueous acetonitrile (75 % v/v)		
Column flow rate	1.0 mL/min		
Column temperature	40 °C		
Detection wavelength	495 nm		
Elution gradient	Time (min)	% Buffer A	% Buffer B
	0	100	0
	5	95	5
	6	20	80
	12	20	80
	12.5	100	0
	25	100	0

Post-column detection was achieved by monitoring absorbance at 495nm using a flow-through variable wavelength monitor. Hydroxyproline elutes as a discreet peak between four to six minutes following sample injection on the column (**Figure 2.3**), between glutamine (3.5 minutes) and serine (seven to nine minutes). The column running and regeneration time for each sample was 25 minutes.

2.12.5. Quantification of hydroxyproline content

Quantification of the hydroxyproline content in each 100 µL sample injected into the column was determined by comparing peak areas of chromatograms obtained for each sample to the average standard peak areas. This value represents the hydroxyproline levels in the fraction of the acid hydrolysate of the spheroids and was used to calculate the total spheroid collagen based on the hydroxyproline content of the collagen and the dilution factors at the processing steps. Total collagen was expressed as ng/spheroid, assuming that hydroxyproline accounts for 13.5 % of the weight of collagen.

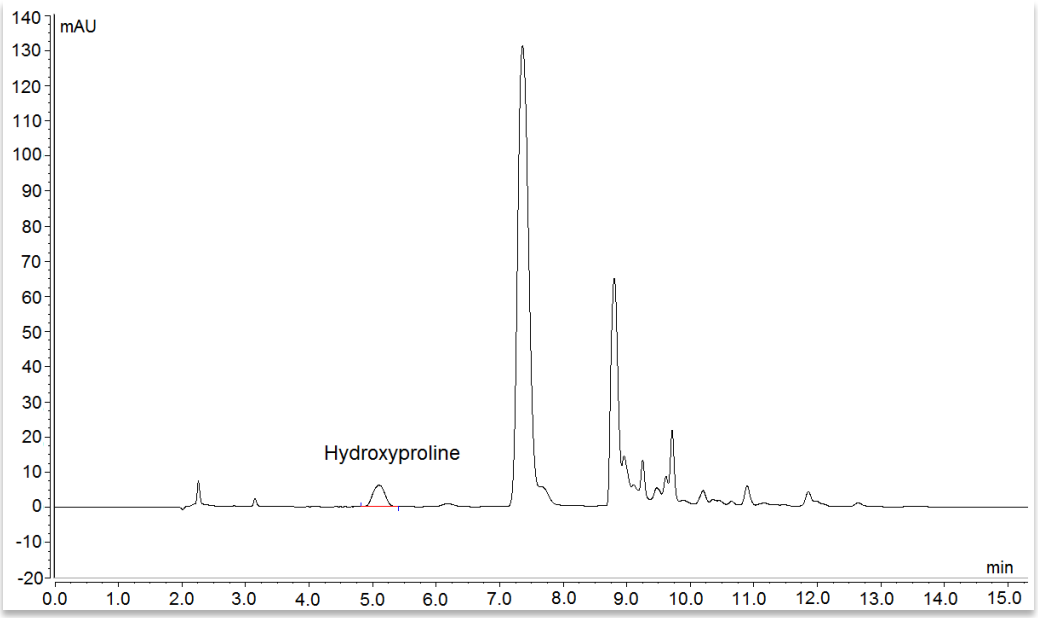

Figure 2. 3. HPLC Chromatogram of a hydroxyproline reference standard.

Hydroxyproline peak is shown between four to six minutes. The concentration of the hydroxyproline standard was 2.5 μM. The area under the hydroxyproline peak is used as reference to calculate hydroxyproline concentrations in unknown samples.

2.13. Zymography

2.13.1. Principle of technique

Zymography is a technique used to analyse the activity of matrix metalloproteinases (MMPs) in biological samples. It involves protein separation under denaturing (sodium dodecyl sulphate, SDS) and non-reducing conditions through a polyacrylamide gel containing a proteolytic substance (in this case, gelatin). The resolved proteins are renatured by the exchange of SDS (an anionic detergent) with Triton X-100 (a non-ionic detergent). Following this, the gel is incubated in a low salt collagenase buffer. The gel is then stained with Coomassie Blue to identify proteolytic activities with clear bands against a blue background (non-degraded gelatin).

2.13.2. Sample preparation

Following spheroid formation, the supernatant was removed and diluted 1:4 with media (DMEM supplemented with 2 mM L-glutamine, 50 U/mL penicillin, 50 μg/mL streptomycin and 0.4 % FBS). The samples were then further diluted 1:1 with Tris-Glycine SDS sample buffer (0.5 M Tris-HCl at pH 6.8 diluted 1:1 with 100 % glycerol; 5 % SDS w/v bromophenol blue). 20 μL of the samples and 2 μL of MMP2 standard control (1 μU; 2B scientific ltd, UK) were then loaded into the wells of Novex 10% Tris-glycine zymogram (0.1 % gelatin) protein gels (Life technologies, UK). The running buffer used was 1x Tris-glycine SDS running buffer. Electrophoresis was performed at 125 V for 90 minutes.

2.13.3. Detecting MMPs

Following electrophoresis the gel was washed with 2.5 % Triton X-100 for one hour and then incubated with 1x low salt collagenase buffer (0.02 % Brij-35 detergent in 0.6 % Tris-base, 1.17 % NaCl, and 0.055 % $CaCl_2$, at pH 7.6 adjusted with concentrated HCl) overnight at 37 ^{o}C. The gels were then incubated with Coomassie blue (0.025 % Coomassie blue in 10 % glacial acetic acid and 50 % methanol) and destain solution (10 % glacial acetic acid with 30 % methanol) for two hours at room temperature. The gels were then sandwiched between two acetate sheets and scanned using transmissive greyscale 300 dpi settings on a flatbed scanner (Epson, UK). The optical density of each band was calculated similarly to Western blots (as mentioned in **Section 2.9.5**). The optical density of each band was normalized to the standard MMP2 control in order to compare between samples.

2.14. PGE_2 ELISA

Prostaglandin E2 Biotrak enzymeimmunoassay system (VWR, UK) was used to measure the levels of PGE_2 in the spheroid supernatants (96 hours post seeding; 1:4 dilution). The ELISA was performed as instructed by the manufacturer's guidelines. Briefly, all reagents were equilibrated to room temperature before use. PGE_2 stock solution was used to prepare working standard concentrations (range from 2.5-320 pg/50μL). Each of the working standard concentrations and the supernatant samples were placed into the appropriate wells of 96-well

microplate provided, pre-coated with sheep anti-mouse IgG. Assay buffer (provided within the kit; 0.1 M phosphate buffer pH 7.5 containing 0.9 % w/v bovine serum albumin and 0.5 % w/v kathon) was used to identify any non-specific binding (NSB). Each well was then treated with anti-PGE_2 antibody (excluding blank and NSB wells) and PGE_2 conjugate (lyophilised PGE_2 conjugated to horseradish peroxidase; excluding blank wells). The microplate was then incubated at room temperature for one hour. Following this, each well was washed thoroughly with the wash buffer provided (0.01 M Phosphate buffer pH 7.5 containing 0.05 % v/v Tween 20) and immediately treated with an enzyme substrate, 3,3',5,5' Tetramethylbenzidine (TMB)/Hydrogen Peroxide. The microplate was then incubated at room temperature on a microplate shaker for 15-30 minutes. The reaction was then halted with the addition of 1 M sulphuric acid. The optical density (OD) was read at 450 nm using an absorbance plate reader.

2.15. Microarray

2.15.1. Principle of technique

A microarray provides quantitative gene expression data by using a collection of microscopic features (generally DNA) acting as probes to target molecules (Miller and Tang, 2009). One common microarray technology used is *in situ*-synthesised oligonucleotide microarrays. These are extremely-high-density microarrays that use different oligonucleotide probes (short single stranded DNA or RNA sequences specific to a particular gene of interest; 25 base pairs in length) which are synthesised directly on the microarray surface (e.g. glass wafer) by using a semiconductor-based photochemical synthesis technology (Dalma-Weiszhausz et al., 2006). One of the most widely used chips containing oligonucleotide probes is Affymetrix GeneChips. Each GeneChip is composed of many probe cells, each of which is specific to one gene and there are millions of oligonucleotide probe copies per probe cell. Each gene is matched to 11 probe cells which are evenly distributed throughout the chip. Each oligonucleotide probe pair is composed of a perfect match (PM) probe and a mismatch (MM) probe (**Figure 2.4A**). PM probes consist of a sequence which is complimentary to the specific gene and therefore is used to measure the gene expression. On the other hand, the MM probe differs from the PM probe by the substitution of a single base, located in the centre of the probe sequence. This helps identify non-specific hybridisation (Miller and Tang, 2009).

Figure 2.4B illustrates the steps involved for Affymetrix microarray. In brief, RNA is extracted from the samples and converted to cDNA. An *in vitro* transcription reaction is then performed to convert the cDNA to biotin-labelled cRNA. The cRNA generated is then fragmented. A hybridisation cocktail is then prepared which includes the probe array controls, fragmented targets, herring sperm DNA (commonly used as a blocking agent in hybridisation experiments), and BSA. The Affymetrix GeneChips are then incubated with this hybridisation cocktail for 16 hours then washed to remove any unbound targets followed by staining with streptavidin phycoerythrin conjugate which is able to detect biotin. The amount of light emitted at 570 nm is proportional to the bound target at each location on the probe array.

2.15.2. Sample preparation

Following spheroid formation of non-IPF (n=10) and IPF (n=10) fibroblasts (24 hours post seeding), ten spheroids were pooled together and washed twice in PBS followed by treatment with 500 μL RNaqueous lysis buffer (Ambion, Life technologies, UK). The samples were then stored at -80 ^{o}C and transported to Epistem (UK) for microarray using Affymetrix GeneChip Human Genome U133 Plus 2.0 Array.

The cDNA generated in the initial steps involved the use of an RNA-Amp kit (Epistem, UK) which was used to convert 10 ng RNA (quantified using a NanoDrop) to poly A cDNA. A bioanalyser (**Section 2.10**) was used to investigate the integrity of the samples (i.e. RNA, cDNA, biotin-labelled fragments) at each step prior to hybridisation.

Four hybridisation controls (BioB, BioC, BioD, and Cre; pre-labelled molecules derived from *E-coli*) were spiked into the samples at increasing concentrations (BioB<BioC<BioD<Cre) prior to hybridisation and biotin-labelling steps, respectively. The data obtained from these controls were used for quality control (QC) analysis (see below). All samples were then processed on the GeneChip as shown in **Figure 2.4** and as described by the manufacturer's instructions.

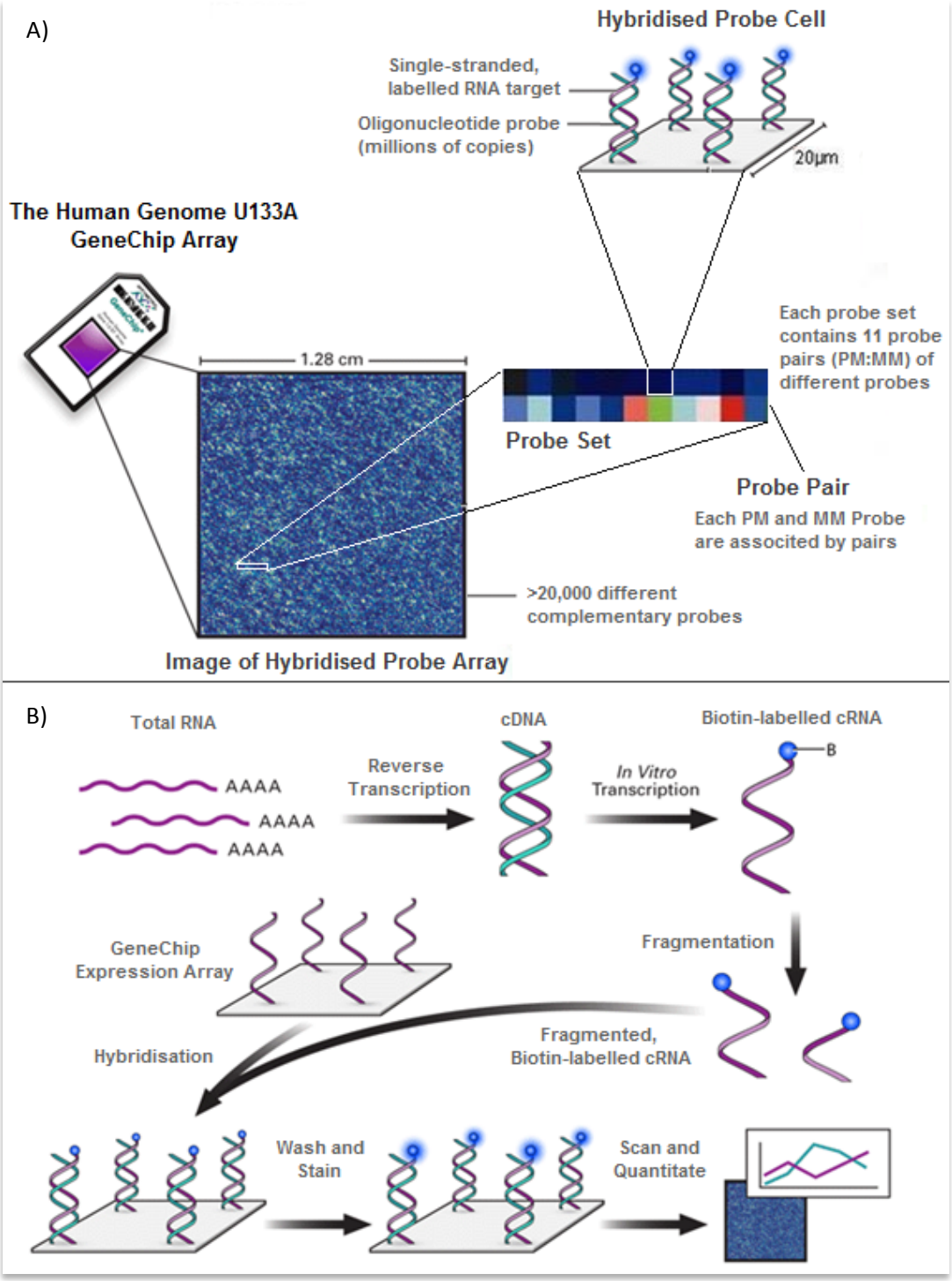

Figure 2. 4. Affymetrix microarray

A) The Human Genome U133A GeneChip Array. B) Microarray protocol. RNA is first extracted from the samples, followed by cDNA formation. An *in vitro* transcription reaction is performed to convert the cDNA to cRNA. The cRNA target is labelled with biotin and fragmented into short sequences. An Affymetrix GeneChip containing oligonucleotide probes is incubated with the target for hybridisation. The chip is washed and stained with a fluorescent statin. Hybridised targets are identified using a GeneChip scanner (Reproduced and adapted with permissions from Affimetrix Ltd).

2.15.3. Data analysis

The data (CEL image files) were processed using Robust Multi-array Average (RMA) in Partek genomic suite (Partek, USA; a comprehensive suite for visualisation and analysis of genomic data). RMA is an algorithm used to background correct, normalise, and summarise the microarray data set (Bolstad et al., 2003). The raw values generated on the array are a mixture of background signal (as a result of optical noise and non-specific binding, i.e. MM probe signal) and PM values. Thus, to determine the true expression of the genes per samples it was vital to background correct the PM values by a non-linear approach which was done on a per-chip basis. The data were normalised using the RMA normalisation approach (i.e. quantile normalisation) in order to allow direct comparisons of multiple chips together.

Following background correction and normalisation of the PM values, the data were then summarised by converting the probe level values to a single expression measure per probe set (i.e. log2 expression). RMA summarisation is based on the assumption that the observed log2 transformed PM values follow a linear additive model (non-parametric regression method) composed of a probe affinity affect (which is assumed to sum to zero), gene specific effect (i.e. expression level, which is estimated using a robust model fitting technique called median polishing that is able to protect against outlier probes), and an error term.

A QC procedure was used in Partek which involved comparing information from the hybridisation controls with the experimental probes on the Affymetrix chips to determine the quality of the microarray data and to detect any samples which did not pass the QC metrics.

Using Partek genomic suite, two factors were considered during ANOVA analysis: condition (i.e. non-IPF and IPF) and gender. Other factors such as batch effect and date of the experiment were removed. The software was also used to perform principal component analysis (PCA), generate dot plots, form heat maps, and perform pathway analysis. Differentially expressed genes with a false discovery rate (FDR) $p<0.05$ (or unadjusted $p<0.01$), and fold change (FC) >2 or <-2 were considered to be statistically significant. String 9.1 (online based software) was used to determine interactions between the differentially expressed genes.

2.16. Statistical analysis

Data shown as percentages were transformed to arcsine (also known as inverse sine) to approximate a Gaussian rather than binomial distribution. In most cases, data are assumed to be normally distributed (Gaussian distribution). However, if the data are in percentages then the values are restricted to lie between 0 to 100 % and such data cannot be used for statistical analysis. Arcsine transformation removes this restriction providing values that lie within a normal distribution which can be used for statistical analysis.

All data in figures are presented as mean values ± standard error of mean, unless indicated otherwise. Statistical analysis was performed between two treatment groups by student's t test, and between multiple treatment groups by one/two way analysis of variance (ANOVA) with Bonferroni post-hoc testing, using GraphPad Prism 5 and/or SigmaPlot 12.3 software. The mean values of various parameters were considered to be significantly different when the p value was less than 0.05. Concentration-response curves were generated using GraphPad Prism (four-parameter, unconstrained, variable slope fit).

CHAPTER 3: RESULTS

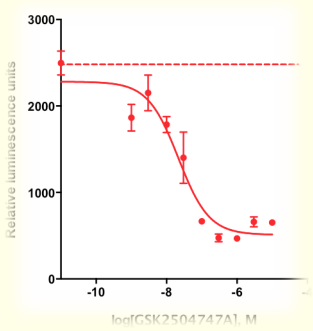

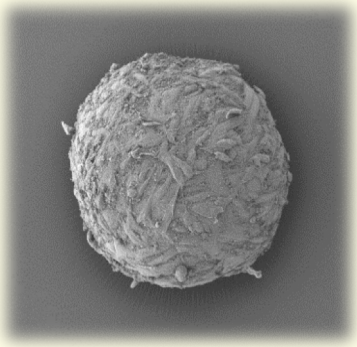

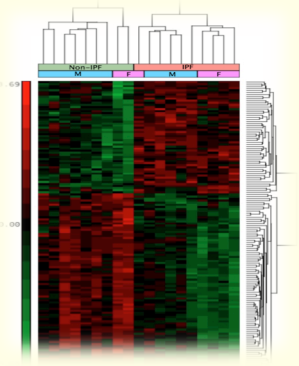

3.1. Fibroblast characterisation and spheroid formation

3.1.1. Introduction

Cell culture systems are indispensable tools required for basic research and for many pre-clinical *in vitro* studies. The classical approach used for many years in numerous laboratories involves culturing cells on plastic (so called static dish culture). This primarily produces adherent 2D cell monolayers which do not reflect the conditions seen *in vivo,* where cells grow within a complex 3D microenvironment (Freed and Vunjak-Novakovic, 1998; Lee et al., 2008). Furthermore, cells in a 2D environment require regular feeding by replacing the overlaid culture medium every 2-3 days (Smalley et al., 2006). In addition, morphological and physiological analyses of cells grow on plastic have shown substantial differences in comparison to their counterparts *in vivo*. Thus, the inconsistency in growth conditions in monolayer cultures and the difference in morphology as well as physiology of the cells, has led to debates regarding the suitability of 2D culture systems as reliable tools for *in vitro* studies. Many groups are now in the process of developing 3D *in vitro* cultures which are considered to be a more representative approach for mimicking *in vivo* conditions. 3D cultures demonstrate a higher degree of structural complexity, similar to tissues and organs. Spheroid cell aggregates and scaffold culture systems are becoming one of the most widely used 3D models for creating 3D complex tissues to understand the pathology of many diseases (in particular cancer), as they can be created with minimal effort (Kunz-Schughart et al., 1998; Friedrich et al., 2009; Fu et al., 2014; Guo et al., 2014a, 2014b; Hsu et al., 2014; Rama-Esendagli et al., 2014; Saar et al., 2014; Subramanian et al., 2014).

For biological studies, the significance of using primary cells instead of cancer cell lines is also becoming widely recognized. Cancer cell lines carry mutations in genes involved in several cellular processes including cell-cycle control, DNA repair, and apoptosis – which can limit their applicability for understanding normal physiology or non-malignant pathology (such as that seen in IPF). A major disadvantage of using primary cells is that the cells cannot be passaged indefinitely due to the onset of replicative senescence. Hence, new primary cells must be isolated regularly. In our laboratory, fibroblasts have been derived from the lung using two alternate isolation protocols. The original protocol involves chopping the lung into small explants (~1 mm^3), which are then cultured in petri dishes and incubated for 2-4 weeks to

allow the outgrowth of fibroblasts. However, this protocol is not only time-consuming, but also results in a relatively low yield of fibroblasts. We have recently investigated an alternative protocol in which whole human lung is trypsinized to derive both primary type II AECs as well as fibroblasts. The fibroblasts grow within 1-2 weeks, the yield is far greater in comparison to the explants, and less selective for proliferative cell subtypes. To date, this protocol has only been used for the isolation of non-IPF fibroblasts. I therefore wished to assess whether this protocol might be suitable for future extraction of fibrotic fibroblasts, or whether it significantly alters the phenotype of the cells. In addition, the spheroid forming capacity of dermal fibroblasts is well documented but to date fibroblasts from the lung have not been used to form spheroids. Therefore, the feasibility of forming spheroids using lung fibroblasts was also investigated.

3.1.2. Non-IPF pHLF-Di cells are myofibroblast-like at baseline

In order to investigate any morphological differences between primary human lung fibroblasts from explant cultures (pHLF-Ex) and from lung digests (pHLF-Di), 10,000 cells were cultured in 96 well plates before serum starvation for 24 hours, followed by TGFβ activation (24 hours). The cells were then fixed for two minutes with 100 % methanol following immunocytochemistry for αSMA, Ki-67, and smoothelin. Ki-67 is a nuclear protein encoded by *MK167*. The precise role of this protein is currently unknown; however it is expressed in all stages of the cell cycle (G1, S, G2, and mitosis) excluding G0 which supports an important role for Ki-67 during proliferation. Therefore in this study, an anti-Ki-67 antibody was used as a marker for proliferation.

Figure 3.1 illustrates that at baseline, non-IPF pHLF-Di have a myofibroblast-like phenotype, since they show an increased appearance of stress fibres and αSMA expression in comparison to non-IPF pHLF-Ex. When treated with TGFβ, non-IPF pHLF-Ex cells show an increase in αSMA expression and stress fibres. However, there was little observable difference in αSMA expression in non-IPF pHLF-Di following TGFβ treatment. In addition, **Figure 3.2** demonstrates phenotypical analysis of non-IPF and IPF pHLF-Ex. Similar to non-IPF pHLF-Ex, IPF fibroblasts also shown an increase in TGFβ-induced αSMA expression. Furthermore, the results also demonstrate that all cells lack smoothelin expression (smooth muscle cell marker), supporting that the cells derived from both isolation methods were not smooth muscle in origin.

Quantitative analyses of **Figures 3.1** and **Figure 3.2** are illustrated in **Figure 3.3A** confirming that non-IPF pHLF-Di have a more myofibroblast phenotype in comparison to pHLF-Ex. In addition, there is no significant difference in αSMA expression between non-IPF pHLF-Ex and IPF pHLF-Ex fibroblasts at baseline (as measured by quantitative image analysis of immunocytofluorescence staining for a-SMA), and both exhibit a comparable elevation in αSMA after addition of exogenous TGFβ. **Figure 3.3B** and **Figure 3.3C** confirm that expected elevation in αSMA protein levels in the presence of TGFβ in non-IPF pHLF-Ex, by western blot.

The effect of TGFβ on fibroblast proliferation was also analysed amongst all cells. **Figure 3.4** illustrates the percentage of Ki-67 positive cells in non-IPF pHLF-Ex and pHLF-Di. At baseline pHLF-Di are more proliferative in comparison to pHLF-Ex despite the fact that both cell isolates are from the same donor. In addition, exogenous TGFβ increased the percentage of Ki-67 positive cells in both pHLF-Ex and pHLF-Di. This result was reproduced in three different donors.

Since there is a clear difference in terms of αSMA and Ki-67 expression at baseline between explant and digest-derived non-IPF cell isolates, it can be hypothesised that similar results may also occur in IPF fibroblasts from trypsin-digested fibrotic lungs. Given that our existing fibroblast biobank has historically been derived from explant cultures, isolation by digestion (associated with significant effects on phenotype) was abandoned as a replacement protocol, despite the greater cell yield. The rest of my project focused on fibroblasts isolated from explants only, and from this point on, pHLF-Ex will be referred to only as pHLF, for simplicity.

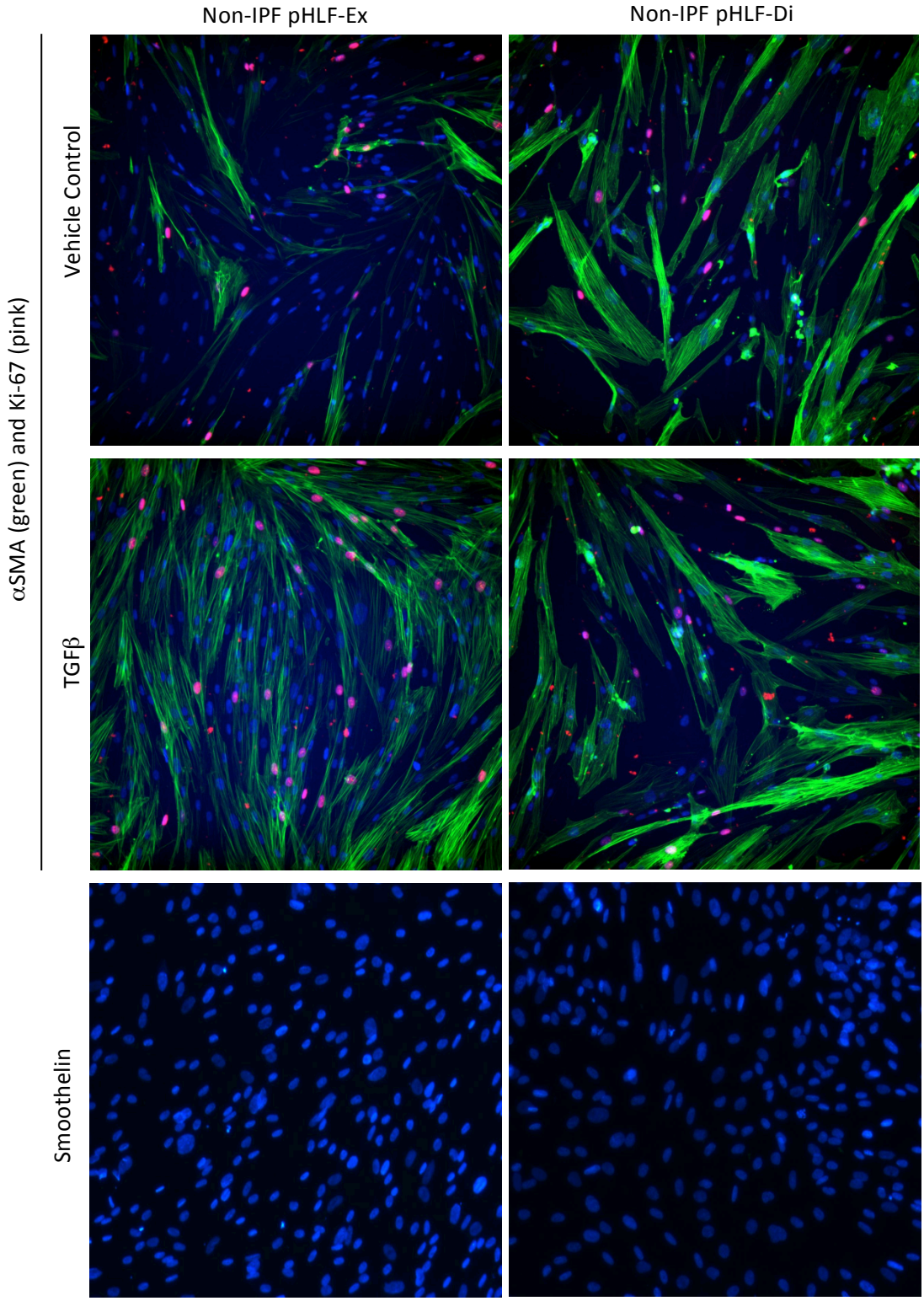

Figure 3. 1. α-SMA, Ki-67, and smoothelin expression in non-IPF pHLF derived from explants and lung digests.

Fibroblasts were cultured in 96 well plates, serum starved for 24 hrs, then stimulated with 1 ng/ml TGF-beta for 24 hrs. Immunocytofluorescence staining of αSMA (green), Ki-67 (pink) and DAPI (blue) is shown. Cells were negative for smoothelin expression. Non-IPF pHLF-Ex, n=3; pHLF-Di, n=3; magnification: x100.

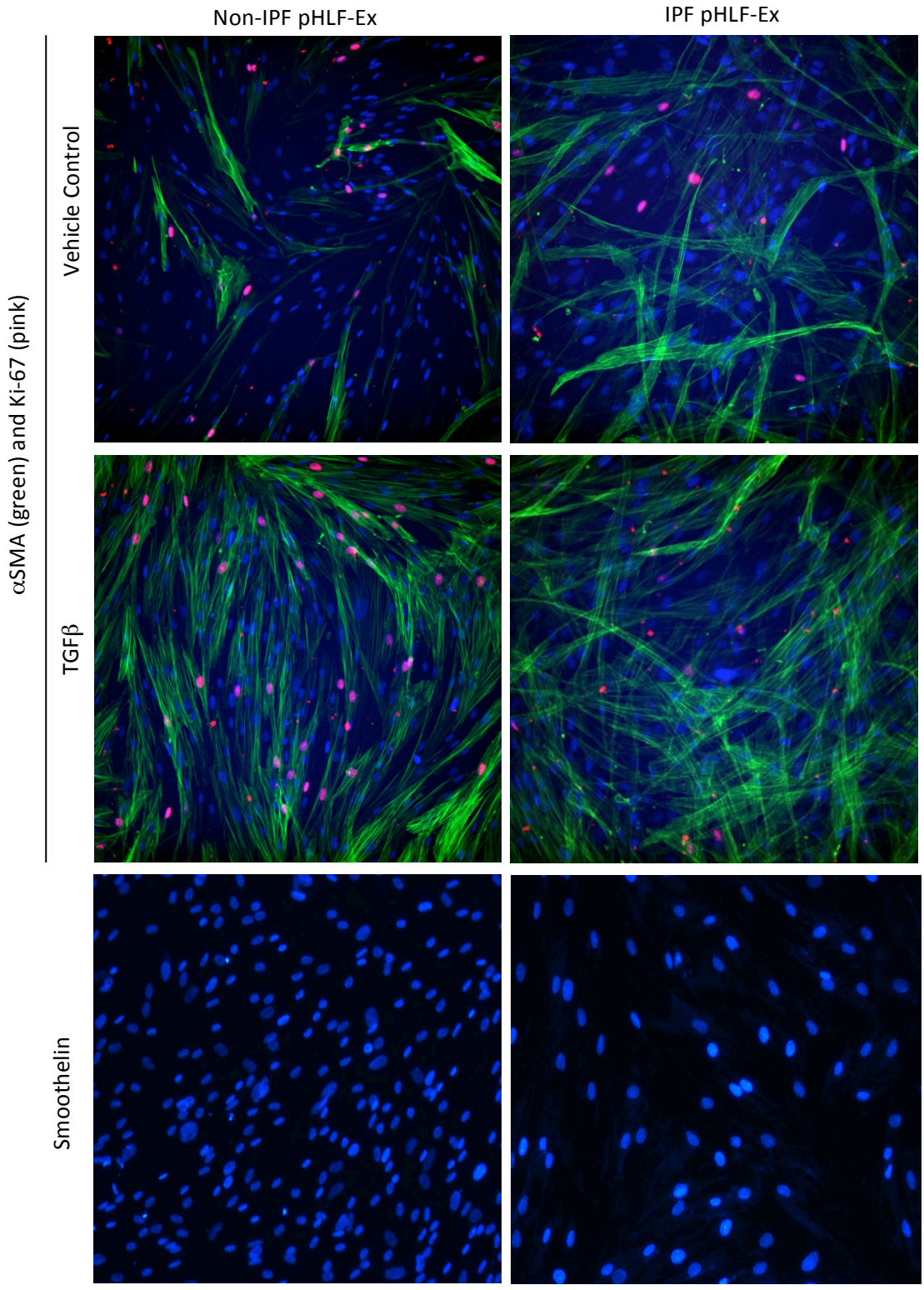

Figure 3. 2. α-SMA, Ki-67, and smoothelin expression in non-IPF and IPF pHLF derived from explant cultures

Fibroblasts were cultured in 96 well plates, serum starved for 24 hrs, then stimulated with 1 ng/ml TGF-beta for 24 hrs. Immunocytofluorescence staining of αSMA (green), Ki-67 (pink) and DAPI (blue) is shown. Cells were negative for smoothelin expression. Non-IPF, n=3; IPF, n=3; magnification: x100.

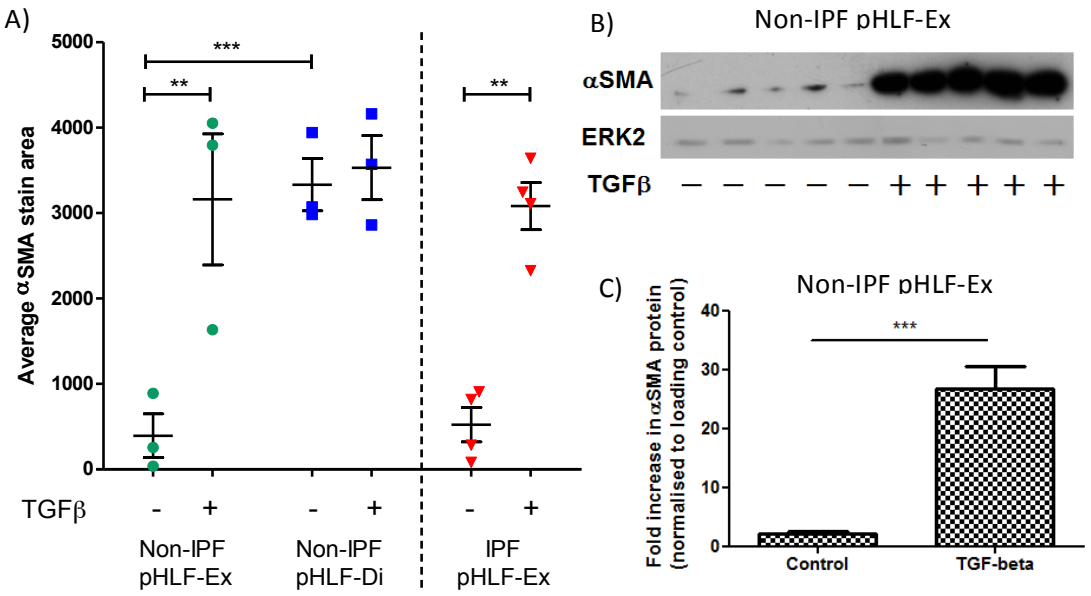

Figure 3. 3. Quantitative analysis of α-SMA expression in primary human lung fibroblasts.

(A) Quantitative data for immunocytofluorescence staining of αSMA in non-IPF pHLF-Ex (n=3), non-IPF pHLF-Di (n=3), and IPF pHLF-Ex (n=4) exogenously treated with 1 ng/ml TGFβ or vehicle control. (B) Western blot illustrating increase in αSMA protein levels in non-IPF pHLF-Ex. (C) Densitometry. ** p<0.01; *** p<0.001

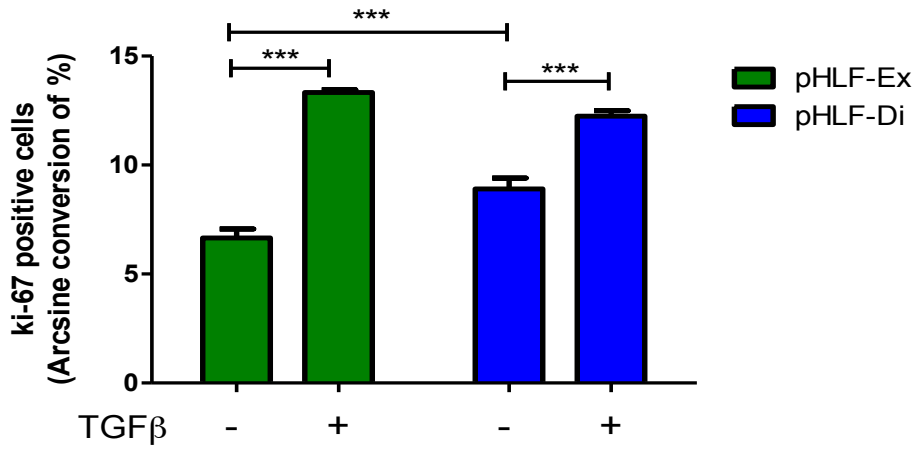

Figure 3. 4. Quantitative analysis of Ki-67 positive cells in non-IPF primary human lung fibroblasts.

Quantitative data for immunocytofluorescence staining of Ki-67 in non-IPF pHLF-Ex (green) and non-IPF pHLF-Di (blue) exogenously treated with 1 ng/ml TGFβ or vehicle control. Data are representative of three donors. *** p<0.001

3.1.3. Non-IPF and IPF fibroblasts aggregate to form spheroids

Non-IPF and IPF pHLF were cultured in 96-well plates (10,000 cells per well) pre-coated with a non-adhesive surface (ultra-low melting point agarose). These were then incubated for 24 hours at 37 ^{o}C with 10 % CO_2. **Figure 3.5A** illustrates phase contrast microscopy images of spheroid formation which were obtained using IncuCyte Zoom (Essen bioscience, UK; see **Section 2.5.3**). As illustrated in **Figure 3.5B**, within 2 hours of seeding, the cells form aggregates which approximately remain the same size (~400 μm) over a 24 hour period. The data are representative of fibroblasts isolated from 10 non-IPF and 10 IPF lung donors. **Figure 3.5C** and **Figure 3.5D** illustrate a macroscopic view of the spheroid and H&E histological staining of an IPF spheroid.

To determine any morphological differences between non-IPF and IPF spheroids, scanning electron microscopy (SEM) and transmission electron microscopy (TEM) were performed, 24 hours post seeding. Spheroid samples were processed by Mark Turmaine (Electron Microscopy Unit, UCL). **Figure 3.6** and **Figure 3.7** illustrate SEM images for non-IPF (n=6) and IPF (n=6) spheroids, respectively. Two out of the six non-IPF donors (donor 1 and 2), in particular, show a more rough/blebbed surface in comparison to all other non-IPF donors - which have a smoother surface with visibly elongated fibroblasts. IPF fibroblast spheroids appear to have a smoother appearance in general, with large, flatter cells. Furthermore, some dead cells (or apoptotic cells) are also present on the surface of both non-IPF and IPF spheroids (cells with a more rounded structure, **Figure 3.8**). Furthermore, IPF spheroids show actin retraction fibres possibly indicating cell migration or contraction. All fibroblast spheroids appeared to have multiple microvilli (**Figure 3.9**). Moreover, fibrillar ECM was evident in some areas of both non-IPF and IPF spheroids (**Figure 3.10**). **Figure 3.11** and **Figure 3.12** illustrate TEM images of non-IPF and IPF spheroids, respectively. Both spheroids show the presence of fibrillar ECM proteins (arrows; most probably fibrillar collagen). In addition, fibroblasts in IPF spheroids appear to be more compact and form junctions (**Figure 3.13**) which were not seen in non-IPF spheroids. These junctions are either tight or adherens junctions. Data are representative of two non-IPF donors and three IPF donors.

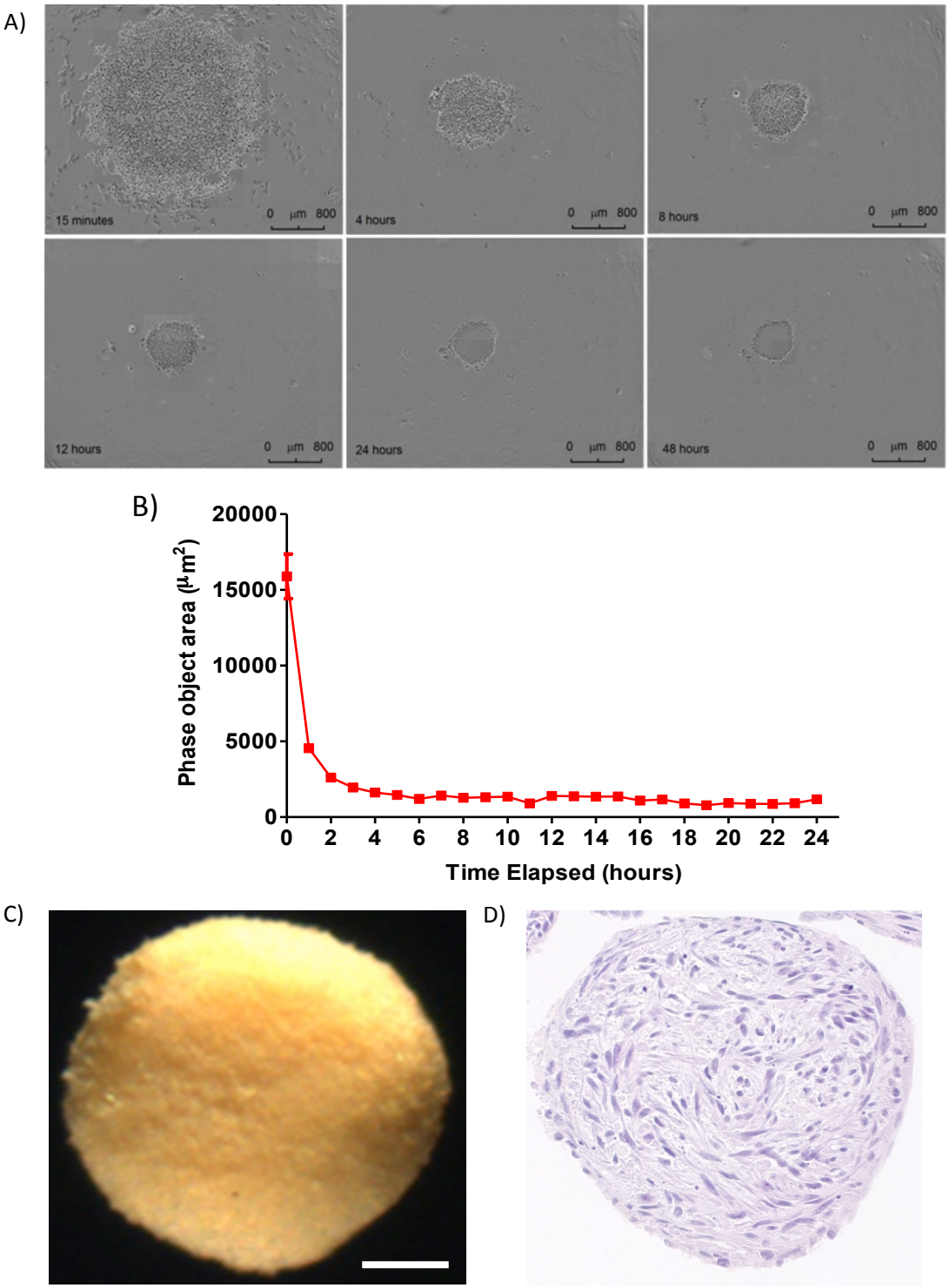

Figure 3. 5. Fibroblast spheroid formation.

Fibroblasts from non-IPF and IPF patients (n=10 and n=10, respectively) have the tendency to form spheroids. (A) Time lapse for spheroid formation (from 15 minutes to 48 hours, post seeding). (B) Phase object area demonstrating size of the spheroid over time, ~400 µm. (C) Macroscopic view of a spheroid. Scale bar = 100 µM. (D) H&E staining. Magnification x10. Representative data shown for one IPF line.

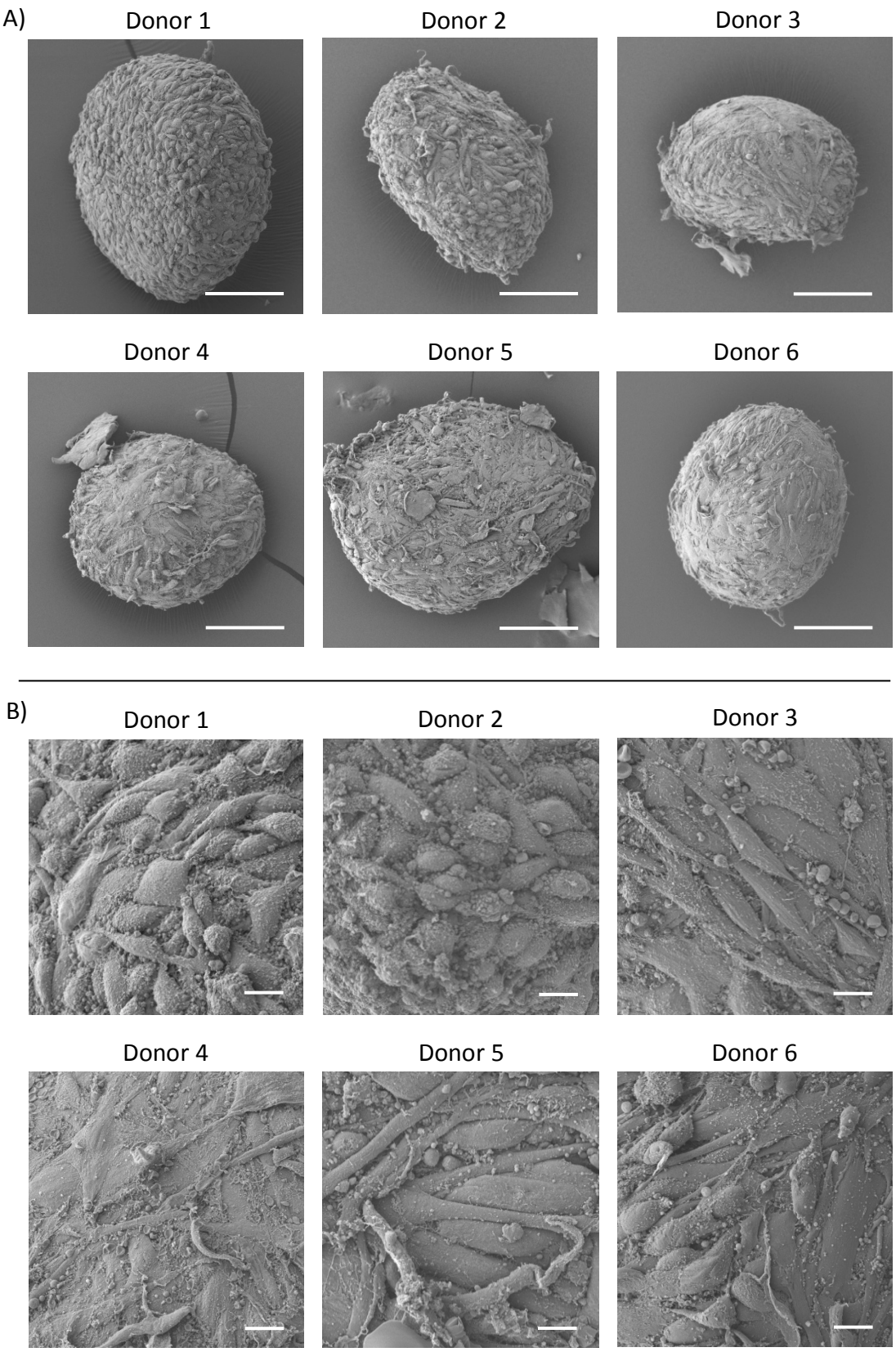

Figure 3. 6. Scanning electron microscopy (SEM) for non-IPF spheroids.

A) Each spheroid represents a different donor (i.e. n=6). Magnification = x200; scale bar = 100 μm. B) Spheroid structures at higher magnification (x1000) for the respective donors. Scale bar = 10 μm.

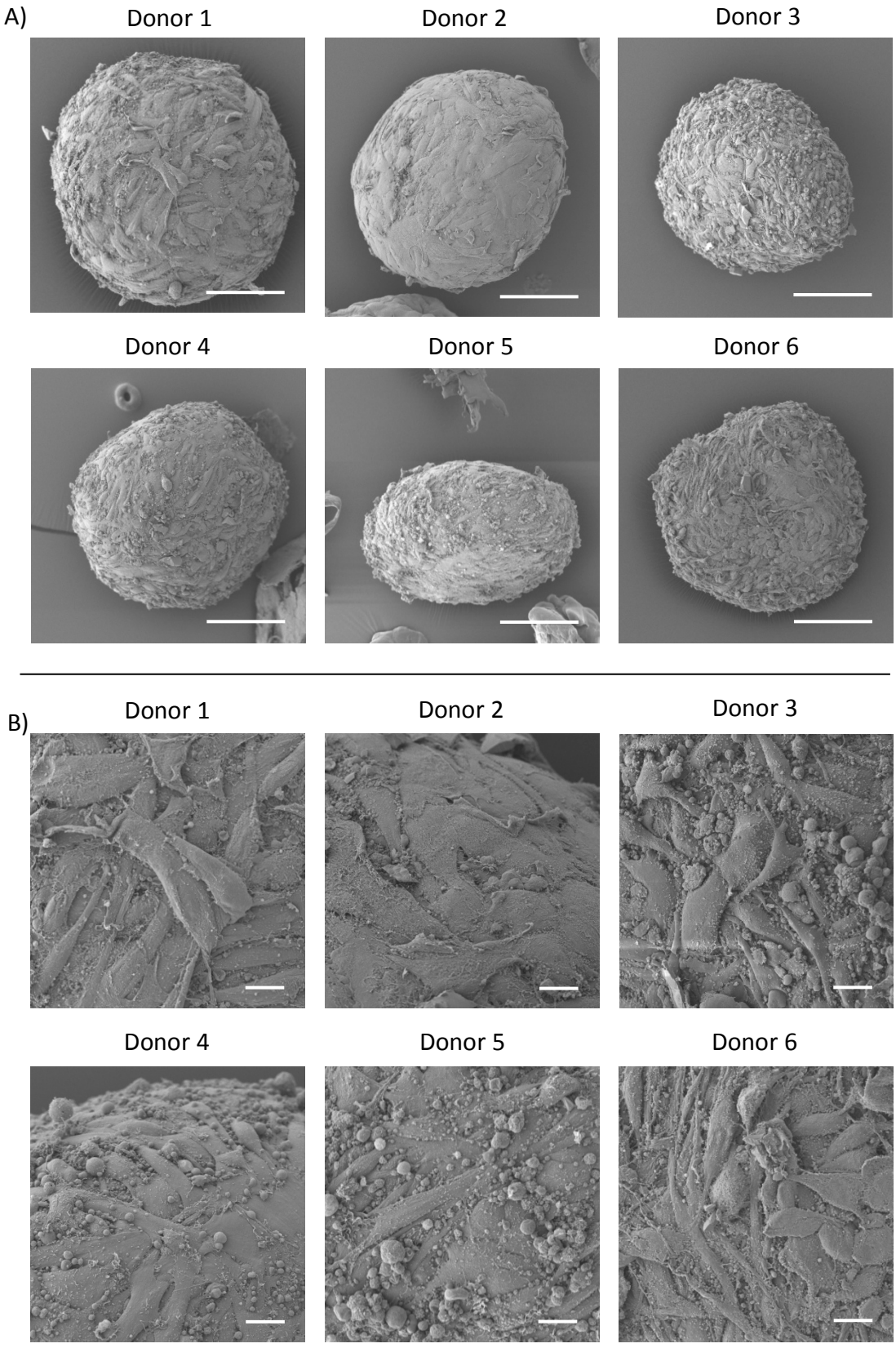

Figure 3. 7. Scanning electron microscopy (SEM) for IPF spheroids.

A) Each spheroid represents a different donor (i.e. n=6). Magnification = x200; scale bar = 100 μm. B) Spheroid structures at higher magnification (x1000) for the respective donors. Scale bar = 10 μm.

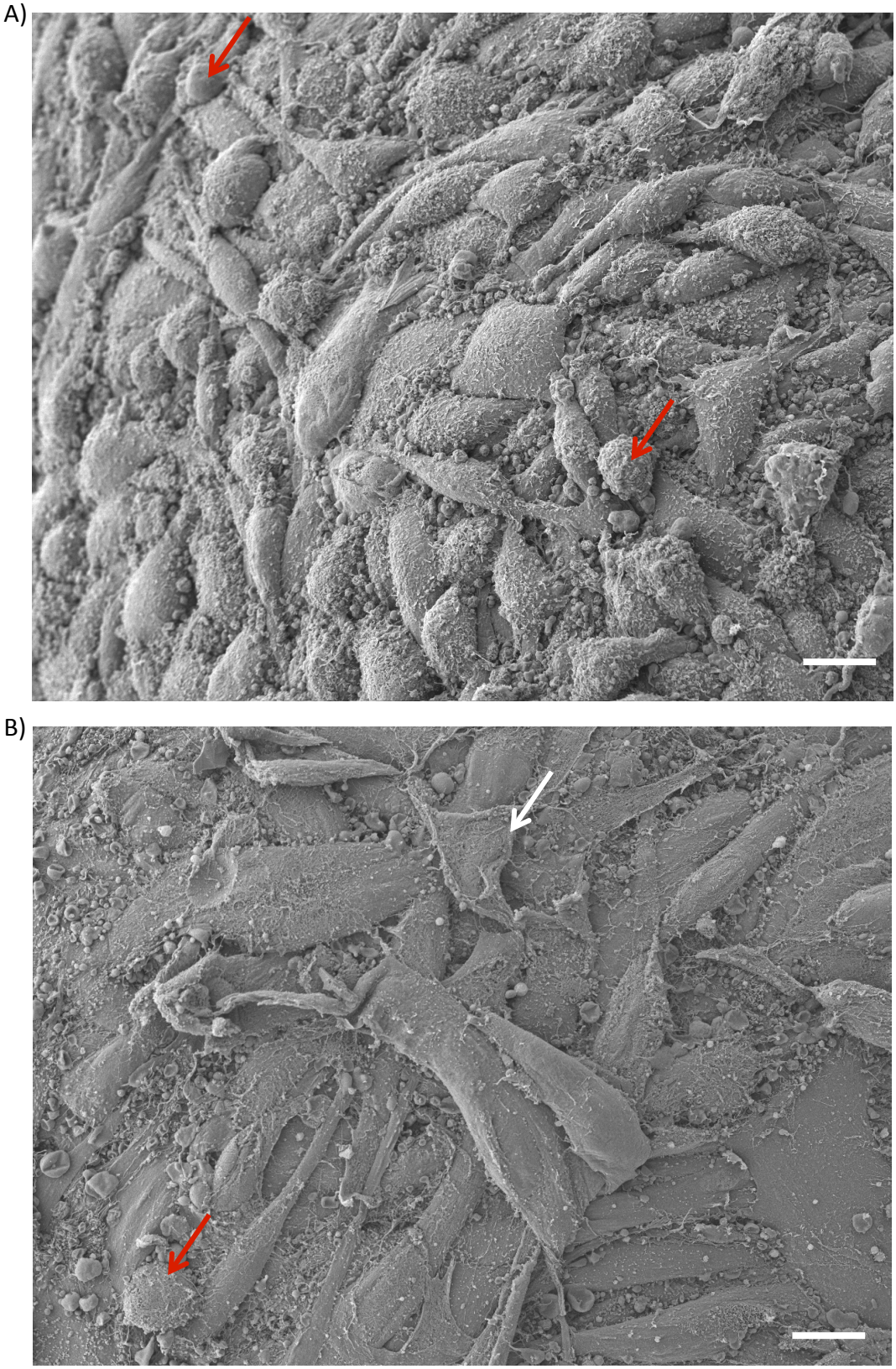

Figure 3. 8. Scanning electron microscopy (SEM) of non-IPF spheroids illustrating probable apoptotic cells.

Cells likely to be undergoing apoptosis are indicated by red arrows of (A) non-IPF and (B) IPF spheroids. White arrow illustrates actin retraction fibres. Scale bar = 10 μm. Magnification x1000

A)

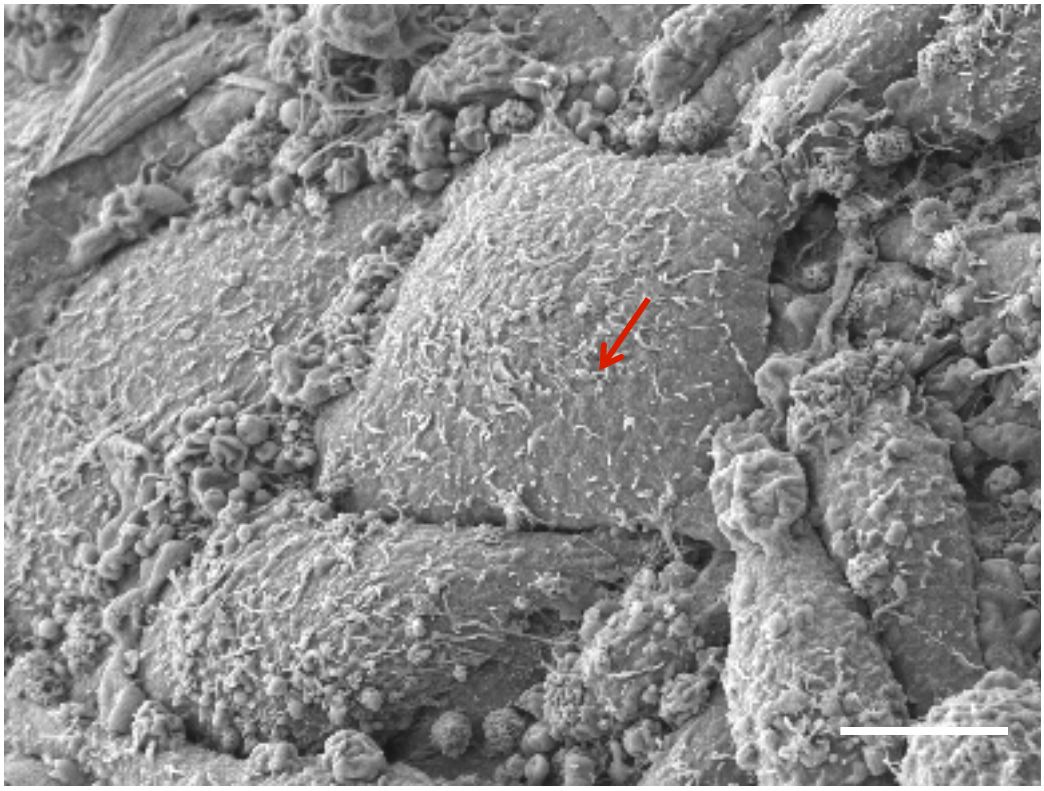

B)

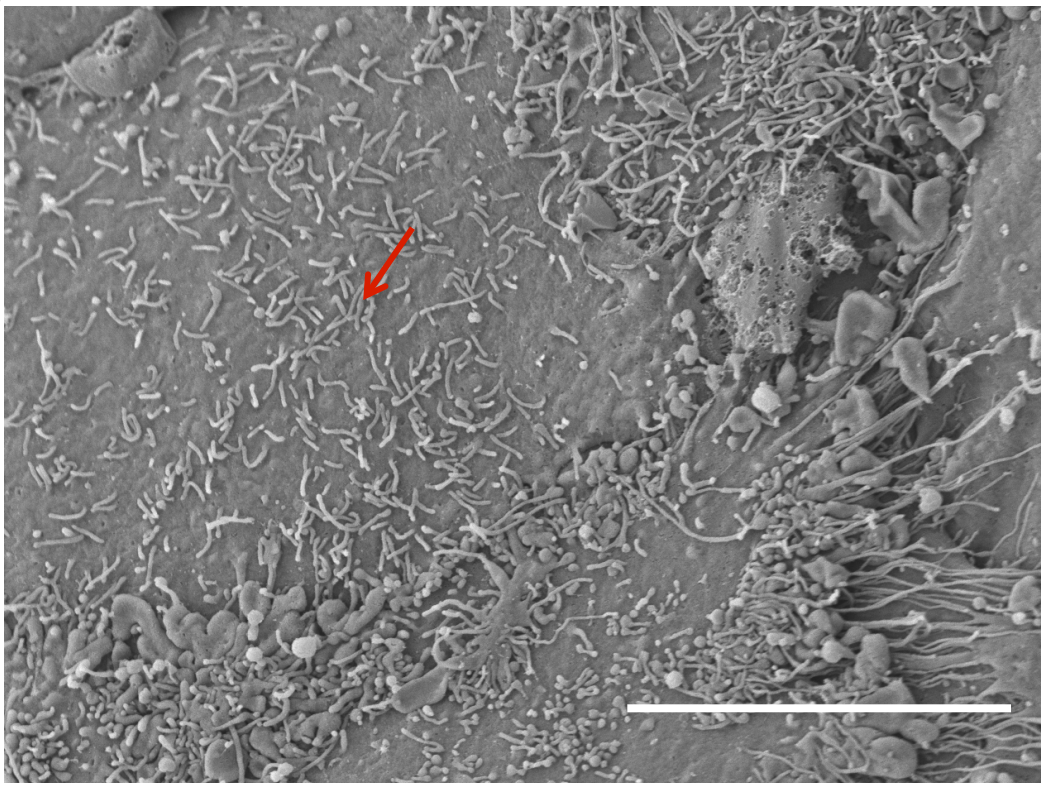

Figure 3. 9. Scanning electron microscopy (SEM) for non-IPF spheroids illustrating microvilli.

Microvilli indicated by red arrows on the surface of both (A) non-IPF and (B) IPF fibroblast spheroids Scale bar = 5 μm. Magnification x2000

A)

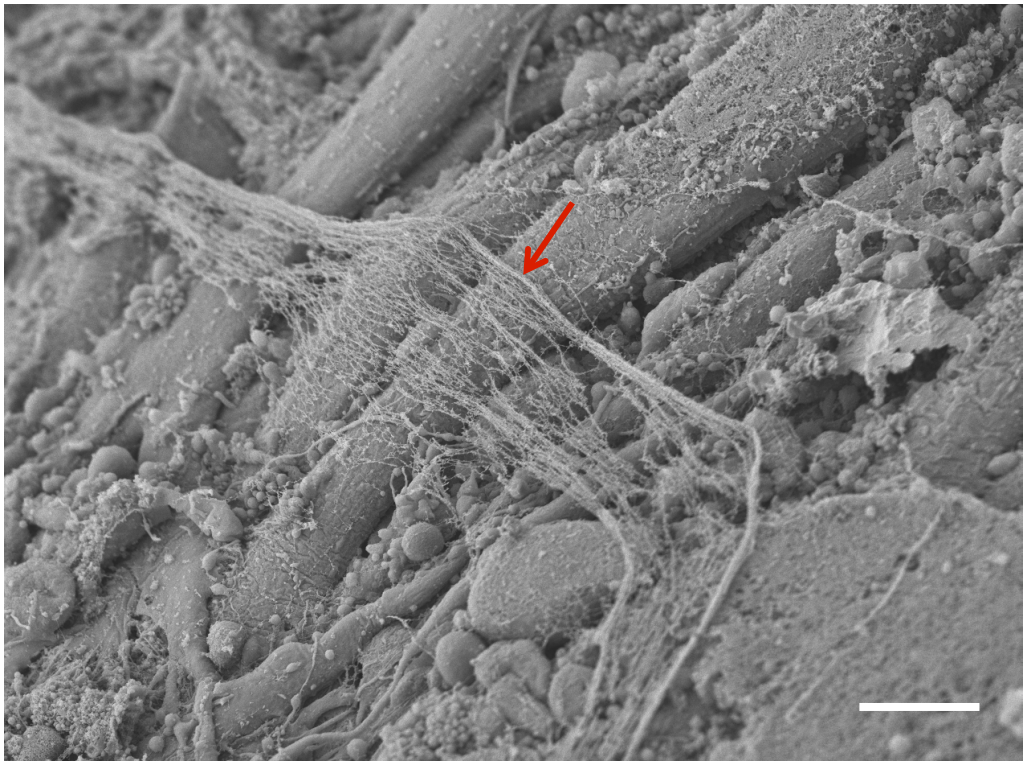

B)

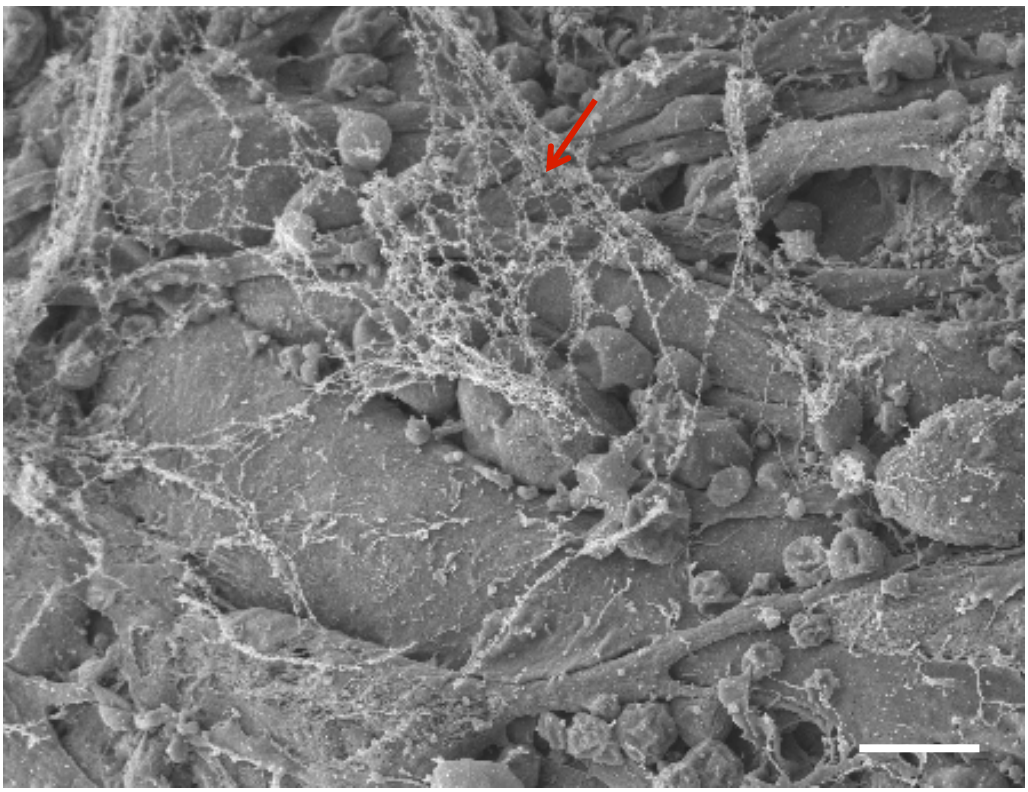

Figure 3. 10. Scanning electron microscopy (SEM) for non-IPF and IPF spheroids illustrating extracellular matrix.

Matrix indicated by red arrows of (A) non-IPF and (B) IPF spheroids. Scale bar = 5 μm. Magnification x3000.

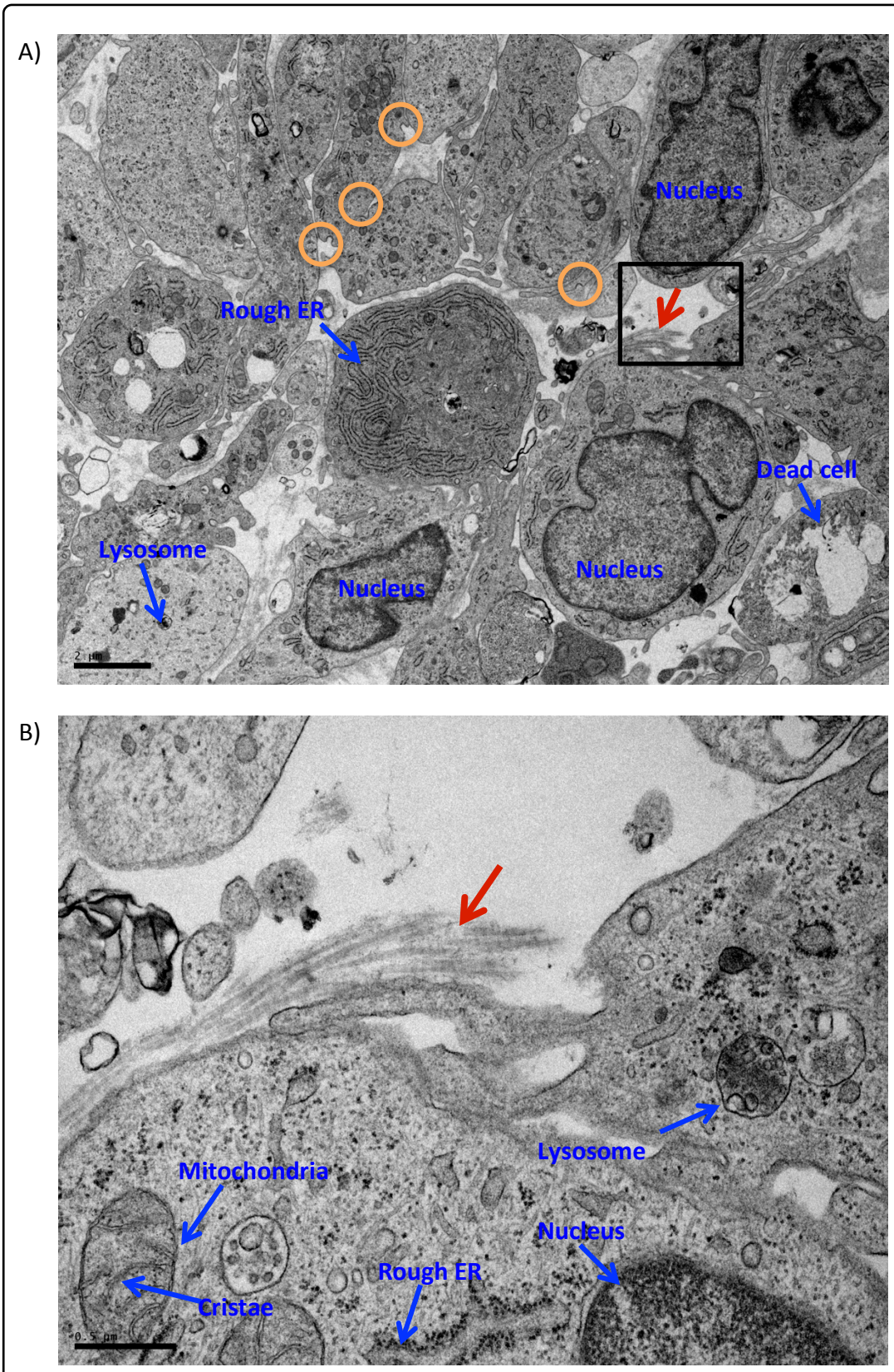

Figure 3. 11. Transmission electron microscopy (TEM) for non-IPF spheroids.

(A) Magnification x8000. Scale bar 2 µm. (B) Greater magnification of black box shown in panel A (x40000). Scale bar 0.5 µm. Fibrillar ECM (red arrows) and invaginations (orange circle) are shown. Data representative of two non-IPF donors.

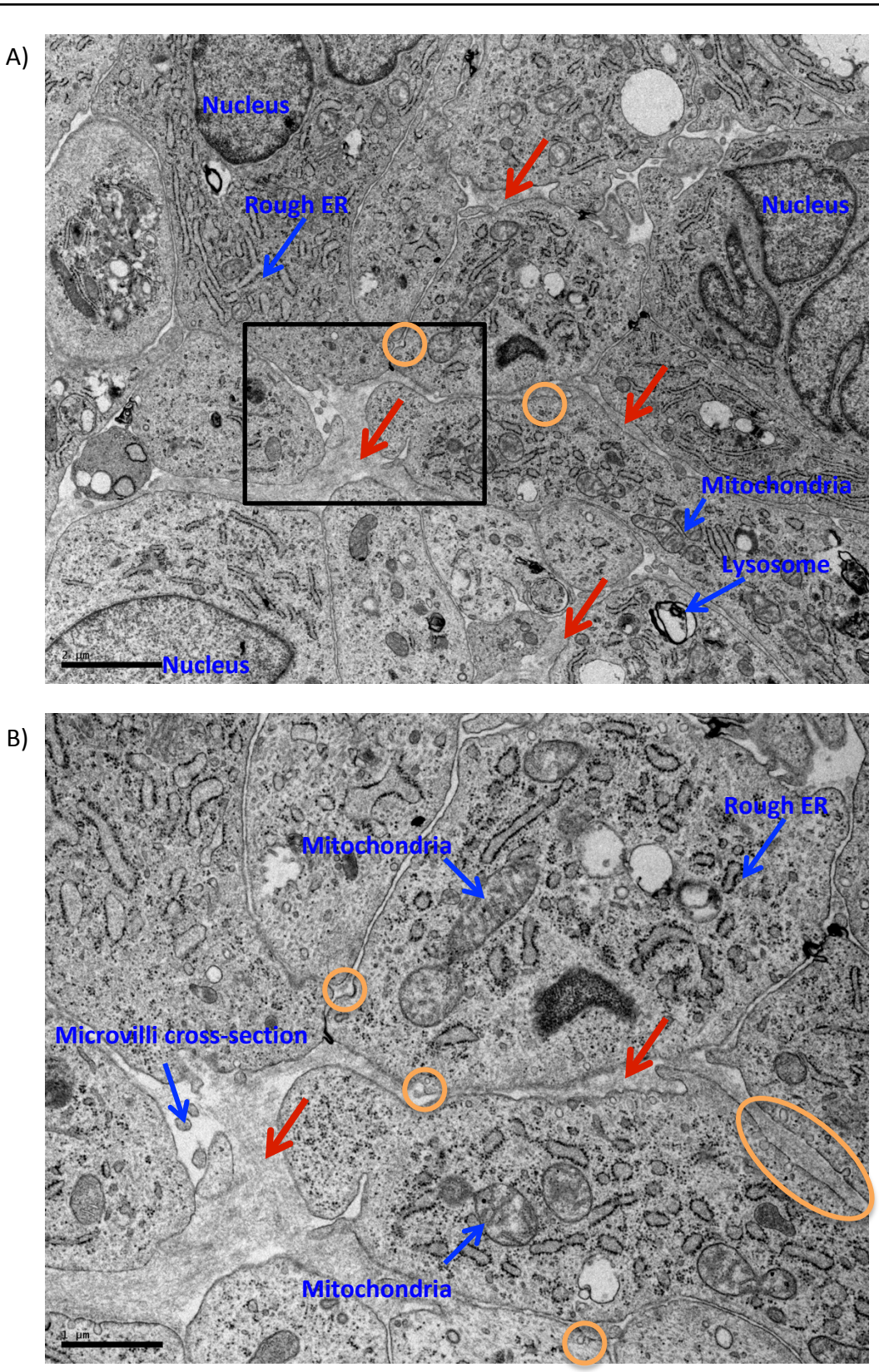

Figure 3. 12. Transmission electron microscopy (TEM) for IPF spheroids.

(A) Magnification x10000. Scale bar 2 μm. (B) Greater magnification of black box shown in panel A (x20000). Scale bar 1 μm. Fibrillar ECM (red arrows) and invaginations (orange circles). Data representative of three IPF donors

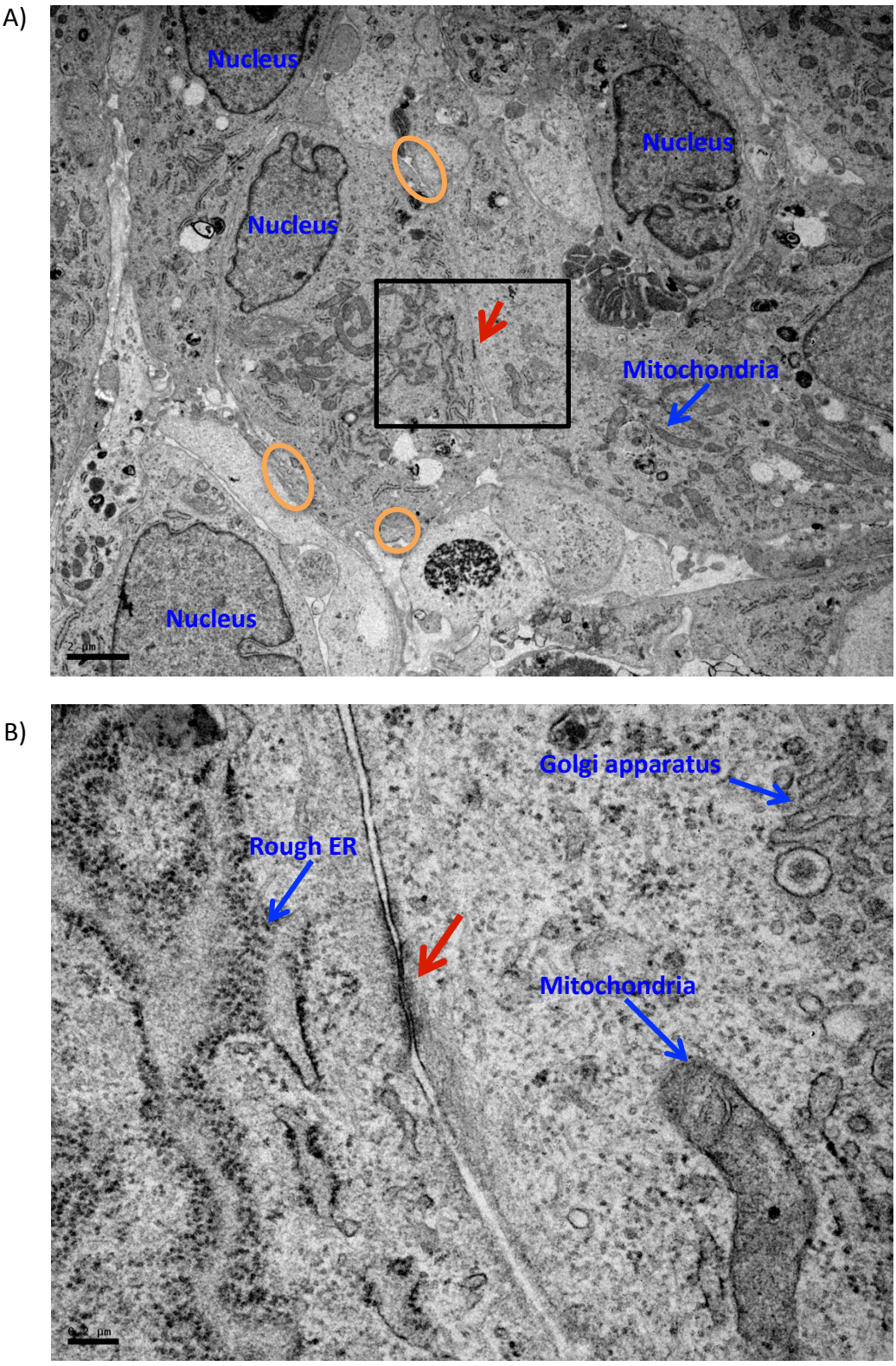

Figure 3. 13. Transmission electron microscopy (TEM) for IPF spheroids illustrating the presence of junctions.

(A) Magnification x6000. Scale bar 2 μm. (B) Greater magnification of black box shown in panel A (x50000). Scale bar 0.2 μm. Junctions (red arrows) and invaginations (orange circles). Data representative of three IPF donors.

3.1.4. Summary

The results described in this section aimed to illustrate any morphological differences between cells isolated using two different isolation protocols and to determine the propensity of lung fibroblasts to form 3D spheroid structure. The results showed:

- Non-IPF pHLF isolated from digested lungs have a more myofibroblastic phenotype with high expression of αSMA and Ki-67 at baseline, in comparison to non-IPF pHLF derived from explant cultures.
- In the presence of TGFβ, αSMA expression increased in both non-IPF and IPF pHLF-Ex, however TGFβ had not effect on αSMA expression of pHLF-Di. Nevertheless, TGFβ accelerated the rate of proliferation in both non-IPF pHLF-Ex and pHLF-Di.

- Both non-IPF and IPF pHLF were able to form spheroids within 24 hours of incubation with the size remaining relatively constant over the subsequent 96 hours.
- Morphologically, IPF spheroids appeared to have a smoother surface in comparison to non-IPF spheroids. However, there were a few similarities including the presence of microvilli and ECM deposits on the surface of the spheroids. Furthermore probable apoptotic cells were also visible on both non-IPF and IPF spheroids.
- TEM analysis demonstrated that IPF fibroblast spheroids were more compact with the presence of tight/adherens junctions which were not evident in non-IPF spheroids. Fibrillar matrix deposits were evident in both non-IPF and IPF spheroids which may potentially be fibrillar collagen.

3.2. Spheroid characterisation part 1: αSMA, Collagen and TGFβ expression

3.2.1. Introduction

Some of the key characteristics shown in the lungs of IPF patients include increased populations of αSMA positive myofibroblasts, excessive production of collagen, and increased synthesis of the potent profibrotic mediator, TGFβ. In order to develop a novel 3D *in vitro* fibrosis model it is vital to investigate whether these features are also evident in the fibroblast spheroids.

3.2.2. IPF spheroids have a myofibroblastic phenotype

As demonstrate earlier in **Section 3.1,** there was no significant difference in baseline expression levels of αSMA in non-IPF and IPF fibroblasts cultured as a 2D monolayer. To investigate whether this was also the case in a 3D system, cells in DMEM with 0.4 % serum and 100μM ascorbic acid were seeded into a 96-well plate (pre-coated with agarose) for 24 hours for spheroid formation and collected for mRNA, protein, and immunohistochemical analysis following 24 hours and 96 hours incubation.

Figure 3.14A illustrates that the mRNA levels of *ACTA2* in IPF spheroids (n=10; red triangles) were significantly greater in comparison to non-IPF spheroids (n=10; green circles) when cultured for 24 hours (1 day; p value <0.05, two-way ANOVA). However, after 96 hours (4 days) of spheroid incubation the mRNA levels between non-IPF and IPF spheroids were not significantly different. Nevertheless, αSMA protein levels (**Figure 3.14B** and **C**) were significantly elevated in IPF spheroids both at 24 hours (6-8 fold increase; p<0.01, two-way ANOVA) and 96 hours (3-6 fold increase; p<0.05, two-way ANOVA) of incubation in comparison to non-IPF (<2 fold). The densitometry data were normalised to loading control (i.e. ERK2). This is also demonstrated immunohistochemically (**Figure 3.14D, E and F**) with strong immunoreactivity shown in IPF spheroid sections (brown staining). In addition, αSMA expression in both non-IPF and IPF spheroids was more or less stable over time with no significant difference in protein levels between 24 hours and 96 hours of spheroid incubation (**Figure 3.14C**). These data suggests that IPF fibroblasts have a more myofibroblastic phenotype in a 3D system, in comparison to non-IPF.

The next step involved investigating the deposition of collagen within these spheroids. As stated earlier, both non-IPF and IPF spheroids seem to show fibrillar ECM deposits which may potentially be collagen (**Section 3.1; Figures 3.11**, **3.12**, and **3.13**). To investigate this, modified Martius Scarlet Blue (MSB) staining was performed to visualise the architecture of connective tissue on non-IPF and IPF spheroids (**Figure 3.15**). The results illustrate clear organisation of the cells in the spheroids with a greater intensity of blue staining (collagen) in IPF spheroids in comparison to non-IPF. To quantify this data, HPLC was performed. **Figure 3.16A** shows that both non-IPF and IPF fibroblasts produce collagen, with slightly elevated levels in IPF spheroids (24 hours post seeding). In non-IPF spheroids, the collagen concentration ranged between 14-88 ng (n=10), whereas the collagen concentration for IPF spheroids ranged between 32-185 ng (n=12; $p<0.05$, student T-test). Furthermore, over time (94 hours) the levels remain relatively stable across the majority of non-IPF or IPF donors (**Figure 3.16B** and **C**, respectively).

Since collagen types I and III are predominately found in the lung (Raghu et al., 1985), the type of collagen deposited by these fibroblast spheroids was investigated. Prior to this, immunohistochemical staining for collagen I and collagen III was performed on sections from both non-IPF (**Figure 3.17**) and IPF formaldehyde-fixed paraffin-embedded lung tissue (**Figure 3.18** and **Figure 3.19**). In non-IPF lung, immunostaining for both collagen I and III localised to AECs and smooth muscle cells surrounding blood vessels (positive for αSMA; **Figure 3.17D**). In IPF lung, both collagen types I and III were present throughout the tissue, including localisation to myofibroblasts (αSMA positive cells) of fibrotic foci. Interestingly, strong immunoreactivity for both collagen types was also evident in the basement membrane underlying bronchial epithelial cells (**Figure 3.19**) which to our knowledge have not been reported before.

Figure 3.20 illustrates that mRNA levels for *COL1A1* and *COL3A1* between non-IPF (n=7) and IPF (n=10) spheroids are not significantly different at both 24 and 96 hours of incubation (two-way ANOVA). **Figure 3.21** shows that both non-IPF and IPF spheroids express collagen type I and collagen type III with slightly stronger immunoreactivity shown in IPF spheroids.

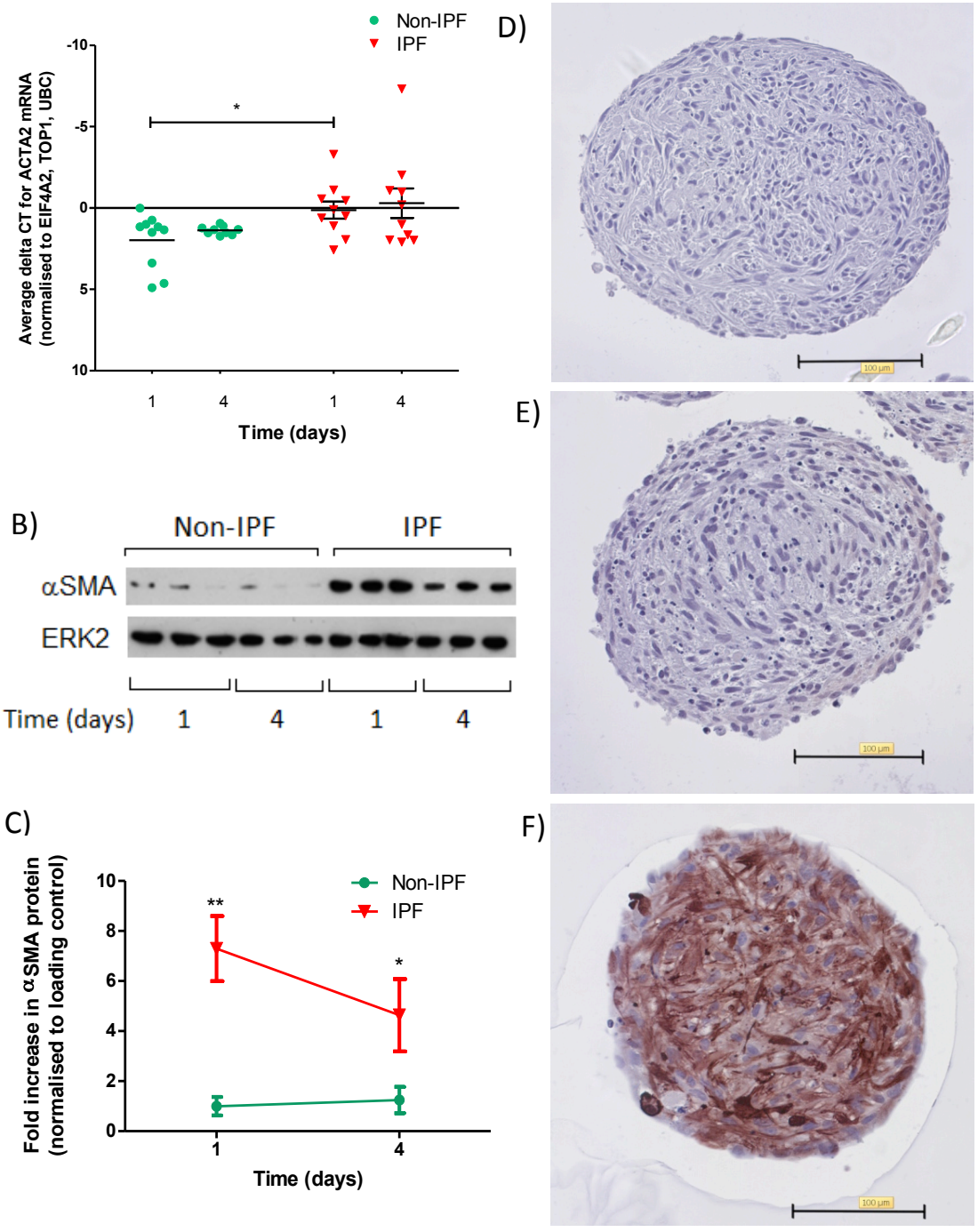

Figure 3. 14. αSMA expression in spheroids.

(A) mRNA levels of *ACTA2* within non-IPF (n=10 donors) and IPF spheroids (n=10). Data, expressed as ΔCt, were normalised to three housekeeping genes (*EIF4A2*, *TOP1*, and *UBC*). (B) Western blot illustrating αSMA protein levels with ERK2 as a loading control. (C) Representative densitometry data shown for one non-IPF and one IPF line. *p<0.05, **p<0.01 (two-way ANOVA. Post hoc test: bonferroni correction). (D) Immunohistochemistry for IgG control, (E) Non-IPF αSMA, and (F) IPF αSMA, 24 hours post seeding. Magnification x200. Scale bar 100 μm. Representative data shown for 4 non-IPF and 6 IPF donors.

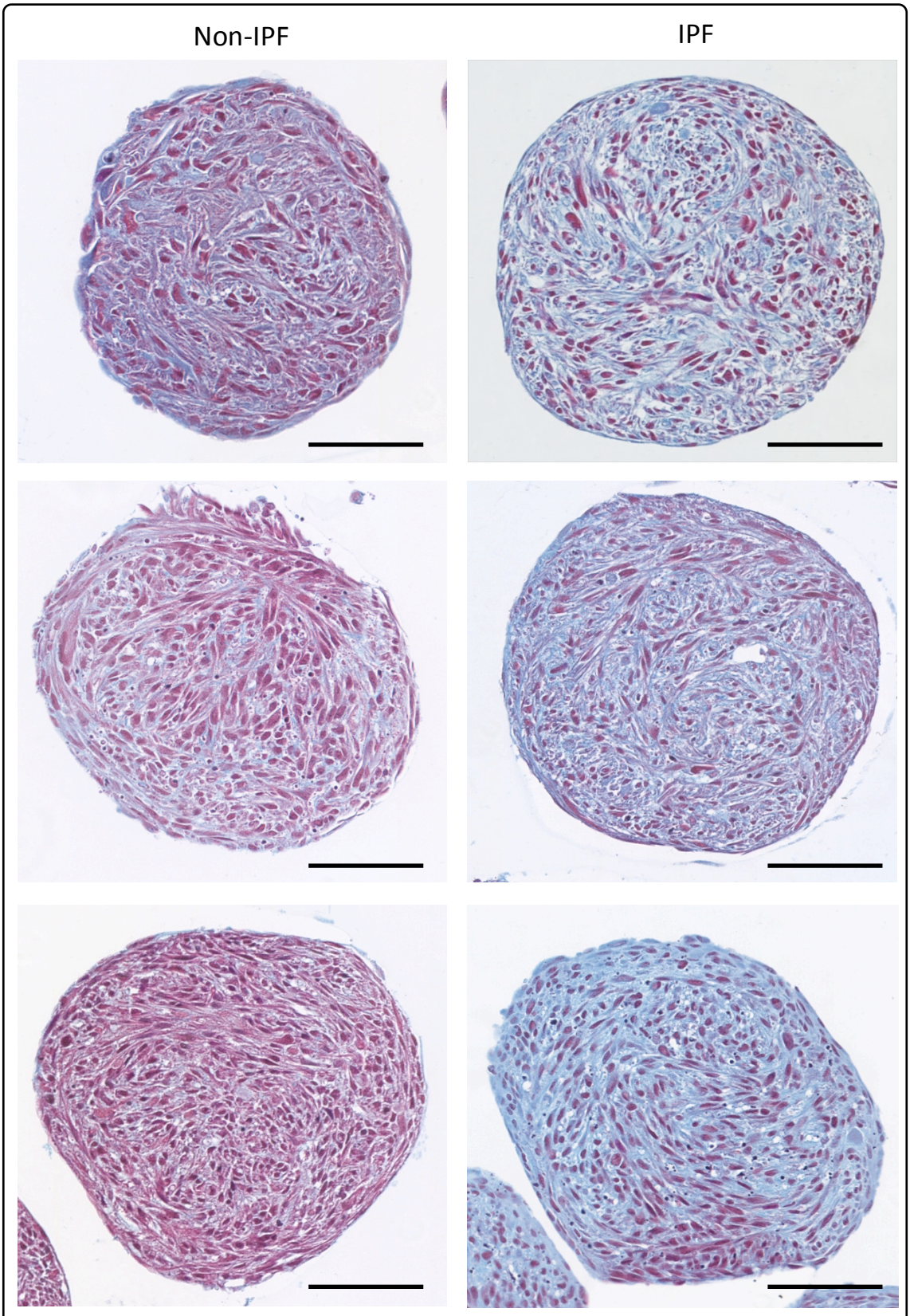

Figure 3. 15. MSB staining for non-IPF and IPF spheroid.

Paraffin-embedded non-IPF (left) and IPF (right) spheroid sections. Each spheroid represents a different donor. Blue indicates collagen deposition. Magnification x200. Scale bar = 100 μm.

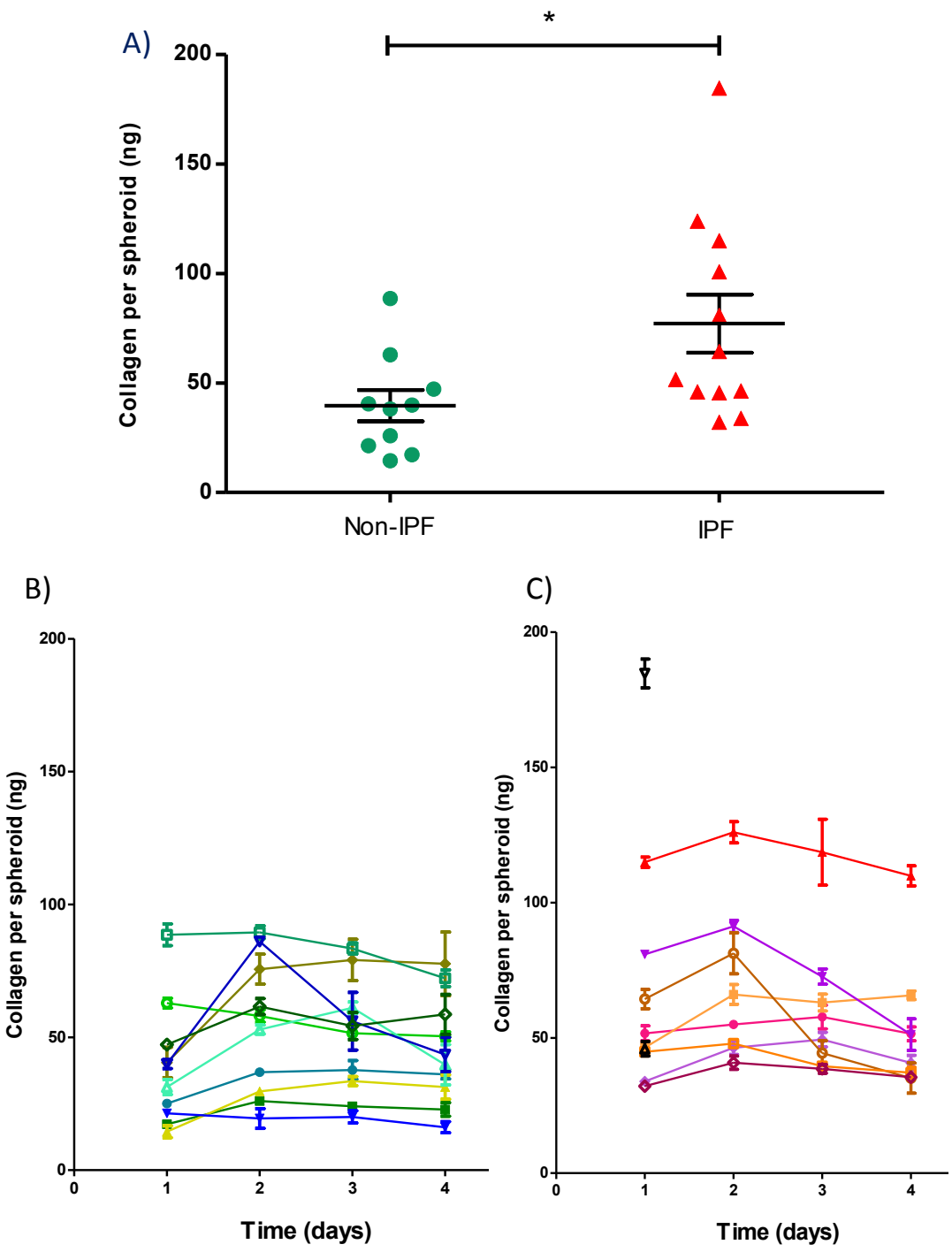

Figure 3. 16. Collagen production in non-IPF and IPF spheroids.

Spheroids were formed and hydrolysed in 6 M HCl for analysis of hydroxyproline levels by HPLC. (A) Collagen levels per spheroid, 24 hours post seeding. Non-IPF spheroids are represented as green circles (n=10) and IPF spheroids are represented as red triangles (n=12). Change in collagen levels over time within non-IPF (B) and IPF spheroids (C). Each line represents an individual patient. * $p<0.05$ (Student T-test).

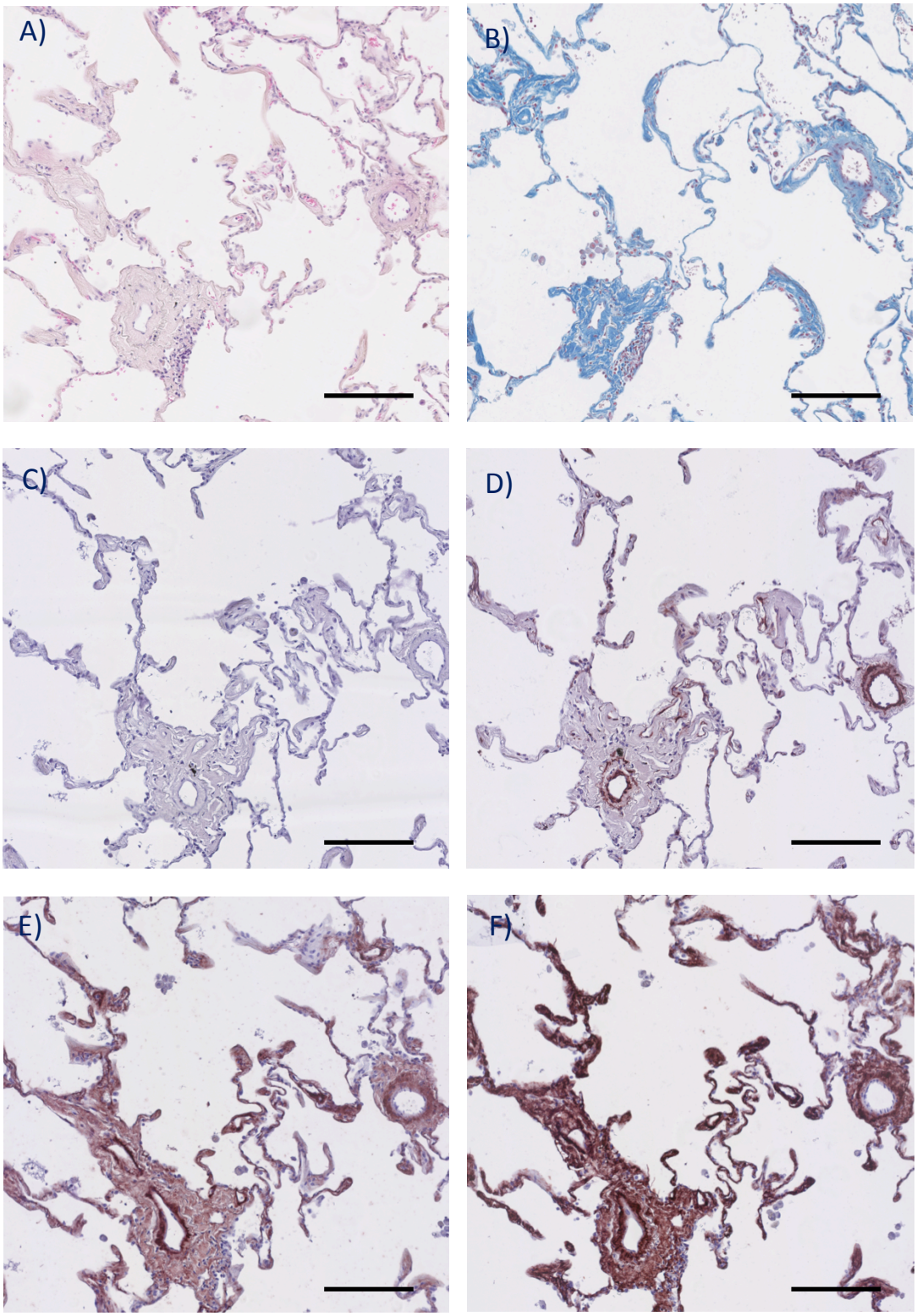

Figure 3. 17. Immunohistochemical staining of paraffin embedded non-IPF lung serial sections.

(A) H&E staining; (B) MSB staining, blue indicates collagen deposition; (C) IgG isotype control; (D) αSMA; (E) collagen type I; (F) collagen type III. Magnification x100. Scale bar = 200 μm

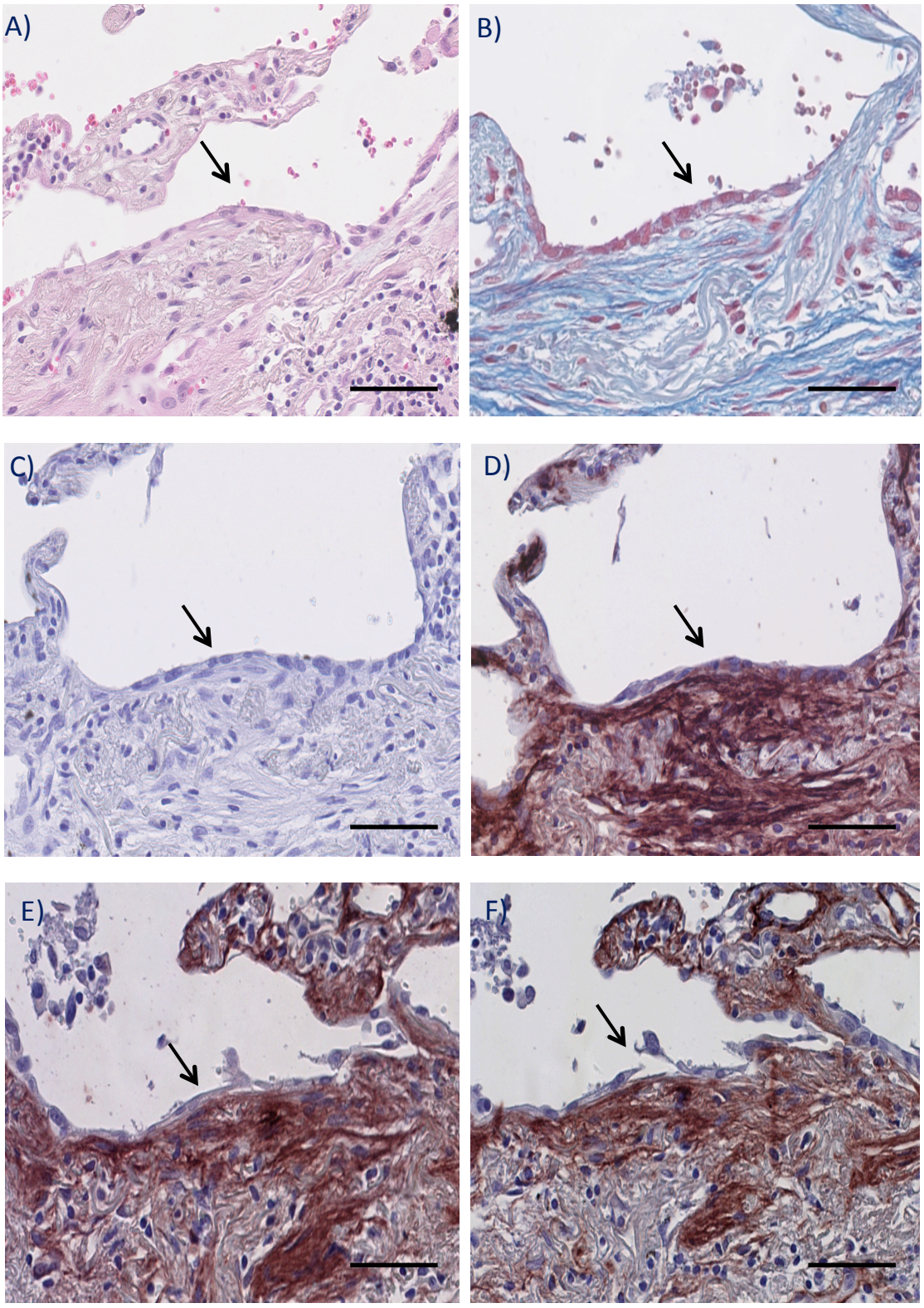

Figure 3. 18. Immunohistochemical staining of a fibrotic focus in paraffin embedded IPF lung serial sections

(A) H&E staining; (B) MSB staining; (C) IgG isotype control; (D) αSMA; (E) collagen type I; (F) collagen type III. Fibrotic focus is indicated by arrows. Magnification x200. Scale bar = 100 μm

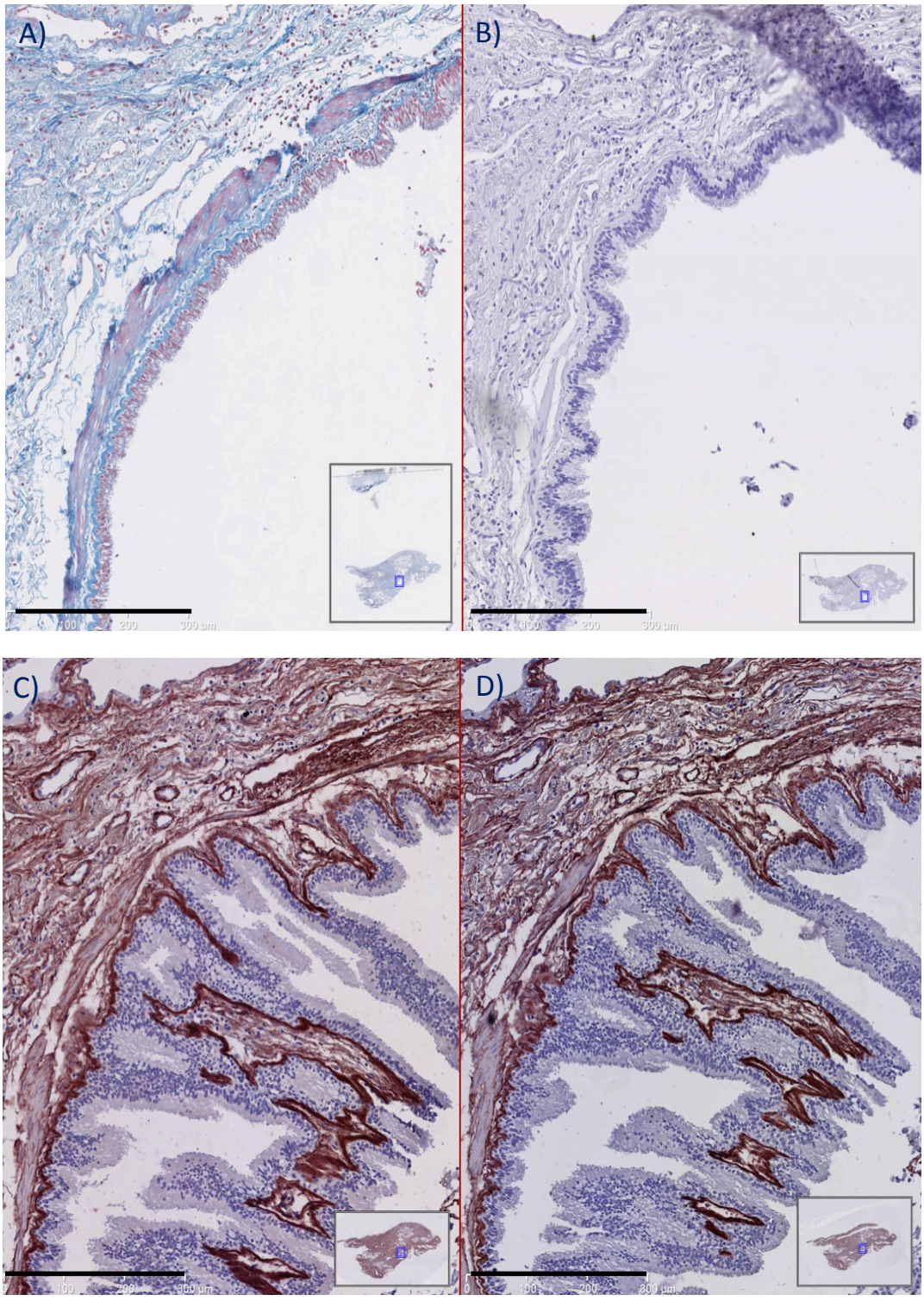

Figure 3. 19. Immunohistochemical staining illustrating collagen types I and III immunoreactivity at the basement membrane of paraffin embedded IPF lung serial sections

(A) MSB staining; (B) IgG isotype control; (C) collagen type I; (D) collagen type III. Magnification x200. Inserts highlight the whole tissue section. Scale bar = 300 μm

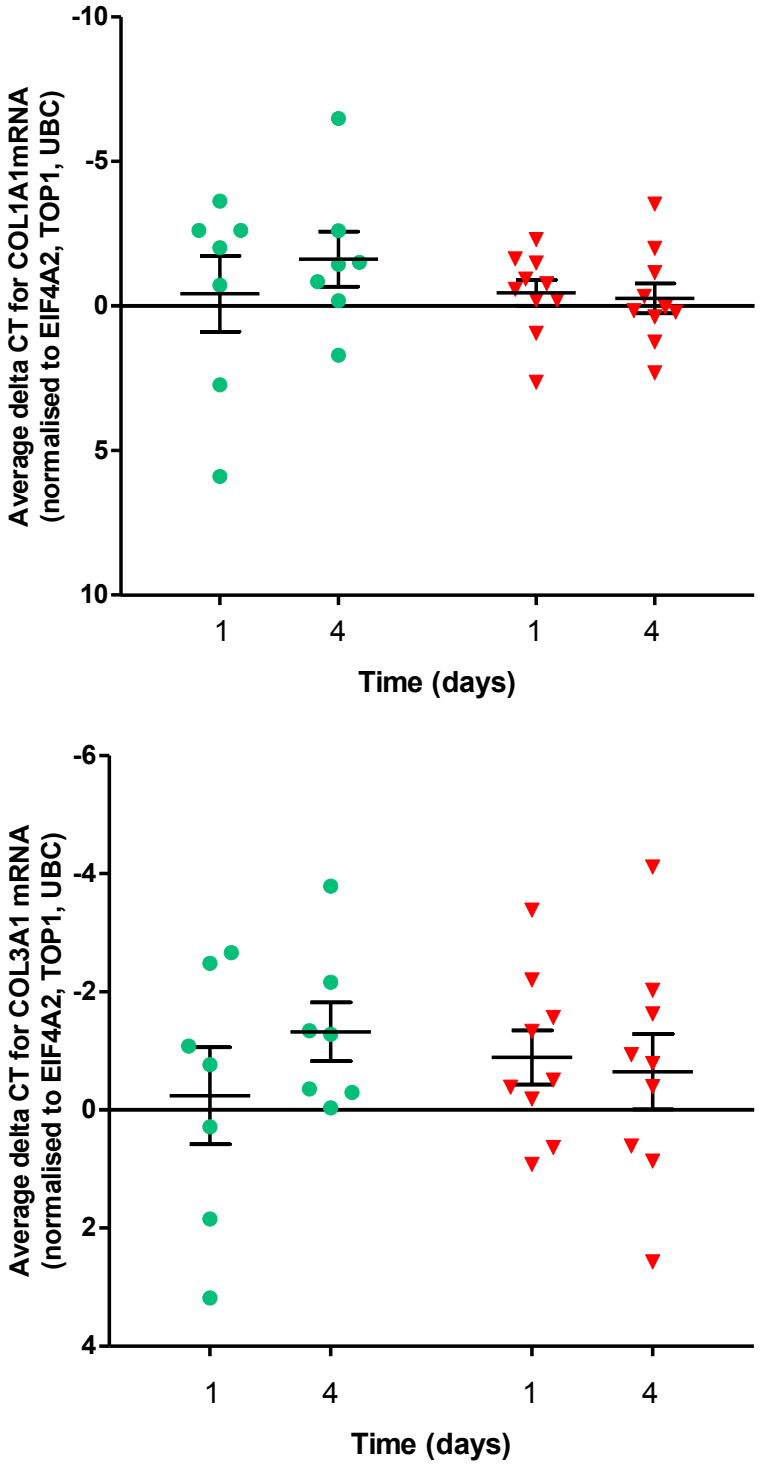

Figure 3. 20. *COL1A1* and *COL3A1* mRNA levels in non-IPF and IPF spheroids.

The mRNA levels of (A) *COL1A1* and (B) *COL3A1* in non-IPF (n=7; green circles) and IPF (n=9; red triangles) spheroids were measured by qRT-PCR. All CT values were normalised to three housekeeping genes based on GeNorm analysis (*EIF4A2, TOP1*, and *UBC*). Each point represents an average result from individual patients.

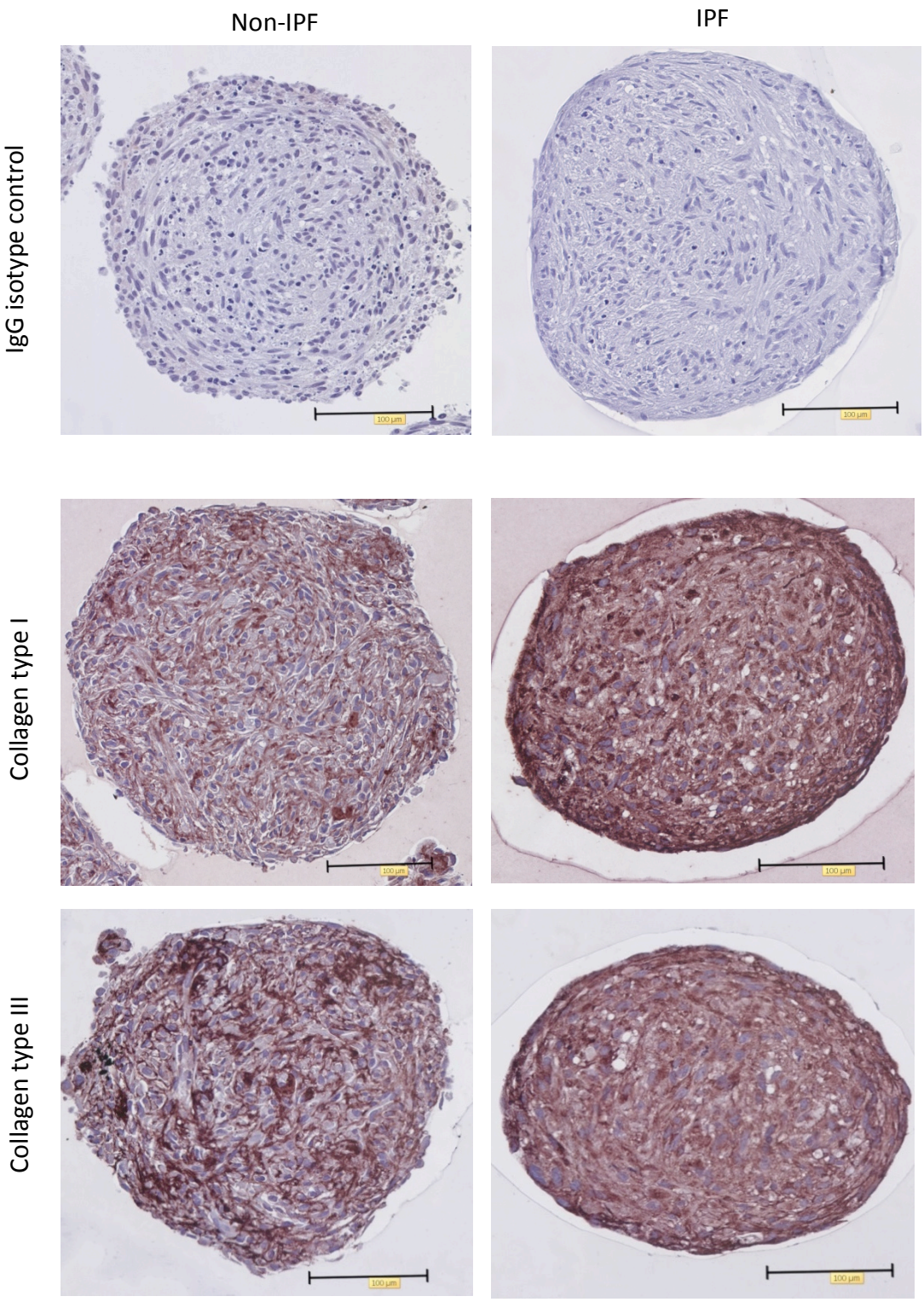

Figure 3. 21. Immunohistochemical staining of collagen types I and III in non-IPF and IPF spheroids.

Paraffin-embedded non-IPF (left) and IPF (right) spheroids were stained with either IgG isotype control or antibodies against collagen type I, or collagen type 3. Magnification x100. Scale bar 100 μm

3.2.3. Spheroids produce high levels of active-TGFβ

TGFβ is widely accepted as a key cytokine involved in the deposition of collagen (Pena et al., 1994; Clark et al., 1997; Garrett et al., 2004; Gu et al., 2007). The current data illustrate that within just 24 hours of spheroid formation, fibroblasts are able to synthesis high levels of collagen (both collagen type I and III). The next step was to investigate whether treating the spheroids exogenously with active TGFβ promotes a further increase in collagen synthesis. The spheroids were cultured for 24 hours in the presence of 1 ng/ml of active TGFβ, prior to analysis. **Figure 3.22** illustrates that exogenous TGFβ had no significant effect on baseline collagen synthesis in either non-IPF or IPF spheroids. Data are representative of two non-IPF and two IPF donors.

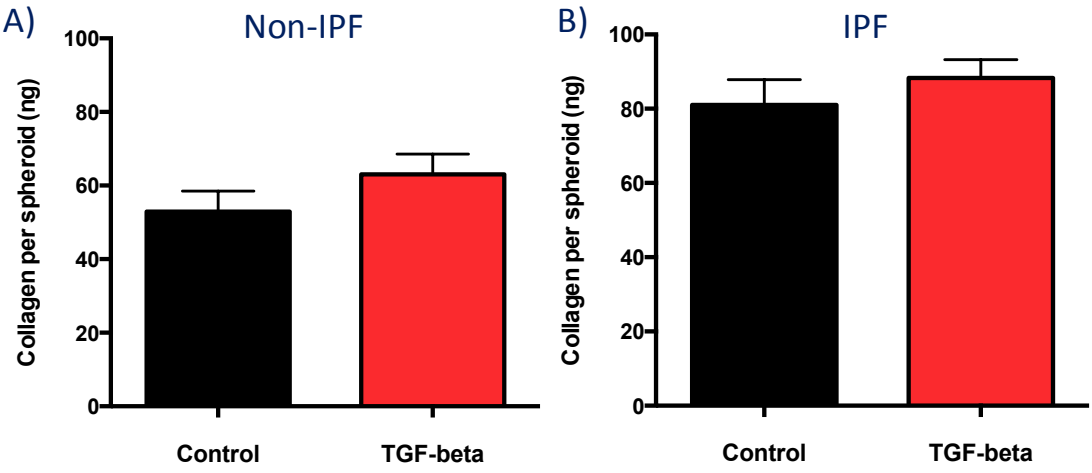

Figure 3. 22. Effect of active TGFβ on collagen synthesis in non-IPF and IPF spheroids.

(A) Non-IPF (n=2) and (B) IPF (n=2) fibroblasts were treated with 1 ng/ml TGFβ. Cells were cultured in agarose-coated 96 well plates and incubated for 24 hours for spheroid formation. HPLC for hydroxyproline was performed following acid hydrolysis of spheroids.

To investigate whether these fibroblast spheroids are capable of synthesising their own active-TGFβ (possibly providing an explanation as to why exogenous TGFβ treatment had no effect on collagen synthesis), a mink lung bioassay was performed to analyse active TGFβ levels in conditioned media (after 24 hrs of spheroid culture). Transformed mink lung epithelial cells (TMLECs) were cultured into 96 well plates (1.6 x 10^4 cells per well) for 3 hours to allow adherence and then washed once in serum free media. TGFβ standard concentrations were

prepared in serum free media. TMLECs were then cultured with either TGFβ standard sample or samples (i.e. conditioned media) for 16 hours. The cells were then lysed and firefly luciferase activity was measured using a luminometer. **Figure 3.23** illustrates the levels of active TGFβ synthesised by the fibroblastic spheroids and secreted into the conditioned medium (24 hours post-seeding). For non-IPF spheroids (n=7) the concentration of active TGFβ in the conditioned medium was <500 pg/mL whilst the concentration for IPF (n=8) ranged between 200-1200 pg/mL. Statistical analysis (Student T-Test) showed there is a significant difference ($p<0.05$) between the levels of active TGFβ in the conditioned media of non-IPF and IPF spheroid.

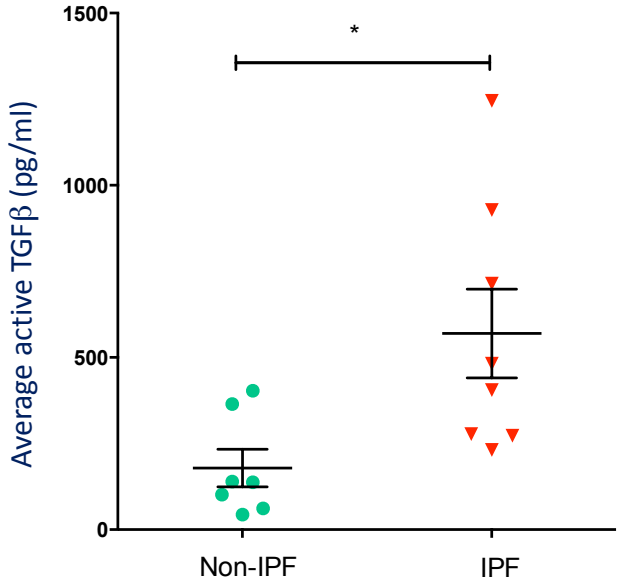

Figure 3. 23. Active TGF-β in conditioned media from non-IPF and IPF spheroids.

Transformed mink lung cells (TMLEC) were cultured with conditioned media of non-IPF (n=7, green circles) and IPF (n=8, red triangles) spheroids (24 hours post-seeding). The TMLC cells were lysed with 1x luciferase reporter buffer followed by the addition of luciferase assay buffer and substrate. The amount of TGFβ produced was then measured using a luminometer. * $p<0.05$, Student T-test.

The experiment was repeated to determine whether active TGFβ was also present in spheroid homogenates and whether the levels changed over time. Conditioned media were collected following 24 hours and 96 hours of spheroid formation. In addition, free-floating spheroids were removed from the culture media and homogenised into 200 μL of fresh serum free media. TMLC cells were treated as described above with TGFβ standard samples, conditioned media, or spheroid homogenates. **Figure 3.24A** illustrates that over 96 hours the levels of

active TGFβ in the conditioned media of IPF spheroids (n=4) is statistically greater in comparison to non-IPF (n=5). In addition, although there is a slight elevation in active TGFβ levels in IPF spheroid supernatants over time (96 hours), this did not reach statistical significance. **Figure 3.24B** demonstrates that active TGFβ is also present within spheroid homogenates in both non-IPF and IPF spheroids with elevated levels in IPF spheroids at both 24 hours ($p<0.001$) and 96 hours ($p<0.01$) of incubation in comparison to non-IPF spheroids. Interestingly however, in IPF spheroids the concentration declines over time (by approximately 50 %). No significant difference is shown in non-IPF spheroids between 24 and 96 hours. Note, the TGFβ levels in the conditioned media shown **Figure 3.24** are consistent with those shown in **Figure 3.23** for the same donors.

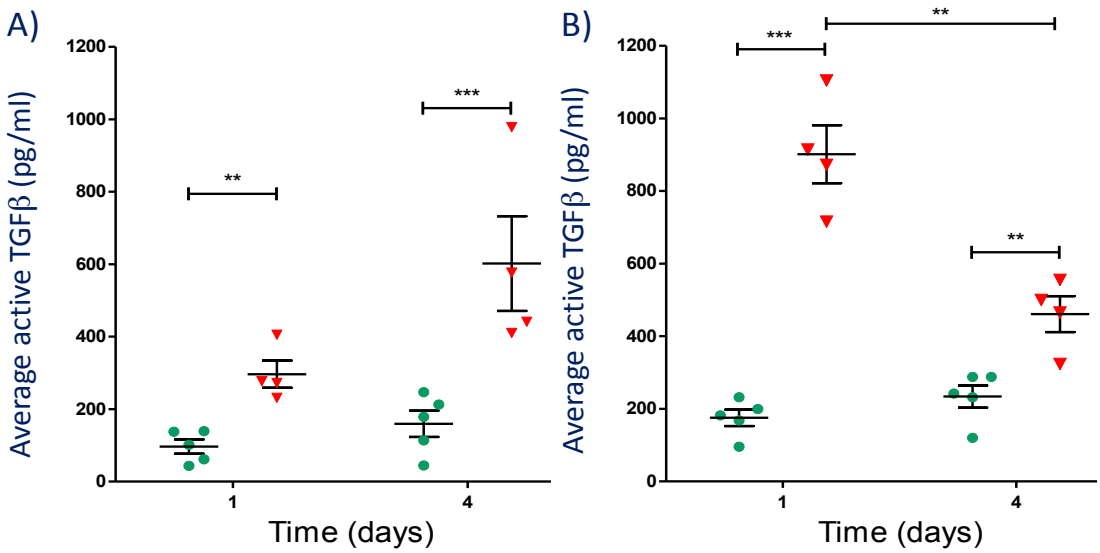

Figure 3. 24. IPF spheroids produce higher levels of active TGFβ.

Spheroids were cultured for 24 hrs (1 day) or 96 hrs (4 days). Transformed mink lung cells (TMLC) were cultured with (A) conditioned media or (B) spheroid homogenates of non-IPF (n=5, green circles) and IPF (n=4, red triangles) spheroids. Luciferase activity was measured by luminescence, and equated to TGFβ concentration by reference to a standard curve. * $p<0.05$, ** $p<0.01$, *** $p<0.001$, Two-way ANOVA (post hoc test: bonferroni correction).

3.2.4. TGFβ activation is independent of TSP-1

Since non-IPF and IPF spheroids are capable of synthesising collagen and active TGFβ (with higher levels in IPF spheroids), the next step was to investigate possible upstream mediators of TGFβ activation. Previous studies have shown TSP-1 (a multifactorial ECM protein) (Armstrong and Bornstein, 2003) is able to activate TGFβ making it readily available to associate with its

receptor and activate downstream signalling events (Crawford et al., 1998; Chen et al., 2009). To address whether this was also the case in this 3D system the spheroids were treated with the TSP-1 inhibitor LSKL. LSKL is an amino acid sequence located near the amino terminal of LAP. A particular tetrapeptide sequence of TSP-1 (KRFK) is able to interact with LSKL resulting in a conformational change in LAP leading to active TGFβ release. Since the conserved LSKL sequence in LAP is necessary for TSP-1 induced TGFβ activation, the addition of a mimetic peptide of this sequence can inhibit the interaction by acting as a competitive antagonist (Xie et al., 2010). As a negative control, a scrambled peptide (SLLK) was used. Cells were seeded for spheroid formation in the presence of either vehicle control (1 % DMSO in 0.4 % media), LSKL, or SLLK at concentrations ranging from 0.0001 μM to 10 μM, for 24 hrs. Spheroids were analysed to determine the collagen content whilst the conditioned media were collected to determine active TGFβ concentrations by performing the mink lung bioassay. As shown in **Figure 3.25** LSKL had no effect on collagen synthesis in either non-IPF (n=2) or IPF (n=1) spheroids and **Figure 3.26** illustrates that this inhibitor had no significant effect on TGFβ activation in non-IPF or IPF spheroids. A slight decline in active TGFβ levels in IPF spheroids was shown with 10 μM of LSKL (based on the curve fit), however statistical analysis (one-way ANOVA) showed this was not significant. This suggests that TGFβ activation and collagen synthesis is not dependent on TSP1.

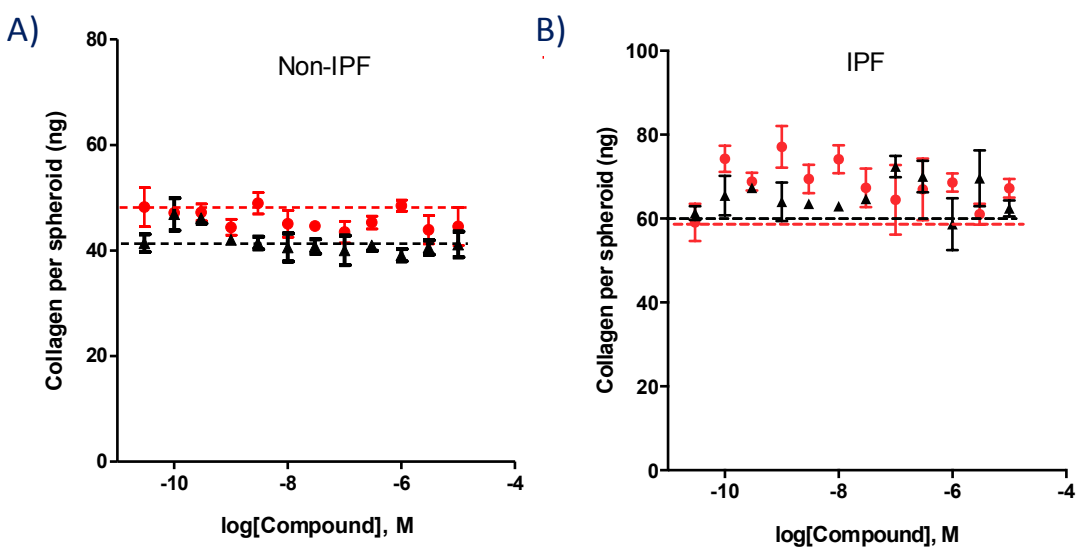

Figure 3. 25. Effect of TSP-1 inhibition (LSKL) on collagen synthesis in non-IPF and IPF spheroids.

Cells were treated with either vehicle control (levels shown as dotted lines), SLLK (black), or LSKL (red) and then cultured for spheroid formation for 24 hours. HPLC was performed on the spheroids to determine collagen content. (A) Non-IPF spheroids (data representative of two donors) and (B) IPF spheroids (n=1).

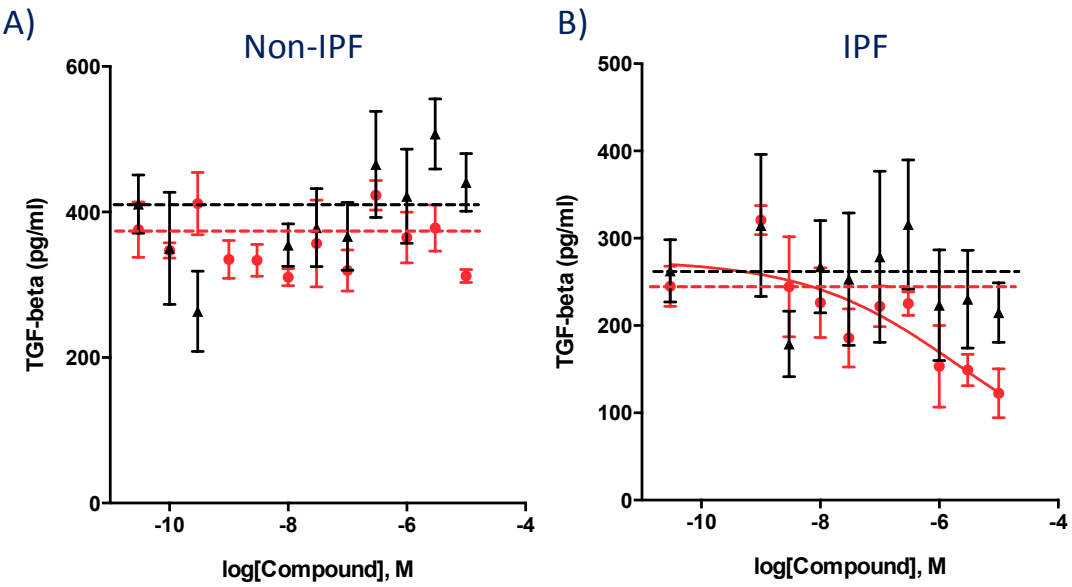

Figure 3. 26. Effect of TSP-1 inhibitor (LSKL) on levels of active TGFβ in non-IPF and IPF spheroids.

Cells were treated with either vehicle control (dotted lines), LSKL (red), or SLLK (negative control; black) and then cultured for spheroid formation for 24 hours. Mink lung bioassay was used to determine the concentration of active TGFβ within the supernatants. (A) Non-IPF spheroids (data representative of two donors) and (B) IPF spheroids (n=1).

3.2.5. TGFβ activation is dependent on integrins with no effect on collagen synthesis

As well as TSP-1, studies have also shown that integrins play a key role in the activation of TGFβ. LAP contains an RGD sequence to which integrins can associate and promote a conformational change in LAP leading to the release of TGFβ from the latency complex. Integrins that have been formally demonstrated to liberate active TGFβ include αvβ3, αvβ5, αvβ6 (present on epithelial cells), and αvβ8 (Munger et al., 1999; Mu, 2002; Asano et al., 2005a, 2005b).

The mRNA levels of *ITGAV, ITGB3, ITGB5,* and *ITGB8* were assessed in both non-IPF and IPF spheroids 24 hours and 96 hours post-seeding. All ΔCt values were normalised to the housekeeping genes *EIF4A2, TOP1*, and *UBC*. **Figure 3.27** illustrates that *ITGAV* and *ITGB5* mRNA levels were statistically greater in IPF spheroids at both time points in comparison to non-IPF ($p<0.01$ and $p<0.05$, respectively; Two-way ANOVA), however *ITGB3* and *ITGB8* mRNA

levels were relatively similar in non-IPF and IPF spheroids. Each point represents average ΔCt values from different donors.

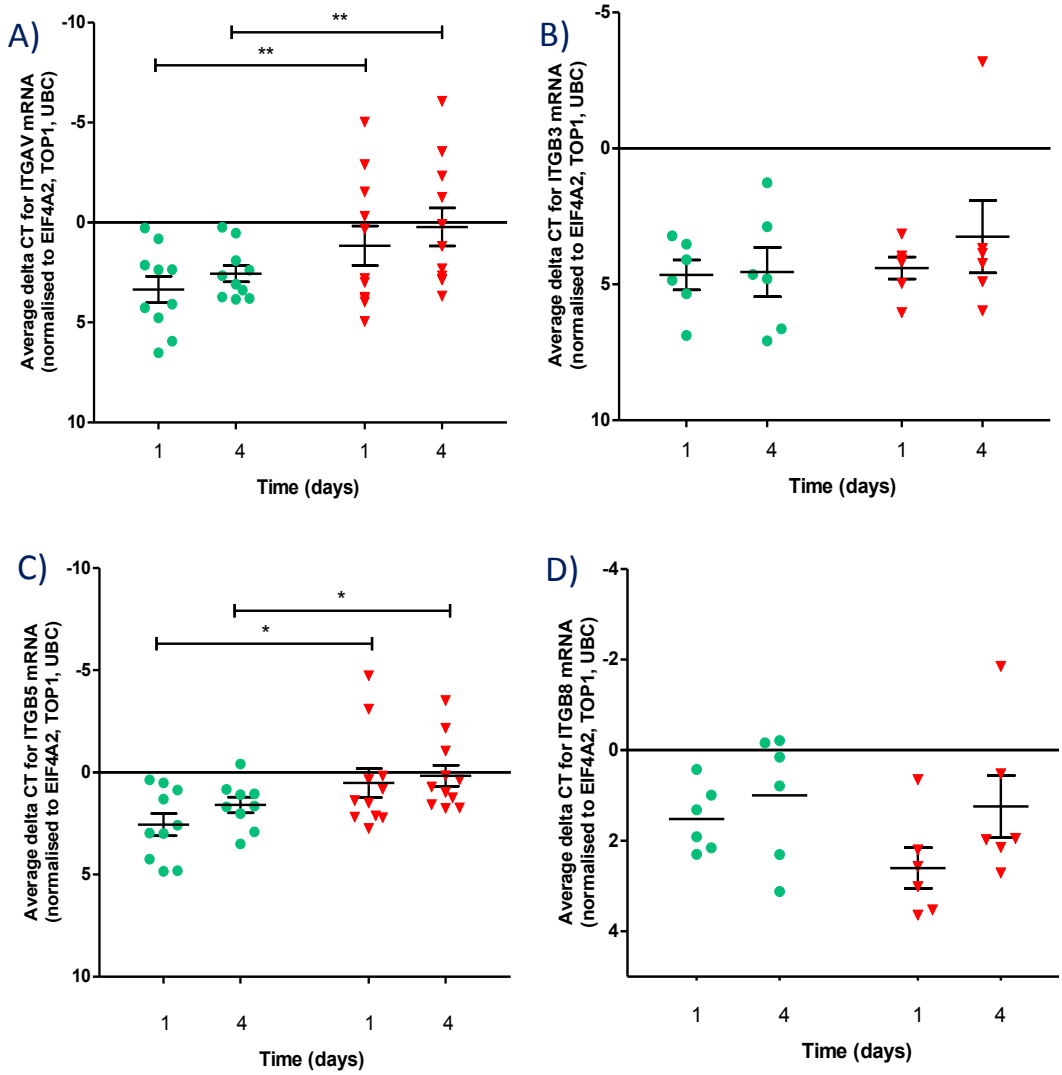

Figure 3. 27. *ITGAV, ITGB3, ITGB5*, and *ITGB8* mRNA levels.

Spheroids were collected 24 – 96 hours post seeding. RNA was extracted from the spheroids for qRT-PCR to analyse the mRNA levels of (A) *ITGAV*, (B) *ITGB3*, (C) *ITGB5*, (D) *ITGB8*. All data points were normalised to three housekeeping genes based on GeNorm analysis (*EIF4A2, TOP1*, and *UBC*). Non-IPF and IPF spheroids are represented as green circles and red triangles, respectively. * p<0.05, ** p<0.01, Two-way ANOVA (post hoc test: bonferroni correction).

To determine the effect of integrins on TGFβ activation and collagen synthesis, three small molecule integrin inhibitors were assessed, all of which were a kind gift from GSK. These were: dual integrin β3/β5 inhibitor, integrin β8 inhibitor, and integrin β3 inhibitor. Spheroids were

treated with the compounds at concentrations ranging from 0.0001 μM to 10 μM for 24 hours either prophylactically (prior to spheroid formation) or therapeutically (24 hours after spheroid formation). The conditioned media were collected to determine the levels of active TGFβ via mink lung bioassay, whilst the spheroids were used to assess collagen content. β3/β5 antagonist) and β8 antagonist had no effect on collagen synthesis in non-IPF or IPF spheroids (**Figure 3.28** and **Figure 3.29**; dotted lines represent collagen levels for spheroids treated with vehicle control). The integrin β3 inhibitor also showed no effect on collagen production in non-IPF spheroids. However, a slight attenuation in collagen synthesis in IPF spheroids was evident at high concentrations of the compound (1-10 μM, with approximately a 30 % attenuation in collagen levels at 10 μM). The IC50 for this compound was calculated as 2.1 μM (variable slope four parameter curve fit; R^2 = 0.178), which is in stark contrast to other *in vitro* assays, where this compound demonstrates highly potency and an IC50 in the nanomolar range (personal communication from Richard Hatley, GSK). The attenuation in collagen synthesis seen here with >1 μM concentration may therefore be the result of toxicity. However, further work is required to confirm this.

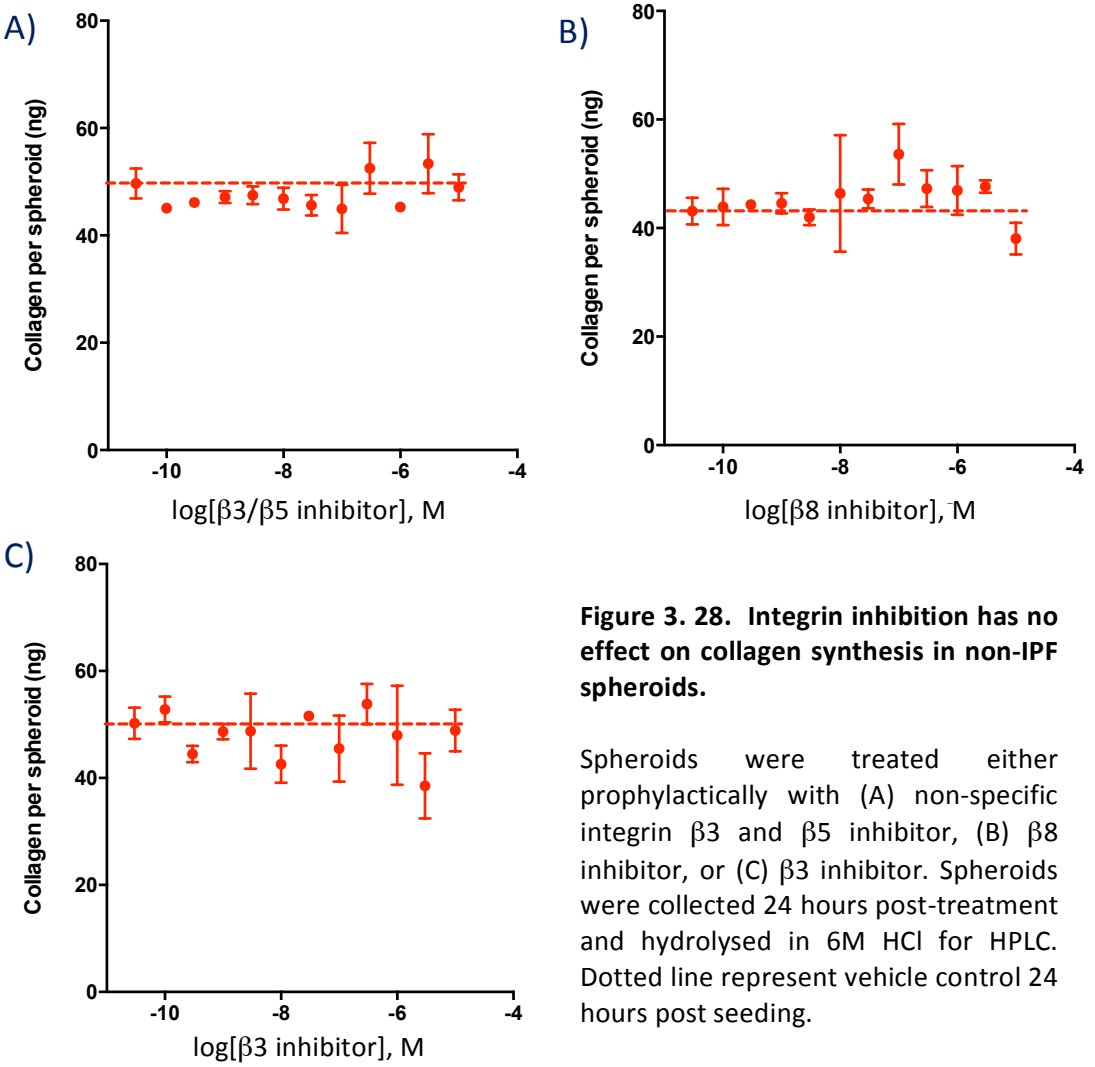

Figure 3. 28. Integrin inhibition has no effect on collagen synthesis in non-IPF spheroids.

Spheroids were treated either prophylactically with (A) non-specific integrin β3 and β5 inhibitor, (B) β8 inhibitor, or (C) β3 inhibitor. Spheroids were collected 24 hours post-treatment and hydrolysed in 6M HCl for HPLC. Dotted line represent vehicle control 24 hours post seeding.

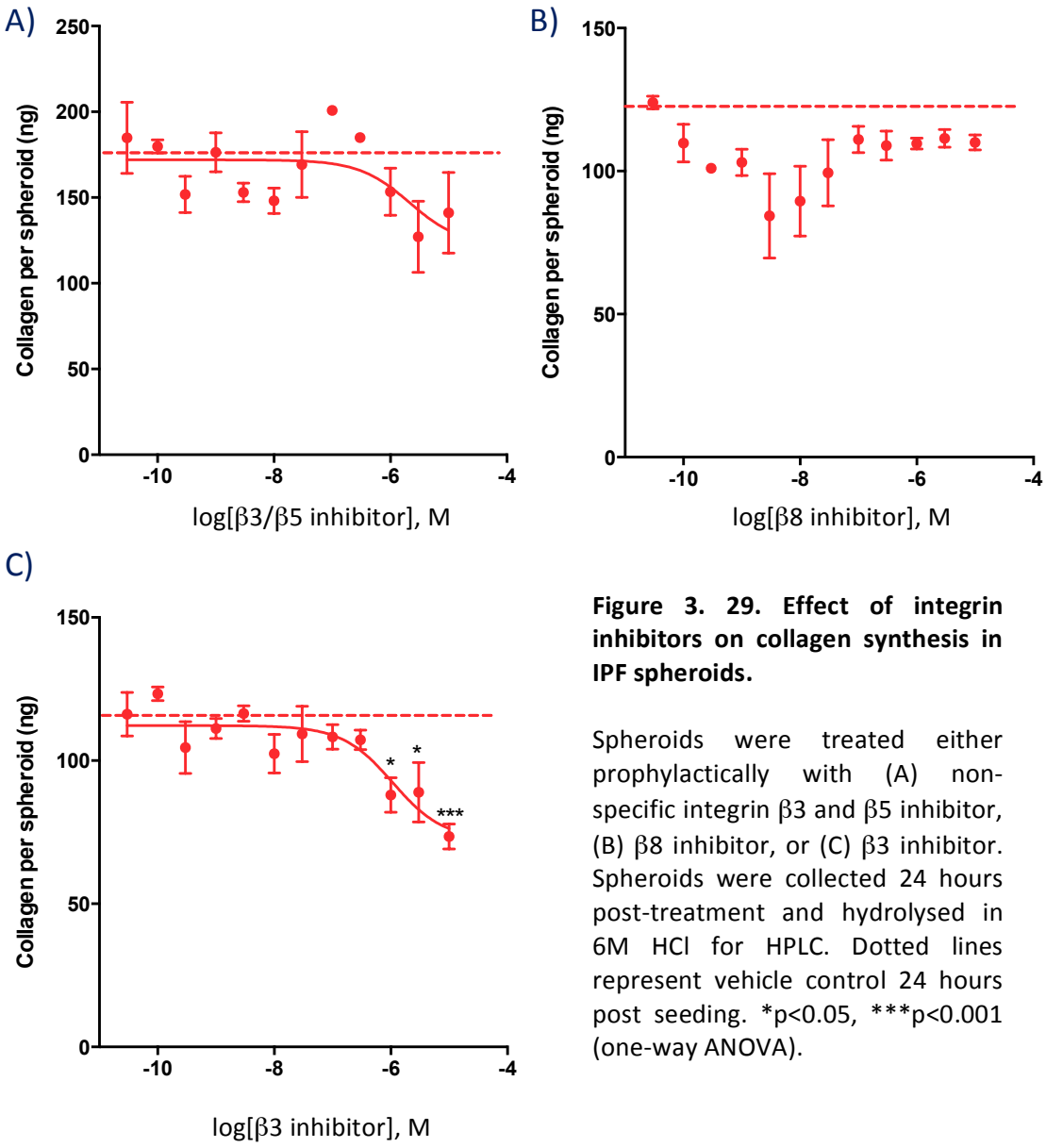

Figure 3. 29. Effect of integrin inhibitors on collagen synthesis in IPF spheroids.

Spheroids were treated either prophylactically with (A) non-specific integrin β3 and β5 inhibitor, (B) β8 inhibitor, or (C) β3 inhibitor. Spheroids were collected 24 hours post-treatment and hydrolysed in 6M HCl for HPLC. Dotted lines represent vehicle control 24 hours post seeding. *p<0.05, ***p<0.001 (one-way ANOVA).

To determine the effect of these compounds on the activation of TGFβ, a mink lung bioassay was performed. **Figure 3.30A** illustrates that the dual β3/β5 antagonist attenuated TGFβ activation with an IC50 of 11.2 μM (R^2 = 0.3017). **Figure 3.30B** shows a concentration-dependent partial attenuation of TGFβ activation (~30 % decrease) in the presence of the β8 antagonist, albeit with an IC50 of 4.75 nM (R^2 = 0.3538). **Figure 3.30C** shows that 10 μM of the β3 inhibitor decreased the levels of active TGFβ by ~50 %. Based on the IC50s for the dual β3/β5 antagonist and β3 inhibitor the data suggests that these compounds have low potency and low efficacy for non-IPF fibroblasts cultured in this 3D system. Nevertheless, β3 inhibitor

did show a partial attenuation in TGFβ activation with a low IC50 suggesting that TGFβ activation in non-IPF spheroids is at least partially dependent on the β8 integrin. The effects seen by the compounds targeting integrins β3 and β5 may potentially be as a result of toxicity however further experimentation of cytotoxicity is required to draw clear conclusions.

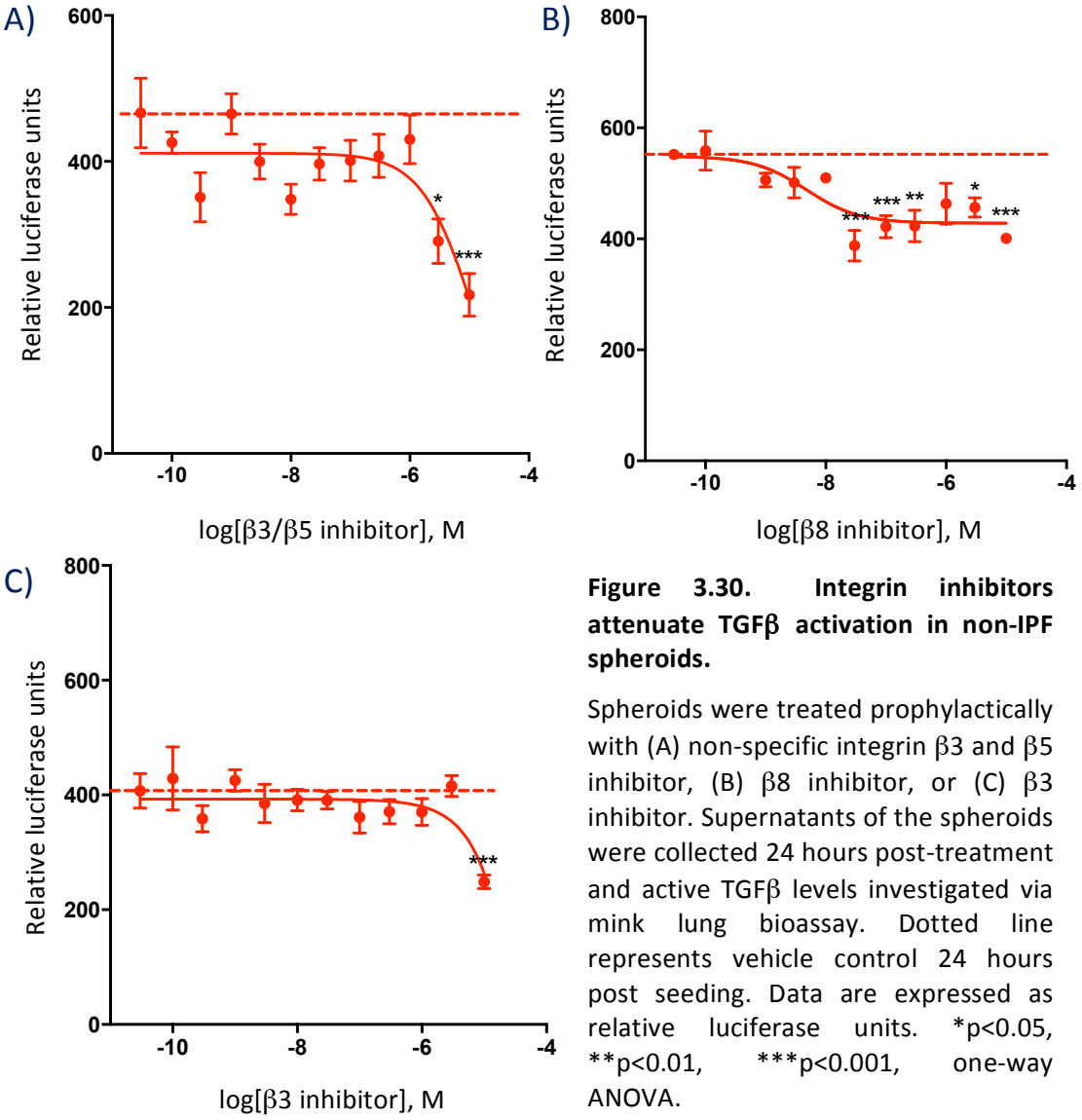

Figure 3.30. Integrin inhibitors attenuate TGFβ activation in non-IPF spheroids.

Spheroids were treated prophylactically with (A) non-specific integrin β3 and β5 inhibitor, (B) β8 inhibitor, or (C) β3 inhibitor. Supernatants of the spheroids were collected 24 hours post-treatment and active TGFβ levels investigated via mink lung bioassay. Dotted line represents vehicle control 24 hours post seeding. Data are expressed as relative luciferase units. *p<0.05, **p<0.01, ***p<0.001, one-way ANOVA.

Figure 3.31 illustrates that all three integrin inhibitors result in a concentration-dependent attenuation in active TGFβ levels in the conditioned media of IPF spheroids. IC50s for β3/β5 inhibitor, β8 inhibitor, and β3 inhibitor were 600 nM (R^2 = 0.6854), 83.6 pM (R^2 = 0.9384), and 21.7 nM (R^2 = 0.8809), respectively. Based on the IC50 values, the β8 integrin inhibitor is more

potent in comparison to β3/β5 inhibitor and β8 inhibitor. In addition, the efficacy of the β8 antagonist is greater in IPF spheroids in comparison to non-IPF spheroids.

Thus, the current data suggest that integrins may promote TGFβ activation in IPF spheroids with partial concentration-dependent attenuation also shown in non-IPF spheroids when treated with the β8 antagonist. However, collagen synthesis in both non-IPF and IPF fibroblast spheroids appears to be largely independent of the activity of the β3, β5 and β8 integrins.

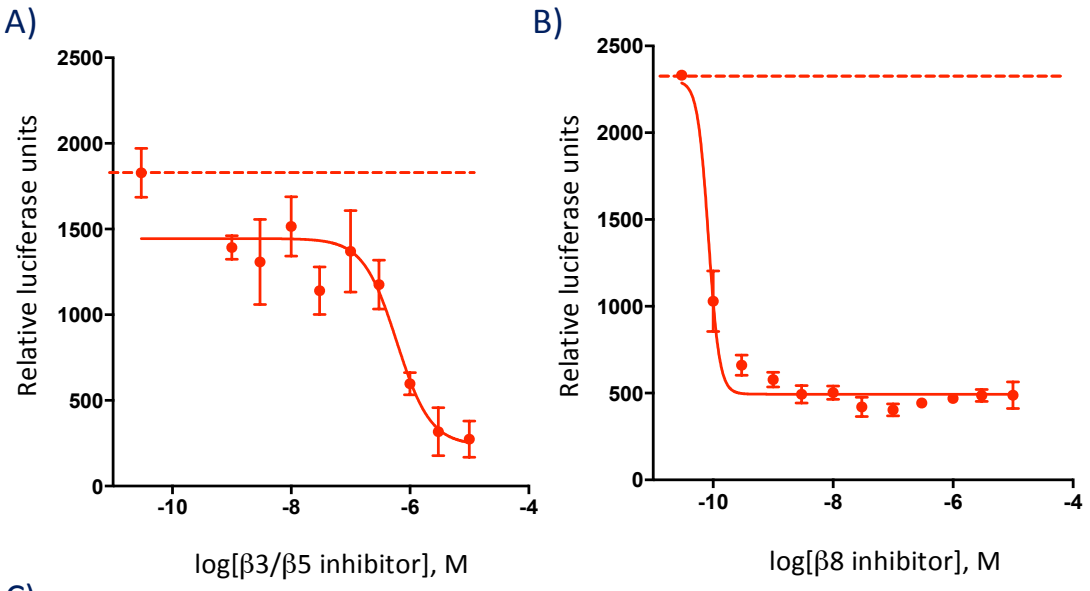

Figure 3. 31. Integrin inhibitors attenuate TGFβ activation in IPF spheroids.

Spheroids were treated either prophylactically with (A) non-specific integrin β3 and β5 inhibitor (IC50 = 600nM), (B) β8 inhibitor (IC50 = 83.6pM), or (C) β3 inhibitor (IC50 = 21.7nM). Supernatants of the spheroids were collected 24 hours post-treatment and were used to determine active TGFβ concentrations via mink lung bioassay. Dotted line represent vehicle control 24 hours post seeding. Data are expressed as relative luciferase units.

3.2.6. Effect of Alk-5 receptor kinase inhibition on collagen synthesis

The above data suggest that blocking the activation of TGFβ (using compounds at relevant concentrations, i.e. <1 μM) has no effect on collagen synthesis. To determine whether antagonising TGFβ signalling has any effect on collagen production, spheroids were treated with a potent and selective ALK5 inhibitor (SB525334A) which has previously been shown to block ALK5 kinase activity *in vitro* with an IC50 of 14.3 nM (Grygielko et al., 2005).

Spheroids were treated with this compound either prophylactically (prior to and during spheroid formation) or therapeutically (24 hours after spheroid formation) at concentrations ranging from 0.0001 μM to 10 μM. **Figure 3.32** illustrates that prophylactic (red) and therapeutic (black) treatment with SB525334A had no effect on collagen production in either non-IPF (n=1) or IPF spheroids (n=1), although an extremely high concentration (10 μM) did result in ~50 % attenuation in IPF spheroids (p<0.0.5; one-way ANOVA) when used prophylactically. Again, this may be due to toxicity, and demonstrates that SB525334A has low potency and efficacy when fibroblasts are cultured as spheroids, in terms of regulating collagen synthesis. Taken together, these data therefore suggest that spheroid collagen production may be independent of TGFβ signalling.

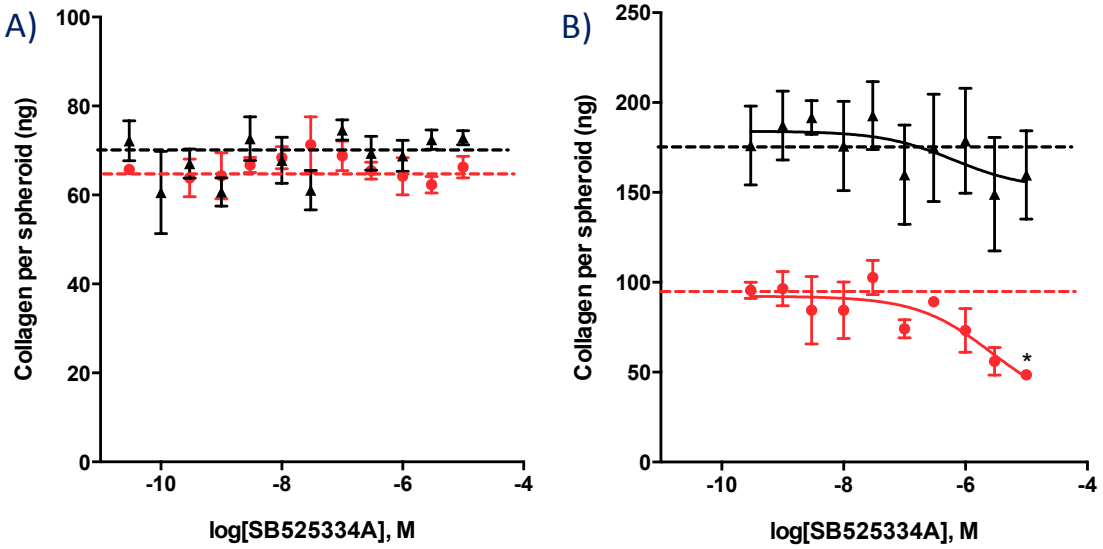

Figure 3. 32. Effect of ALK-5 inhibitor on collagen synthesis in both non-IPF and IPF spheroids.

(A) Non-IPF and (B) IPF spheroids were treated either prophylactically (red) or therapeutically (black) with an ALK-5 inhibitor (SB525334A). Doses ranged from 0.3 nM to 10 μM. Spheroids were collected 24 hours post-treatment and hydrolysed in 6M HCl for HPLC. Dotted line equals vehicle control 24 hours post seeding (red) or 48 hours post seeding (black). * p<0.05, one-way ANOVA.

3.2.7. Summary

This section focused on illustrating phenotypic characteristics of non-IPF and IPF spheroids (i.e. differentiation state, collagen production, and TGFβ activation). The results showed:

- Immunohistochemical analysis, western blotting, and qPCR data demonstrated that αSMA expression is greater in IPF spheroids in comparison to non-IPF suggesting that IPF pHLF have a more myofibroblastic phenotype when cultured as spheroids.
- Collagen I and III expression in IPF lung tissue was evident in several areas including fibrotic foci and basement membrane of bronchial epithelial cells.
- IPF spheroids were able to synthesis higher levels of collagen (types I and III) and active- TGFβ in comparison to non-IPF spheroids.
- The activation of TGFβ was independent of TSP-1 activity in both non-IPF and IPF spheroids.
- Integrin αvβ5 mRNA levels were greater in IPF spheroids in comparison to non-IPF, but there was no significant difference in mRNA levels for *ITGB3* and *ITGB5*
- TGFβ activation in IPF spheroids was partially dependent on β3, β5, and β8 integrin signalling whilst in non-IPF spheroids the activation was partially dependent only on β8 integrin signalling.
- Exogenous TGFβ had no effect on collagen production 24 hours post-seeding and TGFβ activation inhibitors (i.e. TSP-1 or integrin inhibitors) had minimal effect on collagen synthesis in either non-IPF or IPF spheroids.
- A potent ALK5 inhibitor (i.e. SB525334A) also had no effect on collagen synthesis when treated prophylactically or therapeutically. This suggests that in this 3D system the initial collagen deposition by fibroblasts may be independent of TGFβ signalling.

3.3. Spheroid characterisation – proliferation and apoptosis

3.3.1. Introduction

During a normal wound healing response, apoptosis plays an important role as it is involved in the removal of myofibroblasts from the wound site upon wound closure. However, analyses of cells from IPF patients show that epithelial cells undergo apoptosis (Barbas-Filho et al., 2001; Plataki et al., 2005) whereas fibroblasts are more resistant to apoptosis. These observations are not usually perceived in normal human lungs In addition, PGE_2 plays a role in apoptosis imbalance. Previous studies have demonstrated that increased concentrations of PGE_2 promote fibroblasts to become more susceptible to Fas-ligand induced apoptosis. However, fibroblasts from IPF lungs cultured as monolayers have shown low expression of COX2 and PGE_2, making these cells resistant to Fas-ligand induced apoptosis (Maher et al., 2010).

Cell death has previously been studied in spheroids composed of dermal fibroblasts. In contrast to tumour cell spheroids (which continue to grow), dermal fibroblast spheroids do not increase in size. A few days after spheroid formation, dermal fibroblasts begin to decompose by a process coined nemosis (Vaheri et al., 2009). This type of cell death has been described recently as a programmed necrotic-like cell death, with similar morphology features to necrotic cells. However, within the spheroids the cells do not appear to undergo cell death due to hypoxia (a common cause of necrosis), yet they lack certain apoptotic markers, such as Bcl and caspase-3. In fact, the cells within spheroids had elevated COX2 expression. Thus, COX2 induction and production of prostaglandins (i.e. PGE_2, 6-keto-$PGF_{1\alpha}$, $PGF_{2\alpha}$, and PGD_2) are hallmarks of nemosis. However, cell death in spheroid structures has not been investigated in fibroblasts from non-IPF and IPF lung donors. Thus, in this study, the level of cell death within spheroids was investigated, which involved the use of the TUNEL assay (a commonly used assay to detect DNA fragmentation). In addition, the proliferation of fibroblasts within the spheroids was also examined.

3.3.2. Fibroblasts cultured as spheroids are non-proliferative

Spheroids were formed, fixed in 4 % PFA, and embedded into paraffin wax at four different time points (24, 48, 72, and 96 hours). 2 μm thick sections were cut using a microtome for histological analysis. Ki-67 antibody was used to identify proliferating cells. As a positive

control, pHLF were cultured as a monolayer on glass chamber slides (50,000 cells per well) followed by fixation in 100 % methanol for 2 min. Immunofluorescent staining was performed on both spheroid sections and monolayer cells on the same day. **Figure 3.33** illustrates that both non-IPF (n=10) and IPF (n=10) pHLF in monolayer cultures proliferate (similar to section 3.1.2). However, Ki-67 positive cells were not detected within the spheroids. **Figure 3.33** illustrates images for the 96 hour time point however similar results were evident at 24, 48, and 72 hours. This suggests that pHLF cultured as spheroids are non-proliferating.

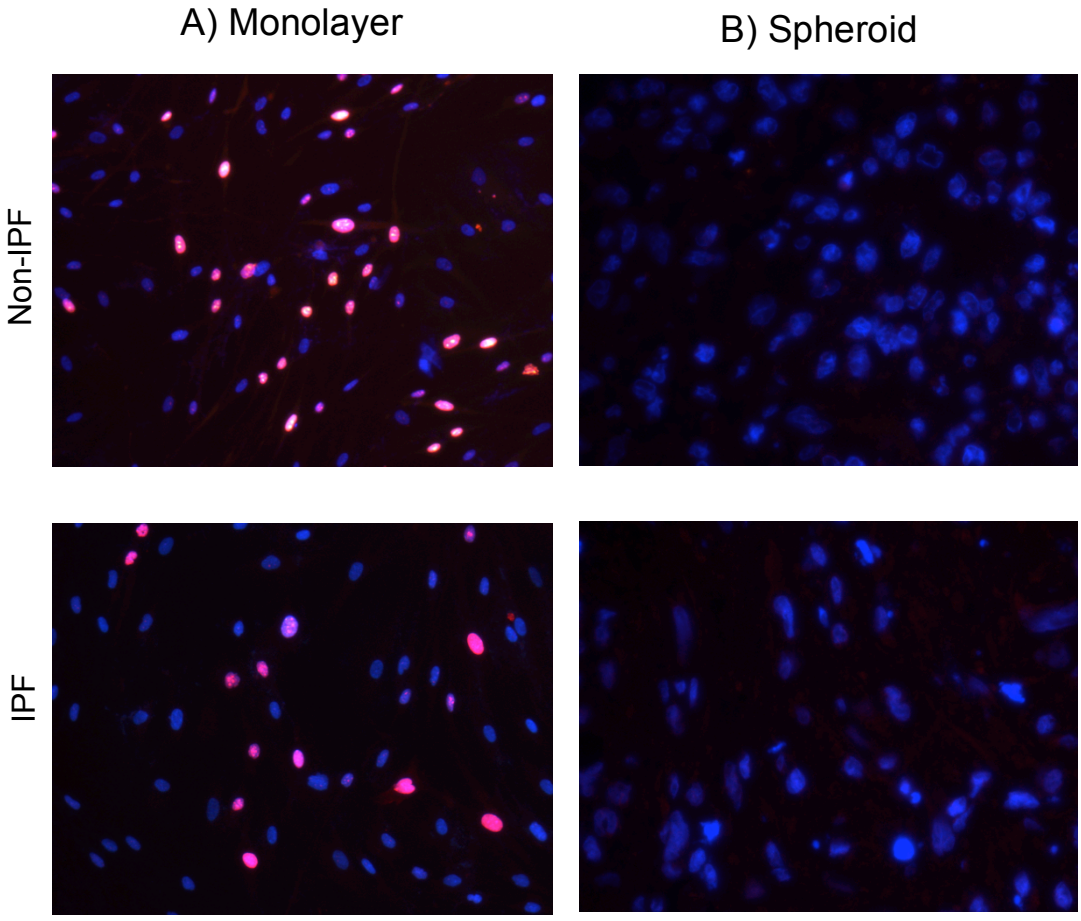

Figure 3. 33. Proliferation of primary human lung fibroblasts in monolayer culture and within 3D spheroid structures.

Immunofluorescence staining for Ki-67 (orange) with nuclei counterstained using DAPI (blue) on (A) chamber slides of monolayer cultures in the presence of 0.4 % FBS; and (B) Formalin-fixed paraffin embedded sections of fibroblast spheroids (4 days post spheroid formation). Magnification x200.

3.3.3. Non-IPF pHLF are more apoptotic in comparison to IPF

The next step was to investigate whether pHLF within spheroids undergo cell death over time (24-96 hours). This was determined by quantifying the number of TUNEL positive cells in serial sections of paraffin embedded spheroids. For statistical analysis, the percentage of TUNEL positive cells was transformed to arcsine (also known as inverse sine) to approximate a Gaussian rather than binomial distribution.

Figure 3.34A and **Figure 3.34B** illustrate that the number of TUNEL positive cells within non-IPF spheroids significantly increases over time following 3-4 days of incubation ($p<0.001$). In contrast, the percentage of TUNEL positive cells in the IPF spheroids was significantly lower (~10 % of the total number of nuclei) in comparison to non-IPF four days post spheroid formation ($p<0.01$).

To determine whether the size of the spheroid had any effect on the percentage of TUNEL positive cells, spheroids were also formed with different cell densities (10,000, 50,000, and 100,000 cells), incubated for four days followed by 4 % PFA fixation and then embedded into paraffin wax. **Figure 3.34C** illustrates that the cell density had no effect on the percentage of TUNEL positive cells in either non-IPF (n=1) or IPF spheroids (n=1). Since a significant difference was clearly illustrated at four days the experiment was repeated in multiple donors (cell density = 10,000; non-IPF n=6; IPF n=5; **Figure 3.34D**) which illustrates that fibrotic fibroblasts are less apoptotic in comparison to non-IPF in a 3D structure ($p<0.01$).

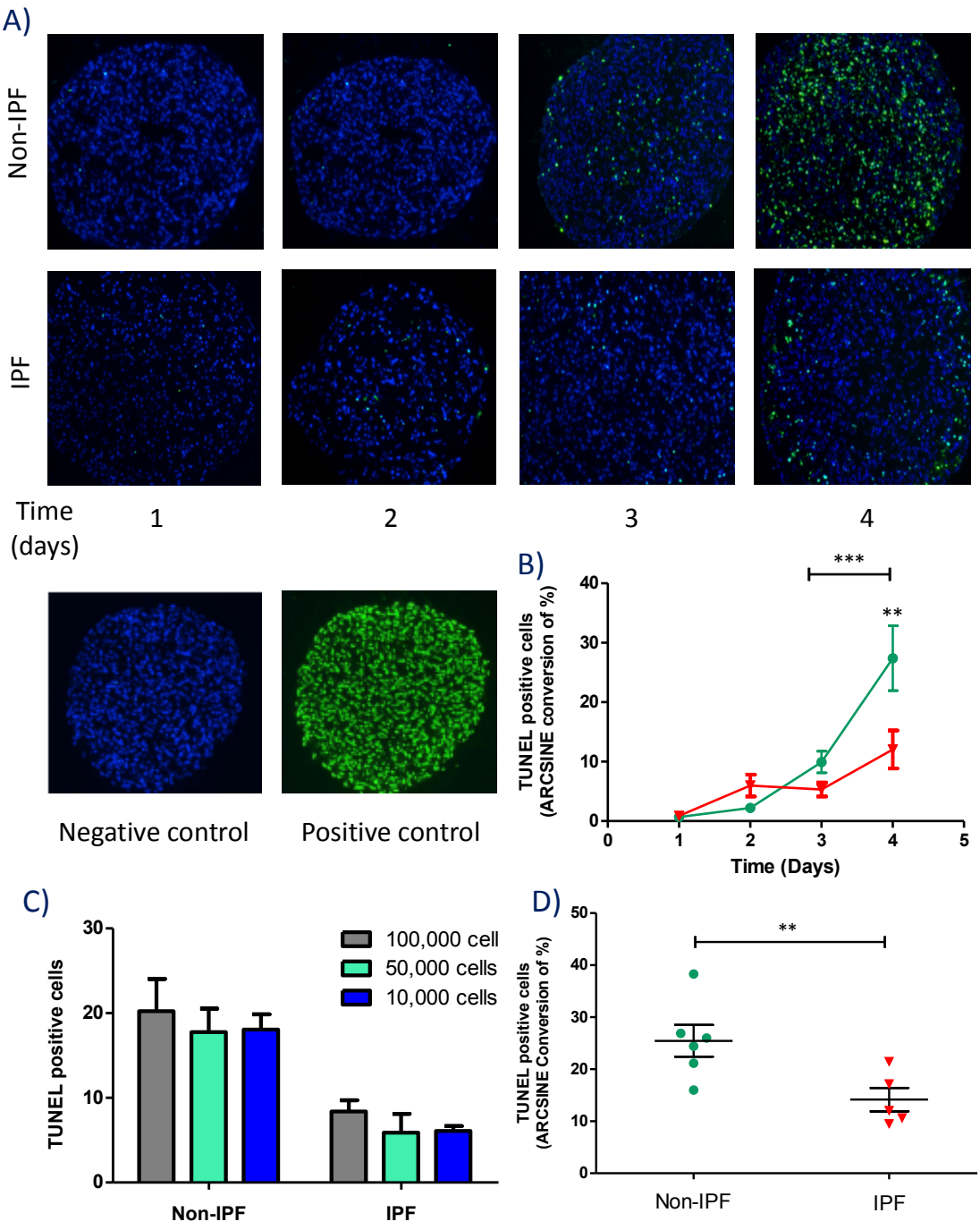

Figure 3. 34. TUNEL positive cells within non-IPF and IPF spheroids.

(A) Spheroids were collected at various time points (24-96 hours) and apoptotic cells were identified on sections by TUNEL. Dead/dying cells are indicated in green and DAPI nuclear staining is shown in blue. Images for negative and positive controls (DNase treated) are shown on the bottom left. Magnification x10. (B) Percentage of TUNEL positive cells were quantified using Image J. Data are representative data of one non-IPF (green) and one IPF donor (red). Three spheroid sections were analysed per donor. (C) Cell density has no effect on the percentage of TUNEL positive cells four days post-seeding. (D) Less DNA fragmentation is detected in IPF spheroids (n=5, green circles) in comparison to non-IPF (n=6; red triangles) four days post-seeding. **p<0.01, *** p<0.0001.

3.3.4. COX-1 inhibition attenuates apoptosis of non-IPF spheroids

Since the current data show that non-IPF fibroblast spheroids are more apoptotic over time in comparison to IPF, the next step was to investigate the COX status of these spheroids by measuring the levels of PGE_2. As mentioned before, COX2 is an enzyme essential for the formation of PGE_2 within lungs and promotes fibroblast cell death in monolayer cultures. In addition, IPF patients have reduced concentrations of PGE_2 in their lung. Furthermore, previous work illustrated that dermal fibroblast spheroids undergo nemotic like death due to the induction of COX2. Thus, it was pertinent to investigate whether this was also the case in lung fibroblast spheroids.

Figure 3.35 illustrates mRNA levels of *PTGS1* (COX1) and *PTGS2* (COX2) in non-IPF (n=5) and IPF (n=8) spheroids. No statistical difference was detected across all donors for both genes. In order to determine the COX status, spheroids were cultured for 4 days and the conditioned media were collected to perform a PGE_2 ELISA. **Figure 3.36A** illustrates high levels of PGE_2 production by non-IPF (n=12) spheroids in comparison to non-IPF (n=8) spheroids ($p<0.05$, student T-test). With the exception of one IPF donor, the concentration of PGE_2 production by all other IPF donors was <1 ng/mL whereas for non-IPF spheroids the concentration ranged between 1-19 ng/mL.

To investigate which COX isoform is involved in PGE_2 synthesis, pHLF were treated with 1 μg/mL indomethacin (non-specific inhibitor for COX) or 5 μg/mL NS398 (COX2 inhibitor) prior to spheroid formation. These concentrations were chosen based on previous experiments performed in our laboratory. The amount of PGE_2 in the conditioned medium of the spheroid cultures was then measured following four days of incubation. **Figure 3.36B** illustrates that in the presence of indomethacin, PGE_2 synthesis was attenuated in non-IPF spheroids by 100 % ($p<0.001$; student T-test) however, surprisingly, NS398 had no effect. **Figure 3.36C** and **D** demonstrate the effect of these compounds on the percentage of TUNEL positive cells in non-IPD spheroids. As shown, indomethacin attenuated the total percentage of cell death (by two-fold) following four days of culture, however NS398 again had no effect. These data suggest that COX1 may play a more central role in fibroblast cell death in this 3D system.

To further investigate this, non-IPF pHLF were treated with additional specific COX inhibitors: SC560 (COX1 specific inhibitor) and CAY10404 (COX2 specific inhibitor) prior to spheroid formation. **Figure 3.37** illustrates the effect of these compounds as well as indomethacin on PGE_2 synthesis in three different non-IPF donors. Both indomethacin (red) and SC560 (blue)

attenuated PGE_2 synthesis at day four. The IC50 for indomethacin across the three donors ranged between 0.15-3.18 nM and the IC50 for SC560 ranged from 0.05-3.82 nM. In contrast, CAY10404 attenuated PGE_2 synthesis only at extremely high concentrations (3-10 μM) across the three donors. Based on previous literature, CAY10404 is an extremely potent compound *in vitro* with, usually, nanomolar potency. However, in this 3D system the efficacy and potency of CAY10404 is very low suggesting that PGE_2 synthesis in non-IPF spheroids is primarily COX1 dependent.

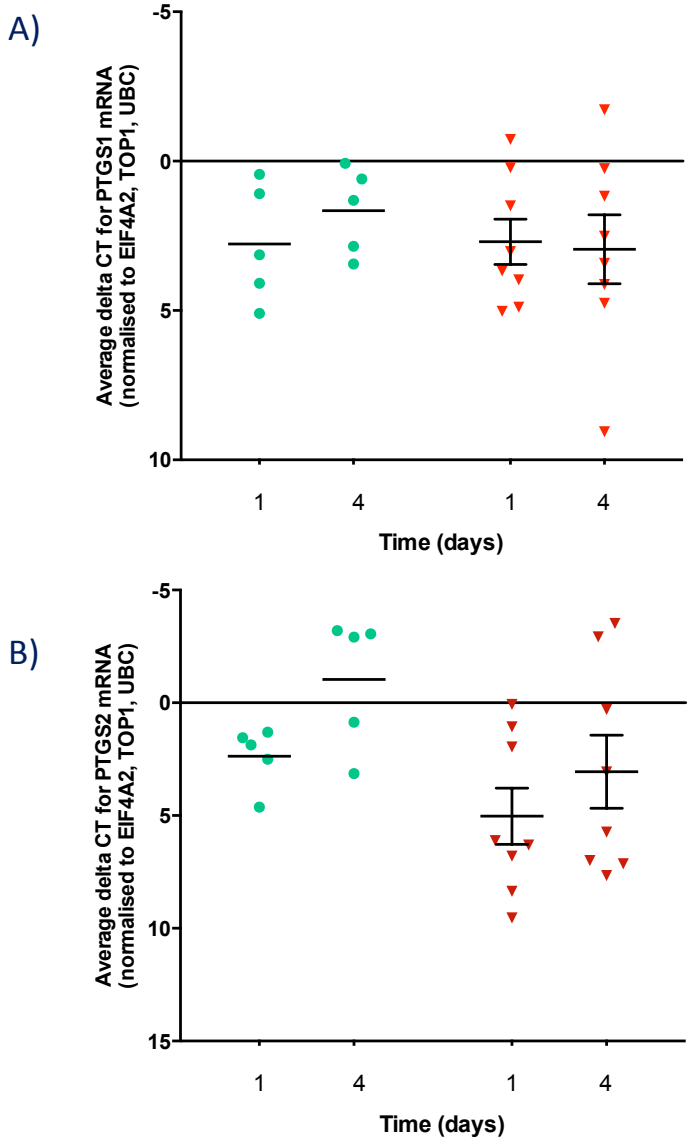

Figure 3. 35. PTGS1 and PTGS2 mRNA levels in non-IPF and IPF spheroids.

Spheroids were collected 24 – 96 hours post seeding. RNA was extracted from the spheroids for qRT-PCR to analyse the mRNA levels of (A) *PTGS1* and (B) *PTGS2*. All data points were normalised to three housekeeping genes based on GeNorm analysis (*EIF4A2, TOP1*, and *UBC*). Non-IPF and IPF spheroids are represented as green circles and red triangles, respectively.

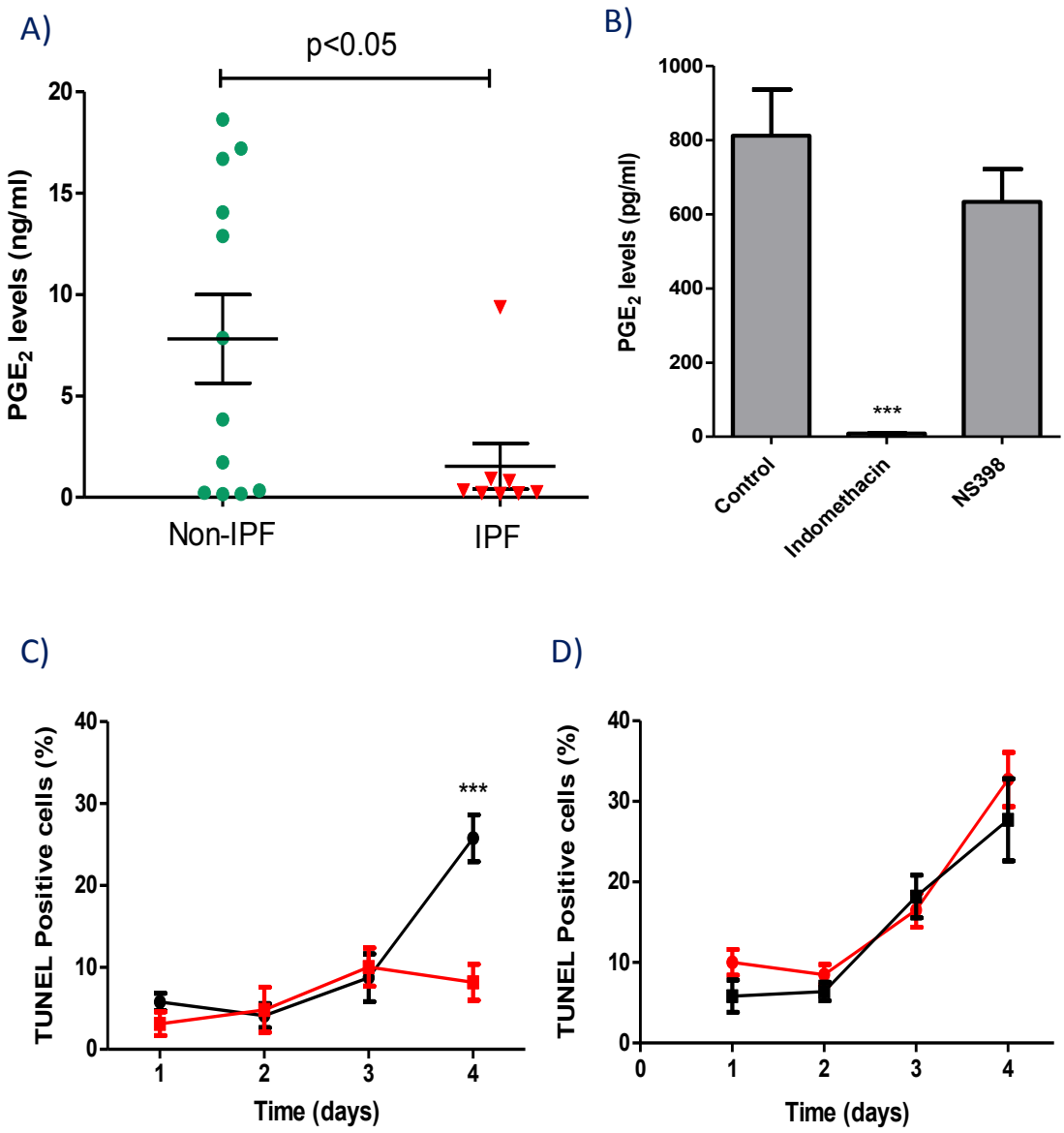

Figure 3. 36. PGE_2 levels in non-IPF and IPF spheroids and the effects of non-specific COX inhibitors.

(A) PGE_2 levels were measured in the supernatant of both control (n=12) and IPF (n=8) spheroids 96 hours post seeding. (B) Non-IPF fibroblasts (n=2) were treated with either vehicle control (DMSO), indomethacin (1 μg/ml), or NS398 (5 μg/ml) and then seeded for spheroid formation and left to incubate for 96 hours before analysing the PGE_2 levels within the supernatants. The spheroids were then fixed and sectioned to investigate the effect of (C) indomethacin and (D) NS398 on the percentage of apoptotic cells by using the TUNEL assay to identify DNA fragmentation. Red represents the effect of the compound and black represents vehicle control. Three spheroid sections were analysed per donor/condition *** p<0.001 (statistical test was performed on % after arcsine conversion).

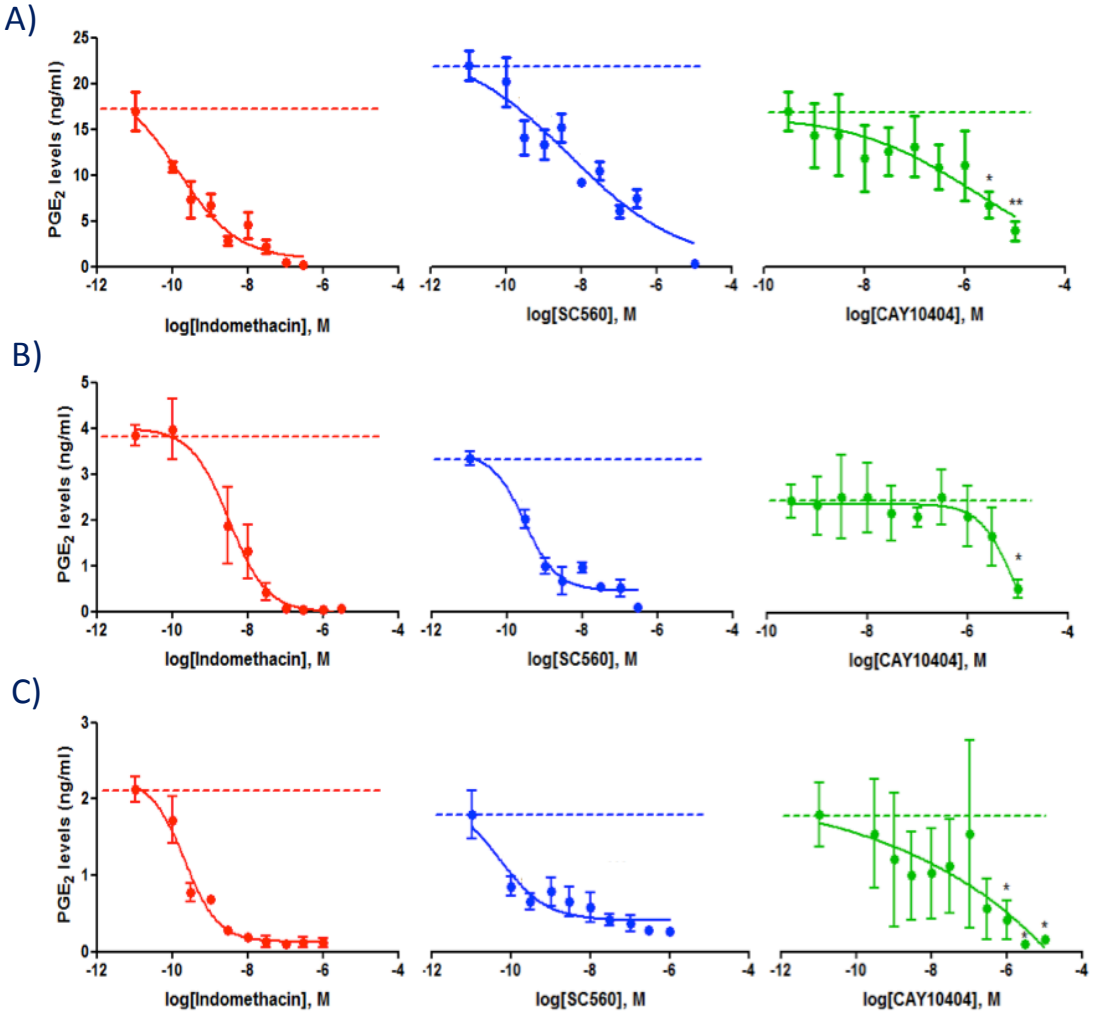

D)

Donor	Indomethacin		SC560		CAY10404	
	IC50	R^2	IC50	R^2	IC50	R^2
A	0.15 nM	0.8270	3.82 nM	0.7835	1.50 μM	0.3723
B	3.18 nM	0.8633	0.30 nM	0.901	7.70 μM	0.3215
C	0.21 nM	0.9162	0.05 nM	0.6926	-	-

Figure 3. 37. Effects of specific COX inhibitors on PGE_2 levels in non-IPF spheroids.

Non-IPF fibroblasts (n=3) were treated with indomethacin (red), SC560 (blue) or CAY10404 (green) and seeded into an agarose coated 96-well plate for spheroid formation. Spheroids were cultured for 96 hours. PGE_2 levels within the conditioned media were analysed (A), (B), and (C) represent three different donors. Dotted lines represent vehicle control (DMSO). *p<0.05, **p<0.01, *** p<0.001. (D) Table illustrating IC50 and R^2 values.

To investigate the effect of these COX-specific compounds on apoptosis/nemesis, a TUNEL assay was performed. **Figure 3.38** shows that in the presence of indomethacin and SC560 non-IPF pHLF cell death is attenuated (IC50 = 96 pM and 93.6 pM, respectively). However,

CAY10404 had no effect, supporting the notion that fibroblast cell death in this 3D system is dependent on COX1 activity.

A)

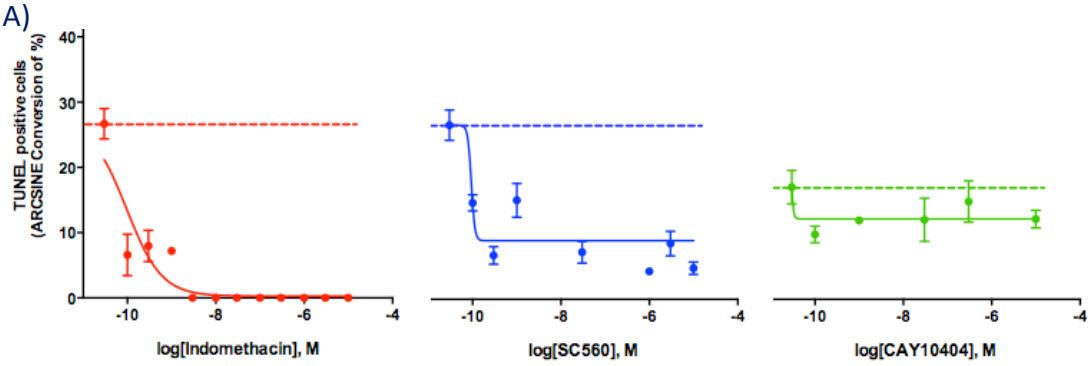

B)

Indomethacin		SC560		CAY10404	
IC50	R^2	IC50	R^2	IC50	R^2
96 pM	0.8163	93.6 pM	0.6109	-	-

Figure 3. 38. Effects of specific COX inhibitors on spheroid cell death.

(A) Non-IPF fibroblasts were treated with indomethacin (red), SC560 (blue), or CAY10404 (green) and then seeded for spheroid formation and left to incubate for 96 hours before embedding into paraffin wax. 2μm thick sections were cut and TUNEL assay was performed. Cell count was performed by using Image J. Dotted lines represent vehicle control (DMSO). *p<0.05, **p<0.01, *** p<0.001 (one-way ANOVA). (B) Table illustrating IC50 and R^2 values.

3.3.5. COX-1 inhibition accelerates collagen synthesis in non-IPF spheroids

To determine the effect of COX inhibitors on collagen synthesis, spheroids treated with indomethacin, SC560, and CAY10404 were hydrolysed in 6M HCl (four days post treatment) to perform HPLC. **Figure 3.39** illustrates that in the presence of indomethacin the collagen levels increased in all three donors. The EC50 for donor A and C were 0.1 nM and 352 nM, respectively. Based on the curve-fit used (i.e. variable slope, four parameter) the software was unable to calculate the IC50 for donor B. Nevertheless, indomethacin was able to increase collagen synthesis even at low dose, which was statically significant following one-way ANOVA analysis. Similar to indomethacin, SC560 also resulted in an increase in collagen synthesis in all three donors however the levels increased by approximately two-fold (which is much greater in comparison to the spheroids treated with indomethacin). The EC50 for all three donors ranged between 2.1 – 922 nM. A slight elevation in collagen production was also detected by CAY10404 however this was only evident at high concentrations 3 – 10 μM in two donors ($p<0.05$, one-way ANOVA). Thus, COX1 inhibition accelerates collagen synthesis.

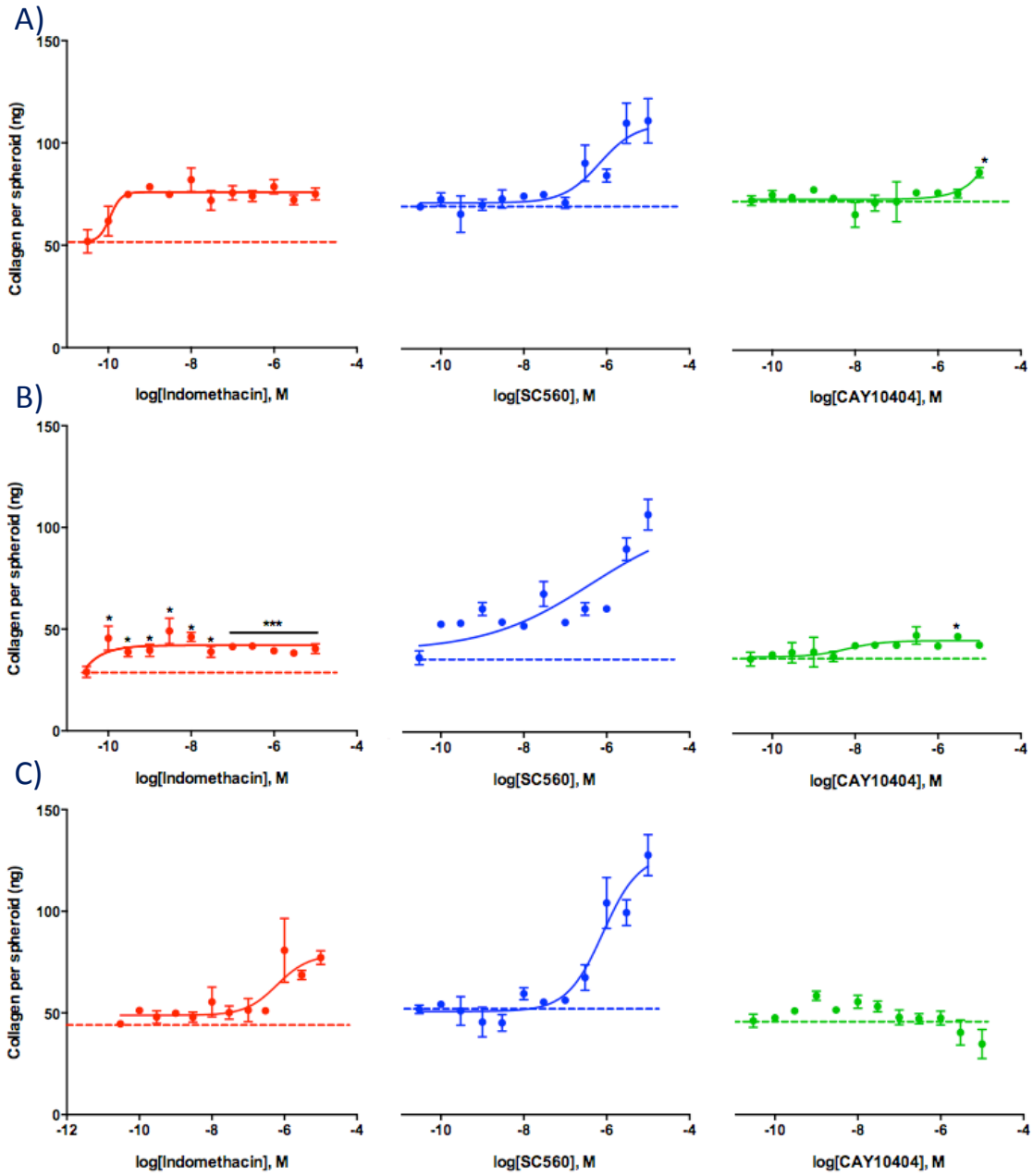

Donor	Indomethacin		SC560		CAY10404	
	IC50	R^2	IC50	R^2	IC50	R^2
A	0.1nM	0.5458	2.1 mM	0.6188	7.7 mM	-
B	-	-	428.3 nM	0.6370	-	-
C	352nM	0.5281	922 nM	0.7987	-	-

Figure 3. 39. Effects of specific COX inhibitors on collagen levels in non-IPF spheroids.

Non-IPF fibroblasts (n=2) were treated with either indomethacin (red), SC560 (blue) or CAY10404 (green)) and then seeded for spheroid formation and left to incubate for 96 hours before analysing hydroxyproline levels within the spheroid by HPLC. (A), (B), and (C) represent three different donors. Dotted lines represent vehicle control (DMSO). *$p<0.05$ (D) Table illustrating EC50 and R^2 values.

3.3.6. PGE_2 attenuates collagen synthesis in spheroids via EP2 receptors

To determine the prophylactic and therapeutic effects of PGE_2 on collagen synthesis, non-IPF and IPF pHLF were treated with PGE_2 prior to spheroid formation or 24 hours after spheroid formation. The cultures were incubated with PGE_2 for 24 hours before analysis by HPLC. **Figure 3.40** illustrates that PGE_2 is able to attenuate collagen synthesis in both non-IPF and IPF spheroids in a concentration-dependent manner. The IC50 in IPF spheroids (10.26nM) is greater in comparison to non-IPF spheroids (2.06nM) suggesting that PGE_2 has a greater potency in non-IPF spheroids in comparison to IPF. No statistical significance was detected in spheroids treated with PGE_2 24 hrs post-spheroid formation (therapeutic treatment; black) in IPF spheroids. However, in non-IPF spheroids, 10 μM PGE_2 did show a statically significant attenuation in collagen synthesis ($p<0.001$; one-way ANOVA).

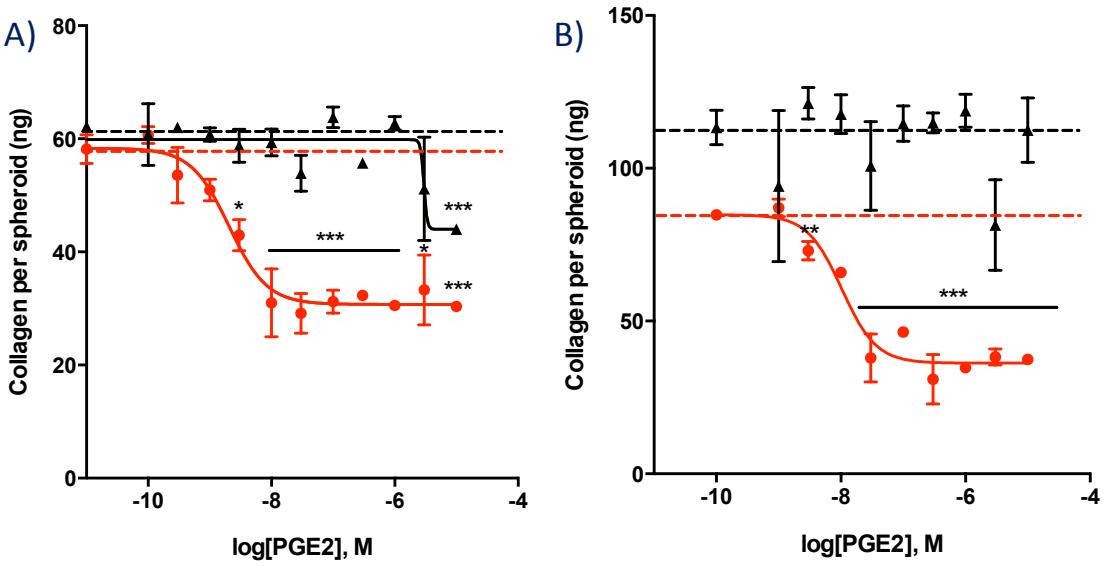

C)

Donor	Prophylactic	Therapeutic
A (Non-IPF)	2.06 nM	3 μM
B (IPF)	10.26 nM	-

Figure 3. 40. PGE_2 attenuates collagen synthesis in both non-IPF and IPF spheroids.

(A) Non-IPF and (B) IPF spheroids were treated either prophylactically (red) or therapeutically (green) with PGE_2. Spheroids were collected 24 hours post-treatment and hydrolysed in 6M HCl for HPLC. Dotted line illustrates vehicle control 24 hours post seeding (red) or 48 hours post seeding (black). C) PGE_2 IC50 in each donor *p<0.05, **p<0.01, ***p<0.001

There are four PGE_2 receptors: EP1, EP2, EP3, and EP4. Activation of EP1 and EP3 results in smooth muscle cell contraction, whilst EP2 and EP4 mediate cell relaxation and promote fibroblast apoptosis in monolayer cultures via the activation of adenylate cyclase (Bozyk and Moore, 2011; Brock, 2014). In non-IPF and IPF spheroids, mRNA levels for all four receptors were quantified. As shown in **Figure 3.41** there were no significant differences in mRNA levels of all four genes between non-IPF and IPF spheroids at either 24 hours or 96 hours. However, there was an elevation in *PTGER4* mRNA levels over time in both non-IPF and IPF spheroids ($p<0.05$, two-WAY ANOVA). It is important to note that the mRNA levels for *PTGER3* were undetectable in 3/6 non-IPF donors, and these data points are not presented on the graph. Based on the ΔCT values, the mRNA levels for *PTGER2* and *PTGER4* are statistically greater in comparison to *PTGER1* and *PTGER3* in both non-IPF and IPF spheroids.

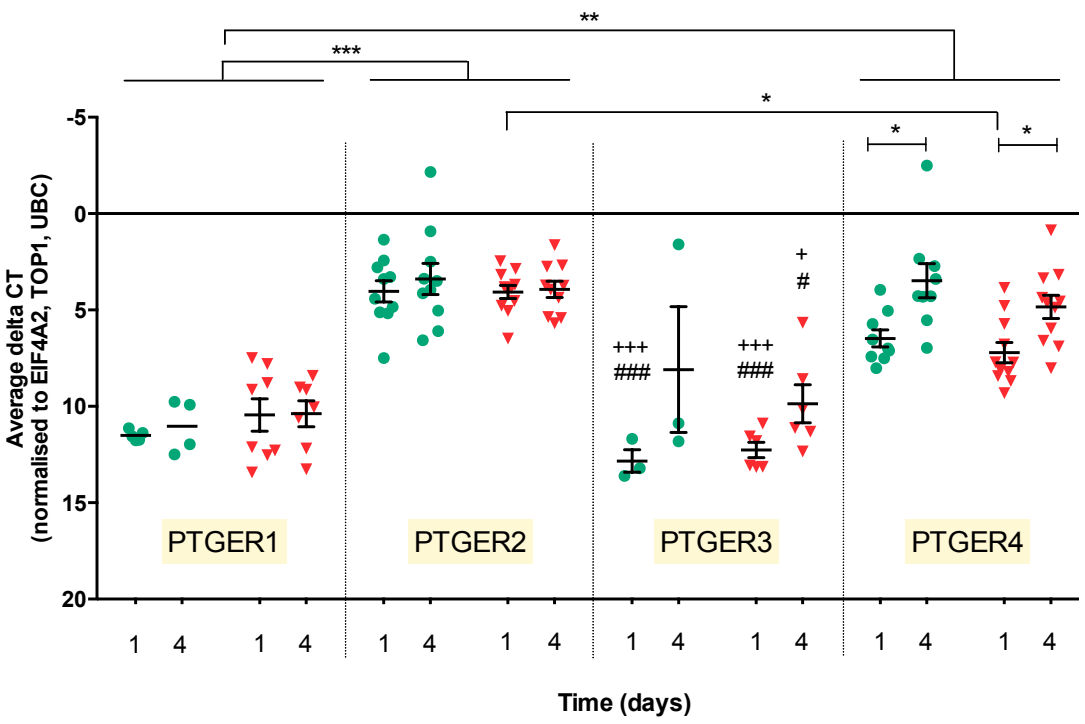

Figure 3. 41. EP receptor mRNA levels in non-IPF and IPF spheroids.

Spheroids were collected 24 – 96 hours post seeding. RNA was extracted from the spheroids for qRT-PCR to analyse the mRNA levels of *PTGER1, PTGER2, PTGER3*, and *PTGER4*. All data points were normalised to three housekeeping genes based on GeNorm analysis (*EIF4A2, TOP1*, and *UBC*). Non-IPF and IPF spheroids are represented as green circles and red triangles, respectively. *p<0.05, **p<0.01, ***p<0.001, +p<0.05 (*PTGER2* vs. *PTGER3*), +++p<0.001 (*PTGER2* vs. *PTGER3*), #p<0.05 (*PTGER3* vs. *PTGER4*), ###p<0.001 (*PTGER3* vs. *PTGER4*).

To determine which EP receptor is activated by PGE_2 to attenuate collagen synthesis and promote fibroblast cell death, non-IPF and IPF spheroids were treated with EP2 and EP4 receptor agonists and antagonists all of which were a kind gift from GSK (Stevenage). These included dual EP2/4 agonists, EP2 agonist, EP2 antagonist, EP4 agonist, and EP4 antagonist. Cells were treated with the compounds prior to spheroid formation and collagen content was investigated 24 hours post-treatment. **Figure 3.42** and **Figure 3.43** illustrate a concentration-dependent attenuation in collagen synthesis when treated with EP2/4 dual agonists or EP2 agonist in both non-IPF and IPF spheroids, respectively. EP2 and EP4 antagonists had no effect on collagen synthesis in either non-IPF or IPF spheroids. The EP4 agonist attenuated collagen production only after using high concentrations of the compound (3 – 10 μM; $p<0.05$, one-way ANOVA) with an IC50 of 1 μM. Based on previous *in vitro* assays, the EP4 agonist is normally highly potent with an IC50 of around 1 nM (personal communication from Richard Hatley, GSK). However, in this 3D culture the IC50 is 1000-fold greater suggesting that the EP4 agonist has a low potency in this vitro assay. Thus, the data illustrates that PGE_2 may attenuate collagen synthesis via EP2 receptor signalling and since antagonising EP2 receptor showed no effect on collagen synthesis it suggests PGE_2 does not affect collagen production at baseline.

3.3.7. Spheroid cell death is dependent on EP2 receptor signalling

To determine the effect of EP2 agonist on apoptosis, four days post spheroid formation, a TUNEL assay was performed on 2μm thick paraffin embedded spheroid sections. **Figure 3.44** illustrates that in the presence of this compound the percentage of TUNEL positive cells increase in a concentration-dependent manner for non-IPF spheroids with an EC50 of 7.2 nM. In addition, 10 μM of EP2 agonist resulted in 100% cell death. An increase in cell death in IPF spheroids was also evident in the presence of 100 pM EP2 agonist, however this elevation only resulted in approximately 20 % cell death (which is similar to baseline non-IPF spheroid cell death). A rise in EP2 agonist concentration did not result in further increase in the percentage of TUNEL positive cells. This suggests that non-IPF spheroid cell death is dependent on EP2 receptor signalling, and it may be partially-dependent on EP2 signalling in IPF spheroids.

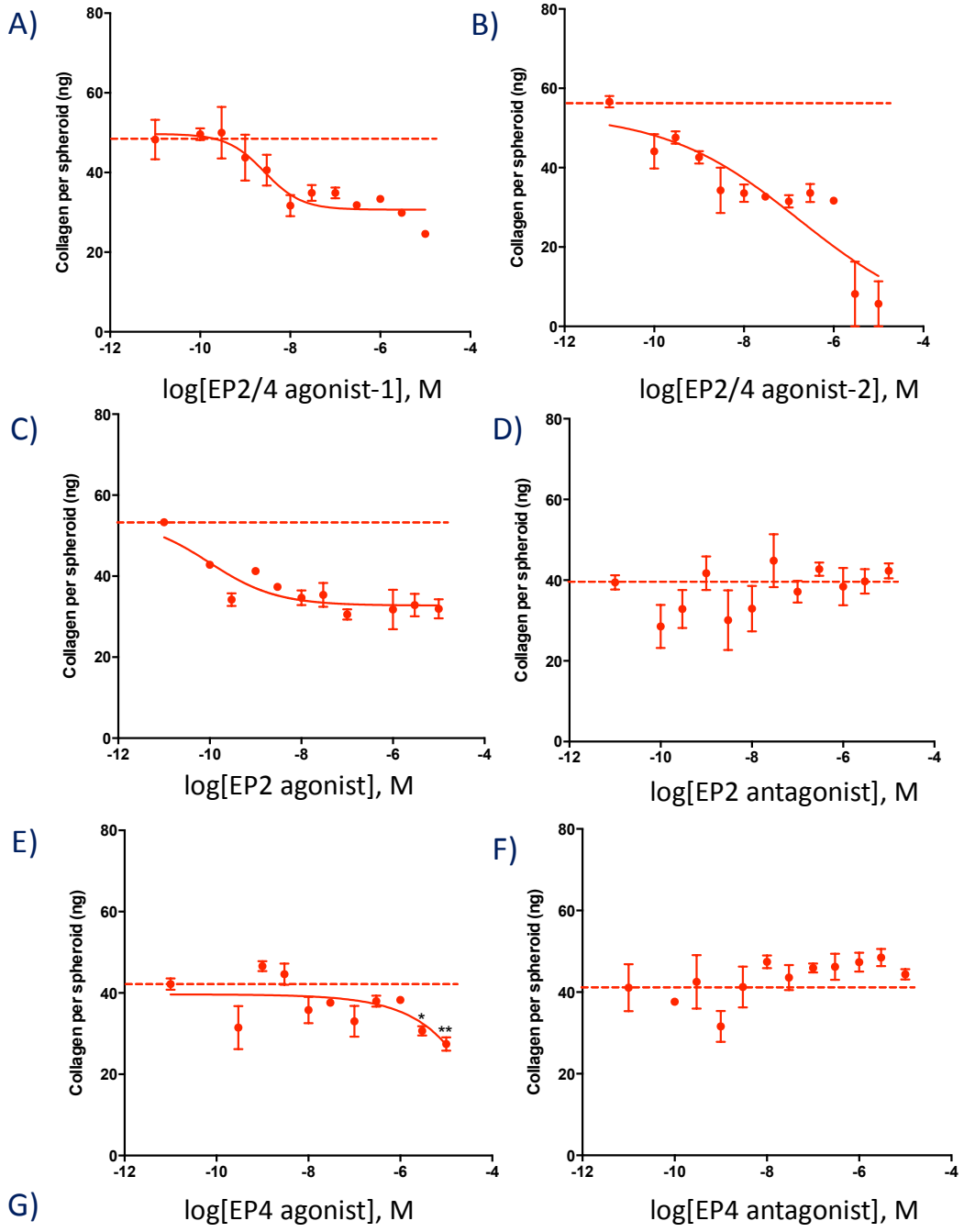

Compound	IC50	R^2
Dual EP2/EP4 agonist-1	2.7 nM	0.6217§
Dual EP2/EP4 agonist-2	169.3 nM	0.6923
EP2 agonist	97.1 pM	0.5615

Figure 3. 42. Effect of EP2 and EP4 compounds on collagen synthesis in non-IPF spheroids.

Non-IPF fibroblasts (n=1) were treated with (A) and (B) dual EP2/4 agonists (C) EP2 agonist, (D) EP2 antagonist, (E) EP4 agonist, or (F) EP4 antagonist. Spheroids were collected 24 hours post-treatment and hydrolysed in 6M HCl for HPLC. Dotted line represents vehicle control 24 hours post seeding). (G) Table illustrating IC50 and R^2 values.

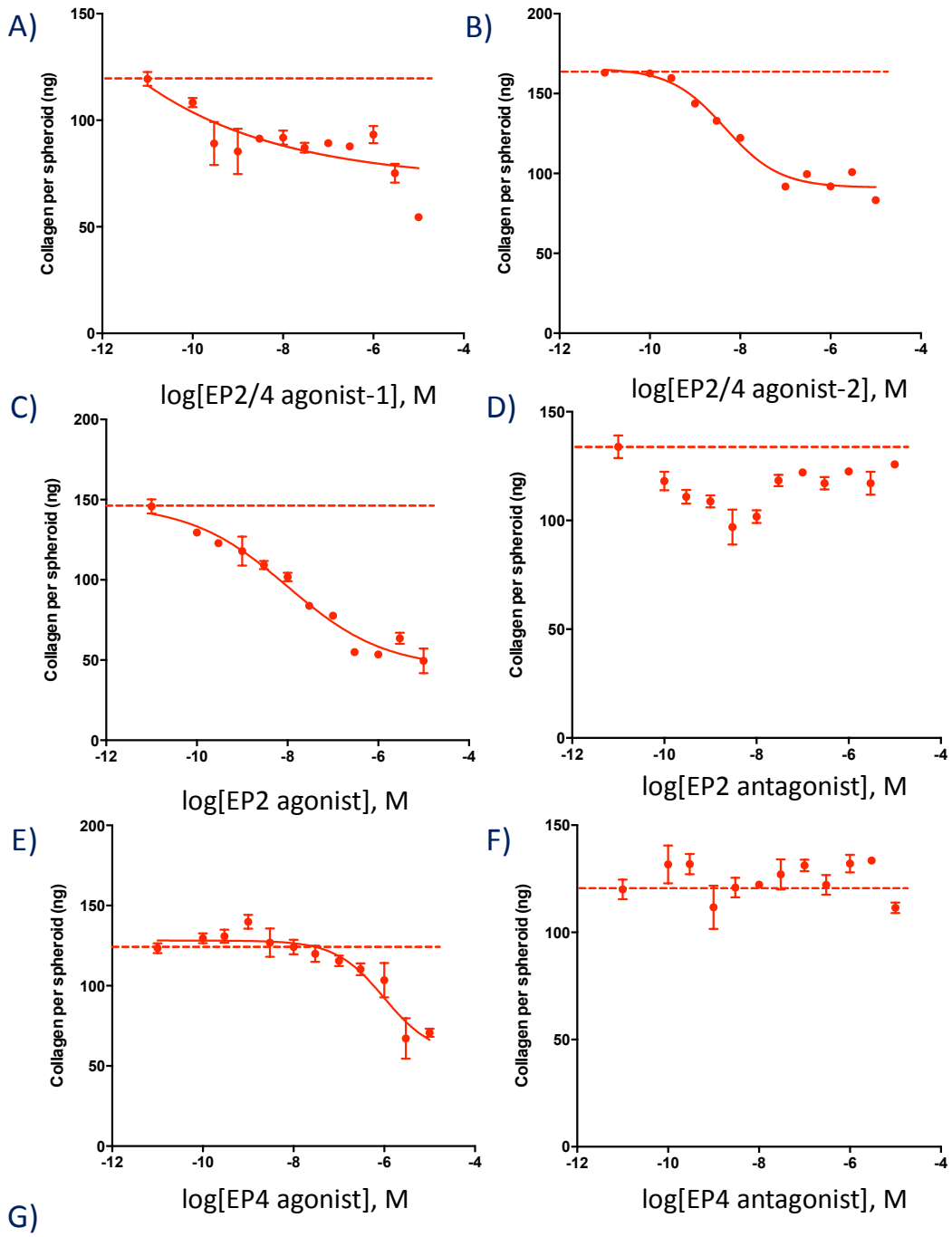

G)

Compound	IC50	R^2
Dual EP2/EP4 agonist-1	10 nM	0.5086
Dual EP2/EP4 agonist-2	4.6 nM	0.9729
EP2 agonist	9.9 nM	0.9411
EP4 agonist	1 μM	0.8147

Figure 3. 43. Effect of EP2 and EP4 compounds on collagen synthesis in IPF spheroids.

IPF fibroblasts (n=1) were treated with (A) and (B) dual EP2/4 agonists C) EP2 agonist, (D) EP2 antagonist, (E) EP4 agonist, or (F) EP4 antagonist. Spheroids were collected 24 hours post-treatment and hydrolysed in 6M HCl for HPLC. Dotted line represents vehicle control 24 hours post seeding). (G) Table illustrating IC50 and R^2 values.

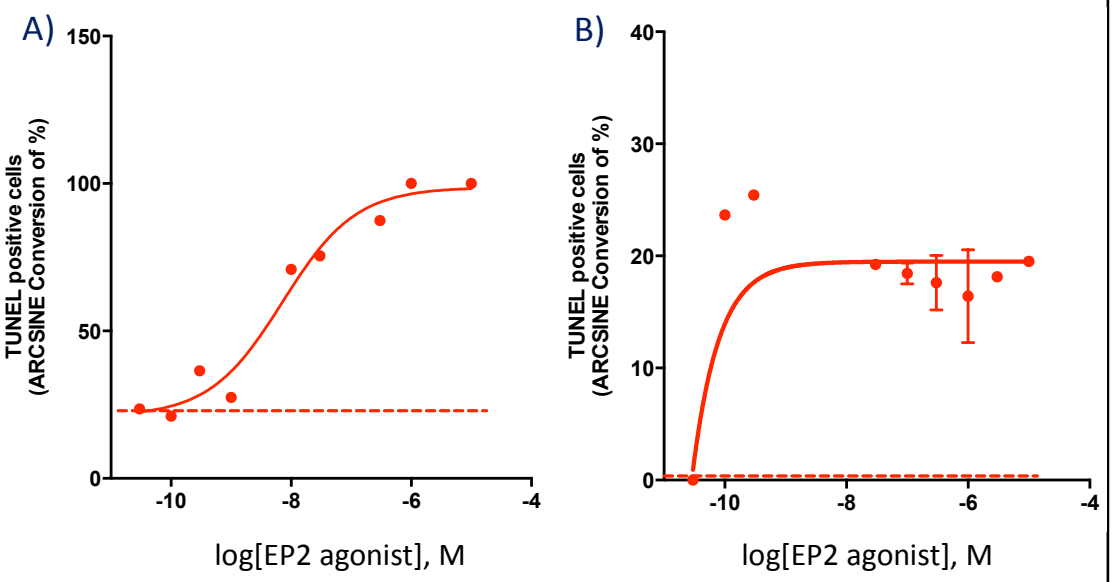

Figure 3. 44. Effects of EP2 agonist on cell viability in non-IPF and IPF spheroids

(A) Non-IPF fibroblasts (EC50 = 7.2 nM) and (B) IPF fibroblasts (EC50 = 0.05 pM) were treated with EP2 agonist, seeded for spheroid formation, and then left to incubate for 96 hours before embedding into paraffin wax. 2 μm thick sections were cut and TUNEL assay was performed. Cell count was performed by using Image J. Dotted lines represent vehicle control (DMSO). Three spheroid sections were analysed per donor/condition.

3.3.8. Summary

In this section the following has been demonstrated:

- Both non-IPF and IPF fibroblast spheroids are non-proliferative when cultured for 24-96 hours.
- Non-IPF fibroblast spheroids are more apoptotic and produce high levels of PGE_2 in comparison to IPF fibroblast spheroids, following four days of incubation.
- *PTGS1* and *PTGS2* mRNA levels are not statistically different between non-IPF and IPF spheroids.
- Non-IPF spheroids treated with a COX1 specific inhibitor (SC560) attenuated PGE_2 synthesis and reduced the percentage of TUNEL positive cells. In addition, COX1 inhibition increased collagen production in non-IPF spheroids. On the other hand, COX2 specific inhibitors (NS398 and CAY10404) showed only moderate effects at extremely high concentrations (low potency).
- In the presence of PGE_2, collagen production was attenuated in both non-IPF and IPF spheroids (prophylactic treatment, 24 hours). However, following therapeutic PGE_2 treatment no effect was evident.
- Non-IPF and IPF spheroids have higher *PTGER2* and *PTGER4* mRNA levels in comparison to *PTGER1* and *PTGER3* mRNA. Levels of *PTGER4* mRNA increase over time in both non-IPF and IPF spheroids.
- Collagen synthesis and cell viability is dependent on EP2 receptor signalling as EP2 agonist attenuated collagen production and promoted cell death in both non-IPF and IPF spheroids. On the other hand EP4 agonist had minimal effect.

3.4. Microarray analysis of non-IPF and IPF spheroids

3.4.1. Spheroid cell death is dependent on EP2 receptor signalling

Microarray is a high-throughput gene expression profiling technique which involves hybridisation of labelled target RNA or DNA to oligonucleotide probes attached to a solid surface, allowing the detection of gene expression within a given sample. This technique has been used extensively for biological research in the past 10 years (Lipshutz et al., 1995; Schena et al., 1995) to understand mechanisms for several diseases including lung cancer (Beer et al., 2002) and breast cancer (Sweet-Cordero et al., 2005). In addition, microarray has been performed on samples from IPF patients. Such samples include peripheral blood (which identified MMP1 and MMP7 as potential biomarkers for IPF) and lung biopsies of IPF patients, categorised as rapid or slow progressors (which in rapid progressors, has identified several genes involved in oxidative stress, apoptosis, cell migration/proliferation, cancer, and fibroblast/smooth muscle cell specific genes (Selman et al., 2006, 2007; Rosas et al., 2008). Furthermore, in our laboratory, microarray has been performed on monolayer fibroblast cultures from patients diagnosed with IPF and system sclerosis, which has identified a number of differentially expressed genes relevant to these diseases (Ian Garner, UCL; personal communication).

So far my data support a clear phenotypic difference between non-IPF and IPF fibroblasts cultured in a 3D system, whereby IPF spheroids have a more myofibroblast-like phenotype, produce higher levels of active TGFβ, synthesise higher levels of collagen, and are less apoptotic in comparison to non-IPF spheroids. Although several studies (including 2D *in vitro* cultures) have supported the role of TGFβ in collagen synthesis, in this 3D system, collagen synthesis seems to be largely independent of TGFβ signalling. The next step of this project involved performing microarray data analysis to identify differentially expressed genes within non-IPF and IPF spheroids and determine key biological pathway(s) which may be involved in the causing morphological and phenotypical differences.

3.4.2. Quality control

24 hours post-seeding (~16 hours post-spheroid formation), ten spheroids from each donor were pooled and lysed using 500 μL RNaqueous lysis buffer. The samples were then

transported to Epistem (UK) subjected to Affymetrix GeneChip oligonucleotide microarray analysis (details of the method can be found in **Section 2.15**). In total there were 20 samples, each from a different donor (non-IPF, n=10; IPF, n=10). Details of each sample are shown in **Table 3.1**. Following RNA extraction, an Agilent Bioanalyzer was used to determine the RNA Integrity Number (RIN) – a measure of the RNA quality. All samples had a RIN above 7, suggesting good RNA integrity (see **Appendix 1**). Following this the samples were further processed and hybridised to Affymetrix GeneChip® Human Genome U133+2 arrays.

The quality of the raw data generated was assessed by background correcting the intensity reading by using the Robust Multi-array Average (RMA) algorithm (with median polishing). This removed any background fluorescence as a result of non-specific binding of labelled samples. The data were then quantile normalised (to adjust the data for technical differences as opposed to biological variations between each sample), and log2 transformed, all performed using Partek Genomic Suite. Boxplots and histograms were generated to visualise the spread of the data as well as compare and contrast the probe intensity between the arrays of the dataset. As illustrated in **Figure 3.45A** and **B** there were no obvious outliers suggesting there were no problems with the probe intensity levels within the array. **Figure 3.45C** and **D** illustrate the QC metrics for each sample, which involved comparing the experimental probes on the Affymetrix chips with the spiked-in hybridisation controls. All samples passed the QC at this stage.

Table 3. 1. Microarray sample information

Sample/ Donor	Condition	Gender	Passage	Collagen (ng)	Location of experiment	Date of experiment	Array batch
1	Non-IPF	M	6	<50	GSK	12/06/2013	1
2	IPF	F	5	>50	UCL	11/06/2013	1
3	Non-IPF	F	6	<50	UCL	22/06/2013	1
4	IPF	M	5	<50	GSK	02/07/2013	1
5	Non-IPF	M	6	<50	UCL	22/06/2013	1
6	IPF	M	6	<50	GSK	02/07/2013	1
7	IPF	F	7	<50	UCL	08/06/2013	1
8	Non-IPF	M	4	>50	UCL	11/06/2013	1
9	IPF	M	6	<50	UCL	04/08/2013	1
10	Non-IPF	M	6	<50	UCL	06/06/2013	1
11	IPF	F	5	>50	GSK	02/07/2013	2
12	Non-IPF	M	5	>50	UCL	07/08/2013	2
13	Non-IPF	M	5	<50	UCL	04/08/2013	2
14	IPF	M	5	<50	GSK	02/07/2013	2
15	Non-IPF	M	6	<50	UCL	08/06/2013	2
16	IPF	M	6	<50	GSK	17/06/2013	2
17	Non-IPF	F	5	<50	UCL	22/06/2013	2
18	IPF	F	7	>50	UCL	11/06/2013	2
19	Non-IPF	M	5	<50	UCL	04/08/2013	2
20	IPF	F	6	>50	UCL	18/06/2013	2

Each sample is composed of primary human lung fibroblasts spheroids from different donors. These spheroids were either generated at GSK or UCL (which is indicated in the table as location of the experiment). RNA from non-IPF and IPF patients was randomised between array batches. As well as collecting spheroid samples for microarray, additional samples were subsequently collected to determine the collagen levels by measuring hydroxyproline content using HPLC.

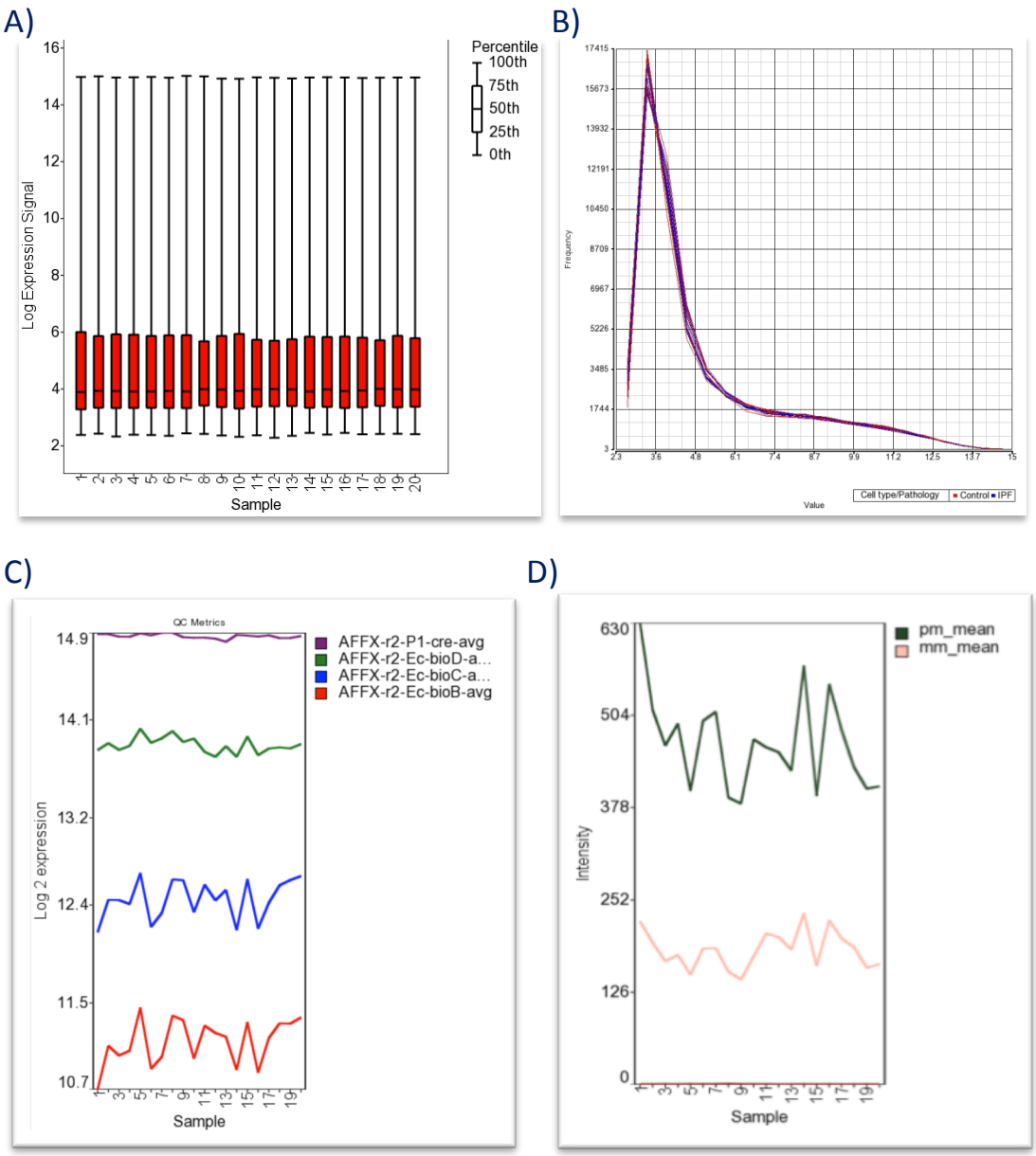

Figure 3. 45. Microarray Quality Control (QC) analysis.

(A) Box plots of log2 expression values following normalisation and summarisation. (B) Histogram after normalisation, showing frequencies at probe intensity. (C) Log2 expression of hybridisation labelling controls. (D) Intensity of perfect match and mismatch probe sets.

3.4.3. Principal Component Analysis (PCA)

PCA is a mathematical algorithm used to reduce the microarray data to a manageable number of dimensions by identifying directions (or principle components) which retain as much of the

variation as possible in the data (Jolliffe, 2002). Using a few principal components (ideally two or three, which account for the largest variations in the data) provides each sample with a value which can be plotted to visually assess difference and similarities between all samples (Price et al., 2006; Ringner, 2008).

Based on the QC results, PCA was performed on all 20 samples (**Figure 3.46**). However, one outlier was clearly identified (circled in **Figure 3.46**). This sample was from non-IPF donor 8 (**Table 3.1**). **Figure 3.47** illustrates the same PCA, re-plotted to highlight any distribution according to cell passage number; donor 8 was the only sample derived at passage 4 (red, circled) whilst all other samples ranged between passages 5-7. Due to this outlier result, donor 8 was excluded from the remainder of the microarray data analysis.

PCA was then performed again without sample 8 (19 out of 20 samples in total) which is illustrated in **Figure 3.48**. After re-running this analysis, a slight batch affect was visible. A batch effect may result due to minuscule differences in any number of non-biological variables (such as change in atmospheric ozone levels, different technicians running the batches, and reagents from different lots) (Fare et al., 2003). Passage number and location of experiment were also assessed on this PCA plot (**Figure 3.49** and **Figure 3.50**, respectively). Passage number showed no distinctive effect. **Figure 3.50** illustrates grouping of five samples from GSK illustrating a slight effect depending on the location of the experiment. Gender of the samples showed no significant grouping (**Figure 3.51**). Based on these results, a further PCA was performed following the removal of the batch effect and the location bias from the experiment using Partek (**Figure 3.52**), which demonstrated a better random distribution of the samples according to batch/location.

After this removal, a clear separation of non-IPF and IPF spheroid groups was evident (**Figure 3.53**), particularly in principal components 1 and 2 (accounting for around 24 % of the variation between datasets). This suggests that the overall gene expression patterns in both groups are separable by microarray. In addition, a slight gender effect was also evident (**Figure 3.54**). Following PCA, hierarchical clustering was then performed to discriminate differentially expressed genes in non-IPF and IPF spheroids (**Section 3.4.4**).

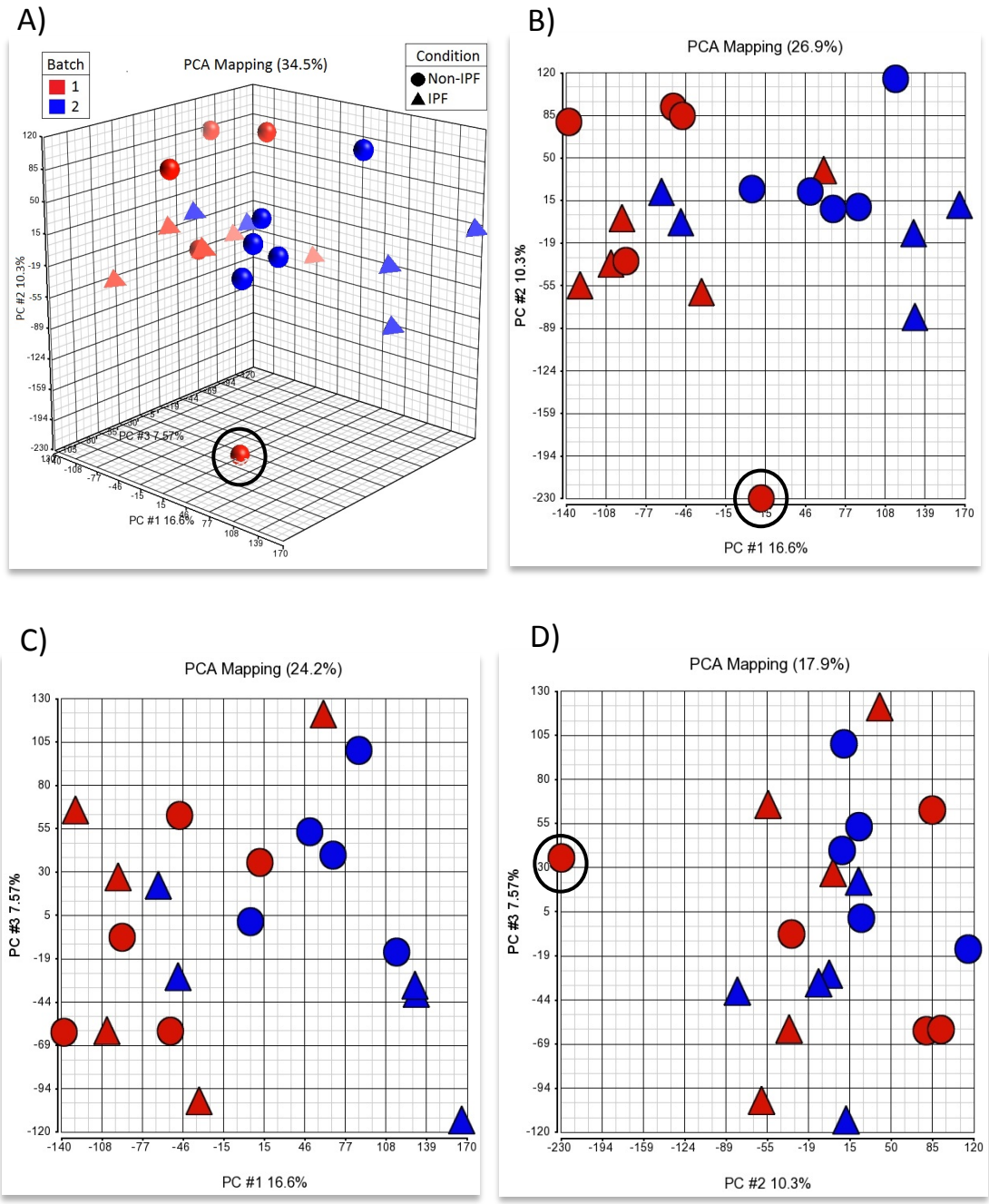

Figure 3. 46. Principle component analysis (PCA) plots for non-IPF and IPF spheroid microarray data.

(A) Three-dimensional PCA plot. Proportion of variance explained: PC1, 16.6 % (x-axis); PC2, 10.3 % (y-axis); PC3, 7.57 % (z-axis). (B-D) Two-dimensional PCA plots for the same data: (B) PC1 vs. PC2; (C) PC1 vs. PC3; (C) PC2 vs. PC3. ANOVA factors: gender and condition (i.e. non-IPF and IPF). Batch effect was not removed. Red = Batch 1; blue = Batch 2; circle/sphere = non-IPF (n=10); triangle/tetrahedron = IPF (n=10). From the 20 samples one outlier is clearly visible in A, B, and D (circled in black). This sample is from a non-IPF donor and from batch 1 of the microarray hybridisations.

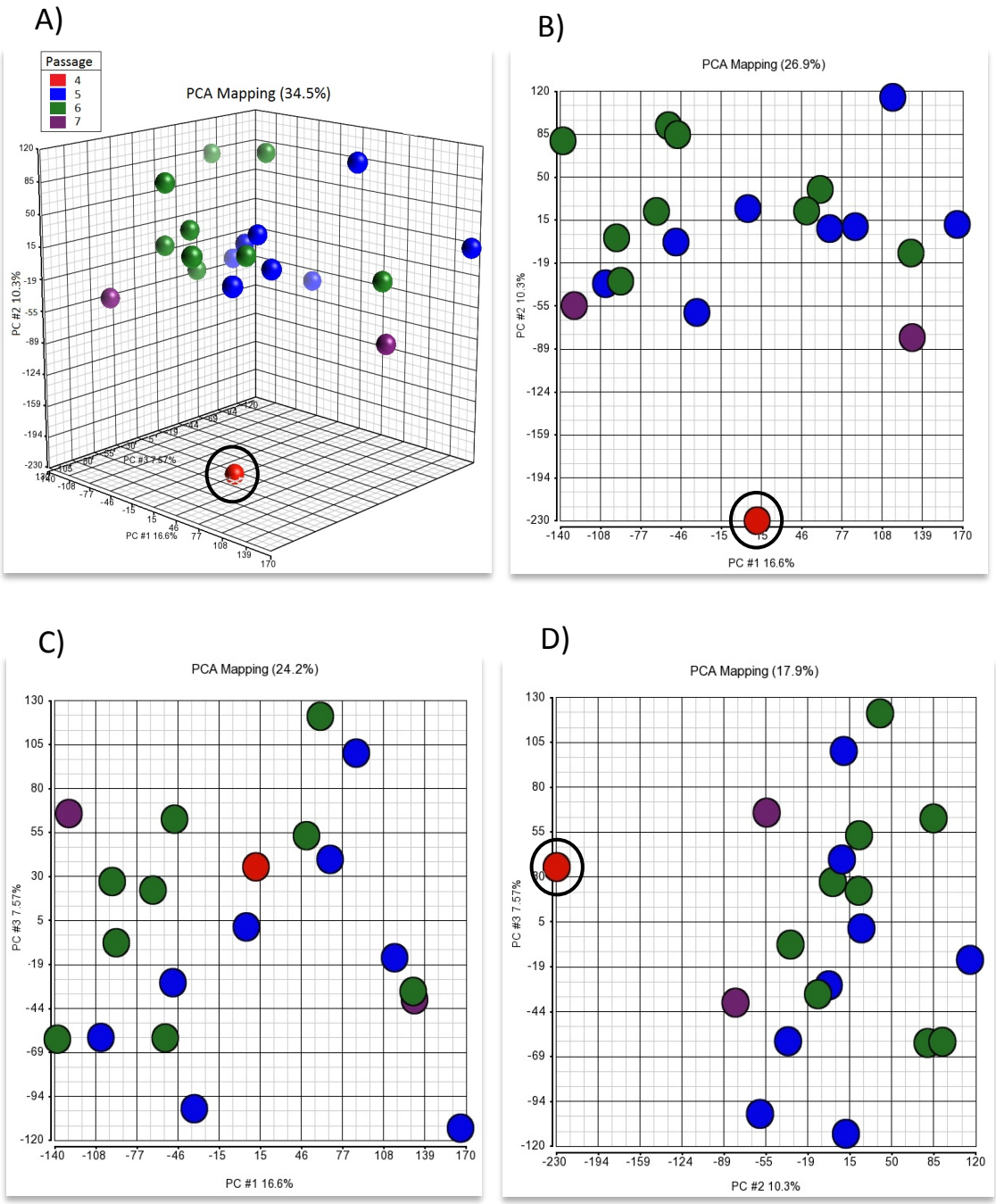

Figure 3. 47. Principle component analysis (PCA) plots for non-IPF and IPF spheroid microarray data illustrating the effect of passage.

The same PCA analysis from Figure 3.46 was re-plotted to indicate cell passage number. (A) Three-dimensional PCA plot. Proportion of variance explained: PC1, 16.6 % (x-axis); PC2, 10.3 % (y-axis); PC3, 7.57 % (z-axis). (B-D) Two-dimensional PCA plots for the same data: (B) PC1 vs. PC2; (C) PC1 vs. PC3; (C) PC2 vs. PC3. ANOVA factors: gender and condition (i.e. non-IPF and IPF). Batch effect was not removed. Red = passage 4; blue = passage 5; green = passage 6; purple = passage 7. Non-IPF, n=10; IPF, n=10. The clear outlier in A, B, and D (red) is the only line derived at passage 4.

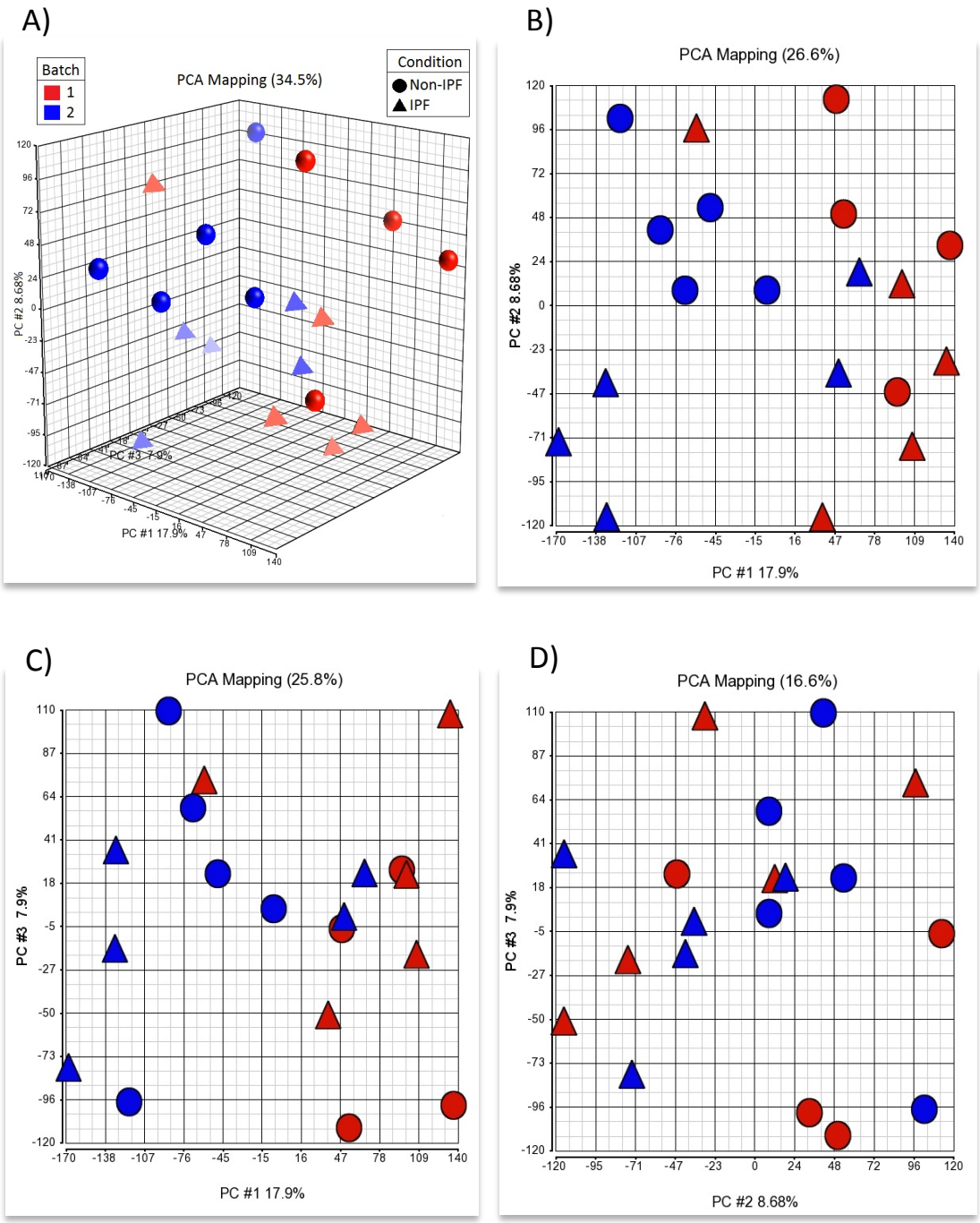

Figure 3. 48. Principle component analysis (PCA) plots for non-IPF and IPF spheroid microarray data (after removing sample 8) illustrating a slight batch effect.

(A) Three-dimensional PCA plot. Proportion of variance explained: PC1, 17.9 % (x-axis); PC2, 8.68 % (y-axis); PC3, 7.9 % (z-axis). (B-D) Two-dimensional PCA plots for the same data: (B) PC1 vs. PC2; (C) PC1 vs. PC3; (C) PC2 vs. PC3. ANOVA factors: gender and condition (i.e. non-IPF and IPF). Batch effect was not removed. Red = batch 1; blue = batch2; circle/sphere = non-IPF (n=9); triangle/tetrahedron = IPF (n=10). Two sample populations, as a result of a batch effect, are slightly visible in B and C.

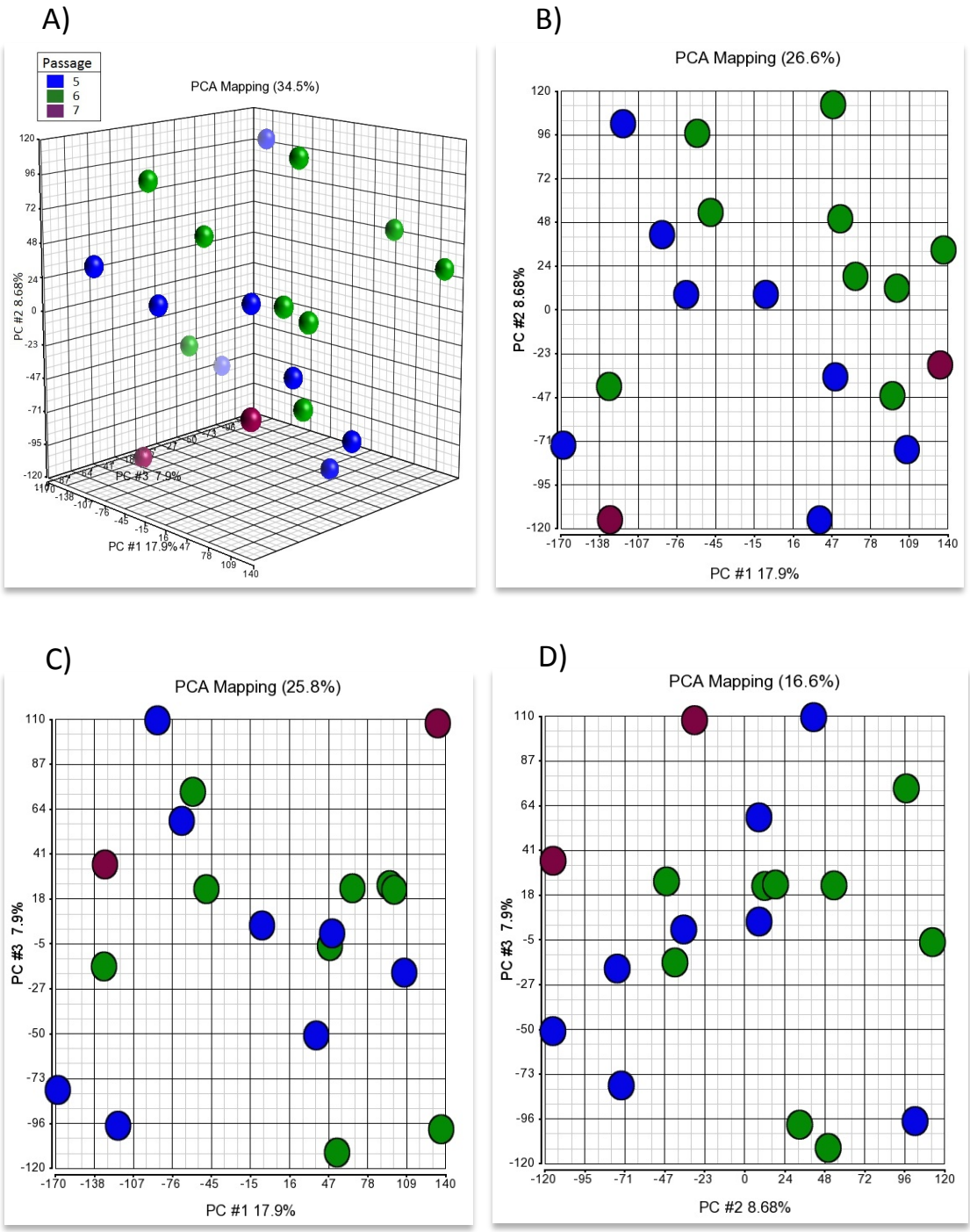

Figure 3. 49. Cell passage showed no obvious effect on the principle component analysis (PCA) plots for non-IPF and IPF spheroid microarray data.

The same PCA analysis from Figure 3.48 was re-plotted to indicate cell passage number. (A) Three-dimensional PCA plot. Proportion of variance explained: PC1, 17.9 % (x-axis); PC2, 8.68 % (y-axis); PC3, 7.9 % (z-axis). (B-D) Two-dimensional PCA plots for the same data: (B) PC1 vs. PC2; (C) PC1 vs. PC3; (C) PC2 vs. PC3. ANOVA factors: gender and condition (i.e. non-IPF and IPF). Batch effect was not removed. Blue = passage 5; green = passage 6; purple = passage 7. Non-IPF, n=9; IPF, n=10.

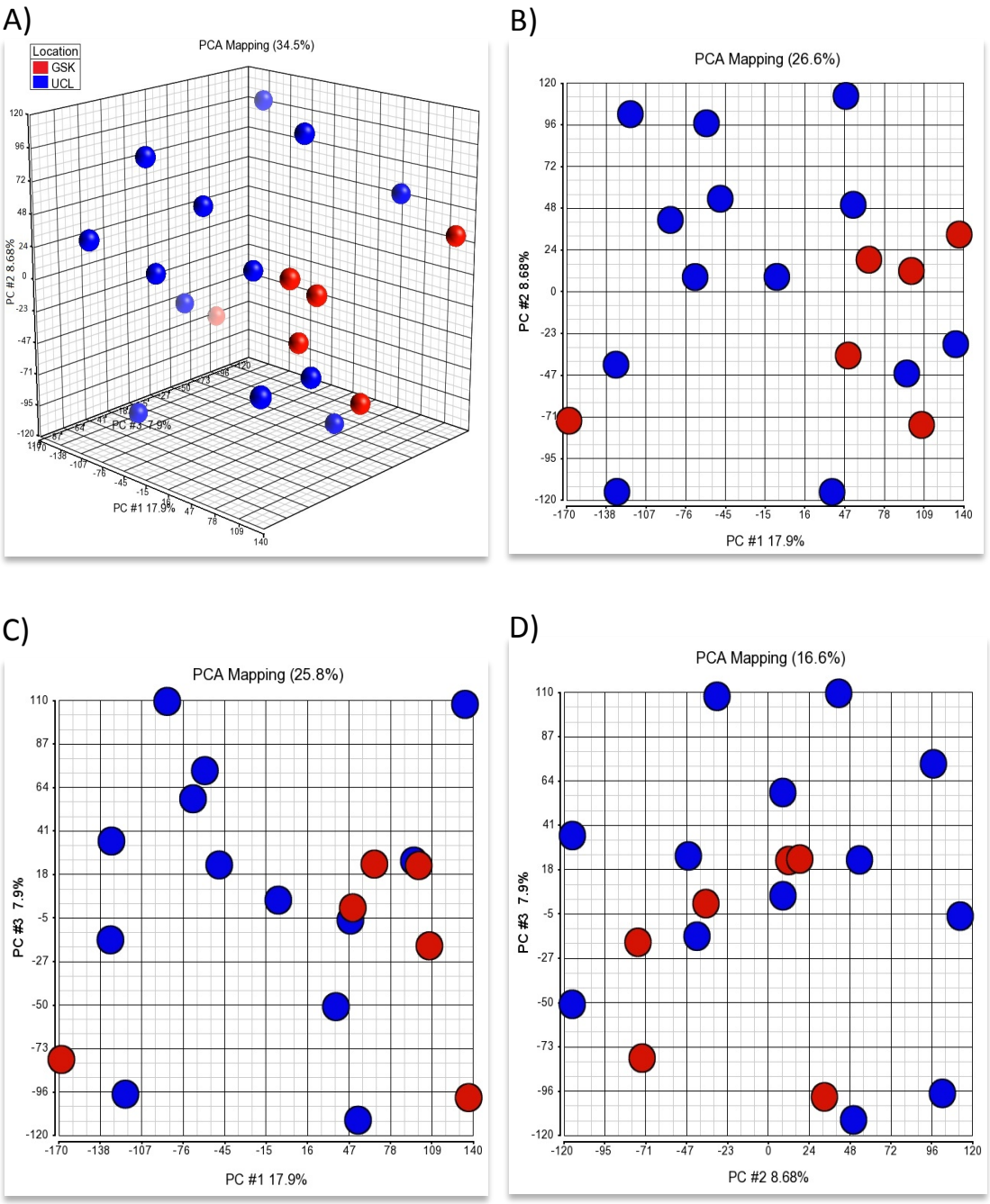

Figure 3. 50. Location of experiment had a slightly discernible effect on the principle component analysis (PCA) plots for non-IPF and IPF spheroid microarray data.

The same PCA analysis from Figure 3.48 was re-plotted to indicate the location of spheroid production. (A) Three-dimensional PCA plot. Proportion of variance explained: PC1, 17.9 % (x-axis); PC2, 8.68 % (y-axis); PC3, 7.9 % (z-axis). (B-D) Two-dimensional PCA plots for the same data: (B) PC1 vs. PC2; (C) PC1 vs. PC3; (C) PC2 vs. PC3. ANOVA factors: gender and condition (i.e. non-IPF and IPF). Batch effect was not removed. Red = GSK (GlaxoSmithKline); blue = UCL (University College London). Non-IPF, n=9; IPF, n=10.

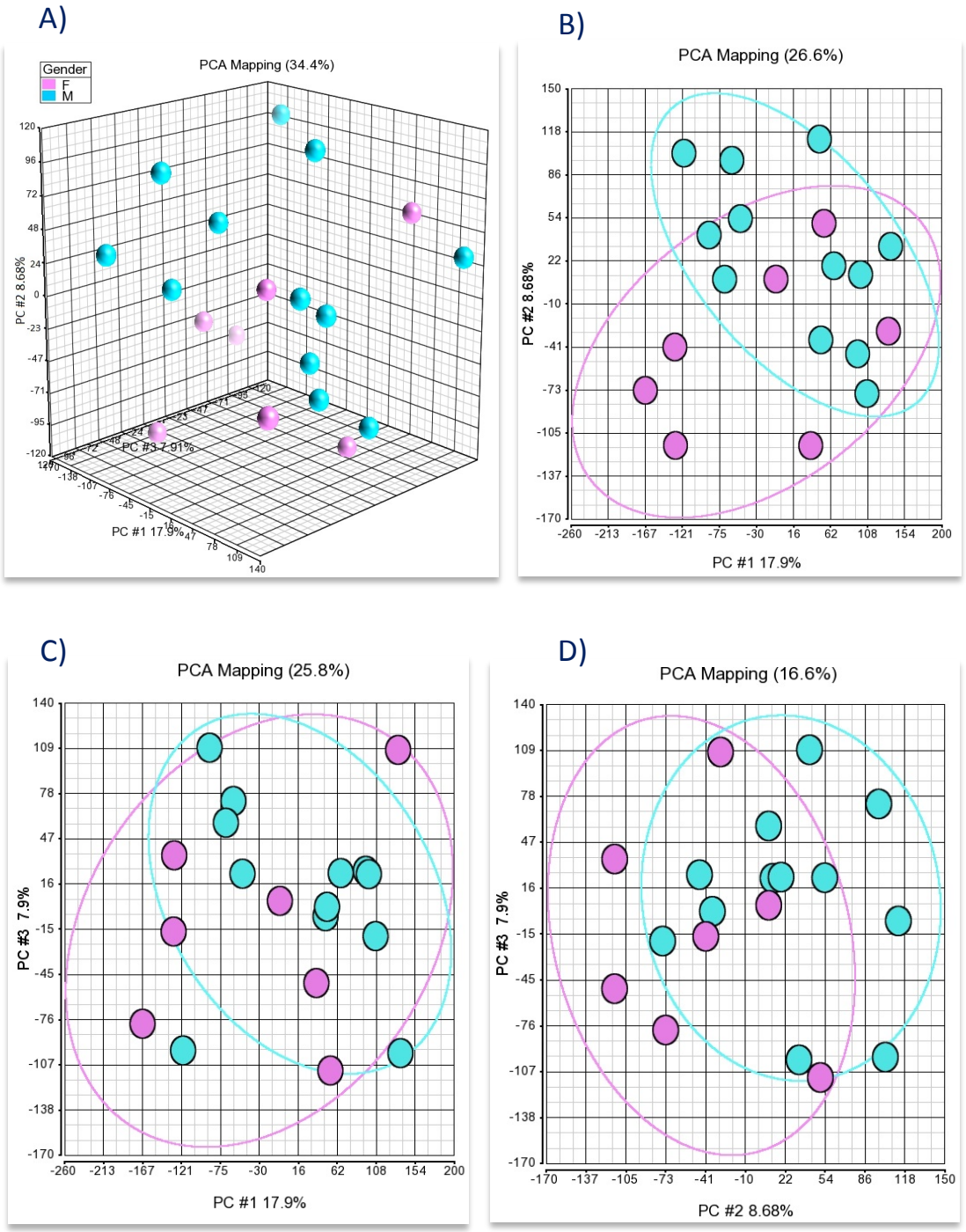

Figure 3. 51. Principle component analysis (PCA) plots illustrating the effect of gender on gene expression for non-IPF and IPF spheroids.

The same PCA analysis from Figure 3.48 was re-plotted to indicate distribution of gender amongst the samples on the PCA plot. (A) Three-dimensional PCA plot. Proportion of variance explained: PC1, 17.9 % (x-axis); PC2, 8.68 % (y-axis); PC3, 7.9 % (z-axis). (B-D) Two-dimensional PCA plots for the same data: (B) PC1 vs. PC2; (C) PC1 vs. PC3; (C) PC2 vs. PC3. ANOVA factors: gender and condition (i.e. non-IPF, n=9; and IPF, n=10). Batch effect was not removed. Pink = female; blue = male. Ellipses were applied using Partek Genomics Suite to help visualise the groupings.

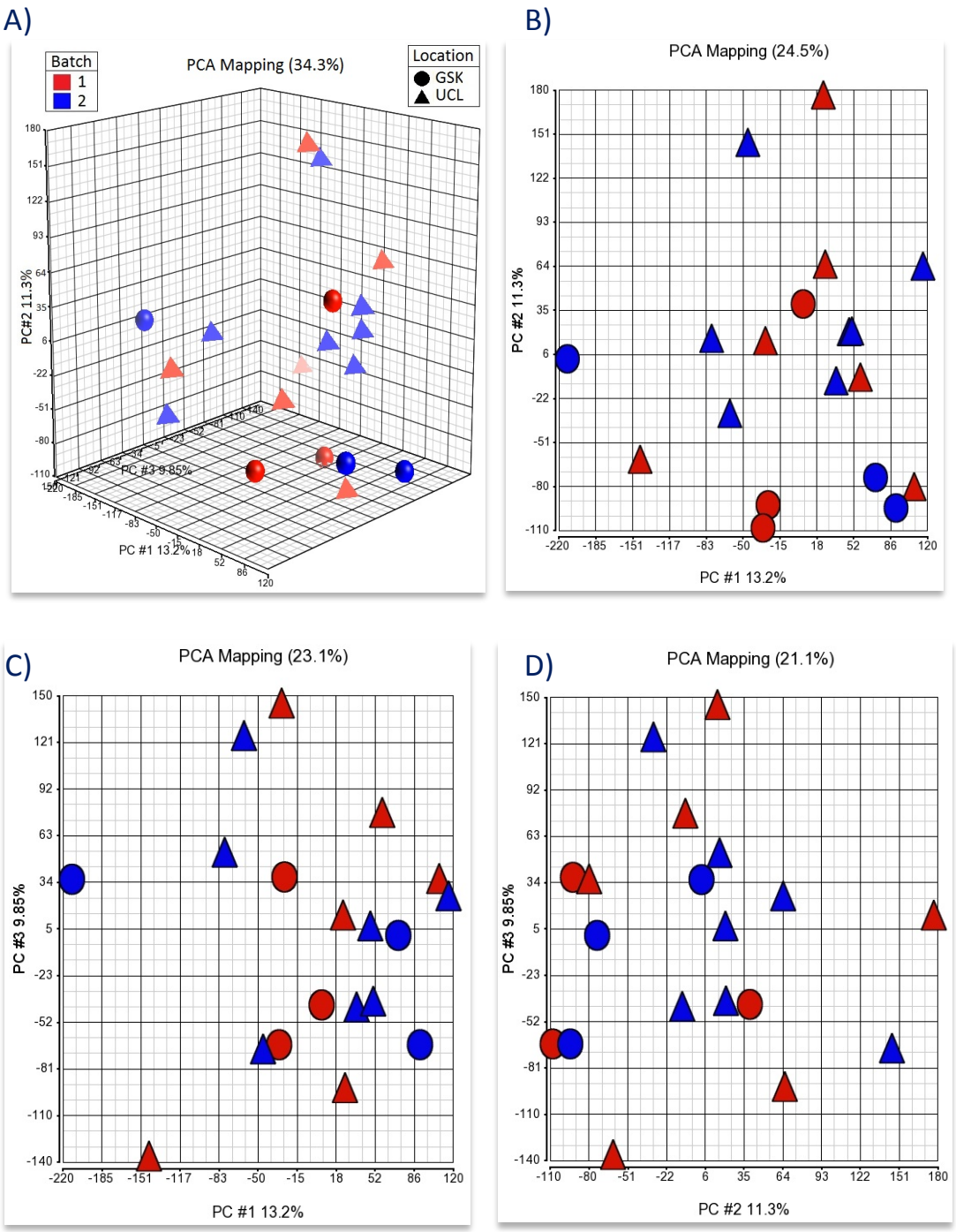

Figure 3. 52. Principle component analysis (PCA) plots for non-IPF and IPF spheroid microarray data after the removal of batch and location bias.

(A) Three-dimensional PCA plot. Proportion of variance explained: PC1, 13.2 % (x-axis); PC2, 11.3 % (y-axis); PC3, 9.85 % (z-axis). (B-D) Two-dimensional PCA plots for the same data: (B) PC1 vs. PC2; (C) PC1 vs. PC3; (C) PC2 vs. PC3. ANOVA factors: gender and condition (i.e. non-IPF, n=9; and IPF, n=10). Batch and location bias effects were removed. Red = batch 1; blue = batch2; circle/sphere = GSK (GlaxoSmithKline); triangle/tetrahedron = UCL (University College London).

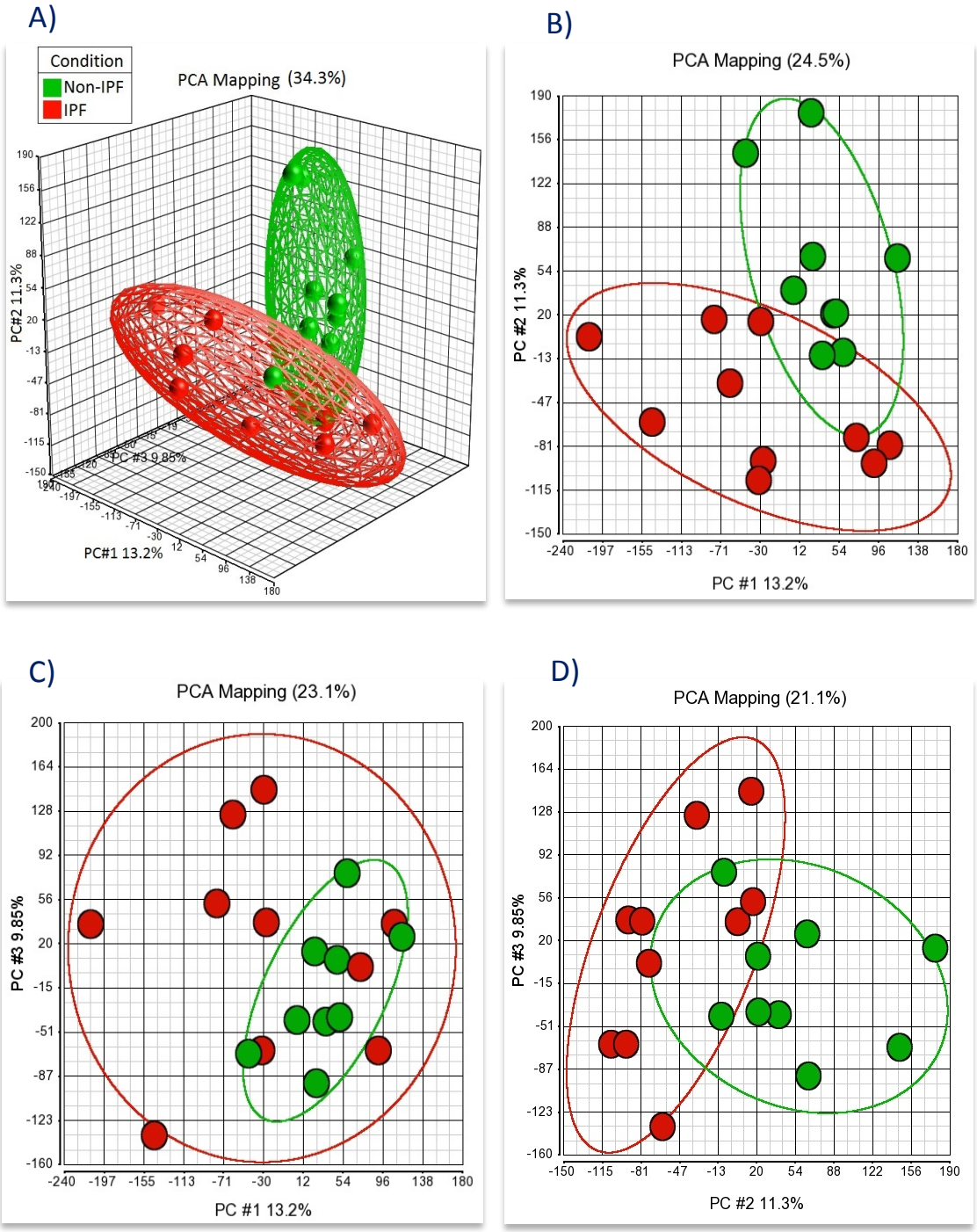

Figure 3. 53. Principle component analysis (PCA) plots illustrating clear separation of non-IPF and IPF spheroid gene expression after the removal of batch and location effects.

The same PCA analysis from Figure 3.52 was re-plotted to indicate the distribution of non-IPF and IPF samples on the PCA plot. (A) Three-dimensional PCA plot. Proportion of variance explained: PC1, 13.2 % (x-axis); PC2, 11.3 % (y-axis); PC3, 9.85 % (z-axis). (B-D) Two-dimensional PCA plots for the same data: (B) PC1 vs. PC2; (C) PC1 vs. PC3; (C) PC2 vs. PC3. ANOVA factors included condition effect (i.e. non-IPF and IPF). Batch and location effects were removed. Green = non-IPF (n=9); red = IPF (n=10). Ellipsoids/ellipses were applied using Partek Genomics Suite to help visualise the groupings.

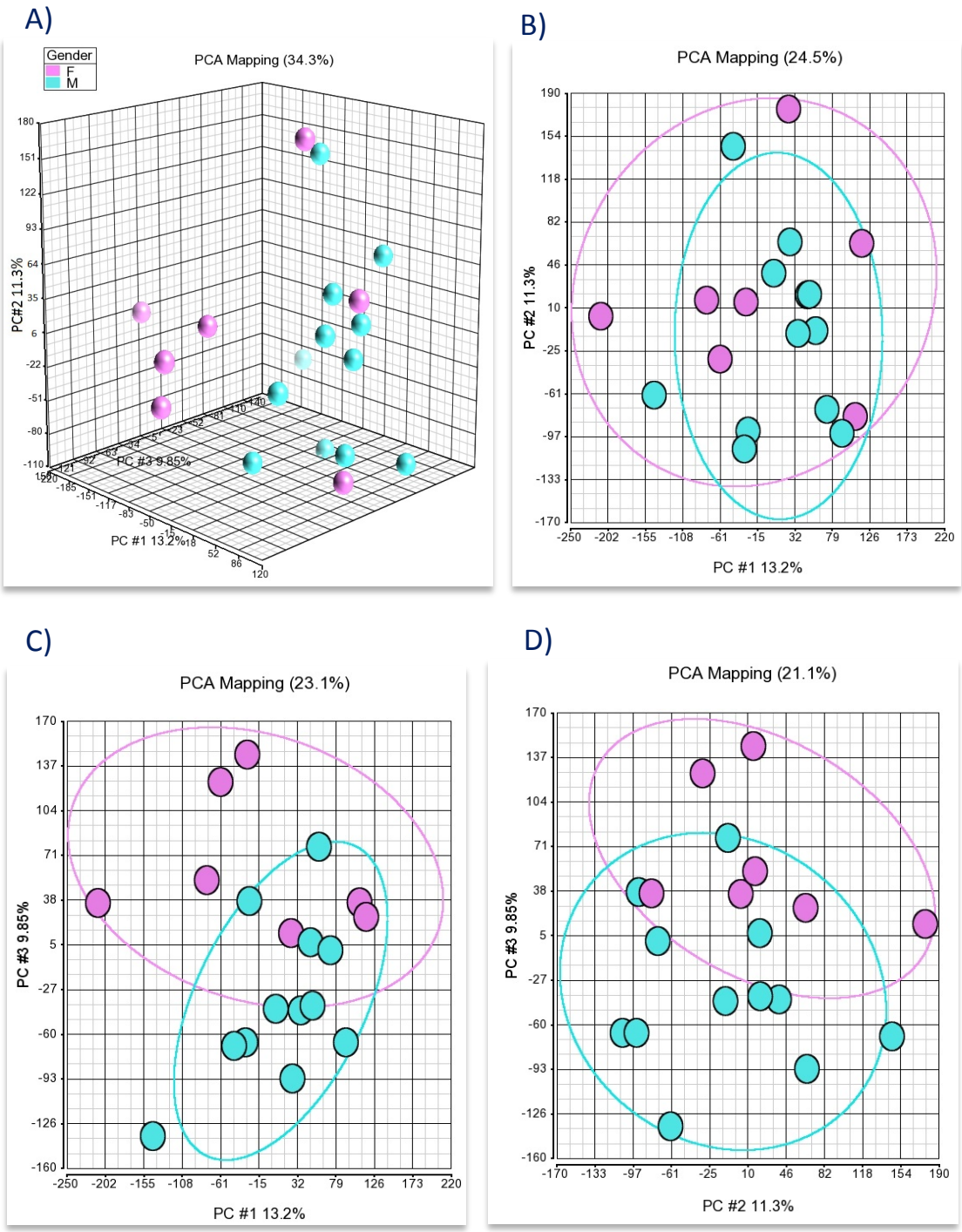

Figure 3. 54. Principle component analysis (PCA) plots illustrating a slight gender effect in gene expression of non-IPF and IPF spheroids after the removal of batch and location effects.

The same PCA analysis from Figure 3.52 was re-plotted to indicate the distribution of gender amongst the samples on the PCA plot. (A) Three-dimensional PCA plot. Proportion of variance explained: PC1, 13.2 % (x-axis); PC2, 11.3 % (y-axis); PC3, 9.85 % (z-axis). (B-D) Two-dimensional PCA plots for the same data: (B) PC1 vs. PC2; (C) PC1 vs. PC3; (C) PC2 vs. PC3. ANOVA factors included condition effect (i.e. non-IPF and IPF). Batch and location effects were removed. Pink = female; blue = male. Ellipses were applied using Partek Genomics Suite to help visualise the groupings.

3.4.4. Visualisation and pathway analysis

Hierarchical clustering is an approach used to identify groups (or clusters) of genes with similar expression profiles (in response to the same environmental factors) to build a hierarchy. **Figure 3.55** illustrates a heat map with hierarchical clustering for the 138 differentially expressed genes in non-IPF (n=9) and IPF (n=10) spheroid samples identified following two-way ANOVA with a fold change of >2 or <-2 and a p value (including false discovery rate [FDR]) of <0.05. Red indicates up-regulated genes, green represents down-regulated genes, and black illustrates genes with no difference in expression. The results illustrate clear separation of differentially expressed genes clustered into two groups (i.e. non-IPF and IPF). There is also evidence of gender clustering in non-IPF and IPF cohorts

Out of the 138 genes, 76 had known functions, whilst 66 genes were unknown (see **Appendix 2**, **Table A1**). The top three differentially expressed genes are shown in **Figure 3.56** which were: *PRR14L* (proline rich 14-like, unknown function), *CTSB* (cathepsin B), and *PTGER3* (prostaglandin E2 receptor 3).

STRING 9.1 (freely available online software tool) was used to retrieve known protein-protein interactions (encoded by the 72 genes with known function). As illustrated in **Figure 3.57**, very little interaction between the differentially expressed genes was evident (grey line indicates co-expression; blue line indicates protein binding; black line indicates evidence of interaction). Partek pathway analysis was also used to determine groups of genes that are regulated in a co-ordinate fashion within a particular biological pathway. This was based on the pathway enrichment score (the negative log/base 10 of the average enrichment p-value derived from the Fisher's Exact test). The software identified 27 pathways with an enrichment p<0.05 by utilising the Kegg databases for human (See **Appendix 2, Table A2).** The database is a collection of pathway maps which represent our knowledge on molecular interaction and reaction networks for genetic information processing, metabolism, cellular processes, human diseases, environmental information processing, organismal systems, and drug development. Based on the analysis phototransduction pathway showed the highest enrichment score of 7.3, however only three genes from this pathway were present in the list of differentially expressed genes. These were *CALM1, CALM2*, and *CALM3* which are involved in encoding the calcium-modulated proteins, calmodulin 1, calmodulin 2, and calmodulin 3, respectively (also known as phosphorylase kinase delta). Calmodulin is also involved in several other pathways including metabolism, apoptosis, inflammation, and smooth muscle contraction all of which showed

high enrichment scores with p<0.05. Metabolic pathways showed the highest number of genes regulated which were *CS* (citrate synthase), *IMPDH2* (Inosine-5'-monophosphate dehydrogenase 2), *MTHFR* (methylenetetrahydrofolate reductase), *P4HA1* (prolyl 4-hydroxylase subunit alpha 1), *SPTLC2* (serine palmitoyltransferase), *SYNJ2* (synaptojanin 2), and *XDH* (xanthine dehydrogenase; **Figure 3.58**).

Since only a limited number of genes showed differential expression following two-way ANOVA with a fold change of >2 or <-2 and a p value with false discovery rate (FDR) of <0.05, the analysis was also repeated by performing two-way ANOVA with a fold change of >2 or <-2 and a p value (unadjusted) of <0.01. Based on these less stringent criteria, 730 genes showed differential expression (**Figure 3.59**). Unlike the previous analysis, the clustering of non-IPF and IPF is less well defined and the gender effect is less apparent.

Figure 3.61 illustrates interactions between the differentially regulated genes with more protein-protein interactions evident in comparison to **Figure 3.57**. Partek pathway analysis identified 31 pathways with an enrichment p<0.05 (by utilising the KEGG database) of which the 'Influenza A' pathway showed the highest enrichment score of 7.2 (see **Appendix 2, Table A3**). Within this pathway 12 genes from the list of differentially expressed genes were identified. These included: *CASP1, CCL2, DDX58, IFIH1, IL1A, IL33, MX1, OAS2, OAS3, PIK3R1, PML*, and *PRKCB* (**Figure 3.61**).

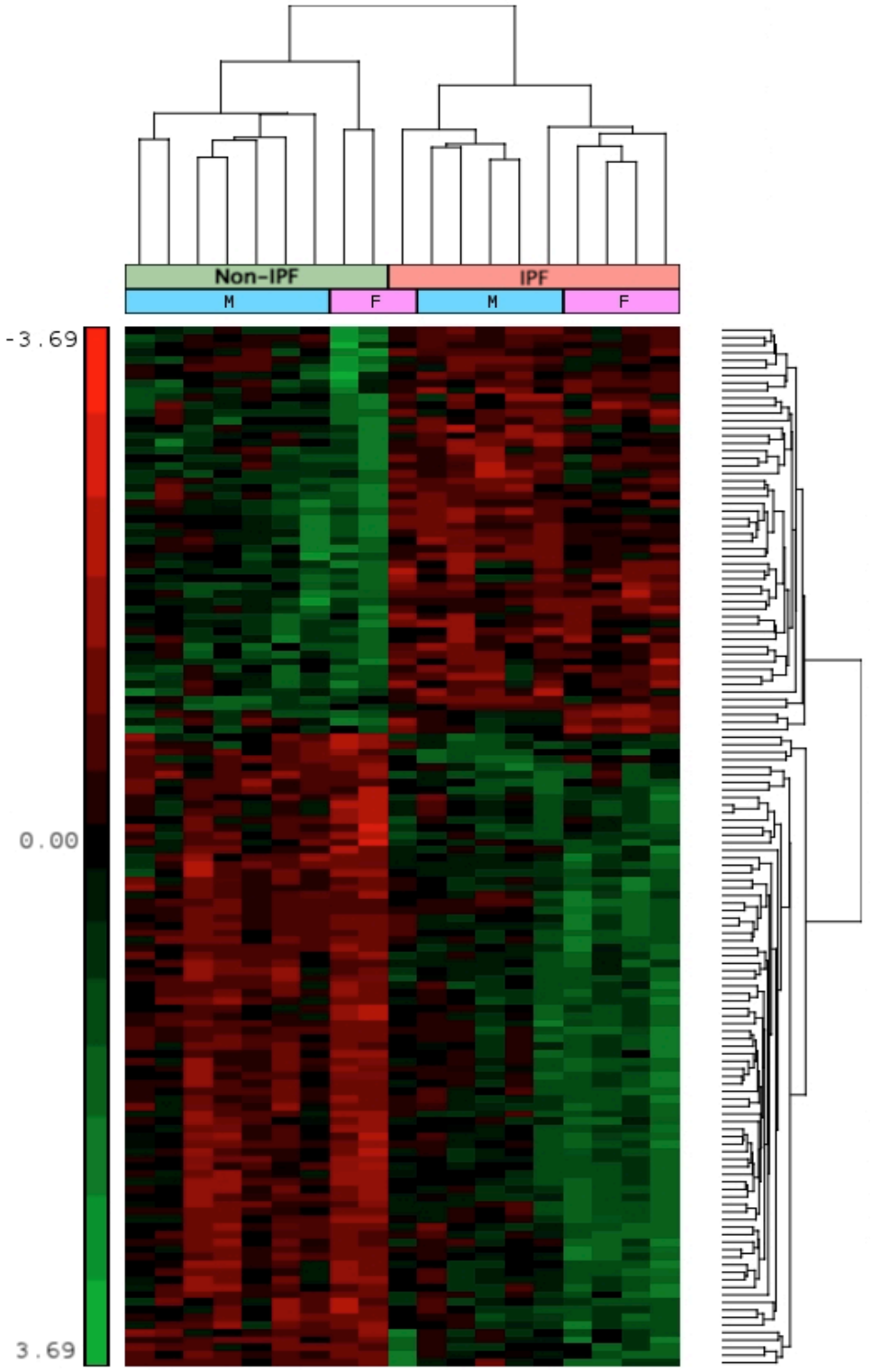

Figure 3. 55. Hierarchical clustering for differentially expressed genes in non-IPF and IPF fibroblast spheroids.

Clear separation of differentially expressed genes clustered into two group (i.e. non-IPF and IPF). There is also evidence of gender clustering in non-IPF and IPF cohorts (M = male; F = female). Red indicates upregulated genes, green represents downregulated genes, and black indicates genes with no difference in regulation. Fold change >2 or <-2 with FDR and $p<0.05$. In total 138 genes were identified.

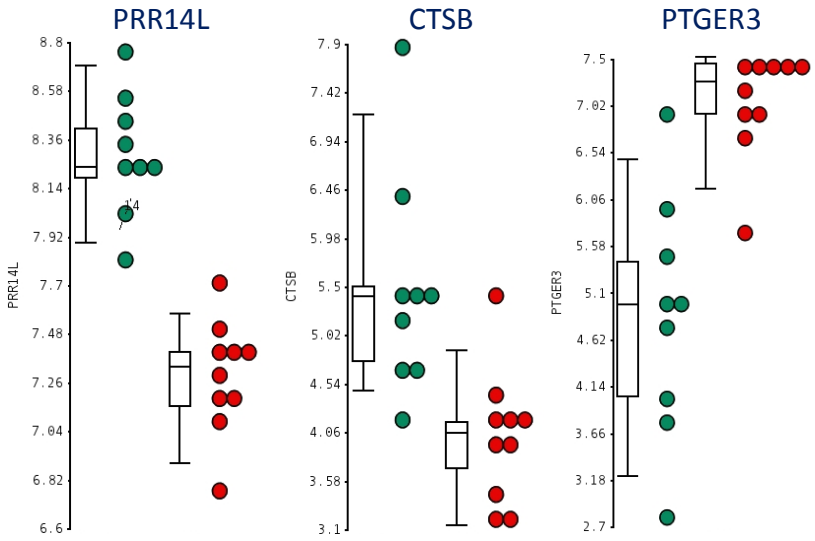

Figure 3. 56. Distribution of gene intensity values for the top three differentially expressed genes across all non-IPF and IPF spheroid samples following microarray data analysis.

Non-IPF (green; n=9) vs. IPF (red; n=10), FDR P<0.05, fold change >2 or <-2.

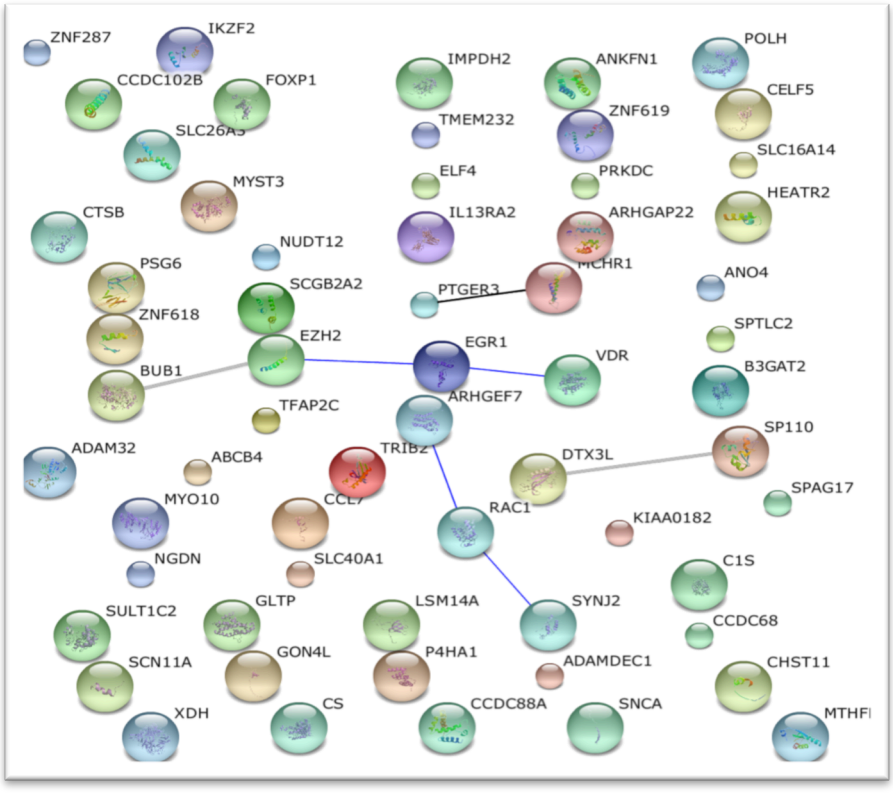

Figure 3. 57. Known protein-protein interaction identified using STRING 9.1.

Each circle represents an individual protein encoded by the differentially expressed genes in non-IPF and IPF spheroids (fold change >2 or <-2 with FDR and p<0.05). Grey lines indicate co-expression; blue lines indicate protein binding; black line indicates evidence of action. This selection of differentially expressed genes appears to have very little direct interaction.

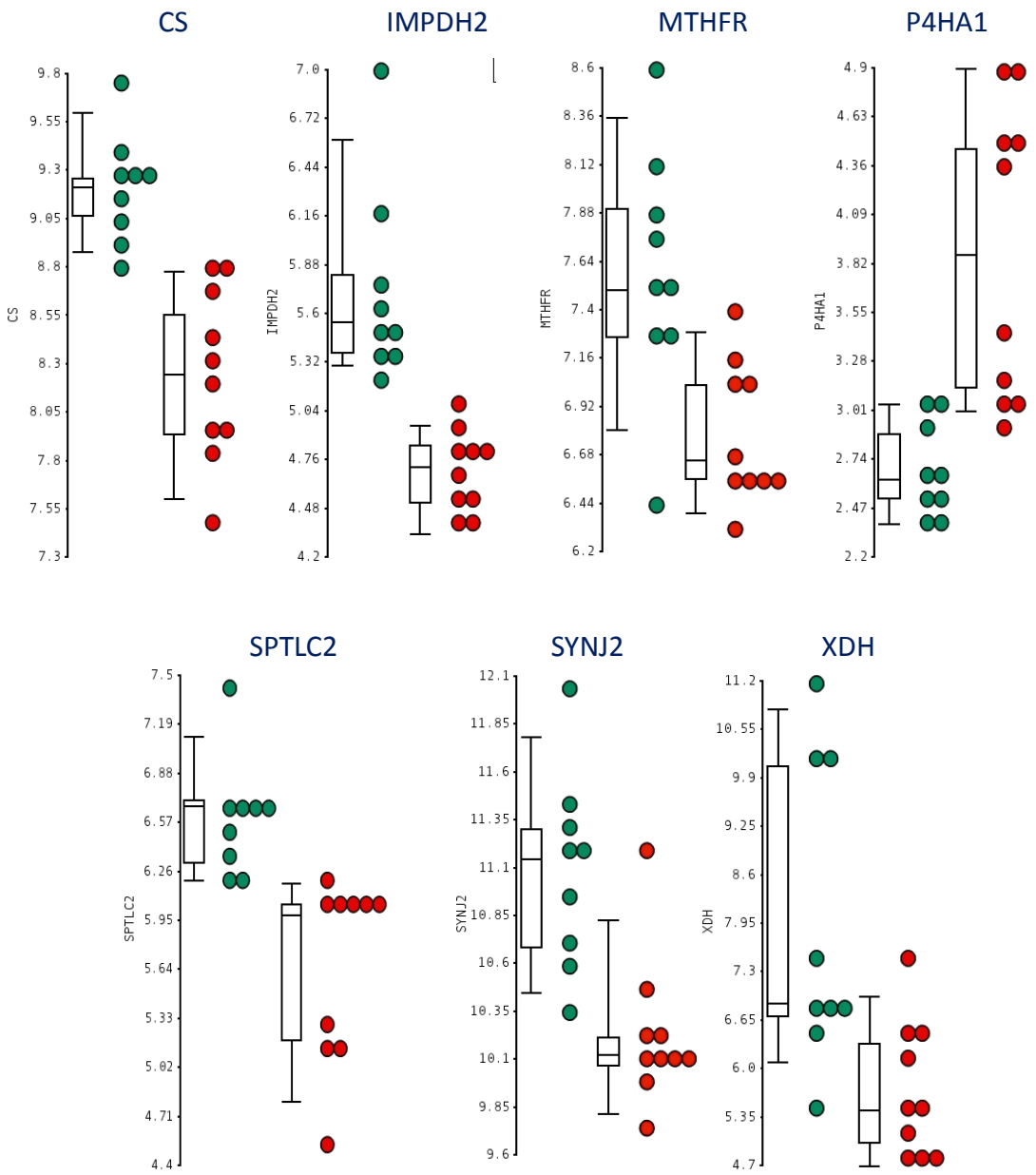

Figure 3. 58. Distribution of gene intensity values for the differentially expressed genes involved in metabolic pathway across all non-IPF and IPF spheroid samples following microarray data analysis.

Non-IPF (green; n=9) vs. IPF (red; n=10), FDR p<0.05, fold change >2 or <-2.

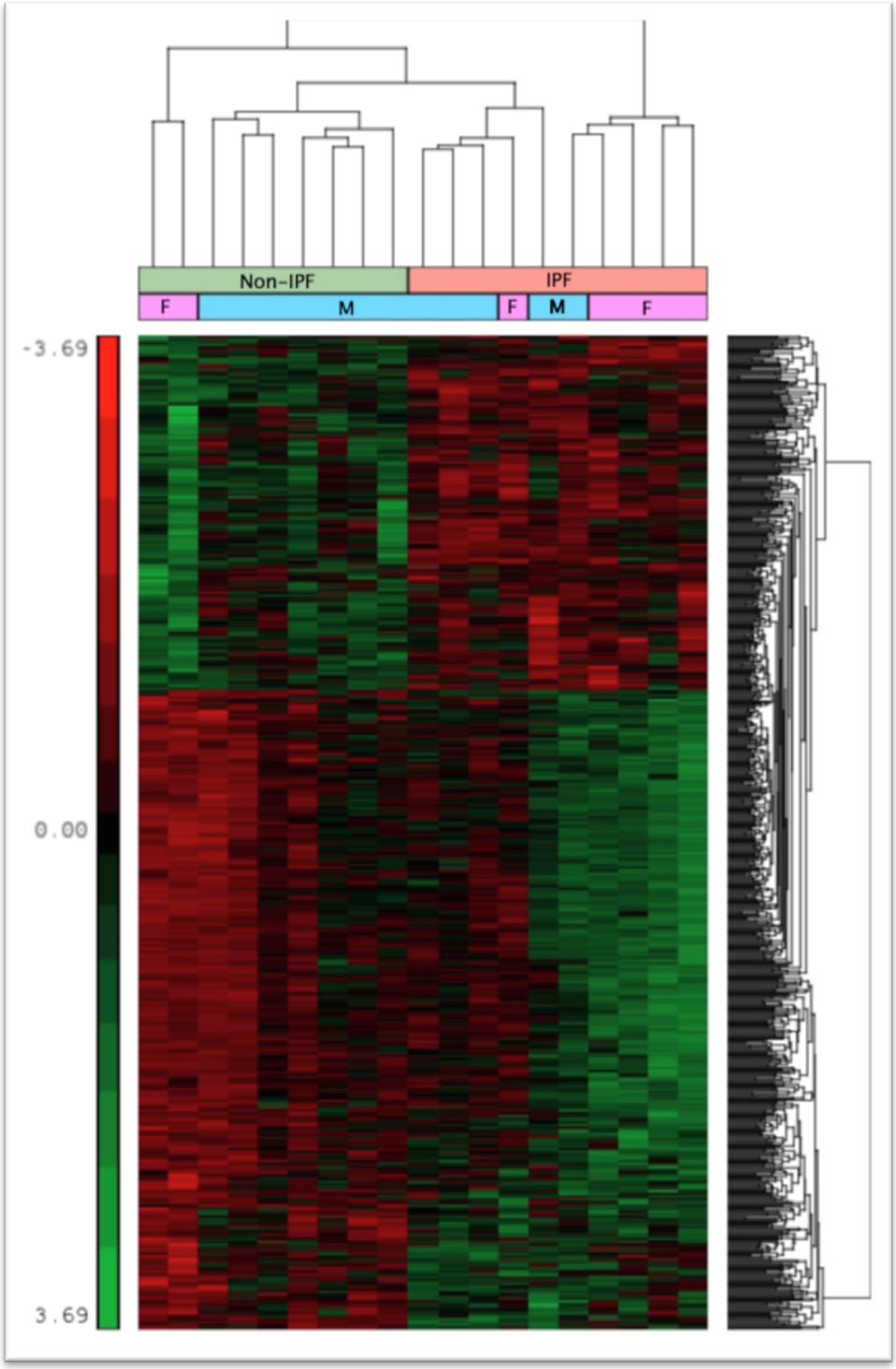

Figure 3. 59. Hierarchical clustering for differentially expressed genes in non-IPF and IPF fibroblast spheroids.

The clustering of non-IPF and IPF is less well-defined and the gender effect is less apparent when using the following threshold: fold change >2 or <-2, unadjusted, $p<0.01$. In total 730 genes were identified. Red indicates upregulate genes, green represents down regulated genes, and black indicates genes with no difference in regulation.

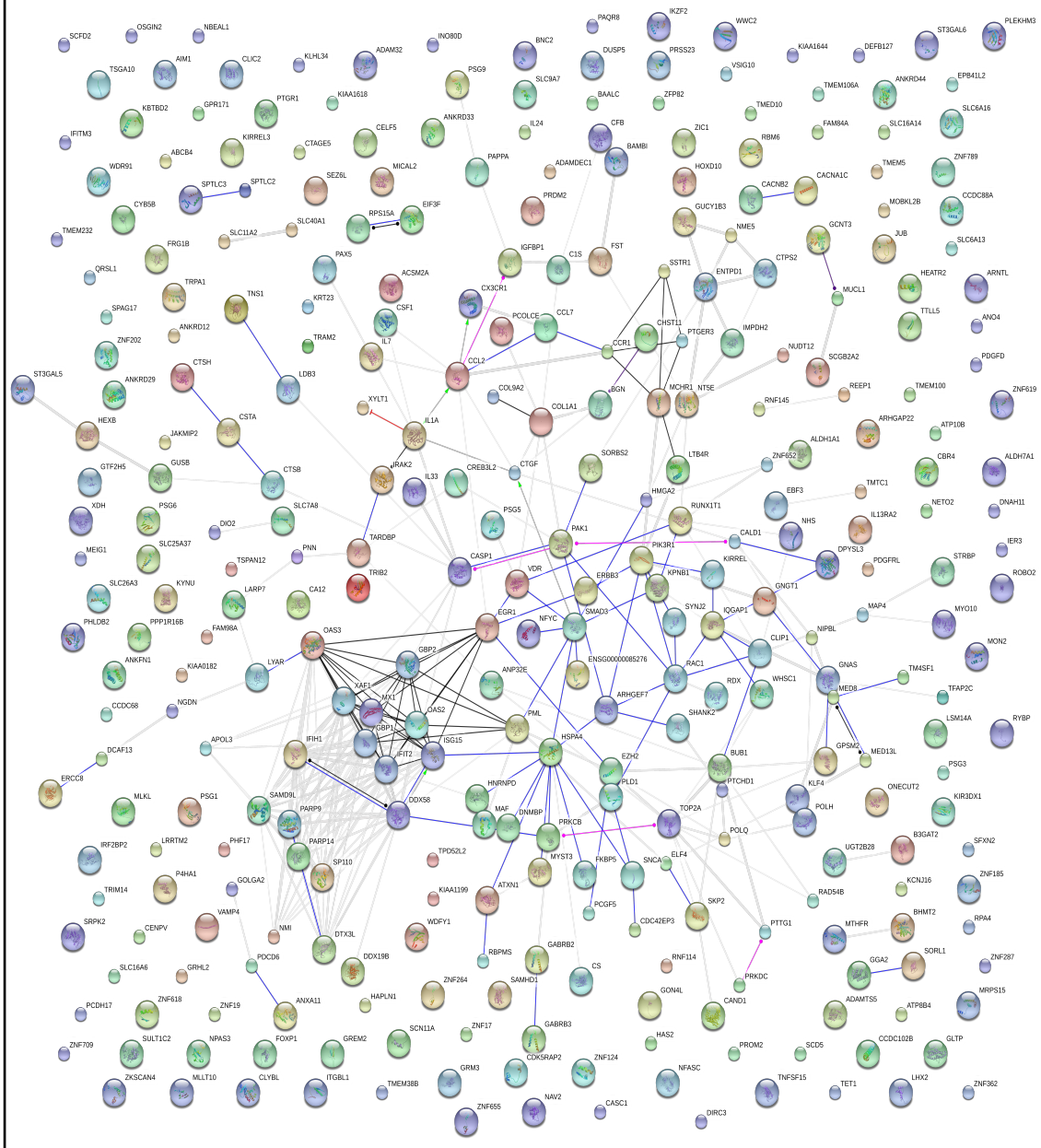

Figure 3. 60. Known protein-protein interactions identified using STRING 9.1.

Each circle represents an individual protein encoded by the differentially expressed genes in non-IPF and IPF spheroids (fold change >2 or <-2 with unadjusted p<0.01). Grey lines indicate co-expression; blue lines indicates protein binding; black line indicates evidence of action; pink line represents post-translational modifications; green indicates activation; yellow represents expression with inhibition.

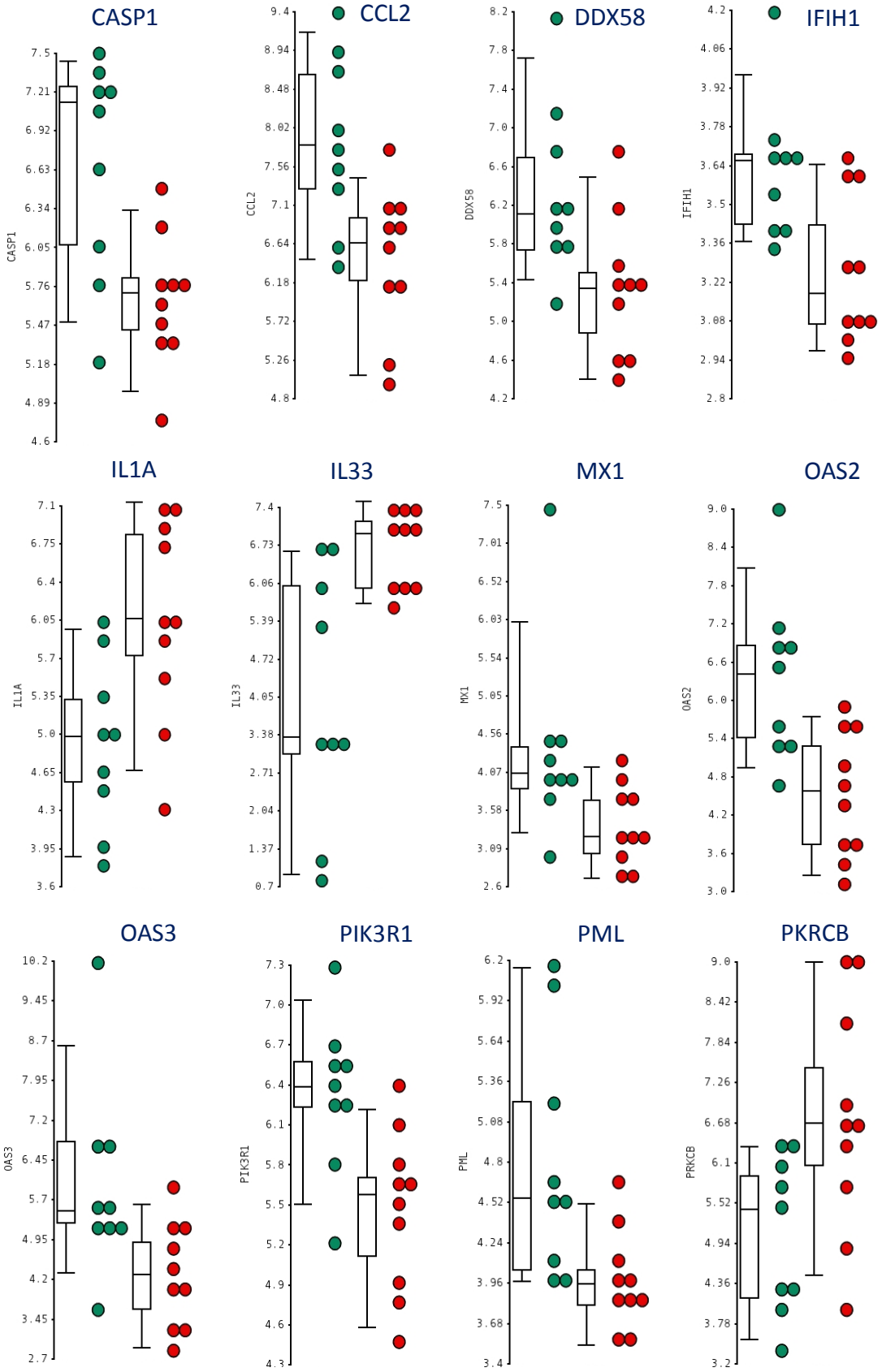

Figure 3. 61. Distribution of probe intensity values of genes involved in Influenza A across all non-IPF and IPF spheroid samples following microarray data analysis.

Non-IPF (green; n=9) vs. IPF (red; n=10), unadjusted p<0.01, fold change >2 or <-2.

3.4.5. Summary

In this section the following were demonstrated:

- All RNA samples were technically of high quality, however only 19 out of 20 samples were taken forward for analysis as one sample was identified as a clear outlier by PCA.
- Removal of batch and location bias resulted in a clear separation between non-IPF and IPF samples by PCA.
- 138 differentially expressed genes were identified between non-IPF and IPF samples with FDR and $p<0.05$ and fold change >2 or <-2. However, only 72 had known functions and only a few protein-protein interactions were detected using STRING 9.1. The top three differentially expressed genes were *PRR14L, CTSB,* and *PTGER3*.
- Partek pathway analysis illustrated the phototransduction pathway with the highest enrichment score however, genes involved in encoding calmodulin were the only ones detected in this pathway. Metabolic pathways showed the most number of differentially expressed genes.
- 730 genes passed the threshold of $p<0.01$ (unadjusted) and fold change of >2 or <-2, of which 414 genes encoded proteins with known functions. More protein-protein interactions were evident in comparison to previous analysis, of which a majority were either co-expressed or known to directly interact with one another.
- Partek pathway analysis demonstrated the 'Influenza A' pathway with the highest enrichment score. 12 genes (*CASP1, CCL2, DDX58, IFIH1, IL1A, IL33, MX1, OAS2, OAS3, PIK3R1, PML*, and *PRKCB*) were identified in the list of differentially expressed probes belonging to this pathway. Future work will involve further analysis of these genes identified by performing qRT-PCR.

3.5. Medium-throughput compound screening

3.5.1. Introduction

Effective treatment for halting the progression of IPF is currently unavailable (although two therapies are now available which have some impact on slowing progression, i.e. pirfenidone and nintedanib). However, numerous research and lead compounds have been developed based on several *in vivo* and *in vitro* studies on lung fibrosis. GSK have generated a focused compound toolbox (known as the 'fibrosis toolbox') composed of 182 compounds that target many different pathways which may potentially be involved in the initiation/progression of this lethal disorder. Such pathways include TGFβ signalling, prostanoid signalling, and developmental pathways (e.g. Wnt and Shh signalling pathways). Screening of these compounds is currently being performed at GSK using other *in vitro* models of fibrosis (i.e. scar-in-a-jar and lung slices). To investigate the effect of these compounds on fibroblast cultured as spheroids a medium-throughput screening was performed. This involved culturing non-IPF (n=1) and IPF (n=1) fibroblasts for spheroid formation with a 10 μM concentration of each of the 182 compounds, in a 96well plate format. The primary end point involved determining total collagen content by performing HPLC. Compounds that showed 50 % or more change in collagen synthesis from baseline, were considered as a 'hit'. In this section the effects of some compounds will be highlighted. Due to confidentiality, only a more limited repertoire of the toolbox will be described.

3.5.2. Targeting collagen biosynthetic pathway

Lysyl oxidase (LOX) is an amine oxidase which catalyses the covalent crosslinking of collagen fibres. Previous studies have illustrated that mice treated with anti-lysyl oxidase-like (LOXL)-2 reduced the fibrotic burden (i.e. decline in disease-associated fibroblasts, reduced synthesis of growth factors, decrease in cross-linked collagenous matrix, and reduced TGFβ signalling) following bleomycin administration. Thus, it has been postulated that *in vivo* LOXL2 may mediate the activation of fibroblasts via catalysing crosslinking of fibrillar collagen and a corresponding increase in tension of the local matrix, leading to the release of active TGFβ from its latent form (Barry-Hamilton et al., 2010). Therefore, it was hypothesised that antagonising LOX activity might also decrease collagen deposition within fibroblast spheroids. However, as shown in **Figure 3.62** LOX and LOXL2 antagonists (at 10μM) only partially

attenuated collagen production (<25 % change from baseline) in non-IPF spheroids, little or no effect seen in IPF spheroids. In addition, **Figure 3.62** also illustrates the effect of heat shock protein 47 (HSP47) inhibitor on collagen synthesis. HSP47 is a collagen-specific molecular chaperone which transiently binds to procollagen in the ER and dissociates in the Golgi to facilitate triple helix formation (Ishida and Nagata, 2011). Previous studies in experimental animal fibrosis models have illustrated that reduced expression of HSP47 resulted in an attenuation in collagen synthesis (Sunamoto et al., 1998; Nishino et al., 2003; Hagiwara et al., 2007a, 2007b; Obata et al., 2012). Furthermore, recent studies have illustrated elevated levels of HSP47 in serum of IPF patients experiencing acute exacerbations (Kakugawa et al., 2013). Thus, it was hypothesised that inhibition of HSP47 activity would attenuate collagen synthesis within spheroids. Spheroids treated with 10 μM GSK-1, in fact reported a slight elevation in collagen production in both non-IPF and IPF spheroids (approximately 10 % change from baseline). The fibrosis toolbox also consisted of bone morphogenetic protein (BMP)-1 antagonists. Unlike most BMPs, BMP1 does not belong to the TGFβ superfamily. In fact, BMP-1 contributes to matrix stiffness by promoting the cleavage and activation of LOX. Furthermore, studies have demonstrated the BMP1 is able to associate with a matricellular protein known as periostin which localises BMP1 to the provisional ECM deposition (Maruhashi et al., 2010). Recently two studies have demonstrated elevated levels of periostan in the circulation and lungs of IPF patients (Okamoto et al., 2011; Naik et al., 2012). My results illustrate that BMP1 inhibitors GSK-4 and GSK-5 reduced collagen production in non-IPF spheroids. Furthermore, GSK-5 also attenuated collagen synthesis in IPF spheroids by ~45 %.

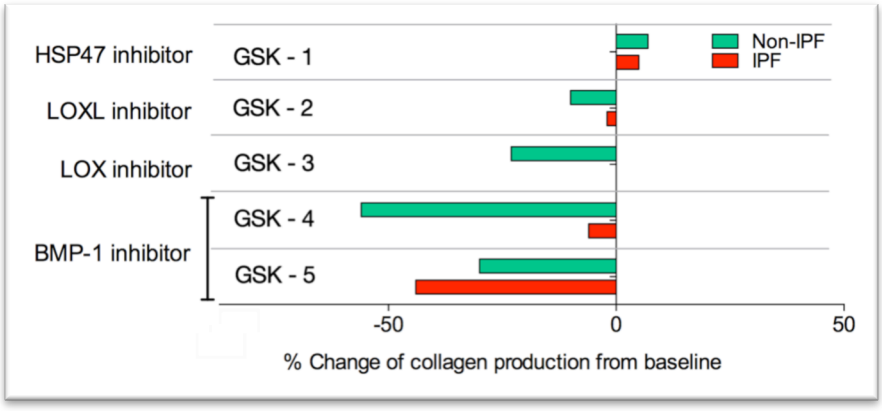

Figure 3. 62. Effects of HSP47, LOX, and BMP-1 inhibitors on collagen synthesis.

Non-IPF (green; n=1) and IPF (red; n=1) spheroids were prophylactically treated with the potential anti-fibrotic compounds shown (10 μM). Spheroids were collected 24 hours post-treatment and hydrolysed in 6 M HCl for HPLC analysis of hydroxyproline levels.

3.5.3. Targeting TGFβ signalling pathway

As stated previously, TGFβ is a potent pro-fibrotic cytokine. Several studies have supported the role of TGFβ in collagen synthesis. However the current data illustrated in this thesis suggest that collagen production is independent of TGFβ signalling in fibroblasts spheroids. This is also supported by data for a majority of the compounds targeting the TGFβ signalling pathway within the fibrosis toolbox (**Figure 3.63**). Nevertheless, some compounds did show over 50 % attenuation in collagen synthesis including a pan αv integrin antagonist (100 % attenuation in non-IPF spheroids) and a non-specific ALK-4/5/7 antagonist (100 % attenuation in IPF spheroids). Since there were a few hits in the compounds targeting the TGFβ signalling pathway further investigations are needed to investigate the IC50/EC50 of these compounds in multiple donors. This is because during the compound screening, the spheroids were treated with one high concentration. Thus, the effects seen could merely be due to toxicity.

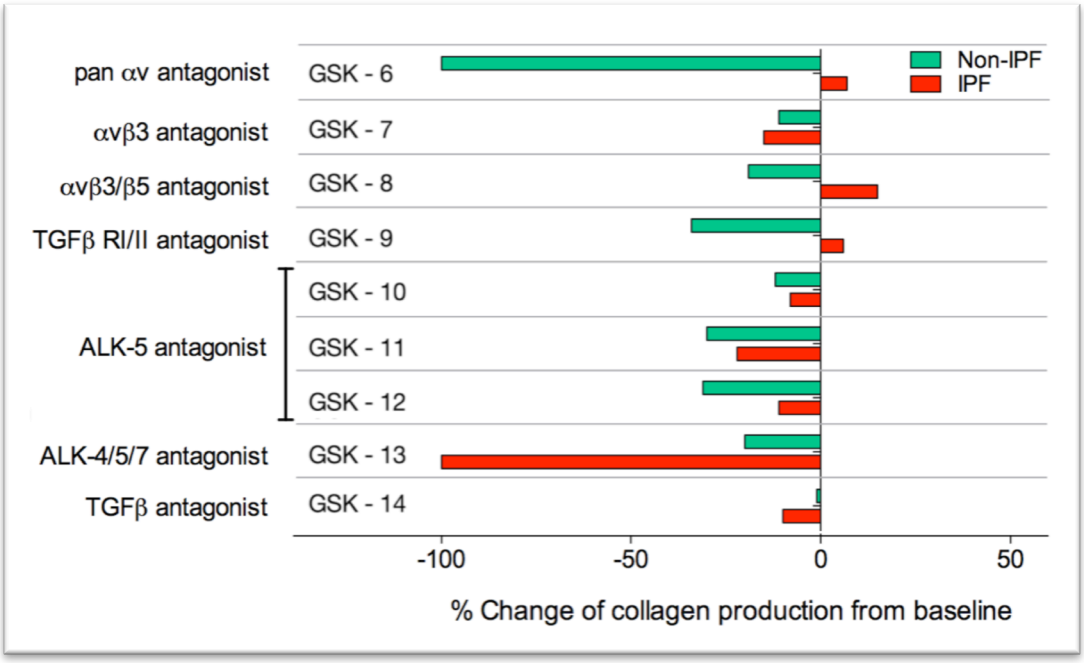

Figure 3. 63. Effects of compounds targeting TGFβ signalling on collagen synthesis in non-IPF and IPF spheroids.

Non-IPF (green; n=1) and IPF (red; n=1) spheroids were prophylactically treated with anti-fibrotic compounds (10 μM) targeting the TGF-beta receptors and integrins. Spheroids were collected 24 hours post-treatment and hydrolysed in 6 M HCl for HPLC analysis of hydroxyproline levels.

3.5.4. Targeting the eicosanoid pathway

The eicosanoid pathway involves the generation of prostaglandins, thromboxanes, and leukotrienes which are synthesised following the metabolism of arachidonic acid. Several *in vitro* and *in vivo* studies have illustrated the role of prostaglandins (i.e. PGE_2, PGI_2, and $PGF_{2\alpha}$) and leukotrienes in the pathogenesis of IPF (some of which have already been described). A number of the compounds within the toolbox also targeted the eicosanoid pathway. As illustrated in **Section 3.3**, PGE_2 plays a key role in spheroid apoptosis and collagen synthesis. This is also demonstrated in **Figure 3.64** whereby the addition of PGE_2 resulted in 80 % and 100 % attenuation of collagen synthesis in non-IPF and IPF spheroids, respectively. In addition, dual EP2/EP4 agonists and EP2 specific agonists also resulted in a hit (full dose responses for GSK-16, GSK-21, GSK-23, GSK-24, GSK-27, and GSK-32 compounds can be seen in **Section 3.3**, **Figure 3.42** and **Figure 3.43**).

Moreover, the $PGF_2\alpha$ receptor (FP) antagonist showed a >50 % increased production in collagen synthesis in IPF spheroids. Studies have illustrated that the plasma concentration of $PGF_{2\alpha}$ metabolite (15-keto-dihydro $PGF_2\alpha$) is elevated in IPF patients (Aihara et al., 2013). Furthermore, $PGF_{2\alpha}$ can potentiate PF via its receptor (FP) in bleomycin-induced lung fibrosis model (Oga et al., 2009). Thus, the increased collagen synthesis in IPF spheroids in the presence of FP antagonists contrasts with these previously published studies, and would benefit from further investigation.

5-LO antagonist and leukotriene D4 receptor antagonist also showed hits with increased production in collagen synthesis in comparison to baseline, in non-IPF spheroids only. Leukotrienes are products of lipoxygenase (i.e. 5-LO) which play a role in the host defence system against infection and invasion of foreign bodies (Yokomizo et al., 2001). BALF and lung tissues of IPF patients show elevated levels of LTB_4 (Wardlaw et al., 1989; Wilborn et al., 1996).

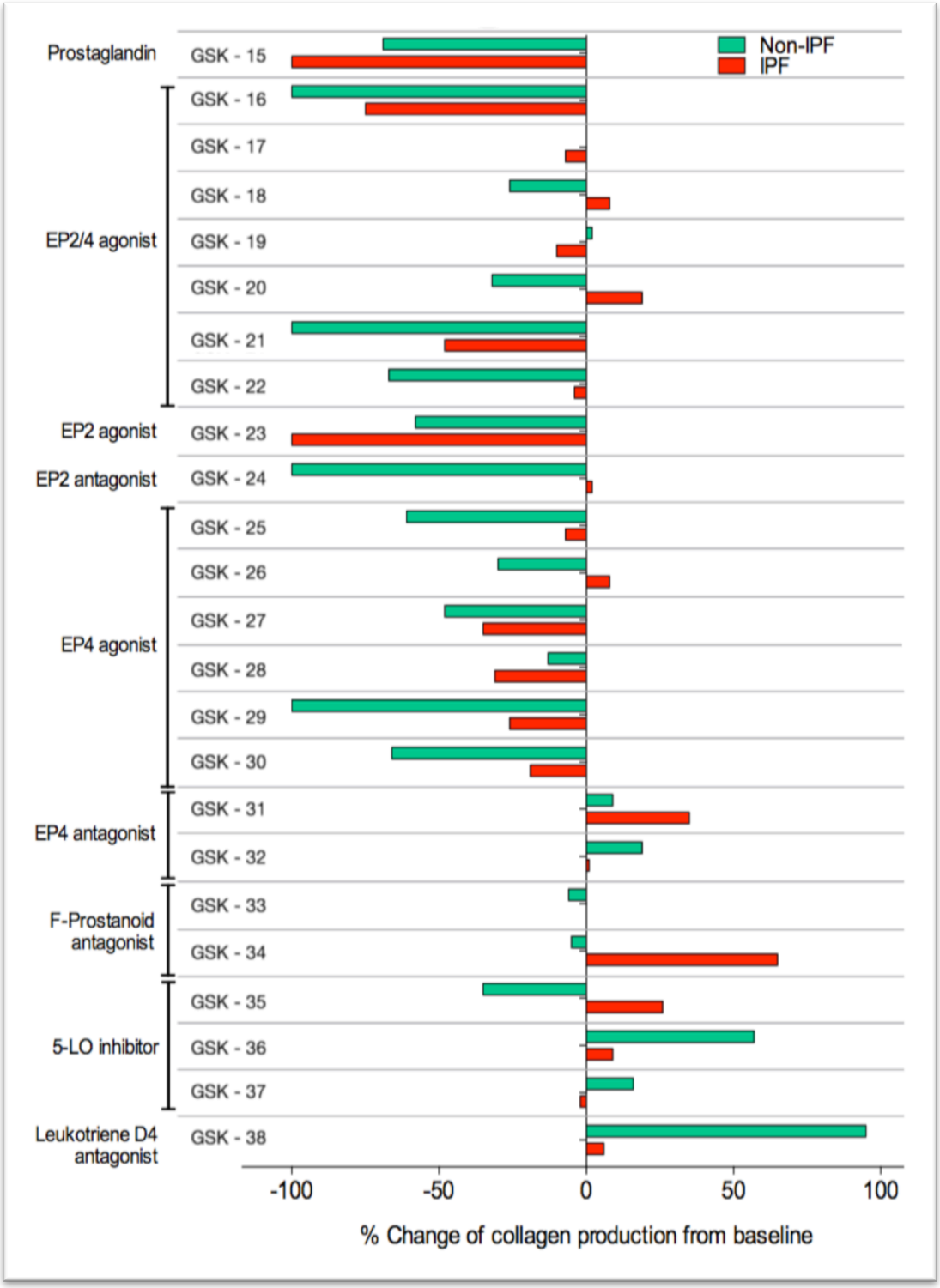

Figure 3. 64. Effect of compounds targeting eicosanoid pathway on collagen synthesis in spheroids.

Non-IPF (green; n=1) and IPF (red; n=1) spheroids were prophylactically treated with anti-fibrotic compounds (10 μM) targeting eicosanoid receptors. Spheroids were collected 24 hours post-treatment and hydrolysed in 6 M HCl for HPLC analysis of hydroxyproline levels.

3.5.5. Targeting ion channels

The fibrosis toolbox also consisted of compounds targeting the following ion channels: Ca^{2+}, $K_{Ca}3.1$, and Na^{+} channels. Ion channels have become an attractive therapeutic target in numerous chronic diseases however only a few studies have illustrated the effect of ion channels in models of PF. For instance, recent unpublished data by Rahaman et al. (2014) on Ca^{2+} channels (i.e. TRVP4; transient receptor potential vanilloid 4), illustrated that both human and murine fibroblasts express TRVP4 and knockdown/antagonism of this receptor (via siRNA or use of antagonist) abrogates TGFβ-induced myofibroblast differentiation and reduces the expression levels of collagen type I and PAI-1. In addition, TRVP4 knockout mice were protected from bleomycin induced PF suggesting a potential role for calcium channels in fibrogenesis (abstract submitted for conference proceedings by Rahaman et al., 2014).

$K_{Ca}3.1$ channel (calcium activated potassium channel) plays an essential role in calcium signalling by maintaining a negative membrane potential during cell activation (Fanger et al., 2001) thus modulating the activity of many cells including smooth muscle cells (Shepherd et al., 2007), mast cells (Cruse et al., 2006), and lymphocytes (Ghanshani et al., 2000). Studies on renal fibrosis have illustrated that pharmacological inhibition or genetic deletion of KCa3.1 prevents surgically-induced renal fibrosis in mice by targeting myofibroblasts, resulting in the decline in fibroblast proliferation and collagen synthesis (Grgic et al., 2009). In addition, a recent study by Roach et al. illustrated that IPF patients express high levels of $K_{Ca}3.1$ channel, and that TGFβ activated myofibroblasts had elevated $K_{Ca}3.1$ ion channel currents; pharmacological inhibition of $K_{Ca}3.1$ resulted in anti-fibrotic effects *in vitro* (i.e. attenuated collagen production and reduced fibroblast proliferation). These data support $K_{Ca}3.1$ channels as a potential target for IPF (Roach et al., 2013).

Figure 3.65 illustrates that the Ca^{2+} channel blockers attenuated collagen synthesis by >50 % in non-IPF spheroids however in IPF spheroids only minimal effects were seen. In addition the Na^{+} channel blocker increased collagen synthesis in non-IPF spheroids by 50 % and again minimal effect was shown in IPF spheroids. The $K_{Ca}3.1$ antagonist showed minimal effects in either non-IPF or IPF spheroids, with slight increase in collagen synthesis.

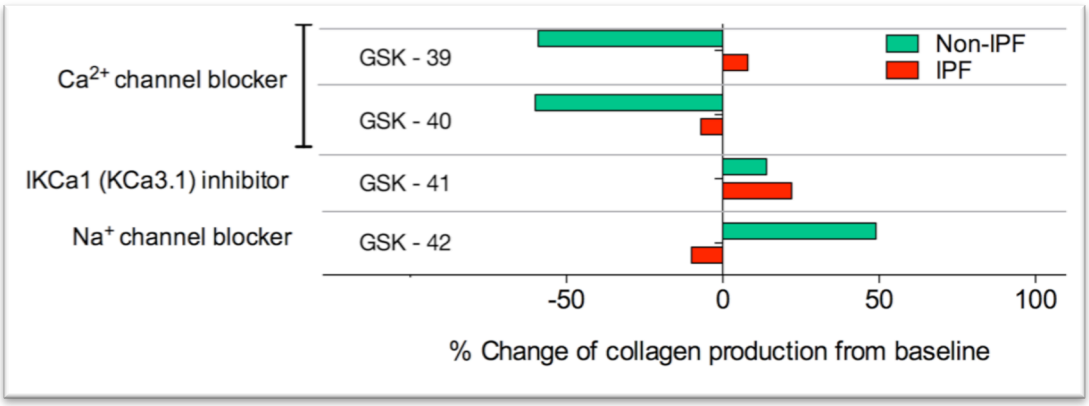

Figure 3. 65. Effect of compounds targeting ion channels on collagen synthesis in spheroids.

Non-IPF (green; n=1) and IPF (red; n=1) spheroids were prophylactically treated with anti-fibrotic compounds (10 μM). Spheroids were collected 24 hours post-treatment and hydrolysed in 6M HCl for HPLC analysis of hydroxyproline levels.

3.5.6. Targeting cytokines

Several chemokines and cytokines have been implicated in modulating different phases of the pathogenesis of lung fibrosis (namely fibrogenesis and inflammation). These include TGFβ (already described), macrophage migration inhibitory factor (MIF), monocyte chemotactic protein-1 (MCP-1/CCL2), and tumour necrosis factor-α (TNF-α).

MIF is a pleotropic proinflammatory cytokine synthesised by several cells including epithelial cells, macrophages, endothelial cells, neutrophils, lymphocytes, and eosinophils. This cytokine is considered as multifactorial as its role has been implicated in the inhibition of apoptosis (Morand, 2005), promotion of fibroblast migration and proliferation (Dewor et al., 2007), and induction of MMPs (Yu et al., 2007). Furthermore, studies have also illustrated elevated levels of MIF in BALF of IPF patients in comparison to control subjects. Positive immunostaining for MIF has been illustrated in areas of active fibrosis (i.e. fibrotic foci) and diffuse cellular infiltrates (Bargagli et al., 2009) supporting MIF as a potential therapeutic target.

CCL2 belongs to the C-C chemokine superfamily of small proteins produced by several cells including fibroblasts, monocytes/macrophages, and epithelial cells (Suga et al., 1999). CCL2 is primarily considered as a potent chemoattractant for monocytes, natural killer cells, and T-cells. However, it also plays a role in the activation of fibroblasts, promoting ECM production via the induction of TGFβ (Gharaee-Kermani and Phan, 2005) and contributing to excessive

collagen synthesis (Moore et al., 2005b). In IPF patients, protein and mRNA levels of CCL2 are elevated (Moore et al., 2001). Furthermore, CCL2 levels are statistically greater in serum and BALF of IPF subjects in comparison to healthy controls (Suga et al., 1999). *In vivo* studies have illustrated that mice deficient for the main CCL2 receptor (CCR2) and mice treated with anti-CCL2 gene therapy are protected from bleomycin induced PF (Smith et al., 1995; Inoshima et al., 2004). Together, these findings support the idea that CCL2 plays a vital role in the development of fibroproliferative lung disease and may also be considered as a potential target for the treatment of IPF.

TNFα has both inflammatory and fibrogenic properties and similar to MIF and CCL2, TNFα is also highly expressed in the lungs of IPF patients. Functional polymorphisms of TNFα have been linked to an increased risk of developing IPF (Datta et al., 2011). Several *in vivo* studies have supported that TNFα is a potential target for IPF. For instance, bleomycin-induced PF is diminished in mice injected with anti-TNFα antibodies (Piguet et al., 1989). Moreover, overexpression of TNF increases ECM protein deposition in the pulmonary interstitium (Miyazaki et al., 1995). Based on these findings a randomized, placebo-controlled phase II trial was performed which recruited 65 IPF patients to assess the safety and efficacy of a recombinant human TNFα receptor which inactivates TNFα (Etanercept). Unfortunately, no significant improvement was detected in IPF patients when measuring the change in FVC, DLCO, and P(A-a)O_2 at rest (as the primary endpoints) (Raghu et al., 2008).

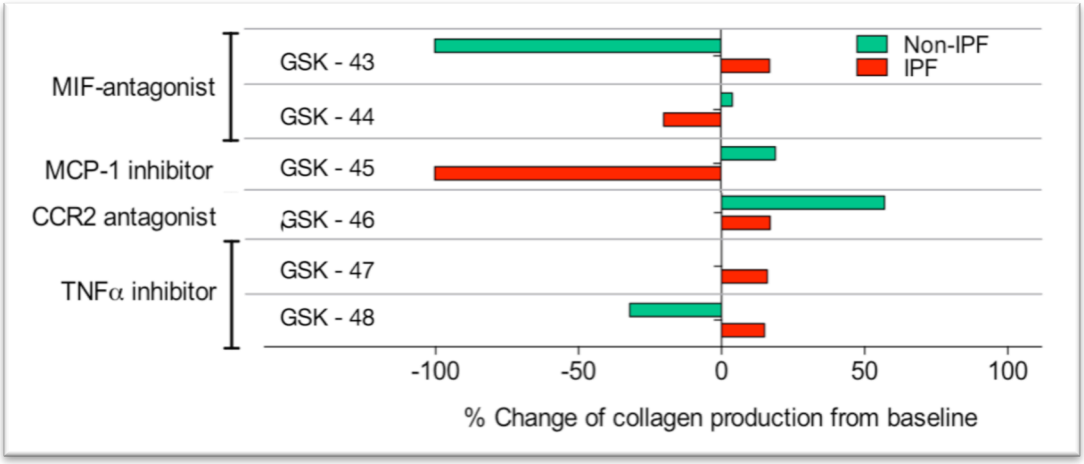

Figure 3. 66. Effect of compounds targeting cytokine receptors on collagen synthesis in spheroids.

Non-IPF (green; n=1) and IPF (red; n=1) spheroids were prophylactically treated with anti-fibrotic compounds (10 μM). Spheroids were collected 24 hours post-treatment and hydrolysed in 6M HCl for HPLC analysis of hydroxyproline levels.

The fibrosis toolbox consisted of compounds targeting receptors for MIF, MCP-1/CCL2, CCR2, and TNFα. Three positive hits were detected: MIF antagonist in non-IPF spheroids (100 % inhibition in collagen synthesis), MCP-1 inhibitor in IPF spheroids (100 % inhibition), and CCR2 antagonist in non-IPF spheroids (~60 % elevation in collagen production; **Figure 3.66**). TNFα inhibitor showed minimal effects in non-IPF and IPF spheroids supporting the results from the phase II clinical trial described above.

3.5.7. Targeting developmental pathways

Many studies have focused on the role of developmental pathways in the pathogenesis of IPF. Such include Wnt/β-catenin and Sonic hedgehog (Shh) pathways, both of which are strongly activated in IPF lung tissues (Chilosi et al., 2003; Bolanos et al., 2012). The toolbox composed compounds targeting these pathways: Tankyrase-1 inhibitor, Wnt inhibitor, and smoothened (Smo) antagonist. Tankyrase-1 is a poly-ADP-ribosyltransferase which is involved in the activation of the Wnt pathway by mediating poly-ADP-ribosylation of two components of the β-catenin destruction complex (AXIN1 and AXIN2).

As shown in **Figure 3.67A,** the tankyrase inhibitor GSK-50 attenuated collagen synthesis in non-IPF spheroids by 52 %. However minimal effect was evident in IPF spheroids. 10 μM GSK-49 also had little effect on collagen synthesis in either non-IPF or IPF spheroids. The Wnt inhibitor (GSK-51) attenuated collagen synthesis by ~90 % in non-IPF spheroids. A full concentration response of this compound in non-IPF (n=1) and IPF (n=2) spheroids is shown in **Figure 3.67B** and **Figure 3.67C, Figure 3.67D** respectively (for **Figure 3.67B** and **D** the donors were the same as the ones used in the screening). Based on these concentration response curves, the compound attenuated collagen synthesis >50 % in non-IPF spheroids and in IPF spheroids (one out of two donors), but only at high doses ranging between 3-10 μM. Both Smo antagonists (GSK-52 and GSK-53) completely abolished collagen production in IPF spheroids (100 % attenuation). A slight attenuation in collagen production was also evident in non-IPF spheroids (between 40-50 %). Given that Smo antagonist has a profound affect on collagen synthesis in IPF spheroids in comparison to non-IPF, further validation is necessary.

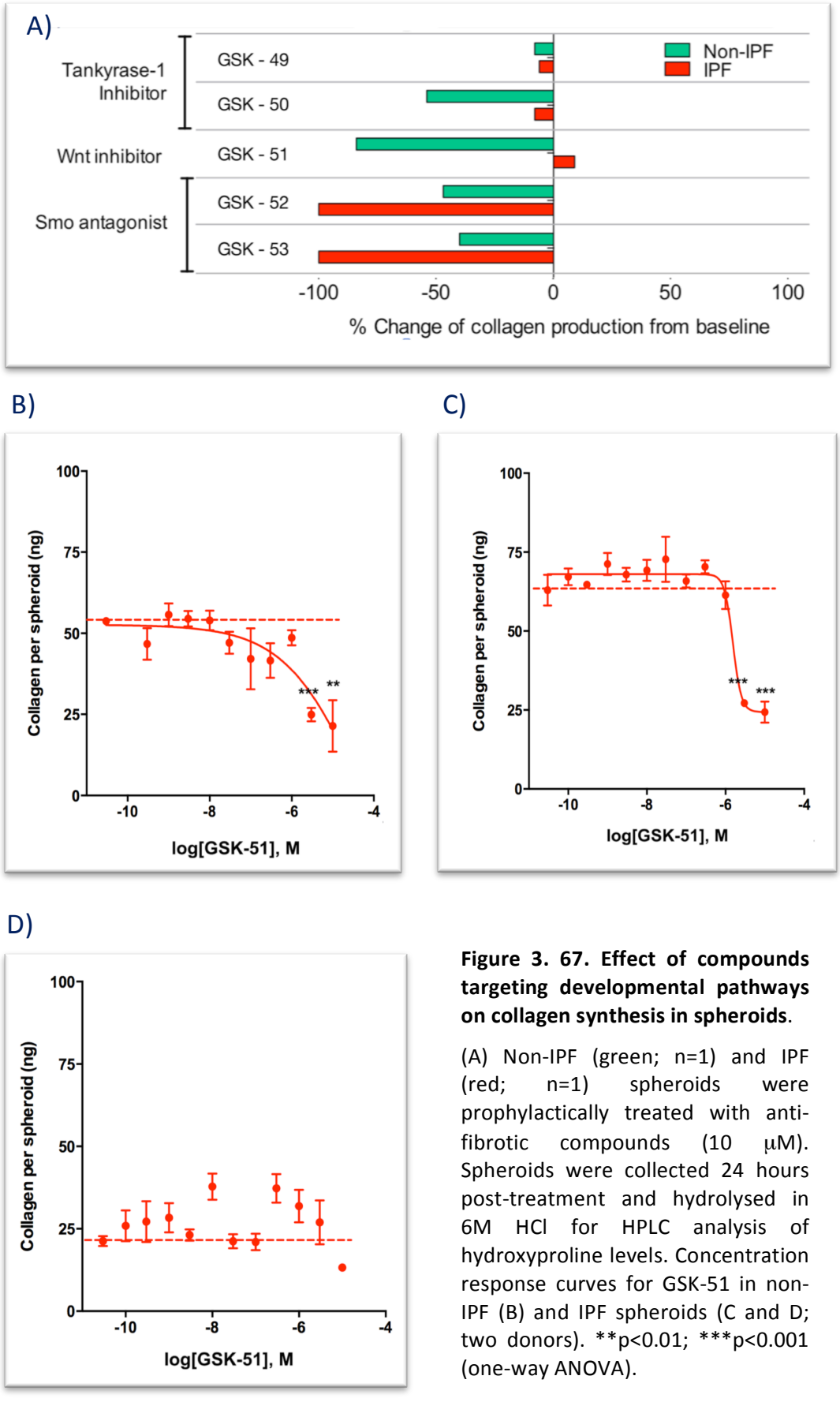

Figure 3. 67. Effect of compounds targeting developmental pathways on collagen synthesis in spheroids.

(A) Non-IPF (green; n=1) and IPF (red; n=1) spheroids were prophylactically treated with anti-fibrotic compounds (10 μM). Spheroids were collected 24 hours post-treatment and hydrolysed in 6M HCl for HPLC analysis of hydroxyproline levels. Concentration response curves for GSK-51 in non-IPF (B) and IPF spheroids (C and D; two donors). **p<0.01; ***p<0.001 (one-way ANOVA).

3.5.8. Targeting PI3K/Akt/mTOR pathway

PI3K is a lipid kinase which is activated in response to receptor tyrosine kinases, G protein coupled receptors/cytokine receptors and Ras. PI3K has been classified into three groups of which class I has been the most extensively studied. Class I PI3Ks are dimeric enzymes which are composed of catalytic and regulatory subunits. There are four isoforms for the catalytic subunit: p110α, p110β, p110δ, and p110γ which have both unique and overlapping roles in physiological and diseased states. Upon activation PI3K generates phosphoinositide products (i.e. phosphatidylinositol 3,4,5-trisphosphate, PIP3) from phosphatidylinositol 4,5-bisphosphate (PIP2) which promotes the translocation of Akt from the cytosol to the cell membrane. PDK1 and mTOR-rictor complex (mTORC-2) phosphorylate the translocated Akt at Thr308 and Ser473, respectively. Activated Akt then inactivates TSC2 (tuberous sclerosis complex 2, also known as tuberin) to prevent the inhibition of mTORC1. Active mTORC1 regulates transcriptional, translational and post-translationalactivity for a variety of cellular processes including metabolism, migration, growth, survival, differentiation, and cytoskeletal organisation (Cantley, 2002; Carracedo and Pandolfi, 2008).

Although the PI3K/Akt/mTOR pathway has been studied extensively in cancer, recently this pathway has become of great interest to understanding the pathogenesis of IPF. Studies have pinpointed a key role of the PI3K in the proliferation and differentiation of lung fibroblasts treated with TGFβ whereby inhibition of PI3K (in particular PI3K p110α and p110γ) activity abrogated TGFβ-induced proliferation of αSMA positive cells (Conte et al., 2011). Furthermore, studies have also illustrated strong immunostaining of downstream effectors of mTOR (e.g. p-S6) in fibroblasts of the fibrotic foci in IPF lung tissue sections (Xu et al., 2013). More recently, research has shown that aberrant Akt/mTOR kinases desensitise IPF fibroblasts to type-I collagen matrix-induced cell death (Nho and Hergert, 2014). These studies support PI3K/Akt/mTOR pathway as a target for modulating IPF progression.

The fibrosis toolbox also comprised compounds targeting this pathway. As shown in **Figure 3.67** two compounds showed a hit, both of which are non-specific mTORC 1/2 inhibitors: GSK-56 and GSK-57. The former compound attenuated collagen synthesis in both non-IPF and IPF spheroids by 58 and 64 %, respectively. However, the latter compound abolished collagen production in non-IPF spheroids with minimal effects shown in IPF spheroids. Furthermore, inhibition of PI3K β/δ had minimal effect on collagen production in either non-IPF or IPF spheroids.

Effect of GSK-X on spheroid formation

Another compound used to investigate the effect of the PI3K/Akt/mTOR pathway in pHLF of non-IPF and IPF subjects using the three-dimensional spheroid model was GSK-X (note, due to confidentiality the exact compound ID has been altered in this thesis). This is a highly potent inhibitor for class I PI3Ks and mTOR which has shown many anti-fibrotic effects in both *in vitro* and *in vivo* models of fibrosis (unpublished confidential data in our lab and at GSK).

Timelapse spheroid images were taken by incubating fibroblasts in the IncuCyte Zoom. Microscopic view of the cells cultured with GSK-X (**Figure 3.69**) illustrates that increasing concentration of this compound caused an increase in phase object area, which represents a reduction in the degree of cellular aggregation. These results were observed for both non-IPF and IPF fibroblasts, up to 24 hours post-seeding (and at concentrations above 0.3 μM). This is also demonstrated quantitatively in **Figure 3.70** (6-24 hours of incubation).

Effect of GSK-X on pro-collagen synthesis.

Pro-collagen production was assessed in primary human lung fibroblasts cultured as spheroids by measuring the accumulation of hydroxyproline within the spheroids. GSK-X significantly reduced levels of pro-collagen in IPF (n=3/5, IC50= 2.2 nM to 94.3 nM; **Figure 3.71**) and non-IPF (n=3, IC50= 0.71 nM to 85.7 nM; **Figure 3.72)** spheroid preparations. However, this effect was only shown when treated prophylactically. Two IPF lines were treated with GSK-X 24 hours after spheroid formation (**Figure 3.71C** and **Figure 3.71D)** and collected for analysis after a further 24 hours of incubation with the compound. The data show that the baseline levels of pro-collagen are slightly elevated 48 hours post-seeding in comparison to 24 hours post-seeding in the IPF spheroids.

In addition, the data illustrate that this compound had no effect on pro-collagen synthesis when used therapeutically at low concentrations (0.1 nM-0.1 μM). However at higher doses (0.3-10 μM) there was a slight attenuation in collagen synthesis in one of the IPF donors (**Figure 3.72C**). Since this was only shown in one donor (**Figure 3.71C**), further work is required to conclude the therapeutic effects of this compound in multiple donors.

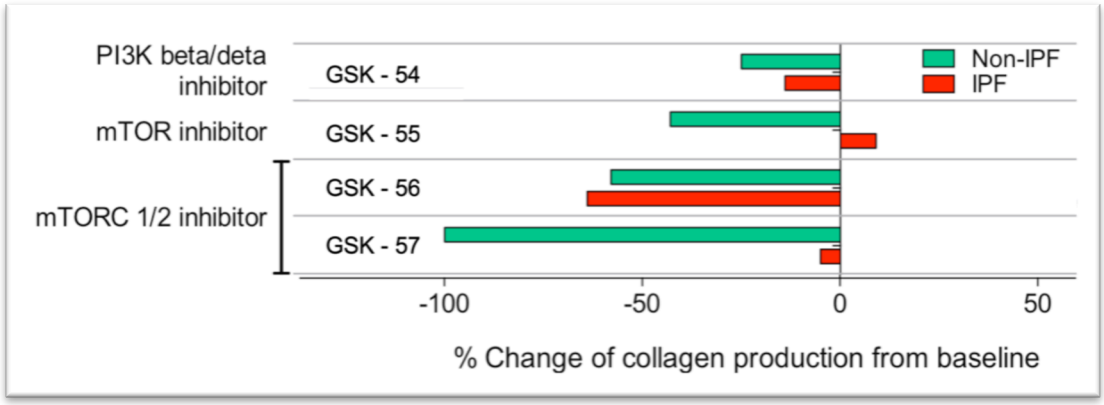

Figure 3. 68. Effect of compounds targeting PI3K pathway on collagen synthesis in spheroids.

Non-IPF (green; n=1) and IPF (red; n=1) spheroids were prophylactically treated with anti-fibrotic compounds (10 μM). Spheroids were collected 24 hours post-treatment and hydrolysed in 6 M HCl for HPLC analysis of hydroxyproline levels.

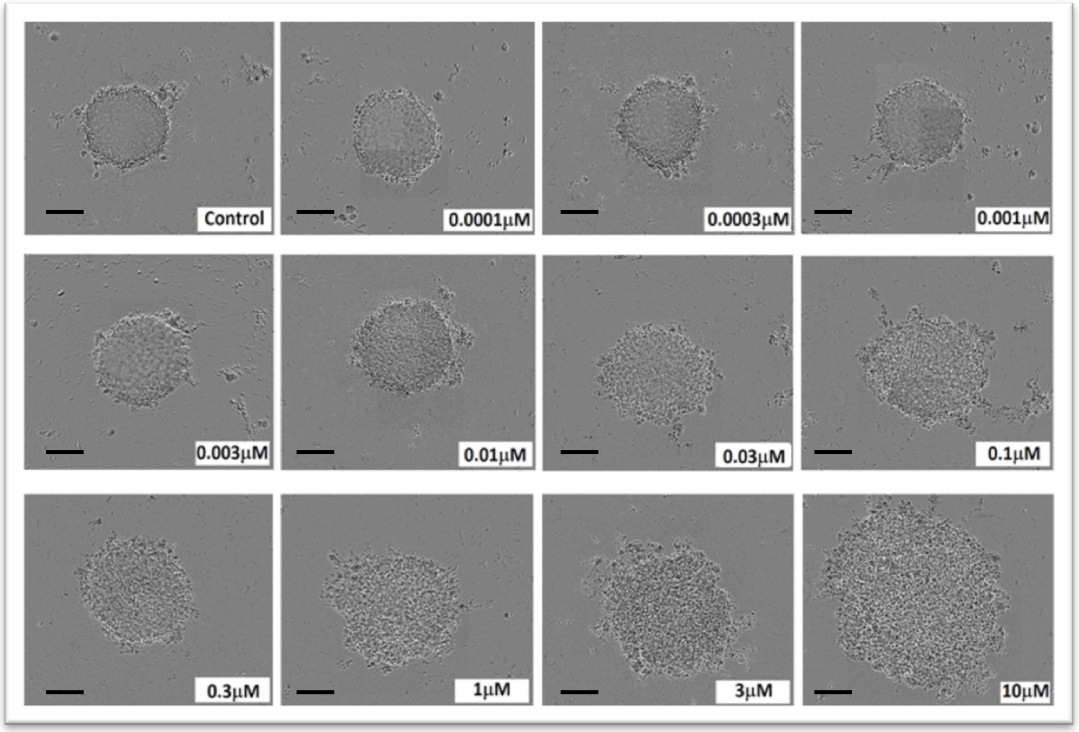

Figure 3. 69. Microscopic view of spheroid formation in the presence of GSK-X.

Increasing concentrations of GSK-X inhibited fibroblast aggregation from non-IPF (n=2) and IPF (n=3) subjects up to 24 hours post seeding, at doses ranging from 0.03 μM to 10 μM). Scale bar, 200 μm. Representative data shown for one IPF line.

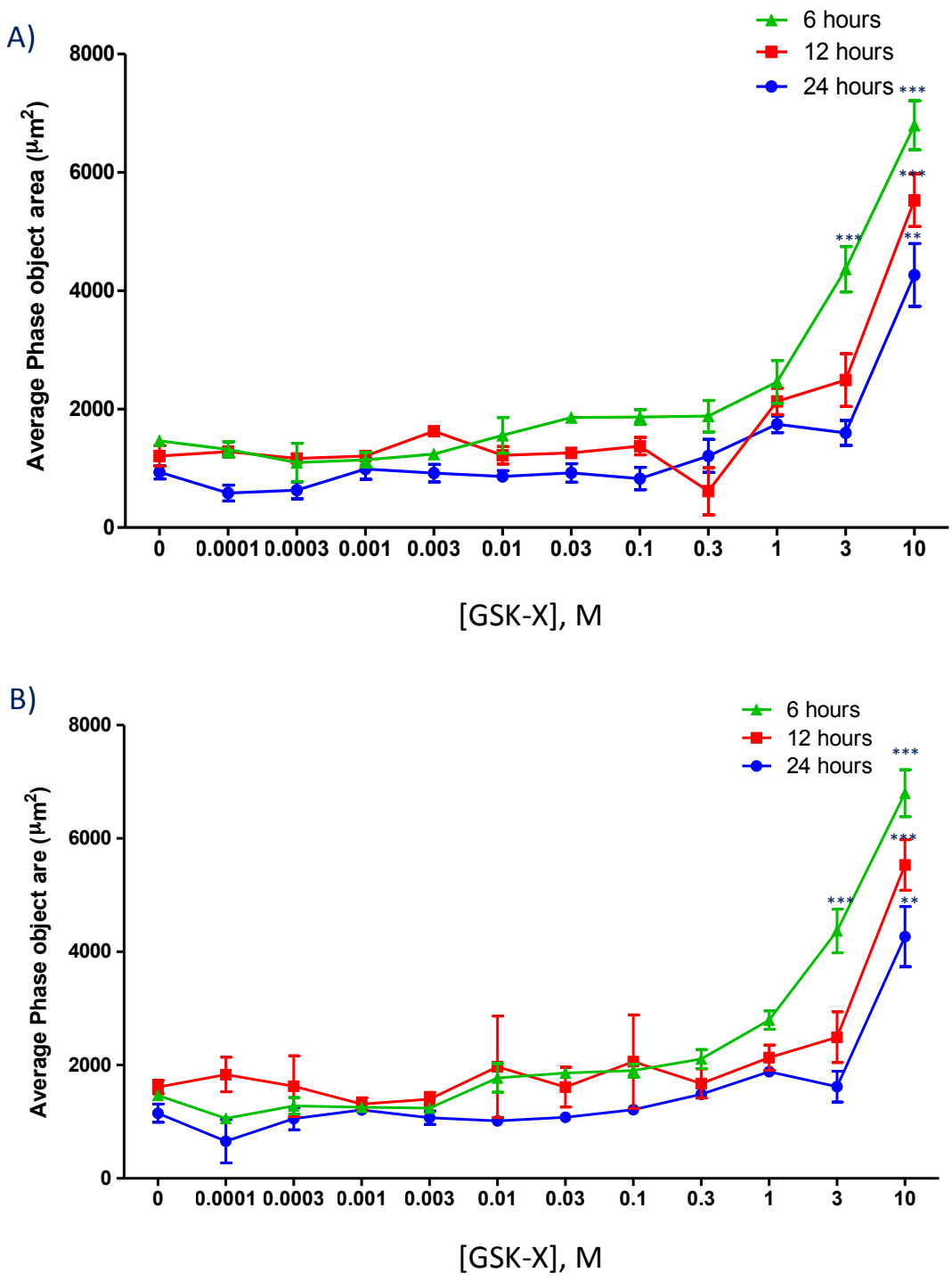

Figure 3. 70. Spheroid formation in the presence of GSK-X.

Increasing concentrations of GSK-X inhibited spheroid formation (illustrated as an increase in average phase object area, number of technical replicates = 8). This is demonstrated in both (A) non-IPF (n=2) and (B) IPF (n=3) subjects, 6 hours (green), 12 hours (red), and 24 hours (blue) post seeding (concentration ranging from 0.03 µM to 10 µM). Representative data shown for one non-IPF and one IPF line. **p<0.01, ***p<0.001

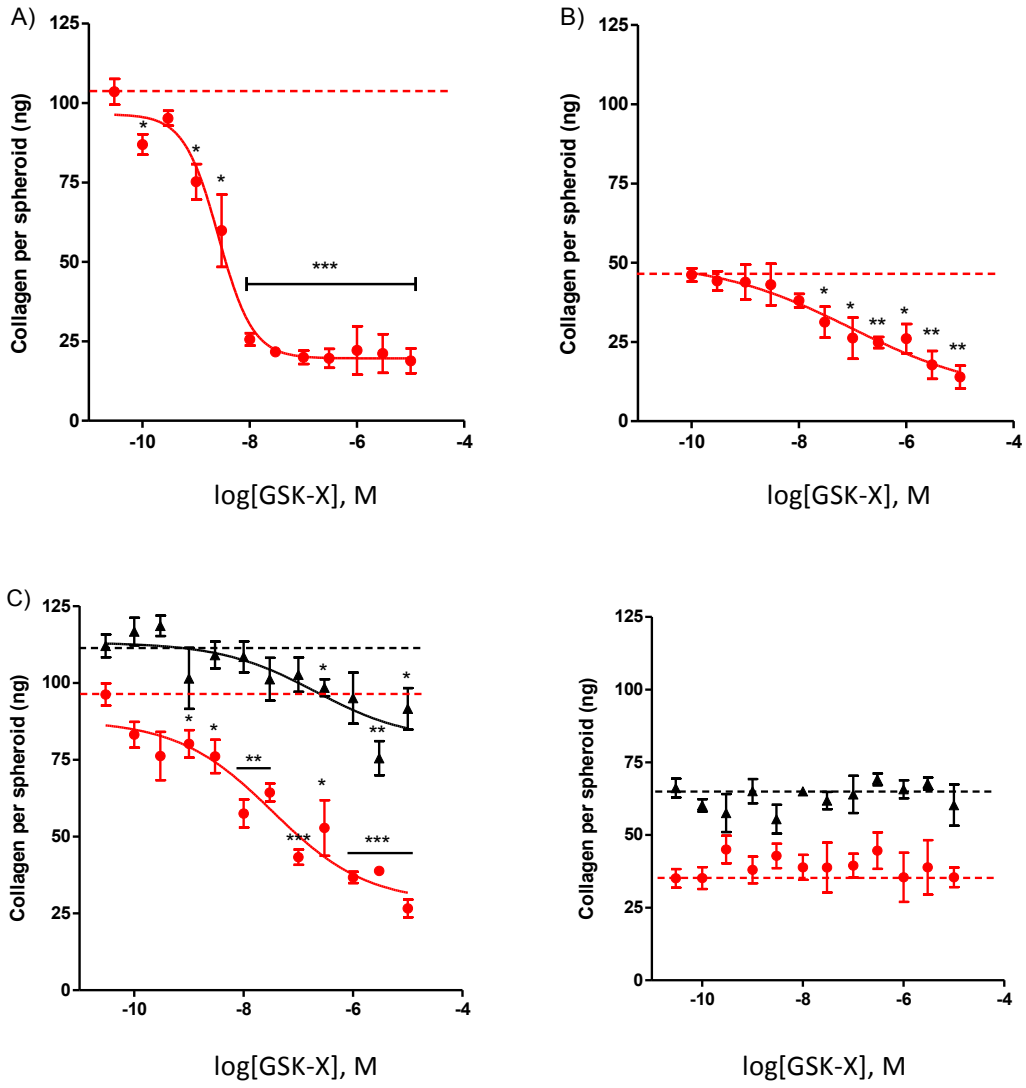

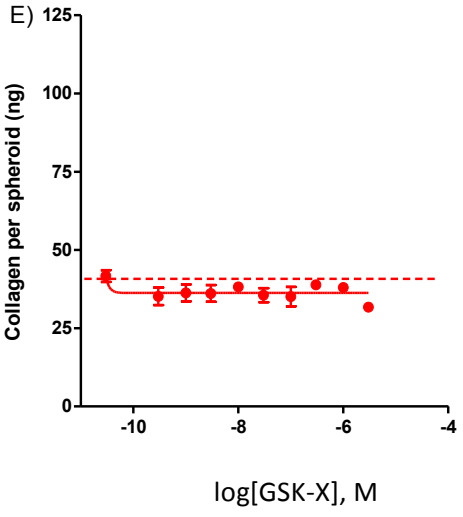

Figure 3. 71. Effect of GSK-X on pro-collagen accumulation within IPF fibroblast spheroids.

Primary human lung fibroblasts from five IPF donors (A-E) were treated with GSK-X (0.3 nM to 10 μM) at the time of culturing in 96 well plates (pre-coated with agarose) to allow spheroid formation (red curves). IC50 values were (A) 2.2 nM, (B) 94.3nM, and (C) 33.8 nM. Black curves represent pro-collagen production of fibroblast spheroids which were treated 24 hours post-seeding/following spheroid formation and incubated for a further 24 hours post-treatment (therapeutic treatment; IC50 for donor C =0.21 μM). Data are expressed as mean ± S.E.M. of 4 replicates. The values *p<0.05, **p<0.01 and ***p<0.001 denote statistical significance of the indicated data compared to spheroids treated with vehicle (DMSO, dotted line).

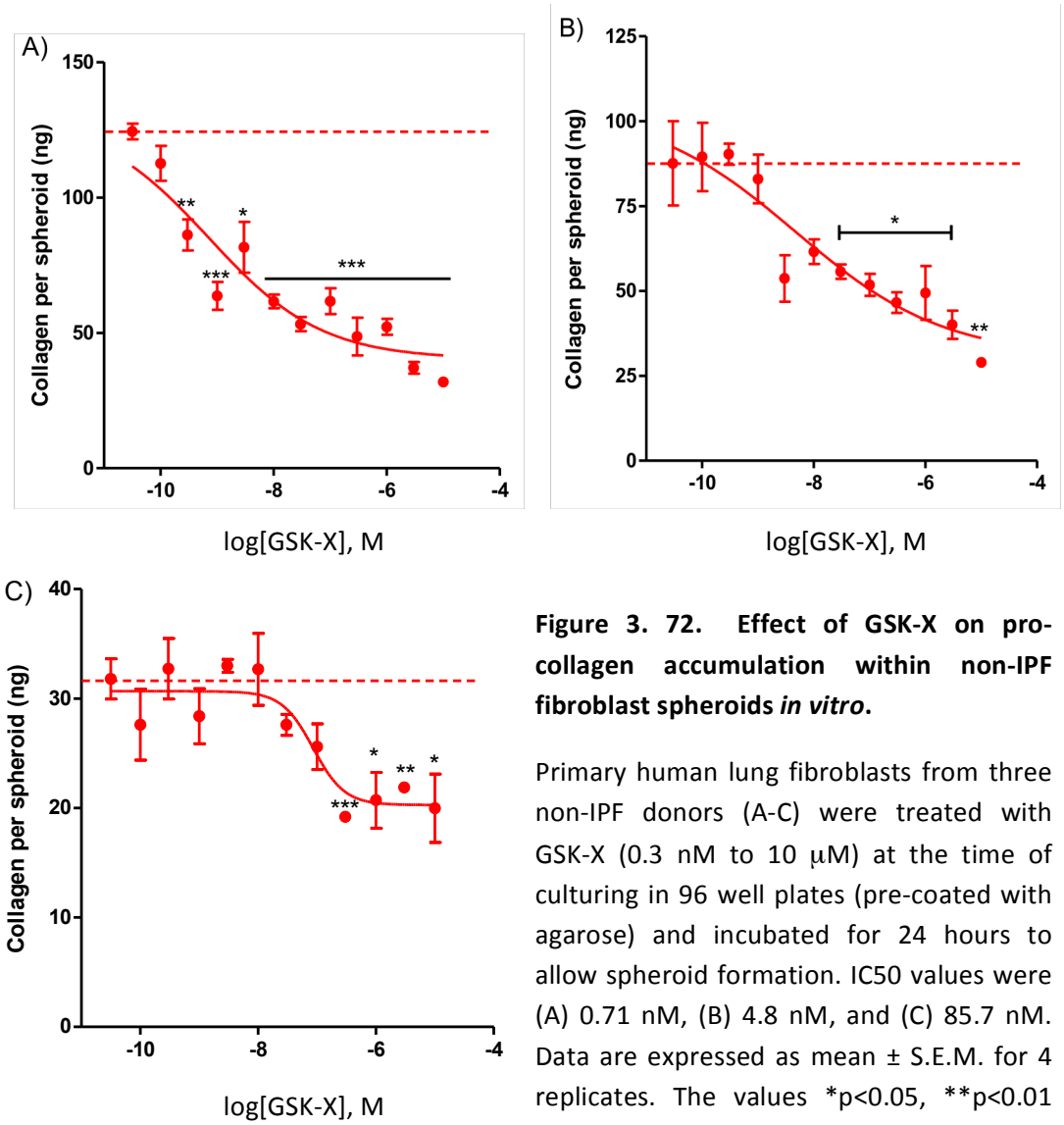

Figure 3. 72. Effect of GSK-X on pro-collagen accumulation within non-IPF fibroblast spheroids *in vitro*.

Primary human lung fibroblasts from three non-IPF donors (A-C) were treated with GSK-X (0.3 nM to 10 μM) at the time of culturing in 96 well plates (pre-coated with agarose) and incubated for 24 hours to allow spheroid formation. IC50 values were (A) 0.71 nM, (B) 4.8 nM, and (C) 85.7 nM. Data are expressed as mean ± S.E.M. for 4 replicates. The values *p<0.05, **p<0.01 and ***p<0.001 denote statistical significance of the indicated data compared to spheroids treated with vehicle (DMSO, dotted line).

3.5.9. Summary

This section focused on analysing microarray data derived from non-IPF and IPF spheroids, which illustrated:

- Several hits (>50 % change in collagen synthesis from baseline) were identified in compounds from the fibrosis toolbox including compounds targeting: integrin αv, ALK-4/5/7, PAI-1, EP2 receptor, EP4 receptor, F-prostanoid, 5-LO, leukotriene D4, Ca^{2+} channels, Na+ channels, MIF, CCL2, CCR2, tankyrase-1, Wnt, Smo, and PI3K/mTOR.
- The effect of GSK-X on spheroid formation was analysed for both non-IPF (n=2) and IPF fibroblasts (n=3). Increasing concentrations of GSK-X inhibited fibroblast aggregation after 6, 12, and 24 hours of incubation (concentration ranging from 0.3 μM to 10 μM).
- The ability of GSK-X to inhibit pro-collagen production by non-IPF and IPF spheroids was assessed by a high-performance liquid chromatography (HPLC) assay for hydroxyproline. Three out of the five IPF donors that formed spheroids showed a significant attenuation in procollagen synthesis when treated with GSK-X prophylactically (IC50 2.2 nM to 94.3 nM). Furthermore, non-IPF spheroids (n=3) also showed an attenuation in procollagen production (IC50 of 0.71 nM to 85.7 nM). In conclusion, GSK-X inhibits fibroblast aggregation and pro-collagen synthesis in both non-IPF and IPF spheroids.

CHAPTER 4: DISCUSSION

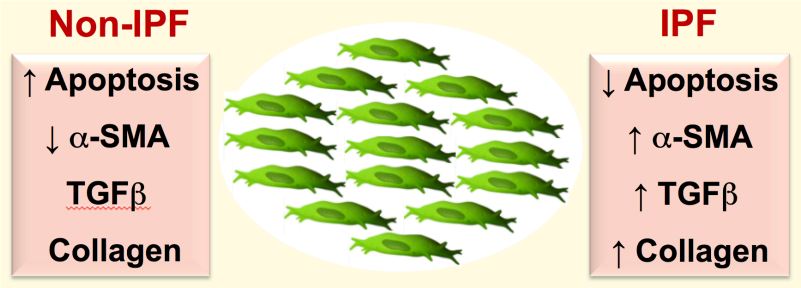

4.1. Overview

Idiopathic pulmonary fibrosis (IPF) is the most common form of pulmonary fibrosis (PF) with an unknown aetiology and just two treatment options (Pirfenidone and Nintedanib) which can slow, but not halt, progression of the disease (King et al., 2014; Richeldi et al., 2014). Currently the literature suggests that dysregulated epithelial mesenchymal crosstalk may play a key role in the development of this ultimately fatal disease. Increasing evidence suggests that repetitive injury to the lung alveolar epithelial cells (AECs) and destruction of the alveolar-capillary basement membrane results in the migration, proliferation and activation of fibroblasts and their deposition of extracellular matrix proteins, which disrupts the lung architecture. Several *in vivo* animal models have been developed in order to understand the pathology of this disease. The most common murine model used in research today involves the administration of bleomycin (Moeller et al., 2008). *In vitro* monolayer cultures are routinely used to address the underlying cell biology. Both *in vivo* and 2D *in vitro* studies have led to the identification of cells and mediators that may play a key role in the disease, including transforming growth factor (TGF)-β and prostaglandin (PG)-E_2. However, there are a number of disadvantages of using such models. For instance, *in vivo* models are highly expensive, often variable and difficult to manipulate (Moraes et al., 2011). In addition, it is widely considered that they have so far failed to be predictive of the eventual clinical outcome of targeted therapies, although the use of appropriate dosing strategies does improve the clinical predictive value (Scotton and Chambers, 2010) . Furthermore, both *in vivo* and 2D *in vitro* cultures are unable to recapitulate some of the characteristic features seen in IPF patients, including fibrotic foci – which correlate with the progression of the disorder (Enomoto et al., 2006). Therefore, it would be highly beneficial to produce a novel *in vitro* model which would mimic fibrotic foci, in order to investigate the mechanisms involved in the progression of this disease, and with the potential to be a more predictive pre-clinical tool for assaying lead compounds. This thesis therefore examined the following hypothesis:

'3D spheroid cultures of fibroblasts will provide a more representative *in vitro* model system for drug screening in IPF'

To address this hypothesis the initial experiments of this thesis aimed to investigate which particular fibroblast isolation protocol was convenient and ideal to use in order to generate the 3D model. The results illustrated that primary human lung fibroblasts (pHLF) isolated from

control (or non-IPF) lung explants (pHLF-Ex) and from trypsin-digested lungs (pHLF-Di) exhibited phenotypic differences. Despite the beneficial aspects of increased cell yields from pHLF-Di, we decided to continue the project with pHLF-Ex to provide better comparisons with existing IPF fibroblast lines and data. The next aim was to determine the potential for both non-IPF and IPF fibroblasts to produce spheroid structures when cultured on a low-adhesive surface. The results indicated that both were able to form spheroids within just 24 hours of incubation with a few morphological differences. Spheroids were characterised by determining the αSMA expression, their ability to produce matrix and active TGFβ, and also their rate of proliferation/apoptosis. As indicated in the results, IPF spheroids had a more myofibroblastic phenotype which expressed high levels of αSMA, synthesised high levels of collagen, and also produced high levels of active TGFβ. However, although the spheroids were capable of synthesising their own active TGFβ, for the first time the results in this thesis demonstrated that collagen synthesis was not wholly dependent on endogenous TGFβ signalling. In addition, non-IPF spheroids were prone to apoptosis which was dependent on EP2 receptor signalling, activated by cyclooxygenase (COX)-1 mediated PGE_2. Moreover, both non-IPF and IPF spheroids were non-proliferative. Furthermore, microarray data analysis and the medium-throughput screening identified potential targets which require further validation. In summary, IPF fibroblast spheroids may represent a novel assay system for pre-clinical drug evaluation; this chapter will discuss these findings and their implications in further detail.

4.2. Isolation methods affect the characteristics of fibroblasts

Myofibroblasts are contractile and highly synthetic, spindle-shaped cells characterised by the *de novo* expression of alpha smooth muscle actin (α-SMA) positive stress fibres. These cells play a vital role in reconstruction of connective tissue following injury and are fundamental cells involved in the development of fibrosis (Hinz et al., 2001a; Gabbiani, 2003; Desmouliere et al., 2005). In normal physiology, injury to the lung epithelium causes inflammation and results in differentiation of fibroblasts to myofibroblasts as part of the normal wound healing response. This differentiation has been suggested to occur in a two phases. The first phase involves the fibroblasts acquiring a migratory phenotype and developing focal adhesions and contractile bundles in response to cytokines (Werner and Grose, 2003), mechanical properties, and organisation of the extracellular matrix (ECM) (Hinz and Gabbiani, 2003b). The contractile bundles formed are referred to as stress fibres, composed of cytoplasmic actins which are structural components of the cytoskeleton in non-muscle cells. Researchers have termed such mesenchymal cells as proto-myofibroblasts in order to distinguish these cells from quiescent fibroblasts (Tomasek et al., 2002; Baum and Duffy, 2011). The second phase involves the proto-myofibroblasts expressing αSMA, and such cells are termed differentiated myofibroblasts. Studies have demonstrated that αSMA expression is controlled by growth factors (e.g. TGFβ), ECM proteins, and the mechanical microenvironment (Tomasek et al., 2002). This increase in αSMA expression augments the contractile activity of the cells, which has an important role in the remodelling of connective tissue (Hinz et al., 2001a). Stress fibres and αSMA expression are common characteristic features used to distinguish between fibroblasts and myofibroblasts (Phan, 2008). Once the tissue is repaired the contractile activity of myofibroblasts is terminated, αSMA expression is reduced, and the cells undergo a programmed cell death, termed apoptosis (Desmouliere et al., 1995). Thus, cell death is an important process during the normal wound healing response. However, in patients with IPF, the activity of myofibroblasts persists, which eventually leads to disruption of the lung architecture.

In our laboratory, the standard protocol used to isolate primary human lung fibroblasts (a non-clonal heterogeneous cell population) involved growing fibroblasts from small ($<1mm^3$) explants over a period of 2-4 weeks. The more recent protocol investigated during this thesis, involved using trypsin to digest the lung sample, while isolating both fibroblasts and primary

type II AECs. The latter protocol not only isolates cells more rapidly, but also gave a far greater yield in comparison to the explant protocol. My results illustrate that fibroblasts isolated using the latter protocol (i.e. pHLF-Di) have a more myofibroblast-like phenotype at baseline in comparison to pHLF-Ex, as these cells show greater αSMA protein expression and the presence of stress fibres. In addition, pHLF-Di cells have the tendency to grow at a faster rate in comparison to pHLF-Ex cells at baseline. These differences between the two cell isolates may have arisen directly due to the activity of the trypsin-EDTA used in the isolation protocol. While commonly used in tissue culture for cell detachment, trypsin is also able to activate a seven-transmembrane domain G-protein coupled receptor, protease activated receptor (PAR)-2, on several cell types including fibroblasts. This activation is mediated via the cleavage of a specific site on the N-terminus of PAR-2 (Olejar and Nouza, 1999; Akers et al., 2000), exposing a tethered ligand which then binds to the second extracellular loop of the receptor resulting in a conformational change and activating intracellular signalling cascades (Dery et al., 1998). As well as trypsin, other trypsin-like proteases (i.e. tryptase) can also activate PAR-2 in fibroblasts – which can result in fibroblast differentiation. Therefore, the presence of stress fibres in pHLF-Di may have resulted due to lengthy exposure to trypsin, resulting in PAR-2–mediated activation.

TGFβ is a pleiotropic regulatory cytokine ubiquitously expressed in it's latent form (bound to the latency associated peptide, LAP) by all cells/tissues sequestered in the matrix (linked to the latent TGFβ binding protein, LTBP) and is considered as the primary mediator involved in wound healing (Lee et al., 2006). Furthermore, there is compelling evidence that TGFβ plays a crucial role in the pathogenesis of IPF, as it is known as a potent mediator for myofibroblast differentiation and proliferation. The results in this project illustrated that TGFβ activation upregulated αSMA expression and stress fibre formation in pHLF-Ex, as expected, however TGFβ had no effect on pHLF-Di. Previously in our lab it has been demonstrated that control pHLF-Ex at higher passage number (>10) have increased αSMA expression and reduced TGFβ responsiveness. Therefore, it is feasible that frequent treatment of cells with trypsin (during routine passage) may not only play a role in altering the cell phenotype but also some of the cells' responses to certain mediators (in this case TGFβ). The high baseline level of αSMA expression, and lack of change in the presence of TGFβ suggests that the vast majority of pHLF-Di cells are already directed towards a myofibroblasts phenotype during the isolation process. Although TGFβ had no effect on αSMA expression in pHLF-Di, the cytokine did increase the rate of proliferation (similar to pHLF-Ex) illustrating that these cells still respond to this

exogenous stimulus. The increase in proliferation rate in response to TGFβ may have resulted via the activation of a Smad-independent pathway (i.e. PI3K/Akt/mTOR signalling pathway) (Conte et al., 2011; Fagone et al., 2011).

Since αSMA is a marker for not only myofibroblasts but also smooth muscle cells, it was vital to investigate whether the population of cells isolated from both protocols were actually in fact fibroblasts/myofibroblasts. This involved performing immunocytochemistry for the detection of smoothelin. Despite previous work from our lab reporting that smoothelin may be expressed in myofibroblasts (Chambers et al., 2003), it is generally accepted that smoothelin is a marker for differentiated smooth muscle cells (van der Loop et al., 1996; Krämer et al., 2001; Nam et al., 2012). The results in this thesis also support this idea, as all cells (both at baseline and TGFβ treated) were negative for smoothelin.

Despite the benefits of the trypsin-digestion protocol (higher yield of fibroblasts, faster isolation, faster proliferation), pHLF-Di were not used for the rest of the project due to the deviation in phenotype compared with the traditional isolation protocol, and hence potential for comparison with the existing biobank of fibroblast lines. Thus, for the rest of the project pHLF-Ex from non-IPF and IPF lung tissues were used to produce a novel 3D *in vitro* model system.

It is worth noting that in 2D monolayer culture, several studies have illustrated that IPF fibroblasts have a more myofibroblasts-like phenotype with increased expression of αSMA and stress fibres at baseline, in comparison to control cells. However in this study the results demonstrated no statistical difference in αSMA expression between non-IPF and IPF fibroblasts, with or without TGFβ when cultured as a monolayer. A possible reason for these contrasting results may be related to the passage number of the cells. As already mentioned, cells at a high passage have increased αSMA expression and reduced responsiveness to TGFβ, which may result from mechanical tension or due to continuous treatment with trypsin. However, at low passage the cells are considered to receive less culture stress - have lower αSMA expression with an increased response to TGFβ. In this project, all cells (including IPF) were cultured at low passages which may explain why there was no statistical difference in αSMA expression between non-IPF and IPF fibroblasts. Other possible reasons for these contradictory results may be donor-to-donor variation (i.e. age, gender, stage of disease progression) and the lung region from which the IPF fibroblasts were isolated (i.e. fibrotic region or less affected/unaffected lung parenchyma).

4.3. Spheroid characterisation

4.3.1. Non-IPF and IPF fibroblast spheroids are morphologically different

Tissue engineering has become an area of great interest over the past decade and many 3D *in vitro* models have been developed to study diseases including cancer. Such models have included the generation of spheroids or the use of more high-throughput microfluidics systems which not only mimic certain physiological features but also have the great advantage of being used for high-throughput drug screening (Scotton, 2011). However, at present no 3D *in vitro* model has been developed to specifically study IPF. Therefore, the aim of this project was to develop a model which mimics one of the hallmark pathological features of IPF, namely fibrotic foci.

Videomicroscopy and electron microscopy (EM) demonstrated that fibroblasts (from both non-IPF and IPF patients) are able to form spheroids when cultured on a non-adhesive surface within just 24 hours of incubation. In addition, the size of the spheroids remained relatively constant (~400 μM in diameter) over 96 hour window of culture investigated. Morphologically IPF spheroids have a smoother surface with larger elongated flatter cells in comparison to non-IPF, which appear to have a rougher surface with smaller, more-rounded cells. In addition, IPF fibroblasts form tight junctions when cultured in this 3D system which was not evident in the non-IPF spheroids (as demonstrated by transmission electron microscopy, TEM), providing evidence of cell-cell communication and adhesion only in IPF spheroids. Furthermore, TEM analysis also illustrated fibrillar deposits which are likely to be ECM proteins.

4.3.2. IPF spheroids have a myofibroblast phenotype

Based on these morphological differences, the next step was to determine the expression of αSMA. The data illustrate that αSMA expression is greater in IPF spheroids in comparison to non-IPF. These data are in support of previous published studies illustrating that IPF fibroblasts have a myofibroblast phenotype. It is important to note that the IPF cells used to form spheroids were from the same donors and grown at the same passage as those cultured as monolayers (see **Sections 3.1** and **4.2**). This suggests that although the results show that IPF fibroblasts have similar αSMA levels to non-IPF fibroblasts when cultured on plastic, in this 3D system, the same IPF cells acquire a myofibroblast phenotype suggesting that cell-cell or cell-

matrix interaction may play an additional key role in mediating the differentiation of IPF fibroblasts (Hinz et al., 2004).

4.3.3. IPF spheroids produce high levels of collagen

Excessive collagen deposition is the key feature shown in the lungs of IPF patients, particularly in areas of active fibrosis (i.e. fibrotic foci). As stated above, EM illustrated fibrillar ECM deposition, suggesting that spheroids may potentially synthesise their own matrix. To address this hydroxyproline content was measured. Hydroxyproline (in particular 4-hydroxyproline, 4-Hyp) is the major amino acid present in all collagen types and its measurement is commonly used to determine the total concentration of collagen within biological samples (Kliment et al., 2011). The results illustrated that in the absence of any exogenous stimuli, both non-IPF and IPF spheroids were capable of synthesising their own matrix (i.e. collagen) within just 24 hours of culture, with statistically greater levels seen in IPF spheroids. This is an intriguing result as other *in vitro* assays for pulmonary fibrosis (i.e. 2D monolayer cultures and the scar-in-a-jar assay) require the addition of exogenous mediators (such as TGFβ), often at supra-physiological concentrations, to stimulate collagen production (Chen and Raghunath, 2009). In addition, since IPF spheroids have an increased αSMA expression, elevated collagen deposition in these spheroids support the concept that αSMA positive myofibroblasts are highly synthetic for collagen (Hinz et al., 2001a; Hinz and Gabbiani, 2003b; Scotton and Chambers, 2007; Hinz, 2010).

In most donors, the spheroid collagen levels remained relatively stable over 96 hours, however there were a few exceptions where the collagen levels either declined or elevated over time. These results highlight one issue of donor-to-donor variation. In addition, a decline in collagen synthesis over time in some donors (in particular some of the non-IPF donors) may have resulted due to the increase cell death within the spheroids as a result of increased production of PGE_2 (Casini et al., 1984; Fine et al., 1989), which will be discussed in greater detail in **Section 4.3.5**. Another potential explanation may be the increase in activity of matrix metalloproteinases (MMPs), in particular MMP2 (see **Appendix 4**). MMPs are matrix-degrading enzymes which are synthesised by fibroblasts in order to control matrix turnover during the initiation and resolution phases following injury. As shown in **Appendix 4**, MMP2 levels increase over time in both non-IPF and IPF spheroids, thus may degrade the collagen levels over the 96 hours of culture. Studies have demonstrated that IPF patients have elevated levels of MMPs in comparison to control subjects which would imply greater matrix degradation,

however, this does not occur in the lungs of IPF patients due to elevated levels of tissue inhibitor of metalloproteinases (TIMPs) (Montaño et al., 1989; Fukuda et al., 1998; Selman, 2000; Greenlee et al., 2007; Dancer et al., 2011). The results in **Appendix 4** illustrate that although there is an increase in MMP2 levels over time there is no statistical difference between non-IPF and IPF spheroids. A possible reason for this is the limited number of donors used to measure MMP2 levels; also the IPF fibroblasts used to investigate MMP levels happened to be those donors which produced lower collagen levels (i.e. <50 ng per spheroid, which is similar to the mean level in non-IPF spheroids). Therefore, further experiments should be performed in the donors which produce high levels of collagen (>50 ng), and TIMP levels would also need to be investigated, before drawing clearer conclusions.

There are a number of explanations why some fibroblast spheroids from IPF patients produced high collagen levels (>50 ng) whilst others produced lower levels (<50 ng): 1) fibroblasts may have been isolated from patients who experienced either a slow or a rapid progression of their disease, 2) the cell isolates may have been taken from different regions of the IPF lung (i.e. less effected areas or fibrotic regions), 3) passage number or cell population doubling (defined as the total number of times a population of cells have doubled since they were initially isolated *in vitro*).

There are 28 types of collagen present within the human body, of which collagen types I and III are considered to be the most abundant in the lung (McAnulty and Laurent, 1987; Lodish et al., 2000). This has also been demonstrated in this thesis with strong immunoreactivity of collagen I and III in both control and fibrotic lung tissue sections, particularly in areas with evidence of αSMA expression – again supporting the concept that myofibroblasts are synthetic for collagen. In IPF lung tissue sections immunoreactivity for collagen I and III was illustrated in the fibrotic foci. Interestingly, strong staining was also shown in the basement membrane underlying the bronchial epithelial cells, which to our knowledge has not been reported previously.

The next step was to identify which collagen type is synthesised by the fibroblasts cultured in the 3D spheroid system. The results showed that both non-IPF and IPF spheroids express collagen types I and III. Although on the transcriptional level there was no statistical difference in *COL1A1* and *COL3A1* mRNA levels, IPF spheroids appeared to show slightly stronger immunoreactivity in comparison to non-IPF spheroid sections. This is in accord with previous studies illustrating that at a translational level a large set of genes are regulated in IPF samples and the differential expression cannot be appreciated at the transcriptional level (Larsson et

al., 2008). Since the immunostaining was not quantified, further experiments are required to provide quantitative analysis illustrating the difference in collagen I and III expression in non-IPF and IPF spheroids. This could be done by determining the levels of procollagen carboxy-terminal pro-peptides (PICP and PIIICP, respectively). These are considered as surrogate markers for collagen synthesis, and are elevated in BALF of IPF patients (reviewed in (Dancer et al., 2011)).

A number of endogenous paracrine and autocrine mediators may be involved in promoting collagen synthesis in these spheroids including increased production of TGFβ, PDGF, IGF1, and EGF and reduced synthesis of anti-fibrotic mediators such as PGE_2. The next section will discuss the effect of TGFβ signalling on collagen synthesis.

4.3.4. Fibroblast spheroids produce active TGFβ

As stated above, TGFβ is well recognised for promoting the synthesis of collagen both *in vivo* and *in vitro*, thus the next step was to determine whether treating the spheroids exogenously with active TGFβ would accelerate collagen synthesis. Surprisingly however, exogenous TGFβ had no effect on collagen production in both non-IPF and IPF spheroids. This lead to the hypothesis that fibroblasts cultured as spheroids might produce their own active TGFβ (in contrast to what is seen in monolayer culture). To investigate this hypothesis, active TGFβ levels were measured in both spheroid homogenates and conditioned media by using the mink lung bioassay. This assay involves the use of transformed mink lung epithelial cell (TMLECs) which are stably transfected with a truncated plasminogen activator inhibitor (PAI)-1 promoter fused to the firefly luciferase reporter gene. The activity of luciferase increases when exposed to TGFβ in a dose-dependent manner (Abe et al., 1994).

The results showed that both non-IPF and IPF spheroids synthesise their own active TGFβ with higher levels shown in IPF spheroids following 24 and 96 hours of culture. Over time, the concentration remains relatively constant in non-IPF spheroids, however in IPF spheroid homogenates active-TGFβ levels decline. Possible explanations could be that over time TGFβ signalling is initiating a negative feedback loop resulting in TGFβ internalisation for degradation (Mitchell et al., 2004; Vilar et al., 2006) or that the TGFβ is being predominantly secreted into the media over time. A slight elevation of active TGFβ levels is indeed evident in the conditioned media from IPF spheroid cultures over 96 hours of incubation however this increase does not reach statistical significance. Another possible explanation could be that

there may be autocrine/paracrine signals within the spheroid which downregulate TGFβ expression.

4.3.5. Integrins mediate TGFβ activation in spheroids

Various processes have been proposed to activate latent TGFβ, including heat, reactive oxygen species, acidic pH, matrix metalloproteinases (MMPs), thrombospondin (TSP)-1, and integrins. In this project the involvement of TSP-1 and integrins was investigated. TSP-1 is a large, disulphide-linked homotrimeric protein which is considered to be a major activator for both small and large forms of latent TGFβ (Raugi et al., 1987; O'Shea et al., 1990; Reed et al., 1995; Yehualaeshet et al., 1999; Nakerakanti, 2012). The association of the TSP-1 KRFK motif with the LSKL sequence of the latency associated peptide (LAP) results in a conformation change in the TGFβ latency complex leading to the release of active TGFβ dimer. Treatment with a mimetic LSKL peptide inhibits TSP-1 mediated TGFβ activation *in vitro* (Xie et al., 2010), however my results demonstrated that the LSKL mimetic peptide had no effect on TGFβ activation or collagen synthesis in either non-IPF or IPF spheroids suggesting that another mechanism is predominant in promoting TGFβ activation in this 3D system.

Integrins are transmembrane linker cell surface receptors composed of α and β subunits which regulate bi-directional signalling. Previous studies have illustrated six out of 24 integrins are able to associate with the RGD sequence in LAP: αvβ1, αvβ3, αvβ5, αvβ6, αvβ8, and α8β1. However, αvβ3 (Asano et al., 2005a), αvβ5 (Asano et al., 2005b), αvβ6 (Munger et al., 1999) and αvβ8 (Mu, 2002) are the only integrins which have been formally demonstrated to release active TGFβ. Integrins αvβ3, αvβ5, and αvβ8 are expressed in fibroblasts (supported by the results in this thesis, confirming their expression by qRT-PCR). Although all three integrins anchor to the RGD sequence to facilitate TGFβ activation, the mechanisms by which this occurs are different. For instance, integrins αvβ3 and αvβ5 result in a conformational change in the latency complex as a result of cell traction leading to the release of the homodimeric TGFβ (Asano et al., 2005a, 2005b; Wipff et al., 2007). Integrin αvβ8, on the other hand, presents the latent complex to cell surface MMPs (MT1-MMP or MMP14) which degrades LAP and releases active TGFβ into the extracellular milieu (Mu, 2002).

The results in this thesis demonstrated that integrin αvβ5 mRNA levels were greater in IPF spheroids in comparison to non-IPF. Since IPF spheroids have a myofibroblast phenotype the increase in αvβ5 mRNA levels may support previously published data illustrating that αvβ5

mediates fibroblast differentiation to myofibroblasts via TGFβ activation (Scotton et al., 2009; Zhou et al., 2010). In addition, αvβ5 expression localises to areas positive for αSMA expression, in particular fibrotic foci, suggesting that αvβ5 may have an important role in the development of IPF (Scotton et al., 2009). The elevated αvβ5 mRNA levels in IPF spheroids therefore reflects what is seen in fibrotic foci.

The mRNA levels for integrins αvβ3 and αvβ8 were also assessed however there were no statistical differences between non-IPF and IPF spheroids. This led to the hypothesis that collagen synthesis by fibroblast spheroids is dependent on integrin αvβ5-mediated TGFβ activation. To investigate this hypothesis the spheroids were treated with integrin inhibitors. Due to the lack of availability of a specific integrin αvβ5 small molecule inhibitor, a selective β3/β5 dual inhibitor was used. In addition, β3 and β8 integrin inhibitors were also assessed. The results illustrated that in non-IPF spheroids, treatment with αvβ8 inhibitor partially attenuated TGFβ activation (high potency with low efficacy). Furthermore, the dual β3/β5 inhibitor and β3 inhibitor also caused a decline in TGFβ activation, however this only occurred at extremely high concentration of the compounds. In other *in vivo* and *in vitro* model systems, these integrin inhibitor compounds were highly potent with IC50s in the nanomolar range (personal communication from Richard Hatley, GSK). However, in this system the non-specific β3/β5 inhibitor and β3 inhibitor appeared to have low potency in blocking TGFβ activation with an effect shown only at micromolar concentration. This affect is likely to be the result of toxicity of the compounds, however further investigations are required to confirm this. Nevertheless, since β8 inhibition did show some attenuation in TGFβ activation, it suggests that in non-IPF spheroids TGFβ activation is partially dependent on the αvβ8 integrin. However, this partial attenuation suggests that another mechanism is also involved in activating TGFβ, which could include the β5 integrin (not directly interrogated here) or MMPs, both of which have previously shown to associate to LAP and release active TGFβ. Further experiments must be performed to investigate this, which could potentially involve treating the spheroids with GM6001 (a potent pan-MMP inhibitor) or a specific β5 antagonist (which to our knowledge has not yet been developed) or a neutralising antibody. In IPF spheroids however, both integrin β3 and β8 inhibition abolished TGFβ activation with high potency. Integrin β3/β5 inhibitor also blocked the activation however at low potency. This suggests TGFβ activation in IPF spheroids is highly dependent on integrins β3 and β8.

4.3.6. Collagen synthesis may be independent of TGFβ signalling

Despite the impact of β3 and β8 inhibition on TGFβ activation, there was no subsequent effect on collagen synthesis, suggesting that in this system collagen synthesis was not dependent on integrin-mediated TGFβ activation. These findings are in support with previously published *in vivo* data which illustrated that mice null for αvβ3 and αvβ5 are not protected from bleomycin-induced PF (reviewed in (Tatler and Jenkins, 2012)).

As stated before, active TGFβ exert its cellular effects via the activation of its receptor which can induce multiple pro-fibrotic effects. Active TGFβ interacts with TGFβ receptor type II (TBRII) which then phosphorylates and dimerises with TGFβ receptor I (TBR1/ALK5). This forms an active ligand-response complex which initiates pro-fibrotic responses in fibroblasts via canonical (Smad-dependent pathway) and non-canonical signalling pathways (i.e. MAPK, and PI3K/Akt pathways; reviewed in (Sakai and Tager, 2013)). Several studies support the role of TGFβ in promoting collagen synthesis via the activation of its receptor, ALK-5. For instance, bleomycin-induced PF mice show a significant attenuation in collagen synthesis, following the treatment with a potent ALK5 inhibitor (i.e. SB525334A) (Scotton et al., 2013) via the reduction Smad2/3 translocation into the nucleus. In addition, reduced Smad 2/3 signalling also decreases CTGF production and attenuates myofibroblasts proliferation (Higashiyama et al., 2007). Unexpectedly, in this spheroid system ALK-5 inhibition had no effect on collagen synthesis (following either prophylactic or therapeutic treatment). These data suggest that although TGFβ signalling is postulated to be the major cytokine stimulating pro-fibrogenic responses, when fibroblasts are cultured as spheroids the initial impetus for collagen synthesis may not be dependent on TGFβ signalling. One thing to note is that this experiment was only performed using one non-IPF donor and one IPF donor which were the same donors used to investigate the effect of β3 and β5 integrin inhibitors on TGFβ production (described above). Due to donor-donor variation and fibroblast heterogeneity, it is vital this experiment is subsequently repeated in multiple donors to further support this observation. In addition, the lack of effect following therapeutic treatment may possibly suggest that the compound is unable to penetrate the spheroid to show its effects. Thus, further research is required to determine whether compounds are capable of penetrating the matrix rich spheroids. This could involve treating the spheroids with a labelled substance to assess its penetration (see Future Directions **Section 5.1.8**).

Although my data suggests that TGFβ may not be essential for the initial collagen production in these spheroids it does not rule out the fact that the TGFβ may be vital in mediating other pro-fibrotic and pro-inflammatory effects. For example, as stated before IPF spheroids have a myofibroblast phenotype. Since IPF spheroids produce high levels of active TGFβ in comparison to non-IPF spheroids we can postulate that TGFβ is involved in promoting fibroblast differentiation which would support several published data. However, further investigations would be necessary before drawing conclusions which could involve determining the effect of antagonising TGFβ receptor signalling (by using an ALK-5 inhibitor) on αSMA expression in the spheroids. In addition, previous studies have shown that TGFβ is involved in upregulating the expression of collagen crosslinking genes (such as transglutaminase 2, TGM2) resulting in overstabilisation of ECM and potentially leading to stiffer matrix (George et al., 1990; Schittny et al., 1997; Ritter and Davies, 1998; Quan et al., 2005). Thus, it could be hypothesised that in this 3D system TGFβ plays a role in maturation of ECM. Furthermore, TGFβ activation has also been implicated in fibroblast survival by mediating PI3K/Akt signalling pathway and inhibiting PGE_2-mediated cell death (Nakerakanti, 2012). However, further investigations will be necessary to determine the precise role of active TGFβ in this 3D system.

4.3.7. Non-IPF spheroids are prone to cell death

Following a normal wound healing response and after the tissue has been repaired, activated fibroblasts are cleared from the site of injury by undergoing apoptosis (Desmouliere et al., 1995). Apoptosis is a programmed cell death involving the activation of caspases which cleave key cellular components required for normal cell function. Such components include cytoskeletal proteins (e.g. actin filaments) and nuclear proteins (e.g. lamins) which result in cell shrinkage, bleb formation, and chromatin condensation. In addition, activated caspase-3 may also initiate the activity of DNase via the activity of caspase-activated DNase (CAD) which results in DNA fragmentation. In turn, apoptotic bodies form which are phagocytosed and degraded.

Fibroblast apoptosis is considered to be critical for prevention of the pathological scarring seen in the lungs of IPF patients (Thannickal and Horowitz, 2006). When activated fibroblasts persist in the tissue due to abnormal apoptotic mechanisms, undesirable fibrosis occurs which is one of the key hallmarks of fibrotic foci (Kuhn and McDonald, 1991; Moodley et al., 2004; Bühling et al., 2005). Compelling evidence reveals that fibroblasts derived from the lungs of IPF

patients are resistant to apoptosis, in particular Fas ligand (FasL)-induced apoptosis (Tanaka et al., 2002; Moodley et al., 2004; Bühling et al., 2005; Huang et al., 2009) which has a pivotal role in the pathogenesis of pulmonary fibrosis (Kuwano et al., 1999b). Fibroblast resistance to FasL-induced apoptosis can result from limited expression of PGE_2 (Maher et al., 2010). In addition, studies on murine models and patients with pulmonary fibrosis have highlighted the importance of histone modifications in the development of fibroblast resistance to apoptosis suggesting novel approaches to therapy for fibroproliferative disorders (Huang et al., 2013).

To investigate whether fibroblasts cultured as spheroids undergo apoptosis, the percentage of nuclei undergoing fragmentation was measured by using terminal deoxynucleotidyl transferase dUTP nick end labelling (TUNEL) assay. This assay is dependent on the activity of terminal deoxynucleotidyl transferase (TdT) which catalyses the addition of dUTP molecules (conjugated to a fluorescent marker) to the fragmented DNA, visualised using fluorescence microscopy. The results illustrated that after 96 hours in culture there was a significant increase in the percentage of cells with fragmented DNA in non-IPF spheroids. In contrast, fibrotic spheroids were less prone to cell death in this 3D system. This supports previous studies demonstrating that IPF fibroblasts are resistant to apoptosis (Maher et al., 2010). However, unlike 2D monolayer cultures, fibroblasts in spheroid do not require the addition of an exogenous mediator to induce apoptosis (i.e. Fas-ligand). In fact, these spheroids are capable of synthesising their own anti-fibrotic mediators to mediate this programmed cell death. Thus, non-IPF and IPF spheroids are reminiscent of the fibroblast aggregates seen in a healing wound following lung injury in control and fibrotic patients, respectively. This would add credence to the use of spheroids as a relevant model for pulmonary fibrosis.

It is also important to note that TUNEL positive cells were randomly distributed throughout the spheroids and not focused in the centre, where oxygen tension would be lowest. In addition, the size of the spheroids did not have a significant effect on the percentage of TUNEL positive cells. These findings suggest that hypoxia may not be the cause of cell death within the spheroids and the cells are unlikely to be necrotic (non-programmed cell death). However, further analysis would be required to confirm this, which could involve measuring the expression of hypoxia markers (such as hypoxia induced factor-1α, HIF-1α) (Carmeliet et al., 1998; Iyer et al., 1998). In addition, to further confirm that the cells are undergoing apoptosis additional studies can be performed which could involve measuring apoptotic markers (such as FasL and cleaved caspase 3).

There are a number of possible reasons which could explain why IPF spheroids are less apoptotic in comparison to non-IPF. One possible reason is the IPF spheroids synthesis high levels of active TGFβ which has previously been reported to promote fibroblast cell survival *in vitro* via the activation of PI3K/Akt pathway (reviewed in (Zhang, 2009). Another possible explanation is that IPF spheroids express high levels of CC chemokine ligand 2 (CCL2, also known as monocyte chemotactic protein-1, MCP1) transcriptionally (see **Appendix 6, Figure A11** which illustrates high CCL2 mRNA levels in IPF spheroids in comparison to non-IPF) which has previously shown to mediate fibroblast survival by regulating interleukin (IL)-6/STAT3 pathway (Liu et al., 2007). Furthermore, reduced expression of anti-fibrotic mediators (such as PGE_2) may also play a key role in protecting IPF fibroblasts from apoptosis. This will be discussed in detail in the next section.

4.3.8. EP2 receptor signalling via COX1-mediated PGE_2 synthesis promotes fibroblast cell death in spheroids

PGE_2 is an antifibrotic lipid mediator derived from arachidonic acid metabolism via the activity of COX. It is the most abundant prostanoid found in the lung, where it is synthesised by many cells including fibroblasts (Wilborn et al., 1995). PGE_2 inhibits fibroblast proliferation (Elias et al., 1985; Bitterman et al., 1986), differentiation (Kolodsick et al., 2003), migration (White et al., 2005), and collagen production (Fine et al., 1989). Furthermore, in epithelial cells, PGE_2 acts as a potent pro-survival mediator (Nishihara et al., 2003; Tessner et al., 2004). Several studies have illustrated that patients diagnosed with IPF have a relative deficiency in PGE_2 synthesis (Wilborn et al., 1995; Keerthisingam et al., 2001; Petkova et al., 2003). The results in this thesis also support this, as non-IPF spheroids produced high levels of PGE_2 four days post spheroid formation, whilst PGE_2 levels were deficient in IPF spheroids. Previous studies have illustrated that TGFβ-induced fibroblast differentiation is dependent on integrin signalling involving focal adhesion kinase (FAK), however in the presence of PGE_2, TGFβ-induced FAK phosphorylation in diminished which in turn limits Akt pathway and prevents fibroblast differentiation (Kolodsick et al., 2003; Thomas et al., 2007). These findings may also partly explain why non-IPF spheroids lack a myofibroblast phenotype, as the increased PGE_2 levels may diminish TGFβ induced myofibroblast differentiation in this 3D system.

Although there is a clear difference in PGE_2 synthesis between control and fibrotic spheroids, transcriptionally the mRNA levels for COX1 and COX2 between non-IPF and IPF spheroids were not statistically different. This contradicts many studies illustrating reduced COX levels in IPF

lung tissue samples in comparison to control samples (Petkova et al., 2003). Nevertheless, since this was only interrogated at the transcriptional level, further investigations are required to determine protein levels of COX1 and COX2 within these spheroids.

The next step was to identify which COX isoform is involved in PGE_2 synthesis by the fibroblast spheroids. In this thesis, the results demonstrated that non-IPF fibroblast cell death is dependent on the activity of COX1 rather than COX2 when cultured as 3D spheroid structures. This data contradicts previously studies which demonstrated the role of COX2 in mediating fibroblast apoptosis *in vitro* (Maher et al., 2010) which suggests that fibroblasts cultured in this 3D system behave differently to fibroblasts cultured as a monolayer. Nevertheless, some studies have supported the role of COX2/PGE_2 mediated cell death within spheroids composed of dermal fibroblasts (Bizik et al., 2004; Vaheri et al., 2009). A possible reason for these contradicting results is the type of compound used and the concentration. Many studies (including the ones described above) used NS398 to determine the effect of COX activity on fibroblast apoptosis. This compound has been classified as a COX2 specific inhibitor with an IC50 of 1.77 μM for human recombinant COX2. However, based on manufacturer's literature this compound may also have off target effects on COX1 activity (IC50 value of 75 μM). The concentration of the compound used in both studies was 15 μM (or 5 μg/mL) which is relatively high in comparison to the IC50 values stated. Thus, it could be speculated that the results shown in those studies may in fact be due to the activity of COX1. In this thesis I also used NS398 and my results illustrated that NS398 had no effect on apoptosis. In addition, I also used more specific COX1 and COX2 inhibitors. These were SC560 (700 fold selectivity for COX1 with an IC50 of 9 nM, according to manufacturer's description) and CAY10404 (500,000 fold selectivity for COX2 with an IC50 of <1 nM). In the presence of these more selective compounds my data supported the role of COX1 mediated apoptosis of fibroblast spheroids. In order fully appreciate the role of COX1 in pHLF apoptosis further studies could be performed on 2D monolayer cultures using these highly specific compounds.

Four receptors for PGE_2 have been described (EP1, EP2, EP3, and EP4) all of which are G-protein coupled receptors (GPCR). Activation of EP1 and EP3 promote smooth muscle cell contraction by increasing in intracellular Ca^{2+} concentration and decreases cAMP levels, respectively. On the other hand, EP2 and EP4 receptor signalling elevate cAMP levels which activates downstream signalling molecules to mediate smooth muscle cell relaxation, increase apoptosis, decrease cell proliferation, and attenuate collagen synthesis (reviewed in (Bozyk and Moore, 2011)). My data demonstrated that prophylactic treatment with PGE_2 attenuated

collagen production in both non-IPF and IPF spheroids (with greater potency shown in non-IPF spheroids), although both express similar levels of *PTGER2* and *4* mRNA, as well as lower levels of *PTGER1* and *3*. However, only treatment with a small molecule EP2 receptor agonist attenuated collagen synthesis in either non-IPF or IPF spheroids in a concentration-dependent manner (with slightly higher potency seen in non-IPF spheroids). This supports published data substantiating the importance of EP2 receptor signalling in attenuating collagen synthesis (Huang et al., 2007). Given that the fibroblasts also showed high levels of *PTGER4* mRNA we would have expected PGE_2 to also have some effect via this receptor. However the results illustrated that in the presence of EP4 agonist or antagonist collagen synthesis did not occur. A possible explanation for this could be that translational levels of EP4 may be low thus the expression of this protein on the membrane surface may be low in comparison to EP2 receptors.

Based on these findings it was also assumed that an EP2 antagonist would allow increased collagen deposition within the spheroids compared to baseline levels. However this was not the case, suggesting that although PGE_2-mediated EP2 receptor activation may decrease collagen production in the 3D system after exogenous PGE_2 treatment, the excessive collagen deposition is not otherwise attenuated by endogenous PGE_2 signalling at baseline. A possible reason for this could be that at early stage of spheroid formation the PGE_2 levels are too low and EP2 receptor signalling is not active. Therefore, antagonising an inactive receptor would not show effect. Based on these findings it can be proposed that, the non-IPF spheroids may to some extent represent what is seen in a normal wound healing process (i.e. promote the synthesis of a provisional matrix following cell-to-cell contact and then eventually undergo apoptosis via increased production of PGE_2).

Unsurprisingly, a small molecule EP2 agonist reduced the viability of non-IPF fibroblast spheroids in a dose-dependent manner akin to exogenous treatment with PGE_2, however it had a more limited impact on the percentage of TUNEL positive cells in IPF spheroids. Although at the transcriptional level there was no statistical difference in *PTGER2* expression between non-IPF and IPF spheroids, there may be a difference at the translational level (Larsson et al., 2008), and it could be hypothesised EP2 receptor protein levels are lower in IPF spheroids in comparison to non-IPF, although this would require further validation.

Previous studies have illustrated that *PTGER2* mRNA levels are lower in IPF fibroblasts in comparison to non-IPF which is as a result of DNA hypermethylation (Moore et al., 2005a;

Huang et al., 2008b, 2010). However, my data contrast these studies, which possibly suggest that following cell-to-cell contact DNA methylation of the *PTGER2* gene is altered. However further research is required to investigate this.

4.3.9. Fibroblast spheroids are non-proliferative

In monolayer culture, fibroblasts (normal and fibrotic) derived from human lungs have the ability to proliferate. In order to investigate whether similar results are shown within 3D spheroids, immunocytofluorescence labelling was conducted to detect Ki-67 positive cells. Ki-67 is a nuclear protein with an unknown function, however it has shown to be expressed in all stages of the cell cycle (G1, S, G2, and mitosis) excluding G0. This supports a possible role for Ki-67 during proliferation which is one the main reason why it is considered as a proliferation marker. In 3D cultures, fibroblasts (from both normal and fibrotic lung) did not proliferate. Such observations have also been observed in dermal fibroblasts which also form non-proliferating spheroids (Bizik et al., 2004). The non-proliferative property of non-IPF fibroblast spheroids may be due to the increased synthesis of PGE_2 and low levels of active TGFβ, both of which have previously shown to affect fibroblast proliferation by affecting the PI3K/Akt pathway (Keerthisingam et al., 2001; Wilkes et al., 2005; Takai et al., 2013).

However, since the IPF spheroids also showed no sign of proliferation (despite having low levels of PGE_2 and high levels of TGFβ) it could be postulated the cells do not proliferate as a result of contact inhibition. Contact inhibition is defined as the termination of ruffling and forward movement in the filopodia (cytoplasmic projections extending beyond the leading edge lamellipodia) following cell-to-cell contact (Abercrombie, 1979; Heckman, 2009) which has previously been described in human fibroblast (Wieser and Oesch, 1986). However the precise mechanism/signalling processes involved in causing contact inhibition is currently unknown. Nevertheless, studies have postulated the role of cell adhesion molecules (such as cadherins) in mediating contact inhibition via the activation of the Hippo pathway. This pathway is involved in the regulation of cell proliferation and apoptosis. This pathway involves the activation of a kinase cascade, where Mst1/2 kinases and Sav1 form a complex to phosphorylate and activate LATS1/2 kinase. This in turn phosphorylates and inhibits the transcription co-activators YAP and TAZ leading to an inhibition of cell proliferation. However, when YAP and TAZ are dephosphorylated they can translocate into the nucleus and interact with transcription factors to promote cell proliferation and inhibit apoptosis (Yu and Guan, 2013). Studies have illustrated that components of tight and adherens junctions are able to

associate with YAP/TAZ preventing its translocation into the nucleus thus inhibit cell proliferation. Disruption of these tight and adherens junctions result in the induction of YAP/TAZ nuclear localisation, promoting cell proliferation. Since IPF spheroids have shown tight/adherens junctions it can be hypothesised that these junctions are regulating the Hippo pathway in the fibroblast spheroids leading to contact inhibition. However, further work is required to investigate the role of this signalling pathway in the pHLF cultured as spheroids.

4.4. Microarray data analysis

4.4.1. Overview

Gene expression microarray technology has revolutionised the field of molecular biology by allowing the detection of expression patterns and interactions of thousands of genes simultaneously, by using multiple probes to assay each transcript. Although this technique is increasingly robust for the detection of genes/pathways whose expression changes in response to specific perturbations, there are still some concerns with regards to the reliability, which is why quantitative and qualitative validation are often necessary (Kerr, 2003).

Microarray analysis has been used extensively to compare transcriptional profiles of lung samples from control subjects with those from patients diagnosed with IPF (Pardo et al., 2005), nonspecific interstitial pneumonitis (NSIP), and hypersensitivity pneumonitis (Selman et al., 2006) – all of which focused on differences in mRNA abundance. In addition, analysis has also been performed on myofibroblasts isolated from control and IPF lungs (Kaminski and Friedman, 2002; Renzoni et al., 2004; Selman et al., 2007). Furthermore, ongoing work in our laboratory has been investigating transcriptional profiles of monolayer fibroblast cultures from lungs of IPF and system sclerosis patients.

Since this report has highlighted phenotypic differences between non-IPF and IPF fibroblast spheroids (i.e. cell death, collagen deposition and TGFβ activation), we decided to analyse the transcriptional profiles of the spheroids to determine possible pathways that may be dysregulated in IPF spheroids, resulting in the phenotypical changes described. Interestingly, while performing quality control of the array data, Principal Component Analysis (PCA) revealed a major sample outlier (which was subsequently excluded from further analysis); this

sample comprised a non-IPF fibroblast line from a low passage culture (i.e. passage 4, in comparison to the remainder fibroblast spheroids cultured at passage 5-7). As stated previously, cell passage can affect cell behaviour, differentiation state and senescence, and may also have early effects on the transcriptome.

Another quality control PCA plot also illustrated slight batch and location effects. Minor differences in non-biological variables (such as reagent lot, operator, and even changes in atmospheric ozone levels) can affect the gene expression microarray results (Fare et al., 2003; Chen et al., 2011). The term 'batch' refers to the microarrays that have been processed at the same time at one site using the same array platform. The term 'batch effect' refers to cumulative errors induced by these time- and place-dependent experimental variations. Batch effects in microarray studies are extremely common and almost inevitable, primarily due to the fact that the majority of the available microarray platforms can only assay <20 samples at one time (Chen et al., 2011). In addition, the location at which the spheroid experiments were initially formed can also affect the array also due to place-dependent variations (e.g. lot number of the reagents used). Since the spheroid samples were generated at two different locations (i.e. UCL and GSK) and processed in two batches, variation due to these effects was removed by using a statistical algorithm within Partek Genomics Suite.

After applying these quality control measures, the PCA plot then demonstrated that there was a clear difference between non-IPF and IPF spheroid samples. However, only 138 differentially expressed genes were identified (false discovery rate, FDR, $p<0.05$ and fold change >2 or <-2). From this list 76 genes encoded proteins with known functions. Compared to other microarray published data the number of differentially expressed genes is this system is quite low (Selman et al., 2006; Lindahl et al., 2013). There are a number of possible reasons that could explain why only a few genes were differentially expressed. The most obvious reason is that fibroblasts spheroid is a completely different system in comparison to monolayer fibroblast cultures. Thus difference in gene expression profile is entirely justifiable.

Another possible reason that could explain why a low number of differentially expressed genes were detected is the presence of noise within the samples created by donor-to-donor variations (e.g. gender, age, medical status, medication taken by the patients, and smoking status). Due to patient confidentiality it was difficult to obtain the complete medical reports for all of the donors, which was one reason why these factors were not taken into account during the analysis.

Furthermore, my data illustrated that within just 24 hours of spheroid formation, both non-IF and IPF spheroids are capable of synthesising their own active TGFβ and collagen. Thus, to some extent both non-IPF and IPF spheroids behave similarly following cell-to-cell contact at the early stage of spheroid formation (irrespective with the fact that active TGFβ and collagen levels were greater in IPF spheroids). Therefore, since the microarray samples only composed of spheroids cultured for 24 hours, it may not be entirely surprising to see a low number of differentially expressed genes at that particular time point. However, after 96 hours non-IPF spheroids undergo apoptosis whilst IPF spheroids remain fairly resistant. Therefore, it may be of great interest to perform another microarray study where spheroids are cultured for 96 hours which could potentially lead to the detection of more differentially expressed genes and could help identify a specific pathway.

Moreover, previously published microarray data studies on non-IPF and IPF myofibroblasts revealed a greater number of differentially expressed genes at the level of ribosomal recruitment than at the level of transcript abundance, suggesting that pathological translation control is a major characteristic of IPF myofibroblasts (Larsson et al., 2008). Similar may also be the case in this 3D system which may also explain the low levels of differed genes at the transcriptional level.

4.4.2. Differentially expressed genes

The top three differentially expressed genes identified were *PRR14L* (proline rich 14-like), *CTSB* (cathepsin B), and *PTGER3* (prostaglandin E2 receptor 3). Currently the function of *PRR14L* is unknown. However many studies have illustrated the importance of cathepsin B and EP3 receptor signalling in pulmonary fibrosis which will be described below.

Cathepsins are a class of proteases primarily involved in lysosomal end stage degradation of endocytosed proteins (Turk et al., 2012). In addition, cathepsins also play a role in degrading ECM proteins (Lecaille et al., 2002; Novinec and Lenarčic, 2013). Their proteolytic activity is regulated by their inhibitors (i.e. steins, kininogens, and cystatins, all of which belong to the cystatins superfamily) (Abrahamson et al., 2003; Turk et al., 2008) which suggests that the balance between cathepsins and cystatins may be important for the degradation of ECM components. Studies have demonstrated increased cathepsin production in many chronic lung diseases including asthma and cystic fibrosis which contribute to the remodelling of ECM and basement membrane (Lalmanach et al., 2006). Furthermore, studies have illustrated that deficiency in cathepsin activity exacerbated lung fibrosis thus overexpression of cathapsin may

be beneficial as a therapeutic strategy for the treatment of pulmonary fibrosis which could aid in the ECM degradation (Lalmanach et al., 2006; Quinn et al., 2010). The results fro the microarray study in this thesis illustrated that transcriptionally CTSB levels are low in IPF in comparison to non-IPF spheroids. This is in support with a recent study published which also demonstrated reduced cathepsin B levels in differentiated lung fibroblasts. It has been shown that intracellular cathepsin B contributes in the TGFβ mediated differentiation of lung fibroblasts via intracellular processing of pro-TGFβ to its mature form. Following release and activation of TGFβ, the canonical Smad signalling pathway initiates myofibrogenesis. Furthermore the same study demonstrated that Smad-signalling regulates the expression of cystatin C which inhibits the activity of extracellular cathepsin leading to reduced ECM degradation (Kasabova et al., 2014). This provides evidence of a negative feedback look for the activity of cathepsin B. Since IPF spheroids spontaneously synthesis TGFβ it can be proposed that reduced *CTSB* may be as a result of this negative feedback loop, contributing to increased collagen levels. However, further validation is required.

As stated before, EP3 receptors which mediate cellular activity via the inhibition of acetylate cyclase resulting in reduced cAMP levels. My current qPCR data has illustrated that there is no significant difference in *PTGER3* mRNA levels between non-IPF and IPF spheroids. However, the microarray data illustrated that *PTGER3* levels are elevated in IPF spheroids. There are several possible reasons for these contradicting data which will be discussed later in **Section 4.4.5**. However, these contradicting results support the need of further validation regarding the expression of this gene.

4.4.2. Pathway analysis

Following the identification of the differentially expressed genes, Partek pathway analysis was then performed to provide an enrichment score. This is a formal statistical evaluation of the dataset which assesses the overlap of the differentially expressed genes with those in each pathway in a database of pathways (Subramanian et al., 2005). In this case the Kegg (Kyoto encyclopaedia of genes and genomes) pathway database was used. Based on this analysis, several pathways were identified including some that are highly topical in understanding the pathogenesis of pulmonary fibrosis. These include phosphatidylinositol signalling, calcium signalling, vascular smooth muscle contraction, cell cycle, Notch signalling, vascular endothelial growth factor (VEGF) signalling pathway, chemokine signalling pathway, inositol phosphate metabolism, metabolic pathways, cell adhesion, mitogen-activated protein kinases (MAPK) signalling, and the PI3K-Akt signalling pathway.

Although these pathways were identified following the enrichment analysis, in many cases only a single differentially expressed gene was detected for each pathway listed (**Appendix 2**). In addition, the pathway with the highest enrichment score was the phototransduction pathway (involved in processing light in the retina of the eye). However, the three genes detected in this pathway are all involved in encoding calmodulin (calcium modulated protein; **Figure A7, K**). This protein not only plays a role in the phototransduction pathway but also in several other processes including smooth muscle contraction (Masuda et al., 1984), calcium signalling pathway, cell migration (Verploegen et al., 2002), inflammation (Nakashima et al., 1986), phosphatidylinositol signalling system (MacNicol et al., 1990), and ras signalling (Villalonga et al., 2002). This suggests that data analysis based solely on enrichment scores may sometimes be misleading (particularly when the number of differentially expressed genes is small) or unhelpful. The enrichment analysis is also dependent on the accuracy of the pathway databases and how up-to-date they are.

4.4.3. Differentially expressed genes involved in metabolic pathways

The pathway that consisted of the most differentially expressed genes was the metabolic pathway. Seven genes belonged to this pathway group: *CS* (citrate synthase), *IMPDH2* (Inosine-5'-monophosphate dehydrogenase 2), *MTHFR* (methylenetetrahydrofolate reductase), *P4HA1* (prolyl 4-hydroxylase subunit alpha 1), *SPTLC2* (serine palmitoyltransferase), *SYNJ2* (synaptojanin 2), and *XDH* (xanthine dehydrogenase). Although these genes belong to metabolic pathways none of them form any direct protein-protein interactions. However, there are a few indirect protein-protein associations (**Appendix 2; Figure A5**). Each of theses genes will be discussed briefly below.

CS encodes for citrate synthase which is located in mitochondria and commonly used as a marker for the presence of intact mitochondria. This enzyme plays a vital role in the Krebs cycle by catalysing the conversion of acetyl-CoA and oxaloacetate into citrate. It has been postulated that factors affecting the Krebs cycle can profoundly influence the cellular energetics of a cell and may therefore affect fibroblast cell growth and proliferation (Emblom-Callahan et al., 2010). Based on the microarray results *CS* regulation is low in IPF spheroids in comparison to non-IPF spheroids (**Figure A5, J**) which suggests that IPF fibroblasts may exhibit defects in respiratory activity with potentially reduced ATP levels (Lin et al., 2012). This result contradicts previously published data illustrating elevated ATP content in BALF of IPF patients in comparison to control subjects. Furthermore, in bleomycin-induced PF mice and *in vitro* assays (involving epithelial cells) ATP has been postulated as a major endogenous danger signal

as it results in IL-1β maturation leading to lung fibrosis (Riteau et al., 2010). However, as stated these finding were demonstrated in epithelial cells. The expression of CS and ATP and the role of Krebs cycle in fibrotic pHLF have not been demonstrated. Thus, further investigations and validations would be necessary to investigate this.

IMPDH2 encodes the rate limiting enzyme inosine-5'-monophosphate (IMP)-dehydrogenase 2 which is involved in the *de novo* guanine nucleotide biosynthesis. The encoded protein catalyses NAD-dependent oxidation of IMP into xanthine-5'-monophosphate (XMP) which is then converted into guanosine-5'-monophosphate (GMP). Thus, this enzyme plays a vital role in the maintenance of cellular guanine deoxy- and ribonucleotide pools essential for the synthesis of genomic material (i.e. of DNA and RNA). Microarray data illustrate that this gene is high in non-IPF spheroids in comparison to IPF (**Figure A8, K**). This could suggest two things – either there is a potential deficit in generating genomic material in IPF spheroids or in non-IPF spheroids this gene is upregulated to increase to pool of genomic material as a consequence of cell-to-cell contact. However, further validation is required before drawing any conclusions.

MTHFR encodes for methylenetetrahydrofolate reductase, an enzyme involved in processing amino acids, particularly the conversion of homocysteine to methionine. Similar to *IMPDH2*, this gene is also low in IPF spheroids in comparison to non-IPF (**Figure A8, D**) suggesting defects in processing amino acids in IPF spheroids.

P4HA1 encodes for prolyl 4-hyroxylase (P4H), an enzyme involved in the hydroxylation of proline resulting in the formation of 4-hydroxyproline which plays a vital role in proper folding of newly synthesised procollagen chains. This gene is upregulated in IPF spheroids in comparison to non-IPF (**Figure A9, C**) which correlates with previously published findings as well as the results in this thesis illustrating that IPF spheroids produce high levels of collagen in comparison to non-IPF.

SPTLC2 encodes for serine palmitoyltransferase, a key enzyme for sphingolipid metabolism (Hanada, 2003). This gene is downregulated in IPF spheroids in comparison to non-IPF (**Figure A10, L**). Sphingolipids are one of the three classes of lipids found in the cell membrane which (along with cholesterol and proteins) form lipid rafts (Lahiri and Futerman, 2007). These form liquid-ordered phases in the lipid bilayer (Lingwood and Simons, 2010). Many sphingolipids, particularly sphingosine 1-phosphate (S1P) and ceramide, are recognised as critical mediators of various basic cellular processes involved in tissue responses to injury. Such processes include cell survival, migration, proliferation, contraction, gene expression, and cell-cell

interactions (Ishii et al., 2004; Hannun and Obeid, 2008; Rivera and Chun, 2008). In addition, recent studies have substantiated the role of S1P in regulating the development of tissue fibrosis in several organ systems including lungs. For instance, inhibition of $S1P_1$ receptor signalling worsened bleomycin-induced pulmonary fibrosis indicating that this pathway acts as an endogenous inhibitor of fibrogenesis in the lungs (Shea et al., 2010). In addition *in vitro* studies have shown that S1P attenuates fibroblast chemotaxis (Goparaju et al., 2005) and conveys autocrine and paracrine protection of epithelial cells (i.e. A549s) (Schnitzer et al., 2009). Further evidence that sphingolipids may regulate the development of lung fibrosis comes from studies showing increased activity of sphingomyelin-degrading enzyme acid sphingomyelinase (ASM) in the lungs of mice following intratracheal bleomycin challenge. Furthermore, mice genetically deficient for this enzyme demonstrated an attenuation of lung fibrosis in this model (Dhami et al., 2010). Thus, dysregulation in the S1P pathway could potentially contribute to decreased fibroblast apoptosis and increased epithelial cell apoptosis which are key cellular features observed in lung fibrosis (reviewed in (Shea, 2012)). As well as illustrating anti-fibrotic effects, several studies have also demonstrated contradicting data whereby S1P signalling can induce TGFβ –induced fibroblast differentiation (Kono et al., 2007). Since the microarray results illustrate a downregulation in the enzyme involved in sphingolipid metabolism it could potentially suggest that dysregulation of the sphingolipid pathway may be relevant for some of the phenotypical features seen in IPF spheroids, and this is worthy of further investigation

SYNJ2 encodes for synaptojanin-2 which is a member of the inositol-polyphosphate 5-phosphatase which is involved in blocking clatherin-mediated endocytosis. To date the effect of this protein on fibrosis has never been studied before. However, since this gene is downregulated in IPF spheroids in comparison to non-IPF (**Figure A6, E**) further investigations and validations could be performed.

4.4.4. Differentially expressed genes involved in influenza

Since only a small number of differentially expressed genes were identified overall, which resulted in minimal identification of protein-protein interactions (based on String 9.1 analysis), it was decided to perform the analysis again with $p<0.01$ (a more stringent p-value, but unadjusted/without FDR) and a fold change of <-2 or >2. Based on these criteria 730 genes passed the threshold, of which 414 genes encoded proteins with known functions. More protein-protein interactions were also evident in comparison to the previous analysis. Bizarrely, Partek pathway analysis demonstrated the Influenza A pathway with the highest

enrichment score. 12 genes (*CASP1, CCL2, DDX58, IFIH1, IL1A, IL33, MX1, OAS2, OAS3, PIK3R1, PML,* and *PRKCB*) were identified in the list of differentially expressed probes belonging to this pathway.

Influenza A virus is a genus of the orthomyxoviridae family of viruses which causes an acute respiratory illness known as influenza (commonly referred to as 'the flu'). Clinical presentations include fever, cough, and dyspnoea. In addition, majority of patients have clinically apparent pneumonia (Bay et al., 2007) which die of progressive respiratory failure. There are several subtypes of this virus of which the H5N1 subtype has previously been shown to result in pulmonary fibrosis in mice infected with this virus (Qiao et al., 2009). This provided evidence that this virus may possibly play a role in the pathogenesis of pulmonary fibrosis. Since this pathway was identified with the highest enrichment score further validation of the microarray results is vital. This would involve performing qRT-PCR of the differentially expressed genes. In addition the effect of this pathway on the phenotype of non-IPF and IPF spheroids (i.e. collagen synthesis, active TGFβ production, and apoptosis) also should be investigated.

One thing to note is that the fibroblasts were not exposed to influenza A virus in this 3D spheroid system. Therefore, the detection of this pathway following the enrichment analysis was unexpected. Furthermore, although the 12 genes detected belong to the Influenza A pathway, some of those genes are functionally linked to many other pathways. For example, *CASP1* encodes caspase 1 which plays a key role in the activation of IL-1β (Denes et al., 2012). IL-33 is a member of the IL-1 family however unlike IL-1β, IL33 activity is not dependent of caspase 1. Both IL1β and IL33 are pro-inflammatory and pro-fibrotic cytokines. In addition, CCL2 is also a chemoattractant cytokine which exerts pro-fibrotic effects on fibroblasts by stimulating ECM production (discussed in more detail in **Section 4.5.5**).

4.4.5. Microarray analysis contradict some qRT-PCR results.

Since previous qRT-PCR analysis of non-IPF and IPF spheroids illustrated some differences between the two (such as differential mRNA levels for *ACTA2*, *ITGAV*, and *ITGB5*), it was expected that these genes would also be detected after performing microarray data analysis. However, this was not the case. In addition, qRT-PCR data for *PTGER3* expression (gene involved in encoding PGE_2 receptor EP3) illustrated that there was no statistical difference between non-IPF and IPF spheroids, however microarray data analysis suggested this gene was differentially expressed with an upregulation seen in IPF spheroids. There are a number of

possible reasons which could explain these differences. For instance, since the samples in the microarray included only one replicate from each donor, it could suggest that some of the array data may have resulted due to chance. Another possible reason for these contradicting results is the method used to isolate RNA. For qRT-PCR Trizol reagent was used however for microarray studies RNaqueous lysis buffer was used for RNA isolation. Thus, for direct comparisons between qRT-PCR and microarray analysis it would be ideal to use the same RNA isolation protocol (something that could be considered in the future). In addition, studies have shown that qRT-PCR is actually more sensitive for detecting small changes in gene expression in comparison to microarrays which could also explain the contradicting results and also support the importance of thorough validation of the microarray data (Wang et al., 2006; Allanach et al., 2008).

4.5. Medium-throughput compound screening

4.5.1. Overview

High/medium-throughput screening is the process of testing a large number of diverse compounds against disease targets to identify 'hits' (Liu et al., 2004). GlaxoSmithKline (GSK) has developed a library composed of 182 compounds which target several pathways potentially involved in the initiation and/or the progression of IPF. This compound library was termed the 'fibrosis toolbox'. A medium-throughput screening was performed which involved treating the non-IPF and IPF spheroids prophylactically with each compound at high concentration (10 μM). The primary endpoint involved determining total spheroid collagen content by HPLC. Due to confidentiality, only a selected subgroup of compounds were analysed and presented in this thesis. The results illustrated a number of hits (or >50 % change in baseline collagen synthesis) within the compound library some of which will be discussed in detail below. It is important to note that all these compounds require further validation, as there is the potential for these 'hits' to have arisen due to toxicity.

4.5.2. Targeting collagen crosslinking

BMP-1 has been reported to play a key role in matrix stiffening by promoting the cleavage and activation of a collagen crosslinking enzyme known as lysyl oxidase (LOX). LOX catalyses the

oxidation of lysine residues in elastin and collagen, which lead to the formation of intra- and intermolecular crosslinks vital for ECM stabilisation (Grimsby et al., 2010). Elevated activity of LOX has previously been reported in PF or models thereof (Almassian et al., 1991; Kagan and Li, 2003). For instance, studies have illustrated that bleomycin-exposed human foetal lung fibroblasts had an upregulation in LOX levels (Chen et al., 2010). Furthermore, a rise in LOX activity elevates bleomycin-induced total lung hydroxyproline in rats (Counts et al., 1981). Moreover, antagonising LOX and LOXL2 activity has previously been shown to attenuate bleomycin-induced PF in hamsters (Kagan, 2000), reduce the production of growth factors, and attenuate TGFβ signalling due to reduced matrix stiffness (Barry-Hamilton et al., 2010). Thus, these findings support the concept that targeting the pathway involved in collagen crosslinking (i.e. BMP-1, LOX, and LOXL2) could be an attractive therapeutic angle for IPF. Based on these findings, an allosteric inhibitor of LOXL2 (GS-6624, formerly known as AB0024) has been developed and evaluated in a phase I clinical trial as a potential compound for the treatment of IPF (clinicaltrials.gov identifier NCT01362231) and a phase II trial is scheduled.

My results illustrated that targeting BMP-1 could attenuate collagen synthesis with a profound effect seen in non-IPF spheroids. On the other hand, antagonising LOX and LOXL2 activity showed minimal effects. This is clearly in contrast to the published data stated above. A possible reason for this could be that the fibroblasts in these spheroids do not express high levels of LOX and LOXL2. This assumption is based on the fact that these genes showed low expression by microarray analysis, confirmed by qRT-PCR analysis showing a low level of mRNA levels for LOXL2 (see **Appendix 5, Figure A10**). Another possible assumption could be that crosslinking has no impact on the amount of collagen synthesised in this system. It is important to note that HPLC is used primarily to measure hydroxyproline levels which correlate to collagen synthesis, it does not measure collagen cross-linking. So it may be entirely feasible that the collagen within the spheroids is not cross-linked at that particular time point (24 hours of spheroid formation). However, further studies are required to determine collagen cross-linking within the spheroids.

4.5.3. Targeting TGFβ signalling pathway

As stated previously, my data illustrate that spheroids are capable of synthesising their own active TGFβ, however collagen production appeared to be independent of TGFβ signalling. Several compounds in the fibrosis toolbox targeted TGFβ activation and receptor signalling (i.e. ALK-5 antagonist, TGFβ antagonist, β3 antagonist, and dual β3/β5 antagonist dual TGFβRI/II

antagonist) and these also showed similar results with little or no effect on collagen synthesis. This further supports the notion that another mechanism/mediator may be involved in promoting collagen production (see **Section 4.3.6**), at least at this early timepoint following spheroid formation.

Interestingly however, a pan integrin αv antagonist completely abolished collagen synthesis in non-IPF spheroids with little effect seen in IPF. This potentially suggests that in non-IPF spheroids blocking all αv integrins in fibroblast spheroids (i.e. αvβ3, αvβ5, and αvβ8) plays a role in collagen production. As stated before, my data illustrates that β3 and β8 integrins partially affect TGFβ activation, but have no effect on collagen synthesis. Thus, it could be postulated that the effects seen through αv antagonist may be primarily due to blocking αvβ5 integrin which would support previously published data (Scotton et al., 2009). Therefore, to investigate this further it is essential to determine the effect of β5 integrin on collagen synthesis (potentially by using a neutralising antibody). Another possible explanation for this result is that in the presence of pan αv antagonist the cell-matrix interaction is altered which may lead to knock-on effects on cell biosynthetic pathways. However, since this compounds used in this library were at an extremely high concentration it is entirely feasible that the result for integrin αv antagonist may have occurred due to toxicity.

In addition, although antagonising ALK-5 receptor had no effect on collagen production, an ALK-4/5/7 antagonist attenuated collagen synthesis in IPF spheroids with minimal effect shown in non-IPF. ALK-4 (ACVR-1B) and ALK-7 (ACVR-1C) are also transmembrane receptor serine/threonine kinases (similar to ALK-5) which are activated in the presence of activin-A. In addition, nodal has also shown to be a ligand for ALK-4 and ALK7. Similar to TGFβ (types I, II, and III), activin-A and nodal also belong to the TGFβ superfamily which mediate the activation of the canonical Smad pathway.

Several studies have implicated a role for activin in the pathogenesis of PF. For instance, bleomycin-induced PF mice show enhanced expression of activin A, particularly in fibroblasts and alveolar macrophages at areas of fibrotic change (Matsuse et al., 1995; Aoki et al., 2005) These results were subsequently confirmed in humans, with enhanced activin A expression shown in patients with conditions associated with interstitial pulmonary fibrosis (Matsuse et al., 1996). In addition, activin A induces lung fibroblast proliferation, differentiation, and increases the ability of fibroblasts to contract collagen gels *in vitro* (Ohga et al., 1996, 2000). Furthermore, studies on other fibrotic diseases such as systemic sclerosis have demonstrated

an increase procollagen production and expression of *COL1A1* mRNA following the activation of the activin A-ALK4-Smad-dependent pathway, which also increased the expression of CTGF (Takagi et al., 2011). Moreover, a recent study demonstrated an attenuation in bleomycin-induced PF (with reduced collagen accumulation, tissue damage, and inflammation) following the administration of follistatin (a protein involved in sequestering activins and hindering their biological activity) (Aoki et al., 2005). All these findings support a functional role of activin in the pathogenesis of pulmonary fibrosis. Since the results in the toolbox illustrated a complete block in collagen synthesis for IPF spheroids in the presence of an ALK-4/5/7 antagonist it can be hypothesised that in this 3D system the collagen synthesis is more dependent on activin-ALK4/7-mediated Smad signalling rather than ALK5-dependent TGFβ signalling. It also highlights the potential of a combinatorial approach, targeting all three receptors in order to attenuate collagen production within the IPF spheroids. In non-IPF spheroids this antagonist showed minimal effects on collagen production; this could be due to reduced expression of these receptors, or suggests that collagen production in non-IPF fibroblast spheroids is dependent on a different mechanism (e.g. PDGF). Thus, further studies are required to determine to expression of these receptors in the fibroblast spheroids and produce concentration-response curves of this compound in non-IPF and IPF spheroids, since therapeutics with differential effects in IPF vs. non-IPF could be highly beneficial.

4.5.4. Targeting the eicosanoid pathway

My results have demonstrated a role for COX1-PGE_2-EP2 signalling in fibroblast spheroid apoptosis and collagen synthesis which has already been discussed in **Section 4.3.8**. In addition, the toolbox also identified compounds which support the role of EP2 receptor signalling in attenuating collagen production in both non-IPF and IPF spheroids. However, there were a few contradicting results. For instance, in the toolbox screen, an EP2 receptor antagonist completely abolished the synthesis of collagen in non-IPF spheroids. However, when a full concentration-response curve was subsequently developed for this compound using fibroblasts from the same donor, no effect on collagen production was seen. This is a clear example of a false positive result (which may have resulted due to technical issues with HPLC), and supports the importance of further validating compounds showing a 'hit', in addition to repeat the experiments with additional donors.

The screening also identified prostaglandin F receptor which, following inhibition, exaggerated collagen production in IPF spheroids but had no effect on non-IPF. This result does not support previously published data as $PGF_{2\alpha}$ has been detected at high levels in IPF patients (Aihara et

al., 2013) and FP receptor signalling accelerates bleomycin-induced pulmonary fibrosis (independently of TGFβ) (Oga et al., 2009). This may be a false positive result but does require further validation. However, it is important to note that single cell-based *in vitro* assay systems are likely to show some difference and may have more flaws in comparison to the more complex *in vivo* systems which are composed of multiple cells types which affect fibroblast cell behaviour. Thus, increased $PGF_2\alpha$ levels shown in IPF patients and bleomycin-induced PF mice may be as a result of other cell types (e.g. epithelial cells).

In addition, the toolbox also consisted of compounds targeting 5-lipoxygenase (5-LO) and leukotriene (LT)-D_4. 5-LO is a rate-limiting enzyme essential for the synthesis of leukotriene's which promote fibroblast proliferation, chemotaxis, and collagen production (Ozaki et al., 1992; Wilborn et al., 1996). Leukotriene-deficient mice show protection from PF (Peters-Golden et al., 2002) and LTD_4 stimulates collagen synthesis *in vitro* following TGFβ-mediated fibroblast differentiation. Thus, it was expected that antagonising the leukotriene pathway would attenuate collagen synthesis. However, the results from the screening did not support this. In fact, antagonising this pathway exaggerated collagen production in non-IPF spheroids, although no effect was shown in IPF spheroids. This suggests that in this 3D system, the leukotriene pathway may play a protective role in preventing over production of collagen following cell-to-cell contact. However, further work is required to investigate this.

4.5.5. CCL2/MCP-1 antagonist

MCP-1 (also known as CCL2) is primarily considered as a potent chemoattractant for T-cells, monocytes and natural killer cells. However, several studies have demonstrated the role of this chemokine in direct activation of fibroblasts, resulting in ECM production via the induction of TGFβ (Gharaee-Kermani et al., 1996; Hogaboam et al., 1998; Moore et al., 2005b). In addition, BALF of IPF patients has elevated levels of CCL2 (Suga et al., 1999) and CC-chemokine receptor 2 (CCR2; the major receptor for CCL2) knockout mice are protected against FITC- and bleomycin-induced pulmonary fibrosis (Moore et al., 2001; Okuma et al., 2004) which further support the role of this chemokine in fibrosis. Recently, a randomised double-blinded placebo-controlled phase II trial was completed, to evaluate the safety and efficacy of an anti-CCL2 antibody in IPF patients (CNTO 888; clinicaltrials.gov identifier NCT00786201), although the results have not yet been reported.

The toolbox screening results illustrated that in the presence of a CCL2/MCP1 inhibitor, collagen synthesis in IPF spheroids was completely abolished. This same compound had very

little effect on non-IPF spheroids. A possible reason for this difference may relate to the fact that IPF fibroblasts express high levels of CCL2 in comparison to non-IPF, at least at the levels of mRNA (see qRT-PCR data in **Appendix 6**). This supports that CCL2/MCP1 may be a potential therapeutic target, however further validation is necessary.

4.5.6. Targeting Smoothened (Smo)

The Hedgehog signalling pathway plays an essential role in embryonic development, tissue patterning, and organogenesis (Riobo and Manning, 2007). Three hedgehog homologs have been identified in mammals of which Sonic Hedgehog (Shh) is the most broadly expressed and involved in patterning the lung (Litingtung et al., 1998; Pepicelli et al., 1998). In brief, SHH binding to its receptor (PTCH1) relieves Smo repression, and results in Smo-dependent downstream signalling events which culminate in activation of transcription factors (e.g. GLI).

Studies in human adult lungs have discovered overexpression of Shh in the alveolar epithelium of patients diagnosed with IPF and other idiopathic interstitial pneumonias (Coon et al., 2006; Fitch et al., 2011; Bolanos et al., 2012). However, the Shh receptor (PTCH1) and downstream signalling molecules (i.e. GLI1 and Smo) are expressed in mesenchymal cells in the fibrotic foci, which supports an epithelial-mesenchymal crosstalk. Furthermore, Shh promotes fibroblast migration, proliferation and enhance collagen synthesis; Shh signalling is also involved in fibroblast resistance to apoptosis. These findings suggest that targeting the Sonic hedgehog pathway may be a promising therapeutic strategy for IPF. The results in this thesis also support this as targeting Smo abolished collagen synthesis in IPF spheroids with a partial inhibition shown in non-IPF. This suggests that Shh signalling pathway is active in IPF spheroids. However, since these fibroblast spheroids are not in contact with epithelial cells (which are thought to express Shh) it could be suggested that the fibroblasts in this system may also express Shh which result in an autocrine and/or paracrine activation of the pathway. However further investigations for the expression of all the proteins involved in the Shh signalling pathway in this spheroid system is required.

4.5.7. Targeting the PI3K/Akt/mTOR pathway

The PI3K/Akt/mTOR pathway has recently become of great interest in understanding the pathogenesis of IPF. PI3K plays a key role in mediating TGFβ-treated lung fibroblast differentiation and proliferation (Conte et al., 2011). In addition, strong immunoreactivity for downstream effectors of mTOR (e.g. p-S6) have been illustrated in fibroblasts of the fibrotic foci (Xu et al., 2013). More recently, research has proposed that Akt/mTOR kinases play a role

in the desensitisation of IPF fibroblasts to type-I collagen matrix-induced cell death (Nho and Hergert, 2014). These studies support PI3K/Akt/mTOR pathway as a target for modulating IPF progression and currently compounds targeting this pathway are being investigated for clinical application.

This thesis also investigated the effect of a similar compound (GSK-X) on pHLF of non-IPF and IPF subjects using my three-dimensional spheroid model. As shown in the results, prophylactic treatment of this compound attenuated both spheroid formation and collagen synthesis of non-IPF and IPF pHLF (in a concentration-dependent manner). Collagen attenuation was detected at very low concentrations of the compound. However, at high concentrations (above 0.3 μM), the fibroblasts were unable form cellular aggregates. This may have possibly resulted due to toxicity. In addition, the results showed that the IC50 differed from donor to donor, most likely due to simple donor-to-donor variations.

The ability of this compound to have therapeutic effects in this spheroid model was also investigated, however, in line with other compounds investigated (e.g. ALK5 inhibitor) GSK-X showed no effect on collagen synthesis when given therapeutically. As mentioned previously, this could be due to an inability of the compound to penetrate the spheroid, or a general issue where reversal of the established collagen deposition was not amenable to modulation. Nevertheless, the current data for this model supports that targeting PI3K/Akt/mTOR signalling pathway may be a potential therapeutic agent to prevent the progression of the disease.

Furthermore, the medium throughput screening identified mTORC1/2 as a potential target for attenuating collagen production. However, PI3K β/δ inhibitor had minimal effect on collagen production in both non-IPF and IPF spheroids. This suggests that collagen synthesis may be dependent of mTORC2-mediated Akt activation (independent of PI3K activity) which supports that mTORC2 may be a potential therapeutic target. However further validation is necessary to investigate this.

4.6. Conclusions

The aim of this thesis was to develop a novel 3D *in vitro* model system to use as an assay for drug screening in IPF. The work presented here reports the finding that pHLF are capable of spontaneously synthesising their own matrix (i.e. collagen) and high levels of active TGFβ when cultured as spheroids, within just 24 hours of cell-to-cell contact. Furthermore, the results also illustrated that non-IPF pHLF spontaneously produce anti-fibrotic mediators (i.e. PGE_2) to promote fibroblast apoptosis, by four days after spheroid formation (**Figure 4.1**); however, IPF spheroids were less prone to cell death.

This thesis also illustrated some intriguing findings which to a certain extent contradict our current understanding regarding the pathogenesis of IPF:

- In 2D *in vitro* models pHLF proliferate, however in this 3D system the cells were non-proliferative which may have either resulted from the release of anti-fibrotic mediators (i.e. PGE_2) or as a result of cell-to-cell interaction leading to contact inhibition.
- Reduced expression of both COX1 and COX2 have been reported in IPF and previously published data have primarily focused on the role of COX2-mediated PGE_2 synthesis in fibroblast apoptosis (since COX2 is considered as an inducible enzyme). However, in this thesis PGE_2 synthesis was dependent primarily on the activity of COX1.
- Although several studies support the role of TGFβ as a potent cytokine involved in collagen production, in this spheroid model TGFβ does not appear to play a dominant role in the initiation of collagen production.

These findings provide new insight to the way pHLF behave following direct cell-to-cell contact when cultured as a 3-D spheroid. It is important to note however that *in vitro* assay systems involving the use of a single cell type are likely to show some phenotypical differences in comparison to the more complex *in vivo* systems which are composed of multiple cells types releasing several mediators. In fact, the addition of another cell type into the model can lead to dramatic phenotypic changes. For instance, when spheroids were co-cultured with epithelial cells (see **Section 5.2** for preliminary data) pHLF showed signs of proliferation and non-IPF spheroids were protected from apoptosis which suggests an epithelial-mesenchymal crosstalk. Thus, although the fibroblast spheroid model does provide some convincing and intriguing results it's important to appreciate that in a more complex system the results may be different.

Medium-throughput drug screening identified a number of potential therapeutic targets including EP2/4 compounds, an integrin αv inhibitor, Smo antagonists, MCP-1 inhibitor, and mTORC 1/2 inhibitors. However, since these compounds were screened at a relatively high concentration, it is feasibly that some of the effects seen are false positives as a result of toxicity. Determining toxic effects of these compounds was one of the major challenges faced with this model, as all of the commercially available cell viability assays tested, failed to show any meaningful data; TUNEL was not a sufficiently high-throughput approach for this purpose. Therefore, in order to fully appreciate fibroblast spheroids as a useful assay for drug screening in IPF the optimisation of a spheroid-compatible cell viability assay would be necessary. One potential approach could involve the use of the IncuCyte which captures live content phase contrast imaging of the spheroids. With this method any compounds that lead to a failure in the formation of cell aggregates may possibly be considered as toxic. An additional challenge faced with this 3D model was determining any effect of compounds used after spheroid formation (therapeutic dosing) – a potential reason for this could be the inability of the compounds penetrating the matrix-rich spheroids. However, further investigations are necessary to determine this.

The major novelty of this model system is that the spheroids do not require the addition of exogenous mediators (e.g. FasL to induce apoptosis, or TGFβ as a pro-fibrotic stimulus) to show the effects described, which differs from all other *in vitro* models of PF. Taken together, these findings support that this 3D system may be a more physiological model in comparison to 2D monolayer cultures, for studying the pathogenesis of IPF.

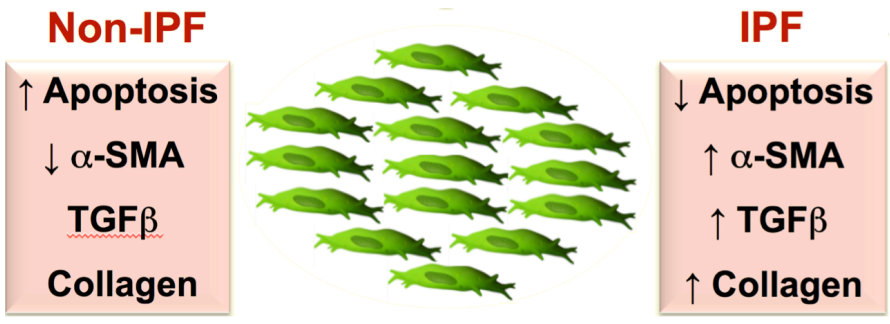

Figure 4. 1: Schematic summarising phenotypic differences between non-IPF and IPF spheroids.

IPF spheroids have a myofibroblast-like phenotype (increased expression of αSMA) and are resistant to apoptosis in comparison to non-IPF spheroids. Both non-IPF and IPF spheroids spontaneously synthesise collagen and active TGFβ with higher levels seen in IPF spheroids.

CHAPTER 5: FUTURE DIRECTIONS &

PRELIMINARY WORK

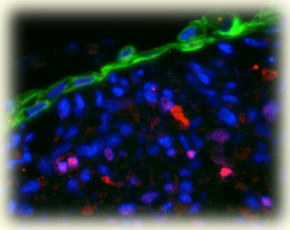

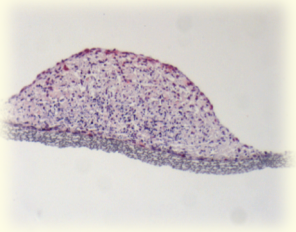

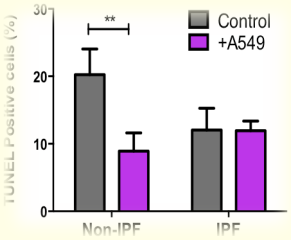

5.1. Furture work

This thesis has investigated several phenotypic characteristics of primary human lung fibroblasts (pHLF) cultured as spheroids, and has provided convincing data to support the hypothesis that fibroblast spheroids may be used as a useful assay for compound screening for drugs targeting idiopathic pulmonary fibrosis (IPF). However, further studies are necessary to address some of the questions arising from the current data (some of which have previously been mentioned in the Discussion section). These are outlined below:

5.1.1. Investigate the expression levels of collagen type I and III

The data in this thesis demonstrated that both non-IPF and IPF spheroids are capable of synthesising collagen within just 24 hours of spheroid formation, with elevated levels seen in IPF spheroids. The data also illustrated that transcriptionally there was no significant difference in *COL1A1* and *COL3A1* mRNA levels, however immunohistochemical staining illustrated a stronger immunoreactivity for both types in IPF spheroids, plus greater levels of hydroxyproline in IPF spheroids. To further clarify these data, and to confirm the post-transcription regulation of collagen production, further experiments are required to measure the levels of procollagen carboxy-terminal pro-peptides PICP and PIIICP, which are considered as surrogate markers for collagen type I and type III respectively.

5.1.2. Investigate EP receptor expression

The data in this thesis illustrated that non-IPF spheroids are prone to apoptosis, which is dependent on the activity of COX1 and EP2 receptor signalling. However, in the presence of an EP2 agonist, only a partial increase in the percentage of apoptotic cells in IPF spheroids was detected. This suggests that even in the presence of an EP2 agonist the IPF spheroids are still resistant to apoptosis. One possibility for this could be that the repertoire of EP receptor expression is altered in IPF spheroids, at the protein level. As with *COL1A1*/*COL3A1* above, qRT-PCR data showed no statistical significance between non-IPF and IPF spheroids in terms of *PTGER2* mRNA levels; difference in the expression of these receptors at the translational level (Larsson et al., 2008) should therefore be investigated. Approaches to knock down EP receptor expression (using sienna), followed by assessment of spheroid formation and apoptosis would also be of interest.

5.1.3. Determine the effect of other prostanoids on the phenotype of fibroblast spheroids

As well as PGE_2, previous studies have also demonstrated the effects of other prostanoids on fibroblast behaviour, such as the anti-fibrotic effects of prostacyclin (PGI_2) *in vitro* (Stratton et al., 2001; Kohyama et al., 2002a) and in the bleomycin-induced pulmonary fibrosis mouse model (Lovgren et al., 2006). Therefore, the effect of this prostanoid in fibroblast spheroids could also be examined to determine whether targeting PGI_2 receptor signalling has a more profound effect on IPF spheroid apoptosis and collagen synthesis.

Furthermore, although the COX expression in IPF patients is low, high levels of $PGF_2\alpha$ has been detected in plasma and bronchoalveolar lavage fluid (BALF) of IPF patients (Aihara et al., 2013). Based on the fibrosis toolbox data, antagonising the receptor for $PGF_2\alpha$ (FP receptor) resulted in an increase in collagen deposition. Since this result contrasts with published data, further experiments on this should be performed including producing full-dose response curves of spheroids treated with the compound.

5.1.4. Determine the role of αvβ5 antagonist on collagen synthesis and TGFβ activation

Spheroids are capable of synthesising their own active TGFβ, which appears to be at least partially dependent on the activity of β3 and β8 integrins. Since a compound specifically targeting αvβ5 was unavailable, and given that αvβ5 mRNA levels were greater in IPF spheroids in comparison to non-IPF, the effect of an αvβ5-specific neutralising antibody could be investigated (in terms of TGFβ activation). In addition, although antagonising β3 and β8 integrins had no effect on collagen synthesis, the fibrosis toolbox identified a pan-αv antagonist which completely abolished collagen production in non-IPF and IPF spheroids; further validation of this compound could be performed. Taken together, these experiments would shed light on the role of these integrins for TGFβ activation in a 3D microenvironment.

5.1.5. Investigate the effect of other pro-fibrotic mediators on collagen synthesis

The results further illustrated that in the presence of a potent ALK5 antagonist (i.e. SB-525334A), collagen synthesis was not attenuated - which suggests that another mediator is involved in driving the initial synthesis of collagen within these spheroids. Possibilities could include platelet-derived growth factor (PDGF), epidermal growth factor (EGF), and insulin

growth factor (IGF)-1, all of which have previously been reported to be involved in promoting myofibroblast proliferation, chemotaxis, cell adhesion, cell survival, and collagen production (Boström et al., 1996; Bonner, 2004; Hetzel et al., 2005; Hung et al., 2013b). An investigation of expression levels (mRNA and protein) and antagonism of these potentially key mediators would be extremely interesting.

5.1.6. Validate microarray data analysis

Microarray data analysis identified several differentially-expressed genes between non-IPF and IPF spheroids, particularly those involved in metabolic pathways and those involved in the response to influenza (i.e. major pro-inflammatory mediators, such as IL-1β). These genes require further validation by performing qRT-PCR and western blotting. Furthermore, studies are now beginning to realise that differences in mRNA abundance often poorly correlate with protein levels (Anderson and Seilhamer, 1997; Gygi et al., 1999; Larsson et al., 2008) – as is also suggested by the *COL1A1*/*COL3A1* data presented in this thesis. Therefore, another potential future study could involve performing microarray on ribosome-bound RNA samples, which is a method previously described as a more useful approach to understand translational regulation of genes (Larsson et al., 2008).

In addition, there are a number of publically-available microarray datasets which have transcriptionally-profiled either IPF/control lung tissue, or cells derived from IPF tissue (including fibroblasts). Alongside data from our laboratory, which is currently investigating the transcriptional profile of IPF and non-IPF fibroblasts grown in monolayer culture, it would be highly informative to investigate the potential overlap (or enrichment) of genes in the spheroid array data, with these other microarray datasets. This would also help clarify whether gene signatures present in the IPF spheroids are relevant to the actual disease process.

5.1.7. Further validation of some key compounds in the fibrosis toolbox and development of a high-throughout cell viability assay

The fibrosis toolbox identified a number of potential targets which attenuated collagen synthesis. Such compounds include ALK4/5/7 receptor antagonist, MCP1 receptor antagonist, Smoothelin (Smo) inhibitor, and mTORC 1/2 antagonist. In addition, the screening also identified targets which exaggerated collagen production including, glucocorticosteroid receptor (GR) antagonist, vitamin K antagonist, and MMP2 inhibitor. These compounds also require further validation.

Since the spheroids were treated with the compounds at a relatively high concentration (10 μM), it is feasible that some of the effects shown could be due to toxicity. Therefore it is also vital to investigate the toxicity of these compounds, if this assay is going to be useful for pre-clinical compound screening. The TUNEL assay is not a sufficiently high-throughput method for this, so another cell viability assay is necessary. Two such cell viability assays have already been assessed in this spheroid model, with minimal success. These were the Alamar Blue assay and the acid phosphatase (APH) assay. Alamar Blue is a blue dye composed of resazurin (a non-toxic cell permeable compound) which is reduced to resorufin in living cells. This reduction reaction can then be quantified by measuring the fluorescence. This assay has previously been used in cancer spheroids showing positive results (Cheng et al., 2012). However in this fibroblast spheroid system, the assay failed to work. A possible reason could be that although resazurin is cell permeable, it may not be able to penetrate through the matrix-rich environment in the spheroid. The APH assay is based on quantifying acid phosphatase activity in the cell cytosol. Viable cells are capable of hydrolysing p-nitro phenyl phosphate (pNPP) to p-nitrophenol and its absorption (at 405 nm) is directly proportional to the cell number. Previous studies have demonstrated that this assay is a useful cell viability tool for spheroids (Friedrich et al., 2007). However, once again in this 3D system the APH assay showed no effect possibly due to the same reason as the Alamar Blue assay (i.e. an inability of pNPP penetrating the spheroids). Therefore, a more reliable spheroid cell viability assay is required to investigate compound toxicity.

5.1.8. Investigate the ability of compounds to penetrate spheroids for therapeutic treatment

Current data involving the treatment of spheroids with antagonists and agonists mainly illustrated effects shown after prophylactic treatment of the compound. However, when the spheroids were treated 24 hours after spheroid formation, no such effects were evident. This raises the question of whether the compounds can even penetrate the matrix-rich spheroids. Therefore, in order to determine therapeutic targets it is vital to investigate this. One approach could involve using a fluorescent label tagged to a compound, which can be easily detected under the fluorescence microscope to determine the extent of diffusion into the spheroid, or using a dye such as Evans Blue, which readily associates with proteins and again can be easily detected/analysed under the microscope.

5.1.9. Investigate the stiffness of spheroids

Mechanical cues inherent to stiff growth substrates are just as essential as chemical compositions in affecting cellular behaviour (such as growth, differentiation, and apoptosis) (Tomasek et al., 2002; Hinz and Gabbiani, 2003a, 2003b; Georges and Janmey, 2005; Engler et al., 2006; Janmey et al., 2009). Studies have shown that the elastic modulus in most normal tissues ranges from 0.5-15 kPa, whereas in a fibrotic tissue the stiffness can be 10-100 times greater (Discher et al., 2005; Georges and Janmey, 2005; Hinz, 2010; Balestrini et al., 2012). In addition, several studies have reported that fibroblasts show distinct functional behaviours, dependant on substrate stiffness (Goffin et al., 2006; Hinz, 2006). Furthermore, reducing the substrate stiffness diminishes stress fibre tension and results in the removal of αSMA from the stress fibres (Goffin et al., 2006). Since IPF spheroids have a myofibroblast phenotype and produce high levels of collagen in comparison to non-IPF it could be hypothesised that these spheroids are stiffer in comparison to non-IPF. It would be highly informative to use an approach such as atomic force microscopy to investigate the elastic modulus (stiffness) of non-IPF and IPF spheroids.

5.1.10. The feasibility of co-culturing fibroblast spheroids with epithelial cells to determine epithelial-mesenchymal crosstalk

As mentioned previously, the main aim of my project was to mimic fibrotic foci, which are aggregates of myofibroblasts underlying hyperplastic epithelial cells. This thesis has focused solely on fibroblasts cultured as 3D spheroids. Therefore, the next aim of this project would be to investigate whether these fibroblast spheroids behave differently when co-cultured with epithelial cells, and to determine the epithelial-mesenchymal crosstalk. The next section in this thesis will illustrate some preliminary results of non-IPF fibroblast spheroids co-cultured with epithelial cells (in submerged culture and at air-liquid interface), and this should be further investigated to improve the physiological relevance of this *in vitro* assay system.

5.2. Preliminary work: Spheroid co-culture – submerged

Current data in this thesis show that non-IPF fibroblast spheroids are more apoptotic in comparison to IPF, which supports previously published studies. However, to date it has not been demonstrated whether co-culture of epithelial cells with fibroblast spheroids has any effect on the viability of the fibroblasts in this 3D system, or vice versa. Therefore, as well as determining the feasibility of co-culturing fibroblast spheroids with epithelial cells, preliminary work was performed to address this issue. The epithelial cells line used were A549 alveolar epithelial cells and primary human bronchiolar epithelial cells (HBECs). A549 cells are derived from a human lung adenocarcinoma, but are commonly used by many researchers to study ATII cell function, as well as to study apoptosis, adhesion, and cell cycle mechanisms in cancer cells (Smith, 1977).

Non-IPF (n=1) and IPF (n=1) fibroblasts were cultured for spheroid formation for 24 hours. Following this, the spheroids were then co-cultured with 5000 epithelial cells (A549 cells or HBECs, in separate experiments), added directly to the well containing a spheroid. After an additional three days of incubation, the spheroids were fixed with 4 % PFA for 20 minutes, processed, and then embedded into paraffin wax. **Figures 5.1**, **5.2, 5.3,** and **5.4** demonstrate that in the presence of A549s or HBECs, a small population of fibroblasts within the spheroids (both non-IPF and IPF) were positive for the proliferation marker Ki-67. In addition, **Figure 5.5** illustrates that upon co-culturing fibroblast spheroids with epithelial cells (A549s or HBECs) in submerged culture, non-IPF fibroblast survival is supported – bringing the rate of apoptosis down to the level seen in fibrotic spheroids. Epithelial cells did not however further decrease the percentage of TUNEL positive cells within IPF spheroids. This supports the notion that there may be dysregulated epithelial-mesenchymal crosstalk in IPF patients, as fibrotic fibroblasts seem to promote their own survival and therefore do not require additional factors from the epithelium, in contrast to normal spheroids. However, fibroblasts within both non-IPF and IPF spheroids did show signs of proliferation in the presence of epithelial cells. Such results contrast with previous studies, which show the role of epithelial cells in fibroblast apoptosis in 2D culture (Lama et al., 2002).

Unlike most cells within the human body, AECs express both COX1 and COX2 constitutively (Lama et al., 2002; Bozyk and Moore, 2011). In addition, previous studies have demonstrated that monolayer co-culture systems involving both AECs and control lung fibroblasts result in

fibroblast cell death, a decrease in cell proliferation, and a decrease in collagen production (Lama et al., 2002). This occurs downstream of PGE_2 receptor signalling (i.e. $G\alpha_i$-coupled EP2 receptors) (Kolodsick et al., 2003; Huang et al., 2007, 2008b). However, this has only been demonstrated in 2D cultures and as mentioned above, the results in this thesis provide contrasting observations of increased fibroblast proliferation and reduced apoptosis in the presence of epithelial cells.

A possible explanation is that if the epithelial cells increase PGE_2 production, then PGE_2 could signal via the activation of other PGE_2 receptors (i.e. EP1 and EP3), both of which are expressed by fibroblasts, in addition to EP2. EP1 and EP3 can play a key role in fibroblast cell survival and proliferation in patients with acute lung injury. Furthermore, it has been suggested that the activation of these receptors occurs when the PGE_2 concentration falls within a particular range (10^{-9} to 10^{-7} M) (Bozyk and Moore, 2011). Thus, it could be hypothesised that in 3D cultures, epithelial cells inhibit apoptosis and promote proliferation via increased PGE_2 production and hence the activation of additional PGE_2 receptors. However, further work is required to investigate this hypothesis and understand the crosstalk between the two cells in greater detail.

Another possible reason why fibroblasts in 3D structures respond differently in comparison to 2D monolayer cultures may be due to the difference in matrix stiffness. Culturing cells on tissue culture treated plastic has limitations for understanding fibroblast cell biology, as the stiffness of the plastic is approximately 20,000 times greater in comparison to that experienced by cells within a normal lung (~2 kPa), 1000 times greater than fibrotic lung (~40 kPa), and 8 times greater than bone (5000 kPa). Thus, such differences in results may have resulted due to the difference in culture systems. The spheroid model does recapitulate the proliferation feature of fibroblasts in fibrotic foci. Many studies including recent unpublished data by Dr. Paul Mercer (UCL) have illustrated that in a fibrotic focus a small population of mesenchymal cells are proliferative (positive for Ki-67 by immunohistochemistry), lending support that this 3D spheroid model may be a useful model that mimics a fibrotic focus.

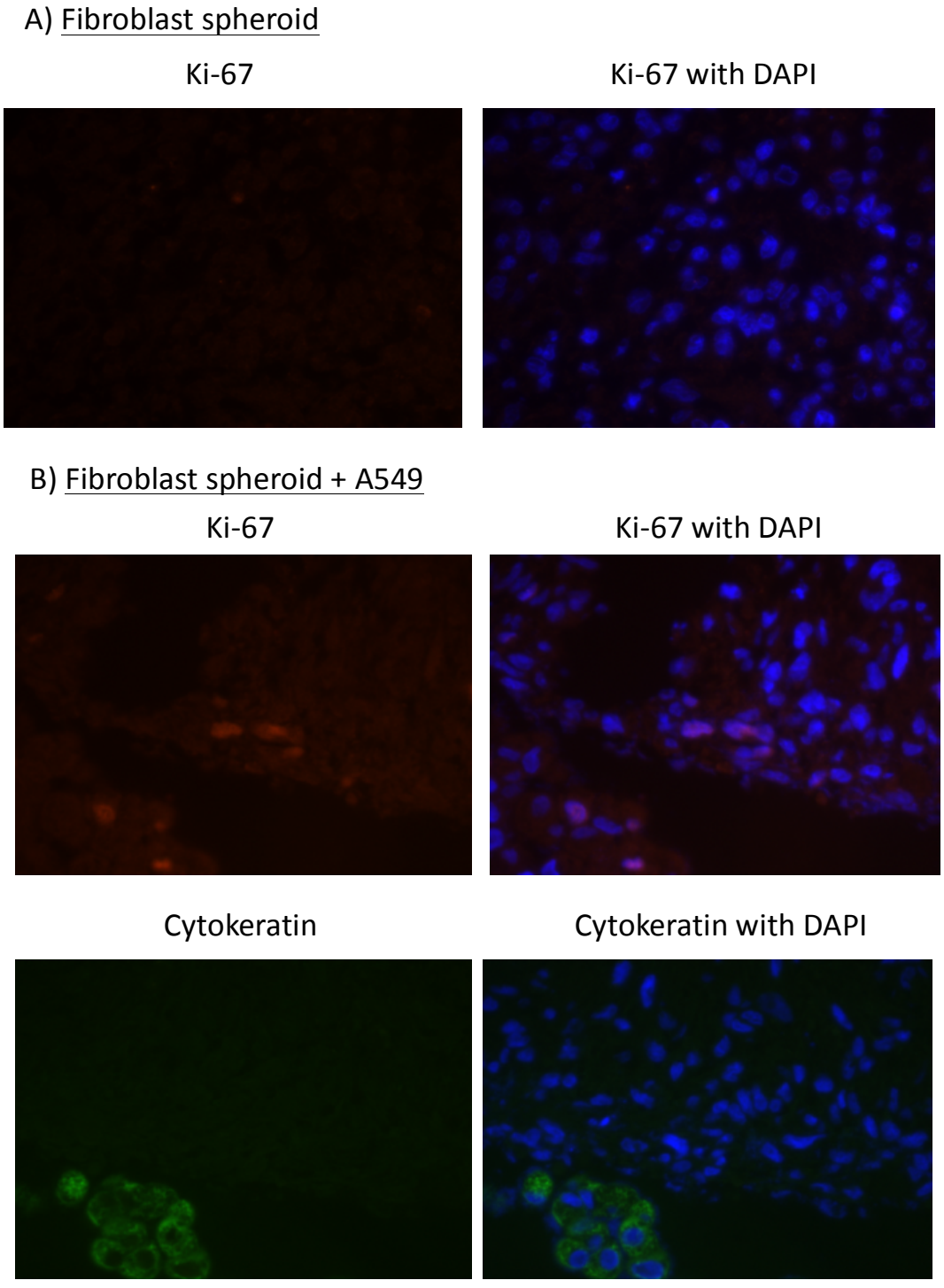

Figure 5. 1. Proliferation of non-IPF fibroblasts within the 3 dimensional spheroid structures with and without A549.

(A) Immunofluorescence staining for Ki-67 (orange) with DAPI (blue) as the nuclear counterstain on paraffin sections of non-IPF fibroblast spheroids (four days post spheroid formation) did not highlight any Ki-67+ cells in the spheroid culture alone. Magnification x200. (B) Spheroids co-cultured with A549s (5,000 epithelial cells per spheroid) had a positive signal for Ki-67 (orange staining) within both the epithelial cytokeratin+ (green staining) compartment (identified on serial section), as well as in fibroblasts within the spheroid. Magnification x200.

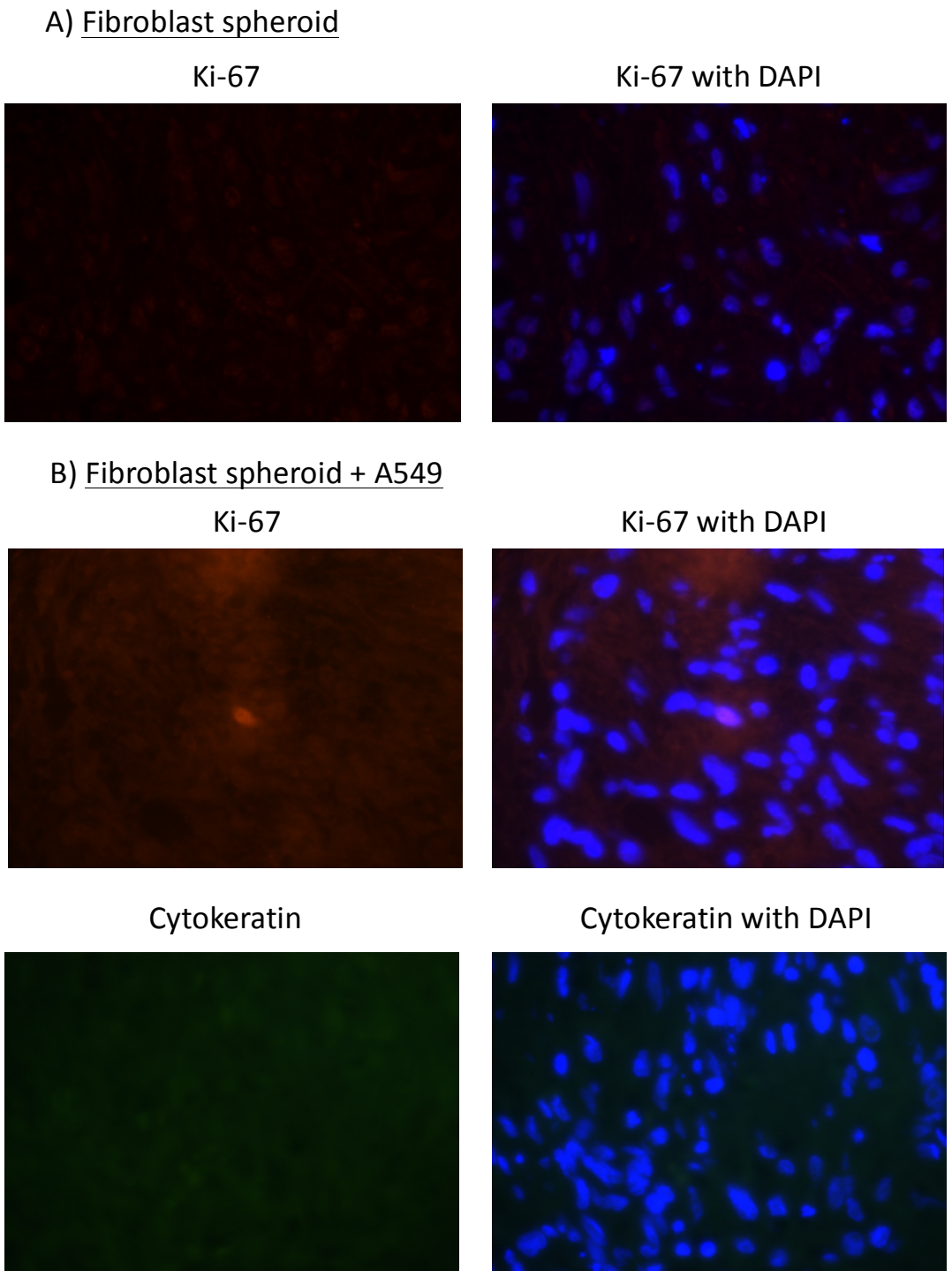

Figure 5. 2. Proliferation of IPF fibroblasts within the 3 dimensional spheroid structures with and without A549.

(A) Immunofluorescence staining for Ki-67 (orange) with DAPI (blue) as the nuclear counterstain on paraffin sections of IPF fibroblast spheroids (four days post spheroid formation) did not highlight any Ki-67+ cells in the spheroid culture alone. Magnification x200. (B) Spheroids co-cultured with A549s (5,000 epithelial cells per spheroid) had a positive signal for Ki-67 (orange staining) within both the epithelial cytokeratin+ (green staining) compartment (identified on serial section), as well as in fibroblasts within the spheroid. Magnification x200.

A) Fibroblast spheroid

Ki-67

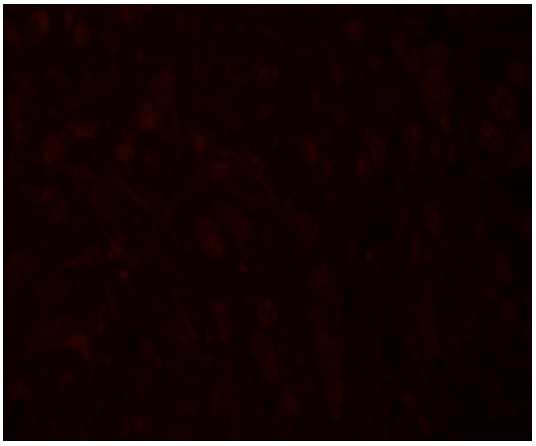

Ki-67 with DAPI

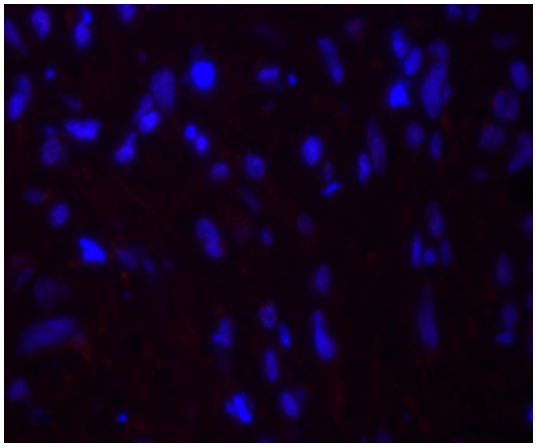

B) Fibroblast spheroid + A549

Ki-67

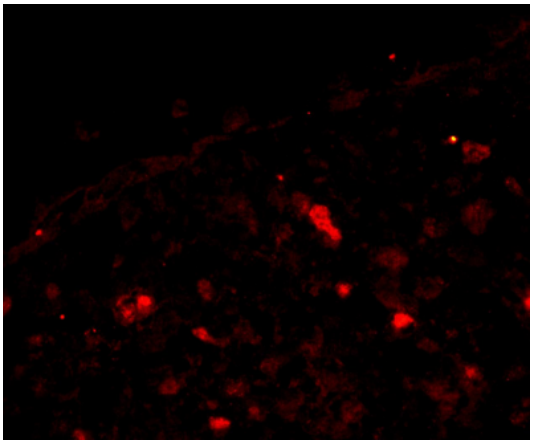

Cytokeratin

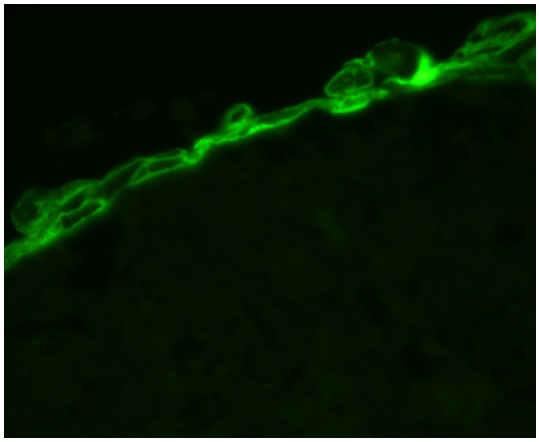

Ki-67 + Cytokeratin + DAPI

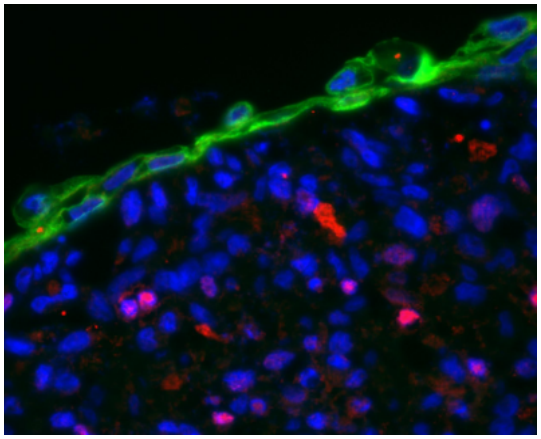

Figure 5. 3. Proliferation of non-IPF fibroblasts within the 3 dimensional spheroid structures with and without HBECs.

(A) Immunofluorescence staining for Ki-67 (orange) with DAPI (blue) as the nuclear counterstain on paraffin sections of non-IPF fibroblast spheroids (four days post spheroid formation) did not highlight any Ki-67+ cells in the spheroid culture alone. Magnification x200. (B) Spheroids co-cultured with HBECs (5,000 epithelial cells per spheroid) had a positive signal for Ki-67 (orange staining) within both the epithelial cytokeratin+ (green staining) compartment (identified on serial section), as well as in fibroblasts within the spheroid. Magnification x200.

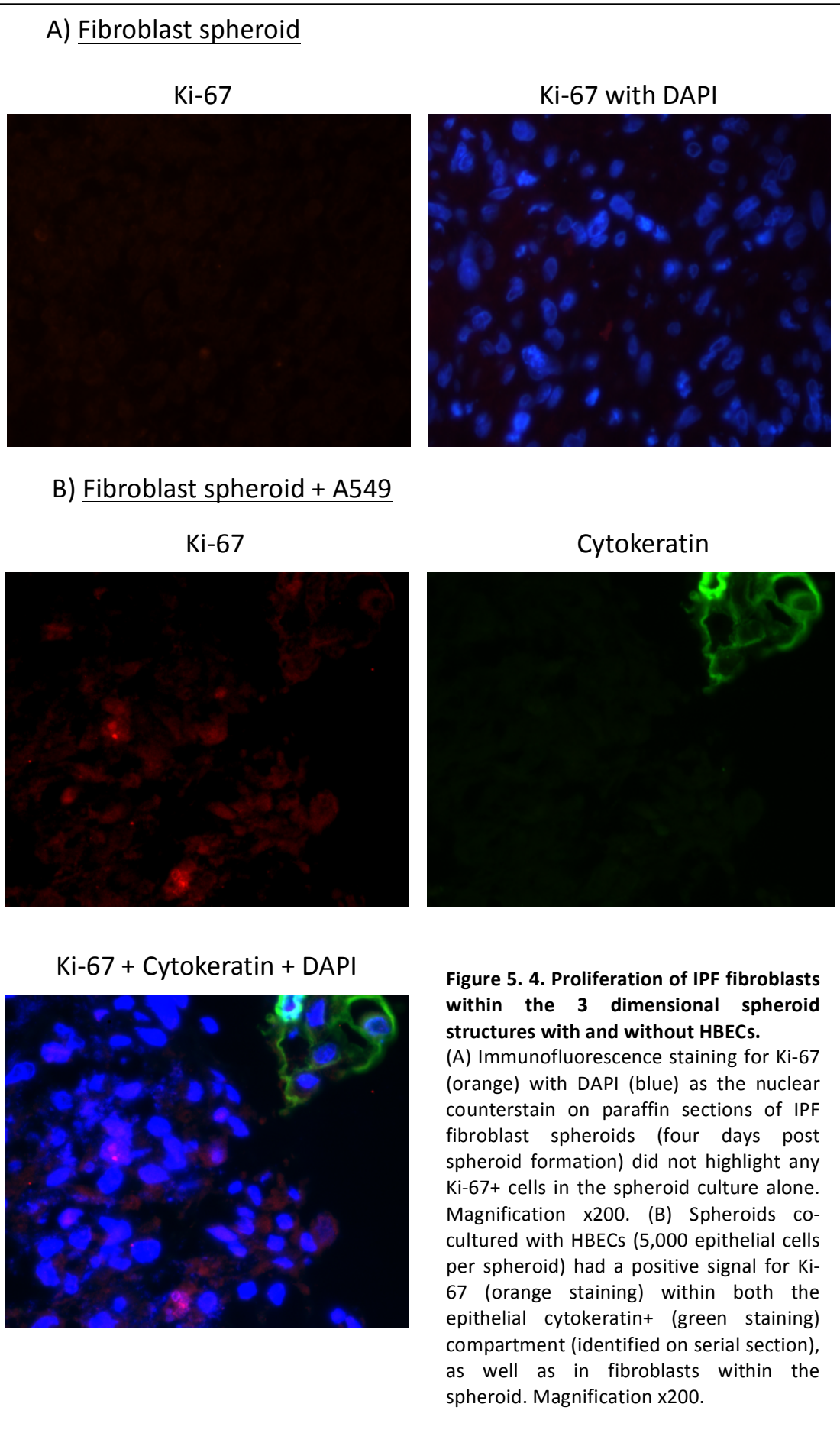

Figure 5. 4. Proliferation of IPF fibroblasts within the 3 dimensional spheroid structures with and without HBECs.
(A) Immunofluorescence staining for Ki-67 (orange) with DAPI (blue) as the nuclear counterstain on paraffin sections of IPF fibroblast spheroids (four days post spheroid formation) did not highlight any Ki-67+ cells in the spheroid culture alone. Magnification x200. (B) Spheroids co-cultured with HBECs (5,000 epithelial cells per spheroid) had a positive signal for Ki-67 (orange staining) within both the epithelial cytokeratin+ (green staining) compartment (identified on serial section), as well as in fibroblasts within the spheroid. Magnification x200.

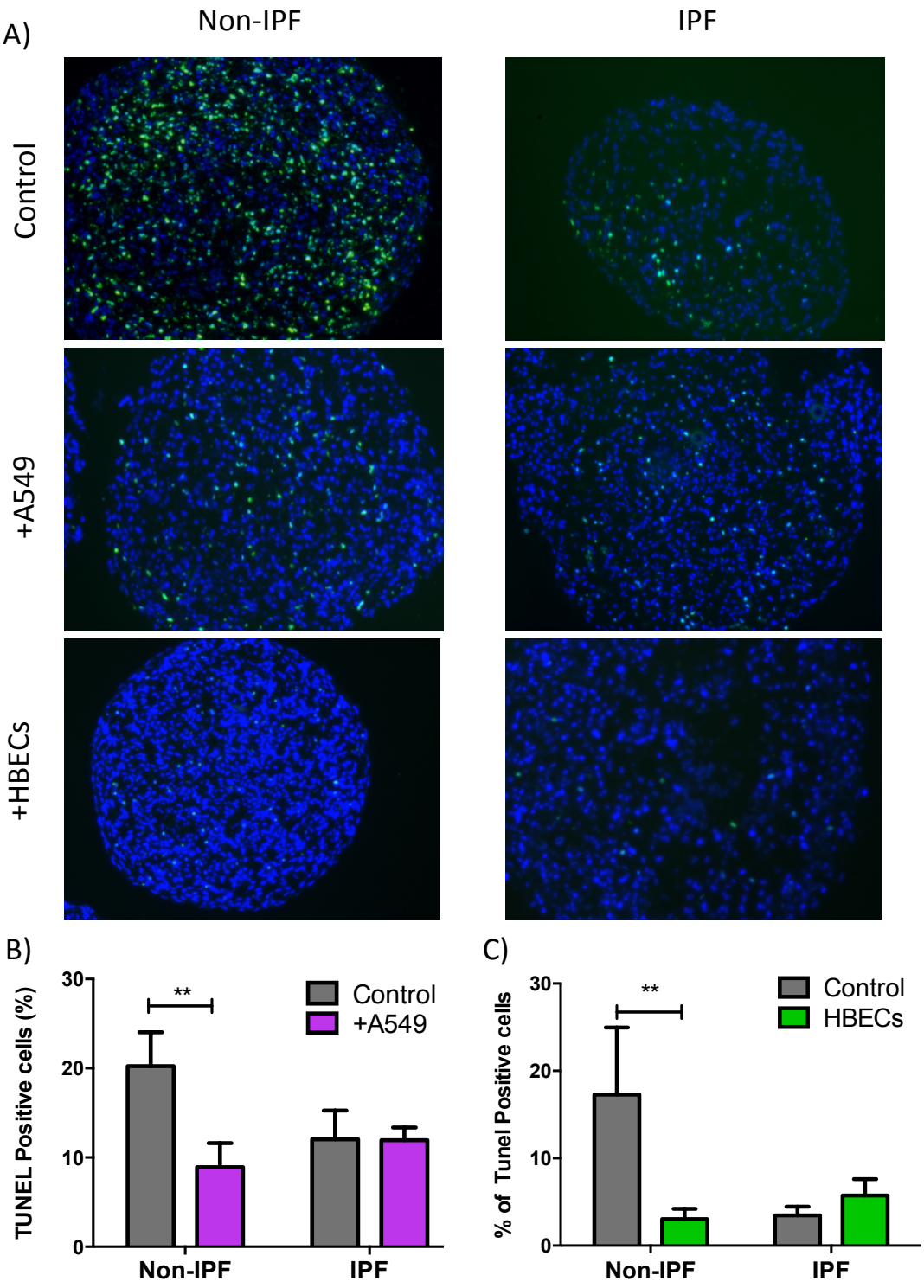

Figure 5. 5. Percentage of TUNEL positive cells in non-IPF and IPF spheroids with and without epithelial cell co-culture.

(A) TUNEL staining of paraffin embedded spheroid sections four days post spheroid formation. Green indicates cell death; blue is DAPI. Magnification x100. Percentage of TUNEL positive cells were quantified in spheroids co-cultured with (B) A549 and (C) HBECs. ** $p<0.01$

5.3. Spheroid co-culture: air-liquid interface

So far I have only demonstrated the effect of epithelial cells in submerged culture. To better understand epithelial-mesenchymal crosstalk, it would be beneficial to grow epithelial cells in an environment which more closely resembles the normal physiological situation within the human lung, namely by developing a model in which the epithelial cells are grown at air-liquid interface (ALI).

Many researchers use transwells to grow monolayer epithelial cells at ALI (Lee et al., 2005, 2008). Thus, in this pilot project a similar concept was applied, to establish a model in which the epithelial cells (at air-liquid interface) coat the fibroblast spheroids. Spheroids were generated as previously described, and following 24 hours incubation they were transferred into transwell inserts containing different types of membranes (**Table 5.1**; 20 spheroids per 12 well insert and 10 spheroids per 24 well insert). Spheroids were then incubated for another 24 hours (10 % CO_2, 37 ^{o}C) before the addition of epithelial cells (A549s), 5x10^{5} per 24-well and 1x10^{6} cells per 12-well insert. The aim then was to allow the A549s to reach confluence and form tight junctions before removing the medium from the upper insert to establish ALI (**Figure 5.6**).

Table 5.1 Types of transwells

Membrane type	Transwell size	Pore size (um)	Supplier
Collagen coated PTFE (equimolar mixture types I and III collagen)	12 well	0.4	VWR
Matrigel coated	12 well	0.4	BD Bioscience
Polyester	12 well	0.4	VWR

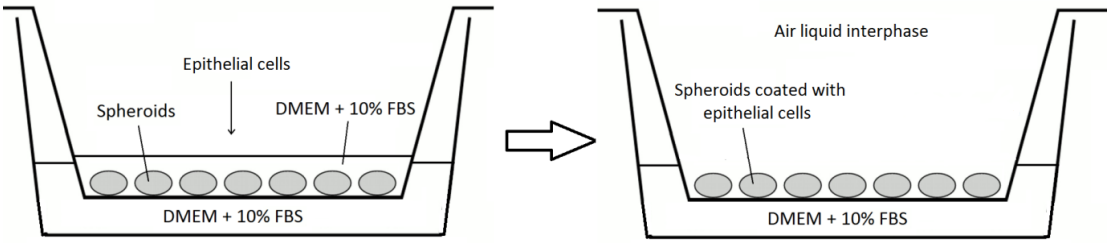

Figure 5. 6. Schematic of 3D spheroid model at ALI.

Spheroids were formed by seeding 100,000 fibroblasts per well in a 96-well plate pre-coated with agarose, and then incubating for 24 hours. The spheroids were then transferred into the top insert of a transwell. After 24 hours, the spheroids were co-cultured with epithelial cells. Once confluence was reached, the medium from the top insert was removed to establish air-liquid interface.

Figure 5.7 illustrates the appearance of non-IPF spheroids cultured on the following membranes: polyester, collagen-coated, and matrigel-coated. Most of the spheroids cultured on polyester alone did not adhere firmly, thus it was difficult to establish a coating of co-cultured epithelial cells (**Figure 5.7A**). Spheroids did adhere to the matrigel coated membrane, however within 24 hours of incubation the spheroids degraded the surrounding matrigel (**Figure 5.7B**), creating a halo. This may have resulted from significant matrix metalloproteinase production, in particular MMP2 (which plays a key role in degrading collagen; see **Appendix 4**).

Figure 5.7C shows an H&E stained section of non-IPF spheroids co-cultured with A549s on collagen-coated transwells. As shown in the figure, the spheroids firmly adhered to the collagen within 24 hours, in comparison to polyester or matrigel-coated membranes. After 24 hours, $5x10^5$ A549 cells were cultured on top, which required a switch from their routine culture in F12K/10 % FBS at 37 ^oC with 5 % CO_2 into DMEM/10 % FBS at 37 ^oC with 10 % CO_2. The cells were incubated for 6 days to reach confluence; however the morphology of the epithelial cells changed (**Figure 5.8**) and they also failed to reach full confluence (remaining ~50 % confluent), so ALI was not established. It is important to note that $5x10^5$ A549s would normally be sufficient for an epithelial monolayer ALI culture. Growth of the A549 cells may have been impaired by culture in DMEM/10 % FBS at 37 ^oC with 10 % CO_2, and this is an issue that would require further optimisation. In addition, continuing this work using primary epithelial cells (i.e. HBECs and primary human type II AECs) in co-culture with both non-IPF and IPF spheroids would be highly informative.

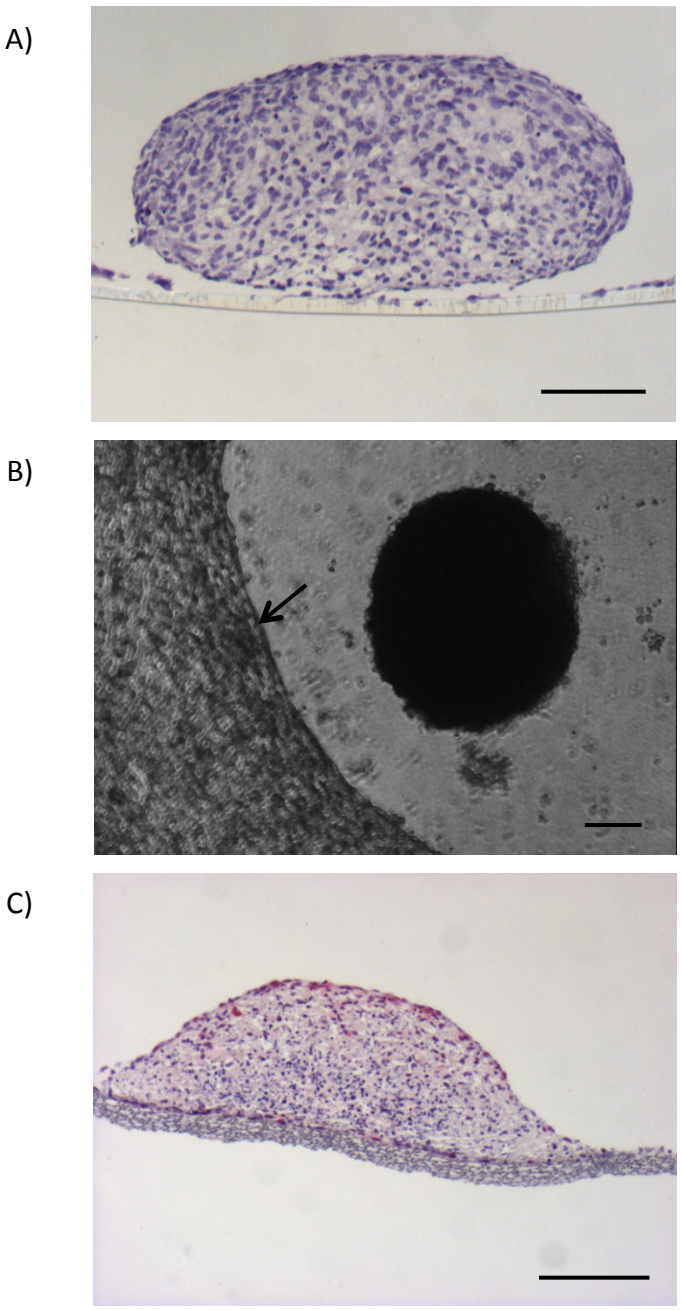

Figure 5. 7. Fibroblast spheroid and epithelial cell co-culture system in transwells.

Non-IPF spheroids were formed and transferred into transwells (polyester, matrigel, or collagen coated). A549 cells were cultured on top of the spheroids. (A) H&E staining of spheroids + A549s co-cultured on polyester transwells. (B) Microscopic view of spheroid only, cultured on matrigel-coated transwells. Arrow represents the margin of matrigel degradation surrounding a spheroid. (C) H&E stained sections of spheroids + A549s co-cultured on collagen-coated transwell. Scale bar, 100 µm.

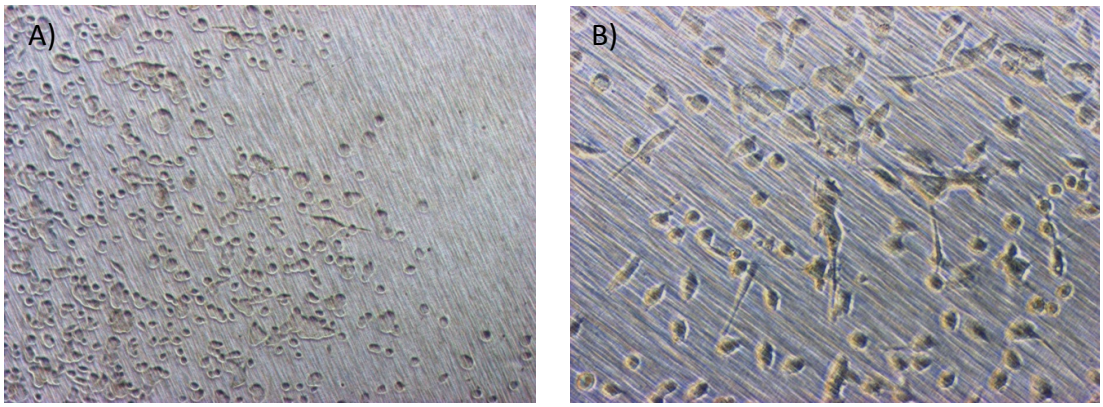

Figure 5. 8. Morphology of A549s on collagen coated membrane.

A) A549 cells cultured without spheroids (control). B) A549 cells co-cultured with non-IPF spheroids. A549 cells were incubated for six days in DMEM + 10 % FBS at 37 ^{o}C with 10 % CO_2. Cells appear more elongated. Magnification x10

5.4. Future directions for the spheroid co-culture model

In these preliminary studies it was demonstrated that epithelial cells appear able to promote fibroblast cell survival and proliferation within the spheroids. However, the results were obtained using cells from only one patient. Therefore, the future work would involve reproducing and validating these results using more non-IPF and IPF fibroblasts from multiple donors in co-culture with, wherever possible, epithelial cells derived from the same patient (feasible for HBECs, but not primary ATII cells).

Furthermore, previous studies involving 2D monolayers have illustrated that AECs from IPF patients are susceptible to Fas-ligand induced apoptosis (Maher et al., 2010). However, in the preliminary work above, the effect fibroblasts have on the survival of AECs was not interrogated; thus the next aim would be to determine whether fibroblast spheroids promote the apoptosis or survival of AECs. In addition, it has not been demonstrated whether AECs promote fibroblast spheroid survival by direct cell-to-cell contact or via a soluble mediator. Therefore, this will also need further investigation.

A number of technical challenges remain regarding the co-culture of spheroids and epithelial cells, particularly at air-liquid interface. Further work would optimise the timing of epithelial

cell addition and culture conditions, and subsequent transfer to ALI, as well as post-processing for analysis (including fixation protocols, sectioning and suchlike).

Microarray data analysis could also be performed to determine transcriptional changes of the fibroblast spheroids when co-cultured with epithelial cells, which could potentially provide vital information in understanding key pathways involved in epithelial-mesenchymal crosstalk, also leading to the identification of potential therapeutic targets.

REFERENCE

References

Botelho, A.L., Mitta, C.M., Lira, J.C., Ramirez, R., Chaves, M., Barreiro, L., et al. (2012). Role of Sonic Hedgehog in idiopathic pulmonary fibrosis. Am J Physiol Lung Cell Mol Physiol 303: 1078–90.

Bonnans, C., Sharma, R.A., Bernard, M., and Speed, T.P. (2008). A comparison of normalization methods for high density oligonucleotide array data based on variance and bias. Bioinformatics 24: 180–186.

Boyle, J.E., Lindroos, P.M., Rice, A.B., Zhang, L., Zaldin, D.C., and Berner, J.C. (1999). Prostaglandin-E2 counteracts interleukin-1beta-stimulated upregulation of platelet-derived growth factor alpha-receptor on rat pulmonary myofibroblasts. Am. J. Respir. Cell Mol. Biol. 20: 459–469.

Boyle, P.E., and Moore, B.B. (2011). Prostaglandin E2 and the pathogenesis of pulmonary fibrosis. Am J Respir Cell Mol Biol. 45: 445–452.

Brock, T.G. (2014). EP2 & EP4 - Sibling PGE2 Receptors.

Brock, T.G., McNish, R.W., Maruyama, P., Coffey, M.J., and Peters-Golden, M. (2003). Prolonged leukotriene synthesis in cultured murine macrophages. Mediation by nitric oxide and prostaglandins. Prostaglandins Other Lipid Mediat. 71: 131–145.

Brown, P.D., Wakefield, L.M., Levinson, A.D., and Sporn, M.B. (1990). Physicochemical activation of recombinant latent transforming growth factor-beta's 1, 2, and 3. Growth Factors 3: 35–43.

Burt, R.K., Yamazaki, M., and Morabito, M. (1996). Ultrastructure of size-regulated heterospheroids composed of human keratinocytes and fibroblasts. J Dermatol Sci. 12: 193–199.

Caniggia, I., Han, R., Liu, J., Wang, J., Tanswell, A.K., and Post, M. (1995). Differential expression of collagen-binding receptors in fetal rat lung cells. Am J Physiol 268: 1136–1143.

Carafoli, F., Bihan, D., Stathopoulos, S., Konstantz, A.D., Kostazkvi, M., Farndale, R.W., et al. (2009). Crystallographic insight into collagen recognition by discoidin domain receptor 2. Structure. 17: 1573–1581.

Chakraborty, S., Chopra, P., Antti, S. V, Doolidar, S.G., and Ray, A. (2014). Emerging therapeutic interventions for idiopathic pulmonary fibrosis. Expert Opin Investig Drugs 833–910.

Chambers, R.C. (2008). Procoagulant signalling mechanisms in lung inflammation and fibrosis: novel opportunities for pharmacological intervention? Br J Pharmacol. 153 Suppl: S367–S378.

Chambers, R.C., Leoni, P., Kaminski, N., Laurent, G.J., and Heller, R.A. (2003). Global expression profiling of fibroblast responses to transforming growth factor-beta1 reveals the induction of inhibitor of differentiation-1 and provides evidence of smooth muscle cell phenotypic switching. Am J Pathol 162: 533–546.

Chapman, H.A., Allen, C.L., and Stone, O.L. (1986). Abnormalities in pathways of alveolar fibrin turnover among patients with interstitial lung disease. Am. Rev. Respir. Dis. 132: 437–443.

References

Charlton, S., Bassols, A., Stanley, K., Ohta, M., Greenberger, J., and Massague, J. (1988). Heterodimeric transforming growth factor beta. Biological properties and interaction with three types of cell surface receptors. J Biol Chem 263: 10783–9.

Chen, C.Z., and Raghunath, M. (2009). Focus on collagen: in vitro systems to study fibrogenesis and antifibrosis state of the art. Fibrogenesis Tissue Repair 2: 7–.

Chen, Y., Wang, X., Wang, D., Tian, L., Lu, L., Tao, S., et al. (2009). A TGF-b synthetic peptide inhibits bleomycin-induced lung fibrosis in mice. Exp. Toxicol. Pathol. 61: 59–65.

Chilosi, M., Poletti, V., Murer, B., Lestani, M., Cancellieri, A., Montagna, L., et al. (2002). Abnormal re-epithelialization and lung remodeling in idiopathic pulmonary fibrosis: the role of deltaN-p63. Lab. Invest. 82: 1335–1345.

Cho, M., Smith, D., Brenton, M., Pensak, S., and Kopp, J. (2007). Pirfenidone slows renal function decline in patients with focal segmental glomerulosclerosis. Clin J Am Soc Nephrol 2: 906–913.

Choi, K., Lee, K., Ryu, S.-W., Im, M., Kook, K.H., and Choi, C. (2012). Pirfenidone inhibits transforming growth factor-β1-induced fibrogenesis by blocking nuclear translocation of Smads in human retinal pigment epithelial cell line ARPE-19. Mol. Vis. 18: 1810–19.

Chung, M.J., Liu, T., Ullenbruch, M., and Phan, S.H. (2007). Antiapoptotic effect of found in inflammatory zone (Fizz)1 on mouse lung fibroblasts. J. Pathol. 212: 180–187.

Churchill, L., Chilton, F.H., Rossi, J.M., Bascom, R., Hubbard, W.C., and Proud, D. (1989). Cyclooxygenase metabolism of endogenous arachidonic acid by cultured human tracheal epithelial cells. Am. Rev. Respir. Dis. 140: 449–459.

Clark, R.A.F., McCoy, G.A., Folkvord, J.M., and McPherson, J.M. (1997). TGF-?1 stimulates cultured human fibroblasts to proliferate and produce tissue-like fibroplasia: A fibronectin matrix-dependent event. J. Cell. Physiol. 170: 69–80.

Collard, H.R. (2010). The age of idiopathic pulmonary fibrosis. Am J Respir Crit Care Med. 181: 771–772.

Cool, C.D., Grotheup, S.D., Rei, P.R., Hansen, P.M., Stewart, J.S., and Brown, K.K. (2006). Fibroblast foci are not discrete sites of lung injury or repair: the fibroblast reticulum. Am J Respir Crit Care Med. 174: 654–658.

Corbel, M., Berthiaume, L., and Lussier, G. (1977). Formation of spheroids by cultured human thyroid cells). Rev Can Biol. 36: 291–299.

Corbel, M., Lanchou, J., Germain, N., Malfettani, Y., Boichot, E., and Lagente, V. (2001). Modulation of airway remodeling-associated mediators by the antifibrotic compound, pirfenidone, and the matrix metalloproteinase inhibitor, batimastat, during acute lung injury in mice. Eur. J. Pharmacol. 426: 113–121.

Corrin, B., Dewar, A., Rodriguez-Roisin, R., and Turner-Warwick, M. (1985). Fine structural changes in cryptogenic fibrosing alveolitis and asbestosis. J. Pathol. 147: 107–119.

References

Cottin, V., Cinetani, B., Valsani, D., Wallaert, B., Cadranel, J., Dalphin, J.-C., et al. (2014). Diagnosis and management of idiopathic pulmonary fibrosis: French practical guidelines. Eur. Respir. Rev. 23: 193–214.

Coward, W.R., Saini, G., and Jenkins, G. (2010). The pathogenesis of idiopathic pulmonary fibrosis. Ther Adv Respir Dis. 4: 367–388.

Coward, W.R., Watts, K., Feghali-Bostwick, C.A., Knox, A., and Pang, L. (2009). Defective Histone Acetylation Is Responsible for the Diminished Expression of Cyclooxygenase 2 in Idiopathic Pulmonary Fibrosis. Mol. Cell. Biol. 29: 4325–4339.

Crawford, S.E., Stellmach, V., Murphy-Ullrich, J.E., Ribeiro, S.M.F., Lawler, J., Hynes, R.O., et al. (1998). Thrombospondin-1 is a major activator of TGF-β1 in vivo. Cell 93: 1159–1170.

Cruse, G., Duffy, S.M., Brightling, C.E., and Bradding, P. (2006). Functional KCa3.1 K+ channels are required for human lung mast cell migration. Thorax 61: 880–885.

Culo, F., Yuhas, J.M., and Sedman, A.J. (1980). Multicellular tumour spheroids: a model for combined in vivo/in vitro assay of tumour immunity. Br J Cancer 41: 500–512.

Dalma-Weiszhausz, D.D., Warrington, J., Tanimoto, E.Y., and Miyada, C.G. (2006). [1] The Affymetrix GeneChip® Platform: An Overview. Methods Enzymol. 410: 3–28.

Danner, R.C. a, Wood, J.W., and Trickett, D.B. (2011). Metalloproteinases in idiopathic pulmonary fibrosis. Eur. Respir. J. 38: 1461–7.

Datta, A., Scotton, C.J., and Chambers, R.C. (2011). Novel therapeutic approaches for pulmonary fibrosis. Br J Pharmacol. 163: 141–172.

Degryse, A.L., and Lawson, W.E. (2011). Progress toward improving animal models for idiopathic pulmonary fibrosis. Am J Med Sci. 341: 444–449.

Degryse, A.L., Tanjore, H., Xu, X.C., Polosukhin, V. V, Jones, B.R., McMahon, F.B., et al. (2010). Repetitive intratracheal bleomycin models several features of idiopathic pulmonary fibrosis. Am. J. Physiol. Lung Cell. Mol. Physiol. 299: 1442–1452.

Dery, O., Corvera, C.U., Steinhoff, M., and Bunnett, N.W. (1998). Proteinase-activated receptors: novel mechanisms of signaling by serine proteases. Am J Physiol 274: C1429–C1452.

Desmouliere, A., Chaponnier, C., and Gabbiani, G. (2005). Tissue repair, contraction, and the myofibroblast. Wound Repair Regen. 13: 7–12.

Desmouliere, A., Redard, M., Darby, I., and Gabbiani, G. (1995). Apoptosis mediates the decrease in cellularity during the transition between granulation tissue and scar. Am J Pathol. 146: 56–66.

Discher, D.E., Janmey, P., and Wang, Y.-L. (2005). Tissue cells feel and respond to the stiffness of their substrate. Science 310: 1139–1143.

Abe, M., Harpel, J.G., Metz, C.N., Nunes, I., Loskutoff, D.J., and Rifkin, D.B. (1994). An assay for transforming growth factor-beta using cells transfected with a plasminogen activator inhibitor-1 promoter-luciferase construct. Anal.Biochem. *216*: 276–284.

Abercrombie, M. (1979). Contact inhibition and malignancy. Nature *281*: 259–262.

Abrahamson, M., Alvarez-Fernandez, M., and Nathanson, C.M. (2003). Cystatins. Biochem. Soc. Symp. *70*: 179–199.

Adds, J., Larkcom, E., and Miller, R. (2001). The pulmonary system. In Respiratory and Coordination, (London: Nelson Thornes Ltd), p 138.

Ahluwalia, N., Shea, B.S., and Tager, A.M. (2014). New Therapeutic Targets in Idiopathic Pulmonary Fibrosis: Aiming to Rein in Runaway Wound Healing Responses. Am. J. Respir. Crit. Care Med.

Aihara, K., Handa, T., Oga, T., Watanabe, K., Tanizawa, K., Ikezoe, K., et al. (2013). Clinical Relevance of Plasma Prostaglandin F2 alpha Metabolite Concentrations in Patients with Idiopathic Pulmonary Fibrosis. PLoS One *8*:

Akers, I.A., Parsons, M., Hill, M.R., Hollenberg, M.D., Sanjar, S., Laurent, G.J., et al. (2000). Mast cell tryptase stimulates human lung fibroblast proliferation via protease-activated receptor-2. Am.J.Physiol Lung Cell Mol.Physiol *278*: L193–L201.

Allanach, K., Mengel, M., Einecke, G., Sis, B., Hidalgo, L.G., Mueller, T., et al. (2008). Comparing microarray versus RT-PCR assessment of renal allograft biopsies: Similar performance despite different dynamic ranges. Am. J. Transplant. *8*: 1006–1015.

Allen JT, S.M. (2002). Growth factors in idiopathic pulmonary fibrosis: relative roles. Respir Res *3*: 13.

Almassian, B., Trackman, P.C., Iguchi, H., Boak, A., Calvaresi, D., and Kagan, H.M. (1991). Induction of lung lysyl oxidase activity and lysyl oxidase protein by exposure of rats to cadmium chloride: properties of the induced enzyme. Connect. Tissue Res. *25*: 197–208.

Anderson, L., and Seilhamer, J. (1997). A comparison of selected mRNA and protein abundances in human liver. In Electrophoresis, pp 533–537.

Andersson-Sjoland, A., Alba, C.G. de, Nihlberg, K., Becerril, C., Ramirez, R., Pardo, A., et al. (2008). Fibrocytes are a potential source of lung fibroblasts in idiopathic pulmonary fibrosis. Int.J.Biochem.Cell Biol. *40*: 2129–2140.

Aoki, F., Kurabayashi, M., Hasegawa, Y., and Kojima, I. (2005). Attenuation of bleomycin-induced pulmonary fibrosis by follistatin. Am. J. Respir. Crit. Care Med. *172*: 713–720.

Appleby, S.B., Ristimäki, A., Neilson, K., Narko, K., and Hla, T. (1994). Structure of the human cyclo-oxygenase-2 gene. Biochem. J. *302 (Pt 3*: 723–727.

Armanios, M.Y., Chen, J.J., Cogan, J.D., Alder, J.K., Ingersoll, R.G., Markin, C., et al. (2007). Telomerase mutations in families with idiopathic pulmonary fibrosis. N.Engl.J.Med. *356*: 1317–1326.

Armstrong, L.C., and Bornstein, P. (2003). Thrombospondins 1 and 2 function as inhibitors of angiogenesis. In Matrix Biology, pp 63–71.

Asano, Y., Ihn, H., Yamane, K., Jinnin, M., Mimura, Y., and Tamaki, K. (2005a). Increased expression of integrin alpha(v)beta3 contributes to the establishment of autocrine TGF-beta signaling in scleroderma fibroblasts. J. Immunol. *175*: 7708–7718.

Asano, Y., Ihn, H., Yamane, K., Jinnin, M., Mimura, Y., and Tamaki, K. (2005b). Involvement of alphavbeta5 integrin-mediated activation of latent transforming growth factor beta1 in autocrine transforming growth factor beta signaling in systemic sclerosis fibroblasts. Arthritis Rheum. *52*: 2897–2905.

ATS, and ERS (2002). American Thoracic Society/European Respiratory Society International Multidisciplinary Consensus Classification of the Idiopathic Interstitial Pneumonias. This joint statement of the American Thoracic Society (ATS), and the European Respiratory Society (E. Am.J.Respir.Crit Care Med. *165*: 277–304.

Baker, B.M., and Chen, C.S. (2012). Deconstructing the third dimension - how 3D culture microenvironments alter cellular cues. J. Cell Sci. *125*: 3015–3024.

Balestrini, J.L., Chaudhry, S., Sarrazy, V., Koehler, A., and Hinz, B. (2012). The mechanical memory of lung myofibroblasts. Integr. Biol. *4*: 410.

Barbas-Filho, J. V, Ferreira, M.A., Sesso, A., Kairalla, R.A., Carvalho, C.R., and Capelozzi, V.L. (2001). Evidence of type II pneumocyte apoptosis in the pathogenesis of idiopathic pulmonary fibrosis (IFP)/usual interstitial pneumonia (UIP). J. Clin. Pathol. *54*: 132–138.

Bargagli, E., Olivieri, C., Nikiforakis, N., Cintorino, M., Magi, B., Perari, M.G., et al. (2009). Analysis of macrophage migration inhibitory factor (MIF) in patients with idiopathic pulmonary fibrosis. Respir. Physiol. Neurobiol. *167*: 261–267.

Barry-Hamilton, V., Spangler, R., Marshall, D., McCauley, S., Rodriguez, H.M., Oyasu, M., et al. (2010). Allosteric inhibition of lysyl oxidase-like-2 impedes the development of a pathologic microenvironment. Nat. Med. *16*: 1009–1017.

Bartram, U., and Speer, C.P. (2004). The role of transforming growth factor beta in lung development and disease. Chest *125*: 754–765.

Baum, B.J., Moss, J., Breul, S.D., Berg, R.A., and Crystal, R.G. (1980). Effect of cyclic AMP on the intracellular degradation of newly synthesized collagen. J. Biol. Chem. *255*: 2843–2847.

Baum, J., and Duffy, H.S. (2011). Fibroblasts and myofibroblasts: what are we talking about? J.Cardiovasc.Pharmacol. *57*: 376–379.

Baumgartner, K.B., Samet, J.M., Stidley, C.A., Colby, T. V, and Waldron, J.A. (1997). Cigarette smoking: a risk factor for idiopathic pulmonary fibrosis. Am. J. Respir. Crit. Care Med. *155*: 242–248.

Bay, A., Etlik, O., Oner, A.F., Unal, O., Arslan, H., Bora, A., et al. (2007). Radiological and clinical course of pneumonia in patients with avian influenza H5N1. Eur. J. Radiol. *61*: 245–250.

Beer, D.G., Kardia, S.L.R., Huang, C.-C., Giordano, T.J., Levin, A.M., Misek, D.E., et al. (2002). Gene-expression profiles predict survival of patients with lung adenocarcinoma. Nat. Med. *8*: 816–824.

Berahim, Z., Moharamzadeh, K., Rawlinson, A., and Jowett, A.K. (2011). Biologic interaction of three-dimensional periodontal fibroblast spheroids with collagen-based and synthetic membranes. J.Periodontol. *82*: 790–797.

Bertozzi, P., Astedt, B., Zenzius, L., Lynch, K., LeMaire, F., Zapol, W., et al. (1990). Depressed bronchoalveolar urokinase activity in patients with adult respiratory distress syndrome. N. Engl. J. Med. *322*: 890–897.

Bichay, T.J., Adams, E.G., Inch, W.R., Adams, W.J., Brewer, J.E., and Bhuyan, B.K. (1990). HPLC and flow cytometric analyses of uptake of adriamycin and menogaril by monolayers and multicell spheroids. Sel Cancer Ther. *6*: 153–166.

Bitterman, P.B., Wewers, M.D., Rennard, S.I., Adelberg, S., and Crystal, R.G. (1986). Modulation of alveolar macrophage-driven fibroblast proliferation by alternative macrophage mediators. J. Clin. Invest. *77*: 700–708.

Bizik, J., Kankuri, E., Ristimaki, A., Taieb, A., Vapaatalo, H., Lubitz, W., et al. (2004). Cell-cell contacts trigger programmed necrosis and induce cyclooxygenase-2 expression. Cell Death.Differ. *11*: 183–195.

Bolanos, A.L., Milla, C.M., Lira, J.C., Ramirez, R., Checa, M., Barrera, L., et al. (2012). Role of Sonic Hedgehog in idiopathic pulmonary fibrosis. Am J Physiol Lung Cell Mol Physiol *303*: L978–90.

Bolstad, B.M., Irizarry, R.A., Åstrand, M., and Speed, T.P. (2003). A comparison of normalization methods for high density oligonucleotide array data based on variance and bias. Bioinformatics *19*: 185–193.

Bonner, J.C. (2004). Regulation of PDGF and its receptors in fibrotic diseases. Cytokine Growth Factor Rev. *15*: 255–273.

Boström, H., Willetts, K., Pekny, M., Levéen, P., Lindahl, P., Hedstrand, H., et al. (1996). PDGF-A signaling is a critical event in lung alveolar myofibroblast development and alveogenesis. Cell *85*: 863–873.

Boyle, J.E., Lindroos, P.M., Rice, A.B., Zhang, L., Zeldin, D.C., and Bonner, J.C. (1999). Prostaglandin-E2 counteracts interleukin-1beta-stimulated upregulation of platelet-derived growth factor alpha-receptor on rat pulmonary myofibroblasts. Am. J. Respir. Cell Mol. Biol. *20*: 433–440.

Bozyk, P.D., and Moore, B.B. (2011). Prostaglandin E2 and the pathogenesis of pulmonary fibrosis. Am.J.Respir.Cell Mol.Biol. *45*: 445–452.

Brock, T.G. (2014). EP2 & EP4 - Sibling PGE2 Receptors.

Brock, T.G., McNish, R.W., Mancuso, P., Coffey, M.J., and Peters-Golden, M. (2003). Prolonged lipopolysaccharide inhibits leukotriene synthesis in peritoneal macrophages: Mediation by nitric oxide and prostaglandins. Prostaglandins Other Lipid Mediat. *71*: 131–145.

Brown, P.D., Wakefield, L.M., Levinson, A.D., and Sporn, M.B. (1990). Physicochemical activation of recombinant latent transforming growth factor-beta's 1, 2, and 3. Growth Factors *3*: 35–43.

Bühling, F., Wille, A., Röcken, C., Wiesner, O., Baier, A., Meinecke, I., et al. (2005). Altered expression of membrane-bound and soluble CD95/Fas contributes to the resistance of fibrotic lung fibroblasts to FasL induced apoptosis. Respir. Res. *6*: 37.

Butt, K.I., Yamazaki, M., and Manabe, M. (1996). Ultrastructure of size-regulated hetero-spheroids composed of human keratinocytes and fibroblasts. J.Dermatol.Sci. *11*: 239–249.

Caniggia, I., Han, R., Liu, J., Wang, J., Tanswell, A.K., and Post, M. (1995). Differential expression of collagen-binding receptors in fetal rat lung cells. Am.J.Physiol *268*: L136–L143.

Cantley, L.C. (2002). The phosphoinositide 3-kinase pathway. Science *296*: 1655–1657.

Carafoli, F., Bihan, D., Stathopoulos, S., Konitsiotis, A.D., Kvansakul, M., Farndale, R.W., et al. (2009). Crystallographic insight into collagen recognition by discoidin domain receptor 2. Structure. *17*: 1573–1581.

Carafoli, F., and Hohenester, E. (2013). Collagen recognition and transmembrane signalling by discoidin domain receptors. Biochim.Biophys.Acta *1834*: 2187–2194.

Carmeliet, P., Dor, Y., Herbert, J.M., Fukumura, D., Brusselmans, K., Dewerchin, M., et al. (1998). Role of HIF-1alpha in hypoxia-mediated apoptosis, cell proliferation and tumour angiogenesis. Nature *394*: 485–490.

Carracedo, A., and Pandolfi, P.P. (2008). The PTEN-PI3K pathway: of feedbacks and cross-talks. Oncogene *27*: 5527–5541.

Casini, A., Nieri, S., Banchetti, E., Ricci, O.E., Calabrò, A., and Surrenti, C. (1984). Effect of PGE2 and indomethacin on human fibroblast collagen production. Boll. Soc. Ital. Biol. Sper. *60*: 1141–1144.

Chakraborty, S., Chopra, P., Ambi, S. V, Dastidar, S.G., and Ray, A. (2014). Emerging therapeutic interventions for idiopathic pulmonary fibrosis. Expert.Opin.Investig.Drugs 893–910.

Chambers, R.C. (2008). Procoagulant signalling mechanisms in lung inflammation and fibrosis: novel opportunities for pharmacological intervention? Br.J.Pharmacol. *153 Suppl*: S367–S378.

Chambers, R.C., Leoni, P., Blanc-Brude, O.P., Wembridge, D.E., and Laurent, G.J. (2000). Thrombin is a potent inducer of connective tissue growth factor production via proteolytic activation of protease-activated receptor-1. J. Biol. Chem. *275*: 35584–35591.

Chambers, R.C., Leoni, P., Kaminski, N., Laurent, G.J., and Heller, R.A. (2003). Global expression profiling of fibroblast responses to transforming growth factor-betal reveals the induction of inhibitor of differentiation-1 and provides evidence of smooth muscle cell phenotypic switching. Am J Pathol *162*: 533–546.

Chapman, H.A., Allen, C.L., and Stone, O.L. (1986). Abnormalities in pathways of alveolar fibrin turnover among patients with interstitial lung disease. Am. Rev. Respir. Dis. *133*: 437–443.

Cheifetz, S., Bassols, A., Stanley, K., Ohta, M., Greenberger, J., and Massague, J. (1988). Heterodimeric transforming growth factor beta. Biological properties and interaction with three types of cell surface receptors. J Biol Chem *263*: 10783–9.

Chen, C., Grennan, K., Badner, J., Zhang, D., Gershon, E., Jin, L., et al. (2011). Removing batch effects in analysis of expression microarray data: An evaluation of six batch adjustment methods. PLoS One *6*:

Chen, C.Z., and Raghunath, M. (2009). Focus on collagen: in vitro systems to study fibrogenesis and antifibrosis state of the art. Fibrogenesis.Tissue Repair *2*: 7–.

Chen, L.J., Li, W.D., Li, S.F., Su, X.W., Lin, G.Y., Huang, Y.J., et al. (2010). Bleomycin induces upregulation of lysyl oxidase in cultured human fetal lung fibroblasts. Acta Pharmacol.Sin.

Chen, Y., Wang, X., Weng, D., Tian, L., Lv, L., Tao, S., et al. (2009). A TSP-1 synthetic peptide inhibits bleomycin-induced lung fibrosis in mice. Exp. Toxicol. Pathol. *61*: 59–65.

Cheng, N.C., Wang, S., and Young, T.H. (2012). The influence of spheroid formation of human adipose-derived stem cells on chitosan films on stemness and differentiation capabilities. Biomaterials *33*: 1748–1758.

Chilosi, M., Poletti, V., Murer, B., Lestani, M., Cancellieri, A., Montagna, L., et al. (2002). Abnormal re-epithelialization and lung remodeling in idiopathic pulmonary fibrosis: the role of deltaN-p63. Lab. Invest. *82*: 1335–1345.

Chilosi, M., Poletti, V., Zamò, A., Lestani, M., Montagna, L., Piccoli, P., et al. (2003). Aberrant Wnt/beta-catenin pathway activation in idiopathic pulmonary fibrosis. Am. J. Pathol. *162*: 1495–1502.

Cho, M., Smith, D., Branton, M., Penzak, S., and Kopp, J. (2007). Pirfenidone slows renal function decline in patients with focal segmental glomerulosclerosis. Clin J Am Soc Nephrol *2*: 906–913.

Choi, K., Lee, K., Ryu, S.-W., Im, M., Kook, K.H., and Choi, C. (2012). Pirfenidone inhibits transforming growth factor-β1-induced fibrogenesis by blocking nuclear translocation of Smads in human retinal pigment epithelial cell line ARPE-19. Mol. Vis. *18*: 1010–20.

Choi, S.-C., Kim, G.-H., Lee, S.J., Park, E., Yeo, C.-Y., and Han, J.-K. (2014). Regulation of Activin/Nodal Signaling by Rap2-Directed Receptor Trafficking. Dev. Cell *15*: 49–61.

Chung, M.J., Liu, T., Ullenbruch, M., and Phan, S.H. (2007). Antiapoptotic effect of found in inflammatory zone (FIZZ)1 on mouse lung fibroblasts. J. Pathol. *212*: 180–187.

Churchill, L., Chilton, F.H., Resau, J.H., Bascom, R., Hubbard, W.C., and Proud, D. (1989). Cyclooxygenase metabolism of endogenous arachidonic acid by cultured human tracheal epithelial cells. Am. Rev. Respir. Dis. *140*: 449–459.

Clark, R.A.F., McCoy, G.A., Folkvord, J.M., and McPherson, J.M. (1997). TGF-??1 stimulates cultured human fibroblasts to proliferate and produce tissue-like fibroplasia: A fibronectin matrix-dependent event. J. Cell. Physiol. *170*: 69–80.

Collard, H.R. (2010). The age of idiopathic pulmonary fibrosis. Am.J.Respir.Crit Care Med. *181*: 771–772.

Conte, E., Fruciano, M., Fagone, E., Gili, E., Caraci, F., Iemmolo, M., et al. (2011). Inhibition of PI3K prevents the proliferation and differentiation of human lung fibroblasts into myofibroblasts: The role of class I P110 isoforms. PLoS One *6*:

Cool, C.D., Groshong, S.D., Rai, P.R., Henson, P.M., Stewart, J.S., and Brown, K.K. (2006). Fibroblast foci are not discrete sites of lung injury or repair: the fibroblast reticulum. Am.J.Respir.Crit Care Med. *174*: 654–658.

Coon, D.R., Roberts, D.J., Loscertales, M., and Kradin, R. (2006). Differential epithelial expression of SHH and FOXF1 in usual and nonspecific interstitial pneumonia. Exp. Mol. Pathol. *80*: 119–123.

Corbeil, M., Berthiaume, L., and Lussier, G. (1977). [Formation of spheriods by cultured human diploid cells]. Rev.Can.Biol. *36*: 291–298.

Corbel, M., Lanchou, J., Germain, N., Malledant, Y., Boichot, E., and Lagente, V. (2001). Modulation of airway remodeling-associated mediators by the antifibrotic compound, pirfenidone, and the matrix metalloproteinase inhibitor, batimastat, during acute lung injury in mice. Eur. J. Pharmacol. *426*: 113–121.

Corrin, B., Dewar, A., Rodriguez-Roisin, R., and Turner-Warwick, M. (1985). Fine structural changes in cryptogenic fibrosing alveolitis and asbestosis. J. Pathol. *147*: 107–119.

Cottin, V., Crestani, B., Valeyre, D., Wallaert, B., Cadranel, J., Dalphin, J.-C., et al. (2014). Diagnosis and management of idiopathic pulmonary fibrosis: French practical guidelines. Eur. Respir. Rev. *23*: 193–214.

Counts, D.F., Evans, J.N., Dipetrillo, T.A., Sterling, K.M., and Kelley, J. (1981). Collagen lysyl oxidase activity in the lung increases during bleomycin-induced lung fibrosis. J. Pharmacol. Exp. Ther. *219*: 675–678.

Coward, W.R., Saini, G., and Jenkins, G. (2010). The pathogenesis of idiopathic pulmonary fibrosis. Ther.Adv.Respir.Dis. *4*: 367–388.

Coward, W.R., Watts, K., Feghali-Bostwick, C.A., Knox, A., and Pang, L. (2009). Defective Histone Acetylation Is Responsible for the Diminished Expression of Cyclooxygenase 2 in Idiopathic Pulmonary Fibrosis. Mol. Cell. Biol. *29* : 4325–4339.

Crawford, S.E., Stellmach, V., Murphy-Ullrich, J.E., Ribeiro, S.M.F., Lawler, J., Hynes, R.O., et al. (1998). Thrombospondin-1 is a major activator of TGF-β1 in vivo. Cell *93*: 1159–1170.

Cruse, G., Duffy, S.M., Brightling, C.E., and Bradding, P. (2006). Functional KCa3.1 K+ channels are required for human lung mast cell migration. Thorax *61* : 880–885.

Culo, F., Yuhas, J.M., and Ladman, A.J. (1980). Multicellular tumour spheroids: a model for combined in vivo/in vitro assay of tumour immunity. Br.J.Cancer *41*: 100–112.

Dalma-Weiszhausz, D.D., Warrington, J., Tanimoto, E.Y., and Miyada, C.G. (2006). [1] The Affymetrix GeneChip?? Platform: An Overview. Methods Enzymol. *410*: 3–28.

Dancer, R.C. a, Wood, a M., and Thickett, D.R. (2011). Metalloproteinases in idiopathic pulmonary fibrosis. Eur. Respir. J. *38*: 1461–7.

Datta, A., Scotton, C.J., and Chambers, R.C. (2011). Novel therapeutic approaches for pulmonary fibrosis. Br.J.Pharmacol. *163*: 141–172.

Degryse, A.L., Tanjore, H., Xu, X.C., Polosukhin, V. V, Jones, B.R., McMahon, F.B., et al. (2010). Repetitive intratracheal bleomycin models several features of idiopathic pulmonary fibrosis. Am. J. Physiol. Lung Cell. Mol. Physiol. *299*: L442–L452.

Denes, A., Lopez-Castejon, G., and Brough, D. (2012). Caspase-1: is IL-1 just the tip of the ICEberg? Cell Death Dis. *3*: e338.

Dery, O., Corvera, C.U., Steinhoff, M., and Bunnett, N.W. (1998). Proteinase-activated receptors: novel mechanisms of signaling by serine proteases. Am.J.Physiol *274*: C1429–C1452.

Desmouliere, A., Chaponnier, C., and Gabbiani, G. (2005). Tissue repair, contraction, and the myofibroblast. Wound.Repair Regen. *13*: 7–12.

Desmouliere, A., Redard, M., Darby, I., and Gabbiani, G. (1995). Apoptosis mediates the decrease in cellularity during the transition between granulation tissue and scar. Am.J.Pathol. *146*: 56–66.

Dewor, M., Steffens, G., Krohn, R., Weber, C., Baron, J., and Bernhagen, J. (2007). Macrophage migration inhibitory factor (MIF) promotes fibroblast migration in scratch-wounded monolayers in vitro. FEBS Lett. *581*: 4734–4742.

Dhami, R., He, X., and Schuchman, E.H. (2010). Acid sphingomyelinase deficiency attenuates bleomycin-induced lung inflammation and fibrosis in mice. Cell Physiol Biochem *26*: 749–760.

Discher, D.E., Janmey, P., and Wang, Y.-L. (2005). Tissue cells feel and respond to the stiffness of their substrate. Science *310*: 1139–1143.

Dorr, R.T. (1992). Bleomycin pharmacology: mechanism of action and resistance, and clinical pharmacokinetics. Semin.Oncol. *19*: 3–8.

Dougher, A.M., Wasserstrom, H., Torley, L., Shridaran, L., Westdock, P., Hileman, R.E., et al. (1997). Identification of a heparin binding peptide on the extracellular domain of the KDR VEGF receptor. Growth Factors *14*: 257–268.

Dunkern, T.R., Feurstein, D., Rossi, G.A., Sabatini, F., and Hatzelmann, A. (2007). Inhibition of TGF-?? induced lung fibroblast to myofibroblast conversion by phosphodiesterase inhibiting drugs and activators of soluble guanylyl cyclase. Eur. J. Pharmacol. *572*: 12–22.

Dunsmore, S.E., and Rannels, D.E. (1996). Extracellular matrix biology in the lung. Am.J.Physiol *270*: L3–27.

Eckes, B., Zweers, M.C., Zhang, Z.G., Hallinger, R., Mauch, C., Aumailley, M., et al. (2006). Mechanical tension and integrin alpha 2 beta 1 regulate fibroblast functions. J.Investig.Dermatol.Symp.Proc. *11*: 66–72.

Edwards, D.R., Murphy, G., Reynolds, J.J., Whitham, S.E., Docherty, A.J., Angel, P., et al. (1987). Transforming growth factor beta modulates the expression of collagenase and metalloproteinase inhibitor. EMBO J. *6*: 1899–1904.

Elias, J.A., Rossman, M.D., Zurier, R.B., and Daniele, R.P. (1985). Human alveolar macrophage inhibition of lung fibroblast growth. A prostaglandin-dependent process. Am. Rev. Respir. Dis. *131*: 94–99.

Elliott, N.T., and Yuan, F. (2011). A review of three-dimensional in vitro tissue models for drug discovery and transport studies. J.Pharm.Sci. *100*: 59–74.

Emblom-Callahan, M.C., Chhina, M.K., Shlobin, O.A., Ahmad, S., Reese, E.S., Iyer, E.P.R., et al. (2010). Genomic phenotype of non-cultured pulmonary fibroblasts in idiopathic pulmonary fibrosis. Genomics *96*: 134–145.

Engler, A.J., Sen, S., Sweeney, H.L., and Discher, D.E. (2006). Matrix Elasticity Directs Stem Cell Lineage Specification. Cell *126*: 677–689.

Enomoto, N., Suda, T., Kato, M., Kaida, Y., Nakamura, Y., Imokawa, S., et al. (2006). Quantitative analysis of fibroblastic foci in usual interstitial pneumonia. Chest *130*: 22–29.

Erbes, R., Schaberg, T., and Loddenkemper, R. (1997). Lung function tests in patients with idiopathic pulmonary fibrosis. Are they helpful for predicting outcome? Chest *111*: 51–57.

Ermert, L., Ermert, M., Goppelt-Struebe, M., Walmrath, D., Grimminger, F., Steudel, W., et al. (1998). Cyclooxygenase isoenzyme localization and mRNA expression in rat lungs. Am. J. Respir. Cell Mol. Biol. *18*: 479–488.

Fagone, E., Conte, E., Gili, E., Fruciano, M., Pistorio, M.P., Furno, D. Lo, et al. (2011). Resveratrol inhibits transforming growth factor-β-induced proliferation and differentiation of ex vivo human lung fibroblasts into myofibroblasts through ERK/Akt inhibition and PTEN restoration. Exp. Lung Res. *37*: 162–174.

Fanger, C.M., Rauer, H., Neben, A.L., Miller, M.J., Rauer, H., Wulff, H., et al. (2001). Calcium-activated potassium channels sustain calcium signaling in T lymphocytes. Selective blockers and manipulated channel expression levels. J. Biol. Chem. *276*: 12249–12256.

Fare, T.L., Coffey, E.M., Dai, H., He, Y.D., Kessler, D.A., Kilian, K.A., et al. (2003). Effects of atmospheric ozone on microarray data quality. Anal. Chem. *75*: 4672–4675.

Farkas, L., Gauldie, J., Voelkel, N.F., and Kolb, M. (2010). Pulmonary Hypertension and Idiopathic Pulmonary Fibrosis - A Tale of Angiogenesis, Apoptosis and Growth Factors. Am.J.Respir.Cell Mol.Biol. 1–15.

Fennema, E., Rivron, N., Rouwkema, J., Blitterswijk, C. van, and Boer, J. De (2013). Spheroid culture as a tool for creating 3D complex tissues. Trends Biotechnol. *31*: 108–115.

Fine, A., Poliks, C.F., Donahue, L.P., Smith, B.D., and Goldstein, R.H. (1989). The differential effect of prostaglandin E2 on transforming growth factor-beta and insulin-induced collagen formation in lung fibroblasts. J. Biol. Chem. *264* : 16988–16991.

Fitch, P.M., Howie, S.E., and Wallace, W.A. (2011). Oxidative damage and TGF-beta differentially induce lung epithelial cell sonic hedgehog and tenascin-C expression: implications for the regulation of lung remodelling in idiopathic interstitial lung disease. Int. J. Exp. Pathol. *92*: 8–17.

Flaherty, K.R., Colby, T. V, Travis, W.D., Toews, G.B., Mumford, J., Murray, S., et al. (2003). Fibroblastic foci in usual interstitial pneumonia: idiopathic versus collagen vascular disease. Am.J.Respir.Crit Care Med. *167*: 1410–1415.

Ford-Hutchinson, A.W., Gresser, M., and Young, R.N. (1994). 5-Lipoxygenase. Annu. Rev. Biochem. *63*: 383–417.

Frankel, S.K., Cosgrove, G.P., Cha, S.-I., Cool, C.D., Wynes, M.W., Edelman, B.L., et al. (2006). TNF-alpha sensitizes normal and fibrotic human lung fibroblasts to Fas-induced apoptosis. Am. J. Respir. Cell Mol. Biol. *34*: 293–304.

Freed, L.E., and Vunjak-Novakovic, G. (1998). Culture of organized cell communities. Adv. Drug Deliv. Rev. *33*: 15–30.

Friedrich, J., Eder, W., Castaneda, J., Doss, M., Huber, E., Ebner, R., et al. (2007). A reliable tool to determine cell viability in complex 3-d culture: the acid phosphatase assay. J. Biomol. Screen. Off. J. Soc. Biomol. Screen. *12*: 925–937.

Friedrich, J., Seidel, C., Ebner, R., and Kunz-Schughart, L.A. (2009). Spheroid-based drug screen: considerations and practical approach. Nat. Protoc. *4*: 309–324.

Fu, C.-Y., Tseng, S.-Y., Yang, S.-M., Hsu, L., Liu, C.-H., and Chang, H.-Y. (2014). A microfluidic chip with a U-shaped microstructure array for multicellular spheroid formation, culturing and analysis. Biofabrication *6*: 015009.

Fujishima, S., Shiomi, T., Yamashita, S., Yogo, Y., Nakano, Y., Inoue, T., et al. (2010). Production and activation of matrix metalloproteinase 7 (matrilysin 1) in the lungs of patients with idiopathic pulmonary fibrosis. Arch. Pathol. Lab. Med. *134*: 1136–1142.

Fukuda, Y., Ishizaki, M., Kudoh, S., Kitaichi, M., and Yamanaka, N. (1998). Localization of matrix metalloproteinases-1, -2, and -9 and tissue inhibitor of metalloproteinase-2 in interstitial lung diseases. Lab. Investig. *78*: 687–698.

Gabbiani, G. (2003). The myofibroblast in wound healing and fibrocontractive diseases. J.Pathol. *200*: 500–503.

García, L., Hernández, I., Sandoval, A., Salazar, A., Garcia, J., Vera, J., et al. (2002). Pirfenidone effectively reverses experimental liver fibrosis. J. Hepatol. *37*: 797–805.

García-Alvarez, J., Ramirez, R., Sampieri, C.L., Nuttall, R.K., Edwards, D.R., Selman, M., et al. (2006). Membrane type-matrix metalloproteinases in idiopathic pulmonary fibrosis. Sarcoidosis Vasc. Diffuse Lung Dis. *23*: 13–21.

Garrett, Q., Khaw, P.T., Blalock, T.D., Schultz, G.S., Grotendorst, G.R., and Daniels, J.T. (2004). Involvement of CTGF in TGF-β1-stimulation of myofibroblast differentiation and collagen matrix contraction in the presence of mechanical stress. Investig. Ophthalmol. Vis. Sci. *45*: 1109–1116.

Gentry, L.E., Lioubin, M.N., Purchio, A.F., and Marquardt, H. (1988). Molecular events in the processing of recombinant type 1 pre-pro-transforming growth factor beta to the mature polypeptide. Mol. Cell. Biol. *8*: 4162–4168.

George, M.D., Vollberg, T.M., Floyd, E.E., Stein, J.P., and Jetten, A.M. (1990). Regulation of transglutaminase type II by transforming growth factor-beta 1 in normal and transformed human epidermal keratinocytes. J. Biol. Chem. *265*: 11098–104.

Georges, P.C., and Janmey, P.A. (2005). Cell type-specific response to growth on soft materials. J. Appl. Physiol. *98*: 1547–1553.

Ghanshani, S., Wulff, H., Miller, M.J., Rohm, H., Neben, A., Gutman, G.A., et al. (2000). Up-regulation of the IKCa1 potassium channel during T-cell activation: Molecular mechanism and functional consequences. J. Biol. Chem. *275*: 37137–37149.

Gharaee-Kermani, M., Denholm, E.M., and Phan, S.H. (1996). Costimulation of fibroblast collagen and transforming growth factor beta1 gene expression by monocyte chemoattractant protein-1 via specific receptors. J. Biol. Chem. *271*: 17779–17784.

Gharaee-Kermani, M., Hu, B., Phan, S.H., and Gyetko, M.R. (2009). Recent advances in molecular targets and treatment of idiopathic pulmonary fibrosis: focus on TGFbeta signaling and the myofibroblast. Curr.Med.Chem. *16*: 1400–1417.

Gharaee-Kermani, M., McCullumsmith, R.E., Charo, I.F., Kunkel, S.L., and Phan, S.H. (2003). CC-chemokine receptor 2 required for bleomycin-induced pulmonary fibrosis. Cytokine *24*: 266–276.

Gharaee-Kermani, M., and Phan, S.H. (2005). Molecular mechanisms of and possible treatment strategies for idiopathic pulmonary fibrosis. Curr. Pharm. Des. *11*: 3943–3971.

Gilbert, P.M., Havenstrite, K.L., Magnusson, K.E.G., Sacco, A., Leonardi, N.A., Kraft, P., et al. (2010). Substrate elasticity regulates skeletal muscle stem cell self-renewal in culture. Science *329*: 1078–1081.

Gleizes, P.E., Munger, J.S., Nunes, I., Harpel, J.G., Mazzieri, R., Noguera, I., et al. (1997). TGF-beta latency: biological significance and mechanisms of activation. Stem Cells *15*: 190–197.

Goffin, J.M., Pittet, P., Csucs, G., Lussi, J.W., Meister, J.-J., and Hinz, B. (2006). Focal adhesion size controls tension-dependent recruitment of alpha-smooth muscle actin to stress fibers. J. Cell Biol. *172*: 259–268.

Goparaju, S.K., Jolly, P.S., Watterson, K.R., Bektas, M., Alvarez, S., Sarkar, S., et al. (2005). The S1P2 receptor negatively regulates platelet-derived growth factor-induced motility and proliferation. Mol. Cell. Biol. *25*: 4237–4249.

Greenlee, K.J., Werb, Z., and Kheradmand, F. (2007). Matrix metalloproteinases in lung: multiple, multifarious, and multifaceted. Physiol Rev. *87*: 69–98.

Grgic, I., Kiss, E., Kaistha, B.P., Busch, C., Kloss, M., Sautter, J., et al. (2009). Renal fibrosis is attenuated by targeted disruption of KCa3.1 potassium channels. Proc. Natl. Acad. Sci. U. S. A. *106*: 14518–14523.

Gribbin, J., Hubbard, R.B., I, J. Le, Smith, C.J., West, J., and Tata, L.J. (2006). Incidence and mortality of idiopathic pulmonary fibrosis and sarcoidosis in the UK. Thorax *61*: 980–985.

Grimsby, J.L., Lucero, H.A., Trackman, P.C., Ravid, K., and Kagan, H.M. (2010). Role of lysyl oxidase propeptide in secretion and enzyme activity. J. Cell. Biochem. *111*: 1231–1243.

Gross, T.J., and Hunninghake, G.W. (2001). Idiopathic pulmonary fibrosis. N.Engl.J.Med. *345*: 517–525.

Grotendorst, G.R., Smale, G., and Pencev, D. (1989a). Production of transforming growth factor beta by human peripheral blood monocytes and neutrophils. J. Cell. Physiol. *140*: 396–402.

Grotendorst, G.R., Soma, Y., Takehara, K., and Charette, M. (1989b). EGF and TGF-alpha are potent chemoattractants for endothelial cells and EGF-like peptides are present at sites of tissue regeneration. J. Cell. Physiol. *139*: 617–623.

Grygielko, E.T., Martin, W.M., Tweed, C., Thornton, P., Harling, J., Brooks, D.P., et al. (2005). Inhibition of gene markers of fibrosis with a novel inhibitor of transforming growth factor-beta type I receptor kinase in puromycin-induced nephritis. J. Pharmacol. Exp. Ther. *313*: 943–951.

Gu, L., Zhu, Y.J., Yang, X., Guo, Z.J., Xu, W.B., and Tian, X.L. (2007). Effect of TGF-beta/Smad signaling pathway on lung myofibroblast differentiation. Acta Pharmacol.Sin. *28*: 382–391.

Gullberg, D., Gehlsen, K.R., Turner, D.C., Ahlen, K., Zijenah, L.S., Barnes, M.J., et al. (1992). Analysis of alpha 1 beta 1, alpha 2 beta 1 and alpha 3 beta 1 integrins in cell--collagen

interactions: identification of conformation dependent alpha 1 beta 1 binding sites in collagen type I. EMBO J. *11*: 3865–3873.

Guo, L., Ge, J., Zhou, Y., Wang, S., Zhao, R.C.H., and Wu, Y. (2014a). Three-dimensional spheroid-cultured mesenchymal stem cells devoid of embolism attenuate brain stroke injury after intra-arterial injection. Stem Cells Dev. *23*: 978–89.

Guo, W.M., Loh, X.J., Tan, E.Y., Loo, J.S.C., and Ho, V.H.B. (2014b). Development of a magnetic 3D spheroid platform with potential application for high-throughput drug screening. Mol. Pharm. *11*: 2182–2189.

Gurujeyalakshmi, G., Hollinger, M.A., and Giri, S.N. (1999). Pirfenidone inhibits PDGF isoforms in bleomycin hamster model of lung fibrosis at the translational level. Am. J. Physiol. *276*: L311–L318.

Gygi, S.P., Rochon, Y., Franza, B.R., and Aebersold, R. (1999). Correlation between protein and mRNA abundance in yeast. Mol. Cell. Biol. *19*: 1720–1730.

Hagimoto, N., Kuwano, K., Inoshima, I., Yoshimi, M., Nakamura, N., Fujita, M., et al. (2002). TGF-beta 1 as an enhancer of Fas-mediated apoptosis of lung epithelial cells. J. Immunol. *168*: 6470–6478.

Hagiwara, S., Iwasaka, H., Matsumoto, S., and Noguchi, T. (2007a). Antisense oligonucleotide inhibition of heat shock protein (HSP) 47 improves bleomycin-induced pulmonary fibrosis in rats. Respir. Res. *8*: 37.

Hagiwara, S., Iwasaka, H., Matsumoto, S., and Noguchi, T. (2007b). Introduction of antisense oligonucleotides to heat shock protein 47 prevents pulmonary fibrosis in lipopolysaccharide-induced pneumopathy of the rat. Eur. J. Pharmacol. *564*: 174–180.

Han, M.K., Murray, S., Fell, C.D., Flaherty, K.R., Toews, G.B., Myers, J., et al. (2008). Sex differences in physiological progression of idiopathic pulmonary fibrosis. Eur.Respir.J. *31*: 1183–1188.

Hanada, K. (2003). Serine palmitoyltransferase, a key enzyme of sphingolipid metabolism. Biochim. Biophys. Acta - Mol. Cell Biol. Lipids *1632*: 16–30.

Hannun, Y.A., and Obeid, L.M. (2008). Principles of bioactive lipid signalling: lessons from sphingolipids. Nat. Rev. Mol. Cell Biol. *9*: 139–150.

Hara, S., Kamei, D., Sasaki, Y., Tanemoto, A., Nakatani, Y., and Murakami, M. (2010). Prostaglandin E synthases: Understanding their pathophysiological roles through mouse genetic models. Biochimie *92*: 651–659.

Harper, K.A., and Tyson-Capper, A.J. (2008). Complexity of COX-2 gene regulation. Biochem. Soc. Trans. *36*: 543–545.

Hecht, S.M. (2000). Bleomycin: new perspectives on the mechanism of action. J.Nat.Prod. *63*: 158–168.

Hecker, L., and Thannickal, V.J. (2011). Nonresolving fibrotic disorders: idiopathic pulmonary fibrosis as a paradigm of impaired tissue regeneration. Am. J. Med. Sci. *341*: 431–434.

Heckman, C.A. (2009). Contact inhibition revisited. J. Cell. Physiol. *220*: 574–575.

Heikkinen, J., Risteli, M., Wang, C., Latvala, J., Rossi, M., Valtavaara, M., et al. (2000). Lysyl hydroxylase 3 is a multifunctional protein possessing collagen glucosyltransferase activity. J.Biol.Chem. *275*: 36158–36163.

Heldin, C.H., and Moustakas, A. (2012). Role of Smads in TGF?? signaling. Cell Tissue Res. *347*: 21–36.

Hempel, S.L., Monick, M.M., He, B., Yano, T., and Hunninghake, G.W. (1994a). Synthesis of prostaglandin H synthase-2 by human alveolar macrophages in response to lipopolysaccharide is inhibited by decreased cell oxidant tone. J. Biol. Chem. *269*: 32979–32984.

Hempel, S.L., Monick, M.M., and Hunninghake, G.W. (1994b). Lipopolysaccharide induces prostaglandin H synthase-2 protein and mRNA in human alveolar macrophages and blood monocytes. J. Clin. Invest. *93*: 391–396.

Henry, M.T., McMahon, K., Mackarel, A.J., Prikk, K., Sorsa, T., Maisi, P., et al. (2002). Matrix metalloproteinases and tissue inhibitor of metalloproteinase-1 in sarcoidosis and IPF. Eur. Respir. J. Off. J. Eur. Soc. Clin. Respir. Physiol. *20*: 1220–1227.

Hermanns, M.I., Unger, R.E., Kehe, K., Peters, K., and Kirkpatrick, C.J. (2004). Lung epithelial cell lines in coculture with human pulmonary microvascular endothelial cells: development of an alveolo-capillary barrier in vitro. Lab. Investig. *84*: 736–752.

Hetzel, M., Bachem, M., Anders, D., Trischler, G., and Faehling, M. (2005). Different effects of growth factors on proliferation and matrix production of normal and fibrotic human lung fibroblasts. Lung *183*: 225–237.

Higashiyama, H., Yoshimoto, D., Kaise, T., Matsubara, S., Fujiwara, M., Kikkawa, H., et al. (2007). Inhibition of activin receptor-like kinase 5 attenuates Bleomycin-induced pulmonary fibrosis. Exp. Mol. Pathol. *83*: 39–46.

Higashiyama, S., Abraham, J.A., and Klagsbrun, M. (1993). Heparin-binding EGF-like growth factor stimulation of smooth muscle cell migration: dependence on interactions with cell surface heparan sulfate. J. Cell Biol. *122*: 933–940.

Hilberg, F., Roth, G.J., Krssak, M., Kautschitsch, S., Sommergruber, W., Tontsch-Grunt, U., et al. (2008). BIBF 1120: triple angiokinase inhibitor with sustained receptor blockade and good antitumor efficacy. Cancer Res. *68*: 4774–4782.

Hinz, B. (2006). Masters and servants of the force: the role of matrix adhesions in myofibroblast force perception and transmission. Eur.J.Cell Biol. *85*: 175–181.

Hinz, B. (2007). Formation and function of the myofibroblast during tissue repair. J. Invest. Dermatol. *127*: 526–537.

Hinz, B. (2010). The myofibroblast: Paradigm for a mechanically active cell. J. Biomech. *43*: 146–155.

Hinz, B., Celetta, G., Tomasek, J.J., Gabbiani, G., and Chaponnier, C. (2001a). Alpha-smooth muscle actin expression upregulates fibroblast contractile activity. Mol.Biol.Cell *12*: 2730–2741.

Hinz, B., and Gabbiani, G. (2003a). Cell-matrix and cell-cell contacts of myofibroblasts: role in connective tissue remodeling. Thromb.Haemost. *90*: 993–1002.

Hinz, B., and Gabbiani, G. (2003b). Mechanisms of force generation and transmission by myofibroblasts. Curr.Opin.Biotechnol. *14*: 538–546.

Hinz, B., and Gabbiani, G. (2010). Fibrosis: recent advances in myofibroblast biology and new therapeutic perspectives. F1000.Biol.Rep. *2*: 78–.

Hinz, B., Mastrangelo, D., Iselin, C.E., Chaponnier, C., and Gabbiani, G. (2001b). Mechanical tension controls granulation tissue contractile activity and myofibroblast differentiation. Am. J. Pathol. *159*: 1009–1020.

Hinz, B., Phan, S.H., Thannickal, V.J., Galli, A., Bochaton-Piallat, M.-L., and Gabbiani, G. (2007). The myofibroblast: one function, multiple origins. Am. J. Pathol. *170*: 1807–1816.

Hinz, B., Pittet, P., Smith-Clerc, J., Chaponnier, C., and Meister, J.-J. (2004). Myofibroblast development is characterized by specific cell-cell adherens junctions. Mol. Biol. Cell *15*: 4310–4320.

Hisatomi, K., Mukae, H., Sakamoto, N., Ishimatsu, Y., Kakugawa, T., Hara, S., et al. (2012). Pirfenidone inhibits TGF-beta1-induced over-expression of collagen type I and heat shock protein 47 in A549 cells. BMC Pulm Med *12*: 24.

Hodges, R.J., Jenkins, R.G., Wheeler-Jones, C.P.D., Copeman, D.M., Bottoms, S.E., Bellingan, G.J., et al. (2004). Severity of lung injury in cyclooxygenase-2-deficient mice is dependent on reduced prostaglandin E(2) production. Am. J. Pathol. *165*: 1663–1676.

Hodgson, U., Laitinen, T., and Tukiainen, P. (2002). Nationwide prevalence of sporadic and familial idiopathic pulmonary fibrosis: evidence of founder effect among multiplex families in Finland. Thorax *57*: 338–342.

Hogaboam, C.M., Steinhauser, M.L., Chensue, S.W., and Kunkel, S.L. (1998). Novel roles for chemokines and fibroblasts in interstitial fibrosis. In Kidney International, pp 2152–2159.

Hojo, S., Fujita, J., Yoshinouchi, T., Yamanouchi, H., Kamei, T., Yamadori, I., et al. (1997). Hepatocyte growth factor and neutrophil elastase in idiopathic pulmonary fibrosis. Respir. Med. *91*: 511–516.

Horton, M.A. (1997). The alpha v beta 3 integrin “vitronectin receptor.” Int.J.Biochem.Cell Biol. *29*: 721–725.

Hsiao, A.Y., Tung, Y.C., Kuo, C.H., Mosadegh, B., Bedenis, R., Pienta, K.J., et al. (2012). Micro-ring structures stabilize microdroplets to enable long term spheroid culture in 384 hanging drop array plates. Biomed. Microdevices *14*: 313–323.

Hsu, S. hui, Ho, T.T., Huang, N.C., Yao, C.L., Peng, L.H., and Dai, N.T. (2014). Substrate-dependent modulation of 3D spheroid morphology self-assembled in mesenchymal stem cell-endothelial progenitor cell coculture. Biomaterials *35*: 7295–7307.

Hu, B., Wu, Z., and Phan, S.H. (2003). Smad3 mediates transforming growth factor-beta-induced alpha-smooth muscle actin expression. Am.J.Respir.Cell Mol.Biol. *29*: 397–404.

Huang, S., Wettlaufer, S.H., Hogaboam, C., Aronoff, D.M., and Peters-Golden, M. (2007). Prostaglandin E(2) inhibits collagen expression and proliferation in patient-derived normal lung fibroblasts via E prostanoid 2 receptor and cAMP signaling. Am.J.Physiol Lung Cell Mol.Physiol *292*: L405–L413.

Huang, S.K., Fisher, A.S., Scruggs, A.M., White, E.S., Hogaboam, C.M., Richardson, B.C., et al. (2010). Hypermethylation of PTGER2 confers prostaglandin E2 resistance in fibrotic fibroblasts from humans and mice. Am. J. Pathol. *177*: 2245–2255.

Huang, S.K., Scruggs, a M., Donaghy, J., Horowitz, J.C., Zaslona, Z., Przybranowski, S., et al. (2013). Histone modifications are responsible for decreased Fas expression and apoptosis resistance in fibrotic lung fibroblasts. Cell Death Dis. *4*: e621.

Huang, S.K., Wettlaufer, S.H., Chung, J., and Peters-Golden, M. (2008a). Prostaglandin E2 inhibits specific lung fibroblast functions via selective actions of PKA and Epac-1. Am. J. Respir. Cell Mol. Biol. *39*: 482–489.

Huang, S.K., Wettlaufer, S.H., Hogaboam, C.M., Flaherty, K.R., Martinez, F.J., Myers, J.L., et al. (2008b). Variable prostaglandin E2 resistance in fibroblasts from patients with usual interstitial pneumonia. Am.J.Respir.Crit Care Med. *177*: 66–74.

Huang, S.K., White, E.S., Wettlaufer, S.H., Grifka, H., Hogaboam, C.M., Thannickal, V.J., et al. (2009). Prostaglandin E(2) induces fibroblast apoptosis by modulating multiple survival pathways. FASEB J. *23*: 4317–4326.

Huh, D., Matthews, B.D., Mammoto, A., Montoya-Zavala, M., Hsin, H.Y., and Ingber, D.E. (2010). Reconstituting organ-level lung functions on a chip. Science (80-.). *328*: 1662–1668.

Hung, C., Linn, G., Chow, Y.H., Kobayashi, A., Mittelsteadt, K., Altemeier, W.A., et al. (2013a). Role of lung pericytes and resident fibroblasts in the pathogenesis of pulmonary fibrosis. Am.J.Respir.Crit Care Med. *188*: 820–830.

Hung, C.F., Rohani, M.G., Lee, S.S., Chen, P., and Schnapp, L.M. (2013b). Role of IGF-1 pathway in lung fibroblast activation. Respir.Res. *14*: 102–.

Huse, M., Muir, T.W., Xu, L., Chen, Y.G., Kuriyan, J., and Massague, J. (2001). The TGF beta receptor activation process: an inhibitor- to substrate- binding switch. Mol Cell *8*: 671–82.

Ichikawa, O., Osawa, M., Nishida, N., Goshima, N., Nomura, N., and Shimada, I. (2007). Structural basis of the collagen-binding mode of discoidin domain receptor 2. EMBO J. *26*: 4168–4176.

Idell, S., Peters, J., James, K.K., Fair, D.S., and Coalson, J.J. (1989). Local abnormalities of coagulation and fibrinolytic pathways that promote alveolar fibrin deposition in the lungs of baboons with diffuse alveolar damage. J. Clin. Invest. *84*: 181–193.

Illman, S.A., Lehti, K., Keski-Oja, J., and Lohi, J. (2006). Epilysin (MMP-28) induces TGF-beta mediated epithelial to mesenchymal transition in lung carcinoma cells. J. Cell Sci. *119*: 3856–3865.

Inoshima, I., Kuwano, K., Hamada, N., Hagimoto, N., Yoshimi, M., Maeyama, T., et al. (2004). Anti-monocyte chemoattractant protein-1 gene therapy attenuates pulmonary fibrosis in mice. Am. J. Physiol. Lung Cell. Mol. Physiol. *286*: L1038–L1044.

Ishida, Y., and Nagata, K. (2011). Hsp47 as a collagen-specific molecular chaperone. Methods Enzymol. *499*: 167–182.

Ishii, I., Fukushima, N., Ye, X., and Chun, J. (2004). Lysophospholipid receptors: signaling and biology. Annu. Rev. Biochem. *73*: 321–354.

Iyer, N. V, Kotch, L.E., Agani, F., Leung, S.W., Laughner, E., Wenger, R.H., et al. (1998). Cellular and developmental control of O2 homeostasis by hypoxia-inducible factor 1 alpha. Genes Dev. *12*: 149–162.

Iyer, S.N., Gurujeyalakshmi, G., and Giri, S.N. (1999). Effects of pirfenidone on transforming growth factor-beta gene expression at the transcriptional level in bleomycin hamster model of lung fibrosis. J. Pharmacol. Exp. Ther. *291*: 367–373.

Janmey, P.A., Winer, J.P., Murray, M.E., and Wen, Q. (2009). The hard life of soft cells. Cell Motil. Cytoskeleton *66*: 597–605.

Jenkins, R.G., Su, X., Su, G., Scotton, C.J., Camerer, E., Laurent, G.J., et al. (2006). Ligation of protease-activated receptor 1 enhances α v β 6 integrin – dependent TGF-β activation and promotes acute lung injury. J. Clin. Incestigation *116*: 1606–1614.

Jeon, N.L., Dertinger, S.K.W., Chiu, D.T., Choi, I.S., Stroock, A.D., and Whitesides, G.M. (2000). Generation of Solution and Surface Gradients Using Microfluidic Systems. Langmuir *16*: 8311–8316.

Jesudason, R., Sato, S., Parameswaran, H., Araujo, A.D., Majumdar, A., Allen, P.G., et al. (2010). Mechanical forces regulate elastase activity and binding site availability in lung elastin. Biophys. J. *99*: 3076–3083.

John, J., Throm Quinlan, A., Silvestri, C., and Billiar, K. (2010). Boundary stiffness regulates fibroblast behavior in collagen gels. In Annals of Biomedical Engineering, pp 658–673.

Jolliffe, I.T. (2002). Principal Component Analysis.

Jordana, M., Särnstrand, B., Sime, P.J., and Ramis, I. (1994). Immune-inflammatory functions of fibroblasts. Eur. Respir. J. Off. J. Eur. Soc. Clin. Respir. Physiol. *7*: 2212–2222.

Kadler, K.E., Baldock, C., Bella, J., and Boot-Handford, R.P. (2007). Collagens at a glance. J.Cell Sci. *120*: 1955–1958.

Kagan, H.M. (2000). Intra- and extracellular enzymes of collagen biosynthesis as biological and chemical targets in the control of fibrosis. Acta Trop. *77*: 147–152.

Kagan, H.M., and Li, W. (2003). Lysyl oxidase: Properties, specificity, and biological roles inside and outside of the cell. J. Cell. Biochem. *88*: 660–672.

Kage, H., and Borok, Z. (2012). EMT and interstitial lung disease: a mysterious relationship. Curr. Opin. Pulm. Med. *18*: 517–23.

Kakugawa, T., Yokota, S.-I., Ishimatsu, Y., Hayashi, T., Nakashima, S., Hara, S., et al. (2013). Serum heat shock protein 47 levels are elevated in acute exacerbation of idiopathic pulmonary fibrosis. Cell Stress Chaperones *18*: 581–90.

Kalluri, R., and Weinberg, R.A. (2009). The basics of epithelial-mesenchymal transition. J.Clin.Invest *119*: 1420–1428.

Kaminski, N., and Friedman, N. (2002). Practical approaches to analyzing results of microarray experiments. Am. J. Respir. Cell Mol. Biol. *27*: 125–132.

Kaner, R.J., Ladetto, J. V, Singh, R., Fukuda, N., Matthay, M.A., and Crystal, R.G. (2000). Lung overexpression of the vascular endothelial growth factor gene induces pulmonary edema. Am. J. Respir. Cell Mol. Biol. *22*: 657–664.

Kang, L., Chung, B.G., Langer, R., and Khademhosseini, A. (2008). Microfluidics for drug discovery and development: from target selection to product lifecycle management. Drug Discov.Today *13*: 1–13.

Kapanci, Y., Ribaux, C., Chaponnier, C., and Gabbiani, G. (1992). Cytoskeletal features of alveolar myofibroblasts and pericytes in normal human and rat lung. J. Histochem. Cytochem. *40*: 1955–1963.

Kardassis, D., Murphy, C., Fotsis, T., Moustakas, A., and Stournaras, C. (2009). Control of transforming growth factor beta signal transduction by small GTPases. FEBS J. *276*: 2947–2965.

Kasabova, M., Joulin-Giet, A., Lecaille, F., Gilmore, B.F., Marchand-Adam, S., Saidi, A., et al. (2014). Regulation of TGF-β1-Driven Differentiation of Human Lung Fibroblasts: Emerging Roles of Cathepsin B and Cystatin C. J. Biol. Chem.

Kasai, H., Allen, J.T., Mason, R.M., Kamimura, T., and Zhang, Z. (2005). TGF-beta1 induces human alveolar epithelial to mesenchymal cell transition (EMT). Respir. Res. *6*: 56.

Kasper, M., and Haroske, G. (1996). Alterations in the alveolar epithelium after injury leading to pulmonary fibrosis. Histol. Histopathol. *11*: 463–483.

Kaur, P., Ward, B., Saha, B., Young, L., Groshen, S., Techy, G., et al. (2011). Human Breast Cancer Histoid: An In Vitro 3-Dimensional Co-culture Model That Mimics Breast Cancer Tissue. J.Histochem.Cytochem. *59*: 1087–1100.

Kawanami, O., Ferrans, V.J., and Crystal, R.G. (1982). Structure of alveolar epithelial cells in patients with fibrotic lung disorders. Lab. Invest. *46*: 39–53.

Kayed, H., Kleeff, J., Keleg, S., Jiang, X., Penzel, R., Giese, T., et al. (2006). Correlation of glypican-1 expression with TGF-beta, BMP, and activin receptors in pancreatic ductal adenocarcinoma. Int. J. Oncol. *29*: 1139–1148.

Keerthisingam, C.B., Jenkins, R.G., Harrison, N.K., Hernandez-Rodriguez, N.A., Booth, H., Laurent, G.J., et al. (2001). Cyclooxygenase-2 Deficiency Results in a Loss of the Anti-Proliferative Response to Transforming Growth Factor-β in Human Fibrotic Lung Fibroblasts and Promotes Bleomycin-Induced Pulmonary Fibrosis in Mice. Am. J. Pathol. *158*: 1411–1422.

Kelley, J., Fabisiak, J.P., Hawes, K., and Absher, M. (1991). Cytokine signaling in lung: transforming growth factor-beta secretion by lung fibroblasts. Am. J. Physiol. *260*: L123–L128.

Kerr, M.K. (2003). Design considerations for efficient and effective microarray studies. Biometrics *59*: 822–828.

Kim, K.K., Kugler, M.C., Wolters, P.J., Robillard, L., Galvez, M.G., Brumwell, A.N., et al. (2006). Alveolar epithelial cell mesenchymal transition develops in vivo during pulmonary fibrosis and is regulated by the extracellular matrix. Proc. Natl. Acad. Sci. U. S. A. *103*: 13180–13185.

King Jr., T.E., Pardo, A., and Selman, M. (2011). Idiopathic pulmonary fibrosis. Lancet *378*: 1949–1961.

King Jr., T.E., Schwarz, M.I., Brown, K., Tooze, J.A., Colby, T. V, Waldron Jr., J.A., et al. (2001). Idiopathic pulmonary fibrosis: relationship between histopathologic features and mortality. Am.J.Respir.Crit Care Med. *164*: 1025–1032.

King, T.E., Bradford, W.Z., Castro-Bernardini, S., Fagan, E. a, Glaspole, I., Glassberg, M.K., et al. (2014). A Phase 3 Trial of Pirfenidone in Patients with Idiopathic Pulmonary Fibrosis. N. Engl. J. Med. 2083–2092.

Kirk, J.M., Heard, B.E., Kerr, I., Turner-Warwick, M., and Laurent, G.J. (1984). Quantitation of types I and III collagen in biopsy lung samples from patients with cryptogenic fibrosing alveolitis. Coll. Relat. Res. *4*: 169–182.

Kliment, C.R., Englert, J.M., Crum, L.P., and Oury, T.D. (2011). A novel method for accurate collagen and biochemical assessment of pulmonary tissue utilizing one animal. Int.J.Clin.Exp.Pathol. *4*: 349–355.

Koff, A., Ohtsuki, M., Polyak, K., Roberts, J.M., and Massagué, J. (1993). Negative regulation of G1 in mammalian cells: inhibition of cyclin E-dependent kinase by TGF-beta. Science *260*: 536–539.

Kohyama, T., Ertl, R.F., Valenti, V., Spurzem, J., Kawamoto, M., Nakamura, Y., et al. (2001). Prostaglandin E(2) inhibits fibroblast chemotaxis. Am. J. Physiol. Lung Cell. Mol. Physiol. *281*: L1257–L1263.

Kohyama, T., Liu, X., Kim, H.J., Kobayashi, T., Ertl, R.F., Wen, F.-Q., et al. (2002a). Prostacyclin analogs inhibit fibroblast migration. Am. J. Physiol. Lung Cell. Mol. Physiol. *283*: L428–L432.

Kohyama, T., Liu, X., Wen, F.-Q., Zhu, Y.K., Wang, H., Kim, H.J., et al. (2002b). PDE4 inhibitors attenuate fibroblast chemotaxis and contraction of native collagen gels. Am. J. Respir. Cell Mol. Biol. *26*: 694–701.

Koli, K., Saharinen, J., Hyytiäinen, M., Penttinen, C., and Keski-Oja, J. (2001). Latency, activation, and binding proteins of TGF-β. Microsc. Res. Tech. *52*: 354–362.

Kolodsick, J.E., Peters-Golden, M., Larios, J., Toews, G.B., Thannickal, V.J., and Moore, B.B. (2003). Prostaglandin E2 inhibits fibroblast to myofibroblast transition via E. prostanoid receptor 2 signaling and cyclic adenosine monophosphate elevation. Am.J.Respir.Cell Mol.Biol. *29*: 537–544.

Konigshoff, M., Balsara, N., Pfaff, E.M., Kramer, M., Chrobak, I., Seeger, W., et al. (2008). Functional Wnt signaling is increased in idiopathic pulmonary fibrosis. PLoS.One. *3*: e2142–.

Konigshoff, M., and Eickelberg, O. (2010). WNT signaling in lung disease: a failure or a regeneration signal? Am.J.Respir.Cell Mol.Biol. *42*: 21–31.

Kono, Y., Nishiuma, T., Nishimura, Y., Kotani, Y., Okada, T., Nakamura, S.-I., et al. (2007). Sphingosine kinase 1 regulates differentiation of human and mouse lung fibroblasts mediated by TGF-beta1. Am. J. Respir. Cell Mol. Biol. *37*: 395–404.

Korfei, M., Ruppert, C., Mahavadi, P., Henneke, I., Markart, P., Koch, M., et al. (2008). Epithelial endoplasmic reticulum stress and apoptosis in sporadic idiopathic pulmonary fibrosis. Am. J. Respir. Crit. Care Med. *178*: 838–846.

Krämer, J., Quensel, C., Meding, J., Cardoso, M.C., and Leonhardt, H. (2001). Identification and characterization of novel smoothelin isoforms in vascular smooth muscle. J. Vasc. Res. *38*: 120–32.

Kubota, S., Takezawa, T., Mori, Y., and Takakuwa, T. (1992). [A new method of in vitro chemosensitivity test using multicellular spheroids of cholangiocarcinoma cell line cocultured with fibroblasts]. Nihon Geka Gakkai Zasshi *93*: 960–963.

Kuhn, C., and McDonald, J.A. (1991). The roles of the myofibroblast in idiopathic pulmonary fibrosis. Ultrastructural and immunohistochemical features of sites of active extracellular matrix synthesis. Am J Pathol *138*: 1257–1265.

Kukkola, L., Hieta, R., Kivirikko, K.I., and Myllyharju, J. (2003). Identification and characterization of a third human, rat, and mouse collagen prolyl 4-hydroxylase isoenzyme. J.Biol.Chem. *278*: 47685–47693.

Kunz-Schughart, L.A., Heyder, P., Schroeder, J., and Knuechel, R. (2001). A heterologous 3-D coculture model of breast tumor cells and fibroblasts to study tumor-associated fibroblast differentiation. Exp.Cell Res. *266*: 74–86.

Kunz-Schughart, L.A., Kreutz, M., and Knuechel, R. (1998). Multicellular spheroids: a three-dimensional in vitro culture system to study tumour biology. Int.J.Exp.Pathol. *79*: 1–23.

Kuwano, K., Hagimoto, N., Kawasaki, M., Yatomi, T., Nakamura, N., Nagata, S., et al. (1999a). Essential roles of the Fas-Fas ligand pathway in the development of pulmonary fibrosis. J. Clin. Invest. *104*: 13–19.

Kuwano, K., Miyazaki, H., Hagimoto, N., Kawasaki, M., Fujita, M., Kunitake, R., et al. (1999b). The involvement of Fas-Fas ligand pathway in fibrosing lung diseases. Am. J. Respir. Cell Mol. Biol. *20*: 53–60.

Lahiri, S., and Futerman, A.H. (2007). The metabolism and function of sphingolipids and glycosphingolipids. Cell. Mol. Life Sci. *64*: 2270–2284.

Lalmanach, G., Diot, E., Godat, E., Lecaille, F., and Hervé-Grépinet, V. (2006). Cysteine cathepsins and caspases in silicosis. In Biological Chemistry, pp 863–870.

Lama, V., Moore, B.B., Christensen, P., Toews, G.B., and Peters-Golden, M. (2002). Prostaglandin E2 synthesis and suppression of fibroblast proliferation by alveolar epithelial cells is cyclooxygenase-2-dependent. Am.J.Respir.Cell Mol.Biol. *27*: 752–758.

Lamande, S.R., and Bateman, J.F. (1999). Procollagen folding and assembly: the role of endoplasmic reticulum enzymes and molecular chaperones. Semin. Dev.Biol. *10*: 455–464.

Lammi, L., Ryhänen, L., Lakari, E., Risteli, J., Pääkkö, P., Kahlos, K., et al. (1999). Type III and type I procollagen markers in fibrosing alveolitis. Am. J. Respir. Crit. Care Med. *159*: 818–823.

Lanone, S., Zheng, T., Zhu, Z., Liu, W., Lee, C.G., Ma, B., et al. (2002). Overlapping and enzyme-specific contributions of matrix metalloproteinases-9 and -12 in IL-13–induced inflammation and remodeling. J. Clin. Invest. *110*: 463–474.

Lareu, R.R., Arsianti, I., Subramhanya, H.K., Yanxian, P., and Raghunath, M. (2007a). In vitro enhancement of collagen matrix formation and crosslinking for applications in tissue engineering: a preliminary study. Tissue Eng. *13*: 385–391.

Lareu, R.R., Subramhanya, K.H., Peng, Y., Benny, P., Chen, C., Wang, Z., et al. (2007b). Collagen matrix deposition is dramatically enhanced in vitro when crowded with charged macromolecules: The biological relevance of the excluded volume effect. FEBS Lett. *581*: 2709–2714.

Larsson, O., Diebold, D., Fan, D., Peterson, M., Nho, R.S., Bitterman, P.B., et al. (2008). Fibrotic myofibroblasts manifest genome-wide derangements of translational control. PLoS One *3*:

Last, J.A., and Reiser, K.M. (1984). Collagen biosynthesis. Environ.Health Perspect. *55*: 169–177.

Laurent, G.J., and Shapiro, S.J. (2006). Encyclpedia of Respiratory Medicine, Four-Volume Set. -.

Lawson, W.E., Crossno, P.F., Polosukhin, V. V, Roldan, J., Cheng, D.-S., Lane, K.B., et al. (2008). Endoplasmic reticulum stress in alveolar epithelial cells is prominent in IPF: association with altered surfactant protein processing and herpesvirus infection. Am. J. Physiol. Lung Cell. Mol. Physiol. *294*: L1119–L1126.

Lecaille, F., Kaleta, J., and Brömme, D. (2002). Human and parasitic Papain-like cysteine proteases: Their role in physiology and pathology and recent developments in inhibitor design. Chem. Rev. *102*: 4459–4488.

Lee, C.G., Cho, S.J., Kang, M.J., Chapoval, S.P., Lee, P.J., Noble, P.W., et al. (2004). Early growth response gene 1-mediated apoptosis is essential for transforming growth factor beta1-induced pulmonary fibrosis. J. Exp. Med. *200*: 377–389.

Lee, C.G., Kang, H.-R., Homer, R.J., Chupp, G., and Elias, J.A. (2006). Transgenic modeling of transforming growth factor-beta(1): role of apoptosis in fibrosis and alveolar remodeling. Proc. Am. Thorac. Soc. *3*: 418–423.

Lee, E.J., Park, S.J., Kang, S.K., Kim, G.-H., Kang, H.-J., Lee, S.-W., et al. (2012). Spherical Bullet Formation via E-cadherin Promotes Therapeutic Potency of Mesenchymal Stem Cells Derived From Human Umbilical Cord Blood for Myocardial Infarction. Mol. Ther. *20*: 1424–1433.

Lee, J., Cuddihy, M.J., and Kotov, N.A. (2008). Three-dimensional cell culture matrices: state of the art. Tissue Eng. Part B. Rev. *14*: 61–86.

Lee, M.K., Yoo, J.W., Lin, H., Kim, Y.S., Kim, D.D., Choi, Y.M., et al. (2005). Air-liquid interface culture of serially passaged human nasal epithelial cell monolayer for in vitro drug transport studies. Drug Deliv. *12*: 305–311.

Leitinger, B. (2003). Molecular analysis of collagen binding by the human discoidin domain receptors, DDR1 and DDR2. Identification of collagen binding sites in DDR2. J.Biol.Chem. *278*: 16761–16769.

Leitinger, B. (2011). Transmembrane collagen receptors. Annu. Dev.Biol. *27*: 265–290.

Li, L., and Lu, Y. (2011). Optimizing a 3D Culture System to Study the Interaction between Epithelial Breast Cancer and Its Surrounding Fibroblasts. J.Cancer *2*: 458–466.

Lin, C.-C., Cheng, T.-L., Tsai, W.-H., Tsai, H.-J., Hu, K.-H., Chang, H.-C., et al. (2012). Loss of the respiratory enzyme citrate synthase directly links the Warburg effect to tumor malignancy. Sci. Rep. *2*: 785.

Lindahl, G.E., Stock, C.J., Shi-Wen, X., Leoni, P., Sestini, P., Howat, S.L., et al. (2013). Microarray profiling reveals suppressed interferon stimulated gene program in fibroblasts from scleroderma-associated interstitial lung disease. Respir. Res. *14*: 80.

Lingwood, D., and Simons, K. (2010). Lipid rafts as a membrane-organizing principle. Science *327*: 46–50.

Lipshutz, R.J., Morris, D., Chee, M., Hubbell, E., Kozal, M.J., Shah, N., et al. (1995). Using oligonucleotide probe arrays to access genetic diversity. Biotechniques *19*: 442–447.

Litingtung, Y., Lei, L., Westphal, H., and Chiang, C. (1998). Sonic hedgehog is essential to foregut development. Nat. Genet. *20*: 58–61.

Liu, B., Li, S., and Hu, J. (2004). Technological advances in high-throughput screening. Am. J. Pharmacogenomics *4*: 263–276.

Liu, R.-M. (2008). Oxidative stress, plasminogen activator inhibitor 1, and lung fibrosis. Antioxid. Redox Signal. *10*: 303–319.

Liu, X., Das, A.M., Seideman, J., Griswold, D., Afuh, C.N., Kobayashi, T., et al. (2007). The CC chemokine ligand 2 (CCL2) mediates fibroblast survival through IL-6. Am. J. Respir. Cell Mol. Biol. *37*: 121–128.

Lodish, H., Berk, A., and SL, Z. (2000). "Collagen: The Fibrous Proteins of the Matrix" in Molecular Cell Biology. 4th edition. -.

Loop, F.T. van der, Schaart, G., Timmer, E.D., Ramaekers, F.C., and Eys, G.J. van (1996). Smoothelin, a novel cytoskeletal protein specific for smooth muscle cells. J. Cell Biol. *134*: 401–411.

Lovgren, A.K., Jania, L.A., Hartney, J.M., Parsons, K.K., Audoly, L.P., Fitzgerald, G.A., et al. (2006). COX-2-derived prostacyclin protects against bleomycin-induced pulmonary fibrosis. Am. J. Physiol. Lung Cell. Mol. Physiol. *291*: L144–L156.

Lovgren, A.K., Kovacs, J.J., Xie, T., Potts, E.N., Li, Y., Foster, W.M., et al. (2011). {beta}-Arrestin Deficiency Protects Against Pulmonary Fibrosis in Mice and Prevents Fibroblast Invasion of Extracellular Matrix. Sci.Transl.Med. *3*: 74ra23–.

MacNicol, M., Jefferson, A.B., and Schulman, H. (1990). Ca2+/calmodulin kinase is activated by the phosphatidylinositol signaling pathway and becomes Ca2(+)-independent in PC12 cells. J. Biol. Chem. *265* : 18055–18058.

Maeyama, T., Kuwano, K., Kawasaki, M., Kunitake, R., Hagimoto, N., Matsuba, T., et al. (2001). Upregulation of Fas-signalling molecules in lung epithelial cells from patients with idiopathic pulmonary fibrosis. Eur. Respir. J. *17*: 180–9.

Maher, T.M., Evans, I.C., Bottoms, S.E., Mercer, P.F., Thorley, A.J., Nicholson, A.G., et al. (2010). Diminished prostaglandin E2 contributes to the apoptosis paradox in idiopathic pulmonary fibrosis. Am.J.Respir.Crit Care Med. *182*: 73–82.

Maki, J.M., Sormunen, R., Lippo, S., Kaarteenaho-Wiik, R., Soininen, R., and Myllyharju, J. (2005). Lysyl oxidase is essential for normal development and function of the respiratory system and for the integrity of elastic and collagen fibers in various tissues. Am.J.Pathol. *167*: 927–936.

Mammoto, T., Jiang, E., Jiang, A., and Mammoto, A. (2013). Extracellular matrix structure and tissue stiffness control postnatal lung development through the lipoprotein receptor-related protein 5/Tie2 signaling system. Am.J.Respir.Cell Mol.Biol. *49*: 1009–1018.

Marchand-Adam, S., Marchal, J., Cohen, M., Soler, P., Gerard, B., Castier, Y., et al. (2003). Defect of hepatocyte growth factor secretion by fibroblasts in idiopathic pulmonary fibrosis. Am J Respir Crit Care Med *168*: 1156–1161.

Margadant, C., and Sonnenberg, A. (2010). Integrin-TGF-beta crosstalk in fibrosis, cancer and wound healing. EMBO Rep. *11*: 97–105.

Maruhashi, T., Kii, I., Saito, M., and Kudo, A. (2010). Interaction between periostin and BMP-1 promotes proteolytic activation of lysyl oxidase. J. Biol. Chem. *285*: 13294–13303.

Masuda, H., Owaribe, K., Hayashi, H., and Hatano, S. (1984). Ca2+-dependent contraction of human lung fibroblasts treated with triton X-100: A role of Ca2+-calmodulin-dependent phosphorylation of myosin 20,000-dalton light chain. Cell Motil. *4*: 315–331.

Matrisian, L.M. (1990). Metalloproteinases and their inhibitors in matrix remodeling. Trends Genet. *6*: 121–125.

Matsuo, T., Takabatake, M., and Matsuo, N. (1997). The effects of growth factors on multicellular spheroids formed by chick embryonic retinal cells. Acta Med.Okayama *51*: 251–260.

Matsuse, T., Fukuchi, Y., Eto, Y., Matsui, H., Hosoi, T., Oka, T., et al. (1995). Expression of immunoreactive and bioactive activin A protein in adult murine lung after bleomycin treatment. Am. J. Respir. Cell Mol. Biol. *13*: 17–24.

Matsuse, T., Ikegami, A., Ohga, E., Hosoi, T., Oka, T., Kida, K., et al. (1996). Expression of immunoreactive activin A protein in remodeling lesions associated with interstitial pulmonary fibrosis. Am. J. Pathol. *148*: 707–713.

Mbonye, U.R., and Song, I. (2009). Posttranscriptional and posttranslational determinants of cyclooxygenase expression. BMB Rep. *42*: 552–560.

McAnulty, R.J., and Laurent, G.J. (1987). Collagen synthesis and degradation in vivo. Evidence for rapid rates of collagen turnover with extensive degradation of newly synthesized collagen in tissues of the adult rat. Coll. Relat. Res. *7*: 93–104.

McCall-Culbreath, K.D., and Zutter, M.M. (2008). Collagen receptor integrins: rising to the challenge. Curr.Drug Targets. *9*: 139–149.

McKeown, S., Richter, A.G., O'Kane, C., McAuley, D.F., and Thickett, D.R. (2009). MMP expression and abnormal lung permeability are important determinants of outcome in IPF. Eur. Respir. J. Off. J. Eur. Soc. Clin. Respir. Physiol. *33*: 77–84.

Meltzer, E.B., and Noble, P.W. (2008). Idiopathic pulmonary fibrosis. Orphanet.J.Rare.Dis. *3*: 8–
.

Miki, H., Mio, T., Nagai, S., Hoshino, Y., Nagao, T., Kitaichi, M., et al. (2000). Fibroblast contractility: usual interstitial pneumonia and nonspecific interstitial pneumonia. Am. J. Respir. Crit. Care Med. *162*: 2259–2264.

Miller, M.B., and Tang, Y.W. (2009). Basic concepts of microarrays and potential applications in clinical microbiology. Clin.Microbiol.Rev. *22*: 611–633.

Mitchell, H., Choudhury, A., Pagano, R.E., and Leof, E.B. (2004). Ligand-dependent and -independent Transforming Growth Factor-β Receptor Recycling Regulated by Clathrin-mediated Endocytosis and Rab11. Mol. Biol. Cell *15* : 4166–4178.

Miyazaki, Y., Araki, K., Vesin, C., Garcia, I., Kapanci, Y., Whitsett, J.A., et al. (1995). Expression of a tumor necrosis factor-α transgene in murine lung causes lymphocytic and fibrosing alveolitis: A mouse model of progressive pulmonary fibrosis. J. Clin. Invest. *96*: 250–259.

Miyazono, K., and Heldin, C.H. (1991). Latent forms of TGF-beta: molecular structure and mechanisms of activation. Ciba Found. Symp. *157*: 81–89; discussion 89–92.

Miyazono, K., Olofsson, A., Colosetti, P., and Heldin, C.H. (1991). A role of the latent TGF-beta 1-binding protein in the assembly and secretion of TGF-beta 1. EMBO J. *10*: 1091–1101.

Mizuno, K., Hayashi, T., and Bachinger, H.P. (2003). Hydroxylation-induced stabilization of the collagen triple helix. Further characterization of peptides with 4(R)-hydroxyproline in the Xaa position. J.Biol.Chem. *278*: 32373–32379.

Moeller, A., Ask, K., Warburton, D., Gauldie, J., and Kolb, M. (2008). The bleomycin animal model: a useful tool to investigate treatment options for idiopathic pulmonary fibrosis? Int.J.Biochem.Cell Biol. *40*: 362–382.

Montaño, M., Ramos, C., González, G., Vadillo, F., Pardo, A., and Selman, M. (1989). Lung collagenase inhibitors and spontaneous and latent collagenase activity in idiopathic pulmonary fibrosis and hypersensitivity pneumonitis. Chest *96*: 1115–1119.

Moodley, Y.P., Caterina, P., Scaffidi, A.K., Misso, N.L., Papadimitriou, J.M., McAnulty, R.J., et al. (2004). Comparison of the morphological and biochemical changes in normal human lung fibroblasts and fibroblasts derived from lungs of patients with idiopathic pulmonary fibrosis during FasL-induced apoptosis. J. Pathol. *202*: 486–495.

Moodley, Y.P., Misso, N.L.A., Scaffidi, A.K., Fogel-Petrovic, M., McAnulty, R.J., Laurent, G.J., et al. (2003). Inverse effects of interleukin-6 on apoptosis of fibroblasts from pulmonary fibrosis and normal lungs. Am. J. Respir. Cell Mol. Biol. *29*: 490–498.

Moore, B.B., Ballinger, M.N., White, E.S., Green, M.E., Herrygers, A.B., Wilke, C.A., et al. (2005a). Bleomycin-induced E prostanoid receptor changes alter fibroblast responses to prostaglandin E2. J. Immunol. *174*: 5644–5649.

Moore, B.B., and Hogaboam, C.M. (2008). Murine models of pulmonary fibrosis. Am.J.Physiol Lung Cell Mol.Physiol *294*: L152–L160.

Moore, B.B., Kolodsick, J.E., Thannickal, V.J., Cooke, K., Moore, T.A., Hogaboam, C., et al. (2005b). CCR2-mediated recruitment of fibrocytes to the alveolar space after fibrotic injury. Am. J. Pathol. *166*: 675–684.

Moore, B.B., Lawson, W.E., Oury, T.D., Sisson, T.H., Raghavendran, K., and Hogaboam, C.M. (2013). Animal models of fibrotic lung disease. Am. J. Respir. Cell Mol. Biol. *49*: 167–79.

Moore, B.B., Paine, R., Christensen, P.J., Moore, T.A., Sitterding, S., Ngan, R., et al. (2001). Protection from pulmonary fibrosis in the absence of CCR2 signaling. J. Immunol. *167*: 4368–4377.

Moore, B.B., Peters-Golden, M., Christensen, P.J., Lama, V., Kuziel, W.A., Paine, R., et al. (2003). Alveolar epithelial cell inhibition of fibroblast proliferation is regulated by MCP-1/CCR2 and mediated by PGE2. Am. J. Physiol. Lung Cell. Mol. Physiol. *284*: L342–L349.

Moraes, C., Mehta, G., Lesher-Perez, S., and Takayama, S. (2011). Organs-on-a-Chip: A Focus on Compartmentalized Microdevices. Ann. Biomed. Eng. 1–17.

Morand, E.F. (2005). New therapeutic target in inflammatory disease: macrophage migration inhibitory factor. Intern. Med. J. *35*: 419–426.

Moustakas, A., and Heldin, C.-H. (2005). Non-Smad TGF-beta signals. J. Cell Sci. *118*: 3573–3584.

Mu, D. (2002). The integrin alphavbeta8 mediates epithelial homeostasis through MT1-MMP-dependent activation of TGF-beta1. J. Cell Biol. *157*: 493–507.

Mu, Y., Gudey, S.K., and Landström, M. (2012). Non-Smad signaling pathways. Cell Tissue Res. *347*: 11–20.

Munger, J.S., Huang, X., Kawakatsu, H., Griffiths, M.J., Dalton, S.L., Wu, J., et al. (1999). The integrin alpha v beta 6 binds and activates latent TGF beta 1: a mechanism for regulating pulmonary inflammation and fibrosis. Cell *96*: 319–328.

Murad, S., Tajima, S., Johnson, G.R., Sivarajah, S., and Pinnell, S.R. (1983). Collagen synthesis in cultured human skin fibroblasts: effect of ascorbic acid and its analogs. J. Invest. Dermatol. *81*: 158–162.

Murakami, S., Nagaya, N., Itoh, T., Kataoka, M., Iwase, T., Horio, T., et al. (2006). Prostacyclin agonist with thromboxane synthase inhibitory activity (ONO-1301) attenuates bleomycin-induced pulmonary fibrosis in mice. Am. J. Physiol. Lung Cell. Mol. Physiol. *290*: L59–L65.

Murphy, G., Ward, R., Gavrilovic, J., and Atkinson, S. (1992). Physiological mechanisms for metalloproteinase activation. Matrix Suppl. *1*: 224–230.

Mutsaers, S.E., Bishop, J.E., McGrouther, G., and Laurent, G.J. (1997). Mechanisms of tissue repair: From wound healing to fibrosis. Int. J. Biochem. Cell Biol. *29*: 5–17.

Nagata, K. (1996). Hsp47: a collagen-specific molecular chaperone. Trends Biochem. *21*: 22–26.

Naik, P.K., Bozyk, P.D., Bentley, J.K., Popova, A.P., Birch, C.M., Wilke, C.A., et al. (2012). Periostin promotes fibrosis and predicts progression in patients with Idiopathic Pulmonary Fibrosis. AJP Lung Cell. Mol. Physiol.

Nakamura, T., Sugino, K., Titani, K., and Sugino, H. (1991). Follistatin, an activin-binding protein, associates with heparan sulfate chains of proteoglycans on follicular granulosa cells. J. Biol. Chem. *266*: 19432–19437.

Nakashima, J.M., Hyde, D.M., and Giri, S.N. (1986). Effects of a calmodulin inhibitor on bleomycin-induced lung inflammation in hamsters. Biochemical, morphometric, and bronchoalveolar lavage data. Am. J. Pathol. *124*: 528–536.

Nakatani, Y., Hokonohara, Y., Kakuta, S., Sudo, K., Iwakura, Y., and Kudo, I. (2007). Knockout mice lacking cPGES/p23, a constitutively expressed PGE2 synthetic enzyme, are peri-natally lethal. Biochem. Biophys. Res. Commun. *362*: 387–392.

Nakayama, S., Mukae, H., Sakamoto, N., Kakugawa, T., Yoshioka, S., Soda, H., et al. (2008). Pirfenidone inhibits the expression of HSP47 in TGF-beta1-stimulated human lung fibroblasts. Life Sci. *82*: 210–217.

Nakerakanti, S. (2012). The Role of TGF-β Receptors in Fibrosis. Open Rheumatol. J. *6*: 156–162.

Nam, Y.H., Lee, S.K., Sammut, D., Davies, D.E., and Howarth, P.H. (2012). Preliminary study of the cellular characteristics of primary bronchial fibroblasts in patients with asthma: expression of alpha-smooth muscle actin, fibronectin containing extra type III domain A, and smoothelin. J. Investig. Allergol. Clin. Immunol. *22*: 20–27.

Narumiya, S., Sugimoto, Y., and Ushikubi, F. (1999). Prostanoid receptors: structures, properties, and functions. Physiol. Rev. *79*: 1193–1226.

Navaratnam, V., Fleming, K.M., West, J., Smith, C.J., Jenkins, R.G., Fogarty, A., et al. (2011). The rising incidence of idiopathic pulmonary fibrosis in the U.K. Thorax *66*: 462–467.

Nho, R.S., and Hergert, P. (2014). IPF Fibroblasts Are Desensitized to Type I Collagen Matrix-Induced Cell Death by Suppressing Low Autophagy via Aberrant Akt/mTOR Kinases. PLoS One *9*: e94616.

Nicholson, A.G., Fulford, L.G., Colby, T. V, Bois, R.M. du, Hansell, D.M., and Wells, A.U. (2002). The relationship between individual histologic features and disease progression in idiopathic pulmonary fibrosis. Am.J.Respir.Crit Care Med. *166*: 173–177.

Nishihara, H., Kizaka-Kondoh, S., Insel, P.A., and Eckmann, L. (2003). Inhibition of apoptosis in normal and transformed intestinal epithelial cells by cAMP through induction of inhibitor of apoptosis protein (IAP)-2. Proc. Natl. Acad. Sci. *100* : 8921–8926.

Nishino, T., Miyazaki, M., Abe, K., Furusu, A., Mishima, Y., Harada, T., et al. (2003). Antisense oligonucleotides against collagen-binding stress protein HSP47 suppress peritoneal fibrosis in rats. Kidney Int. *64*: 887–896.

Nkyimbeng, T., Ruppert, C., Shiomi, T., Dahal, B., Lang, G., Seeger, W., et al. (2013). Pivotal role of matrix metalloproteinase 13 in extracellular matrix turnover in idiopathic pulmonary fibrosis. PLoS One *8*: e73279.

Noble, P.W., Albera, C., Bradford, W.Z., Costabel, U., Glassberg, M.K., Kardatzke, D., et al. (2011). Pirfenidone in patients with idiopathic pulmonary fibrosis (CAPACITY): two randomised trials. Lancet *377*: 1760–1769.

Noble, P.W., Barkauskas, C.E., and Jiang, D. (2012). Pulmonary fibrosis: patterns and perpetrators. J.Clin.Invest *122*: 2756–2762.

Novinec, M., and Lenarčic, B. (2013). Cathepsin K: A unique collagenolytic cysteine peptidase. Biol. Chem. *394*: 1163–1179.

Nunes, I., Gleizes, P.E., Metz, C.N., and Rifkin, D.B. (1997). Latent transforming growth factor-beta binding protein domains involved in activation and transglutaminase-dependent cross-linking of latent transforming growth factor-beta. J. Cell Biol. *136*: 1151–1163.

O'Shea, K.S., Liu, L.H., Kinnunen, L.H., and Dixit, V.M. (1990). Role of the extracellular matrix protein thrombospondin in the early development of the mouse embryo. J. Cell Biol. *111* : 2713–2723.

Obata, Y., Nishino, T., Kushibiki, T., Tomoshige, R., Xia, Z., Miyazaki, M., et al. (2012). HSP47 siRNA conjugated with cationized gelatin microspheres suppresses peritoneal fibrosis in mice. Acta Biomater. *8*: 2688–2696.

Obberghen-Schilling, E. Van, Roche, N.S., Flanders, K.C., Sporn, M.B., and Roberts, A.B. (1988). Transforming growth factor beta 1 positively regulates its own expression in normal and transformed cells. J. Biol. Chem. *263*: 7741–7746.

Oga, T., Matsuoka, T., Yao, C., Nonomura, K., Kitaoka, S., Sakata, D., et al. (2009). Prostaglandin F(2alpha) receptor signaling facilitates bleomycin-induced pulmonary fibrosis independently of transforming growth factor-beta. Nat. Med. *15*: 1426–1430.

Ohga, E., Matsuse, T., Teramoto, S., Katayama, H., Nagase, T., Fukuchi, Y., et al. (1996). Effects of activin A on proliferation and differentiation of human lung fibroblasts. Biochem Biophys Res Commun *228*: 391–396.

Ohga, E., Matsuse, T., Teramoto, S., and Ouchi, Y. (2000). Activin receptors are expressed on human lung fibroblast and activin A facilitates fibroblast-mediated collagen gel contraction. Life Sci. *66*: 1603–1613.

Okamoto, M., Hoshino, T., Kitasato, Y., Sakazaki, Y., Kawayama, T., Fujimoto, K., et al. (2011). Periostin, a matrix protein, is a novel biomarker for idiopathic interstitial pneumonias. Eur. Respir. J. *37*: 1119–27.

Oku, H., Nakazato, H., Horikawa, T., Tsuruta, Y., and Suzuki, R. (2002). Pirfenidone suppresses tumor necrosis factor-alpha, enhances interleukin-10 and protects mice from endotoxic shock. Eur. J. Pharmacol. *446*: 167–176.

Oku, H., Shimizu, T., Kawabata, T., Nagira, M., Hikita, I., Ueyama, A., et al. (2008). Antifibrotic action of pirfenidone and prednisolone: Different effects on pulmonary cytokines and growth factors in bleomycin-induced murine pulmonary fibrosis. Eur. J. Pharmacol. *590*: 400–408.

Okuma, T., Terasaki, Y., Kaikita, K., Kobayashi, H., Kuziel, W.A., Kawasuji, M., et al. (2004). C-C chemokine receptor 2 (CCR2) deficiency improves bleomycin-induced pulmonary fibrosis by attenuation of both macrophage infiltration and production of macrophage-derived matrix metalloproteinases. J. Pathol. *204*: 594–604.

Olejar, T., and Nouza, K. (1999). Thrombin and trypsin receptors: the same mechanism of signalling on cellular surfaces. Bratisl.Lek.Listy *100*: 75–79.

Orphanet Report Series (2013). Prevalence of rare diseases : bibliographic data.

Ozaki, T., Hayashi, H., Tani, K., Ogushi, F., Yasuoka, S., and Ogura, T. (1992). Neutrophil Chemotactic Factors in the Respiratory Tract of Patients with Chronic Airway Diseases or Idiopathic Pulmonary Fibrosis. Am. Rev. Respir. Dis. *145*: 85–91.

Paine-Saunders, S., Viviano, B.L., Zupicich, J., Skarnes, W.C., and Saunders, S. (2000). glypican-3 controls cellular responses to Bmp4 in limb patterning and skeletal development. Dev. Biol. *225*: 179–187.

Pannu, J., Nakerakanti, S., Smith, E., Dijke, P. ten, and Trojanowska, M. (2007). Transforming growth factor-beta receptor type I-dependent fibrogenic gene program is mediated via activation of Smad1 and ERK1/2 pathways.

Pardo, A., Gibson, K., Cisneros, J., Richards, T.J., Yang, Y., Becerril, C., et al. (2005). Up-Regulation and Profibrotic Role of Osteopontin in Human Idiopathic Pulmonary Fibrosis. PLoS Med *2*: e251.

Pardo, A., Selman, M., and Kaminski, N. (2008). Approaching the degradome in idiopathic pulmonary fibrosis. Int. J. Biochem. Cell Biol. *40*: 1141–1155.

Pena, R.A., Jerdan, J.A., and Glaser, B.M. (1994). Effects of TGF-beta and TGF-beta neutralizing antibodies on fibroblast-induced collagen gel contraction: implications for proliferative vitreoretinopathy. Invest. Ophthalmol. Vis. Sci. *35*: 2804–2808.

Pepicelli, C. V, Lewis, P.M., and McMahon, A.P. (1998). Sonic hedgehog regulates branching morphogenesis in the mammalian lung. Curr. Biol. *8*: 1083–1086.

Peters-Golden, M., Bailie, M., Marshall, T., Wilke, C., Phan, S.H., Toews, G.B., et al. (2002). Protection from pulmonary fibrosis in leukotriene-deficient mice. Am. J. Respir. Crit. Care Med. *165*: 229–235.

Petkova, D.K., Clelland, C.A., Ronan, J.E., Lewis, S., and Knox, A.J. (2003). Reduced expression of cyclooxygenase (COX) in idiopathic pulmonary fibrosis and sarcoidosis. Histopathology *43*: 381–386.

Phan, S.H. (2008). Biology of fibroblasts and myofibroblasts. Proc.Am.Thorac.Soc. *5*: 334–337.

Piguet, P.F., Collart, M.A., Grau, G.E., Kapanci, Y., and Vassalli, P. (1989). Tumor necrosis factor/cachectin plays a key role in bleomycin-induced pneumopathy and fibrosis. J. Exp. Med. *170*: 655–663.

Piguet, P.F., Ribaux, C., Karpuz, V., Grau, G.E., and Kapanci, Y. (1993). Expression and localization of tumor necrosis factor-alpha and its mRNA in idiopathic pulmonary fibrosis. Am J Pathol *143*: 651–5.

Plataki, M., Koutsopoulos, A. V, Darivianaki, K., Delides, G., Siafakas, N.M., and Bouros, D. (2005). Expression of apoptotic and antiapoptotic markers in epithelial cells in idiopathic pulmonary fibrosis. Chest *127*: 266–274.

Poletti, V., Ravaglia, C., and Tomassetti, S. (2014). Pirfenidone for the treatment of idiopathic pulmonary fibrosis. Expert Rev. Respir. Med. 1–7.

Postlethwaite, A.E., Keski-Oja, J., Moses, H.L., and Kang, A.H. (1987). Stimulation of the chemotactic migration of human fibroblasts by transforming growth factor beta. J Exp Med *165*: 251–256.

Price, A.L., Patterson, N.J., Plenge, R.M., Weinblatt, M.E., Shadick, N. a, and Reich, D. (2006). Principal components analysis corrects for stratification in genome-wide association studies. Nat. Genet. *38*: 904–9.

Qiao, J., Zhang, M., Bi, J., Wang, X., Deng, G., He, G., et al. (2009). Pulmonary fibrosis induced by H5N1 viral infection in mice. Respir. Res. *10*: 107.

Quan, G., Choi, J.Y., Lee, D.S., and Lee, S.C. (2005). TGF-beta 1 up-regulates transglutaminase two and fibronectin in dermal fibroblasts: A possible mechanism for the stabilization of tissue inflammation. Arch. Dermatol. Res. *297*: 84–90.

Quinn, D.J., Weldon, S., and Taggart, C.C. (2010). Antiproteases as therapeutics to target inflammation in cystic fibrosis. Open Respir. Med. J. *4*: 20–31.

Rafii, R., Juarez, M.M., Albertson, T.E., and Chan, A.L. (2013). A review of current and novel therapies for idiopathic pulmonary fibrosis. J.Thorac.Dis. *5*: 48–73.

Raghu, G., Brown, K.K., Costabel, U., Cottin, V., Bois, R.M. Du, Lasky, J.A., et al. (2008). Treatment of idiopathic pulmonary fibrosis with etanercept: An exploratory, placebo-controlled trial. Am. J. Respir. Crit. Care Med. *178*: 948–955.

Raghu, G., Chen, Y.Y., Rusch, V., and Rabinovitch, P.S. (1988). Differential proliferation of fibroblasts cultured from normal and fibrotic human lungs. Am. Rev. Respir. Dis. *138*: 703–708.

Raghu, G., Collard, H.R., Egan, J.J., Martinez, F.J., Behr, J., Brown, K.K., et al. (2011). An official ATS/ERS/JRS/ALAT statement: idiopathic pulmonary fibrosis: evidence-based guidelines for diagnosis and management. Am.J.Respir.Crit Care Med. *183*: 788–824.

Raghu, G., Striker, L.J., Hudson, L.D., and Striker, G.E. (1985). Extracellular matrix in normal and fibrotic human lungs. Am. Rev. Respir. Dis. *131*: 281–289.

Raghu, G., Weycker, D., Edelsberg, J., Bradford, W.Z., and Oster, G. (2006). Incidence and prevalence of idiopathic pulmonary fibrosis. Am.J.Respir.Crit Care Med. *174*: 810–816.

Rahaman, S.O., Dominak, L.M., Paruchuri, S., Southern, B.D., Abraham, S., Niese, K.A., et al. (2014). Trpv4 Calcium Channel Deficiency Protects Against Pulmonary Fibrosis In Mice And Abrogates Myofibroblast Differentiation.

Rahimi, R.A., and Leof, E.B. (2007). TGF-?? signaling: A tale of two responses. J. Cell. Biochem. *102*: 593–608.

Rahnama'i, M.S., Kerrebroeck, P.E. V van, Wachter, S.G. de, and Koeveringe, G.A. van (2012). The role of prostanoids in urinary bladder physiology. Nat Rev Urol *9*: 283–290.

Rama-Esendagli, D., Esendagli, G., Yilmaz, G., and Guc, D. (2014). Spheroid formation and invasion capacity are differentially influenced by co-cultures of fibroblast and macrophage cells in breast cancer. Mol. Biol. Rep. 1–8.

Ramos, C., and Becerril, C. (2010). FGF-1 reverts epithelial-mesenchymal transition induced by TGF-β1 through MAPK/ERK kinase pathway. Am. J. … *229*: 222–231.

Ramos, C., Montaño, M., García-Alvarez, J., Ruiz, V., Uhal, B.D., Selman, M., et al. (2001). Fibroblasts from idiopathic pulmonary fibrosis and normal lungs differ in growth rate, apoptosis, and tissue inhibitor of metalloproteinases expression. Am. J. Respir. Cell Mol. Biol. *24*: 591–598.

Raugi, G.J., Olerud, J.E., and Gown, A.M. (1987). Thrombospondin in early human wound tissue. J. Invest. Dermatol. *89*: 551–554.

Reed, M.J., Iruela-Arispe, L., O'Brien, E.R., Truong, T., LaBell, T., Bornstein, P., et al. (1995). Expression of thrombospondins by endothelial cells. Injury is correlated with TSP-1. Am. J. Pathol. *147*: 1068–1080.

Reichsman, F., Smith, L., and Cumberledge, S. (1996). Glycosaminoglycans can modulate extracellular localization of the wingless protein and promote signal transduction. J. Cell Biol. *135*: 819–827.

Reiser, K., McCormick, R.J., and Rucker, R.B. (1992). Enzymatic and nonenzymatic cross-linking of collagen and elastin. FASEB J. *6*: 2439–2449.

Renzoni, E.A., Abraham, D.J., Howat, S., Shi-Wen, X., Sestini, P., Bou-Gharios, G., et al. (2004). Gene expression profiling reveals novel TGFbeta targets in adult lung fibroblasts. Respir. Res. *5*: 24.

Richeldi, L., Bois, R.M. du, Raghu, G., Azuma, A., Brown, K.K., Costabel, U., et al. (2014). Efficacy and Safety of Nintedanib in Idiopathic Pulmonary Fibrosis. Supplement material. N. Engl. J. Med.

Richeldi, L., Costabel, U., Selman, M., Kim, D.S., Hansell, D.M., Nicholson, A.G., et al. (2011). Efficacy of a tyrosine kinase inhibitor in idiopathic pulmonary fibrosis. N. Engl. J. Med. *365*: 1079–87.

Richter, A.G., McKeown, S., Rathinam, S., Harper, L., Rajesh, P., McAuley, D.F., et al. (2009). Soluble endostatin is a novel inhibitor of epithelial repair in idiopathic pulmonary fibrosis. Thorax *64*: 156–161.

Ringner, M. (2008). What is principal component analysis? Nat Biotechnol *26*: 303–304.

Riobo, N.A., and Manning, D.R. (2007). Pathways of signal transduction employed by vertebrate Hedgehogs. Biochem. J. *403*: 369–379.

Risteli, M., Niemitalo, O., Lankinen, H., Juffer, A.H., and Myllyla, R. (2004). Characterization of collagenous peptides bound to lysyl hydroxylase isoforms. J.Biol.Chem. *279*: 37535–37543.

Riteau, N., Gasse, P., Fauconnier, L., Gombault, A., Couegnat, M., Fick, L., et al. (2010). Extracellular ATP is a danger signal activating P2X7 receptor in lung inflammation and fibrosis. Am. J. Respir. Crit. Care Med. *182*: 774–783.

Ritter, S.J., and Davies, P.J. (1998). Identification of a transforming growth factor-beta1/bone morphogenetic protein 4 (TGF-beta1/BMP4) response element within the mouse tissue transglutaminase gene promoter. J. Biol. Chem. *273*: 12798–12806.

Rivera, R., and Chun, J. (2008). Biological effects of lysophospholipids. Rev. Physiol. Biochem. Pharmacol. *160*: 25–46.

Roach, K.M., Duffy, S.M., Coward, W., Feghali-Bostwick, C., Wulff, H., and Bradding, P. (2013). The K+ channel KCa3.1 as a novel target for idiopathic pulmonary fibrosis. PLoS One *8*:

Rock, J.R., Barkauskas, C.E., Cronce, M.J., Xue, Y., Harris, J.R., Liang, J., et al. (2011). Multiple stromal populations contribute to pulmonary fibrosis without evidence for epithelial to mesenchymal transition. Proc. Natl. Acad. Sci. *108* : E1475–E1483.

Rosas, I.O., Richards, T.J., Konishi, K., Zhang, Y., Gibson, K., Lokshin, A.E., et al. (2008). MMP1 and MMP7 as potential peripheral blood biomarkers in idiopathic pulmonary fibrosis. PLoS Med. *5*: 0623–0633.

Ruiz, P.A., and Jarai, G. (2011). Collagen I induces discoidin domain receptor (DDR) 1 expression through DDR2 and a JAK2-ERK1/2-mediated mechanism in primary human lung fibroblasts. J.Biol.Chem. *286*: 12912–12923.

Saar, M., Zhao, H., Nolley, R., Young, S.R., Coleman, I., Nelson, P.S., et al. (2014). Spheroid culture of LuCaP 147 as an authentic preclinical model of prostate cancer subtype with SPOP mutation and hypermutator phenotype. Cancer Lett.

Sagana, R.L., Yan, M., Cornett, A.M., Tsui, J.L., Stephenson, D.A., Huang, S.K., et al. (2009). Phosphatase and tensin homologue on chromosome 10 (PTEN) directs prostaglandin E2-mediated fibroblast responses via regulation of E prostanoid 2 receptor expression. J. Biol. Chem. *284*: 32264–32271.

Saharinen, J., Hyytiäinen, M., Taipale, J., and Keski-Oja, J. (1999). Latent transforming growth factor-beta binding proteins (LTBPs)--structural extracellular matrix proteins for targeting TGF-beta action. Cytokine Growth Factor Rev. *10*: 99–117.

Sakai, N., and Tager, A.M. (2013). Fibrosis of two: Epithelial cell-fibroblast interactions in pulmonary fibrosis. Biochim. Biophys. Acta - Mol. Basis Dis. *1832*: 911–921.

Saleh, F.A., Whyte, M., and Genever, P.G. (2011). Effects of endothelial cells on human mesenchymal stem cell activity in a three-dimensional in vitro model. Eur.Cell Mater. *22*: 242–257.

Salmenperä, P., Kankuri, E., Bizik, J., Sirén, V., Virtanen, I., Takahashi, S., et al. (2008). Formation and activation of fibroblast spheroids depend on fibronectin-integrin interaction. Exp. Cell Res. *314*: 3444–3452.

Samuelsson, B., Morgenstern, R., and Jakobsson, P.-J. (2007). Membrane prostaglandin E synthase-1: a novel therapeutic target. Pharmacol. Rev. *59*: 207–224.

Satoh, W., Takahashi, S., Sassa, F., Fukuda, J., and Suzuki, H. (2009). On-chip culturing of hepatocytes and monitoring their ammonia metabolism. Lab Chip. *9*: 35–37.

Sauk, J.J., Nikitakis, N., and Siavash, H. (2005). Hsp47 a novel collagen binding serpin chaperone, autoantigen and therapeutic target. Front Biosci. *10*: 107–118.

Schegg, B., Hulsmeier, A.J., Rutschmann, C., Maag, C., and Hennet, T. (2009). Core glycosylation of collagen is initiated by two beta(1-O)galactosyltransferases. Mol.Cell Biol. *29*: 943–952.

Schena, M., Shalon, D., Davis, R.W., and Brown, P.O. (1995). Quantitative monitoring of gene expression patterns with a complementary DNA microarray. Science *270*: 467–470.

Schittny, J.C., Paulsson, M., Vallan, C., Burri, P.H., Kedei, N., and Aeschlimann, D. (1997). Protein Cross-linking Mediated by Tissue Transglutaminase Correlates with the Maturation of Extracellular Matrices during Lung Development. Am. J. Respir. Cell Mol. Biol. *17*: 334–343.

Schnitzer, S.E., Weigert, A., Zhou, J., and Brüne, B. (2009). Hypoxia enhances sphingosine kinase 2 activity and provokes sphingosine-1-phosphate-mediated chemoresistance in A549 lung cancer cells. Mol. Cancer Res. *7*: 393–401.

Schroeder, A., Mueller, O., Stocker, S., Salowsky, R., Leiber, M., Gassmann, M., et al. (2006). The RIN: an RNA integrity number for assigning integrity values to RNA measurements. BMC.Mol.Biol. *7*: 3–.

Schuster, U., Buttner, R., Hofstadter, F., and Knuchel, R. (1994). A heterologous in vitro coculture system to study interaction between human bladder cancer cells and fibroblasts. J.Urol. *151*: 1707–1711.

Scotton, C.J. (2011). A breath of fresh air for tissue engineering? Mater. Today *14*: 212–216.

Scotton, C.J., and Chambers, R.C. (2007). Molecular targets in pulmonary fibrosis: the myofibroblast in focus. Chest *132*: 1311–1321.

Scotton, C.J., and Chambers, R.C. (2010). Bleomycin revisited: towards a more representative model of IPF? Am. J. Physiol. - Lung Cell. Mol. Physiol. *299*: L439–L441.

Scotton, C.J., Hayes, B., Alexander, R., Datta, A., Forty, E.J., Mercer, P.F., et al. (2013). Ex vivo micro-computed tomography analysis of bleomycin-induced lung fibrosis for preclinical drug evaluation. Eur.Respir.J. *42*: 1633–1645.

Scotton, C.J., Krupiczojc, M.A., Konigshoff, M., Mercer, P.F., Lee, Y.C., Kaminski, N., et al. (2009). Increased local expression of coagulation factor X contributes to the fibrotic response in human and murine lung injury. J.Clin.Invest *119*: 2550–2563.

Seibold, M.A., Wise, A.L., Speer, M.C., Steele, M.P., Brown, K.K., Loyd, J.E., et al. (2011). A common MUC5B promoter polymorphism and pulmonary fibrosis. N.Engl.J.Med. *364*: 1503–1512.

Selman, M. (2000). TIMP-1, -2, -3, and -4 in idiopathic pulmonary fibrosis. Am J Physiol Lung Cell Mol Physiol *279*: L562–L574.

Selman, M., Carrillo, G., Estrada, A., Mejia, M., Becerril, C., Cisneros, J., et al. (2007). Accelerated variant of idiopathic pulmonary fibrosis: clinical behavior and gene expression pattern. PLoS.One. *2*: e482–.

Selman, M., King, T.E., and Pardo, A. (2001). Idiopathic pulmonary fibrosis: prevailing and evolving hypotheses about its pathogenesis and implications for therapy. In Annals of Internal Medicine, pp 136–151.

Selman, M., and Pardo, A. (2002). Idiopathic pulmonary fibrosis: an epithelial/fibroblastic cross-talk disorder. Respir.Res. *3*: 3–.

Selman, M., and Pardo, A. (2006). Role of epithelial cells in idiopathic pulmonary fibrosis: from innocent targets to serial killers. Proc. Am. Thorac. Soc. *3*: 364–372.

Selman, M., Pardo, A., Barrera, L., Estrada, A., Watson, S.R., Wilson, K., et al. (2006). Gene expression profiles distinguish idiopathic pulmonary fibrosis from hypersensitivity pneumonitis. Am. J. Respir. Crit. Care Med. *173*: 188–198.

Selman, M., Pardo, A., Richeldi, L., and Cerri, S. (2011). Emerging drugs for idiopathic pulmonary fibrosis. Expert.Opin.Emerg.Drugs -.

Serini, G., and Gabbiani, G. (1999). Mechanisms of myofibroblast activity and phenotypic modulation. Exp. Cell Res. *250*: 273–83.

Shannon, J.M., and Hyatt, B.A. (2004). Epithelial-mesenchymal interactions in the developing lung. Annu. Rev. Physiol. *66*: 625–645.

Shea, B.S. (2012). Sphingolipid Regulation of Tissue Fibrosis. Open Rheumatol. J. *6*: 123–129.

Shea, B.S., Brooks, S.F., Fontaine, B.A., Chun, J., Luster, A.D., and Tager, A.M. (2010). Prolonged exposure to sphingosine 1-phosphate receptor-1 agonists exacerbates vascular leak, fibrosis, and mortality after lung injury. Am. J. Respir. Cell Mol. Biol. *43*: 662–673.

Shepherd, M.C., Duffy, S.M., Harris, T., Cruse, G., Schuliga, M., Brightling, C.E., et al. (2007). KCa3.1 Ca2+ activated K+ channels regulate human airway smooth muscle proliferation. Am. J. Respir. Cell Mol. Biol. *37*: 525–531.

Shi, M., Zhu, J., Wang, R., Chen, X., Mi, L., Walz, T., et al. (2011). Latent TGF-beta structure and activation. Nature *474*: 343–349.

Shi, Y., and Massague, J. (2003). Mechanisms of TGF-beta signaling from cell membrane to the nucleus. Cell *113*: 685–700.

Shima, I., Kubota, S., Sasaguri, Y., Hamada, T., Arima, N., Ito, A., et al. (1995). Rearrangement of esophageal-carcinoma cells and stromal fibroblasts in a multicellular spheroid. Int.J.Oncol. *7*: 795–800.

Shrivastava, A., Radziejewski, C., Campbell, E., Kovac, L., McGlynn, M., Ryan, T.E., et al. (1997). An orphan receptor tyrosine kinase family whose members serve as nonintegrin collagen receptors. Mol.Cell *1*: 25–34.

Simon, L.S. (1999). Role and regulation of cyclooxygenase-2 during inflammation. In American Journal of Medicine,.

Sirianni, F.E., Chu, F.S.F., and Walker, D.C. (2003). Human alveolar wall fibroblasts directly link epithelial type 2 cells to capillary endothelium. Am. J. Respir. Crit. Care Med. *168*: 1532–1537.

Smalley, K.M., Lioni, M., and Herlyn, M. (2006). Life ins't flat: Taking cancer biology to the next dimension. Vitr. Cell. Dev. Biol. - Anim. *42*: 242–247.

Smith, B.T. (1977). Cell line A549: a model system for the study of alveolar type II cell function. Am.Rev.Respir.Dis. *115*: 285–293.

Smith, R.E., Strieter, R.M., Zhang, K., Phan, S.H., Standiford, T.J., Lukacs, N.W., et al. (1995). A role for C-C chemokines in fibrotic lung disease. J. Leukoc. Biol. *57*: 782–787.

Soberman Peter, R.J.C. (2006). Revisiting prostacyclin: new directions in pulmonary fibrosis and inflammation. Am. J. Physiol. - Lung Cell. Mol. Physiol. *291*: L142–L143.

Song, S.H., Jong, H.S., Choi, H.H., Inoue, H., Tanabe, T., Kim, N.K., et al. (2001). Transcriptional silencing of Cyclooxygenase-2 by hyper-methylation of the 5' CpG island in human gastric carcinoma cells. Cancer Res. *61*: 4628–4635.

Souchelnytskyi, S., Dijke, P. ten, Miyazono, K., and Heldin, C.H. (1996). Phosphorylation of Ser165 in TGF-beta type I receptor modulates TGF- beta1-induced cellular responses. Embo J *15*: 6231–40.

Spagnolo, P., Rossi, G., and Cavazza, A. (2014). Pathogenesis of idiopathic pulmonary fibrosis and its clinical implications. Expert Rev. Clin. Immunol. *10*: 1005–1017.

Spiro, R.G. (1969). Characterization and quantitative determination of the hydroxylysine-linked carbohydrate units of several collagens. J.Biol.Chem. *244*: 602–612.

Stratton, R., Shiwen, X., Martini, G., Holmes, A., Leask, A., Haberberger, T., et al. (2001). Iloprost suppresses connective tissue growth factor production in fibroblasts and in the skin of scleroderma patients. J. Clin. Invest. *108*: 241–250.

Strieter, R.M., Keeley, E.C., Hughes, M.A., Burdick, M.D., and Mehrad, B. (2009). The role of circulating mesenchymal progenitor cells (fibrocytes) in the pathogenesis of pulmonary fibrosis. J.Leukoc.Biol. *86*: 1111–1118.

Subramanian, A., Tamayo, P., Mootha, V.K., Mukherjee, S., Ebert, B.L., Gillette, M. a, et al. (2005). Gene set enrichment analysis: a knowledge-based approach for interpreting genome-wide expression profiles. Proc. Natl. Acad. Sci. U. S. A. *102*: 15545–50.

Subramanian, K., Owens, D.J., Raju, R., Firpo, M., O'Brien, T.D., Verfaillie, C.M., et al. (2014). Spheroid culture for enhanced differentiation of human embryonic stem cells to hepatocyte-like cells. Stem Cells Dev. *23*: 124–31.

Suga, M., Iyonaga, K., Ichiyasu, H., Saita, N., Yamasaki, H., and Ando, M. (1999). Clinical significance of MCP-1 levels in BALF and serum in patients with interstitial lung diseases. Eur. Respir. J. *14*: 376–82.

Suganuma, H., Sato, A., Tamura, R., and Chida, K. (1995). Enhanced migration of fibroblasts derived from lungs with fibrotic lesions. Thorax *50*: 984–989.

Sunamoto, M., Kuze, K., Tsuji, H., Ohishi, N., Yagi, K., Nagata, K., et al. (1998). Antisense oligonucleotides against collagen-binding stress protein HSP47 suppress collagen accumulation in experimental glomerulonephritis. Lab. Invest. *78*: 967–972.

Sureshbabu, A., Tonner, E., Allan, G.J., and Flint, D.J. (2011). Relative Roles of TGF-beta and IGFBP-5 in Idiopathic Pulmonary Fibrosis. Pulm.Med. *2011*: 517687–.

Sutinen, S., Rainio, P., Huhti, E., and Pokela, R. (1980). Ultrastructure of terminal respiratory epithelium and prognosis in chronic interstitial pneumonia. Eur. J. Respir. Dis. *61*: 325–336.

Sweet-Cordero, A., Mukherjee, S., Subramanian, A., You, H., Roix, J.J., Ladd-Acosta, C., et al. (2005). An oncogenic KRAS2 expression signature identified by cross-species gene-expression analysis. Nat. Genet. *37*: 48–55.

Taguchi, T., and Razzaque, M.S. (2007). The collagen-specific molecular chaperone HSP47: is there a role in fibrosis? Trends Mol.Med. *13*: 45–53.

Taipale, J., Miyazono, K., Heldin, C.H., and Keski-Oja, J. (1994). Latent transforming growth factor-beta 1 associates to fibroblast extracellular matrix via latent TGF-beta binding protein. J. Cell Biol. *124*: 171–181.

Takagi, K., Kawaguchi, Y., Kawamoto, M., Ota, Y., Tochimoto, A., Gono, T., et al. (2011). Activation of the Activin A-ALK-Smad pathway in systemic sclerosis. J. Autoimmun. *36*: 181–188.

Takai, E., Tsukimoto, M., and Kojima, S. (2013). TGF-β1 Downregulates COX-2 Expression Leading to Decrease of PGE2 Production in Human Lung Cancer A549 Cells, Which Is Involved in Fibrotic Response to TGF-β1. PLoS One *8*:

Takezawa, T., Mori, Y., Yonaha, T., and Yoshizato, K. (1993). Characterization of morphology and cellular metabolism during the spheroid formation by fibroblasts. Exp.Cell Res. *208*: 430–441.

Tanaka, T., Yoshimi, M., Maeyama, T., Hagimoto, N., Kuwano, K., and Hara, N. (2002). Resistance to Fas-mediated apoptosis in human lung fibroblast. Eur. Respir. J. Off. J. Eur. Soc. Clin. Respir. Physiol. *20*: 359–368.

Tang, Y.-W., Johnson, J.E., Browning, P.J., Cruz-Gervis, R.A., Davis, A., Graham, B.S., et al. (2003). Herpesvirus DNA is consistently detected in lungs of patients with idiopathic pulmonary fibrosis. J. Clin. Microbiol. *41*: 2633–2640.

Tatler, A.L., and Jenkins, G. (2012). TGF- Activation and Lung Fibrosis. Proc. Am. Thorac. Soc. *9*: 130–136.

Tessner, T.G., Muhale, F., Riehl, T.E., Anant, S., and Stenson, W.F. (2004). Prostaglandin E2 reduces radiation-induced epithelial apoptosis through a mechanism involving AKT activation and bax translocation. J. Clin. Invest. *114*: 1676–1685.

Thannickal, V.J., and Horowitz, J.C. (2006). Evolving concepts of apoptosis in idiopathic pulmonary fibrosis. Proc. Am. Thorac. Soc. *3*: 350–356.

Thannickal, V.J., Toews, G.B., White, E.S., Lynch III, J.P., and Martinez, F.J. (2004). Mechanisms of pulmonary fibrosis. Annu.Rev.Med. *55*: 395–417.

The Idiopathic Pulmonary Fibrosis Clinical Research Network (2014). Randomized Trial of Acetylcysteine in Idiopathic Pulmonary Fibrosis. N. Engl. J. Med. 2093–2101.

Thomas, A.Q., Lane, K., Phillips III, J., Prince, M., Markin, C., Speer, M., et al. (2002). Heterozygosity for a surfactant protein C gene mutation associated with usual interstitial pneumonitis and cellular nonspecific interstitial pneumonitis in one kindred. Am.J.Respir.Crit Care Med. *165*: 1322–1328.

Thomas, P.E., Peters-Golden, M., White, E.S., Thannickal, V.J., and Moore, B.B. (2007). PGE(2) inhibition of TGF-beta1-induced myofibroblast differentiation is Smad-independent but involves cell shape and adhesion-dependent signaling. Am. J. Physiol. Lung Cell. Mol. Physiol. *293*: L417–L428.

Tian, B., Lessan, K., Kahm, J., Kleidon, J., and Henke, C. (2002). beta 1 integrin regulates fibroblast viability during collagen matrix contraction through a phosphatidylinositol 3-kinase/Akt/protein kinase B signaling pathway. J.Biol.Chem. *277*: 24667–24675.

Togo, S., Liu, X., Wang, X., Sugiura, H., Kamio, K., Kawasaki, S., et al. (2009). PDE4 inhibitors roflumilast and rolipram augment PGE2 inhibition of TGF-{beta}1-stimulated fibroblasts. Am. J. Physiol. Lung Cell. Mol. Physiol. *296*: L959–L969.

Tomasek, J.J., Gabbiani, G., Hinz, B., Chaponnier, C., and Brown, R.A. (2002). Myofibroblasts and mechano-regulation of connective tissue remodelling. Nat.Rev.Mol.Cell Biol. *3*: 349–363.

Travis, W.D., Costabel, U., Hansell, D.M., King Jr., T.E., Lynch, D.A., Nicholson, A.G., et al. (2013). An official American Thoracic Society/European Respiratory Society statement: Update of the international multidisciplinary classification of the idiopathic interstitial pneumonias. Am.J.Respir.Crit Care Med. *188*: 733–748.

Tsakiri, K.D., Cronkhite, J.T., Kuan, P.J., Xing, C., Raghu, G., Weissler, J.C., et al. (2007). Adult-onset pulmonary fibrosis caused by mutations in telomerase. Proc.Natl.Acad.Sci.U.S.A *104*: 7552–7557.

Tung, Y.-C., Hsiao, A.Y., Allen, S.G., Torisawa, Y., Ho, M., and Takayama, S. (2011). High-throughput 3D spheroid culture and drug testing using a 384 hanging drop array. Analyst *136*: 473–478.

Turk, V., Stoka, V., and Turk, D. (2008). Cystatins: biochemical and structural properties, and medical relevance. Front. Biosci. *13*: 5406–5420.

Turk, V., Stoka, V., Vasiljeva, O., Renko, M., Sun, T., Turk, B., et al. (2012). Cysteine cathepsins: from structure, function and regulation to new frontiers. Biochim. Biophys. Acta *1824*: 68–88.

Uhal, B.D., Joshi, I., Hughes, W.F., Ramos, C., Pardo, A., and Selman, M. (1998). Alveolar epithelial cell death adjacent to underlying myofibroblasts in advanced fibrotic human lung. Am. J. Physiol. *275*: L1192–L1199.

Vaheri, A., Enzerink, A., Rasanen, K., and Salmenpera, P. (2009). Nemosis, a novel way of fibroblast activation, in inflammation and cancer. Exp.Cell Res. *315*: 1633–1638.

Vancheri, C., Failla, M., Crimi, N., and Raghu, G. (2010). Idiopathic pulmonary fibrosis: a disease with similarities and links to cancer biology. Eur.Respir.J. *35*: 496–504.

Vega, S., Morales, A. V, Ocaña, O.H., Valdés, F., Fabregat, I., and Nieto, M.A. (2004). Snail blocks the cell cycle and confers resistance to cell death. Genes Dev. *18*: 1131–1143.

Verploegen, S., Leeuwen, C.M. Van, Deutekom, H.W.M. Van, Lammers, J.W.J., Koenderman, L., and Coffer, P.J. (2002). Role of Ca2+/calmodulin regulated signaling pathways in chemoattractant induced neutrophil effector functions: Comparison with the role of phosphotidylinositol-3 kinase. Eur. J. Biochem. *269*: 4625–4634.

Vilar, J.M.G., Jansen, R., and Sander, C. (2006). Signal processing in the TGF-beta superfamily ligand-receptor network. PLoS Comput. Biol. *2*: e3.

Villalonga, P., López-Alcalá, C., Chiloeches, A., Gil, J., Marais, R., Bachs, O., et al. (2002). Calmodulin prevents activation of Ras by PKC in 3T3 fibroblasts. J. Biol. Chem. *277*: 37929–37935.

Vogel, W., Gish, G.D., Alves, F., and Pawson, T. (1997). The discoidin domain receptor tyrosine kinases are activated by collagen. Mol.Cell *1*: 13–23.

Vranka, J.A., Sakai, L.Y., and Bachinger, H.P. (2004). Prolyl 3-hydroxylase 1, enzyme characterization and identification of a novel family of enzymes. J.Biol.Chem. *279*: 23615–23621.

Vuga, L.J., Milosevic, J., Pandit, K., Ben-Yehudah, A., Chu, Y., Richards, T., et al. (2013). Cartilage oligomeric matrix protein in idiopathic pulmonary fibrosis. PLoS.One. *8*: e83120–.

Waghray, M., Cui, Z., Horowitz, J.C., Subramanian, I.M., Martinez, F.J., Toews, G.B., et al. (2005). Hydrogen peroxide is a diffusible paracrine signal for the induction of epithelial cell death by activated myofibroblasts. FASEB J. *19*: 854–856.

Walenga, R.W., Kester, M., Coroneos, E., Butcher, S., Dwivedi, R., and Statt, C. (1996). Constitutive expression of prostaglandin endoperoxide G/H synthetase (PGHS)-2 but not PGHS-1 in hum an tracheal epithelial cells in vitro. Prostaglandins *52*: 341–359.

Wang, Y., Barbacioru, C., Hyland, F., Xiao, W., Hunkapiller, K.L., Blake, J., et al. (2006). Large scale real-time PCR validation on gene expression measurements from two commercial long-oligonucleotide microarrays. BMC Genomics *7*: 59.

Wardlaw, A.J., Hay, H., Cromwell, O., Collins, J. V, and Kay, A.B. (1989). Leukotrienes, LTC4 and LTB4, in bronchoalveolar lavage in bronchial asthma and other respiratory diseases. J. Allergy Clin. Immunol. *84*: 19–26.

Wei, B., Cai, L., Sun, D., Wang, Y., Wang, C., Chai, X., et al. (2014). Microsomal Prostaglandin E Synthase-1 Deficiency Exacerbates Pulmonary Fibrosis Induced by Bleomycin in Mice. Molecules *19*: 4967–4985.

Wells, R.G. (2008). The role of matrix stiffness in regulating cell behavior. Hepatology *47*: 1394–1400.

Werner, S., and Grose, R. (2003). Regulation of wound healing by growth factors and cytokines. Physiol Rev. *83*: 835–870.

White, E.S., Atrasz, R.G., Dickie, E.G., Aronoff, D.M., Stambolic, V., Mak, T.W., et al. (2005). Prostaglandin E(2) inhibits fibroblast migration by E-prostanoid 2 receptor-mediated increase in PTEN activity. Am. J. Respir. Cell Mol. Biol. *32*: 135–141.

White, E.S., Atrasz, R.G., Hu, B., Phan, S.H., Stambolic, V., Mak, T.W., et al. (2006). Negative regulation of myofibroblast differentiation by PTEN (Phosphatase and Tensin Homolog Deleted on chromosome 10). Am J Respir Crit Care Med *173*: 112–121.

Whitesides, G.M. (2006). The origins and the future of microfluidics. Nature *442*: 368–373.

Whyte, M., Hubbard, R., Meliconi, R., Whidborne, M., Eaton, V., Bingle, C., et al. (2000). Increased risk of fibrosing alveolitis associated with interleukin-1 receptor antagonist and tumor necrosis factor-alpha gene polymorphisms. Am.J.Respir.Crit Care Med. *162*: 755–758.

Wieser, R.J., and Oesch, F. (1986). Contact inhibition of growth of human diploid fibroblasts by immobilized plasma membrane glycoproteins. J. Cell Biol. *103*: 361–367.

Wilborn, J., Bailie, M., Coffey, M., Burdick, M., Strieter, R., and Peters-Golden, M. (1996). Constitutive activation of 5-lipoxygenase in the lungs of patients with idiopathic pulmonary fibrosis. J Clin Invest *97*: 1827–1836.

Wilborn, J., Crofford, L.J., Burdick, M.D., Kunkel, S.L., Strieter, R.M., and Peters-Golden, M. (1995). Cultured lung fibroblasts isolated from patients with idiopathic pulmonary fibrosis have a diminished capacity to synthesize prostaglandin E2 and to express cyclooxygenase-2. J. Clin. Invest. *95*: 1861–1868.

Wilkes, M.C., and Leof, E.B. (2006). Transforming growth factor beta activation of c-Abl is independent of receptor internalization and regulated by phosphatidylinositol 3-kinase and PAK2 in mesenchymal cultures. J. Biol. Chem. *281*: 27846–27854.

Wilkes, M.C., Mitchell, H., Penheiter, S.G., Doré, J.J., Suzuki, K., Edens, M., et al. (2005). Transforming growth factor-β activation of phosphatidylinositol 3-kinase is independent of Smad2 and Smad3 and regulates fibroblast responses via p21-activated kinase-2. Cancer Res. *65*: 10431–10440.

Willis, B.C., and Borok, Z. (2007). TGF-beta-induced EMT: mechanisms and implications for fibrotic lung disease. Am.J.Physiol Lung Cell Mol.Physiol *293*: L525–L534.

Wilson, R., Lees, J.F., and Bulleid, N.J. (1998). Protein disulfide isomerase acts as a molecular chaperone during the assembly of procollagen. J.Biol.Chem. *273*: 9637–9643.

Winslow, T. (2006). Lungs [Online]. -.

Wipff, P.J., Rifkin, D.B., Meister, J.J., and Hinz, B. (2007). Myofibroblast contraction activates latent TGF-beta1 from the extracellular matrix. J.Cell Biol. *179*: 1311–1323.

Wollin, L., Maillet, I., Quesniaux, V.V., Holweg, A., and Ryffel, B. (2014). Anti-fibrotic and anti-inflammatory activity of the tyrosine kinase inhibitor, nintedanib, in experimental models of lung fibrosis. J. Pharmacol. Exp. Ther. *349*: 209–20.

Worthington, J.J., Klementowicz, J.E., and Travis, M.A. (2011). TGFbeta: a sleeping giant awoken by integrins. Trends Biochem. *36*: 47–54.

Wu, Z., Yang, L., Cai, L., Zhang, M., Cheng, X., Yang, X., et al. (2007). Detection of epithelial to mesenchymal transition in airways of a bleomycin induced pulmonary fibrosis model derived from an alpha-smooth muscle actin-Cre transgenic mouse. Respir. Res. *8*: 1.

Xaubet, A., Ancochea, J., Bollo, E., Fernandez-Fabrellas, E., Franquet, T., Molina-Molina, M., et al. (2013). Guidelines for the diagnosis and treatment of idiopathic pulmonary fibrosis. Sociedad Espanola de Neumologia y Cirugia Toracica (SEPAR) Research Group on Diffuse Pulmonary Diseases. Arch.Bronconeumol. *49*: 343–353.

Xaubet, A., Marin-Arguedas, A., Lario, S., Ancochea, J., Morell, F., Ruiz-Manzano, J., et al. (2003). Transforming growth factor-beta1 gene polymorphisms are associated with disease progression in idiopathic pulmonary fibrosis. Am.J.Respir.Crit Care Med. *168*: 431–435.

Xie, X.S., Li, F.Y., Liu, H.C., Deng, Y., Li, Z., and Fan, J.M. (2010). LSKL, a peptide antagonist of thrombospondin-1, attenuates renal interstitial fibrosis in rats with unilateral ureteral obstruction. Arch. Pharm. Res. *33*: 275–284.

Xu, K., Gui, Y., Ma, A., Tian, X., and Zeng, N. (2013). Mtor Signaling Pathway Contributes To The Pathogenesis Of Pulmonary Fibrosis. Am J Respir Crit Care Med *187*: A1863.

Xu, Y.D., Hua, J., Mui, A., O'Connor, R., Grotendorst, G., and Khalil, N. (2003). Release of biologically active TGF-beta1 by alveolar epithelial cells results in pulmonary fibrosis. Am. J. Physiol. Lung Cell. Mol. Physiol. *285*: L527–L539.

Yamashita, C.M., Dolgonos, L., Zemans, R.L., Young, S.K., Robertson, J., Briones, N., et al. (2011). Matrix metalloproteinase 3 is a mediator of pulmonary fibrosis. Am. J. Pathol. *179*: 1733–1745.

Yehualaeshet, T., O'Connor, R., Green-Johnson, J., Mai, S., Silverstein, R., Murphy-Ullrich, J.E., et al. (1999). Activation of rat alveolar macrophage-derived latent transforming growth factor beta-1 by plasmin requires interaction with thrombospondin-1 and its cell surface receptor, CD36. Am. J. Pathol. *155*: 841–851.

Yokomizo, T., Izumi, T., and Shimizu, T. (2001). Leukotriene B4: metabolism and signal transduction. Arch. Biochem. Biophys. *385*: 231–241.

Yu, F.X., and Guan, K.L. (2013). The Hippo pathway: Regulators and regulations. Genes Dev. *27*: 355–371.

Yu, X., Lin, S.G., Huang, X.R., Bacher, M., Leng, L., Bucala, R., et al. (2007). Macrophage migration inhibitory factor induces MMP-9 expression in macrophages via the MEK-ERK MAP kinase pathway. J Interf. Cytokine Res *27*: 103–109.

Zhang, H.Y., Gharaee-Kermani, M., and Phan, S.H. (1997). Regulation of lung fibroblast alpha-smooth muscle actin expression, contractile phenotype, and apoptosis by IL-1beta. J. Immunol. *158*: 1392–1399.

Zhang, H.Y., Gharaee-Kermani, M., Zhang, K., Karmiol, S., and Phan, S.H. (1996). Lung fibroblast alpha-smooth muscle actin expression and contractile phenotype in bleomycin-induced pulmonary fibrosis. Am. J. Pathol. *148*: 527–537.

Zhang, H.Y., and Phan, S.H. (1999). Inhibition of myofibroblast apoptosis by transforming growth factor beta(1). Am. J. Respir. Cell Mol. Biol. *21*: 658–665.

Zhang, Y.E. (2009). Non-Smad pathways in TGF-beta signaling. Cell Res. *19*: 128–139.

Zhou, Y., Hagood, J.S., Lu, B., Merryman, W.D., and Murphy-Ullrich, J.E. (2010). Thy-1-integrin alphav beta5 interactions inhibit lung fibroblast contraction-induced latent transforming growth factor-beta1 activation and myofibroblast differentiation. J.Biol.Chem. *285*: 22382–22393.

APPENDIX

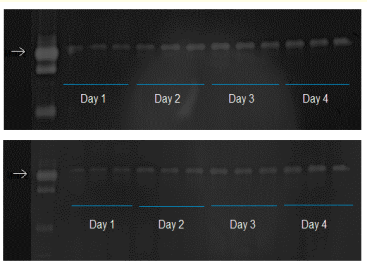

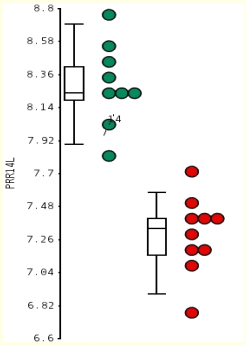

Pathway Name	Enrichment Score	Enrichment p-value	% [illegible] pathway that are present	No. [illegible] in list, in pathway
[illegible]	7.33932	0.000643491	10.3448	3
Pertussis	6.88058	0.00102755	5.26316	4
Phosphatidylinositol [illegible] system	6.64204	0.00130437	4.59627	4
Mineral absorption	5.80381	0.00301604	6.12245	3
Alcoholism	5.77681	0.00309859	2.95858	5
Oocyte meiosis	5.52153	0.00399972	3.63636	4
[illegible] pathway	5.21143	0.00545389	3.33333	4
[illegible]	5.00623	0.00660607	4.61538	3
Long-term potentiation	4.9221	0.00728382	4.47761	3
Amphetamine addiction	4.88108	0.00758884	4.41176	3
Gastric acid secretion	4.6483	0.00957784	4.05405	3
Salivary secretion	4.1469	0.0157817	3.37079	3
Alzheimer's disease	4.09479	0.0166593	2.40964	4
[illegible] pathway	4.08964	0.0167453	3.2967	3
Circadian entrainment	3.94781	0.0192969	3.125	3
Tuberculosis	3.86399	0.0209842	2.24719	4
[illegible]	3.84037	0.0214857	3	3
[illegible] pathway	3.84037	0.0214857	3	3
Calcium [illegible] pathway	3.80927	0.0221643	2.20994	4
Drug metabolism - other enzymes	3.61095	0.0270261	4.65116	2
Caffeine metabolism	3.51989	0.0296026	25	1
Vascular smooth muscle contraction	3.39087	0.0336794	2.32301	3
Olfactory transduction	3.36961	0.0344031	2.5	3
Rap1 [illegible] pathway	3.30307	0.0367701	1.88679	4
Systemic lupus [illegible]	3.28664	0.0373792	2.41935	3
Neurotrophin signaling [illegible] pathway	3.16805	0.0420855	2.30769	3
[illegible] pathway	3.13192	0.0436339	1.79671	4
Insulin [illegible]	2.9845	0.0501649	2.14286	3

APPENDIX 1: RNA integrity for microarray samples

A)

Sample number	[RNA] ng/ul	RIN
1	45.77	9.7
2	25.45	9
3	37.95	9.2
4	13.84	9.3
5	20.55	not calc'd
6	22.98	9
7	15.64	9
8	20.87	8.7
9	13.25	8.9
10	16.84	9.1
11	11.98	8.7
12	16.77	8.6
13	10.46	9.4
14	16.16	9.2
15	11.61	9.2
16	16.07	9.3
17	14.99	9.1
18	16.42	8.5
19	10.11	9.3
20	19.2	8.6
LB	4.85	1.1
HT29	7.91	9.7

B)

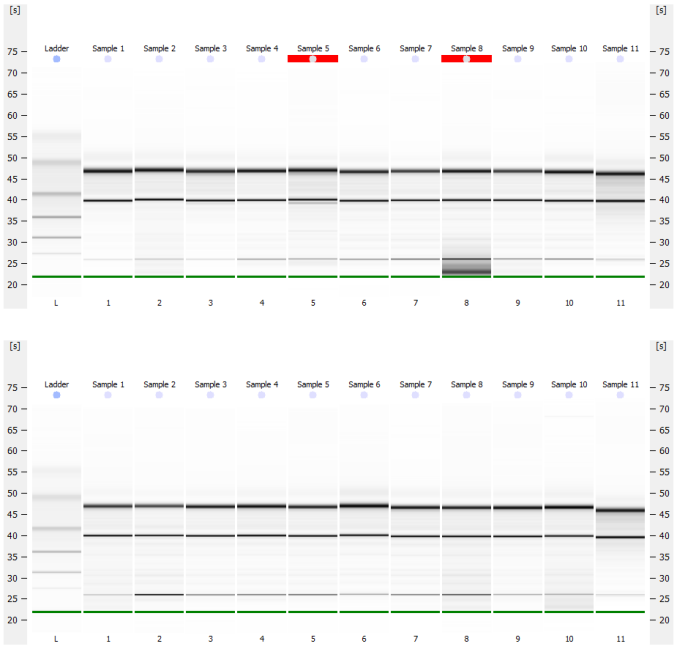

C)

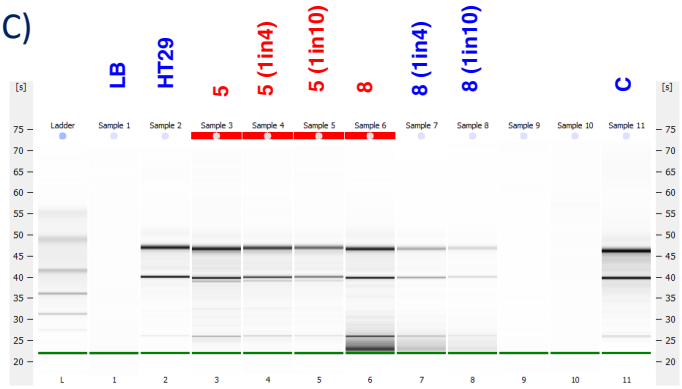

Figure A. 1. RNA yields and quality control

RNA was extracted from non-IPF (n=10) and IPF (n=10) spheroids using RNase aqueous kit. (A) Bioanalyzer and Nanodrop were used to determine the RNA integrity and RNA concentration, respectively. (B) RNA quality was also determined by running the samples on agarose gels. (C) Samples 5 and 8 were re-run on the agarose gel at different dilutions. Lysis buffer (LB) and HT29 were used as negative and positive controls, respectively.

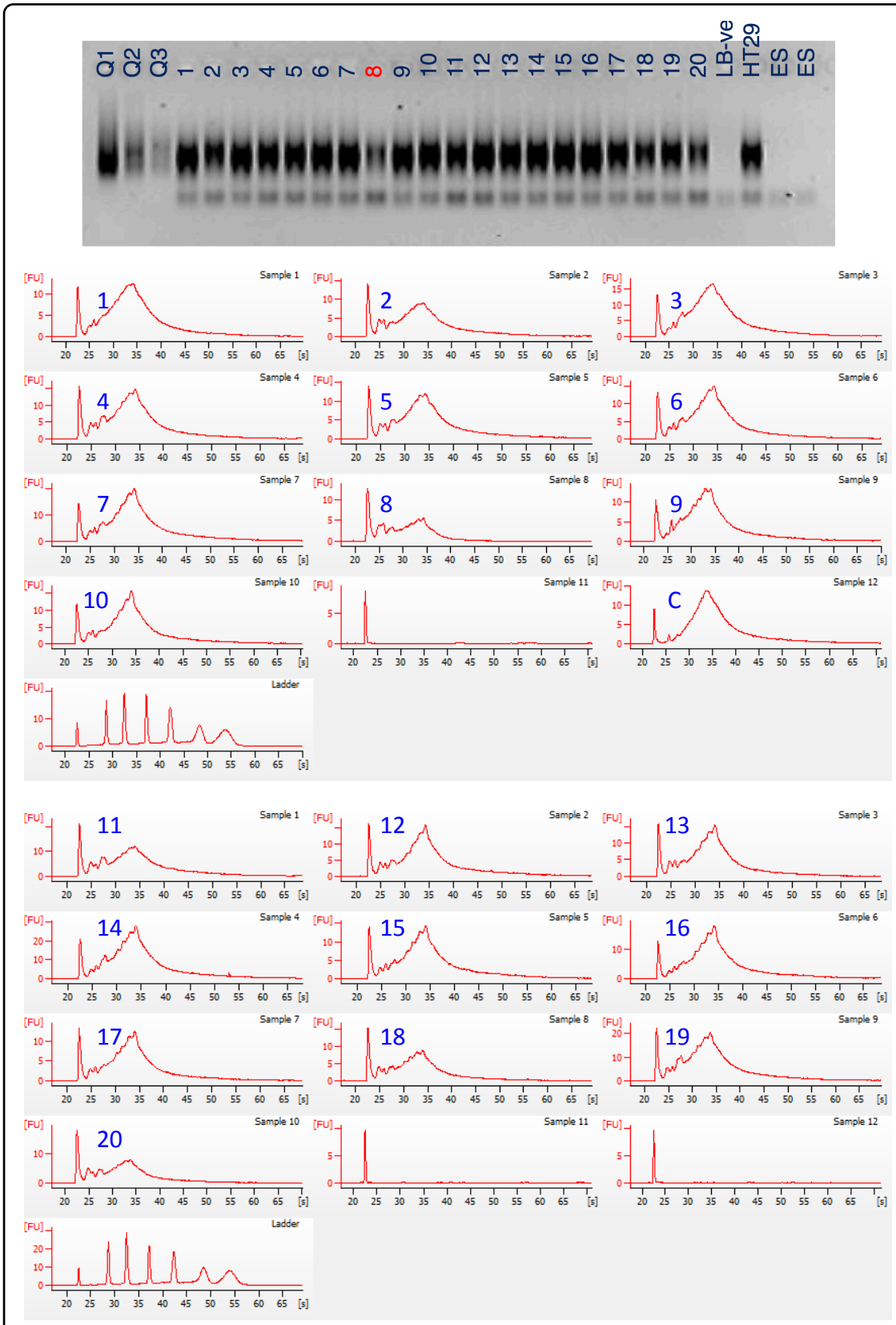

Figure A. 2. Poly A cDNA quality control on agarose gel and bioanalyser.

A) Poly A cDNA samples run on agarose. Lysis buffer (LB) and HT29 were used as controls. ES = empty space. Sample 8 is highlighted in red as this donor was removed from the rest of the microarray analysis. B) Bioanalyser electrograms for non-IPF (n=10) and IPF (n=10) poly A cDNA samples. Each donor is labelled 1-20 (blue). Other than sample 8 all other samples showed good quality for poly A cDNA.

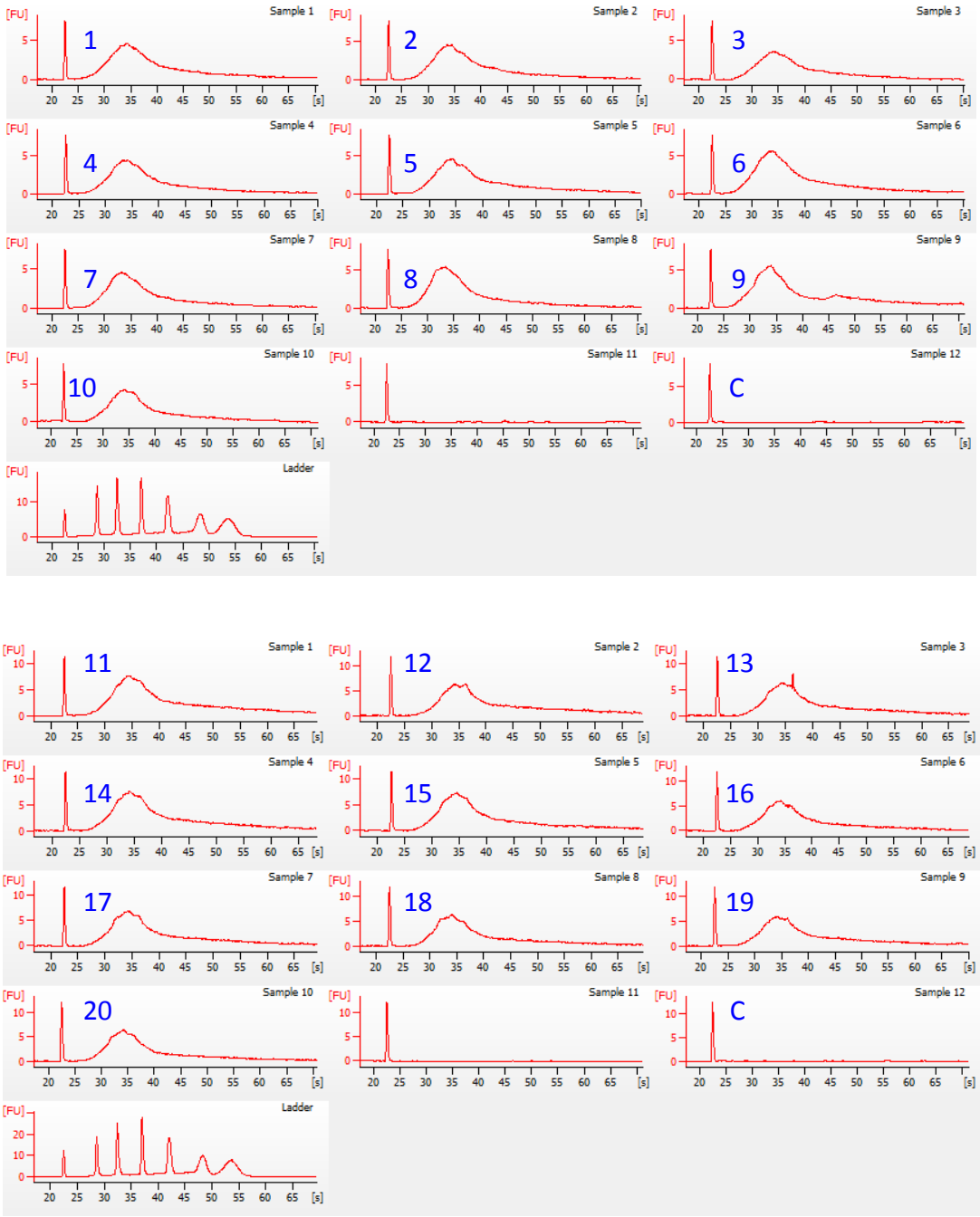

Figure A. 3. Labelled sample quality control on bioanalyser

Bioanalyser electrograms for non-IPF (n=10) and IPF (n=10) cRNA samples following labelling. Each donor is labelled 1-20 (blue). Other samples showed good cRNA labelling which is represented by the peak shown at 35.

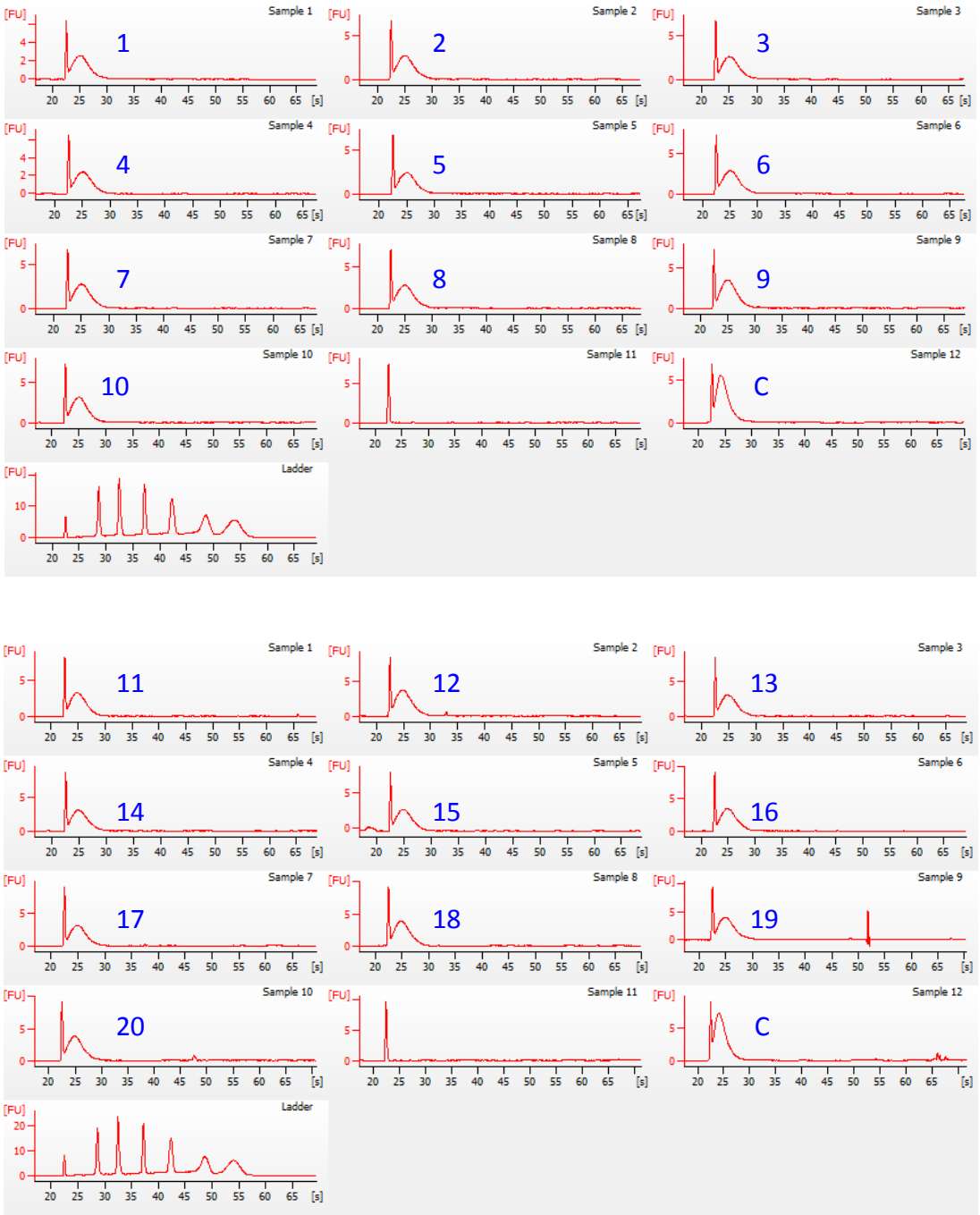

Figure A. 4. Fragmented cRNA sample quality control on bioanalyser

Bioanalyser electrograms for non-IPF (n=10) and IPF (n=10) fragmented cRNA samples. Each donor is labelled 1-20 (blue). The first peak (between 20-25) is the marker. The second peak represent the quality of fragmented cRNA. The lower the peak the less fragmented cRNA is present. In general all samples are fine for hybridisation.

APPENDIX 2: Microarray data analysis

Table A1 illustrates the list of differentially expressed genes following microarray data analysis of non-IPF and IPF spheroids with the following criteria: FDR p<0.05, fold change >2 or <-2. **Figure A5** illustrates protein-protein interactions of the seven differentially expressed genes identified in the microarray data analysis belonging to metabolic pathways.

Table A1: Differentially expressed genes following microarray data analysis of non-IPF and IPF spheroids (FDR p<0.05, FC >2 or <-2)

Gene Symbol	Probeset ID	Gene Title	p-value	Fold-Change	Description
PRR14L	1558097_at	proline rich 14-like	1.35E-06	2.13452	Control up vs. IPF
CTSB	227961_at	cathepsin B	2.19E-06	4.35692	Control up vs. IPF
PTGER3	213933_at	prostaglandin E receptor 3 (subtype EP3)	3.60E-06	-6.97695	Control down vs. IPF
ZNF618	226592_at	zinc finger protein 618	8.55E-06	2.30699	Control up vs. IPF
NUDT12	1562775_at	nudix (nucleoside diphosphate linked moiety X)-type motif 12	1.15E-05	-6.86504	Control down vs. IPF
THRB-IT1 /// THRB-IT1	233130_at	THRB intronic transcript 1 (non-protein coding) /// NULL	1.23E-05	-4.51984	Control down vs. IPF
NGDN	216263_s_at	neuroguidin, EIF4E binding protein	1.59E-05	-7.60476	Control down vs. IPF
SPAG17	233516_s_at	sperm associated antigen 17	1.76E-05	2.34199	Control up vs. IPF
SULT1C2	205343_at	sulfotransferase family, cytosolic, 1C, member 2	2.38E-05	-2.48374	Control down vs. IPF
CS	208660_at	citrate synthase	3.06E-05	2.14768	Control up vs. IPF
TMEM232	1568698_at	transmembrane protein 232	3.12E-05	-5.62409	Control down vs. IPF
ABCB4	1570505_at	ATP-binding cassette, sub-family B (MDR/TAP), member 4	3.69E-05	-10.9506	Control down vs. IPF
PRRC2C	211948_x_at	proline-rich coiled-coil 2C	4.03E-05	2.21755	Control up vs. IPF
B3GAT2	239144_at	beta-1,3-	4.20E-05	-7.14623	Control

		glucuronyltransferase 2 (glucuronosyltransferase S)			down vs. IPF
SCN11A	210853_at	sodium channel, voltage-gated, type XI, alpha subunit	4.22E-05	-7.98132	Control down vs. IPF
XDH	241994_at	xanthine dehydrogenase	4.33E-05	9.82099	Control up vs. IPF
SYNJ2	210612_s_at	synaptojanin 2	4.58E-05	2.1818	Control up vs. IPF
POTEG / POTEM	242912_at	POTE ankyrin domain family, member G /// POTE ankyrin domain family, member M	5.09E-05	-9.27424	Control down vs. IPF
FOXP1	223287_s_at	forkhead box P1	5.14E-05	2.29153	Control up vs. IPF
C9orf38	208077_at	chromosome 9 open reading frame 38	5.19E-05	-4.79021	Control down vs. IPF
CLDN23	228704_s_at	claudin 23	5.82E-05	-6.87981	Control down vs. IPF
ELF4	31845_at	E74-like factor 4 (ets domain transcription factor)	6.18E-05	2.40782	Control up vs. IPF
ADAMDEC1	206134_at	ADAM-like, decysin 1	7.23E-05	-4.44309	Control down vs. IPF
GSE1	212056_at	Gse1 coiled-coil protein	7.44E-05	2.0933	Control up vs. IPF
GLTP	219267_at	glycolipid transfer protein	7.47E-05	-3.10894	Control down vs. IPF
C1S	1555229_a_at	complement component 1, s subcomponent	7.48E-05	3.06672	Control up vs. IPF
CCL7	208075_s_at	chemokine (C-C motif) ligand 7	8.19E-05	2.20444	Control up vs. IPF
CCDC102B	220301_at	coiled-coil domain containing 102B	8.60E-05	-2.43441	Control down vs. IPF
CHST11	226368_at	carbohydrate (chondroitin 4) sulfotransferase 11	8.94E-05	3.38147	Control up vs. IPF
H3F3A / H3F3B / MIR4738	211998_at	H3 histone, family 3A / H3 histone, family 3B (H3.3B) / microRNA 4738	9.07E-05	2.6387	Control up vs. IPF
SLC16A14	238029_s_at	solute carrier family 16, member 14 (monocarboxylic acid transporter 14)	0.000103314	-6.60546	Control down vs. IPF

PRKDC	208694_at	protein kinase, DNA-activated, catalytic polypeptide	0.0001077 4	2.05763	Control up vs. IPF
ANO4	239883_s_a t	anoctamin 4	0.0001081 34	-10.335	Control down vs. IPF
EZH2	203358_s_a t	enhancer of zeste homolog 2 (Drosophila)	0.0001189 76	2.04584	Control up vs. IPF
CALM1 / CALM2 / CALM3	211985_s_a t	calmodulin 1 (phosphorylase kinase, delta) / calmodulin 2 (phosphorylase kinase, delta	0.0001238 22	2.33678	Control up vs. IPF
ARHGEF7	235412_at	Rho guanine nucleotide exchange factor (GEF) 7	0.0001423 26	-9.45404	Control down vs. IPF
MYO10	216222_s_a t	myosin X	0.0001426 38	2.09371	Control up vs. IPF
CCDC68	220180_at	coiled-coil domain containing 68	0.0001433 73	-2.52926	Control down vs. IPF
ARHGAP22	206298_at	Rho GTPase activating protein 22	0.0001454 12	2.55764	Control up vs. IPF
MTHFR	239035_at	methylenetetrahydr ofolate reductase (NAD(P)H)	0.0001485 63	2.0933	Control up vs. IPF
SP110	208012_x_ at	SP110 nuclear body protein	0.0001551 81	2.62068	Control up vs. IPF
SCAND2P	215670_s_a t	SCAN domain containing 2 pseudogene	0.0001734 77	3.10532	Control up vs. IPF
AKIP1 / NUAK2	220987_s_a t	A kinase (PRKA) interacting protein 1 /// NUAK family, SNF1-like kinase, 2	0.0001757 56	5.03172	Control up vs. IPF
EGR1	227404_s_a t	early growth response 1	0.0001852 8	2.14051	Control up vs. IPF
CCDC88A	221078_s_a t	coiled-coil domain containing 88A	0.0001888 81	3.46477	Control up vs. IPF
ANKFN1	1559640_at	ankyrin-repeat and fibronectin type III domain containing 1	0.0001987 11	-10.9947	Control down vs. IPF
ANO4	236420_s_a t	anoctamin 4	0.0002115 07	-7.47891	Control down vs. IPF
IMPDH2	201892_s_a t	IMP (inosine 5'-monophosphate) dehydrogenase 2	0.0002139 39	2.13772	Control up vs. IPF
BUB1	209642_at	BUB1 mitotic checkpoint serine/threonine kinase	0.0002248 22	3.18582	Control up vs. IPF

SLC26A3	215657_at	solute carrier family 26, member 3	0.000226169	-4.28905	Control down vs. IPF
APCDD1L-AS1	1559433_at	APCDD1L antisense RNA 1 (head to head)	0.00025357	2.28726	Control up vs. IPF
PSG6	209738_x_at	pregnancy specific beta-1-glycoprotein 6	0.00026528	-2.34506	Control down vs. IPF
P4HA1	243335_at	prolyl 4-hydroxylase, alpha polypeptide I	0.000287544	-2.34549	Control down vs. IPF
KAT6A	226547_at	K(lysine) acetyltransferase 6A	0.000297076	2.1688	Control up vs. IPF
CELF5	230497_at	CUGBP, Elav-like family member 5	0.000299644	-7.50241	Control down vs. IPF
GON4L	1555913_at	gon-4-like (C. elegans)	0.000310771	2.1787	Control up vs. IPF
ADAM32	1552266_at	ADAM metallopeptidase domain 32	0.000322135	-3.21016	Control down vs. IPF
SCGB2A2	206378_at	secretoglobin, family 2A, member 2	0.000323155	-2.37632	Control down vs. IPF
ZNF619	1552836_at	zinc finger protein 619	0.000324816	2.60859	Control up vs. IPF
TRIB2	202479_s_at	tribbles homolog 2 (Drosophila)	0.000326062	2.4936	Control up vs. IPF
TFAP2C	205286_at	transcription factor AP-2 gamma (activating enhancer binding protein 2 gamma)	0.000350084	-2.5387	Control down vs. IPF
SLC40A1	223044_at	solute carrier family 40 (iron-regulated transporter), member 1	0.000354637	-3.18587	Control down vs. IPF
IKZF2	231929_at	IKAROS family zinc finger 2 (Helios)	0.000362299	2.78964	Control up vs. IPF
ZNF287	220055_at	zinc finger protein 287	0.00036859	2.935	Control up vs. IPF
MCHR1	230498_at	melanin-concentrating hormone receptor 1	0.000370954	2.13084	Control up vs. IPF
RAC1	208641_s_at	ras-related C3 botulinum toxin substrate 1 (rho family, small GTP binding protein Rac1)	0.00037488	2.37692	Control up vs. IPF
DTX3L	225415_at	deltex 3-like (Drosophila)	0.000376426	2.02342	Control up vs. IPF
HEATR2	218460_at	HEAT repeat	0.0004038	2.27094	Control up

		containing 2	3		vs. IPF
IL13RA2	206172_at	interleukin 13 receptor, alpha 2	0.000406164	-3.81747	Control down vs. IPF
POLH	219380_x_at	polymerase (DNA directed), eta	0.000407705	2.02139	Control up vs. IPF
TOLLIP-AS1	1555865_at	TOLLIP antisense RNA 1 (head to head)	0.000409152	3.24508	Control up vs. IPF
CENPA / SLC35F6	204962_s_at	centromere protein A /// solute carrier family 35, member F6	0.000410158	2.00247	Control up vs. IPF
SNCA	204466_s_at	synuclein, alpha (non A4 component of amyloid precursor)	0.000417247	-4.25986	Control down vs. IPF
VDR	204254_s_at	vitamin D (1,25-dihydroxyvitamin D3) receptor	0.000441613	2.21428	Control up vs. IPF
SPTLC2	225095_at	serine palmitoyltransferase, long chain base subunit 2	0.000446234	2.2132	Control up vs. IPF
LSM14A	212131_at	LSM14A, SCD6 homolog A (S. cerevisiae)	0.000454197	2.23246	Control up vs. IPF

Table A 2: Pathway enrichment analysis (Non-IPF vs. IPF: FDR p<0.05, FC >2 or <-2)

Pathway Name	Enrichment Score	Enrichment p-value	% genes in pathway that are present	No. genes in list, in pathway
Phototransduction	7.33932	0.000649491	10.3448	3
Pertussis	6.88058	0.00102755	5.26316	4
Phosphatidylinositol signalling system	6.64204	0.00130437	4.93827	4
Mineral absorption	5.80381	0.00301604	6.12245	3
Alcoholism	5.77681	0.00309859	2.95858	5
Oocyte meiosis	5.52153	0.00399972	3.63636	4
Neurotrophin signalling pathway	5.21143	0.00545389	3.33333	4
Glioma	5.00623	0.00669607	4.61538	3
Long-term potentiation	4.9221	0.00728382	4.47761	3
Amphetamine addiction	4.88108	0.00758884	4.41176	3
Gastric acid secretion	4.6483	0.00957784	4.05405	3
Salivary secretion	4.1489	0.0157817	3.37079	3
Alzheimer's disease	4.09479	0.0166593	2.40964	4
GnRH signalling pathway	4.08964	0.0167453	3.2967	3
Circadian entrainment	3.94781	0.0192969	3.125	3
Tuberculosis	3.86399	0.0209842	2.24719	4
Melanogenesis	3.84037	0.0214857	3	3
Estrogen signalling pathway	3.84037	0.0214857	3	3
Calcium signalling pathway	3.80927	0.0221643	2.20994	4
Drug metabolism – other enzymes	3.61095	0.0270261	4.65116	2
Caffeine metabolism	3.51989	0.0296026	20	1
Vascular smooth muscle contraction	3.39087	0.0336794	2.52101	3
Olfactory transduction	3.36961	0.0344031	2.5	3
Rap1 signaling pathway	3.30307	0.0367701	1.88679	4
Systemic lupus erythematosus	3.28664	0.0373792	2.41935	3
Dopaminergic synapse	3.16805	0.0420855	2.30769	3
Ras signalling pathway	3.13192	0.0436339	1.78571	4
Metabolic pathways	0.583509	0.557937	0.603448	7

Table A 3: Pathway enrichment analysis (Non-IPF vs. IPF: unadjusted p<0.01, FC >2 or <-2)

Pathway Name	Enrichment Score	Enrichment p-value	% genes in pathway that are present	No. of genes in list, in pathway
Influenza A	7.21705	0.000733964	6.85714	12
Amphetamine addiction	6.95352	0.000955263	10.2941	7
Circadian entrainment	6.38428	0.00168788	8.33333	8
Dopaminergic synapse	5.74976	0.00318355	6.92308	9
Phototransduction	5.45483	0.00427559	13.7931	4
GnRH signaling pathway	5.27537	0.00511607	7.69231	7
Vascular smooth muscle contraction	5.05489	0.00637807	6.72269	8
Gastric acid secretion	4.92094	0.00729225	8.10811	6
Pertussis	4.79315	0.00828633	7.89474	6
Estrogen signaling pathway	4.76635	0.00851141	7	7
Phosphatidylinositol signaling system	4.49249	0.0111927	7.40741	6
Ras signaling pathway	4.19253	0.015108	4.91071	11
Glutamatergic synapse	4.09024	0.0167353	6.14035	7
Salivary secretion	4.06062	0.0172384	6.74157	6
GABAergic synapse	4.06062	0.0172384	6.74157	6
Drug metabolism - other enzymes	4.05765	0.0172896	9.30233	4
Glioma	4.05677	0.0173049	7.69231	5
Fc gamma R-mediated phagocytosis	4.01042	0.0181258	6.66667	6
Long-term potentiation	3.93719	0.0195029	7.46269	5
Morphine addiction	3.91233	0.0199938	6.52174	6
Adrenergic signaling in cardiomyocytes	3.78757	0.0226506	5.36913	8
Herpes simplex infection	3.65515	0.0258576	4.94505	9
Mineral absorption	3.62375	0.0266823	8.16327	4
Melanogenesis	3.54838	0.0287712	6	6
Chemokine signaling pathway	3.53276	0.0292242	4.83871	9
Steroid hormone biosynthesis	3.31165	0.0364561	7.40741	4
Measles	3.31076	0.0364884	5.22388	7
Serotonergic synapse	3.14895	0.0428971	5.45455	6
Alcoholism	3.14121	0.0432305	4.73373	8
Glycosphingolipid biosynthesis - ganglio series	3.06899	0.0464681	13.3333	2

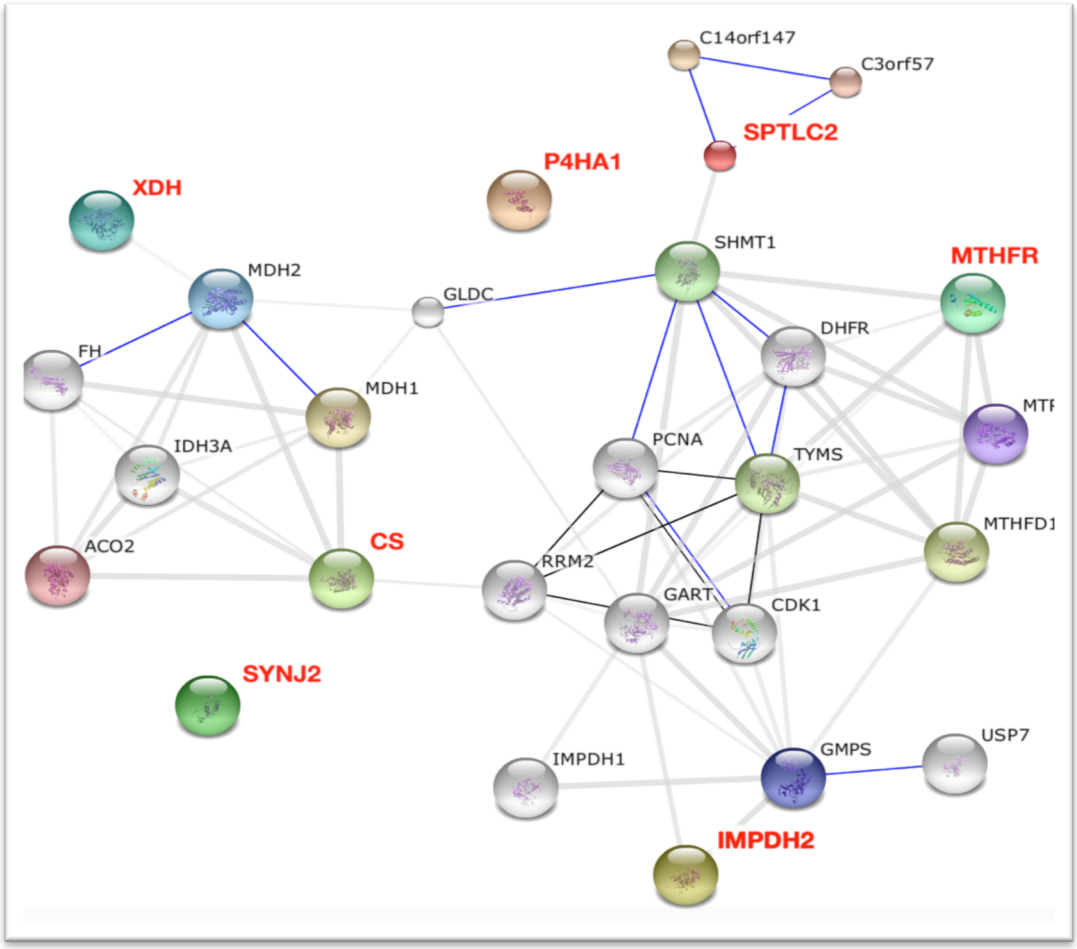

Figure A. 5. Protein-protein interactions of the seven differentially expressed genes identified in the microarray data analysis belonging to metabolic pathways

Each circle represents an individual protein (not differentially expressed following microarray data analysis). The genes highlighted in red were the differentially expressed genes in non-IPF and IPF spheroids (fold change <2 or >-2 with FDR p<0.05) all of which belong to metabolic pathways. Grey lines indicate co-expression; blue lines indicate protein binding.

APPENDIX 3: Fibrosis toolbox

Figure A.6 illustrates compounds within the fibrosis toolbox targeting multiple kinases. A hit was considered if the compound (at 10μM) resulted in >50 % change in collagen synthesis 24 hours post seeding. Due to confidentiality the precise mechanism of action for each compound is unknown. **Figure A.7** illustrates other compounds in the fibrosis toolbox used for medium-throughput screening with their mechanism of actions.

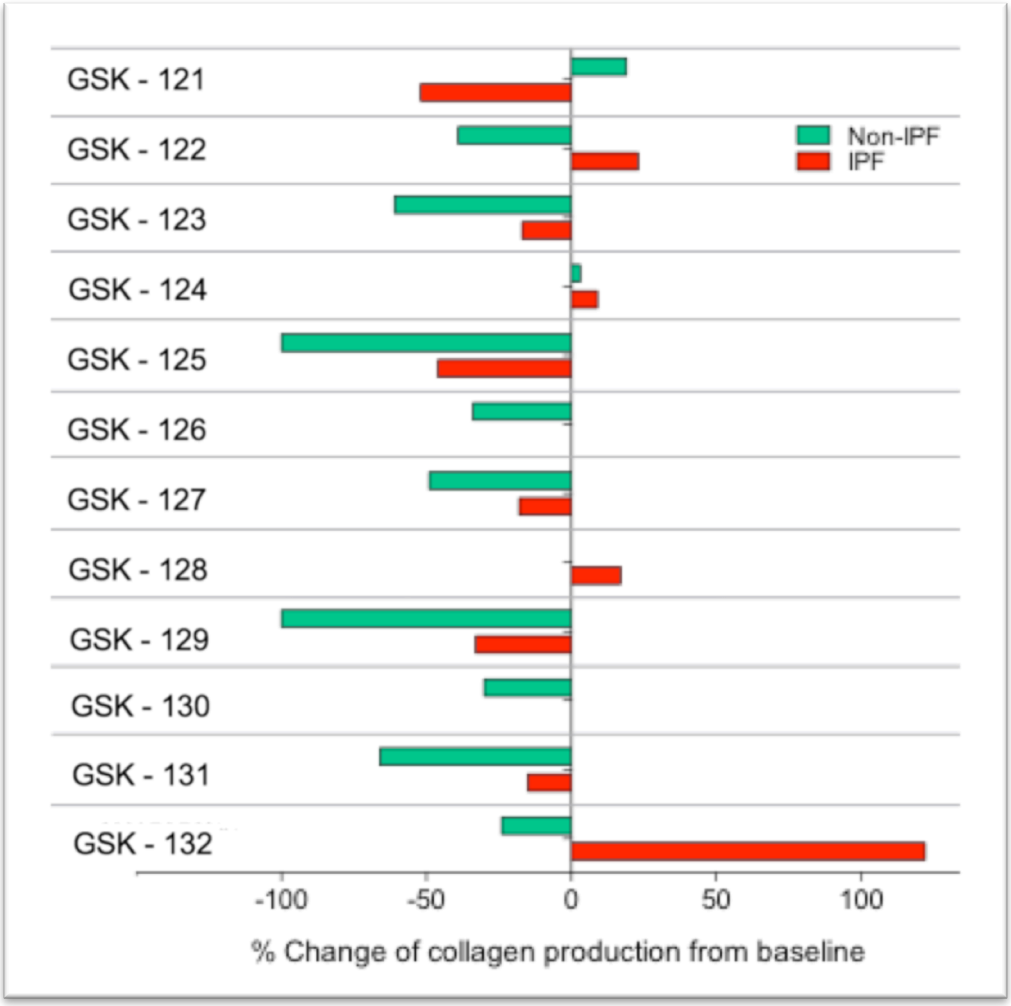

Figure A. 6. Effect of multiple kinase inhibitors on collagen synthesis in spheroids.

Non-IPF (green; n=1) and IPF (red; n=1) spheroids were prophylactically treated with anti-fibrotic compounds (10 μM). Spheroids were collected 24 hours post-treatment and hydrolysed in 6 M HCl for HPLC.

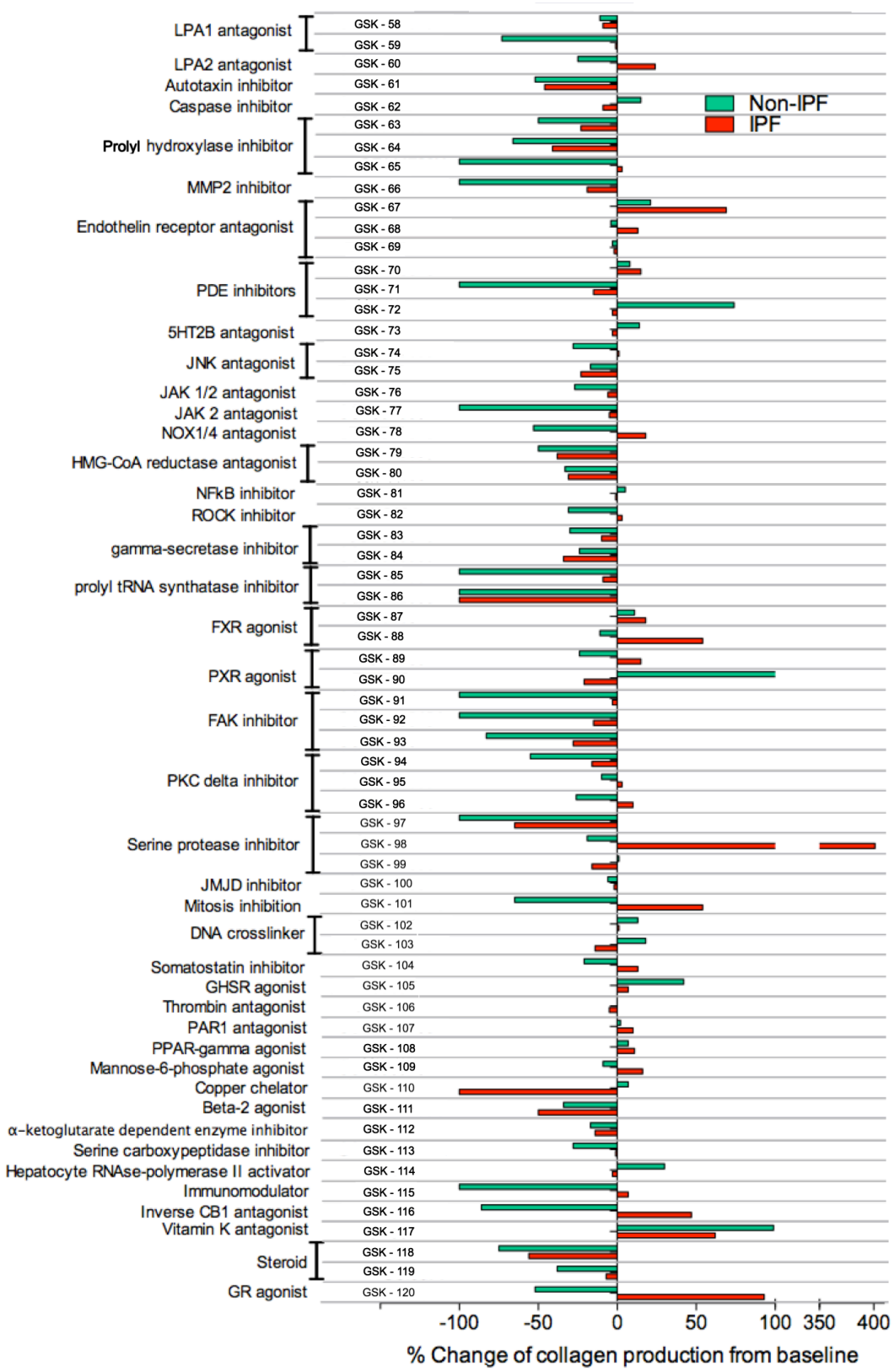

Figure A. 7. Effect of potential therapeutic targets on collagen synthesis in spheroids.

Non-IPF (green; n=1) and IPF (red; n=1) spheroids were prophylactically treated with anti-fibrotic compounds (10 μM). Spheroids were collected 24 hours post-treatment and hydrolysed in 6 M HCl for HPLC.

APPENDIX 4: Non-IPF and IPF spheroids produce MMP2

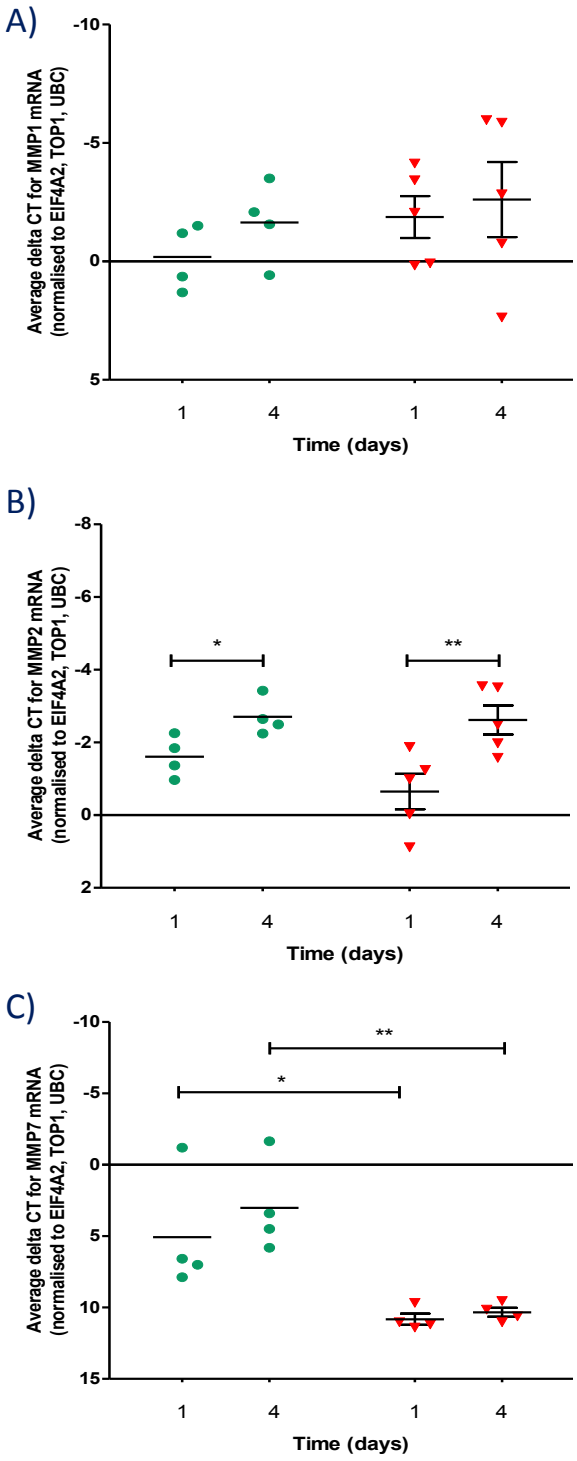

Figure A. 8. *MMP1, MMP2*, and *MMP7* mRNA levels.

Spheroids were collected 24-96 hours post seeding. RNA was extracted from the spheroids for qRT-PCR to analyse the mRNA levels of (A) *MMP1*, (B) *MMP2,* and (C) *MMP7*. All data points were normalised to three housekeeping genes based on GeNorm analysis (*EIF4A2, TOP1*, and *UBC*). Control (n=4) and IPF spheroids (n=5) are represented as green circles and red triangles, respectively. *p<0.05, *p<0.01

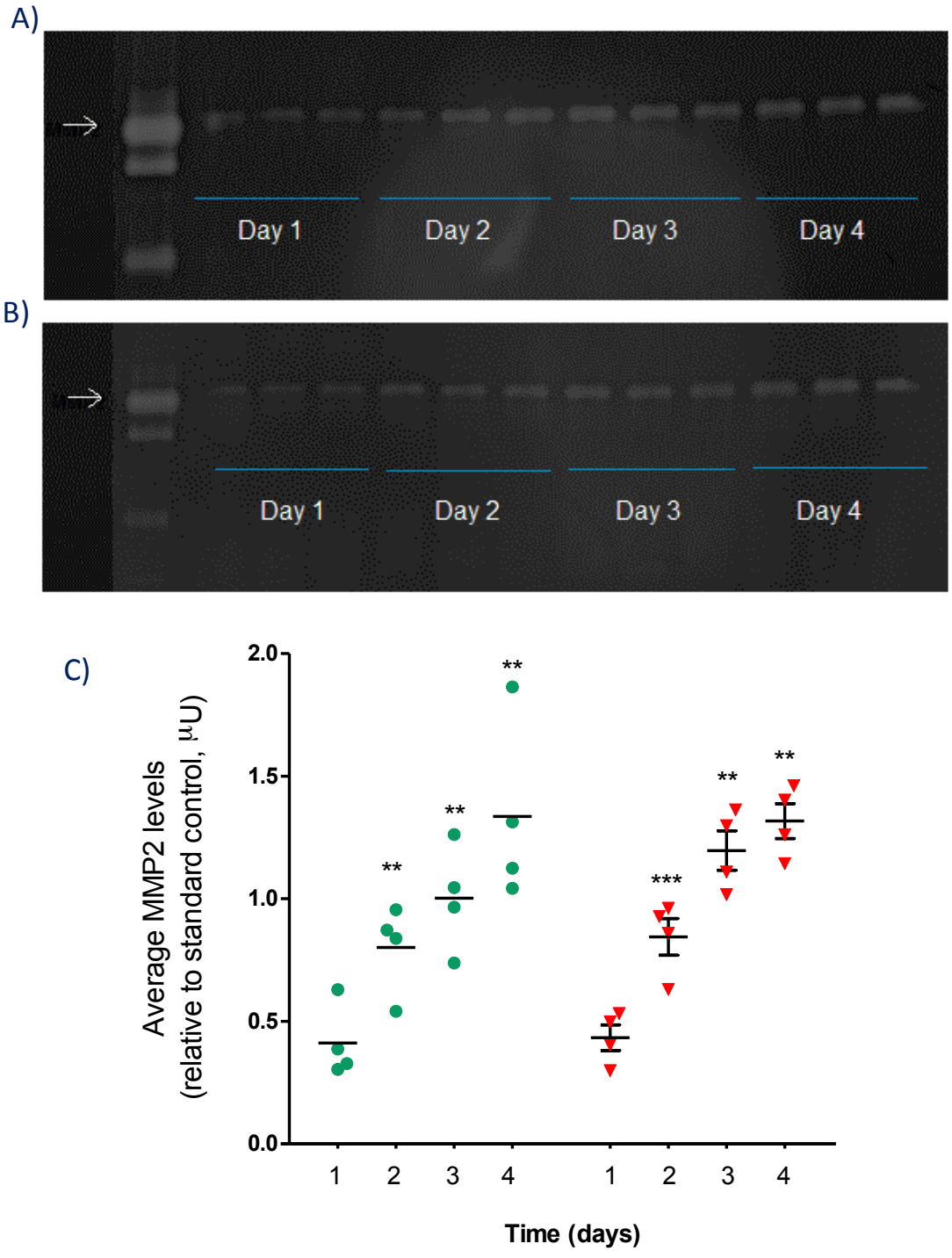

Figure A. 9. MMP2 levels secreted into the conditioned media of spheroids

Zymograms illustrating levels of MMP2 present in the supernatants of (A) non-IPF and (B) IPF spheroids, which were collected 24-96 hours post-seeding. Arrow illustrates MMP2 standard control. (C) Average MMP2 levels relative to MMP2 standard control. Non-IPF (n=4) and IPF spheroids (n=4) are represented as green circles and red triangles, respectively. ** p<0.01, ***p<0.001

APPENDIX 5: LOXL2 mRNA levels in non-IPF and IPF spheroids

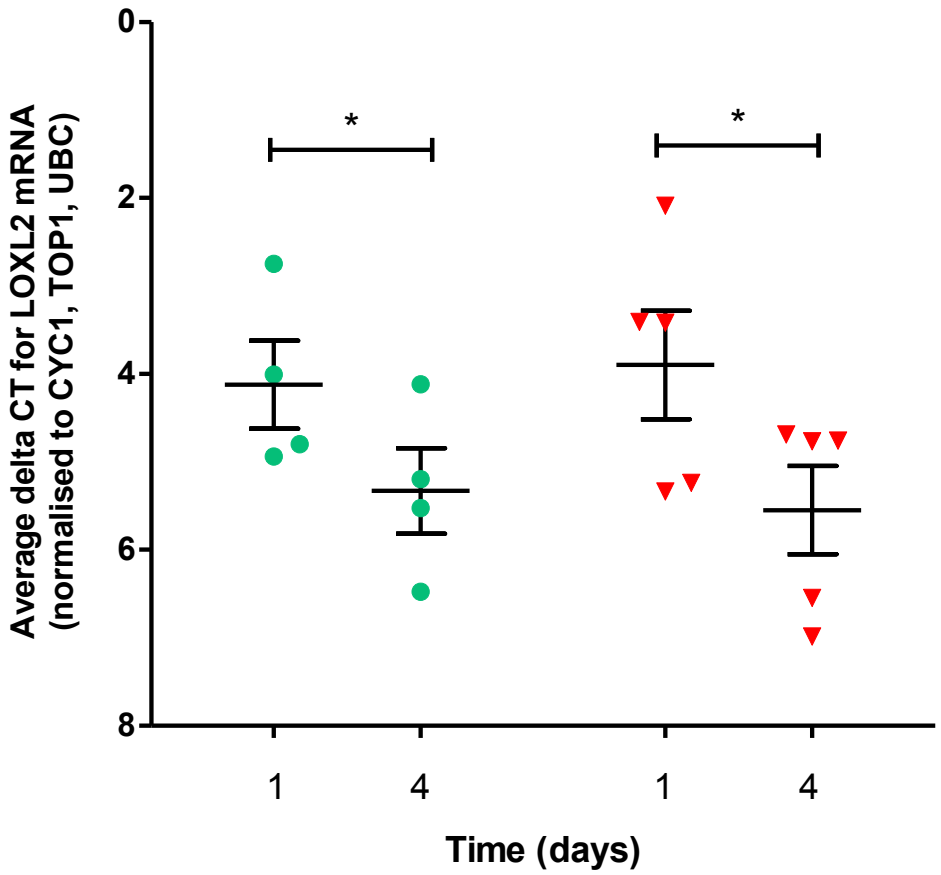

Figure A. 10. *LOXL2* qRT-PCR data for non-IPF and IPF spheroids.

Spheroids were collected 24 hours and 96 hours post seeding. RNA was extracted from the spheroids using Trizol for qRT-PCR to analyse the mRNA levels of *LOXL2*. All data points were normalised to three housekeeping genes based on GeNorm analysis (*CYC1, TOP1*, and *UBC*). Control and IPF spheroids are represented as green circles and red triangles, respectively. (Control, n=4; IPF, n=5). *p <0.05

APPENDIX 6: CCL2 mRNA levels in non-IPF and IPF spheroids

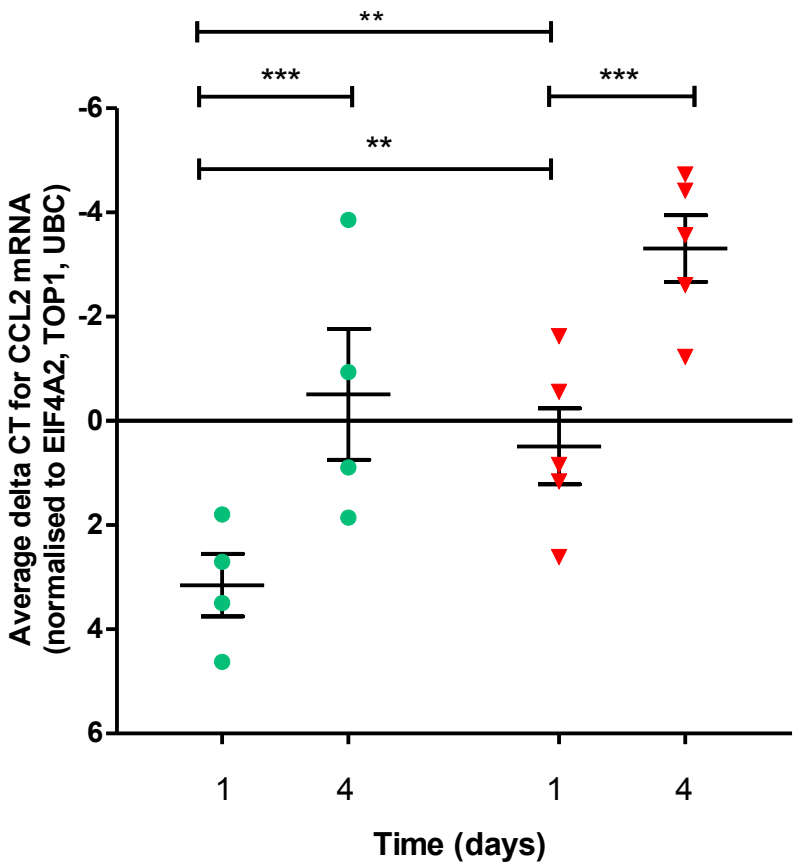

Figure A. 11. *CCL2* qRT-PCR data for non-IPF and IPF spheroids.

Spheroids were collected 24 hours and 96 hours post seeding. RNA was extracted from the spheroids using Trizol for qRT-PCR to analyse the mRNA levels of *CCL2*. All data points were normalised to three housekeeping genes based on GeNorm analysis (*CYC1, TOP1*, and *UBC*). Non-IPF and IPF spheroids are represented as green circles and red triangles, respectively. (Control, n=4; IPF, n=5). *p <0.05

Posters and Presentations

Kanda N., Blanchard A., Chambers R.C., Scotton C.J. Development of novel 3D *in vitro* models of lung fibrosis for studying epithelial-mesenchymal crosstalk

- Poster Presentation at Creative Advance in Fibrosis Therapeutics (CRAFT) Symposium (GSK, Stevenage). November 2011

Kanda N., Nanthakumar C.B., Hatley R., McAnulty R.J., Blanchard A., Chambers R.C., Scotton C.J. Fibroblast spheroids: useful assay for drug evaluation in IPF?

- Poster and flash presentation at CRAFT Symposium (GSK, Stevenage). November 2012
- Presentation at British Association for Lung Research (BALR) conference (Nottingham). July 2013.
- Presentation at London Matrix Group (LMG) symposium (UCL, London). October 2013
- Poster presentation at Infection, Immunology, and Inflammation (III) symposium (UCL, London). October 2013
- Poster presentation at CRAFT Symposium (GSK, Stevenage). January 2014
- Poster presentation at the 18th International Colloquium on Lung and Airway Fibrosis (ICLAF; Canada). September 2014

Prizes

1st Prize poster and flash presentation award: CRAFT symposium (GSK). November 2012

Travel award: BALR conference (Nottingham). July 2013

Runners up poster presentation: **III** symposium (UCL). October 2013

Travel award: ICLAF (Canada). September 2014